ASSEMBLY OF COMPLEX CARBOCYCLIC ARCHITECTURES VIA PALLADIUM AND NICKEL-CATALYZED CYCLIZATIONS

Thesis by

Allison Michelle Stanko

In Partial Fulfillment of the Requirements for

the Degree of

Doctor of Philosophy

CALIFORNIA INSTITUTE OF TECHNOLOGY

Pasadena, California

2024

(Defended April 17th, 2024)

© 2024

Allison Michelle Stanko
ORCID: 0000-0003-0576-3739

To my fiancé, Alex

ACKNOWLEDGEMENTS

My time at Caltech has been the most challenging but also the most rewarding four and a half years of my life. There were many moments when I thought very seriously about quitting, countless times that I asked myself if it was worth it, and many tears shed over failed experiments and feeling "not good enough". I came to Caltech in 2019 to earn my PhD because I truly love organic chemistry, and I couldn't think of anything else that I would rather do than spend the next years of my life in the lab, solving problems that I was excited about and becoming the best scientist that I could be. I want to thank everyone in my life that saw the passion for chemistry within me and helped cultivate it, whether it be through mentorship, emotional support, or personal support. I can say with certainty that I could not have done this alone.

The first people I want to thank are my family; more specifically, the Stanko, Alpert, Ferreira, and Caponetti families. To my parents, Sue and Mike, thank you for the countless times you encouraged me, validated me, and supported me when times were tough. My mom, Sue, is the ultimate hype woman, and her enthusiasm and positivity lifted me out of some really sad times. Thank you for the countless phone conversations, packages full of snacks, hand-painted cards, love, and encouragement. You have no idea how much of an impact these selfless gestures had on my mood, productivity, and success. Thank you to my dad, Mike, for your positive encouragement, and for instilling within me the work ethic that has enabled my success in graduate school. Growing up, I saw time and time again how you never backed down from a challenge, and that you never fretted about having to put in that extra bit of elbow grease to get the job done. The person who taught my dad that sense of bravery and work ethic was my grandpa, Frank. Grandpa Frank (GPF), I want to thank you

for giving me the wisdom to understand the world around me, and the courage to rise above the challenges I've faced over the past 5 years. I want to thank you especially for your extremely wise warning: "Watch out for the alligators". When you first said that to me in high school, I totally laughed it off. But I've come to realize you're right… they're everywhere. My other favorite GPF quote, "You're a racehorse Stanko– don't let the plow horses slow you down", is one that I have repeated to myself time and time again throughout this experience. I love you Grandpa, I'm so grateful to have you in my life. Thank you also to my aunt, Mary, for her love, support, and encouragement. With her ever-present confidence and self-assurance, Mary is an inspiration to me.

To my sister, Elizabeth Alpert, thank you for being a loving sister and a great role model. Through your example, I learned to pursue the things I'm passionate about while loving myself unconditionally and holding onto the things that matter to me in life. To my niece Violet– thank you for the joy you have brought into our lives. I know you're going to grow up and do incredible things. To my brother-in-law, Warren, thank you for your love and support, and for putting up with all the Stanko family shenanigans.

To the Ferreira family, John and Jennifer, thank you for your endless encouragement, positivity, support, and generosity. To Jennifer, thank you for the kind and thoughtful cards, gifts, and messages that brought me joy and kept me going throughout my PhD. To John, thank you for your encouragement, your sage advice, and for inspiring me with stories of your career and successes. You both have made me feel so incredibly loved and accepted into your family.

To my California family– Allison, Andy, and Norah Caponetti, thank you for your love, support, and beautiful memories. Thank you to Allison and Andy for your words of

encouragement, for being fantastic listeners while Alex and I complained about our challenges at work, for all the awesome dinners we enjoyed at your home, and for the adventures we've had together. I can't wait for many more adventures with you both, and with your beautiful daughter Norah.

The next people I'd like to thank aren't technically family, but they certainly have made me feel like it. Thank you to Scott and Silva Virgil for your kindness, support, and generosity. From taking Alex and I to our first opera, to celebrating our engagement, to the most incredible birthday cake I have literally had in my entire life, you two have shared memories with Alex and I that we will have forever. Thank you to Silva for all of the days that you chatted with me and shared your positive energy with me when I stopped by your office. Maybe I never mentioned it to you, but I often came to visit you on days that I was struggling, and your encouragement and kindness lifted me up when I needed it the most. To Scott, thank you for being the most incredible mentor and for sharing your passion for chemistry with me every single day. Thank you for sharing in my excitement about automated reaction setups, for your patience when I asked you to help me with challenging purifications, and for sharing your wisdom and experience with me at every opportunity you had. I truly would not be the chemist I am today without you.

Next, I want to thank my advisor, Brian, for seeing the potential in me and giving me the opportunity to explore the science that I am excited about. I recall the day that I asked to join your lab. That was a really hard day for me, and I will never forget when you said "Ally– I would have been happy to have you two years ago, and I'm happy to have you now." Those words were exactly what I needed to hear in that moment. Thank you for pushing me to be the best scientist I can be, and for the intellectual journey of a lifetime.

I also want to thank my former advisor, Sarah Reisman, for taking me on as a first year and for the lessons that I learned as a young student in your lab. You taught me how to be a more organized and thoughtful chemist, and you inspired me as a highly successful woman in the field of synthetic organic chemistry.

I want to thank the chair of my committee, Professor Hosea Nelson, for your wise advice, thoughtful and challenging questions, and positive attitude. Your recommendation to "push myself out of my scientific comfort zone" is one that will take forward with me as I begin my career as a scientist at Terray. I also want to thank Prof. Kim See, my out of field committee member, for always bringing good questions and good energy to thesis committee meetings.

Thank you to the people who "started it all" for me: my undergraduate advisor Prof. Alison Frontier, and my undergraduate mentor Georgios Alachouzos. Alison welcomed me into her lab with open arms when I was a junior at the University of Rochester, and my memories of the time I spent in her lab are honestly some of the most fun and valuable experiences I have ever had as a scientist and as a person. I want to thank the entire Frontier lab during my time there, George, Connor, Dylan, Eric, Paul, Aleksa, Patrick, and Shukree, for sharing with me your passion and excitement for organic chemistry and making me feel extremely welcome and accepted, despite being the only woman in the lab. Being a part of the group was really what inspired me to attend graduate school in the first place. I want to say a huge thank you to George, my undergraduate mentor. You instilled some fantastic experimental habits in me that I have carried with me throughout my entire graduate career (to this day, I still weigh out my silica before running a column). More importantly, you

pushed me to be the best scientist I could be in the most positive, constructive way possible. I'm incredibly lucky to have had you as a mentor.

To my first mentor at Caltech, Karli Holman, thank you for being a fantastic project partner, and for your support and friendship while I navigated the most difficult time of my life as a first-year graduate student. Thank you for sharing your passion and expertise with me, and for supporting my decision to leave the Reisman lab to join Brian's group. You also instilled in me some fantastic experimental techniques, organizational skills, and smart ideas about lab safety that I am lucky to have carried with me into my time in the Stoltz group.

To my colleagues in the Stoltz lab– thank you for making our lab a truly amazing place to do science. To my fellow 5th year, Melinda, thank you for encouraging me to make the leap and join Brian's lab as a 3rd year, for commiserating with me as we endured our props exams and thesis writing together, and our fun office chats about raves, ski trips, and the best food in LA. Thank you also to my former desk-mate, Veronica Hubble, for making me smile every day and helping me learn the names of heterocycles. To some of my closest friends at Caltech (and in general), Chloe, Kim, and Marva, you brought me sunshine on my darkest days and made lab a fun and positive place to be. Miss Chloe, thank you for our bay dance parties, conversations about the Housewives, listening to rave doof doof music, teaching me how to say "no!", and for laughing with me every day. Because of you, my 5th year was the most fun I have ever had in lab. I am so grateful for your friendship, and I am excited for it to continue growing. To my loyal and brilliant friend Kim, thank you for inspiring me as a scientist, for the countless therapy sessions at twinkle tea, for listening and encouraging me when chemistry wasn't going my way, for chatting with me while I was bored running columns, for feeding me lunch and baked goods, and for being one of my most

caring and loyal friends. I know that we will stay very close in the years to come. To the beautiful Marva, thank you for your empathy, willingness to listen, endless love and generosity, for bringing your flawless energy to lab every single day, and for your inspirational confidence as a woman in STEM. You were there for me through every traumatic lab safety incident, every frustrating day in lab, and of course also to celebrate with me in the joyful moments. To my bay mates– Adrian, Kevin, Samkian the Spider, Christian, and Chloe– thank you for being the "best bay" and for sharing your scientific expertise, positive energy, and excellent taste in music. Thank you especially to Teacher Adrian and Christian– you two were quite literally by my side through every experiment, and it was an absolute pleasure to work next to you two for the past 2.5 years. To Adrian (de Almenara), thank you for being a wonderful project partner, for sharing your endless experimental knowledge with me, and for introducing me to some great soundcloud artists. To the current 4th years in the group- Samir, Jay, Kali, Kevin, Adrian, and Elliot- thank you for inspiring me with your talent and passion and for your friendship and good vibes. Also, to my friends across the hall in the Reisman lab, Stanna and Jordan, thank you for your positive energy and listening ears.

To my friends outside of Caltech– thank you for listening to me complain and for encouraging me and reminding me that it would all be worth it. Thank you to my friends from college, Luke Jenkins, Sarah Hackley, and Stacey Monsell, for all the hours we spent over facetime and for literally traveling 3,000 miles to celebrate my defense with me. I love you guys. Thank you to my bestie Emmy for being one of my biggest cheerleaders, for listening and validating me, for accidental twinning with me on camping trips, and for the most special friendship I have literally had in my entire life. I am so thrilled to be staying in

Los Angeles close to you and Mike, and I can't wait for all our future adventures together. To my amazing friends Melissa and Andrew, thank you for our literal therapy sessions over facetime and beer, for the awesome camping and ski trips together, and for supporting Alex and I over the past few years. To my "bad book bitties"– Sammy, Claire, Jess, Allee, Mikah, Kim, Kelly, Lexie, Cassandra, Dani, and Madeline– thank you for making Tuesday the best day of the week, for giving me your wisdom and perspective, and for being amazingly supportive of me, even though there were many times that I couldn't make it to events and hangouts.

To my sweet and beautiful dog, Astra, I know you will never read this because you literally cannot read, but I promise I will read it to you while I feed you treats: Thank you for the joy you have brought into my life, for the cuddles and kisses when I am sad, for bringing me toys when you are excited, for encouraging me to stop and sniff the flowers, and for being the best dog in the whole damn world. I literally cannot imagine my life without you.

And lastly, to the person whom none of this would be possible without, my fiancé, Alex, thank you for bringing out the best in me, for inspiring me to keep going, and for reminding me of the things that truly matter in life. Thank you for the thousands of hours that you listened to me complain about failed and puzzling experiments, for learning what a TLC is, for the top-notch career coaching/interview prep, for all of the runs to Whole Foods and the meals you delivered to me, for telling me to get back to work and stop doom scrolling, for covering my dog walk for me, for your endless patience on the days when I came home with nothing left to give, for inspiring me with your incredible work ethic and intellect, and for being the most thoughtful, selfless, loving, and generous partner I could ever ask for. Here's to the A-Team, and the adventures that lie ahead of us.

ABSTRACT

Transition metal catalysis can be leveraged to construct challenging chemical bonds with excellent chemo- and stereoselectivity. Herein we describe the discovery of a novel palladium-catalyzed cascade cyclization and a nickel-catalyzed spirocyclization, enabling the assembly of complex carbocyclic architectures. We begin with an introduction describing notable applications of palladium-catalyzed cascade cyclizations in natural product synthesis, enabling the concurrent formation of C–C and C–N bonds in a single synthetic step.

Next, the development of a palladium-catalyzed oxidative Heck/aza-Wacker cascade cyclization is described. This cascade reaction enabled the construction of an all-carbon quaternary center, a C–C bond, and a C–N bond in a single synthetic step. Furthermore, it was employed to build the carbocyclic core of the natural product noraugustamine.

Then, we outline the discovery and optimization of an enantioselective nickel-catalyzed α-spirocyclization of lactones. The established method efficiently and enantioselectively forges 5-, 6-, and 7-membered rings containing all-carbon quaternary centers. This discovery represents an expansion of the synthetic toolkit for enantioselective spirocyclization, providing access to chiral, pharmaceutically relevant spirocyclic products.

Finally, we describe a collaborative project with the Su lab at the University of Arizona in the area of polymer synthesis and gas sensing, where we designed a sensor for the selective detection of gaseous nitric oxide. The sensor's excellent specificity and part-per-trillion level sensitivity was enabled by novel ferrocene-containing polymeric coatings.

PUBLISHED CONTENT AND CONTRIBUTIONS

1. Holman, K. R[†].; **Stanko, A. M.**[†]; Reisman, S. E. Palladium-Catalyzed Cascade Cyclizations Involving C–C and C–X Bond Formation: Strategic Applications in Natural Product Synthesis. *Chem. Soc. Rev.* **2021**, *50* (14), 7891– 7908. https://doi.org/10.1039/D0CS01385D

   [†]These authors contributed equally.

   A.M.S. participated in review conceptualization and scope, reference collection, and manuscript preparation.

2. Holman, K. R.; **Stanko, A. M.**; Richter, M. J. R.; Feng, S. S.; Gessesse, M. N.; Reisman, S. E. Synthesis of Noraugustamine and Development of an Oxidative Heck/Aza-Wacker Cascade Cyclization. *Org. Lett.* **2022**, *24* (16), 3019–3023. https://doi.org/10.1021/acs.orglett.2c00948

   A.M.S. participated in experimental data collection, data analysis, and manuscript preparation.

3. Xu, Y[†].; **Stanko, A. M.** [†]; Cerione, C. S.; Lohrey, T. D.; McLeod, E.; Stoltz, B. M.; Su, J. Low Part-Per-Trillion, Humidity Resistant Detection of Nitric Oxide Using Microtoroid Optical Resonators. *ACS Appl. Mater. Interfaces.* **2024**, *16* (4), 5120– 5128. https://doi.org/10.1021/acsami.3c16012

   [†] These authors contributed equally.

   A.M.S. designed, synthesized, and characterized polymers and led the manuscript preparation.

TABLE OF CONTENTS

CHAPTER 1   **1**

Palladium-Catalyzed Cascade Cyclizations Involving C–C and C–X bond Formation: Strategic Applications in Natural Product Synthesis

CHAPTER 2   **46**

Synthesis of Noraugustamine and Development of an Oxidative Heck/Aza-Wacker Cascade Cyclization

APPENDIX 1   **103**
Spectra Relevant to Chapter 2

CHAPTER 3   **176**
Enantioselective Ni-Catalyzed α-Spirocyclization of Lactones

APPENDIX 2   **304**
Spectra Relevant to Chapter 3

CHAPTER 4   **413**
Low Part-Per-Trillion, Humidity Resistant Detection of Nitric Oxide Using

Microtoroid Optical Resonators

APPENDIX 3   **450**
Spectra Relevant to Chapter 4

ABOUT THE AUTHOR   **463**

LIST OF ABBREVIATIONS

$[\alpha]_d^{23}$	specific rotation at wavelength of sodium D line at 23 degrees celsius
AIBN	Azobisisobutyronitrile
APTES	3-(Aminopropyl) Triethoxysilane
aq	aqueous
CAM	Cerium ammonium molybdate
CGS	Chemiresistive Gas Sensors
$CHCl_3$	Chloroform
CO	Carbon monoxide
COPD	Chronic Obstructive Pulmonary Disease
$Cu(OAc)_2$	Copper(II) acetate
$CuCl_2$	Copper(II) chloride
DAQ	Data Acquisition
DMSO	Dimethyl Sulfoxide
dr	Diastereomeric Ratio
ee	enantiomeric excess
ESI	Electrospray Ionization
Et_2O	Diethyl Ether
FcMA	Ferrocenyl Methacrylate
FDA	Food and Drug Administration
FI	Field Ionization
FLOWER	Frequency Locked Optical Whispering Evanescent Resonator
GPC	Gel Permeation Chromatography
HPLC	High-Performance Liquid Chromatography
HRMS	High Resolution Mass Spectrometry

IR	Infrared Spectroscopy
$KMnO_4$	Potassium permanganate
LDA	Lithium diisopropylamide
LHMDS	Lithium hexamethyldisilazide
LOD	Limit of Detection
MeCN	Acetonitrile
MMA	Methyl Methacrylate
M_n	Number Average Molecular Weight
N	Nitrogen
NO	Nitric oxide
N_2	Nitrogen gas
neoc	Neocuproine
Ni	Nickel
NiBr2(dtbbpy)	Nickel(II) bromide bis(di-tert-butyl2,2'bipyridine)
NMR	Nuclear Magnetic Resonance
NO	Nitric Oxide
O	Oxygen
OAc	Acetate
OTf	Trifluoromethanesulfonate
PCCs	Palladium catalyzed cascade cyclizations
Pd	Palladium
$Pd(TFA)_2$	Palladium(II) trifluoroacetate
PDI	Polydispersity Index
PhBr	Bromobenzene
PMMA	Poly(methyl methacrylate)
ppb	Part-per-billion

ppmv	Parts Per Million by Volume
ppq	Part-per-quadrillion
ppt	Parts Per Trillion
RAFT	Reversible Addition Fragmentation Chain Transfer
RSAW	Rayleigh Surface Acoustic Wave
SWNT	Single Wall Carbon Nanotube
TBME	*tert*-butyl methyl ether
TBS	*tert*-Butyldimethylsilyl
TEC	Thermo Electric Cooler
TFA	Trifluoroacetic acid
THF	Tetrahydrofuran
THP	Tetrahydropyran
TLC	Thin-Layer Chromatography
UV	Ultraviolet
WGM	Whispering Gallery Mode

CHAPTER 1

Palladium-Catalyzed Cascade Cyclizations Involving C–C and C–X

Bond Formation: Strategic Applications in Natural Product Synthesis[†]

1.1   INTRODUCTION

Strategically applied cascade reactions can enable the rapid construction of natural product core structures from simpler starting materials, dramatically shortening and simplifying synthetic plans.[1] As the breadth of palladium-catalyzed C–X (X = O,N) and C–C bond-forming reactions has expanded over the past 30 years, palladium-catalyzed cascade cyclizations (PCCs) have emerged as a powerful strategy to forge multiple rings in a single synthetic operation.[2]

In a cascade (or domino) reaction, multiple bond-forming and/or bond-breaking transformations occur sequentially under a constant set of conditions. In order for a process to be classified as a cascade, the functionality required for the second transformation must be generated as a result of the first.[2] These processes are occasionally referred to as tandem reactions, but there is some controversy to this nomenclature. The term "tandem reaction" has previously been used to describe sequential transformations occurring under a changing set of conditions, so we will abstain from using this term to describe the cascade reactions

covered herein.[3] It has also become customary to name PCCs after known cross-coupling reactions, such as the Heck reaction, with which they share some mechanistic steps. However, we find this nomenclature to be problematic, given that the mechanisms of most cascades are not identical to those of their parent cross-couplings. Therefore, with the exception of named cascade reactions, such as the Larock heteroannulation, we refer to PCCs by their key bond-forming mechanistic steps.

Palladium-catalyzed cascade reactions have been defined mechanistically as consisting of three parts: initiation, relay, and termination (Figure 1.1).[4] An initiation step, for example, nucleopalladation or oxidative addition, generates a carbon- or heteroatom-bound Pd species. This intermediate then undergoes one or more relay steps, such as olefin carbopalladation or carbonylation. A termination step, such as β-hydride elimination or nucleophilic capture, releases the cascade product and regenerates the Pd catalyst.

Figure 1.1 *Mechanistic analogy for palladium-catalyzed cascade reactions.*
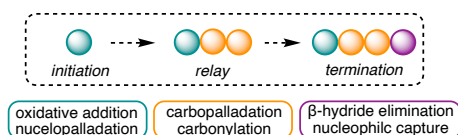
In this review, we demonstrate how the strategic application of PCCs can expedite the total synthesis of complex natural products, enabling the formation of multiple rings and both C–C and C–X bonds in a single synthetic operation. We begin by discussing how carbonylative cascades can be employed to build fused and spirocyclic lactones into carbocyclic frameworks, enabling the synthesis of multiple natural products including (±)-schindilactone A (**3**) and (+)-perseanol (**2**, Figure 1.2). Next, we describe how the Larock

heteroannulation cascade can forge both C–C and either C–O or C–N bonds to construct

indole or benzofuran-containing natural products. Finally, we focus on cascades that are

used to form both C–C and C–N bonds, facilitating the total synthesis of complex alkaloids

such as (+)-mitomycin K (**1**).

Figure 1.2 *Representative natural products synthesized via PCC.*
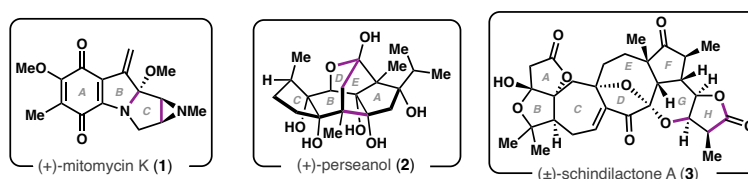
1.2 C–C AND C–O BOND FORMATION: CARBONYLATIVE CASCADES

1.2.1 The Semmelhack Reaction

The Semmelhack reaction was initially developed as a means to investigate the

stereoselectivity of olefin oxypalladation, a key mechanistic step in the Wacker process

(Scheme 1.1a). Following oxypalladation of *cis*-2-butene (**4**), Stille and coworkers sought

to trap the resultant alkylpalladium intermediate (**5**) before it could undergo β-hydride

elimination to form **6**.[5] As carbonylation of alkylpalladium species had previously been

shown to occur at a faster rate than β-hydride elimination, **4** was subjected to typical

Wacker conditions in the presence of carbon monoxide. *Trans*-oxypalladation was

followed by carbonylation and methanol trapping to afford β-methoxyester **7**.

In 1984, Semmelhack and Bodurow applied this cascade to the synthesis of

tetrahydrofuran (THF) and tetrahydropyran (THP) rings from alcohols bearing pendant

olefins.[6] Here, the catalytic cycle is thought to be initiated by intramolecular oxypalladation

of olefin **8** to form alkylpalladium **9** (Scheme 1.1b). Carbonylation and methanol trapping

then afford **11**, and the liberated Pd^0 complex is oxidized by CuCl$_2$ to regenerate Pd^{II}. In

another report, intramolecular trapping of the acyl-Pd^{II} complex was found to give rise to

two rings in a single transformation. In this case, stoichiometric Pd(OAc)$_2$ was used instead

of PdCl$_2$/CuCl$_2$ (Scheme 1.1c).[7] The Semmelhack reaction has since been widely used in

the synthesis of complex natural products due to its mild reaction conditions, functional

group tolerance, and generally high yields.[8]

Scheme 1.1 *Development of the Semmelhack reaction.*
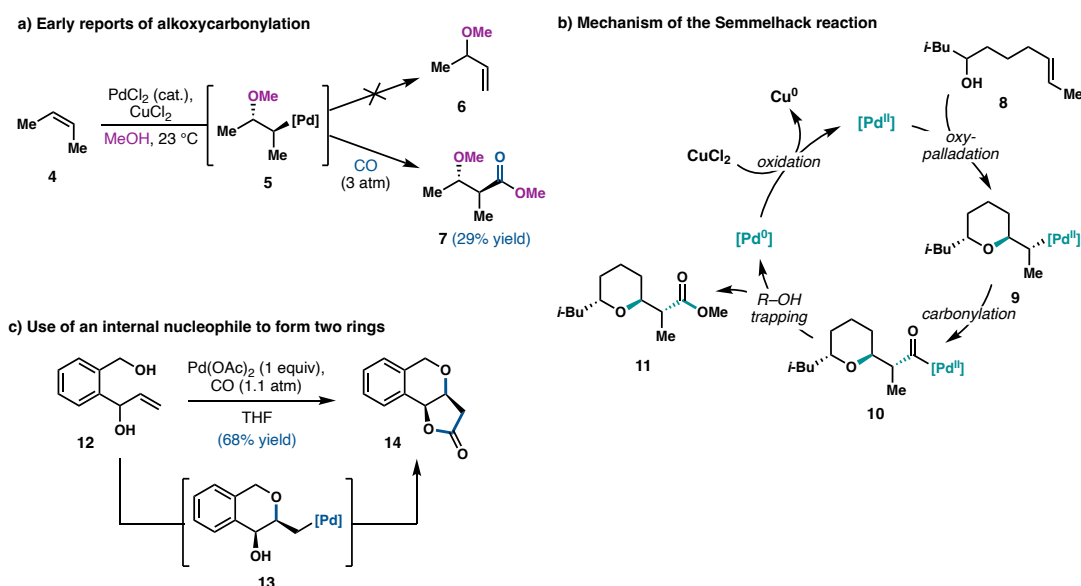
Total Synthesis of (–)-Kumausallene

One notable application of the Semmelhack PCC in natural product synthesis is

Tang and Werness' synthesis of (–)-kumausallene (**15**), a bromoallene-containing

nonisoprenoid sesquiterpene (Scheme 1.2a).[9] Given that previous synthetic approaches by

Overman and Evans were challenged by stereoselective bromoallene formation, Tang and

Werness envisioned a biomimetic approach. Late-stage biomimetic bromoetherification

could selectively afford **15** from (+)-trans-deacetylkumausyne (**16**), the putative

biosynthetic precursor to (–)-kumausallene. Enyne **16** could arise from pseudosymmetric

lactone **17**, which could in turn be formed via Semmelhack reaction of known diol **18**. The

use of a PCC early in the synthesis of **15** would allow rapid entry to the polycyclic

framework by exploiting the symmetry present in the natural product.

Key to the success of this strategy was the robust nature of the Semmelhack reaction

on scale. Indeed, subjection of C2-symmetric diol **18**, accessed in three steps from

acetylacetone, to typical Semmelhack reaction conditions afforded **17** in 87% yield on

gram scale (Scheme 1.2b). With ready access to lactone **17**, it was then elaborated to enyne

16 in seven steps. Finally, upon treatment with N-bromosuccinimide, **16** readily underwent

bromoetherification to afford (–)-kumausallene as a single diastereomer.

Scheme 1.2 *Total synthesis of (–)-kumausallene.*
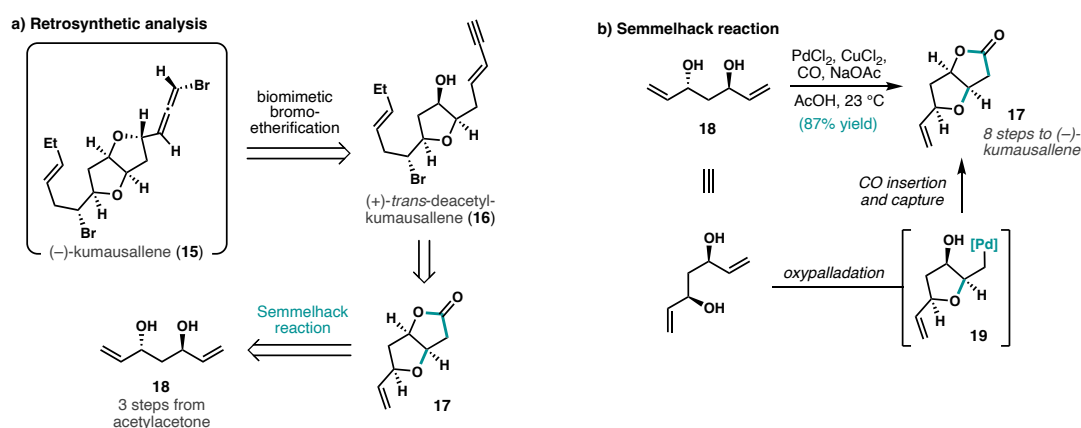
Total Synthesis of (±)-Schindilactone A

Tang, Chen, and Yang's synthesis of (±)-schindilactone A **(3)** further demonstrated

the utility of the Semmelhack reaction in natural product synthesis (Scheme 1.3a).[10]

Schindilactone A was isolated in 1982 from the Schisandraceae family of flowering plants, many species of which have been used in traditional Chinese medicine. With twelve stereogenic centers decorating a highly oxygenated octacyclic framework, **3** is a formidable synthetic target. In contrast to Tang and Werness' synthesis of (–)-kumausallene, wherein the cascade was performed early in the synthesis to rapidly build complexity, here a Semmelhack reaction was used on an advanced substrate.

Retrosynthetically, **3** was first disconnected at the A ring, which was envisioned to arise from aldol addition of an acetyl-protected alcohol to the B ring lactone. Next, a Semmelhack reaction was proposed to form the G and H rings. This disconnection simplified the natural product to pentacyclic compound **21**. The F ring could be installed via a Pauson–Khand reaction, and the central E ring could arise from cross-coupling followed by ring-closing metathesis. The proposed late-stage Semmelhack reaction would be key in constructing two of the final rings of the natural product. However, this strategy would require an especially robust cascade to be able to perform well on highly functionalized **21**.

In prior studies, Chen and Yang found that the Semmelhack reaction could be used to construct the GH ring system of a related natural product. Model substrate **22** underwent Semmelhack reaction to afford **24** in 95% yield (Scheme 1.3b). Encouraged by these studies, advanced intermediate **21** (prepared in 22 steps) was subjected to similar reaction conditions (Scheme 1.3c). By increasing the catalyst loading relative to the model studies (from 30 to 50 mol %), **20** could be obtained in 78% isolated yield. Lactone **20** was then

elaborated to **3** in a six-step sequence to achieve the first total synthesis of (±)-

schindilactone A in 29 steps.

Scheme 1.3 *Total synthesis of (+)-schindilactone A.*

a) Retrosynthetic analysis

b) Model system studies

c) Application to (±)-schindilactone A
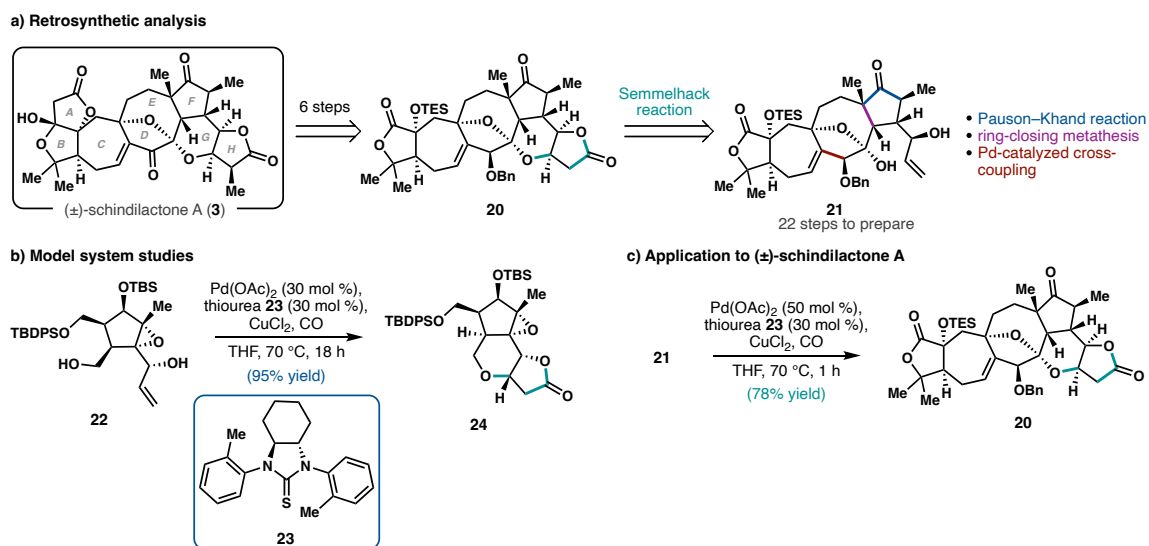
The Semmelhack PCC has been employed in the synthesis of a number of other

natural products: (–)-plakortone D (**25**),[11] (±)-crisamicin A (**26**),[12] (±)-pallambins C and D

(**27**),[13] and (±)-pallambins A and B (**28**, Figure 1.3).[14] Together, these syntheses illustrate

the utility of the Semmelhack reaction to construct the bicyclic lactone motif found in a

variety of natural product classes. Although application of this PCC is limited to lactone

formation, the compatibility of the Semmelhack reaction with both early and late stages of

a synthesis makes it an attractive strategy to synthesize complex, polycyclic systems.

Figure 1.3 *Other natural products synthesized via Semmelhack reaction.*

(–)-plakortone D (**25**)   (±)-crisamicin A (**26**)   (±)-pallambins C and D (**27**)   (±)-pallambins A and B (**28**)
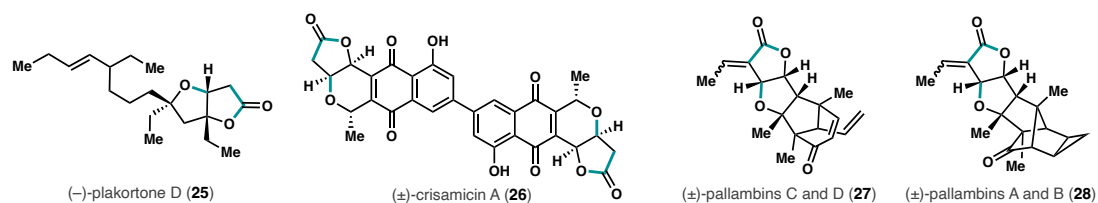
1.2.2 Carbopalladation/Carbonylative Lactonization

Recently, PCCs involving carbopalladation followed by carbonylation have been used in natural product synthesis. This reaction, initially reported by Grigg and coworkers in 1993, shares some common features with the Semmelhack reaction (Scheme 1.4a).[15] Rather than olefin oxypalladation, the initiating step of this cascade is oxidative addition of an aryl or alkenyl halide **(29)** to a Pd^0 species (Scheme 1.4b). Subsequent migratory insertion (i.e., carbopalladation) of a pendant olefin forms the first ring, resulting in alkyl PdII species 32. Carbon monoxide insertion affords acyl Pd^{II} species **33**, then capture by an internal alcohol nucleophile forges the second ring and releases Pd^0. Overall, one C–O and two C–C bonds are formed in a single transformation. This reaction is often referred to in the literature as the "Heck/carbonylative lactonization cascade". However, as we have previously described, this nomenclature is not accurate; the cascade does not involve all of the same mechanistic steps as the Heck reaction. Thus, we refer to this reaction as the carbopalladation/carbonylative lactonization cascade.

Despite their mechanistic similarities, this cascade provides access to structurally distinct scaffolds from the Semmelhack reaction: multiple C–C bonds are formed, enabling construction of a broader variety of ring systems. Additionally, an exogenous stoichiometric oxidant is not required. However, premature carbonylation can be a challenge. In order for this cascade to proceed in high yield, alkene insertion of species **31** must outcompete CO insertion.

Scheme 1.4 *The carbopalladation/carbonylative lactonization cascade.*
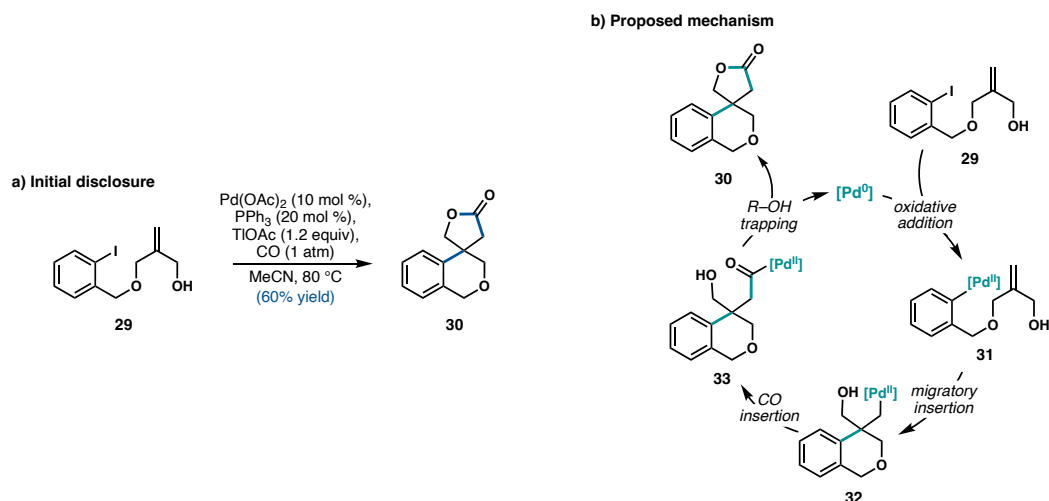
Total Synthesis of (–)-Spinosyn A

The carbopalladation/carbonylative lactonization cascade was first applied to natural product synthesis in Dai and coworkers' synthesis of (–)-spinosyn A (**34**, Scheme 1.5a).[16] (–)-Spinosyn A is the primary component of spinosad, a broadly used insecticide with an excellent environmental profile and low mammalian toxicity. Cross-resistance to spinosad has recently emerged, necessitating an efficient synthetic route to **34** for access to structural analogs. Prior to Dai and coworkers' report, the shortest synthesis of **34** required 31 total steps (23 in the longest linear sequence).

Dai and coworkers envisioned disconnecting **34** through a late-stage palladium-catalyzed carbopalladation/carbonylative macrolactonization cascade. The proposed macrolactonization cascade presented several potential challenges: 5-exo-trig cyclization of the alkenyl- or acyl-Pd intermediates onto the cyclohexene olefin could interfere with desired reactivity, the diastereoselectivity of the olefin carbopalladation was unknown, and

macrocycle formation via the carbopalladation/carbonylative lactonization cascade was unprecedented.

The key strategic steps were initially validated in a simpler model system (Scheme 1.5b). Propargylic acetate **36**, formed via a convergent 1,2-addition, smoothly rearranged under gold catalysis to give **37**. Excitingly, carbopalladation/carbonylative macrolactonization of **37** afforded **38** in 58% yield and 3:1 dr. The 6-membered ring was thought to promote the desired carbopalladation via the Thorpe–Ingold effect, placing the alkenyl iodide and pendant olefin in close proximity.

In light of these promising results, fully elaborated substrate **39** was prepared and subjected to the reaction conditions (Scheme 1.5c). After some reoptimization, including a change in ligand and increased CO pressure, the desired cyclization proceeded in 43% yield to afford 12-membered lactone **40** as a single diastereomer. Macrocycle **40** could be advanced to (–)-spinosyn A in four additional steps, requiring 23 total steps (15 in the longest linear sequence). This synthesis expanded the scope of the carbopalladation/carbonylative macro-lactonization cascade, demonstrating its efficacy in forming fused macrocyclic ring systems. Furthermore, the smooth transition from the model system to the fully functionalized system is a promising indicator that homologous complex substrates may be tolerated in the reaction, enabling the preparation of analogs of **34**.

Scheme 1.5 *Total synthesis of (–)-spinosyn A.*

a) Approach: Late-stage macrolactonization

b) Model studies

c) Carbopalladation/carbonylative lactonization cascade
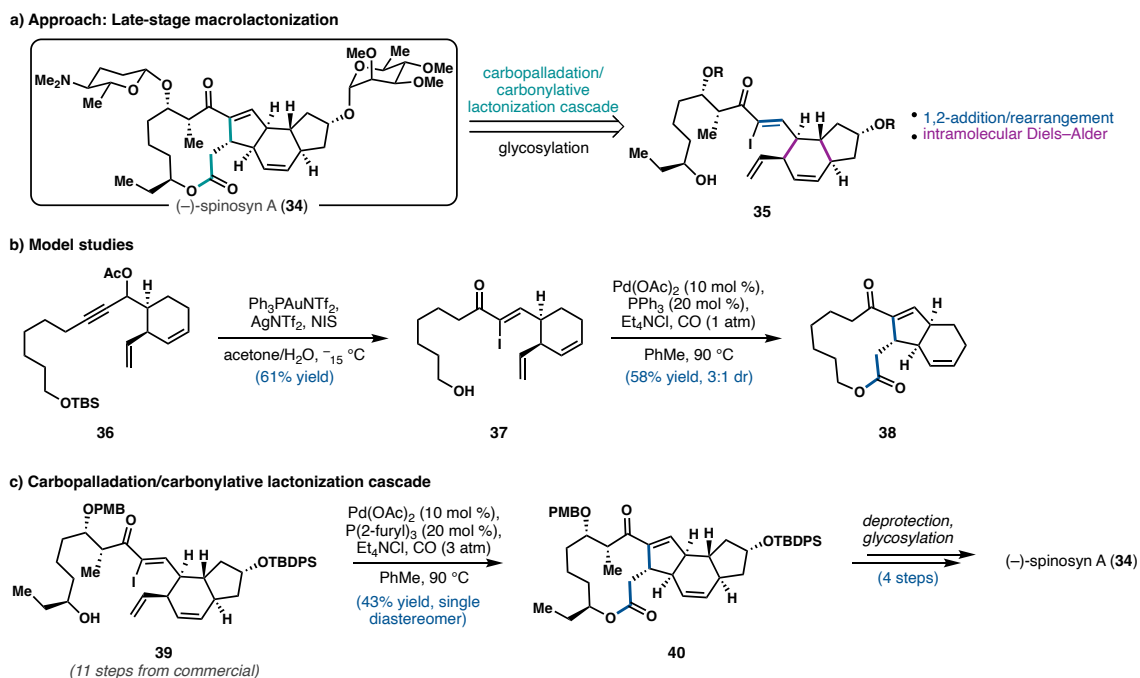
Total Synthesis of (+)-Perseanol

The carbopalladation/carbonylative lactonization cascade was also employed in Reisman and coworkers' synthesis of (+)-perseanol (**2**), an isoryanodane diterpene with potent antifeedant and insecticidal properties (Scheme 1.6a).[17] An approach to the pentacyclic isoryanodane core was developed by Inoue and coworkers; however, no completed syntheses of **2** or other isoryanodane diterpenes had been disclosed. Reisman and coworkers proposed formation of the E ring at a late stage, disconnecting **2** to **41**. A two-part convergent fragment coupling strategy was designed to efficiently access **41**. First, two fragments of similar size and complexity would be united via 1,2-addition of alkenyl iodide **43** to aldehyde **42** (Scheme 1.6b). Next, a palladium-catalyzed carbo-

palladation/carbonylative lactonization cascade of the resulting alcohol **44** would close the

B and D rings to afford **41**.
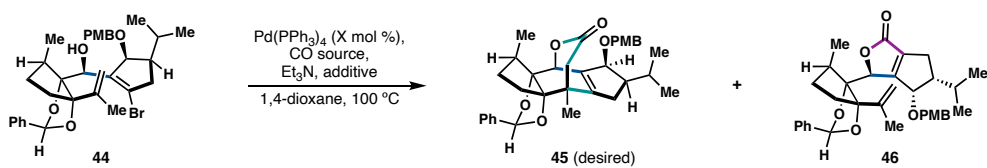
Scheme 1.6 *Strategic Approach to (+)-Perseanol*
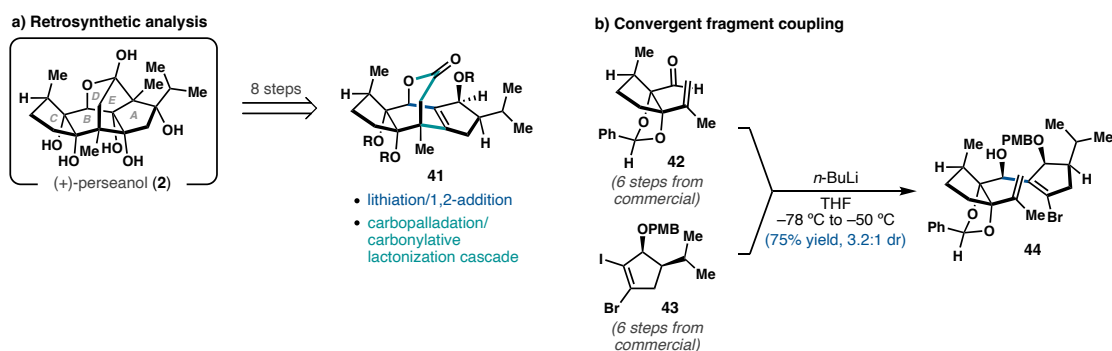
To that end, cyclopentene fragments **42** and **43** were each prepared in six steps from

commercially available substrates and coupled to give secondary alcohol **44** in 75% yield.

With substrate **44** in hand, the carbopalladation/carbonylative lactonization cascade was

investigated (Table 1.1). Initial attempts resulted in recovery of significant amounts of

unreacted starting material (entry 1). Hypothesizing that coordination of CO to palladium

inhibited the rate of oxidative addition, the reaction mixture was stirred at 100 °C for 60

minutes before addition of CO (entry 2). In this case, the desired product **45** was obtained

in modest yield alongside premature carbonylation product **46**. The yield of **45** could be

further improved by increasing the palladium loading to 120 mol % and the prestir time to

90 minutes as well as changing the palladium source (entry 3). Reagents that generate CO

in situ were also tested, in hopes that maintaining low concentration of CO would enable

the use of catalytic amounts of palladium (entries 4–7). The use of N-formylsaccharin in

combination with KF ultimately afforded **45** in 57% yield using 50 mol % catalyst (entry

8). Cascade product **45** was advanced to **2** in 8 additional steps, completing the first total

synthesis of (+)-perseanol in 16 steps (longest linear sequence) from (R)-pulegone.

Table 1.1 *Optimization of carbopalladation/carbonylative lactonization cascade.*

entry	Pd loading (mol %)	CO source	additive	**44** (%)	**45** (%)	**46** (%)
1	50[a]	CO (1 atm), 5 min prestir	-	75	10	5
2	50[a]	CO (1 atm), 60 min prestir	-	50	34	9
3	120	CO (1 atm), 90 min prestir	-	23	48	13
4	50	$Mo(CO)_6$	DBU	85	0	8
5	50	*t*-BuNC	-	90	0	0
6	50	phenyl formate	-	14	7	4
7	50	*N*-formylsaccharin	-	22	31	10
8	50	*N*-formylsaccharin	KF	1	57	14

[a]Pd(P(*t*-Bu)$_3$)$_2$ with 2X mol % P(*p*-F-Ph)$_3$ was used as Pd source

Carbonylative Spirolactonization of Hydroxycyclopropanols: Total Synthesis of α-

Levantenolide and α-Levantanolide

A final example of a carbonylative PCC in natural product synthesis is Zare,

Waymouth, and Dai's synthesis of α-levantenolide (**47**) and α-levantanolide (**48**, Scheme

1.7a).[18] Motivated by a lack of methods to efficiently synthesize oxaspirolactones, the

authors envisioned that readily available hydroxycyclopropanols could be used to access

these valuable materials (Scheme 1.7b). The authors hypothesized that

hydroxycyclopropanol **49** could first engage with a Pd^{II} catalyst, undergoing β-carbon

elimination to form Pd-homoenolate **50**. Ketal formation w›ith a pendant alcohol and

hydroxyl coordination would give rise to **51**, which could form the desired oxaspirolactone

(**52**) after CO insertion and lactonization. An oxidant would then be required to regenerate

Pd^{II}.

Scheme 1.7 *Spirolactonization strategy toward α-levantenolide and α-levantanolide.*
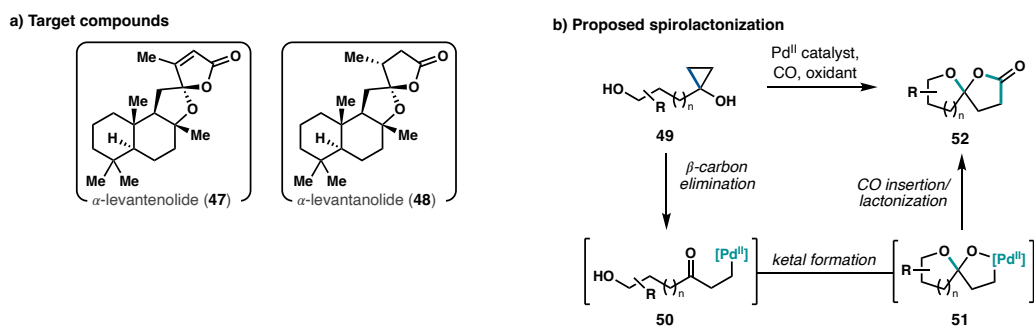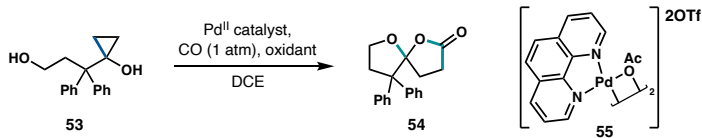
The proposed cascade was developed using model substrate **53** (Table 1.2).

Pd(TFA)$_2$ and [(cinnamyl)PdCl]$_2$ were effective in combination with CO and 2 equivalents

of benzoquinone (entries 1 and 2). Hypothesizing that an electron-deficient palladium

species would facilitate coordination of the cyclolopropanol [Pd(neoc)(OAc)]$_2$(OTf)$_2$ (**55**)

was tested, and the yield improved to 85% (entry 3). A balloon of oxygen could be used in

place of benzoquinone, though the yield was significantly reduced (entry 4). Increasing the

temperature to 50 °C allowed the catalyst loading and reaction time to be reduced, affording

product in 89% yield after only 18 h with 5 mol % catalyst (entry 5). The efficacy of this

reaction was further demonstrated using a set of 23 hydroxycyclopropanol substrates, with

yields ranging from 50 to 99%. Having developed a robust method for the carbonylative

spirocyclization of hydroxycyclopropanols, the authors applied this reaction to the

syntheses of **47** and **48** (Scheme 1.8).

Commercially available (+)-sclareolide (**56**) was converted to cyclopropanol **57** in

57% yield. The spirolactonization cascade proceeded in 53% total yield and required only

2 mol % catalyst; however, a mixture of diastereomers was obtained. The desired

diastereomer, **48**, was isolated in 30% yield. This was consistent with the substrate scope,

Table 1.2 *Development of spirolactonization cascade.*

entry	Pd catalyst (mol %)	oxidant	T (°C)	time (h)	yield (%)
1	Pd(TFA)$_2$ (10)	BQ	23	14	30
2	[(cinnamyl)PdCl]$_2$ (10)	BQ	23	60	66
3	**55** (10)	BQ	23	60	85
4	**55** (10)	O$_2$	23	60	60
5	**55** (5)	BQ	50	18	89

in which spiro[4.4] ring systems were generally synthesized in poor dr, but spiro[4.5]

systems were generally obtained with good dr. Nevertheless, α-levantanolide (**48**) was

obtained in 17% overall yield across two steps. Both diastereomers of spirocyclization

product (**48** and **58**) could be carried forward in a two-step sequence, affording α-

levantenolide (**47**) in four steps and 14% overall yield.

Scheme 1.8 *Total synthesis of α-levantenolide and α-levantanolide.*
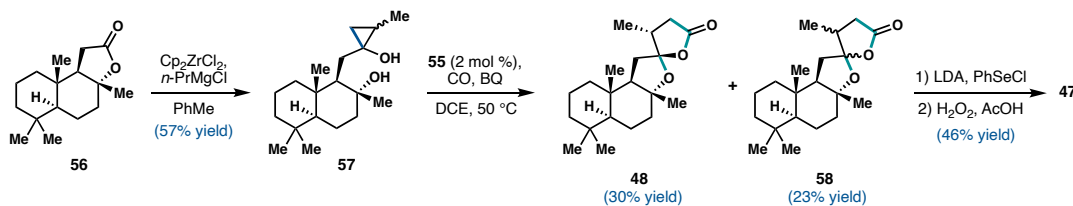
1.3 C–C AND C–O OR C–N BOND FORMATION: LAROCK

HETEROANNULATIONS

Providing access to distinct chemical space from the previously described

carbonylative cascades, the Larock heteroannulation reaction enables the one-step

synthesis of 2,3-disubstituted indoles, benzofurans, and related heterocycles. Multistep

versions of this transformation involving initial cross-coupling of an alkynyl tin or thallium

species onto the aryl ring and then subsequent cyclization to form a 3-substituted indole
were originally established by Taylor, McKillop and Stille.[19] The widely used single-step
heteroannulation method was developed by Larock soon after these initial reports.[20] The
method was later expanded for the synthesis of 1,2-dihydroisoquinolines, benzofurans,
benzopyrans, and isocoumarins.

The proposed mechanism for these reactions involves initial reduction of the Pd^{II}
source to Pd^0, subsequent oxidative addition of the aryl iodide **59**, alkyne coordination and
insertion to give alkenyl Pd species **62**, and reductive elimination to release the indole
product (**63**, Scheme 1.9).[21] If the difference in size between alkyne substituents is large
enough, the annulation occurs with high regioselectivity. Given that the interaction
between the larger substituent (R^L) and a developing Pd–C bond will be less than that
between R^L and a shorter C–C bond, R^L is placed at the 2-position of the indole.

Scheme 1.9 *Proposed catalytic cycle for the Larock heteroannulation cascade.*
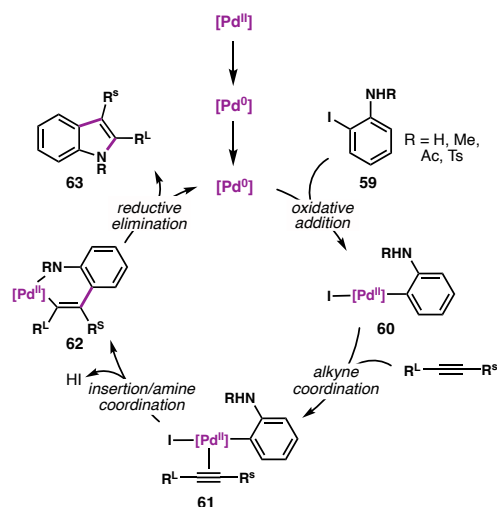
Total Synthesis of Eight Ergot Alkaloids

The 3,4-fused indole motif is present in many bioactive natural products, necessitating streamlined methods for the construction of these scaffolds (Scheme 1.10a). Striving to establish a general strategy for the single-step construction of this moiety, Jia and coworkers developed an intramolecular Larock heteroannulation reaction. They aimed to apply the method to the natural product fargesine (**68**) as a proof of concept.[22] To the authors' delight, the optimization of this method proved simpler than anticipated, as the standard conditions for the Larock indole synthesis furnished the desired 3,4-fused indoles in good to excellent yields (Scheme 1.10a). Furthermore, this method could be used to form both medium-sized rings as well as macrocycles. Additionally, 2-bromoanilines could be employed as substrates in the presence of a MePhos (**79**) or dppp ligand in place of the traditional PPh₃ ligand. Finally, the application of this method enabled the 8-step total synthesis of (±)-fargesine (Scheme 1.10b).

Scheme 1.10 *Development and application of intramolecular Larock heteroannulation method.*
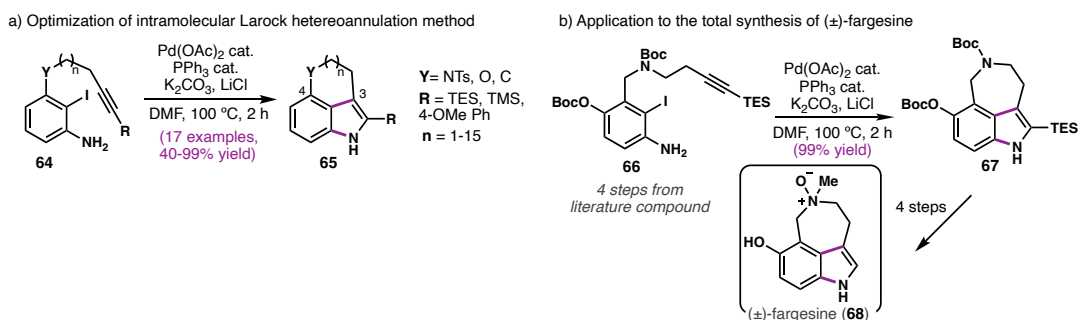
Many natural products produced by ergot fungi also contain the 3,4-fused indole scaffold, and members of this class display diverse and medicinally relevant bioactivities.

In fact, several ergot alkaloids are used in the clinical treatment of migraines and Parkinson's disease, rendering natural products in this class attractive synthetic targets.[23] Demonstrating the synthetic utility of their previously established intramolecular Larock heteroannulation method, Jia and coworkers designed a highly divergent synthetic route for the total syntheses of (±)-festuclavine (**69**), (±)-9-deacetoxy-fumigaclalvine C (**70**), (±)-pibocin A (**71**), (±)-fumigaclavine G (**72**), (±)-dihydrosetoclavine (**73**), (±)-iso-dihydrosetoclavine (**74**), (±)-costaclavine (**75**), and (±)-epi-costaclavine (**76**) from common intermediate **77** (Scheme 1.11).[24] Larock heteroannulation precursor **78** was accessed in 6 steps from commercially available 2-bromo-1-methyl-3-nitrobenzene.

Scheme 1.11 *Abbreviated retrosynthetic strategy for the synthesis of eight ergot alkaloids.*
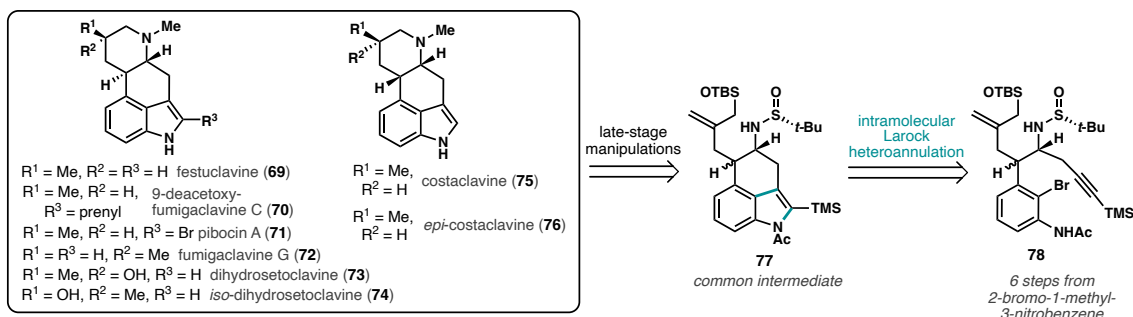
When **78** was subjected to the previously established PCC conditions, the expected heteroannulation product was obtained in 92% yield on gram scale (Scheme 1.12a). Surprisingly, tetracyclic product **80**, the result of an unexpected one-pot Larock heteroannulation/Tsuji–Trost allylation, was also isolated in a trace amount. Because the requisite functionality for the Tsuji–Trost allylation was already present in the starting material, this reaction is most accurately described as a "one-pot" transformation rather

than a cascade. By simply increasing the Pd and ligand loadings, tetracyclic product **80**
was obtained in 65% yield, along with 25% of the Larock heteroannulation product, **77**
(Scheme 1.12b). Impressively, this one-pot transformation established the tetracyclic
framework shared by the target ergot alkaloids and forged two C–N bonds and one C–C
bond in a single synthetic step. Furthermore, this constituted the first example of Tsuji–
Trost allylation utilizing a TBS-protected allylic alcohol. Each ergot alkaloid target was
subsequently accessed from tetracyclic indole **80** in five or fewer steps, demonstrating the
synthetic efficiency and versatility of this divergent synthetic route.

Scheme 1.12 *One-pot Larock heteroannulation cascade/Tsuji-Trost allylation.*
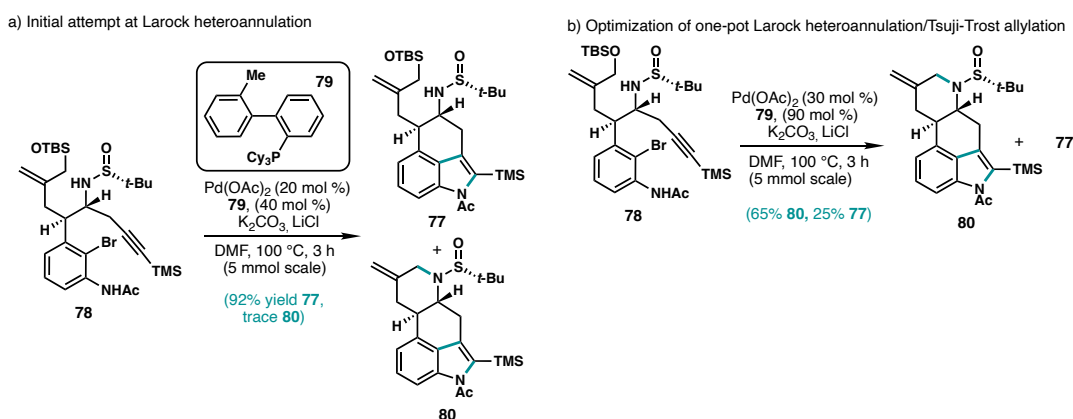
Catalytic Asymmetric Total Synthesis of (–)-Galanthamine and (–)-Lycoramine

In pursuit of (–)-galanthamine and (–)-lycoramine, two benzofuran-containing
Amaryllidaceae alkaloids, the Jia group aimed to expand their intramolecular Larock
heteroannulation methodology for the synthesis of 3,4-fused benzofurans.[25] Screening of
multiple ligands and Pd sources revealed that $Pd_2(dba)_3 \cdot CHCl_3$ and $P(t\text{-Bu})_3 \cdot HBF_4$ were
the optimal reagents (Scheme 1.13). The substrate scope was quite general, enabling the
construction of 6–9-membered rings containing O or N heteroatoms and tolerating various

substitutions at the 2-position. Notably, the desire to utilize the Larock heteroannulation

cascade to construct (–)-galanthamine (**83**) and (–)-lycoramine (**84**) resulted in the

expansion of the substrate scope for this reaction, demonstrating that strategic applications

can have impacts beyond the realm of natural product synthesis.

Scheme 1.13 *Substrate scope of Larock heteroannulation method.*
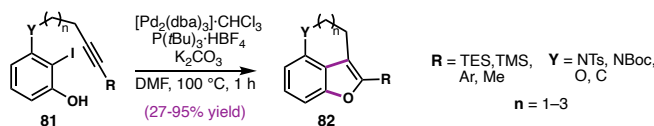
Amaryllidaceae alkaloids **83** and **84** are medicinally relevant targets that have

demonstrated inhibition of acetyl-cholinesterases; in fact, (–)-galanthamine has been used

clinically to treat Alzheimer's disease. Previous approaches aimed to form the "B" or "D"

ring at a late stage in the synthesis. In contrast, Jia and coworkers aimed to construct the

ABD ring system in a single synthetic operation through a palladium-catalyzed Larock

heteroannulation reaction. Retrosynthetically, a late-stage asymmetric Michael

addition/aldol sequence would be used to forge the C ring from benzofuran **86**, which

would be prepared via PCC of iodophenol **87** (Scheme 1.14a). The optimized

heteroannulation cascade translated well to the fully elaborated system, enabling the

catalytic asymmetric total synthesis of (–)-galanthamine and (–)-lycoramine, which were

completed in 14 and 9 steps, respectively (Scheme 1.14b). Although it was two steps longer

than the shortest catalytic asymmetric synthesis of (–)-galanthamine achieved by Zhou and

Xie, the unique retrosynthetic strategy developed by Jia and coworkers led to an expansion

of the substrate scope for the Larock heteroannulation reaction, laying the groundwork for

future applications to the synthesis of medicinally important benzofuran natural products.

Scheme 1.14 *Total synthesis of (–)-galanthamine and (–)-lycoramine.*
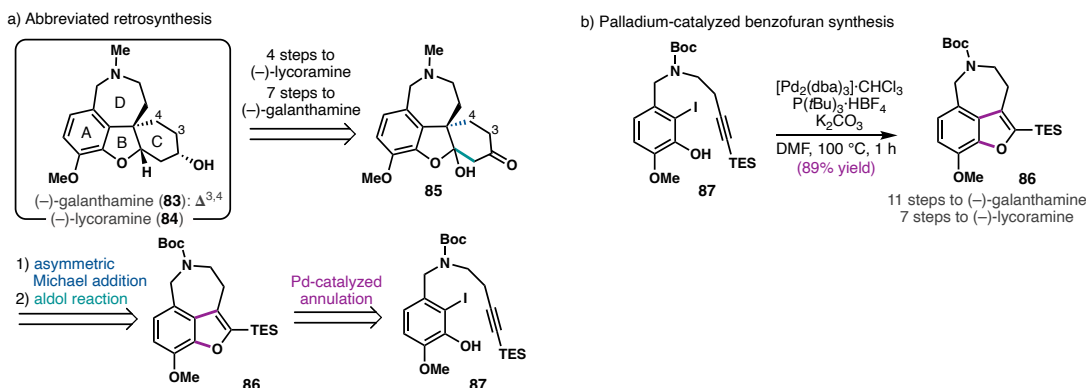
Asymmetric Total Synthesis of (+)-Halenaquinone and (+)-Halenaquinol

To the best of our knowledge, Shibasaki and coworkers' total synthesis of (+)-halenaquinone (**88**) and (+)-halenaquinol (**89**), completed in 1996, was the first published application of PCC in natural product synthesis (Scheme 1.15a).[26,27] This approach featured two key palladium-catalyzed reactions: a one-pot Suzuki cross-coupling/asymmetric Heck coupling and a Larock heteroannulation cascade. The combination of these two palladium-catalyzed cyclization reactions was a creative strategy that enabled the rapid assembly of the pentacyclic core of **88** and **89**.

Retrosynthetically, both targets were derived from compound **90**, the product of the key Larock heteroannulation cascade. The Larock heteroannulation substrate **91** was accessed in 8 step sequence involving multiple oxidations and functional group manipulations of **93**. Compound **93** was accessed via a novel one-pot Suzuki coupling/Heck coupling reaction. Although the authors denote this process as a "cascade", we disagree with this nomenclature, as the requisite functionality for the second Heck coupling is already present in the substrate and is not generated as a result of the first Suzuki

coupling. An impressive transformation nonetheless, this one-pot reaction installed the

benzylic quaternary center of both natural products in 85% ee and 20% yield from triflate

92 (Scheme 15b). Tricyclic product **93** was then advanced to PCC precursor **91** in an eight-

step sequence. The key Larock heteroannulation cascade occurred in a 72% yield. Notably,

this was the first published example of intramolecular Larock annulation, and it was also

the first application to utilize an iodinated diosphenol. This synthetic effort enabled the

short and enantioselective construction of both **88** and **89**, and it demonstrates how the

strategic combination of multiple palladium-catalyzed cyclizations can be utilized to build

complex carbocyclic frameworks from simple starting materials.

Scheme 1.15 *Asymmetric total synthesis of (+)-halenaquinone and (+)-halenaquinol.*

a) Retrosynthetic plan for the total synthesis of (+)-halenaquinone and (+)-halenaquinol

b) One-pot Suzuki coupling/asymmetric Heck coupling and intramolecular Larock heteroannulation cascade
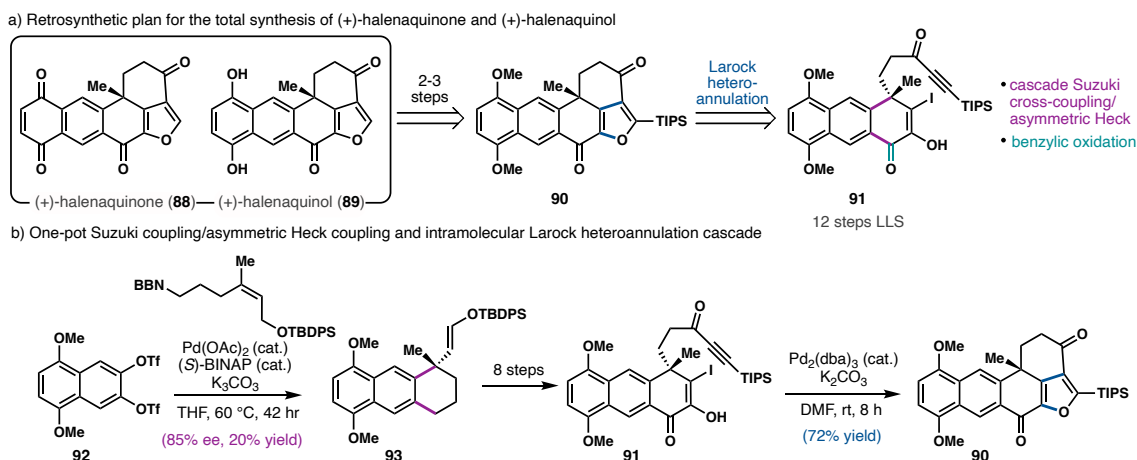
The intramolecular Larock heteroannulation cascade has been applied in several

additional total syntheses (Figure 1.4). The Boger group successfully applied the cascade

for the construction of ergot alkaloids (±)-dihydrolysergic acid (**94**) and (±)-

dihydrolysergol (**95**).[28] In addition, the total syntheses of macrocyclic peptides (±)-

chloropeptin I (**96**) and (±)-chloropeptin II (**97**) were enabled by an intramolecular Larock

macrocyclization using stoichiometric palladium.[29] More recently, Boger and coworkers completed the total synthesis of macrocyclic peptide (±)-streptide (**98**) using a similar transformation, which gave the indole product in 60% yield.[30] These examples demonstrate the robust and highly selective nature of the intramolecular Larock heteroannulation reaction, enabling the formation of 20-membered macrocycles from complex polypeptide substrates.

Figure 1.4 *Additional targets completed via Larock heteroannulation cascade.*

dihydrolysergic acid (**94**)

dihydrolysergol (**95**)

complestatin (chloropeptin II) (**96**)

chloropeptin I (**97**)

streptide (**98**)
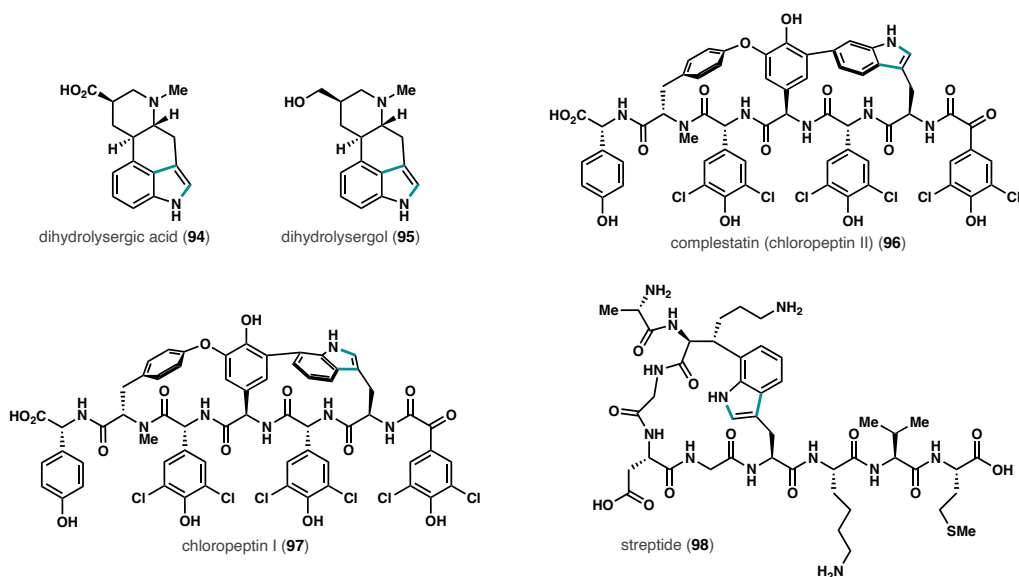
1.4 C–C AND C–N BOND FORMATION: NUCLEOPALLADATION/ CARBOPALLADATION/β-HYDRIDE ELIMINATION CASCADES

Although redox-neutral C–C and C–N bond-forming PCCs have been widely developed and applied, oxidative cascades have received significantly less attention. C–C and C–O bond-forming cascades involving nucleopalladation and subsequent carbopalladation and β-hydride elimination were initially discovered by Larock, although these early examples required stoichiometric palladium.[31] A catalytic, oxidative version of

this transformation was established by Semmelhack, and enantioselective variants were developed soon after.[32,33] The analogous transformation with nitrogen nucleophiles was first reported in the context of chiral indoline synthesis and later applied to the total synthesis of (+)-mitomycin K (**1**).[34] The proposed mechanism of this PCC is initiated by aminopalladation to afford alkylpalladium species **99** (Scheme 1.16). Subsequent carbopalladation of the pendant alkene forms an additional ring, and β-hydride elimination from **100** releases the polycyclic product (**101**). Reductive elimination and oxidation regenerate the Pd^{II} catalyst.

Scheme 1.16 *Proposed catalytic cycle for nucleopalladation/carbopalladation/ β-hydride elimination cascades.*
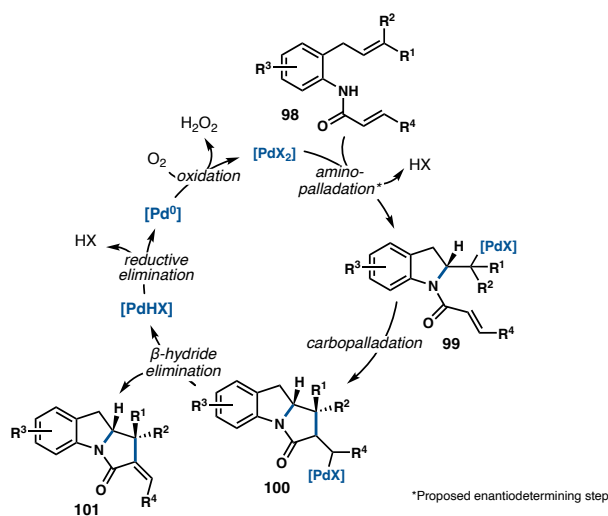
Asymmetric Total Synthesis of (+)-Mitomycin K

The mitomycins are an iconic class of natural products, well known for their small but highly functionalized structure and potent antitumor activity. Mitomycins have a long synthetic history, but the first enantioselective synthesis of (+)-mitomycin K (**1**) was only recently achieved (Scheme 1.17). Retrosynthetically, the authors envisioned the completion of target **1** from precursor azide **102**, which had previously been employed in a racemic synthesis of (±)-mitomycin K. They aimed to derive azide **102** from PCC product **103** via a sequence of functional group manipulations. A key palladium-catalyzed oxidative cascade cyclization of **104** would establish the 6/5/5 fused polycyclic core and constitute the first successful strategic application of their previous established enantioselective oxidative cyclization method.

Scheme 1.17 *Retrosynthetic plan for the synthesis of (+)-mitomycin K.*
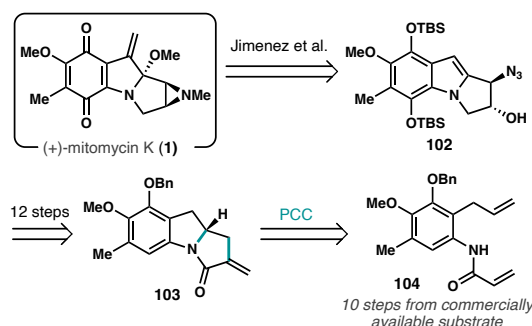
Prior investigations of the key oxidative PCC did not explore arene substituent effects. In this case, substitution at C8 and C5 was desired in order to reduce the number of subsequent oxidation state manipulations (Scheme 1.18). Therefore, the authors aimed to elucidate substituent effects on reaction yield and enantioselectivity. Interestingly, substitution at C5, vicinal to the acrylamide moiety, was found to be detrimental to ee,

whereas benzyl ether substitution at C8, vicinal to the allyl group, was somewhat beneficial, although the rationale for these substituent effects is unclear. The authors obtained cyclization product **103** in 83% ee, which was subsequently advanced to azide **102** in 12 steps. Although the absolute configuration at C9 established by the cyclization was subsequently ablated via oxidation, it was first used to relay the correct absolute configurations at both C1 and C2. Finally, azide **102** was advanced to (+)-mitomycin K using a procedure established by Jimenez et al.

Scheme 1.18 *Key palladium-catalyzed oxidative cascade cyclization.*

19 steps to (+)-mitomycin K
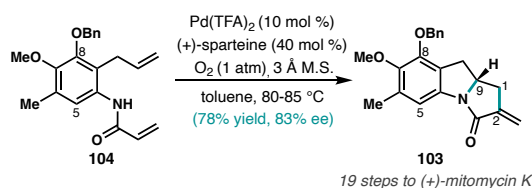
The application of this oxidative PCC enabled the first enantioselective total synthesis of (+)-mitomycin K, demonstrating that PCCs can be a powerful tool for asymmetric synthesis. In addition, the aforementioned oxidative PCC enabled the single-step construction of the polycyclic 6/5/5 scaffold from a much simpler precursor. Unfortunately, the need for multiple oxidation state manipulations and functional group interconversions to obtain desired azide intermediate **102** added many steps to the synthesis. Nevertheless, the authors persevered and successfully constructed enantiopure (+)-mitomycin K in 33 steps from commercial starting materials, completing the first asymmetric total synthesis of this natural product.

1.5. C–C AND C–N BOND FORMATION: CARBOPALLADATION/π-ALLYL CAPTURE

The carbopalladation/π-allyl capture cascade is one of the most widely developed and frequently applied PCCs, accepting a variety of diene or allene substrates and O, C, and N-centered nucleophiles. In the literature, this cascade is often referred to as the Heck insertion/anion capture cascade or the Heck/Tsuji–Trost cascade. We consider it more accurate to refer to these reactions as carbopalladation/π-allyl capture cascades, as their proposed mechanism does not contain all the elementary steps of the Heck coupling or the Tsuji–Trost allylation. The suggested mechanism for these transformations commences with oxidative addition of an alkenyl or aryl halide electrophile, such as **105**, to a Pd^0 complex (Scheme 1.19). The resulting Pd^{II} complex (**106**) participates in the carbopalladation of a diene or allene to give π-allylpalladium^{II} intermediate **107**. This intermediate can then be trapped by a variety of internal or external nucleophiles. This PCC was initially disclosed and extensively developed by Grigg and coworkers, who found that π-allylpalladium^{II} complexes generated from allene or diene insertion could be successfully trapped by hydrides, organozincs, organoborons, organotins, C-, O-, and N-centered nucleophiles.[35] Subsequently, Shibasaki and coworkers developed an enantioselective variant that utilized a Pd(OAc)$_2$ catalyst and chiral (S)-BINAP ligand to promote asymmetric diene insertion followed by stereoselective π-allyl capture by acetate anions or benzylamines.[36,37] They later applied this cascade to the asymmetric total synthesis of natural product (–)-$\Delta^{9(12)}$-capnellene.[38]

Scheme 1.19 *Proposed catalytic cycle for carbopalladation/π-allyl capture cascades.*

Total Synthesis of (–)-Spirotryprostatin B
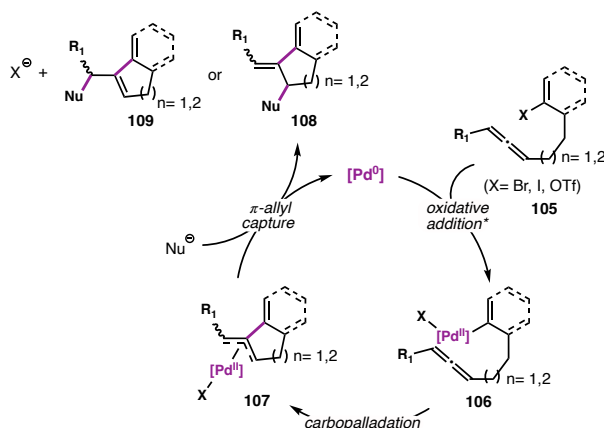
In 2000, the Overman group employed the carbopalladation/π-allyl capture cascade
to synthesize the marine natural product (–)-spirotryprostatin B (110, Scheme 1.20).[39,40]

Scheme 1.20 *Abbreviated retrosynthetic scheme. Compounds denoted with "a"
represent the Z diene/triene, and those with "b" represent the E diene/triene.*
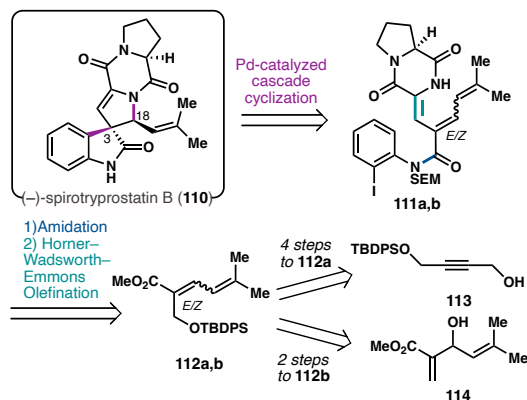
Their original strategy was to employ this PCC in an asymmetric fashion to establish the
correct absolute configurations of both the oxindole C3 all-carbon quaternary center and
the adjacent C18 stereocenter of the spiropyrrolidine ring in a single step. The requisite Z
and E trienes for this key PCC, **111a** and **111b**, respectively, were synthesized via

amidation and Horner–Wadsworth–Emmons olefination of aldehydes derived from **112a**

and **112b**.

Unfortunately, upon exposure of cyclization precursor **111a** to Pd$_2$(dba)$_3$ and

either (*R*) or (*S*)-BINAP, only SEM protected (–)-18-*epi*-spirotryprostatin B (**117**)

and (–)-3-*epi*-spirotryprostatin B (**118**) were obtained, along with byproducts **119**

and **120** resulting from elimination of palladium hydride from the π-allylpalladium

intermediate (Scheme 1.21b).

Scheme 1.21 *Studies toward the total synthesis of (–)-spirotryprostatin B.*
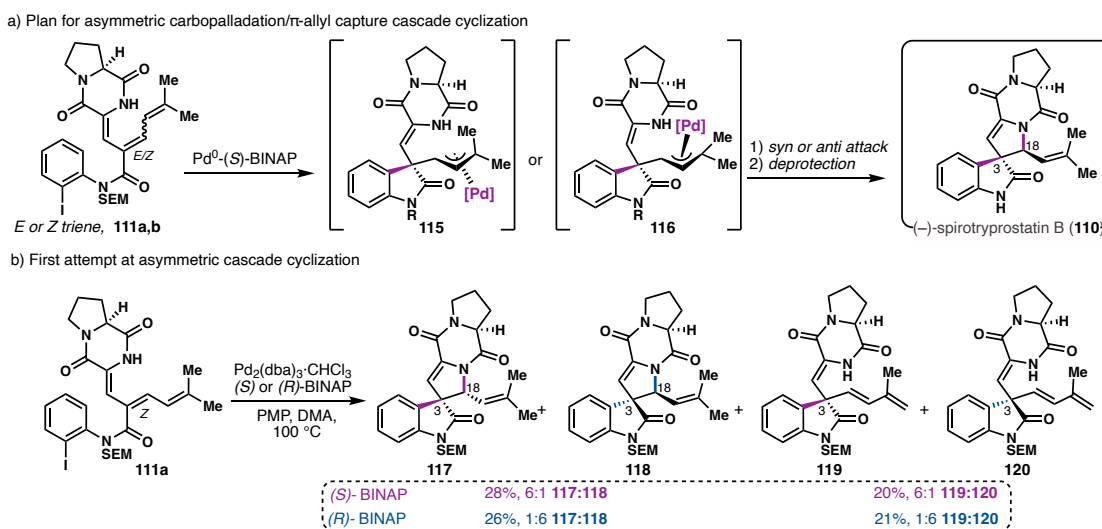
Based on the stereochemical implications of their first attempt, the authors prepared

the (2E)-2,4-hexadienamide precursor **111b**, expecting it to yield SEM-protected (–)-

spirotryprostatin B. Frustratingly, **111b** isomerized under the reaction conditions to the

more stable (2Z) cyclization precursor, yielding products **117** and **118** as before (Scheme

1.22a). To complete their synthesis, the authors performed the cascade cyclization with an

achiral Pd catalyst, allowing the reaction to occur at lower temperature and thereby

preventing isomerization. A 1:1 mixture of SEM protected (–)-spirotryprostatin B (**121**)

and (–)-3,18-epi-spirotryprostatin B (**122**) was obtained in 72% yield (Scheme 1.22b).

Scheme 1.22 *Additional studies toward the total synthesis of (–)-spirotryprostatin B.*

a) Attempt at asymmetric cascade cyclization with "E" triene

b) Successful cascade cyclization with an achiral Pd catalyst
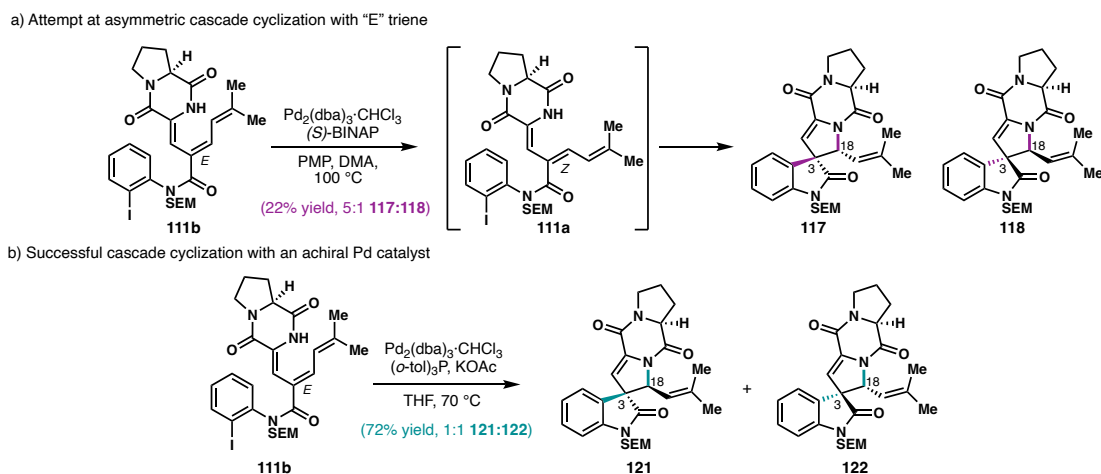
Although the asymmetric variant of this cascade cyclization failed to produce the

desired epimer, the synthetic efficiency of this strategy should not be overlooked. This

palladium-catalyzed cascade installed two of the five rings of the natural product and

established the correct relative configuration of stereocenters C3 and C18 in a single

synthetic operation, allowing the authors to access (–)-spirotryprostatin B in just 11 steps

from a known compound.

Formal Synthesis of Elacomine and Isoelacomine

Following Overman's application of the carbopalladation/π-allyl capture cascade

to the synthesis of (–)-spirotryprostatin B, Takemoto and coworkers applied a related

strategy for the synthesis of elacomine (**123**), a hemiterpene spirooxindole alkaloid

(Scheme 1.23).[41] Although elacomine itself does not exhibit biological activity, the

spiro(pyrrolidine-3,3'-oxindole) scaffold is a common motif in medicinally relevant

natural products. The application of the carbopalladation/π-allyl capture cascade was inspired by their previously established cycloamidation of carbamoyl chlorides with dienes. Compound **125** was identified as the requisite PCC precursor to the natural product, and it was prepared from Heck coupling product **126** in eight steps, including reductive lactone opening, Wittig olefination, and amide installation.

Scheme 1.23. *Retrosynthetic scheme for the formal synthesis of elacomine and isoelacomine.*
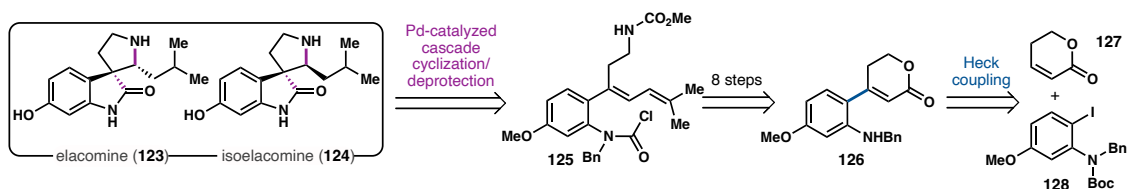
Surprisingly, subjection of carbamoyl chloride **125** to the conditions previously optimized for domino cyclization did not result in the expected cascade product (entry 1, Table 1.3). Instead, **129** was isolated, the product of β-hydride elimination from the π-allylpalladium intermediate. When Bu₄NI was used as an additive, desired PCC product **130** could be isolated, albeit in low yield (entry 2). Changing the ligand to DPPF did not improve the yield of **130** (entry 3), but byproduct **129** was not observed in the absence of Cs_2CO_3 (entry 4), inspiring a screen of acidic conditions. In the presence of catalytic $Bi(OTf)_3$, cyclization product **130** was obtained in 52% yield but with poor dr (entry 7). Ultimately, the Heck reaction and hydroamination were performed separately to improve the yield and dr of spirooxindole **130** formation. When elimination product **129** was subjected to catalytic $Bi(OTf)_3$ and KPF_6, the hydroamination product (**130**) was obtained in 83%

Table 1.3 *Optimization of carbopalladation/ π-allyl capture strategy.*
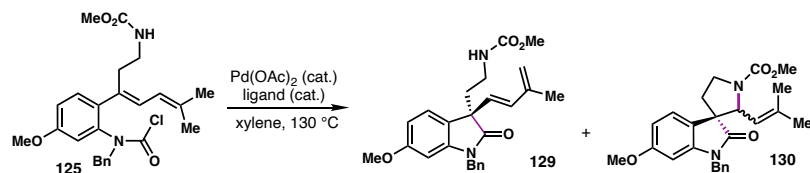
Entry	Ligand	Additives	% **133** (dr)	% **132**
1	PPh$_3$	Cs$_2$CO$_3$	0	86
2	PPh$_3$	Cs$_2$CO$_3$, Bu$_4$NI	11 (1:1)	28
3	DPPF	Cs$_2$CO$_3$	0	84
4	DPPF	–	37 (1:1)	0
5	DPPF	TfOH	17 (1:1)	0
6	DPPF	Hf(OTf)$_4$	33 (5:4)	0
7	DPPF	Bi(OTf)$_3$ *	52 (5:4)	0

*Pd(TFA)$_2$ was used instead of Pd(OAc)$_2$

yield and 3:1 dr (Scheme 1.24). The diastereomeric reaction products were separately converted to elacomine and isoelacomine in just two steps. Despite its practical challenges, the late-stage PCC greatly simplified the synthetic strategy for the total synthesis of elacomine and isoelacomine.

Scheme 1.24 *Bi-catalyzed hydroamination.*
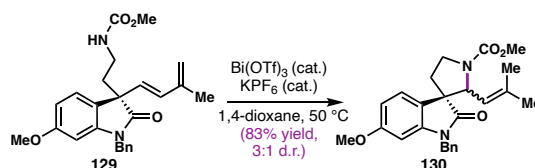
Enantioselective Formal Synthesis of (–)-Aurantioclavine

Nemoto and coworkers were the first to apply the carbopalladation/π-allyl capture PCC to the construction of 3,4-fused tricyclic indoles.[42] This skeleton is ubiquitous in bioactive natural products, including the clavine alkaloids, communesins, and lysergic acid derivatives.[23,43,44] To illustrate proof of concept, the group initially applied the cascade to synthesize the core of dragamacidin E.[45] Soon after, the group published an enantioselective formal synthesis of the ergot alkaloid (–)-aurantioclavine (**131**) realizing

their first completed synthesis involving the cascade (Scheme 1.25).[46] Their key

retrosynthetic disconnections included a palladium-catalyzed carbopalladation/π-allyl

capture cascade to establish the 3,4-fused tricyclic indole scaffold and an organocatalytic

asymmetric aziridination to establish the absolute configuration of the single stereogenic

center in the natural product.

Scheme 1.25 *Enantioselective formal synthesis of (−)-aurantioclavine***.**
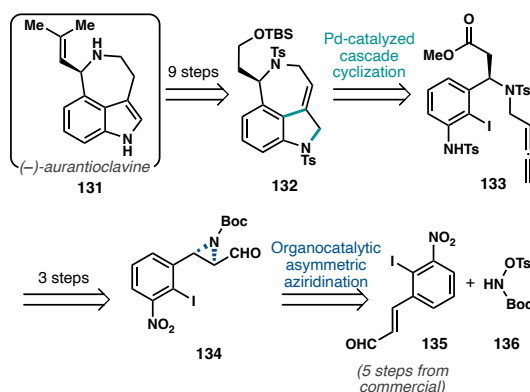
Their first attempt at PCC with substrate **133** unfortunately failed to yield the

desired product; instead, compound **137** was isolated due to elimination of the tosylamido

moiety (Scheme 1.26a). In order to circumvent this undesired reactivity, the authors

reduced the methyl ester to obtain TBS ether **138**, hypothesizing that the lack of an acidic

proton in this substrate would prevent tosylamido elimination. Subjecting **138** to their

established reaction conditions provided the desired product (**132**) in good yield (Scheme

1.26b). Elaboration of **132** to a known intermediate enabled the completion of their 22-step

formal synthesis.

Although mechanistically distinct, this cascade can be strategically similar to the

intramolecular Larock heteroannulation cascade, with the allene acting as an alkyne

surrogate. Because the carbopalladation/π-allyl capture cascade tolerates terminal allenes, this method may be more useful for the synthesis of indoles lacking substitution at the 2-position, whereas the Larock heteroannulation cascade is best suited to indoles with functionality at the 2-position.

Scheme 1.26 *Optimization of carbopalladation/ π-allyl capture cascade.*
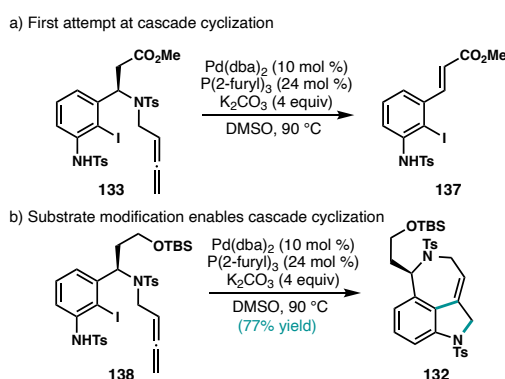
Total Synthesis of (±)-Lysergic acid, (±)-Lysergol, and (±)-Isolysergol

Ergot alkaloids have a rich history as targets for total synthesis, inspiring elegant strategies for the construction of the 3,4-fused tetracyclic indole core. Ohno and coworkers' divergent total synthesis of (±)-lysergic acid (**141**), (±)-lysergol (**139**), and (±)-isolysergol (**140**) via carbopalladation/π-allyl capture cascade constitutes a primary example (Scheme 1.27).[47] The authors aimed to install both the C and D rings of the target alkaloids concurrently through the application of the aforementioned PCC. The allenic amide cyclization substrate **143** would be prepared in a 13-step sequence utilizing a Claisen rearrangement to install the allene and a Mitsunobu reaction to furnish the sulfonamide. The authors encountered their first major challenge when they obtained cyclization substrates **145** and **146** as a mixture of inseparable diastereomers. Therefore, they subjected

Scheme 1.27 *Retrosynthetic plan for the total synthesis of lysergic acid and analogues.*
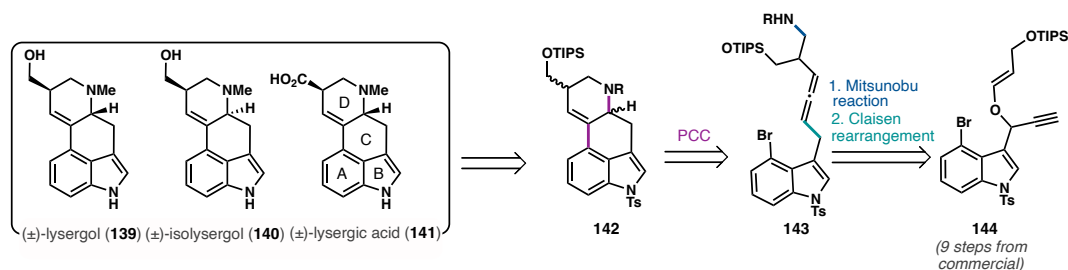
In a 4:1 ratio of diastereomers to a screen of Pd sources, ligands, bases, and solvents (Table 1.4). Although the diastereoselectivity of the reaction could not be improved without a reduction in yield, it was found that the tosylamide substrates **146a** and **146b** provided slightly higher dr than the nosylamides **145a** and **145b** (entries 1 and 4). HPLC separation of nosylamide substrates **145a** and **145b** showed that dr improved slightly when a diasteromerically pure substrate was used (entries 2 and 3).

Table 1.4 *Optimization of the key carbopalladation/π-allyl capture cascade.*

Entry	Substrate	Substrate d.r.	Temperature	Product	Product d.r.	Yield
1	**145**	a:b = 4:1	120°C	**147**	a:b = 74:26	78%
2	**145a**	single diastereomer	120°C	**147**	a:b = 83:17	78%
3	**145b**	single diastereomer	120°C	**147**	a:b = 21:79	67%
4	**146**	a:b = 4:1	100°C	**148**	a:b = 87:13	65%

In a demonstration of perseverance, the authors utilized the lack of diastereoselectivity to their advantage. Nosyl deprotection and N-methylation of **147a** and **147b** yielded a separable mixture of diastereomers from which (±)-isolysergol and (±)-lysergol were derived. Similarly, alcohol deprotection of **148b** and conversion to the

methyl ester gave a separable mixture of diastereomers, the major of which was advanced

to (±)-lysergic acid.

The authors proposed that the major cyclization product (**148a**) could arise from a

pathway involving oxidative addition, aminopalladation, and reductive elimination

(Scheme 1.28). This mechanistic pathway is reminiscent of palladium-catalyzed

carboamination reactions developed by the Wolfe group.[48–50] The minor diastereomer was

proposed to arise from a carbopalladation/π-allyl capture pathway that involved anti

capture of the π-allyl Pd intermediate by nitrogen.

Scheme 1.28 *Proposed mechanistic pathways leading to major and minor*

diastereomers.
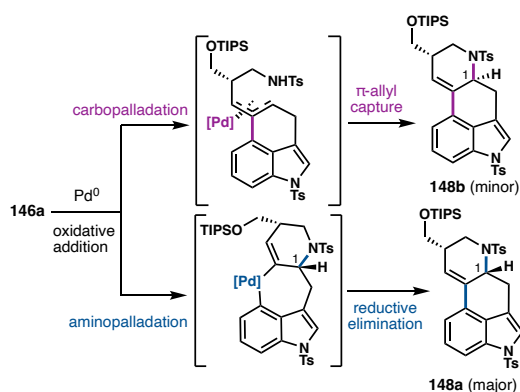
1.6 CONCLUSION

We have highlighted a number of natural product syntheses that utilize palladium-

catalyzed cascade cyclizations, focusing on cascades that close multiple rings and form

both C–X (X = O,N) and C–C bonds in a single synthetic step. Three key strategic

approaches have emerged in our analysis. First, a PCC can be employed early in the

synthesis to rapidly build complexity and establish the core structure of the natural product. This approach is exemplified in the synthesis of (–)-kumausallene (**15**), in which a gram-scale Semmelhack reaction is the fourth step. Second, a PCC can be used at a late stage to construct the final few rings of a natural product. This strategy requires particularly robust and functional group-tolerant cascades. Notable examples highlighted in this review include the syntheses of (±)-schindilactone A (**3**), (–)-spinosyn A (**34**), and (+)-halenaquinone/halenaquinol (**88** and **89**). Third, a PCC can support a convergent synthetic strategy. In this case, an initial fragment coupling step joins two fragments of similar size and complexity. The PCC is then used to forge additional rings between these fragments, tailoring the natural product scaffold. This strategy was employed in the syntheses of (+)-perseanol (**2**) and (–)-spirotryprostatin B (**110**).

Despite the success of PCCs in natural product synthesis, there are some areas which invite further development. Some of the syntheses covered required lengthy functional group interconversion sequences following the key PCC. This may be avoidable in some cases with improved route design; however, it could also indicate a lack of functional group tolerance in the PCC itself. Another interesting extension of the current technology would be the development and application of intermolecular PCCs. Such a cascade could be applied toward a convergent total synthesis, in which the PCC would encompass both the fragment coupling and the scaffold tailoring steps. Finally, expansion of PCCs to other ring systems, such as strained carbocyclic systems and lactams, could enable their use toward a broader variety of natural products. This could potentially facilitate the synthesis of previously inaccessible natural products. Overall, palladium-

catalyzed cascades have been used effectively in the total synthesis of a multitude of natural

products. We anticipate that these reactions will continue to be successfully leveraged in

natural product synthesis due to their power, breadth, and versatility.

1.7   REFERENCES

(1)   Nicolaou, K. C.; Edmonds, D. J.; Bulger, P. G. Cascade Reactions in Total

Synthesis. *Angewandte Chemie International Edition* **2006**, *45* (43), 7134–7186.

(2)   Bunce, R. A. Recent Advances in the Use of Tandem Reactions for Organic

Synthesis. *Tetrahedron* **1995**, *51* (48), 13103–13159.

(3)   Tietze, L. F.; Beifuss, U. Sequential Transformations in Organic Chemistry: A

Synthetic Strategy with a Future. *Angewandte Chemie International Edition in

English* **1993**, *32* (2), 131–163.

(4)   Döndaş, H. A.; Retamosa, M. de G.; Sansano, J. M. Recent Development in

Palladium-Catalyzed Domino Reactions: Access to Materials and Biologically

Important Carbo- and Heterocycles. *Organometallics* **2019**, *38* (9), 1828–1867.

(5)   James, D. E.; Hines, L. F.; Stille, J. K. The Palladium(II) Catalyzed Olefin

Carbonylation Reaction. The Stereochemistry of Methoxypalladation. *J. Am. Chem.

Soc.* **1976**, *98* (7), 1806–1809.

(6)   Semmelhack, M. F.; Bodurow, C. Intramolecular Alkoxypalladation/Carbonylation

of Alkenes. *J. Am. Chem. Soc.* **1984**, *106* (5), 1496–1498.

(7)   Semmelhack, M. F.; Bodurow, C.; Baum, M. Direct Synthesis of Pyran-Lactones Related to Naphthoquinoneantibiotics. *Tetrahedron Letters* **1984**, *25* (30), 3171–3174.

(8)   Ma, K.; Martin, B. S.; Yin, X.; Dai, M. Natural Product Syntheses via Carbonylative Cyclizations. *Nat. Prod. Rep.* **2019**, *36* (1), 174–219.

(9)   Werness, J. B.; Tang, W. Stereoselective Total Synthesis of (−)-Kumausallene. *Org. Lett.* **2011**, *13* (14), 3664–3666.

(10)   Xiao, Q.; Ren, W.-W.; Chen, Z.-X.; Sun, T.-W.; Li, Y.; Ye, Q.-D.; Gong, J.-X.; Meng, F.-K.; You, L.; Liu, Y.-F.; Zhao, M.-Z.; Xu, L.-M.; Shan, Z.-H.; Shi, Y.; Tang, Y.-F.; Chen, J.-H.; Yang, Z. Diastereoselective Total Synthesis of (±)-Schindilactone A. *Angewandte Chemie International Edition* **2011**, *50* (32), 7373–7377.

(11)   Hayes, P. Y.; Kitching, W. Total Synthesis and Absolute Stereochemistry of Plakortone D. *J. Am. Chem. Soc.* **2002**, *124* (33), 9718–9719.

(12)   Li, Z.; Gao, Y.; Tang, Y.; Dai, M.; Wang, G.; Wang, Z.; Yang, Z. Total Synthesis of Crisamicin A. *Org. Lett.* **2008**, *10* (14), 3017–3020.

(13)   Xu, X.-S.; Li, Z.-W.; Zhang, Y.-J.; Peng, X.-S.; Wong, H. N. C. Total Synthesis of (±)-Pallambins C and D. *Chem. Commun.* **2012**, *48* (68), 8517–8519.

(14)   Ebner, C.; Carreira, E. M. Pentafulvene for the Synthesis of Complex Natural Products: Total Syntheses of (±)-Pallambins A and B. *Angewandte Chemie International Edition* **2015**, *54* (38), 11227–11230.

(15) Grigg, R.; Sridharan, V. Spirocycles via Palladium Catalysed Cascade Cyclisation-Carbonylation-Anion Capture Processes. *Tetrahedron Letters* **1993**, *34* (46), 7471–7474.

(16) Bai, Y.; Shen, X.; Li, Y.; Dai, M. Total Synthesis of (−)-Spinosyn A via Carbonylative Macrolactonization. *J. Am. Chem. Soc.* **2016**, *138* (34), 10838–10841.

(17) Han, A.; Tao, Y.; Reisman, S. E. A 16-Step Synthesis of the Isoryanodane Diterpene (+)-Perseanol. *Nature* **2019**, *573* (7775), 563–567.

(18) Davis, D. C.; Walker, K. L.; Hu, C.; Zare, R. N.; Waymouth, R. M.; Dai, M. Catalytic Carbonylative Spirolactonization of Hydroxycyclopropanols. *J. Am. Chem. Soc.* **2016**, *138* (33), 10693–10699.

(19) Rudisill, D. E.; Stille, J. K. Palladium-Catalyzed Synthesis of 2-Substituted Indoles. *J. Org. Chem.* **1989**, *54* (25), 5856–5866.

(20) Larock, R. C.; Yum, E. K.; Refvik, M. D. Synthesis of 2,3-Disubstituted Indoles via Palladium-Catalyzed Annulation of Internal Alkynes. *J. Org. Chem.* **1998**, *63* (22), 7652–7662.

(21) Larock, R. C.; Yum, E. K. Synthesis of Indoles via Palladium-Catalyzed Heteroannulation of Internal Alkynes. *J. Am. Chem. Soc.* **1991**, *113* (17), 6689–6690.

(22) Shan, D.; Gao, Y.; Jia, Y. Intramolecular Larock Indole Synthesis: Preparation of 3,4-Fused Tricyclic Indoles and Total Synthesis of Fargesine. *Angewandte Chemie International Edition* **2013**, *52* (18), 4902–4905.

(23) Liu, H.; Jia, Y. Ergot Alkaloids: Synthetic Approaches to Lysergic Acid and Clavine Alkaloids. *Nat. Prod. Rep.* **2017**, *34* (4), 411–432.

(24) Liu, H.; Zhang, X.; Shan, D.; Pitchakuntla, M.; Ma, Y.; Jia, Y. Total Syntheses of Festuclavine, Pyroclavine, Costaclavine, Epi-Costaclavine, Pibocin A, 9-Deacetoxyfumigaclavine C, Fumigaclavine G, and Dihydrosetoclavine. *Org. Lett.* **2017**, *19* (12), 3323–3326.

(25) Li, L.; Yang, Q.; Wang, Y.; Jia, Y. Catalytic Asymmetric Total Synthesis of (−)-Galanthamine and (−)-Lycoramine. *Angewandte Chemie International Edition* **2015**, *54* (21), 6255–6259.

(26) Kojima, A.; Takemoto, T.; Sodeoka, M.; Shibasaki, M. Catalytic Asymmetric Synthesis of Halenaquinone and Halenaquinol. *J. Org. Chem.* **1996**, *61* (15), 4876–4877.

(27) Kojima, A. Catalytic Asymmetric Synthesis of Halenaquinone and Halenaquinol. *Synthesis* **1998**, *1998* (Sup. 1), 581–589.

(28) Lee, K.; Poudel, Y. B.; Glinkerman, C. M.; Boger, D. L. Total Synthesis of Dihydrolysergic Acid and Dihydrolysergol: Development of a Divergent Synthetic Strategy Applicable to Rapid Assembly of D-Ring Analogs. *Tetrahedron* **2015**, *71* (35), 5897–5905.

(29) Garfunkle, J.; Kimball, F. S.; Trzupek, J. D.; Takizawa, S.; Shimamura, H.; Tomishima, M.; Boger, D. L. Total Synthesis of Chloropeptin II (Complestatin) and Chloropeptin I. *J. Am. Chem. Soc.* **2009**, *131* (44), 16036–16038.

(30) Isley, N. A.; Endo, Y.; Wu, Z.-C.; Covington, B. C.; Bushin, L. B.;
Seyedsayamdost, M. R.; Boger, D. L. Total Synthesis and Stereochemical
Assignment of Streptide. *J. Am. Chem. Soc.* **2019**, *141* (43), 17361–17369.

(31) Larock, R. C.; Lee, N. H. Organopalladium Approaches to Prostaglandins. 11.
Synthesis of PGF2.Alpha. and 12-Epi PGF2.Alpha. by the Controlled, One Step,
Palladium-Promoted, Intermolecular Coupling of Three Different Alkenes. *J. Am.
Chem. Soc.* **1991**, *113* (20), 7815–7816.

(32) Semmelhack, M. F.; Epa, W. R. Catalytic Tandem Oxy-Palladation and Vinylation.
Tetrahedron Letters **1993**, *34* (45), 7205–7208.

(33) Tietze, L. F.; Sommer, K. M.; Zinngrebe, J.; Stecker, F. Palladium-Catalyzed
Enantioselective Domino Reaction for the Efficient Synthesis of Vitamin E.
Angewandte Chemie International Edition **2005**, *44* (2), 257–259.

(34) Gu, Q.-S.; Yang, D. Enantioselective Synthesis of (+)-Mitomycin K by a Palladium-
Catalyzed Oxidative Tandem Cyclization. *Angewandte Chemie International
Edition* **2017**, *56* (21), 5886–5889.

(35) Grigg, R. Heterocycle Synthesis by Palladium Catalysed Cyclisation-Anion Capture
Processes. A Powerful New Strategy. *Journal of Heterocyclic Chemistry* **1994**, *31*
(3), 631–639.

(36) Kagechika, K.; Shibasaki, M. Asymmetric Heck Reaction: A Catalytic Asymmetric
Synthesis of the Key Intermediate for .DELTA.9(12)-Capnellene-
3.Beta.,8.Beta.,10.Alpha.-Triol and .DELTA.9(12)-Capnellene-
3.Beta.,8.Beta.,10.Alpha.,14-Tetrol. *J. Org. Chem.* **1991**, *56* (13), 4093–4094.

(37) Kagechika, K.; Ohshima, T.; Shibasaki, M. Asymmetric Heck Reaction-Anion Capture Process. A Catalytic Asymmetric Synthesis of the Key Intermediates for the Capnellenols. *Tetrahedron* **1993**, *49* (9), 1773–1782.

(38) Ohshima, T.; Kagechika, K.; Adachi, M.; Sodeoka, M.; Shibasaki, M. Asymmetric Heck Reaction−Carbanion Capture Process. Catalytic Asymmetric Total Synthesis of (−)-Δ9(12)-Capnellene. *J. Am. Chem. Soc.* **1996**, *118* (30), 7108–7116.

(39) Overman, L. E.; Rosen, M. D. Total Synthesis of (−)-Spirotryprostatin B and Three Stereoisomers. *Angewandte Chemie International Edition* **2000**, *39* (24), 4596–4599.

(40) Overman, L. E.; Rosen, M. D. Terminating Catalytic Asymmetric Heck Cyclizations by Stereoselective Intramolecular Capture of H3-Allylpalladium Intermediates: Total Synthesis of (−)-Spirotryprostatin B and Three Stereoisomers. *Tetrahedron* **2010**, *66* (33), 6514–6525.

(41) Kamisaki, H.; Nanjo, T.; Tsukano, C.; Takemoto, Y. Domino Pd-Catalyzed Heck Cyclization and Bismuth-Catalyzed Hydroamination: Formal Synthesis of Elacomine and Isoelacomine. *Chemistry – A European Journal* **2011**, *17* (2), 626–633.

(42) Nakano, S.; Inoue, N.; Hamada, Y.; Nemoto, T. Pd-Catalyzed Cascade Cyclization by Intramolecular Heck Insertion of an Allene–Allylic Amination Sequence: Application to the Synthesis of 3,4-Fused Tricyclic Indoles. *Org. Lett.* **2015**, *17* (11), 2622–2625.

(43) Hendrickson, J. B.; Wang, J. A New Synthesis of Lysergic Acid. *Org. Lett.* **2004**, *6* (1), 3–5.

(44) Zuo, Z.; Ma, D. Enantioselective Total Syntheses of Communesins A and B. *Angewandte Chemie International Edition* **2011**, *50* (50), 12008–12011.

(45) Inoue, N.; Nakano, S.; Harada, S.; Hamada, Y.; Nemoto, T. Synthetic Study of Dragmacidin E: Construction of the Core Structure Using Pd-Catalyzed Cascade Cyclization and Rh-Catalyzed Aminoacetoxylation. *J. Org. Chem.* **2017**, *82* (5), 2787–2793.

(46) Nakano, S.; Hamada, Y.; Nemoto, T. Enantioselective Formal Synthesis of (−)-Aurantioclavine Using Pd-Catalyzed Cascade Cyclization and Organocatalytic Asymmetric Aziridination. *Tetrahedron Letters* **2018**, *59* (8), 760–762.

(47) Inuki, S.; Oishi, S.; Fujii, N.; Ohno, H. Total Synthesis of (±)-Lysergic Acid, Lysergol, and Isolysergol by Palladium-Catalyzed Domino Cyclization of Amino Allenes Bearing a Bromoindolyl Group. *Org. Lett.* **2008**, *10* (22), 5239–5242.

(48) Bertrand, M. B.; Wolfe, J. P. Stereoselective Synthesis of N-Protected Pyrrolidines via Pd-Catalyzed Reactions of γ-(N-Acylamino) Alkenes and γ-(N-Boc-Amino) Alkenes with Aryl Bromides. *Tetrahedron* **2005**, *61* (26), 6447–6459.

(49) Yang, Q.; Ney, J. E.; Wolfe, J. P. Palladium-Catalyzed Tandem N-Arylation/Carboamination Reactions for the Stereoselective Synthesis of N-Aryl-2-Benzyl Pyrrolidines. *Org. Lett.* **2005**, *7* (13), 2575–2578.

(50) Mai, D. N.; Wolfe, J. P. Asymmetric Palladium-Catalyzed Carboamination

Reactions for the Synthesis of Enantiomerically Enriched 2-(Arylmethyl)- and 2-

(Alkenylmethyl)Pyrrolidines. *J. Am. Chem. Soc.* **2010**, *132* (35), 12157–12159.

CHAPTER 2

Synthesis of Noraugustamine and Development of an Oxidative Heck/Aza-Wacker Cascade Cyclization

2.1 INTRODUCTION

The Amaryllidaceae alkaloid family of natural products has attracted attention from synthetic chemists due to their diverse structures and biological activities.[1–3] Two representative members are augustamine (**149**) and the *N*-demethyl congener, noraugustamine (**150**), which bear structural features such as an all-carbon quaternary center, a fused pyrrolidine ring, and a bridging benzylidene acetal (Scheme 2.1).[4–6] We

Scheme 2.1 *Retrosynthetic analysis.*
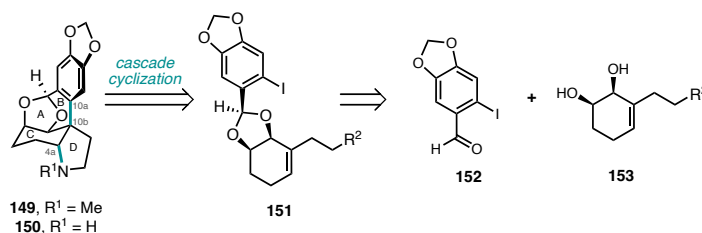
became interested in **149** and **150** as part of a more general program aimed at developing cascade cyclizations that enable the sequenced formation of C–C and C–N bonds.[7] In this context, we envisioned accessing the tetracyclic ABCD core from cyclohexene **153** by either a radical[8,9] or transition metal-catalyzed[10–13] process.[14–16] Here we report our efforts

in this area, which resulted in the development of an oxidative Pd-catalyzed cascade reaction to form a quaternary center and two rings in a single step.

2.2 RESULTS AND DISCUSSION

We first investigated a radical cascade cyclization of aryl iodide **151**. In the proposed cascade, iodine atom abstraction from **151** would be followed by cyclization of the aryl radical onto the olefin. The resulting alkyl radical could then cyclize onto a pendant azide, delivering **149**.[17] To this end, we prepared azide **157** from known cyclohexadiene **154**, which is available in two steps from commercially available starting materials (Scheme 2.2).[18] Following dihydroxylation of **154** with osmium tetroxide, diol **155** was coupled with **152** to afford acetal **156** in moderate yield and good diastereoselectivity.[19] Displacement of the pendant tosylate with sodium azide delivered cyclization substrate **157**.

Scheme 2.2 *Radical cyclization approach.*
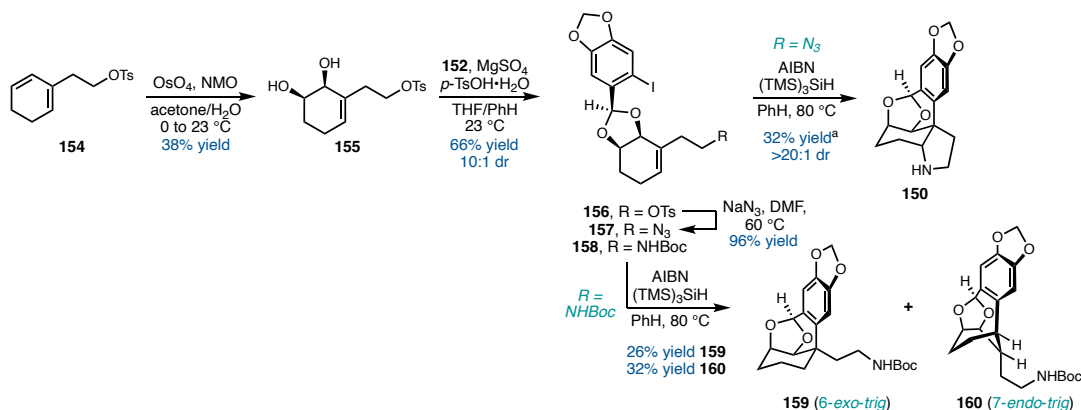
With **157** in hand, we investigated the radical cyclization cascade. We were pleased to find that **150** was obtained in 32% yield upon treatment with AIBN and tris(trimethylsilyl)silane. Despite extensive optimization, efforts to improve the yield of this transformation were unsuccessful (See Experimental Section 2.4.2). We hypothesized

that the low yield resulted from poor regioselectivity in the initial C–C bond-forming

cyclization. Indeed, when **158** was subjected to the optimized conditions, the desired 6-

exo-trig cyclization product **159** (26% yield) was accompanied by a 32% yield of **160**, the

result of a 7-*endo-trig* cyclization process.[20–24]

To address this regioselectivity issue, we hypothesized that use of a transition metal

catalyst might favor the desired isomer. Given the documented preference of Heck

reactions for *exo* over *endo* cyclizations, we subjected **161** to palladium catalysis (Scheme

2.3).[25,26] Gratifyingly, **161** underwent exclusive 6-*exo-trig* Heck cyclization in 58% yield.

Scheme 2.3 *Heck cyclization studies.*
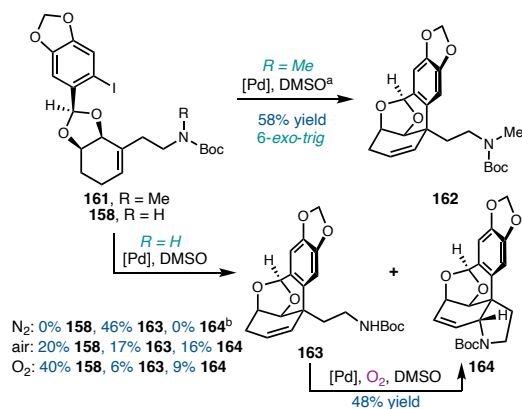
[a]*Pd*(OAc)$_2$ (10 mol %), (*R,R*)-Me-BozPhos (20 mol %), *n*-Bu$_4$NOAc (2 equiv), H$_2$O (200 equiv), DMSO,
120 °C, 18–22 h. [b]Determined by ^{1}H NMR versus 1,3,5-trimethoxybenzene as an internal standard

Substrate **158** performed similarly, affording **163** in 46% yield. When the reaction

was performed open to air, we observed formation of **164**, the result of Heck reaction

followed by aza-Wacker cyclization. Subjection of Heck product **163** to the reaction

conditions, in this case sparging with oxygen, resulted in clean conversion to **164** in 48%

yield. However, the yield of **164** from the single-step cascade cyclization of **158** could not

be improved. Subjection of **158** to the O_2-sparged reaction conditions resulted in increased amounts of unreacted starting material. Unfortunately, use of a sulfonamide, which was anticipated to cyclize faster under the aza-Wacker conditions,[27] resulted in 7-*endo-trig* cyclization (See Experimental Section 2.4.2).

To further investigate the feasibility of a Pd-catalyzed cascade cyclization, we synthesized modified substrate **166** (Scheme 2.4). We envisioned that removing the rigid acetal would favor 6-*exo-trig* cyclization even for sulfonamide substrates by alleviating the ring strain associated with formation of the C10a–C10b bond. We also hypothesized that a cascade process in which both cyclizations are oxidative would be more amenable to optimization; the aza-Wacker cyclization requires a stoichiometric oxidant for catalyst turnover, so the C–C bond-forming cyclization must also be compatible with oxidizing reaction conditions.[28–30] To this end, alkenyl iodide **167** and alkyl bromide **168**, each accessible in one step,[31,32] were coupled to afford **169** in 58% yield on multigram scale.

Scheme 2.4 *Pd-catalyzed cascade cyclization approach.*
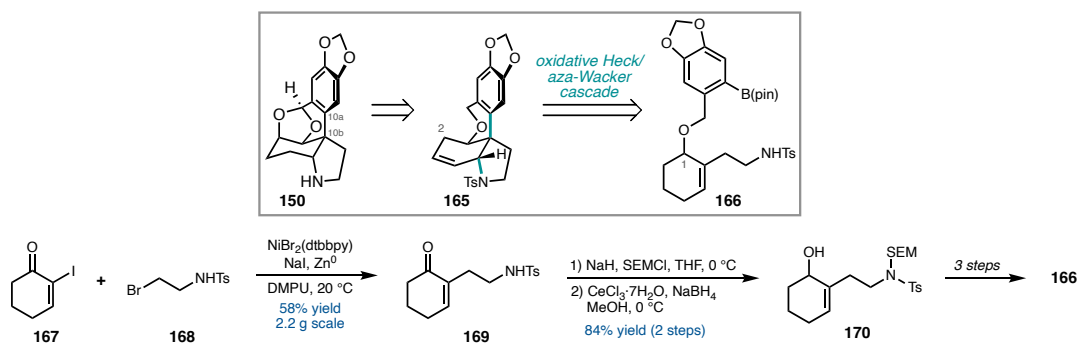
This is a rare example of Ni-catalyzed cross-electrophile coupling using an α-halogenated enone, and further exploration of this transformation is underway.[33–35] SEM protection and

Luche reduction afforded **170**, which was advanced in three steps to substrate **166** (See

Experimental Section 2.3.3).

A broad survey of reaction conditions identified $Pd(OAc)_2$ (10 mol %)/$Cu(OAc)_2$

(40 mol %) in DMSO as optimal, with air as the terminal oxidant and H_2O (5 equiv) as an

additive, affording cascade product **165** in 62% yield (Table 2.1, entry 1). Importantly, no

7-*endo-trig* cyclization was identified under any of the reaction conditions investigated.

Table 2.1 *Optimization of oxidative Heck/aza-Wacker cascade.*
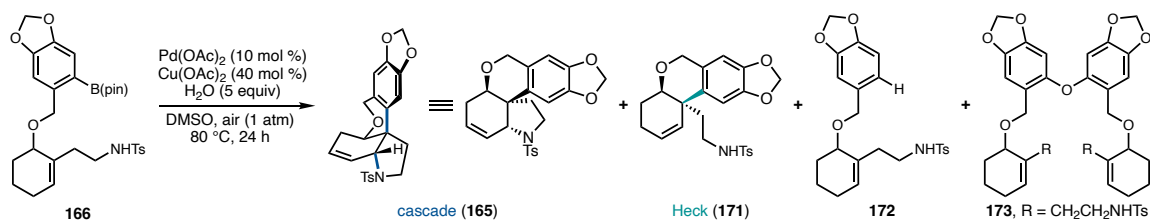
entry	deviation from ideal conditions	165	171	172	173	166
1	none	62	0	4	0	0
2	2 equiv Cu(OAc)$_2$, no air	43	14	8	0	0
3	2 equiv Cu(OAc)$_2$, no Pd(OAc)$_2$, no air	0	0	64	12	0
4	2 equiv Cu(OAc)$_2$, no Pd(OAc)$_2$	0	0	23	46	0
5	1 atm O$_2$ instead of air	38	6	12	4	0
6	1 atm O$_2$ instead of Cu(OAc)$_2$/air	0	10	0	0	57
7	2 equiv BQ instead of Cu(OAc)$_2$/air	0	0	0	0	84
8	H$_2$O omitted	9	8	15	5	0
9	ran at 50 °C instead of 80 °C	11	47	10	0	0

When $Cu(OAc)_2$ was used in stoichiometric quantities as the sole oxidant, conversion of

Heck product **171** to **165** was incomplete (entry 2). In the absence of $Pd(OAc)_2$ and air,

stoichiometric $Cu(OAc)_2$ promoted protodeborylation, forming **172** in 64% yield (entry 3).

Interestingly, stoichiometric $Cu(OAc)_2$ resulted in distinct reactivity under air, instead

furnishing byproduct **173** in 23% yield (entry 4).[36] To suppress these undesired reactions,

alternative oxidants were explored; use of O_2[37] or benzoquinone (BQ)[38] as oxidant resulted

in mostly recovered starting material (entries 5 and 6) When **166** was subjected to catalytic

$Pd(OAc)_2$ and $Cu(OAc)_2$ with O_2 in place of air, **165** was observed in only 38% yield (entry

7). Water was found to be a crucial additive; **165** was formed in only 9% yield when it was

omitted.[39–41] Performing the reaction at lower temperature resulted in poor conversion of

Heck product **171** to **165** (entry 9).

Finally, we explored the scope of the transformation (Scheme 2.5). We were

pleased to find that electron-rich (**26b**) and electron-neutral (**26a** and **26c**) substrates

performed well in the cyclization, with fluorinated substrate **26c** giving the highest yield.

Scheme 2.5 *Additional substrates. Reactions were conducted on 0.05 mmol scale.*

Isolated yields are reported.
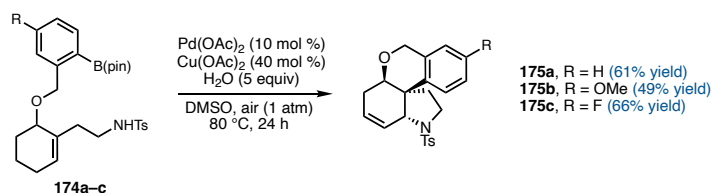
2.3 CONCLUSION

In summary, two cascade cyclization strategies were investigated to form the B and

D rings of the augustamine-type Amaryllidaceae alkaloids. A radical cyclization cascade

enabled access to **150** but displayed poor regioselectivity of the first, C–C bond-forming

step. Efforts to improve the regioselectivity of this cyclization using Pd catalysis

uncovered the feasibility of a Heck/aza-Wacker cascade. This reactivity was further

developed, demonstrating that a Pd-catalyzed oxidative Heck/aza-Wacker cascade enables

construction of an all-carbon quaternary center, a C–N bond, and two rings in a single step.

2.4   EXPERIMENTAL SECTION
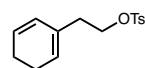
2.4.1 Materials and Methods

Unless otherwise stated, reactions were performed under a N_2 atmosphere using

freshly dried solvents. Tetrahydrofuran (THF), diethyl ether (Et$_2$O), methylene chloride

(CH$_2$Cl$_2$), toluene (PhMe), hexanes, and benzene (C$_6$H$_6$) were dried by passing through

activated alumina columns under a positive pressure of argon. Anhydrous dimethyl

sulfoxide (DMSO) was degassed via three freeze-pump-thaw cycles then stored in a

nitrogen-filled glovebox. Triethylamine (Et$_3$N) was distilled over calcium hydride prior to

use. NiBr$_2$(dtbbpy) was synthesized according to the procedure reported by Shenvi and

coworkers.[1] Cu(OAc)$_2$•H$_2$O was dehydrated by refluxing in acetic anhydride.[2] Unless

otherwise stated, chemicals and reagents were used as received. All reactions were

monitored by thin-layer chromatography using EMD/Merck silica gel 60 F254 pre-coated

plates (0.25 mm) and were visualized by UV, CAM, or KMnO$_4$ staining. Flash column

chromatography was performed as described by Still and coworkers using silica gel (230-

400 mesh, Silicycle).[3] Purified compounds were dried on a high vacuum line (0.2 torr) to

remove trace solvent. ^{1}H and ^{13}C NMR spectra were recorded on a Bruker Avance III HD

with Prodigy cryoprobe (at 400 MHz and 101 MHz, respectively), a Varian 400 MR (at

400 MHz and 101 MHz, respectively), or a Varian Inova 500 (at 500 MHz and 126 MHz,

respectively). ^{1}H NMR and ^{19}F NMR spectra were also recorded on a Varian Inova 300 (at

300 MHz and 282 MHz, respectively). NMR data is reported relative to internal CHCl$_3$

(^{1}H, δ = 7.26), internal CDCl$_3$ (^{13}C, δ = 77.0), or added C$_6$F$_6$ (^{19}F, δ = −164.9). Data for ^{1}H

NMR spectra are reported as follows: chemical shift (δ ppm) (multiplicity, coupling

constant (Hz), integration). Multiplicity and qualifier abbreviations are as follows: s =

singlet, d = doublet, t = triplet, q = quartet, m = multiplet, br = broad. In cases where

residual solvent was present in the NMR spectra, its contribution to the mass of the sample

was calculated by ^{1}H NMR and the yield was adjusted; unless otherwise noted, compounds

are >95% pure. IR spectra were recorded on a Perkin Elmer Paragon 1000 spectrometer

and are reported in frequency of absorption (cm^{-1}). HRMS were acquired from the Caltech

Mass Spectral Facility using fast-atom bombardment (FAB), electrospray ionization (TOF-

ESI), atmospheric pressure chemical ionization (APCI), field desorption (FD), or electron

impact (EI).

2.4.2 Synthesis of (±)-Noraugustamine

Preparation of Cyclohexadiene 154:

 Cyclohexadiene **154** was prepared according to the procedure reported by

Diver and coworkers.[18] Spectral data matched those reported in the literature.

Preparation of Diol 155:
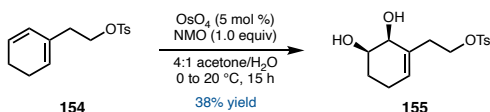
A round-bottomed flask was charged with cyclohexadiene **154** (1.38 g, 5.0 mmol, 1.0

equiv), acetone/H₂O (4:1, 40 mL), and a stir bar then cooled to 0 °C using an ice/water

bath. *N*-Methylmorpholine *N*-oxide (0.581 g, 5.0 mmol, 1.0 equiv) and OsO₄ (2.5% in *t*-

BuOH, 2.5 mL, 0.25 mmol, 0.050 equiv) were added, and the brown mixture was stirred

for 15 h while it was allowed to slowly warm to room temperature. The reaction was quenched with saturated aqueous $Na_2S_2O_3$ (30 mL) and stirred for another hour before it was diluted with EtOAc (40 mL). The aqueous layer was extracted with EtOAc (3 x 40 mL). The combined organic phases were washed with brine (100 mL; aqueous phase was once more extracted with EtOAc), dried over $MgSO_4$, and concentrated. The residue was purified via column chromatography (20 to 33% EtOAc/hexanes) to afford diol **155** (706 mg, 38% yield) as a cloudy, colorless oil. This compound is unstable and must be used shortly after purification; see note in ^{13}C NMR for more information. The sample contained residual EtOAc by NMR and the yield was adjusted accordingly.

^{1}H NMR (400 MHz, CDCl₃): δ 7.77 (d, $J = 8.0$ Hz, 2H), 7.34 (d, $J = 9.2$ Hz, 2H), 5.60 (t, $J = 3.4$ Hz, 1H), 4.26 – 4.14 (m, 2H), 3.94 – 3.87 (m, 1H), 3.78 – 3.65 (m, 1H), 2.62 – 2.48 (m, 1H), 2.44 (s, 3H), 2.42 – 2.38 (m, 1H), 2.21 – 2.12 (m, 1H), 2.03 – 1.96 (m, 1H), 1.76 – 1.52 (m, 2H).

^{13}C NMR (101 MHz, CDCl₃): δ 144.9, 133.3, 132.4, 130.0, 129.1, 128.0, 69.5 (2 overlapping peaks), 68.9, 34.3, 25.4, 23.8, 21.8. The signals at 171.3, 60.6, 21.2, and 14.4 are derived from the residual EtOAc. The lower-intensity signals at 133.8, 119.6, 67.2, 64.6, 30.9, 25.3, and 20.9 are derived from cyclization of the allylic alcohol onto the pendant tosylate and match the previously reported data for this compound.[42] This compound is not present in appreciable amounts in the ^{1}H spectrum, indicating that cyclization likely occurred in the NMR tube following purification.

FTIR (NaCl, thin film): 3378, 2923, 1598, 1439, 1356, 1188, 1175, 1097, 1051, 960, 915, 833, 815 cm^{-1}.

HRMS (APCI) *m/z*: [M – OH]$^+$ Calcd for $C_{15}H_{19}O_4S$ 295.0999; Found 295.0987.

R_f = 0.20 (silica, 50% EtOAc/hexanes, KMnO₄).

Preparation of 6-iodobenzo[*d*][1,3]dioxole-5-carbaldehyde (152):
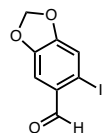
6-iodobenzo[*d*][1,3]dioxole-5-carbaldehyde (**152**) was prepared according to the procedure reported by Crich and Krishnamurthy.[43] Spectral data matched those reported in the literature.

Preparation of acetal 156:
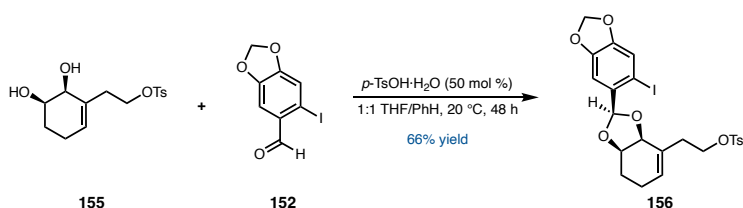
A flame-dried three-necked round bottom flask equipped with two rubber septa, a magnetic stir bar and a gas inlet. This apparatus was placed under an atmosphere of nitrogen then charged with 6-iodobenzo[*d*][1,3]dioxole-5-carbaldehyde (**152**, 1.08 g, 3.9 mmol, 2.0 equiv), *p*-TsOH•H$_2$O (0.186 g, 0.98 mmol, 0.50 equiv), and anhydrous THF (25 mL). The diol (**155**, 0.611 g, 2.0 mmol, 1.0 equiv) was added as a solution in benzene (25 mL) and the resulting pale yellow suspension was stirred for 48 h. The reaction mixture was poured into saturated aqueous NaHCO$_3$ (50 mL) and the aqueous phase was extracted with EtOAc (3 x 50 mL). The combined organic layers were washed with brine (50 mL), dried over MgSO$_4$ and concentrated. NMR analysis of the crude reaction mixture indicated diastereoselectivity of 10:1. The residue was purified via column chromatography (10 to 25% EtOAc/hexanes) to afford **156** (718 mg, 66% yield) as a white foam.

^{1}H NMR (400 MHz, CDCl$_3$): δ 7.73 (d, J = 8.5 Hz, 2H), 7.30 (d, J = 8.2 Hz, 2H), 7.17 (s,

1H), 6.90 (s, 1H), 6.04 – 5.93 (m, 2H), 5.89 (s, 1H), 5.72 (t, J = 4.2 Hz, 1H), 4.34 – 4.27

(m, 2H), 4.19 (dt, J = 9.9, 7.0 Hz, 1H), 4.05 (dt, J = 9.9, 6.6 Hz, 1H), 2.57 – 2.42 (m, 2H),

2.42 (s, 3H), 2.23 – 2.09 (m, 1H), 1.99 – 1.90 (m, 1H), 1.88 – 1.76 (m, 2H).

^{13}C NMR (101 MHz, CDCl$_3$): δ 149.3, 148.6, 144.7, 133.1, 132.7, 130.4, 129.8, 129.1,

127.9, 118.3, 108.3, 106.4, 101.9, 86.1, 74.6, 74.1, 68.8, 33.9, 25.5, 21.7, 21.1.

FTIR (NaCl, thin film): 2900, 2257, 2075, 1919, 1853, 1618, 1598, 1502, 1477, 1415,

1388, 1359, 1307, 1293, 1243, 1188, 1176, 1119, 1097, 1070, 1038, 993, 963, 914, 871,

771, 734 cm^{-1}.

HRMS (APCI) *m/z*: [M + H]$^+$ Calcd for C$_{23}$H$_{24}$IO$_7$S 571.0282; Found 571.0265.

R_f = 0.55 (silica, 33% EtOAc/hexanes, UV/KMnO$_4$).

Preparation of azide 157:
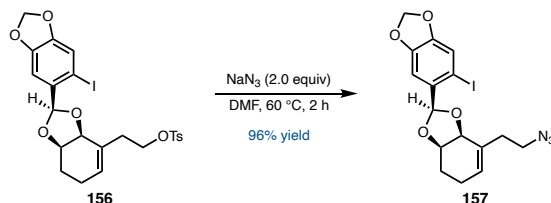
A 25 mL Schlenk flask was charged with the alkyl tosylate (**156**, 372 mg, 0.65 mmol, 1.0

equiv), sodium azide (84.6 mg, 1.3 mmol, 2.0 equiv), and a stir bar. The flask was

evacuated and backfilled with nitrogen three times, and then anhydrous DMF (10 mL) was

added. The suspension was heated to 60 °C using an oil bath for 2 h then cooled to ambient

temperature and quenched with water (10 mL). The aqueous phase was extracted with Et$_2$O

(3 x 20 mL). The combined organic layers were washed with water (20 mL), dried over

MgSO$_4$, and concentrated. The residue was purified via column chromatography (40:1:1

to 30:1:1 hexanes/EtOAc/Et$_2$O) to afford azide **157** (276 mg, 96% yield) as a white oil.

^{1}H NMR (500 MHz, CDCl$_3$): δ 7.21 (s, 1H), 6.99 (s, 1H), 6.02 – 5.94 (m, 3H), 5.89 – 5.79

(m, 1H), 4.45 (d, J = 6.4 Hz, 1H), 4.42 – 4.34 (m, 1H), 3.51 – 3.34 (m, 2H), 2.56 – 2.33

(m, 2H), 2.31 – 2.15 (m, 1H), 2.01 (dq, J = 18.0, 5.0 Hz, 1H), 1.97 – 1.82 (m, 2H).

^{13}C NMR (126 MHz, CDCl$_3$): δ 149.5, 148.7, 132.8, 132.0, 128.9, 118.5, 108.5, 106.7,

101.9, 86.3, 74.8, 74.5, 49.7, 34.2, 25.8, 21.4.

FTIR (NaCl, thin film): 2894, 2357, 2093, 1617, 1500, 1474, 1413, 1388, 1366, 1293,

1241, 1175, 1116, 1069, 1037, 1004, 966, 929, 903, 869, 838, 801 cm^{-1}.

HRMS (APCI) *m/z*: [M – N$_2$ + H]$^+$ Calcd for C$_{16}$H$_{17}$INO$_4$ 414.0197; Found 414.0177.

R_f = 0.57 (silica, 80:10:10 EtOAc/hexanes, UV/KMnO$_4$).

Preparation of Amine S1:
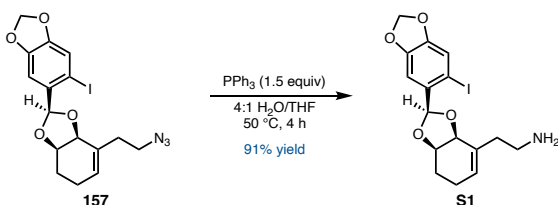
A round-bottomed flask was charged with azide (**157**, 793 mg, 1.80 mmol, 1.0 equiv), PPh$_3$

(707 mg, 2.70 mmol, 1.5 equiv), THF (7 mL), H$_2$O (28 mL), and a stir bar. The reaction

was heated to 50 °C under nitrogen using an oil bath for 3 h then cooled and diluted with

EtOAc (50 mL) and 2 M NaOH (40 mL). The aqueous layer was extracted with EtOAc (3

x 50 mL), then the combined organics were dried over Na$_2$SO$_4$ and concentrated. The

residue was purified via column chromatography (94:5:1 DCM/MeOH/NH₄OH) to afford

S1 as a colorless oil (724 mg, 91% yield).

¹H NMR (400 MHz, CDCl₃): δ 7.19 (s, 1H), 6.98 (s, 1H), 5.95 (s, 3H), 5.76 (t, J = 4.1 Hz,

1H), 4.48 – 4.40 (m, 1H), 4.35 (td, J = 6.3, 4.2 Hz, 1H), 2.97 – 2.74 (m, 2H), 2.36 (dtd, J

= 13.2, 6.6, 1.6 Hz, 1H), 2.29 – 2.14 (m, 2H), 2.04 – 1.92 (m, 1H), 1.85 (dq, J = 7.5, 5.7

Hz, 2H).

¹³C NMR (101 MHz, CDCl₃): δ 148.8, 148.1, 132.5, 132.3, 127.4, 117.9, 107.9, 105.9,

101.3, 85.7, 74.2, 73.9, 39.6, 38.0, 25.5, 20.8.

FTIR (NaCl, thin film): 2905, 1501, 1475, 1413, 1242, 1116, 1068, 1034 cm⁻¹.

HRMS (FD) *m/z*: [M + H]⁺ Calcd for $C_{16}H_{19}NO_4I$ 416.0353; Found 416.0358.

R_f = 0.27 (silica, 80:19:1 DCM/MeOH/NH₄OH, UV/ninhydrin)

Preparation of Carbamate 158:
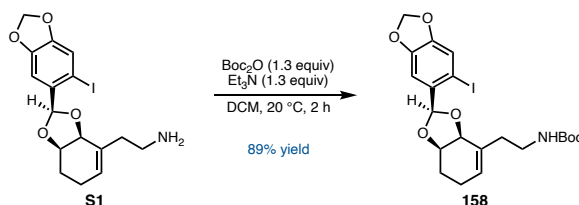
A round-bottomed flask was charged with amine (**S1**, 229 mg, 0.55 mmol, 1.0 equiv),

DCM (2.8 mL), and a stir bar then stirred at ambient temperature. Triethylamine (0.100

mL, 0.72 mmol, 1.3 equiv) was added, followed by di-*tert*-butyl dicarbonate (Boc₂O, 156

mg, 0.72 mmol, 1.3 equiv). The reaction was stirred for 2 h then concentrated. The residue

was purified via column chromatography (20% EtOAc/hexanes) to afford carbamate **158**

(253 mg, 89% yield) as an amorphous white solid.

^{1}H NMR (500 MHz, CDCl$_3$): δ 7.21 (s, 1H), 6.99 (s, 1H), 5.97 (d, J = 1.9 Hz, 3H), 5.82

– 5.74 (m, 1H), 4.66 (s, 1H), 4.47 (d, J = 6.4 Hz, 1H), 4.37 (td, J = 6.4, 4.1 Hz, 1H), 3.43

– 3.20 (m, 2H), 2.52 – 2.34 (m, 1H), 2.23 (dt, J = 14.0, 7.1 Hz, 2H), 2.03 – 1.95 (m, 1H),

1.87 (dq, J = 9.1, 5.5 Hz, 2H), 1.43 (s, 9H).

^{13}C NMR (101 MHz, CDCl$_3$): δ 156.0, 149.3, 148.6, 132.7, 128.4, 118.4, 108.3, 106.3,

101.8, 86.1, 79.0, 74.7, 74.3, 38.8, 35.2, 28.4, 25.9, 21.2.

FTIR (NaCl, thin film): 3362, 2920, 1702, 1502, 1476, 1242, 1168, 1038 cm^{-1}.

HRMS (FD) m/z: [M + •]$^+$ Calcd for C$_{21}$H$_{26}$NO$_6$I 515.0799; Found 515.0828.

R_f = 0.54 (silica, 35% EtOAc/hexanes, UV/anisaldehyde).

Preparation of Carbamate 161:
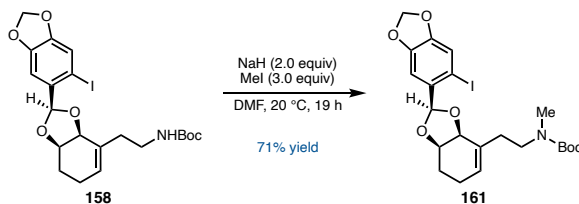
An oven-dried 2-dram vial was charged with a stir bar then pumped into a nitrogen-filled

glovebox. NaH (8.0 mg, 0.30 mmol, 2.0 equiv) was added. The vial was sealed with a

19/38 septum and electrical tape then removed from the glovebox. DMF (0.375 mL) was

added, and the suspension was stirred at 0 °C under nitrogen using an ice/water bath. The

carbamate (**158**, 77.3 mg, 0.15 mmol, 1.0 equiv) was added as a solution in DMF (0.375

mL), then the reaction was warmed to ambient temperature and stirred for 45 min. The

reaction was cooled to 0 °C, iodomethane (28.0 μL, 0.45 mmol, 3.0 equiv) was added, and

then the reaction was warmed to ambient temperature and stirred for an additional 19 h.

The reaction was quenched with water then extracted with EtOAc (3 x 2 mL). The combined organic layers were washed with 1 M LiCl (2 x 2 mL), dried over Na_2SO_4, and concentrated. The residue was purified via column chromatography (15% EtOAc/hexanes) to afford carbamate **161** (56.7 mg, 71% yield) as a sticky, off-white foam.

¹H NMR (400 MHz, CDCl₃): δ 7.20 (s, 1H), 6.99 (s, 1H), 5.97 (d, *J* = 2.0 Hz, 3H), 5.72 (t, *J* = 4.1 Hz, 1H), 4.65 – 4.43 (m, 1H), 4.36 (td, *J* = 6.1, 4.4 Hz, 1H), 3.72 – 3.37 (m, 1H), 3.18 (s, 1H), 2.83 (s, 3H), 2.48 – 2.26 (m, 2H), 2.26 – 2.13 (m, 1H), 1.96 (s, 1H), 1.90 (s, 2H), 1.44 (s, 9H).

¹³C NMR (101 MHz, CDCl₃): δ 155.7, 149.2, 148.5, 132.8 (2 overlapping peaks), 127.9/127.6*, 118.4, 108.4, 106.4, 101.7, 86.1, 79.2/79.1*, 74.7, 74.2/74.0*, 47.9/46.6*, 34.1, 32.7/32.2*, 28.5, 25.8, 21.3. *rotamers

FTIR (NaCl, thin film): 2926, 1694, 1476, 1391, 1242, 1158, 1038 cm⁻¹.

HRMS (FD) *m/z*: [M + •]⁺ Calcd for $C_{22}H_{28}NO_6I$ 529.0956; Found 529.0960.

***R*ₓ** = 0.57 (silica, 35% EtOAc/hexanes, UV/anisaldehyde).

Procedures for Radical Cyclizations

Radical Cyclization: General Procedure 1
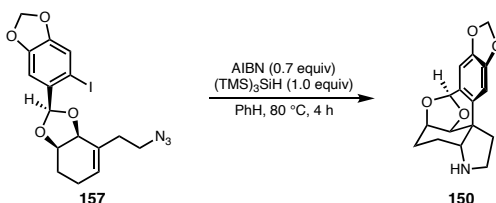
A flame-dried three-necked round-bottomed flask was equipped with a reflux condenser, two rubber septa, and a stir bar under nitrogen. The flask was charged with substrate (0.030

mmol, 1.0 equiv), tris(trimethylsilyl)silane (9.3 µL, 0.030 mmol, 1.0 equiv), and benzene

(2.6 mL) then heated to reflux using an oil bath. AIBN (3.4 mg, 0.021 mmol, 0.7 equiv)

was added over 4 h as a solution in benzene (1.1 mL), then the reaction was concentrated.

Optimization of Radical Cascade

entry	equiv (TMS)$_3$SiH	radical initiator	solvent	T (°C)	t (h)	NMR yield
1	3	AIBN (1 equiv)	PhH	80	4	11%
2	3	V-70 (1 equiv)	PhH	30	50	0%
3	3	Et$_3$B/air (0.25 equiv)	PhH	20	1	trace
4	1.1	ABCN (1 equiv)	PhMe	110	4	11%
5	1	AIBN (1 equiv)	PhH	80	4	10%
6	1	AIBN (1 equiv)	PhH	80	4	23%
7	1	AIBN (0.7 equiv)	PhH	80	4	23%
8	1	AIBN (0.3 equiv)	PhH	80	4	16%
9	1	AIBN (0.7 equiv)	PhH	80	4	32%

Entries 1–5: syringe pump addition of silane and initator over the course of the reaction
Entries 6–8: syringe pump addition of substrate over the course of the reaction
Entry 9: syringe pump addition of AIBN over the course of the reaction

Noraugustamine (150):
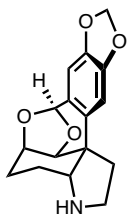
Prepared from azide **157** according to General Procedure 1. The residue was

dissolved in DCM (2 mL) and extracted with 0.1 M HCl (2 x 1 mL). The

aqueous phase was basified to pH 14 with 3 M NaOH then extracted with DCM

(3 x 2 mL). The combined organic extracts were dried over Na$_2$SO$_4$ and concentrated.

Following analysis by ^{1}H NMR to determine yield, several reactions were combined and

purified via column chromatography (20:2:1 DCM/MeOH/Et$_2$O) to give **150** as an

amorphous white solid.

^{1}H NMR (400 MHz, CDCl$_3$): δ 6.77 (s, 1H), 6.62 (s, 1H), 5.93 (d, J = 1.9 Hz, 2H), 5.86

(s, 1H), 4.32 (d, J = 4.5 Hz, 1H), 4.25 (dt, J = 4.6, 4.1 Hz, 1H), 3.52 (dd, J = 4.6, 4.1 Hz,

1H), 3.49 – 3.29 (m, 2H), 2.44 (ddd, J = 13.4, 7.9, 3.9 Hz, 1H), 2.20 – 2.04 (m, 2H), 1.77

(dddd, J = 14.9, 4.3, 4.2, 4.2 Hz, 1H), 1.59 – 1.48 (m, 2H).

^{13}C NMR (101 MHz, CDCl$_3$): δ 148.2, 145.9, 133.5, 129.3, 106.6, 105.1, 101.4, 100.4,

76.2, 74.5, 65.9, 47.1, 43.9, 39.7, 21.6, 18.8.

FTIR (NaCl, thin film): 2920, 1738, 1614, 1503, 1486, 1441, 1377, 1322, 1245, 1077,

1037, 934, 868, 841, 824, 736 cm^{-1}.

HRMS (APCI) *m/z*: [M + H]$^+$ Calcd for C$_{16}$H$_{18}$NO$_4$ 288.1230; Found 288.1221.

R_f = 0.22 (silica, 20:2:1 DCM/MeOH/Et$_2$O, UV/ninhydrin).

Compound 159
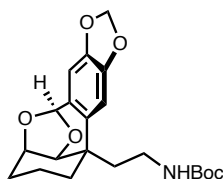
Prepared from carbamate **158** (10.3 mg, 0.020 mmol) according to
General Procedure 1. The residue was dissolved in EtOAc (2 mL) and
saturated aqueous NaHCO$_3$ (2 mL) then extracted with EtOAc (3 x 2

mL). The combined organic extracts were dried over Na$_2$SO$_4$ and concentrated. The residue

was purified via column chromatography (20% EtOAc/hexanes) then preparative TLC

(15/15/70 Et$_2$O/DCM/PhMe) to give **11** as an amorphous white solid (2.0 mg, 25% yield).

^{1}H NMR (400 MHz, CDCl$_3$): δ 6.69 (s, 1H), 6.59 (s, 1H), 5.94 (dd, J = 8.5, 1.4 Hz, 2H),

5.83 (s, 1H), 4.74 (s, 1H), 4.22 (s, 2H), 3.25 – 2.94 (m, 2H), 2.06 (d, J = 13.9 Hz, 1H), 1.97

– 1.84 (m, 2H), 1.73 (dt, J = 14.3, 7.0 Hz, 1H), 1.40 (s, 9H), 1.31 (td, J = 13.6, 2.7 Hz, 4H).

^{13}C NMR (101 MHz, CDCl$_3$): δ 156.0, 148.2, 145.6, 133.8, 106.1, 104.6, 101.2, 100.4,

79.2, 79.0, 74.9, 44.9, 41.3, 38.4, 37.4, 28.6, 27.5, 15.7.

FTIR (NaCl, thin film): 2933, 1708, 1505, 1239, 1172, 1039, 940 cm^{-1}.

HRMS (FD) *m/z*: [M + •]$^+$ Calcd for $C_{21}H_{27}NO_6$ 389.1833; Found 389.1844.

R$_f$ = 0.27 (silica, 40% EtOAc/hexanes, UV/anisaldehyde).

Compound 159
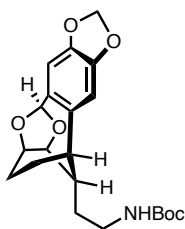
Prepared from carbamate **158** (10.3 mg, 0.020 mmol) according to General Procedure 1. The residue was dissolved in EtOAc (2 mL) and saturated aqueous NaHCO$_3$ (2 mL) then extracted with EtOAc (3 x 2 mL). The combined organic extracts were dried over Na$_2$SO$_4$ and concentrated.

The residue was purified via column chromatography (20% EtOAc/hexanes) then preparative TLC (15/15/70 Et$_2$O/DCM/PhMe) to give **159** as an amorphous white solid (2.1 mg, 26% yield).

^{1}H NMR (400 MHz, CDCl$_3$): δ 6.68 (s, 1H), 6.64 (s, 1H), 5.96 – 5.89 (m, 2H), 5.83 (s, 1H), 4.65 – 4.56 (m, 1H), 4.55 – 4.48 (m, 1H), 4.46 (s, 1H), 3.27 – 3.10 (m, 2H), 2.95 – 2.81 (m, 1H), 2.21 – 2.07 (m, 1H), 2.07 – 1.96 (m, 1H), 1.85 (s, 1H), 1.78 – 1.65 (m, 1H), 1.65 – 1.60 (m, 1H), 1.52 (dd, *J* = 14.1, 7.1 Hz, 2H), 1.43 (s, 9H).

^{13}C NMR (101 MHz, CDCl$_3$): δ 156.2, 147.3, 145.5, 137.7, 133.7, 111.8, 109.2, 106.7, 101.3, 79.3, 75.3 (2 overlapping peaks), 41.6, 38.4, 34.5, 30.8, 28.6, 25.2, 21.6.

FTIR (NaCl, thin film): 3384, 2929, 1700, 1506, 1489, 1364, 1243, 1175, 1120, 1045 cm^{-1}.

HRMS (FD) *m/z*: [M + •]$^+$ Calcd for $C_{21}H_{27}NO_6$ 389.1833; Found 389.1839.

R$_f$ = 0.27 (silica, 40% EtOAc/hexanes, UV/anisaldehyde).

Procedures for Heck Reactions

Heck Cyclization: General Procedure 2

A 1-dram vial was charged with a stir bar and pumped into a nitrogen-filled glovebox. Tetrabutylammonium acetate (30.2 mg, 0.10 mmol, 2.0 equiv) was added, and
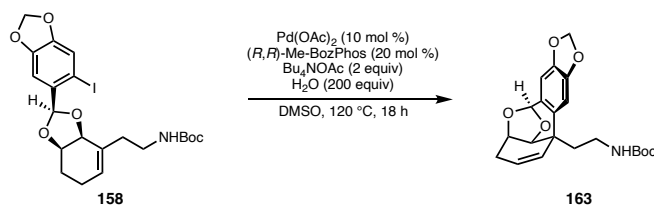
then the aryl iodide (0.050 mmol, 1.0 equiv) was added as a solution in DMSO (0.50 mL). Pd(OAc)$_2$ (1.1 mg, 0.0050 mmol, 0.10 equiv) and (*R*,*R*)-Me-BozPhos (3.2 mg, 0.010 mmol, 0.20 equiv) were added as a solution in DMSO (0.50 mL). The vial was capped and removed from the glovebox. Water (0.18 mL, 10 mmol, 200 equiv) was quickly added, then the reaction was immediately sealed with a Teflon-lined cap and stirred at 120 °C for 18 h using an aluminum heating block. The reaction was cooled to ambient temperature then diluted with EtOAc (2 mL), brine (0.5 mL), and water (1 mL). The aqueous layer was extracted with EtOAc (3 x 2 mL), then the combined organics were washed with water (2 mL), dried over Na$_2$SO$_4$, and concentrated.

Reactions under N$_2$: the above procedure, taking care to minimize the time that the vial is open between adding water and sealing with a Teflon cap.

Reactions under air: stirred open to air for 10 minutes prior to addition of water.

Reactions under O$_2$: sparged with oxygen for 5 minutes prior to addition of water, taking care to minimize the time that the vial is open between sparging and sealing with a Teflon cap.

Compound 162
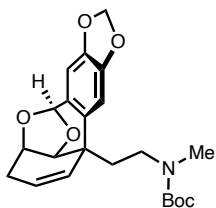
Prepared from carbamate **161** (23.8 mg, 0.045 mmol) according to General Procedure 2 (under N_2). The residue was purified via column chromatography (20% EtOAc/hexanes) to give **162** as an amorphous, white solid (10.4 mg, 58% yield).

^{1}H NMR (400 MHz, CDCl$_3$): δ 6.71 (s, 1H), 6.58 (s, 1H), 5.91 (dd, J = 9.9, 1.4 Hz, 2H), 5.84 (s, 1H), 5.81 – 5.74 (m, 1H), 5.63 – 5.52 (m, 1H), 4.49 – 4.26 (m, 2H), 3.78 – 3.31 (m, 1H), 3.06 – 2.87 (m, 1H), 2.81 (s, 3H), 2.53 (d, J = 17.1 Hz, 1H), 2.32 (d, J = 19.3 Hz, 1H), 2.19 – 2.08 (m, 1H), 1.90 (s, 1H), 1.44 (s, 9H).

^{13}C NMR (101 MHz, CDCl$_3$): δ 155.7, 148.2, 145.5, 133.3, 131.7, 131.1, 124.2, 107.0, 104.7, 101.2, 100.1, 79.5, 77.8, 72.5, 45.7, 40.4, 39.5, 34.4, 28.3.

FTIR (NaCl, thin film): 2924, 1686, 1484, 1394, 1366, 1256, 1159, 1080, 1038, 931, 872 cm^{-1}.

HRMS (FD) m/z: [M + •]$^+$ Calcd for $C_{22}H_{27}NO_6$ 401.1833; Found 401.1828.

R_f = 0.35 (silica, 35% EtOAc/hexanes, UV/anisaldehyde).

Compound 163
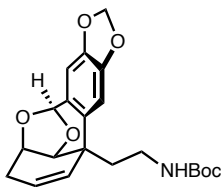
Prepared from carbamate **158** (25.8 mg, 0.050 mmol) according to General Procedure 2 (under N_2). The residue was purified via column chromatography (20% EtOAc/hexanes) to give **163** as an amorphous white solid (9.8 mg, 47% yield).

^{1}H NMR (400 MHz, CDCl$_3$): δ 6.67 (s, 1H), 6.58 (s, 1H), 5.97 – 5.83 (m, 3H), 5.76 (dt, J = 10.7, 1.3 Hz, 1H), 5.56 (ddd, J = 9.9, 4.5, 3.3 Hz, 1H), 4.71 (s, 1H), 4.40 (d, J = 5.1 Hz, 1H), 4.35 (ddd, J = 7.1, 4.9, 2.0 Hz, 1H), 3.33 – 3.17 (m, 1H), 3.17 – 3.05 (m, 1H), 2.61 – 2.47 (m, 1H), 2.37 – 2.24 (m, 1H), 2.12 (ddd, J = 14.2, 8.1, 6.2 Hz, 1H), 1.89 (dt, J = 13.8, 7.1 Hz, 1H), 1.41 (s, 9H).

^{13}C NMR (101 MHz, CDCl$_3$): δ 156.0, 148.2, 145.6, 133.5, 132.0, 131.0, 124.2, 107.2, 104.7, 101.2, 100.0, 79.1, 77.8, 72.4, 42.6, 39.8, 37.1, 28.6, 28.4.

FTIR (NaCl, thin film): 2972, 1708, 1502, 1483, 1365, 1246, 1166, 1078, 1038, 931 cm^{-1}.

HRMS (FD) _m/z_: [M + •]$^+$ Calcd for C$_{21}$H$_{25}$NO$_6$ 387.1676; Found 387.1686.

_R$_f$_ = 0.32 (silica, 35% EtOAc/hexanes, UV/anisaldehyde).

Compound 164
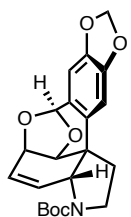
Prepared from carbamate **158** (7.5 mg, 0.019 mmol) according to General Procedure 2 (under O$_2$). The residue was purified via column chromatography (15:15:70 EtOAc/DCM/hexanes) to give **164** as an amorphous white solid (3.6 mg, 48% yield).

^{1}H NMR (400 MHz, CDCl$_3$): δ 6.74 (s, 1H), 6.60 (s, 1H), 6.37 – 6.00 (m, 2H), 5.97 – 5.85 (m, 3H), 4.55 (d, J = 5.6 Hz, 1H), 4.43 (dd, J = 5.6, 2.9 Hz, 1H), 4.21 (s, 1H), 3.80 (s, 1H), 3.54 (td, J = 11.3, 6.7 Hz, 1H), 2.46 (dd, J = 13.0, 6.7 Hz, 1H), 2.16 – 2.06 (m, 1H), 1.49 (s, 9H).

^{13}C NMR (101 MHz, CDCl$_3$): δ 155.0*, 148.2, 146.2, 132.8, 127.7, 127.7, 127.3, 106.9, 105.3, 101.4, 101.0, 80.5*, 73.8, 70.3, 62.8, 46.6*, 46.1, 36.9*, 28.6. *quaternary carbons and/or broad rotamers, difficult to see in ^{13}C NMR (low signal due to poor solubility) but visible by HMBC.

FTIR (NaCl, thin film): 2918, 1691, 1486, 1392, 1244, 1172, 1115, 1078, 1039, 925, 730 cm^{-1}.

HRMS (FD) *m/z*: [M + •]$^+$ Calcd for C$_{21}$H$_{23}$NO$_6$ 385.1520; Found 385.1532.

R_f = 0.42 (silica, 35% EtOAc/hexanes, UV/anisaldehyde).

S3
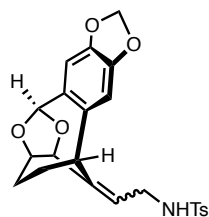
Prepared from sulfonamide **S2** (7.2 mg, 0.013 mmol) according to General Procedure 2 (under N$_2$). The residue was purified via column chromatography (30% EtOAc/hexanes) then preparative TLC (40% EtOAc/hexanes) to give **S3** as a white solid (2.0 mg, 33% yield, 1.2:1 mixture of inseparable olefin isomers). This sample was 91% pure by weight (6% EtOAc, 3% TsNH$_2$, determined by ^{1}H NMR) and the yield has been adjusted accordingly.

^{1}H NMR (400 MHz, CDCl$_3$): δ 7.77 – 7.66 (m, 4H), 7.38 – 7.29 (m, 2H), 7.25 (s, 2H), 6.69 (s, 2H), 6.62 (s, 1H), 6.50 (s, 1H), 6.01 – 5.83 (m, 6H), 5.52 (t, *J* = 7.0 Hz, 1H), 5.47 (t, *J* = 7.2 Hz, 1H), 5.02 (d, *J* = 6.6 Hz, 1H), 4.63 (d, *J* = 7.5 Hz, 1H), 4.59 (dd, *J* = 7.1, 3.4 Hz, 2H), 4.42 (t, *J* = 6.1 Hz, 1H), 4.27 (t, *J* = 6.0 Hz, 1H), 3.84 – 3.68 (m, 3H), 3.68 – 3.54

(m, 2H), 3.35 (d, J = 11.1 Hz, 1H), 2.45 (s, 3H), 2.42 (s, 3H), 2.19 – 2.06 (m, 2H), 2.02 –

1.93 (m, 2H), 1.89 – 1.71 (m, 2H), 1.43 – 1.31 (m, 2H).

^{13}C NMR (101 MHz, CDCl$_3$): δ 147.7, 145.7, 145.6, 143.9, 143.8, 139.2, 138.3, 137.8,

137.0, 136.8, 136.6, 133.6, 133.0, 130.0, 129.9, 127.3, 127.3, 126.6, 126.2, 125.5, 110.3,

110.0, 109.6, 109.5, 107.0, 106.7, 101.5, 101.4, 81.8, 76.1, 76.1, 73.5, 48.4, 40.0, 39.9,

27.1, 26.9, 22.1, 22.0, 21.7, 21.7.

FTIR (NaCl, thin film): 3270, 2924, 1487, 1328, 1240, 1157, 1093, 1036 cm^{-1}.

HRMS (FD) *m/z*: [M + •]$^+$ Calcd for C$_{23}$H$_{23}$NO$_6$S 441.1241; Found 441.1241.

R$_f$ = 0.37 (silica, 40% EtOAc/hexanes, UV/anisaldehyde).

Oxidative Heck/Aza-Wacker Cascade

Substrate Preparation
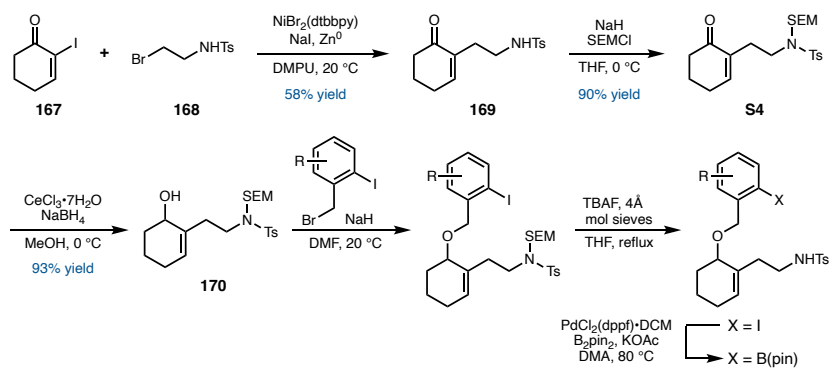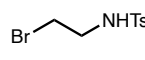
Preparation of 2-iodocyclohex-2-en-1-one (167):
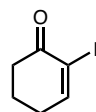
2-iodocyclohex-2-en-1-one (**167**) was prepared according to the procedure

reported by Krafft and Cran.[31] Spectral data matched those reported in the

literature.

Preparation of *N*-(2-bromoethyl)-4-methylbenzenesulfonamide (168):

N-(2-bromoethyl)-4-methylbenzenesulfonamide   (**168**)   was   prepared

according to the procedure reported by Romo and coworkers.[32] Spectral data matched those

reported in the literature.

Preparation of enone 169:
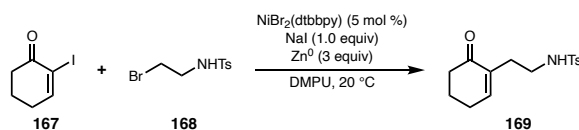
0.1 mmol scale procedure: A flame-dried 1 dram vial was charged with a stir bar, 2-

iodocyclohex-2-en-1-one (**167**, 22.2 mg, 0.10 mmol, 1.0 equiv), *N*-(2-bromoethyl)-4-

methylbenzenesulfonamide (**168**, 41.7 mg, 0.15 mmol, 1.5 equiv), zinc dust (19.6 mg, 0.30

mmol, 3.0 equiv), and NaI (15.0 mg, 0.10 mmol, 1.0 equiv). The vial was pumped into a

nitrogen-filled glovebox, and then $NiBr_2$(dtbbpy) (2.44 mg, 0.050 mmol, 0.05 equiv) and

anhydrous DMPU (0.40 mL) were added. The reaction was sealed with a Teflon-lined cap

and electrical tape then removed from the glovebox and stirred at 20 °C and 700 rpm. After

24 h, the reaction was diluted with EtOAc (5 mL) and 0.5 M HCl (2 mL). The layers were

separated, and the organic layer was washed with water (2 x 2 mL), dried over Na_2SO_4,

and concentrated. ^{1}H NMR with added 1,1,2,2-tetra-chloroethane indicated a 62% yield of

the desired enone. The residue was purified twice by column chromatography (30 to 40%

EtOAc/hexanes) to yield enone **169** (10.0 mg, 34% yield) as an amorphous white solid.

^{1}H NMR (400 MHz, CDCl$_3$): δ 7.72 (dd, J = 8.5, 2.0 Hz, 2H), 7.33 – 7.27 (m, 2H), 6.78

(q, J = 3.3 Hz, 1H), 4.73 (t, J = 6.0 Hz, 1H), 3.14 – 2.96 (m, 2H), 2.42 (d, J = 2.0 Hz, 3H),

2.41 – 2.30 (m, 6H), 1.99 – 1.91 (m, 2H).

^{13}C NMR (101 MHz, CDCl$_3$): δ 200.0, 148.8, 143.4, 137.2, 136.4, 129.8, 127.2, 42.7,

38.4, 30.6, 26.2, 23.0, 21.6.

FTIR (NaCl, thin film): 3277, 2926, 1666, 1426, 1327, 1159, 1094 cm^{-1}.

HRMS (FD) *m/z*: [M + H]$^+$ Calcd for C$_{15}$H$_{20}$NO$_3$S 294.1158; Found 294.1148.

R$_f$ = 0.35 (silica, 50% EtOAc/hexanes, UV/anisaldehyde).

10 mmol scale procedure: A flame-dried 200 mL round-bottomed flask was charged with

a large football-shaped stir bar, 2-iodocyclohex-2-en-1-one (**167**, 2.22 g, 10 mmol, 1.0

equiv), *N*-(2-bromoethyl)-4-methylbenzenesulfonamide (**168**, 4.17 g, 15 mmol, 1.5 equiv),

zinc dust (1.96 g, 30 mmol, 3.0 equiv), NaI (1.50 g, 10 mmol, 1.0 equiv), and NiBr$_2$(dtbbpy)

(244 mg, 0.50 mmol, 0.05 equiv) then sealed with a septum. The flask was evacuated and

backfilled 3x with nitrogen, then anhydrous DMPU (40 mL) was added. The top of the

septum was sealed with parafilm (where the needle had pierced it) and the edges of the

septum were sealed with electrical tape. The reaction was stirred at 20 °C and 700 rpm for

20 h then transferred to a separatory funnel and diluted with EtOAc (300 mL) and 0.5 M

HCl (120 mL). The layers were separated, and the organic layer was washed with water

(150 mL) then saturated aqueous NaHCO$_3$ (150 mL), dried over Na$_2$SO$_4$, and concentrated

onto Celite. The residue was purified via column chromatography (35% EtOAc/hexanes)

to yield enone **169** (2.10 g, 58% yield) as a yellow oil. The sample was 81% pure by weight

(9% EtOAc, 10% TsNH$_2$, determined by ^{1}H NMR) and the yield has been adjusted

accordingly. The sample can be carried forward at this purity; alternatively, an additional

flash column (30 or 35% EtOAc/hexanes) can remove excess TsNH$_2$.

Preparation of SEM-protected enone S4:
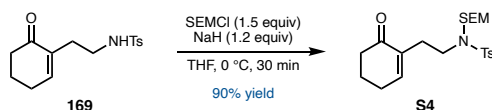
An oven-dried round-bottomed flask and stir bar were pumped into a nitrogen-filled

glovebox. NaH (134 mg, 5.0 mmol, 1.2 equiv) was added, and then the flask was sealed

with a septum and removed from the glovebox. THF (21 mL) was added, and the reaction

was stirred at 0 °C under nitrogen using an ice/water bath. The enone (**169**, 1.23 g, 4.2

mmol, 1.0 equiv) was added dropwise as a solution in THF (21 mL). This solution was

stirred for 10 minutes, and then 2-(trimethylsilyl)ethoxymethyl chloride (SEMCl, 1.12 mL,

6.3 mmol, 1.5 equiv) was added. The reaction was allowed to stir at 0 °C under nitrogen

for 30 min then quenched with brine (5 mL). The reaction was diluted with water (50 mL)

and EtOAc (100 mL). The aqueous layer was extracted with EtOAc (100 mL), then the

combined organic layers were dried over Na$_2$SO$_4$ and concentrated onto Celite. The residue

was purified via column chromatography (20% EtOAc/hexanes) to yield enone **S4** as a

pale yellow oil (1.69 g, 90% yield).

^{1}H NMR (500 MHz, CDCl$_3$): δ 7.83 – 7.62 (m, 2H), 7.33 – 7.21 (m, 2H), 6.78 (t, J = 4.2

Hz, 1H), 4.73 (s, 2H), 3.43 (dd, J = 10.1, 6.9 Hz, 2H), 3.26 (t, J = 7.1 Hz, 2H), 2.50 – 2.44

(m, 2H), 2.41 (s, 3H), 2.36 (td, J = 6.0, 4.3 Hz, 2H), 2.03 – 1.94 (m, 2H), 0.85 (dd, J = 10.1,

6.9 Hz, 2H), –0.02 (s, 9H).

^{13}C NMR (126 MHz, CDCl$_3$): δ 199.4, 147.8, 143.3, 137.8, 136.4, 129.6, 127.5, 78.1,

65.7, 46.1, 38.5, 29.8, 26.3, 23.1, 21.6, 18.0, –1.3.

FTIR (NaCl, thin film): 2949, 1673, 1340, 1248, 1157, 1067, 938, 837, 657 cm^{-1}.

HRMS (FD) *m/z*: [M + •]$^+$ Calcd for C$_{21}$H$_{33}$NO$_4$SSi 423.1894; Found 423.1917.

R$_f$ = 0.44 (silica, 30% EtOAc/hexanes, UV/anisaldehyde).

Preparation of allylic alcohol 170:
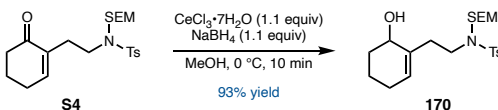
A round-bottomed flask was charged with enone (**S4**, 1.20 g, 2.7 mmol, 1.0 equiv), MeOH

(10.8 mL), cerium chloride heptahydrate (1.11 g, 3.0 mmol, 1.1 equiv), and a stir bar then

stirred at 0 °C under nitrogen using an ice/water bath. Sodium borohydride (112 mg, 3.0

mmol, 1.1 equiv) was added portionwise, and the reaction was stirred at 0 °C for 10 min

then quenched with saturated aqueous NH$_4$Cl. The resulting mixture was diluted with

saturated aqueous Rochelle's salt (250 mL) and Et$_2$O (250 mL) and stirred at 1400 rpm

overnight. The layers were separated, and the aqueous layer was extracted with Et$_2$O (2 x

100 mL). The combined organics were washed with brine (50 mL), dried over MgSO$_4$,

filtered, and concentrated onto Celite. The residue was purified via column

chromatography (20 to 30% EtOAc/hexanes) to afford **170** as a colorless oil (1.07 g, 93%

yield).

^{1}H NMR (500 MHz, CDCl$_3$): δ 7.72 (d, *J* = 8.3 Hz, 2H), 7.27 (d, *J* = 8.1 Hz, 2H), 5.57 (t,

J = 3.9 Hz, 1H), 4.75 (dt, *J* = 12.0, 9.2 Hz, 2H), 4.06 (s, 1H), 3.46 (dd, *J* = 8.2, 6.7 Hz, 2H),

3.33 (t, *J* = 5.6 Hz, 2H), 2.53 – 2.43 (m, 1H), 2.42 (s, 3H), 2.31 (dt, *J* = 14.4, 7.4 Hz, 1H),

2.09 – 1.99 (m, 1H), 1.99 – 1.87 (m, 1H), 1.80 – 1.49 (m, 4H), 0.87 (t, J = 9.7 Hz, 2H), –

0.02 (s, 9H).

^{13}C NMR (126 MHz, CDCl$_3$): δ 143.4, 137.7, 136.1, 129.7, 128.0, 127.4, 78.0, 67.4, 65.7,

46.4, 34.1, 32.4, 25.6, 21.6, 18.2, 18.0, –1.3.

FTIR (NaCl, thin film): 3520, 2936, 1336, 1249, 1157, 1068, 859, 837, 656 cm^{-1}.

HRMS (FD) m/z: [M + •]$^+$ Calcd for C$_{21}$H$_{35}$NO$_4$SSi 425.2051; Found 425.2046.

R_f = 0.25 (silica, 15:15:70 DCM/EtOAc/hexanes, UV).

Preparation of Benzyl Bromides:

5-(bromomethyl)-6-iodobenzo[d][1,3]dioxole **(S5)**,

2-(bromomethyl)-1-iodo-4-methoxybenzene **(S6)**,

and 2-(bromomethyl)-4-fluoro-1-iodobenzene **(S7)**
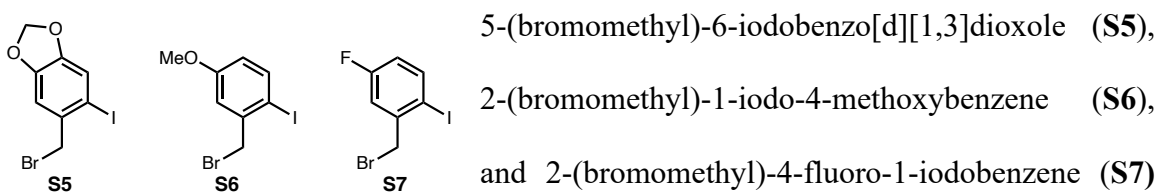
were prepared according to the procedure reported by Lete and coworkers.[44] Spectral data

matched those reported in the literature.

Alkylation: General Procedure 3
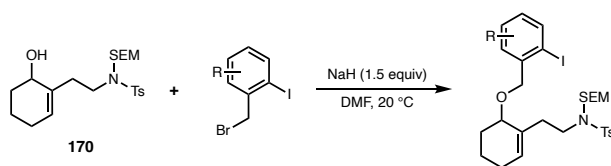
A round-bottomed flask was charged with a stir bar then brought into a nitrogen-filled

glovebox. NaH (72.5 mg, 2.7 mmol, 1.5 equiv) was added. Anhydrous DMF (6 mL) was

added, then the flask was sealed with a septum and electrical tape, removed from the

glovebox, and stirred at 0 °C under nitrogen using an ice/water bath. The alcohol (**170**, 772

mg, 1.8 mmol, 1.0 equiv) was added as a solution in DMF (6 mL) over 6 minutes. The

reaction was stirred at ambient temperature for 10 min, cooled to 0 °C, and then the benzyl

bromide (3.6 mmol, 2.0 equiv) was added slowly as a solution in DMF (6 mL). The reaction

was allowed to warm to ambient temperature, stirred under nitrogen for 18.5 h, then

quenched slowly with water (5 mL) and diluted with EtOAc (50 mL). The layers were

separated, and the aqueous layer was extracted with EtOAc (3 x 50 mL). The combined

organic layers were washed with 1 M LiCl (50 mL), dried over Na_2SO_4, filtered, and

concentrated.

S8
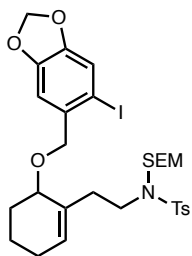
Prepared from alcohol **170** (772 mg, 1.8 mmol, 1.0 equiv) and 5-(bromomethyl)-6-iodobenzo[*d*][1,3]dioxole (**S5**, 1.24 g, 3.6 mmol, 2.0 equiv) according to General Procedure 3. The residue was purified via column chromatography (5 to 10% EtOAc/hexanes) to give **S8** as a colorless oil (806 mg, 64% yield).

¹H NMR (400 MHz, CDCl₃): δ 7.75 – 7.64 (m, 2H), 7.26 – 7.20 (m, 3H), 6.99 (s, 1H),

5.95 (s, 2H), 5.67 – 5.58 (m, 1H), 4.79 – 4.68 (m, 2H), 4.51 (d, J = 11.8 Hz, 1H), 4.34 (d,

J = 11.8 Hz, 1H), 3.83 (s, 1H), 3.47 – 3.37 (m, 2H), 3.32 (ddd, J = 14.0, 9.5, 6.8 Hz, 1H),

3.19 (ddd, J = 14.3, 9.7, 5.0 Hz, 1H), 2.42 (d, J = 8.2 Hz, 1H), 2.39 (s, 3H), 2.30 (dt, J =

14.8, 8.2 Hz, 1H), 2.12 – 1.86 (m, 3H), 1.68 (td, J = 11.9, 7.3 Hz, 3H), 0.90 – 0.78 (m, 2H),

–0.04 (s, 9H).

¹³C NMR (101 MHz, CDCl₃): δ 148.6, 147.9, 143.2, 137.9, 134.7, 134.6, 129.6, 128.7,

127.4, 118.5, 109.9, 101.7, 86.3, 77.7, 74.8, 74.2, 65.5, 46.1, 33.9, 27.4, 25.6, 21.6, 18.2,

18.0, –1.3.

FTIR (NaCl, thin film): 2938, 1477, 1339, 1245, 1157, 1068, 1037, 861, 835 cm⁻¹.

HRMS (FD) *m/z*: [M + •]⁺ Calcd for $C_{29}H_{40}NO_6SSiI$ 685.1385; Found 685.1397.

R_f = 0.50 (silica, 20% EtOAc/hexanes, UV/anisaldehyde).

S9
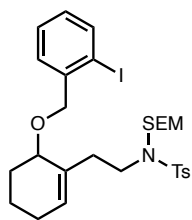
Prepared from alcohol **170** (192 mg, 0.45 mmol, 1.0 equiv) and 1-(bromomethyl)-2-iodobenzene (267 mg, 0.90 mmol, 2.0 equiv) according to General Procedure 3. The residue was purified via column chromatography (8% EtOAc/hexanes) to give **S9** as a colorless oil (218 mg, 74% yield).

¹H NMR (400 MHz, CDCl₃): δ 7.81 (dd, *J* = 7.9, 1.2 Hz, 1H), 7.74 – 7.62 (m, 2H), 7.47

(dd, *J* = 7.7, 1.7 Hz, 1H), 7.32 (td, *J* = 7.5, 1.2 Hz, 1H), 7.23 – 7.18 (m, 2H), 6.97 (td, *J* =

7.6, 1.8 Hz, 1H), 5.65 – 5.59 (m, 1H), 4.79 – 4.67 (m, 2H), 4.60 (d, *J* = 12.2 Hz, 1H), 4.41

(d, *J* = 12.2 Hz, 1H), 3.87 (t, *J* = 4.1 Hz, 1H), 3.45 – 3.37 (m, 2H), 3.33 (ddd, *J* = 14.0, 9.6,

6.8 Hz, 1H), 3.20 (ddd, *J* = 14.3, 9.8, 5.0 Hz, 1H), 2.57 – 2.41 (m, 1H), 2.38 (s, 3H), 2.36

– 2.26 (m, 1H), 2.10 – 1.84 (m, 3H), 1.78 – 1.62 (m, 2H), 1.56 – 1.49 (m, 1H), 0.93 – 0.76

(m, 2H), –0.04 (s, 9H).

¹³C NMR (101 MHz, CDCl₃): δ 143.2, 141.2, 139.1, 137.9, 134.6, 129.6, 129.4, 129.2,

128.7, 128.4, 127.4, 98.2, 77.7, 74.9, 74.5, 65.5, 46.1, 34.0, 27.3, 25.6, 21.6, 18.2, 18.0, –

1.3.

FTIR (NaCl, thin film): 2932, 1343, 1247, 1158, 1068, 836, 751 cm⁻¹.

HRMS (FD) *m/z*: [M + •]⁺ Calcd for $C_{28}H_{40}NO_4SSiI$ 641.1487; Found 641.1505.

***R*ⱼ** = 0.60 (silica, 20% EtOAc/hexanes, UV/anisaldehyde).

S10
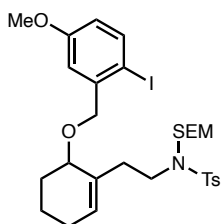
Prepared from alcohol **170** (192 mg, 0.45 mmol, 1.0 equiv) and 2-
(bromomethyl)-1-iodo-4-methoxybenzene (**S6**, 294 mg, 0.90 mmol,
2.0 equiv) according to General Procedure 3. The residue was purified
via column chromatography (8% EtOAc/hexanes) to give **S10** as a

colorless oil (212 mg, 68% yield).

¹H NMR (400 MHz, CDCl₃): δ 7.74 – 7.59 (m, 3H), 7.23 – 7.17 (m, 2H), 7.08 (d, *J* = 3.1

Hz, 1H), 6.58 (dd, *J* = 8.6, 3.1 Hz, 1H), 5.66 – 5.56 (m, 1H), 4.78 – 4.65 (m, 2H), 4.54 (d,

J = 12.5 Hz, 1H), 4.37 (d, *J* = 12.5 Hz, 1H), 3.87 (d, *J* = 4.7 Hz, 1H), 3.76 (s, 3H), 3.46 –

3.37 (m, 2H), 3.36 – 3.29 (m, 1H), 3.19 (ddd, *J* = 14.3, 9.7, 5.0 Hz, 1H), 2.52 – 2.40 (m,

1H), 2.38 (s, 3H), 2.32 (dd, *J* = 14.3, 7.9 Hz, 1H), 2.04 (s, 1H), 2.00 – 1.87 (m, 2H), 1.68

(tdd, *J* = 13.1, 10.9, 4.9 Hz, 2H), 1.60 – 1.47 (m, 1H), 0.90 – 0.76 (m, 2H), –0.05 (s, 9H).

^{13}C NMR (101 MHz, CDCl$_3$): δ 160.5, 143.5, 142.6, 139.8, 138.2, 134.9, 129.9, 129.0,

127.7, 115.7, 115.4, 86.5, 78.0, 75.1, 74.9, 65.8, 55.8, 46.3, 34.4, 27.8, 25.9, 21.9, 18.6,

18.3, –1.0.

FTIR (NaCl, thin film): 2937, 2366, 1456, 1340, 1158, 1068, 841, 680 cm^{-1}.

HRMS (FD) *m/z*: [M + •]$^+$ Calcd for C$_{29}$H$_{42}$NO$_5$SSiI 671.1592; Found 671.1600.

R$_f$ = 0.50 (silica, 20% EtOAc/hexane, UV/anisaldehyde).

S11
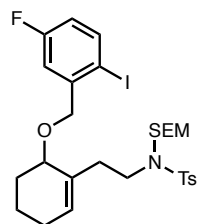
Prepared from alcohol **170** (192 mg, 0.45 mmol, 1.0 equiv) and 2-
(bromomethyl)-4-fluoro-1-iodobenzene (**S7**, 283 mg, 0.90 mmol, 2.0
equiv) according to General Procedure 3. The residue was purified via
column chromatography (5% EtOAc/hexanes) to give **S11** as a colorless

oil (158 mg, 52% yield).

^{1}H NMR (400 MHz, CDCl$_3$): δ 7.73 (dd, *J* = 8.6, 5.5 Hz, 1H), 7.70 – 7.64 (m, 2H), 7.24

– 7.18 (m, 3H), 6.81 – 6.65 (m, 1H), 5.65 (t, *J* = 2.0 Hz, 1H), 4.81 – 4.66 (m, 2H), 4.53 (d,

J = 12.9 Hz, 1H), 4.36 (d, *J* = 13.0 Hz, 1H), 3.89 (t, *J* = 4.0 Hz, 1H), 3.51 – 3.39 (m, 2H),

3.35 (ddd, *J* = 14.1, 9.7, 6.7 Hz, 1H), 3.21 (ddd, *J* = 14.3, 9.8, 5.0 Hz, 1H), 2.50 – 2.40 (m,

1H), 2.37 (s, 3H), 2.36 – 2.28 (m, 1H), 2.04 (s, 1H), 2.01 – 1.88 (m, 2H), 1.75 – 1.63 (m,

2H), 1.58 – 1.50 (m, 1H), 0.90 – 0.75 (m, 2H), –0.04 (s, 9H).

^{13}C NMR (101 MHz, CDCl$_3$): δ 163.4 (d, *J* = 247.2 Hz), 143.7 (d, *J* = 7.2 Hz), 143.2,

140.0 (d, *J* = 7.6 Hz), 137.8, 134.4, 129.6, 128.9, 127.3, 116.3 (d, *J* = 23.8 Hz), 116.3 (d, *J*

= 21.9 Hz), 89.8 (d, J = 3.1 Hz), 77.7, 74.9, 74.4, 65.5, 46.1, 34.1, 27.4, 25.6, 21.6, 18.2,

18.0, –1.3.

^{19}F NMR (282 MHz, CDCl$_3$): δ –116.8.

FTIR (NaCl, thin film): 2936, 1464, 1454, 1341, 1248, 1157, 1072, 944, 859, 836, 655

cm^{-1}.

HRMS (FD) *m/z*: [M + •]$^+$ Calcd for C$_{28}$H$_{39}$NO$_4$SSiFI 659.1392; Found 659.1416.

R_f = 0.63 (silica, 20% EtOAc/hexanes, UV/anisaldehyde).

SEM Deprotection: General Procedure 4
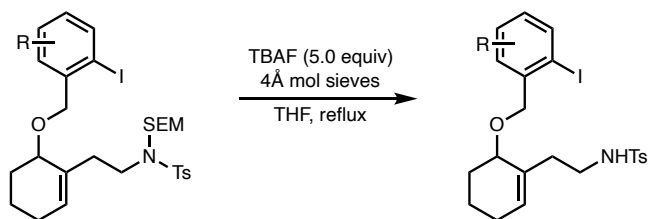
A round-bottomed flask was charged with 4Å molecular sieves (powdered, 260 mg/mmol)

and a stir bar then flame-dried and cooled under nitrogen. The SEM-protected substrate

(0.32 mmol, 1.0 equiv) was added as a solution in anhydrous THF (3.2 mL), followed by

tetrabutylammonium fluoride (1.0 M in THF, 1.6 mL, 1.6 mmol, 5.0 equiv). The reaction

was equipped with a reflux condenser and heated to reflux using an oil bath for 15 h. The

reaction was cooled to ambient temperature then filtered over Celite, taking care to rinse

several times with EtOAc to ensure that the compound fully elutes. The resulting solution

(75 mL) was then quenched with saturated aqueous NaHCO$_3$ (10 mL) and brine (10 mL)

then diluted with water (30 mL). The aqueous layer was extracted with EtOAc (2 x 50 mL),

then the combined organic layers were dried over Na$_2$SO$_4$ and concentrated.

S12
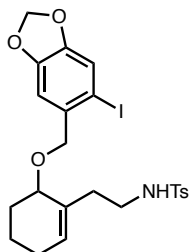
Prepared from **S8** (219 mg, 0.32 mmol) according to General Procedure
4. The residue was purified via column chromatography (20%
EtOAc/hexanes) to give **S12** as an off-white oil (127 mg, 68% yield).

^{1}H NMR (500 MHz, CDCl$_3$): δ 7.65 (d, J = 8.2 Hz, 2H), 7.23 (d, J = 6.6 Hz, 3H), 6.93 (s,

1H), 6.03 – 5.97 (m, 2H), 5.55 (s, 1H), 4.76 (t, J = 5.7 Hz, 1H), 4.48 (d, J = 11.8 Hz, 1H),

4.26 (d, J = 11.8 Hz, 1H), 3.67 (s, 1H), 3.05 (dt, J = 12.0, 6.0 Hz, 1H), 3.01 – 2.86 (m, 1H),

2.42 (s, 3H), 2.40 – 2.32 (m, 1H), 2.13 – 2.07 (m, 1H), 2.03 – 1.88 (m, 3H), 1.73 – 1.58

(m, 3H).

^{13}C NMR (101 MHz, CDCl$_3$): δ 148.7, 148.2, 143.2, 137.1, 134.1, 133.8, 130.1, 129.7,

127.2, 118.6, 109.8, 101.9, 86.5, 74.6, 74.1, 42.2, 34.6, 27.1, 25.6, 21.7, 18.0.

FTIR (NaCl, thin film): 3274, 2931, 1477, 1327, 1232, 1158, 1037, 932, 814, 668 cm^{-1}.

HRMS (TOF-ESI) *m/z*: [M + H]$^+$ Calcd for C$_{23}$H$_{27}$NO$_5$SI 556.0655; Found 556.0668.

R$_f$ = 0.23 (silica, 20% EtOAc/hexanes, UV/anisaldehyde).

S13
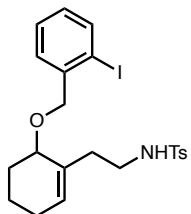
Prepared from **S9** (210 mg, 0.32 mmol) according to General Procedure
4. The residue was purified via column chromatography (20%
EtOAc/hexanes) to give **S13** as a viscous, pale yellow oil (144 mg, 84%

yield).

¹H NMR (400 MHz, CDCl₃): δ 7.81 (dd, J = 7.9, 1.2 Hz, 1H), 7.69 – 7.56 (m, 2H), 7.41

(dd, J = 7.7, 1.8 Hz, 1H), 7.35 (td, J = 7.5, 1.2 Hz, 1H), 7.23 – 7.16 (m, 2H), 7.00 (td, J =

7.6, 1.8 Hz, 1H), 5.56 (t, J = 3.9 Hz, 1H), 4.76 (t, J = 5.7 Hz, 1H), 4.55 (d, J = 12.3 Hz,

1H), 4.30 (d, J = 12.3 Hz, 1H), 3.82 – 3.63 (m, 1H), 3.12 – 2.87 (m, 2H), 2.40 (s, 3H), 2.40

– 2.31 (m, 1H), 2.20 – 2.06 (m, 1H), 2.02 – 1.87 (m, 3H), 1.80 – 1.48 (m, 3H).

¹³C NMR (101 MHz, CDCl₃): δ 143.2, 140.7, 139.3, 137.1, 133.7, 130.2, 129.7, 129.5,

129.4, 128.6, 127.2, 98.3, 74.7, 74.4, 42.1, 34.7, 27.1, 25.6, 21.7, 18.0.

FTIR (NaCl, thin film): 3268, 2928, 2859, 1438, 1324, 1163, 1090, 1012, 814, 749, 661

cm⁻¹.

HRMS (TOF-ESI) *m/z*: [M + H]⁺ Calcd for $C_{22}H_{27}NO_3SI$ 512.0756; Found 512.0786.

R_f = 0.29 (silica, 20% EtOAc/hexanes, UV/anisaldehyde).

S14
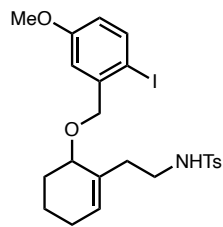
Prepared from **S10** (208 mg, 0.30 mmol) according to General Procedure 4. The residue was purified via column chromatography (25% EtOAc/hexanes) to give **S14** as a viscous, pale yellow oil (121 mg, 72% yield).

¹H NMR (400 MHz, CDCl₃): δ 7.66 (d, J = 8.6 Hz, 1H), 7.61 (d, J = 8.3 Hz, 2H), 7.24 –

7.18 (m, 2H), 7.02 (d, J = 3.1 Hz, 1H), 6.61 (dd, J = 8.7, 3.1 Hz, 1H), 5.66 – 5.49 (m, 1H),

4.81 (t, J = 5.7 Hz, 1H), 4.49 (d, J = 12.6 Hz, 1H), 4.26 (d, J = 12.6 Hz, 1H), 3.81 (s, 3H),

3.69 (t, J = 4.1 Hz, 1H), 3.23 – 2.88 (m, 2H), 2.40 (s, 3H), 2.39 – 2.30 (m, 1H), 2.17 – 2.06

(m, 1H), 2.02 – 1.87 (m, 2H), 1.76 – 1.47 (m, 4H).

^{13}C NMR (101 MHz, CDCl$_3$): δ 160.3, 143.2, 141.8, 139.6, 137.1, 133.6, 130.3, 129.7,

127.2, 115.6, 115.1, 86.2, 74.6, 74.4, 55.6, 42.1, 34.8, 27.1, 25.6, 21.7, 18.0.

FTIR (NaCl, thin film): 3277, 2932, 1467, 1326, 1297, 1160, 1093, 1076, 812, 663 cm^{-1}.

HRMS (TOF-ESI) *m/z*: [M + H]$^+$ Calcd for C$_{22}$H$_{29}$NO$_4$SI 542.0862; Found 542.0883.

R$_f$ = 0.19 (silica, 20% EtOAc/hexanes, UV/anisaldehyde).

S15
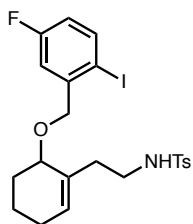
Prepared from **S11** (132 mg, 0.20 mmol) according to General Procedure 4. The residue was purified via column chromatography (15% EtOAc/hexanes) to give **S15** as a colorless oil (85.4 mg, 77% yield).

^{1}H NMR (400 MHz, CDCl$_3$): δ 7.74 (dd, *J* = 8.6, 5.5 Hz, 1H), 7.70 – 7.60 (m, 2H), 7.23

(d, *J* = 8.0 Hz, 2H), 7.16 (dd, *J* = 9.6, 3.1 Hz, 1H), 6.76 (td, *J* = 8.3, 3.1 Hz, 1H), 5.60 (t, *J*

= 1.9 Hz, 1H), 4.66 (t, *J* = 5.8 Hz, 1H), 4.47 (d, *J* = 12.9 Hz, 1H), 4.25 (d, *J* = 13.0 Hz, 1H),

3.78 – 3.67 (m, 1H), 3.17 – 2.92 (m, 2H), 2.48 – 2.30 (m, 4H), 2.18 – 2.06 (m, 1H), 2.03 –

1.84 (m, 3H), 1.75 – 1.50 (m, 3H).

^{13}C NMR (101 MHz, CDCl$_3$): δ 163.4 (d, *J* = 247.8 Hz), 143.3, 143.2 (d, *J* = 7.2 Hz),

140.2 (d, *J* = 7.7 Hz), 137.0, 133.5, 130.3, 129.7, 127.2, 116.6 (d, *J* = 22.0 Hz), 116.3 (d, *J*

= 23.6 Hz), 89.9 (d, *J* = 3.1 Hz), 74.8, 74.3, 42.0, 34.8, 27.1, 25.6, 21.7, 18.0.

^{19}F NMR (282 MHz, CDCl$_3$): δ –116.3.

FTIR (NaCl, thin film): 3268, 2921, 1328, 1158, 1074, 813, 681 cm^{-1}.

HRMS (TOF-ESI) *m/z*: [M + H]$^+$ Calcd for $C_{22}H_{26}NO_3SFI$ 530.0662; Found 530.0649.

R_f = 0.33 (silica, 20% EtOAc/hexanes, UV/anisaldehyde).

Borylation: General Procedure 5
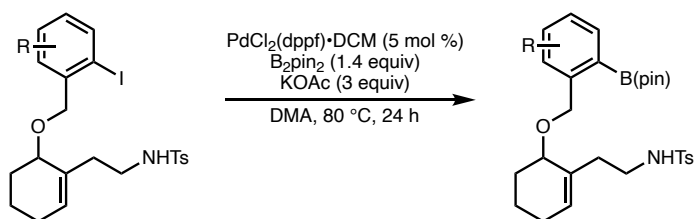
A 2-dram vial was charged with aryl iodide (139 mg, 0.27 mmol, 1.0 equiv) and a stir bar

then pumped into a nitrogen-filled glovebox. Bis(pinacolato)diboron (B_2pin_2, 96.6 mg,

0.38 mmol, 1.4 equiv), PdCl$_2$(dppf)•DCM (11.1 mg, 0.014 mmol, 0.050 equiv), potassium

acetate (80.0 mg, 0.82 mmol, 3.0 equiv), and DMA (2.7 mL) were added, then the vial was

sealed with a Teflon cap and electrical tape and brought out of the glovebox. The reaction

was stirred at 80 °C using an aluminum heating block for 24 h, cooled to ambient

temperature, and then diluted with EtOAc (2 mL) and saturated aqueous NaHCO$_3$ (3 mL).

The layers were partitioned, and the aqueous layer was extracted with EtOAc (3 x 2 mL).

The combined organic layers were washed with 1 M LiCl (2 x 1 mL), filtered over a short

silica plug, and then concentrated onto Celite.

Compound 166
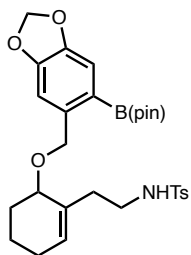
Prepared from **S12** (462 mg, 0.82 mmol) according to General Procedure 5, using a 25 mL round-bottomed flask instead of a 2-dram vial and an oil bath instead of an aluminum heating block. The residue was purified via column chromatography (20% EtOAc/hexanes) to give **166** as a sticky white solid (274 mg, 61% yield).

^{1}H NMR (400 MHz, CDCl$_3$): δ 7.72 – 7.57 (m, 2H), 7.25 – 7.21 (m, 3H), 6.94 (s, 1H), 6.00 – 5.92 (m, 2H), 5.48 (t, J = 3.9 Hz, 1H), 4.97 (t, J = 5.6 Hz, 1H), 4.74 (d, J = 11.6 Hz, 1H), 4.65 (d, J = 11.6 Hz, 1H), 3.64 (t, J = 4.0 Hz, 1H), 3.00 (dq, J = 11.9, 5.9 Hz, 1H), 2.87 (ddt, J = 12.0, 8.4, 5.5 Hz, 1H), 2.40 (s, 3H), 2.33 – 2.23 (m, 1H), 2.03 – 1.86 (m, 4H), 1.72 – 1.62 (m, 1H), 1.56 – 1.43 (m, 2H), 1.31 (d, J = 1.9 Hz, 12H).

^{13}C NMR (101 MHz, CDCl$_3$): δ 150.3, 146.7, 143.0, 140.5, 137.3, 134.4, 129.6, 129.5, 127.2, 114.8, 109.9, 101.2, 83.7, 73.1, 69.2, 42.3, 34.5, 27.3, 25.6, 25.0, 25.0, 21.6, 18.0.

FTIR (NaCl, thin film): 3280, 2932, 1428, 1369, 1319, 1161, 1114, 1041 cm^{-1}.

HRMS (TOF-ESI) *m/z*: [M + H]$^+$ Calcd for C$_{29}$H$_{38}$NO$_7$SB 555.2462; Found 555.2451.

R_f = 0.23 (silica, 20% EtOAc/hexanes, UV/anisaldehyde).

Compound 174a
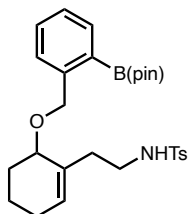
Prepared from **S13** (139 mg, 0.27 mmol) according to General Procedure 5. The residue was purified via column chromatography (15% EtOAc/hexanes) to give **174a** as a viscous, colorless oil (75.0 mg, 53% yield).

¹H NMR (400 MHz, CDCl₃): δ 7.79 (dt, J = 7.3, 1.0 Hz, 1H), 7.66 – 7.54 (m, 2H), 7.47 –

7.38 (m, 2H), 7.31 – 7.23 (m, 1H), 7.23 – 7.15 (m, 2H), 5.49 (t, J = 3.8 Hz, 1H), 4.98 (t, J

= 5.7 Hz, 1H), 4.83 (d, J = 12.0 Hz, 1H), 4.68 (d, J = 12.0 Hz, 1H), 3.66 (t, J = 4.1 Hz, 1H),

2.96 (dq, J = 11.9, 5.9 Hz, 1H), 2.86 (ddt, J = 11.8, 8.2, 5.6 Hz, 1H), 2.39 (s, 3H), 2.26 (dtd,

J = 12.0, 6.3, 1.5 Hz, 1H), 2.04 – 1.88 (m, 3H), 1.72 – 1.45 (m, 4H), 1.34 (d, J = 2.3 Hz,

12H).

¹³C NMR (101 MHz, CDCl₃): δ 144.7, 142.9, 137.3, 136.0, 134.3, 131.3, 129.6, 129.5,

128.8, 127.2, 126.9, 83.8, 73.3, 69.7, 42.2, 34.6, 27.2, 25.6, 25.1, 25.0, 21.6, 18.1.

FTIR (NaCl, thin film): 2933, 1380, 1347, 1222, 1162, 1075, 661 cm⁻¹.

HRMS (TOF-ESI) *m/z*: [M + H]⁺ Calcd for C₂₈H₃₉NO₅SB 512.2642; Found 512.2623.

***R*$_f$** = 0.45 (silica, 25% EtOAc/hexanes, UV/anisaldehyde).

Compound 174b
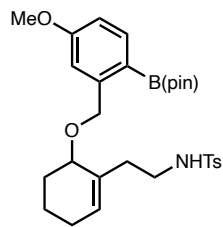
Prepared from **S14** (114 mg, 0.21 mmol) according to General
Procedure 5. The residue was purified via column chromatography (15%
EtOAc/hexanes) to give **174b** as a viscous, colorless oil (48.9 mg, 43%
yield).

¹H NMR (400 MHz, CDCl₃): δ 7.75 (d, J = 8.3 Hz, 1H), 7.67 – 7.58 (m, 2H), 7.20 (d, J =

8.0 Hz, 2H), 7.05 (d, J = 2.5 Hz, 1H), 6.80 (dd, J = 8.3, 2.6 Hz, 1H), 5.48 (t, J = 3.8 Hz,

1H), 5.08 (t, J = 5.6 Hz, 1H), 4.76 (q, J = 12.4 Hz, 2H), 3.84 (s, 3H), 3.66 (t, J = 3.8 Hz,

1H), 3.05 – 2.94 (m, 1H), 2.94 – 2.83 (m, 1H), 2.39 (s, 3H), 2.27 (ddd, J = 12.0, 9.4, 4.2

Hz, 1H), 2.04 – 1.82 (m, 4H), 1.72 – 1.44 (m, 3H), 1.32 (d, J = 2.2 Hz, 12H).

^{13}C NMR (101 MHz, CDCl$_3$): δ 162.2, 147.4, 143.0, 137.9, 137.3, 134.3, 129.7, 129.6,

127.2, 113.9, 112.7, 83.5, 73.3, 69.4, 55.3, 42.3, 34.6, 27.3, 25.7, 25.0, 25.0, 21.6, 18.0.

FTIR (NaCl, thin film): 2930, 1601, 1380, 1347, 1321, 1288, 1161, 1126, 1032 cm^{-1}.

HRMS (TOF-ESI) *m/z*: [M + H]$^+$ Calcd for C$_{29}$H$_{41}$NO$_6$SB 542.2748; Found 542.2728.

R_f = 0.41 (silica, 25% EtOAc/hexanes, UV/anisaldehyde).

Compound 174c
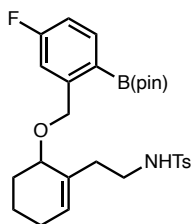
Prepared from **S15** (78.0 mg, 0.14 mmol) according to General Procedure

5. The residue was purified via column chromatography (15%

EtOAc/hexanes) to give **174c** as a colorless oil (55.4 mg, 74% yield).

^{1}H NMR (400 MHz, CDCl$_3$): δ 7.79 (dd, *J* = 8.3, 6.5 Hz, 1H), 7.67 – 7.57 (m, 2H), 7.25

– 7.20 (m, 2H), 7.16 (dd, *J* = 10.4, 2.6 Hz, 1H), 6.94 (td, *J* = 8.4, 2.6 Hz, 1H), 5.54 (t, *J* =

3.9 Hz, 1H), 4.85 (t, *J* = 5.7 Hz, 1H), 4.81 (d, *J* = 12.8 Hz, 1H), 4.68 (d, *J* = 12.8 Hz, 1H),

3.76 – 3.64 (m, 1H), 3.06 – 2.86 (m, 2H), 2.39 (s, 3H), 2.37 – 2.25 (m, 1H), 2.11 – 2.01

(m, 1H), 2.01 – 1.85 (m, 2H), 1.74 – 1.44 (m, 4H), 1.33 (d, *J* = 1.2 Hz, 12H).

^{13}C NMR (101 MHz, CDCl$_3$): δ 165.1 (d, *J* = 250.5 Hz), 148.6 (d, *J* = 7.5 Hz), 143.1,

138.4 (d, *J* = 8.2 Hz), 137.2, 134.1, 129.8, 129.6, 127.2, 115.0 (d, *J* = 21.1 Hz), 113.7 (d, *J*

= 20.0 Hz), 83.9, 74.0, 69.2, 42.1, 34.7, 27.3, 25.6, 25.1, 25.0, 21.6, 18.1.

^{19}F NMR (282 MHz, CDCl$_3$): δ –111.8.

FTIR (NaCl, thin film): 3261, 2930, 1601, 1380, 1346, 1323, 1160, 1104, 857 cm^{-1}.

HRMS (TOF-ESI) *m/z*: [M + H]$^+$ Calcd for C$_{28}$H$_{38}$NO$_5$SFB 530.2548; Found 530.2569.

R_f = 0.30 (silica, 20% EtOAc/hexanes, UV/anisaldehyde).

b) Reaction on 0.015 mmol Scale
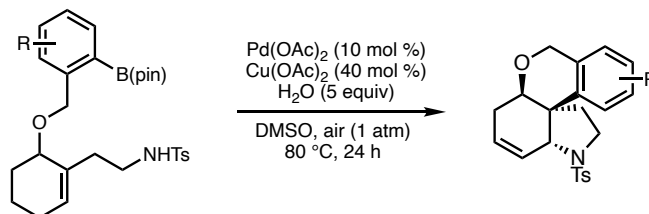
Three oven-dried 1-dram vials were pumped into a nitrogen-filled glovebox. A stock
solution of $Cu(OAc)_2$ (1.09 mg, 0.0060 mmol, 0.40 equiv) in DMSO (0.15 mL) was
prepared in one vial, which was then sealed with a 19/38 septum and electrical tape. A
stock solution of $Pd(OAc)_2$ (0.337 mg, 0.0015 mmol, 0.10 equiv) and substrate (0.015
mmol, 1.0 equiv) in DMSO (0.15 mL) was prepared in another vial, which was sealed the
same way. The final vial was charged with a stir bar, sealed the same way, and then all
three vials were removed from the glovebox. The Cu/DMSO solution was charged with
water (1.35 μL, 0.075 mmol, 5.0 equiv), sonicated until all solids had dissolved, and then
added to the reaction vial. The Pd/substrate/DMSO solution was then added to the reaction
vial. A balloon of compressed air was added, and then the reaction was stirred at 80 °C and
300 rpm using an aluminum heating block for 24 h. The reaction was cooled to ambient
temperature then diluted with EtOAc (2 mL) and 1:1:1 brine/water/1 M HCl (2 mL). The
aqueous layer was extracted with EtOAc (2 x 2 mL), and then the combined organic layers
were washed with water (2 x 2 mL), dried over Na_2SO_4, and concentrated.

c) Reaction on 0.050 mmol Scale: General Procedure 6

Three oven-dried 2-dram vials were pumped into a nitrogen-filled glovebox. A stock

solution of Cu(OAc)₂ (3.63 mg, 0.020 mmol, 0.40 equiv) in DMSO (0.50 mL) was

prepared in one vial, which was then sealed with a 19/38 septum and electrical tape. A

stock solution of Pd(OAc)₂ (1.12 mg, 0.0050 mmol, 0.10 equiv) and substrate (0.050 mmol,

1.0 equiv) in DMSO (0.50 mL) was prepared in another vial, which was sealed the same

way. The final vial was charged with a stir bar, sealed the same way, and then all three

vials were removed from the glovebox. The Cu/DMSO solution was charged with water

(4.50 µL, 0.25 mmol, 5.0 equiv), sonicated until all solids had dissolved, and then added

to the reaction vial. The Pd/substrate/DMSO solution was then added to the reaction vial.

A balloon of compressed air was added, and then the reaction was stirred at 80 °C and 700

rpm using an aluminum heating block for 24 h. The reaction was cooled to ambient

temperature then diluted with EtOAc (3 mL) and 1:1:1 brine/water/1 M HCl (3 mL). The

aqueous layer was extracted with EtOAc (2 x 2 mL), and then the combined organic layers

were washed with water (2 x 2 mL), dried over Na₂SO₄, and concentrated.

d) Characterization of Reaction Products

Compound 165
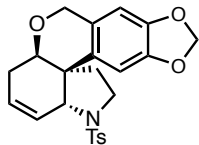
Prepared from **166** (27.8 mg, 0.050 mmol) according to General

Procedure 6. The residue was purified via column chromatography (20%

EtOAc/hexanes) to give **165** as an amorphous white solid (15.0 mg, 59% yield). The

sample contained residual protodeborylation (**172**, 16% by weight, determined by ¹H NMR)

and the yield was adjusted accordingly. An aliquot of the sample was further purified by

preparative TLC (30% EtOAc/hexanes) to afford analytically pure **165** (5.4 mg, 25% yield).

Another sample was recrystallized from Et$_2$O/DCM to obtain crystals suitable for x-ray
diffraction.

^{1}H NMR (400 MHz, CDCl$_3$): δ 7.69 (d, J = 9.0 Hz, 2H), 7.28 (d, J = 2.0 Hz, 2H), 6.37 (s,
1H), 6.19 (s, 1H), 5.87 (dd, J = 5.1, 1.4 Hz, 2H), 5.86 – 5.79 (m, 1H), 5.77 – 5.66 (m, 1H),
4.85 – 4.67 (m, 2H), 4.30 (s, 1H), 3.88 – 3.76 (m, 1H), 3.70 – 3.59 (m, 1H), 3.59 – 3.45
(m, 1H), 2.53 – 2.44 (m, 1H), 2.42 (s, 3H), 2.40 – 2.28 (m, 1H), 2.24 – 2.08 (m, 1H), 1.94
– 1.81 (m, 1H).

^{13}C NMR (101 MHz, CDCl$_3$): δ 146.7, 146.4, 143.4, 136.8, 133.6, 129.7, 127.3, 126.6,
126.6, 124.9, 106.2, 103.8, 101.0, 73.4, 67.5, 64.0, 46.3, 45.7, 33.7, 27.6, 21.7.

FTIR (NaCl, thin film): 2924, 1483, 1334, 1238, 1162, 1108, 1036, 935, 658 cm^{-1}.

HRMS (FD) *m/z*: [M + •]$^+$ Calcd for C$_{23}$H$_{23}$NO$_5$S 425.1291; Found 425.1300.

R$_f$ = 0.32 (silica, 35% EtOAc/hexanes, UV/anisaldehyde).

mp = 180–184 °C

Low-temperature diffraction data (ϕ-and ω-scans) were collected on a Bruker AXS D8

VENTURE KAPPA diffractometer coupled to a PHOTON II CPAD detector with Cu K_α

radiation ($\lambda = 1.54178$ Å) from an IμS micro-source for the structure of compound **165**.

The structure was solved by direct methods using SHELXS[45] and refined against F^2 on all

data by full-matrix least squares with SHELXL-2017[46] using established refinement

techniques.[47] All non-hydrogen atoms were refined anisotropically. All hydrogen atoms

were included into the model at geometrically calculated positions and refined using a
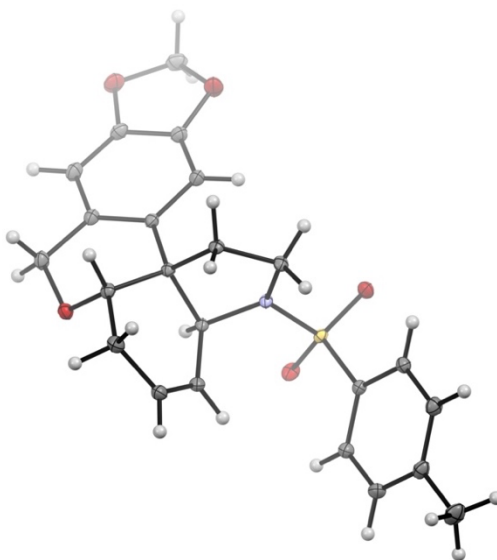
riding model. The isotropic displacement parameters of all hydrogen atoms were fixed to

1.2 times the U value of the atoms they are linked to (1.5 times for methyl groups).

Compound **165** crystallizes in the monoclinic space group P2$_1$/n with one molecule in the

asymmetric unit.

ORTEP drawing of **165** showing thermal ellipsoids at the 50% probability level.

Crystal data and structure refinement for **165**:

Identification code	d20043
Empirical formula	$C_{23}H_{23}NO_5S$
Formula weight	425.48
Temperature/K	100.0
Crystal system	monoclinic
Space group	$P2_1/n$
a/Å	14.402(10)
b/Å	7.842(3)
c/Å	17.774(7)
α/°	90
β/°	105.567(18)
γ/°	90
Volume/Å^3	1933.7(17)
Z	4
ρ_{calc}g/cm^3	1.461
μ/mm^{-1}	0.205
F(000)	896.0
Crystal size/mm^3	0.304 × 0.272 × 0.15
Radiation	MoKα (λ = 0.71073)
2Θ range for data collection/°	4.246 to 70.448
Index ranges	-22 ≤ h ≤ 22, -12 ≤ k ≤ 12, -28 ≤ l ≤ 28

Reflections collected	116660
Independent reflections	8319 [R_{int} = 0.0428, R_{sigma} = 0.0250]
Data/restraints/parameters	8319/0/272
Goodness-of-fit on F^2	1.056
Final R indexes [I>=2σ (I)]	R_1 = 0.0427, wR_2 = 0.1022
Final R indexes [all data]	R_1 = 0.0577, wR_2 = 0.1084
Largest diff. peak/hole / e Å^{-3}	0.57/-0.46

Compound 171
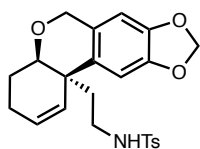
Isolated from optimization table entry 9. The residue was purified via preparative TLC (40% EtOAc/hexanes) to give **171** as an amorphous white solid (1.6 mg, 25% yield).

^{1}H NMR (400 MHz, CDCl$_3$): δ 7.66 (dd, J = 7.6, 1.2 Hz, 2H), 7.31 – 7.26 (m, 2H), 6.62 (s, 1H), 6.32 (s, 1H), 5.90 (dt, J = 11.7, 1.2 Hz, 2H), 5.71 – 5.54 (m, 2H), 5.00 (t, J = 6.2 Hz, 1H), 4.68 (d, J = 15.0 Hz, 1H), 4.46 (d, J = 15.0 Hz, 1H), 3.81 (dd, J = 9.2, 3.4 Hz, 1H), 2.92 – 2.81 (m, 1H), 2.81 – 2.69 (m, 1H), 2.42 (s, 3H), 2.21 – 2.04 (m, 2H), 1.95 – 1.72 (m, 4H).

^{13}C NMR (101 MHz, CDCl$_3$): δ 147.2, 146.0, 143.4, 137.2, 132.9, 131.3, 129.7, 127.2, 126.8, 126.3, 106.5, 104.1, 101.0, 75.0, 64.3, 42.5, 40.1, 39.7, 23.9, 23.4, 21.7.

FTIR (NaCl, thin film): 3272, 2911, 1483, 1324, 1234, 1159, 1038 cm^{-1}.

HRMS (FD) *m/z*: [M + •]$^+$ Calcd for C$_{23}$H$_{25}$NO$_5$S 427.1448; Found 427.1458.

R$_f$ = 0.47 (silica, 40% EtOAc/hexanes, UV/anisaldehyde).

Compound 172
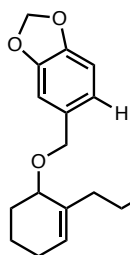
Isolated from optimization table entries 3 and 4. The residue was purified via preparative TLC (40% EtOAc/hexanes) to give **172** as a colorless oil (6.4 mg, 50% yield).

^{1}H NMR (400 MHz, CDCl$_3$): δ 7.71 – 7.60 (m, 2H), 7.26 – 7.24 (m, 2H), 6.79 (s, 1H), 6.76 (s, 2H), 5.96 (s, 2H), 5.50 (t, J = 2.1 Hz, 1H), 5.00 (t, J = 5.6 Hz, 1H), 4.50 (d, J = 11.4 Hz, 1H), 4.25 (d, J = 11.4 Hz, 1H), 3.68 – 3.57 (m, 1H), 3.09 – 2.98 (m, 1H), 2.86 (ddt, J = 11.9, 8.6, 5.3 Hz, 1H), 2.41 (s, 3H), 2.35 – 2.22 (m, 1H), 2.03 – 1.85 (m, 4H), 1.71 – 1.59 (m, 1H), 1.56 – 1.45 (m, 2H).

^{13}C NMR (101 MHz, CDCl$_3$): δ 147.9, 147.4, 143.1, 137.2, 134.0, 132.1, 130.0, 129.6, 127.2, 121.9, 109.0, 108.3, 101.2, 73.2, 70.6, 42.4, 34.6, 26.9, 25.6, 21.6, 17.8.

FTIR (NaCl, thin film): 3279, 2930, 1491, 1442, 1325, 1250, 1160, 1094, 1038, 810 cm^{-1}.

HRMS (FD) m/z: [M + •]$^+$ Calcd for C$_{23}$H$_{27}$NO$_5$S 429.1605; Found 429.1616.

R_f = 0.64 (silica, 40% EtOAc/hexanes, UV/anisaldehyde).

Compound 173
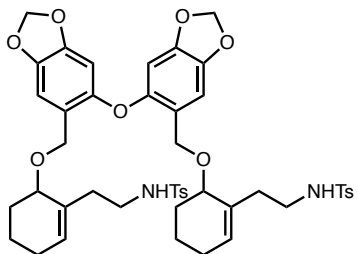
Isolated from optimization table entries 3 and 4. The residue was purified via column chromatography (20:20:60 to 30:30:40 Et$_2$O/DCM/hexanes) to give **173** as a colorless oil (6.3 mg, 24% yield).

^{1}H NMR (400 MHz, CDCl$_3$): δ 7.65 (dd, J = 8.3, 1.8 Hz, 4H), 7.24 (d, J = 8.0 Hz, 4H),

6.89 (s, 2H), 6.30 (s, 2H), 5.97 – 5.92 (m, 4H), 5.47 (t, J = 3.8 Hz, 2H), 5.09 (q, J = 5.1 Hz,

2H), 4.53 (dd, J = 11.4, 6.2 Hz, 2H), 4.41 (dd, J = 11.4, 5.7 Hz, 2H), 3.71 – 3.61 (m, 2H),

3.04 (dqd, J = 12.1, 6.0, 2.0 Hz, 2H), 2.96 – 2.81 (m, 2H), 2.40 (s, 6H), 2.26 (dt, J = 12.4,

6.2 Hz, 2H), 2.00 (ddd, J = 14.5, 8.5, 6.5 Hz, 2H), 1.93 – 1.78 (m, 6H), 1.56 – 1.40 (m,

6H).

^{13}C NMR (101 MHz, CDCl$_3$): δ 149.7, 148.1, 143.8, 143.7, 143.1, 137.3, 137.3, 134.2,

129.6, 129.6, 129.6, 127.2, 121.5, 109.5, 109.5, 101.7, 100.3, 74.1, 74.1, 65.2, 42.4, 42.4,

34.4, 27.0, 25.6, 21.6, 17.9, 17.9.

FTIR (NaCl, thin film): 3277, 2924, 1479, 1426, 1323, 1158, 1091, 1037 cm^{-1}.

HRMS (FD) *m/z*: [M + •]$^+$ Calcd for C$_{46}$H$_{52}$N$_2$O$_{11}$S$_2$ 872.3007; Found 872.3000.

R_f = 0.48 (silica, 50% EtOAc/hexanes, UV/anisaldehyde).

Compound 175a
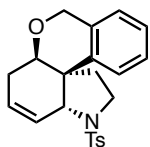
Prepared from **174a** (25.6 mg, 0.050 mmol) according to General Procedure

6. The residue was purified via column chromatography (20%

EtOAc/hexanes) to give **175a** as an amorphous, off-white solid (11.7 mg, 61% yield).

^{1}H NMR (400 MHz, CDCl$_3$): δ 7.73 – 7.64 (m, 2H), 7.26 – 7.22 (m, 3H), 7.13 (td, J = 7.4,

1.2 Hz, 1H), 6.95 – 6.91 (m, 1H), 6.76 (d, J = 8.2 Hz, 1H), 5.83 (dtd, J = 10.2, 2.7, 1.5 Hz,

1H), 5.78 – 5.69 (m, 1H), 4.94 – 4.81 (m, 2H), 4.39 – 4.33 (m, 1H), 3.89 (t, J = 4.0 Hz,

1H), 3.69 (ddd, J = 10.2, 9.5, 5.5 Hz, 1H), 3.57 (td, J = 9.9, 5.9 Hz, 1H), 2.57 – 2.47 (m,

1H), 2.43 (s, 3H), 2.39 – 2.31 (m, 1H), 2.19 (ddd, J = 13.3, 9.6, 5.5 Hz, 1H), 1.97 (ddd, J

= 13.4, 9.5, 6.0 Hz, 1H).

^{13}C NMR (101 MHz, CDCl$_3$): δ 143.3, 140.3, 137.0, 133.2, 129.7, 127.4, 127.0, 126.6,

126.6, 125.8, 124.8, 124.0, 73.4, 67.5, 63.9, 46.2, 45.8, 33.5, 27.7, 21.7.

FTIR (NaCl, thin film): 2924, 1337, 1156, 1098, 1040, 760, 673, 661 cm^{-1}.

HRMS (TOF-ESI) *m/z*: [M + H]$^+$ Calcd for C$_{22}$H$_{24}$NO$_3$S 382.1477; Found 382.1491.

R$_f$ = 0.44 (silica, 35% EtOAc/hexanes, UV/anisaldehyde).

Compound 175b
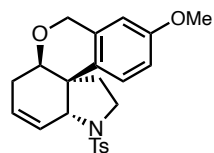
Prepared from **174b** (27.1 mg, 0.050 mmol) according to General

Procedure 6. The residue was purified via column chromatography (20

to 25% EtOAc/hexanes) to give **175b** as a white solid (10.6 mg, 49% yield).

^{1}H NMR (500 MHz, CDCl$_3$): δ 7.67 (d, J = 8.1 Hz, 2H), 7.24 (d, J = 9.4 Hz, 2H), 6.68 (d,

J = 8.6 Hz, 1H), 6.53 – 6.41 (m, 2H), 5.81 (d, J = 10.8 Hz, 1H), 5.76 – 5.68 (m, 1H), 4.90

– 4.76 (m, 2H), 4.32 (s, 1H), 3.86 (t, J = 3.9 Hz, 1H), 3.76 (s, 3H), 3.72 – 3.64 (m, 1H),

3.56 (td, J = 10.0, 5.7 Hz, 1H), 2.57 – 2.48 (m, 1H), 2.44 (s, 3H), 2.40 – 2.30 (m, 1H), 2.24

– 2.13 (m, 1H), 1.98 – 1.88 (m, 1H).

^{13}C NMR (101 MHz, CDCl$_3$): δ 158.0, 143.1, 137.0, 134.4, 132.5, 129.5, 127.2, 126.9,

126.6, 124.6, 113.0, 108.3, 73.5, 67.5, 63.9, 55.2, 45.6, 45.6, 33.3, 27.5, 21.5.

FTIR (NaCl, thin film): 2923, 1500, 1338, 1164, 1094, 1038, 682, 663 cm^{-1}.

HRMS (TOF-ESI) *m/z*: [M + H]$^+$ Calcd for C$_{23}$H$_{26}$NO$_4$S 412.1583; Found 412.1580.

R$_f$ = 0.34 (silica, 35% EtOAc/hexanes, UV/anisaldehyde).

Compound 175c
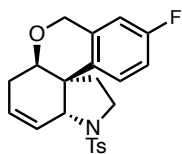
Prepared from **174c** (26.5 mg, 0.050 mmol) according to General Procedure 6. The residue was purified via column chromatography (25% EtOAc/hexanes) to give **175c** as an amorphous white solid (13.5 mg, 66% yield).

^{1}H NMR (400 MHz, CDCl$_3$): δ 7.65 (d, J = 8.6 Hz, 2H), 7.25 (d, J = 8.0 Hz, 2H), 6.71 (dd, J = 8.7, 5.4 Hz, 1H), 6.63 (dd, J = 8.9, 2.7 Hz, 1H), 6.56 (td, J = 8.6, 2.8 Hz, 1H), 5.79 (dtd, J = 10.2, 2.6, 1.3 Hz, 1H), 5.76 – 5.69 (m, 1H), 4.91 – 4.76 (m, 2H), 4.29 (s, 1H), 3.85 (t, J = 3.8 Hz, 1H), 3.77 – 3.64 (m, 1H), 3.57 (td, J = 10.0, 5.5 Hz, 1H), 2.57 – 2.47 (m, 1H), 2.44 (s, 3H), 2.41 – 2.30 (m, 1H), 2.18 (ddd, J = 13.4, 9.8, 5.8 Hz, 1H), 1.96 (ddd, J = 13.4, 9.4, 5.5 Hz, 1H).

^{13}C NMR (101 MHz, CDCl$_3$): δ 160.0 (d, J = 244.8 Hz), 143.3, 137.0, 136.2, 135.2 (d, J = 6.9 Hz), 129.5, 127.5 (d, J = 8.0 Hz), 127.1, 126.4, 124.5, 113.7 (d, J = 21.3 Hz), 110.3 (d, J = 21.6 Hz), 73.5, 67.4, 63.8, 45.8, 45.5, 33.0, 27.6, 21.5.

^{19}F NMR (282 MHz, CDCl$_3$): δ –119.0.

FTIR (NaCl, thin film): 2925, 1496, 1338, 1249, 1160, 1099, 810, 682, 668 cm^{-1}.

HRMS (TOF-ESI) *m/z*: [M + H]$^+$ Calcd for C$_{22}$H$_{23}$NO$_3$SF 400.1383; Found 400.1380.

R_f = 0.40 (silica, 35% EtOAc/hexanes, UV/anisaldehyde).

2.5   REFERENCES

(1)   Nair, J. J.; Bastida, J.; Viladomat, F.; van Staden, J. Cytotoxic Agents of the Crinane

Series of Amaryllidaceae Alkaloids. *Natural Product Communications* **2012**, *7* (12),

1934578X1200701234.

(2)   He, M.; Qu, C.; Gao, O.; Hu, X.; Hong, X. Biological and Pharmacological

Activities of Amaryllidaceae Alkaloids. *RSC Adv.* **2015**, *5* (21), 16562–16574.

(3)   Ding, Y.; Qu, D.; Zhang, K.-M.; Cang, X.-X.; Kou, Z.-N.; Xiao, W.; Zhu, J.-B.

Phytochemical and Biological Investigations of Amaryllidaceae Alkaloids: A

Review. *Journal of Asian Natural Products Research* **2017**, *19* (1), 53–100.

(4)   Machocho, A. K.; Bastida, J.; Codina, C.; Viladomat, F.; Brun, R.; Chhabra, S. C.

Augustamine Type Alkaloids from Crinum Kirkii. *Phytochemistry* **2004**, *65* (23),

3143–3149.

(5)   Pearson, W. H.; Lovering, F. E. Short, Efficient Syntheses of the Amaryllidaceae

Alkaloids (-)-Amabiline and (-)-Augustamine via Intramolecular 2-Azaallyl Anion

Cycloadditions. *J. Am. Chem. Soc.* **1995**, *117* (49), 12336–12337.

(6)   Pearson, W. H.; Lovering, F. E. Assembly of 3a-Arylperhydroindoles by the

Intramolecular Cycloaddition of 2-Azaallyl Anions with Alkenes. Total Syntheses

of (±)-Crinine, (±)-6-Epicrinine, (−)-Amabiline, and (−)-Augustamine. *J. Org.*

Chem. **1998**, *63* (11), 3607–3617.

(7)   Wong, A. R.; Fastuca, N. J.; Mak, V. W.; Kerkovius, J. K.; Stevenson, S. M.;

Reisman, S. E. Total Syntheses of the C19 Diterpenoid Alkaloids (−)-Talatisamine,

(−)-Liljestrandisine, and (−)-Liljestrandinine by a Fragment Coupling Approach. *ACS Cent. Sci.* **2021**, *7* (8), 1311–1316.

(8)   Romero, K. J.; Galliher, M. S.; Pratt, D. A.; Stephenson, C. R. J. Radicals in Natural Product Synthesis. *Chem. Soc. Rev.* **2018**, *47* (21), 7851–7866.

(9)   Hung, K.; Hu, X.; Maimone, T. J. Total Synthesis of Complex Terpenoids Employing Radical Cascade Processes. *Nat. Prod. Rep.* **2018**, *35* (2), 174–202.

(10) Dounay, A. B.; Overman, L. E. The Asymmetric Intramolecular Heck Reaction in Natural Product Total Synthesis. *Chem. Rev.* **2003**, *103* (8), 2945–2964.

(11) Bai, Y.; Davis, D. C.; Dai, M. Natural Product Synthesis via Palladium-Catalyzed Carbonylation. *J. Org. Chem.* **2017**, *82* (5), 2319–2328.

(12) Ohno, H.; Inuki, S. Recent Progress in Palladium-Catalyzed Cascade Cyclizations for Natural Product Synthesis. *Synthesis* **2018**, *50* (04), 700–710.

(13) Holman, K. R.; Stanko, A. M.; Reisman, S. E. Palladium-Catalyzed Cascade Cyclizations Involving C–C and C–X Bond Formation: Strategic Applications in Natural Product Synthesis. *Chem. Soc. Rev.* **2021**.

(14) Nicolaou, K. C.; Chen, J. S. The Art of Total Synthesis through Cascade Reactions. *Chem. Soc. Rev.* **2009**, *38* (11), 2993–3009.

(15) Ardkhean, R.; Caputo, D. F. J.; Morrow, S. M.; Shi, H.; Xiong, Y.; Anderson, E. A. Cascade Polycyclizations in Natural Product Synthesis. *Chem. Soc. Rev.* **2016**, *45* (6), 1557–1569.

(16) Jiang, Y.; McNamee, R. E.; Smith, P. J.; Sozanschi, A.; Tong, Z.; Anderson, E. A.
Advances in Polycyclization Cascades in Natural Product Synthesis. *Chem. Soc.
Rev.* **2021**, *50* (1), 58–71.

(17) Kizil, M.; Murphy, J. A. Stereoselective Preparation of the ABCE Tetracycle of
Aspidospermidine and Related Alkaloids. *J. Chem. Soc., Chem. Commun.* **1995**, No.
14, 1409–1410.

(18) Peppers, B. P.; Kulkarni, A. A.; Diver, S. T. Functional Group Scope in the
Methylene-Free, Tandem Enyne Metathesis. *Org. Lett.* **2006**, *8* (12), 2539–2542.

(19) Willy, W. E.; Binsch, G.; Eliel, E. L. Conformational Analysis. XXIII. 1,3-
Dioxolanes. *J. Am. Chem. Soc.* **1970**, *92* (18), 5394–5402.

(20) Bailey, W. F.; Longstaff, S. C. Cyclization of Methyl-Substituted 6-Heptenyl
Radicals. *Org. Lett.* **2001**, *3* (14), 2217–2219.

(21) Justicia, J.; Oller-López, J. L.; Campaña, A. G.; Oltra, J. E.; Cuerva, J. M.; Buñuel,
E.; Cárdenas, D. J. 7-Endo Radical Cyclizations Catalyzed by Titanocene(III).
Straightforward Synthesis of Terpenoids with Seven-Membered Carbocycles. *J. Am.
Chem. Soc.* **2005**, *127* (42), 14911–14921.

(22) Kamimura, A.; Kotake, T.; Ishihara, Y.; So, M.; Hayashi, T. Kinetic Study of the 7-
Endo Selective Radical Cyclization of N-Tert-Butyl-o-Bromobenzylmethacryl
Amides: Kinetic Investigation of the Cyclization and 1,7-Hydrogen Transfer of
Aromatic Radicals. *J. Org. Chem.* **2013**, *78* (8), 3961–3971.

(23) He, M.; Qu, C.; Ding, B.; Chen, H.; Li, Y.; Qiu, G.; Hu, X.; Hong, X. Total

Synthesis of (±)-8-Oxo-Erythrinine, (±)-8-Oxo-Erythraline, and (±)-Clivonine.

European Journal of Organic Chemistry **2015**, *2015* (15), 3240–3250.

(24) Long, H.; Song, J.; Xu, H.-C. Electrochemical Synthesis of 7-Membered

Carbocycles through Cascade 5-Exo-Trig/7-Endo-Trig Radical Cyclization. *Org.*

Chem. Front. **2018**, *5* (21), 3129–3132.

(25) Beletskaya, I. P.; Cheprakov, A. V. The Heck Reaction as a Sharpening Stone of

Palladium Catalysis. *Chem. Rev.* **2000**, *100* (8), 3009–3066.

(26) Fiser, B.; Cuerva, J. M.; Gómez-Bengoa, E. Baldwin-Type Rules for Metal-

Controlled Intramolecular Migratory Insertions. A Computational Study of Ni, Pd,

and Pt Case. *Organometallics* **2018**, *37* (3), 390–395.

(27) Fix, S. R.; Brice, J. L.; Stahl, S. S. Efficient Intramolecular Oxidative Amination of

Olefins through Direct Dioxygen-Coupled Palladium Catalysis. *Angewandte*

Chemie International Edition **2002**, *41* (1), 164–166.

(28) Karimi, B.; Behzadnia, H.; Elhamifar, D.; Akhavan, P. F.; Esfahani, F. K.; Zamani,

A. Transition-Metal-Catalyzed Oxidative Heck Reactions. *Synthesis* **2010**, *2010*

(09), 1399–1427.

(29) Lee, A.-L. Enantioselective Oxidative Boron Heck Reactions. *Org. Biomol. Chem.*

2016, *14* (24), 5357–5366.

(30) Xie, J.-Q.; Liang, R.-X.; Jia, Y.-X. Recent Advances of Catalytic Enantioselective

Heck Reactions and Reductive-Heck Reactions. *Chinese Journal of Chemistry*

2021, *39* (3), 710–728.

(31) Krafft, M. E.; Cran, J. W. A Convenient Protocol for the α-Iodination of α,β-
Unsaturated Carbonyl Compounds with I2 in an Aqueous Medium. *Synlett* **2005**,
2005 (08), 1263–1266.

(32) Kang, G.; Yamagami, M.; Vellalath, S.; Romo, D. Enantioselective Synthesis of
Medium-Sized Lactams via Chiral α,β-Unsaturated Acylammonium Salts.
Angewandte Chemie International Edition **2018**, *57* (22), 6527–6531.

(33) Anka-Lufford, L. L.; Prinsell, M. R.; Weix, D. J. Selective Cross-Coupling of
Organic Halides with Allylic Acetates. *J. Org. Chem.* **2012**, *77* (22), 9989–10000.

(34) Ackerman, L. K. G.; Lovell, M. M.; Weix, D. J. Multimetallic Catalysed Cross-
Coupling of Aryl Bromides with Aryl Triflates. *Nature* **2015**, *524* (7566), 454–457.

(35) Olivares, A. M.; Weix, D. J. Multimetallic Ni- and Pd-Catalyzed Cross-Electrophile
Coupling To Form Highly Substituted 1,3-Dienes. *J. Am. Chem. Soc.* **2018**, *140* (7),
2446–2449.

(36) Vantourout, J. C.; Miras, H. N.; Isidro-Llobet, A.; Sproules, S.; Watson, A. J. B.
Spectroscopic Studies of the Chan–Lam Amination: A Mechanism-Inspired
Solution to Boronic Ester Reactivity. *J. Am. Chem. Soc.* **2017**, *139* (13), 4769–4779.

(37) Steinhoff, B. A.; Fix, S. R.; Stahl, S. S. Mechanistic Study of Alcohol Oxidation by
the Pd(OAc)2/O2/DMSO Catalyst System and Implications for the Development of
Improved Aerobic Oxidation Catalysts. *J. Am. Chem. Soc.* **2002**, *124* (5), 766–767.

(38) Popp, B. V.; Stahl, S. S. Palladium-Catalyzed Oxidation Reactions: Comparison of
Benzoquinone and Molecular Oxygen as Stoichiometric Oxidants. In

Organometallic Oxidation Catalysis; Meyer, F., Limberg, C., Eds.; *Springer: Berlin, Heidelberg,* **2007**; pp 149–189.

(39) Nishikata, T.; Yamamoto, Y.; Miyaura, N. Conjugate Addition of Aryl Boronic Acids to Enones Catalyzed by Cationic Palladium(II)–Phosphane Complexes. *Angewandte Chemie International Edition* **2003**, *42* (24), 2768–2770.

(40) Amatore, C.; Jutand, A.; Le Duc, G. Kinetic Data for the Transmetalation/Reductive Elimination in Palladium-Catalyzed Suzuki–Miyaura Reactions: Unexpected Triple Role of Hydroxide Ions Used as Base. *Chemistry – A European Journal* **2011**, *17* (8), 2492–2503.

(41) Vachhani, D. D.; Butani, H. H.; Sharma, N.; Bhoya, U. C.; Shah, A. K.; Eycken, E. V. V. der. Domino Heck/Borylation Sequence towards Indolinone-3-Methyl Boronic Esters: Trapping of the σ-Alkylpalladium Intermediate with Boron. *Chem. Commun.* **2015**, *51* (80), 14862–14865.

(42) Stabile, M. R.; Hudlicky, T.; Meisels, M. L. New Chiral Synthon from Bromoethylbenzene: Absolute Stereochemistry of a Biooxidation Metabolite. *Tetrahedron: Asymmetry* **1995**, *6* (2), 537–542.

(43) Crich, D.; Krishnamurthy, V. Radical Dearomatization of Benzene Leading to Phenanthridine and Phenanthridinone Derivatives Related to (±)-Pancratistatin. *Tetrahedron* **2006**, *62* (29), 6830–6840.

(44) Ruiz, J.; Ardeo, A.; Ignacio, R.; Sotomayor, N.; Lete, E. An Efficient Entry to Pyrrolo[1,2-*b*]Isoquinolines and Related Systems through Parham Cyclisation. *Tetrahedron* **2005**, *61* (13), 3311–3324.

(45) Sheldrick, G. M. Phase Annealing in SHELX-90: Direct Methods for Larger

Structures. *Acta Cryst A* **1990**, *46* (6), 467–473.

(46) Sheldrick, G. M. Crystal Structure Refinement with SHELXL. *Acta Cryst C* **2015**,

71 (1), 3–8.

(47) Müller, P. Practical Suggestions for Better Crystal Structures. *Crystallography

Reviews* **2009**, *15* (1), 57–83.

APPENDIX 1

Spectra Relevant to Chapter 2: Synthesis of Noraugustamine and

Development of an Oxidative Heck/Aza-Wacker Cyclization

*Please note, spectra are listed below in the order in which they appear in Section 2.4: Experimental Section
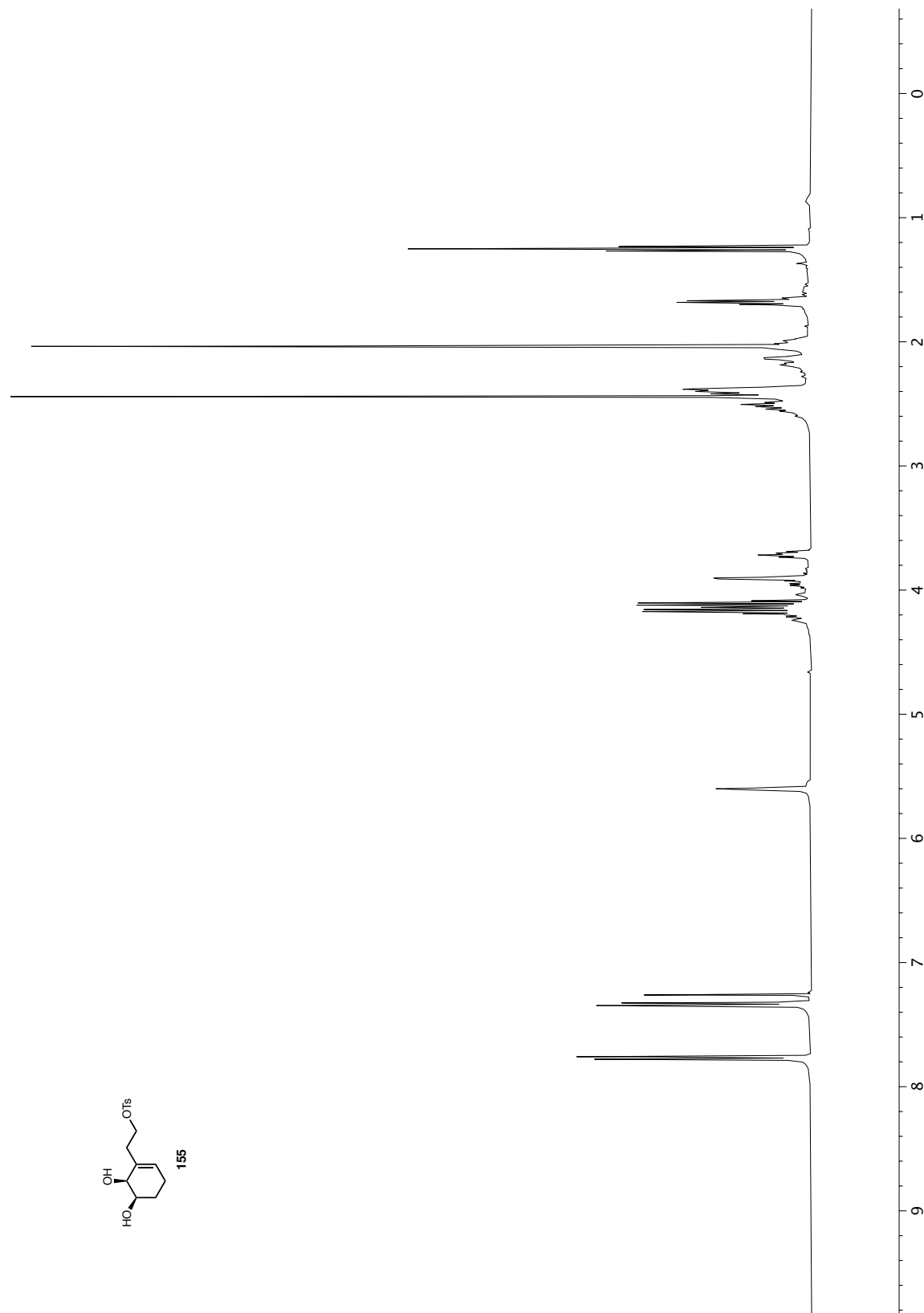
Figure A1.1 ^{1}H NMR (400 MHz, CDCl$_3$) of compound **155.**
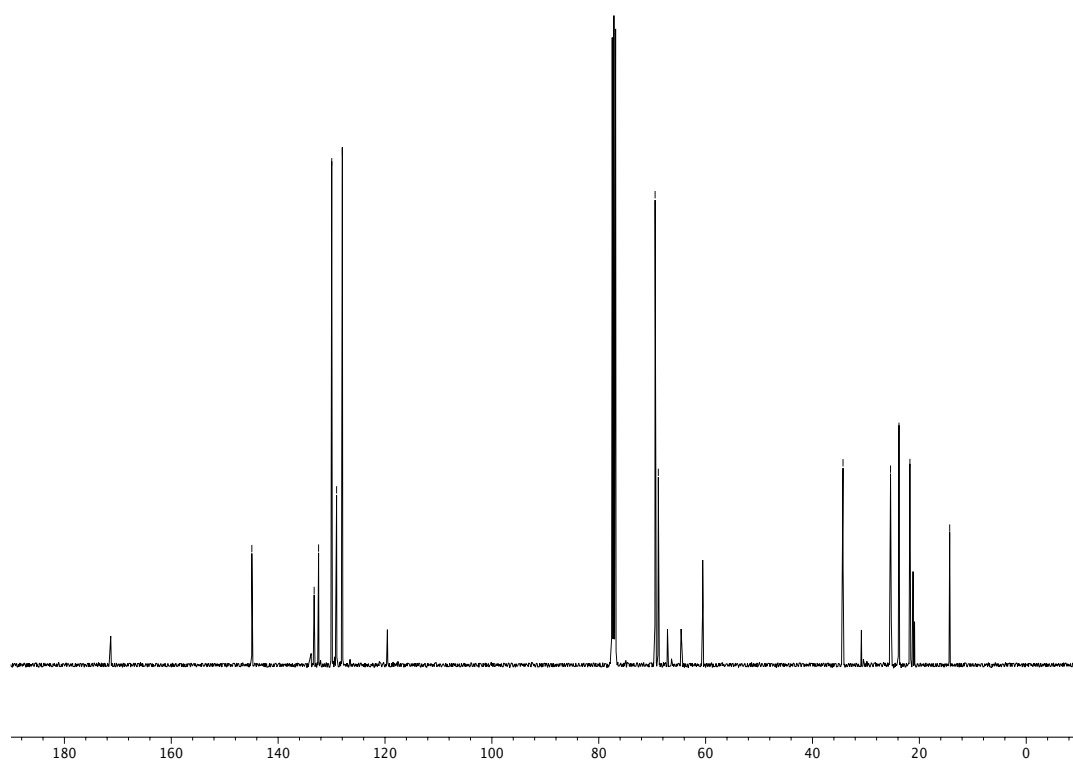
Figure A1.2 ^{13}C NMR (101 MHz, CDCl$_3$) of Compound **155**.
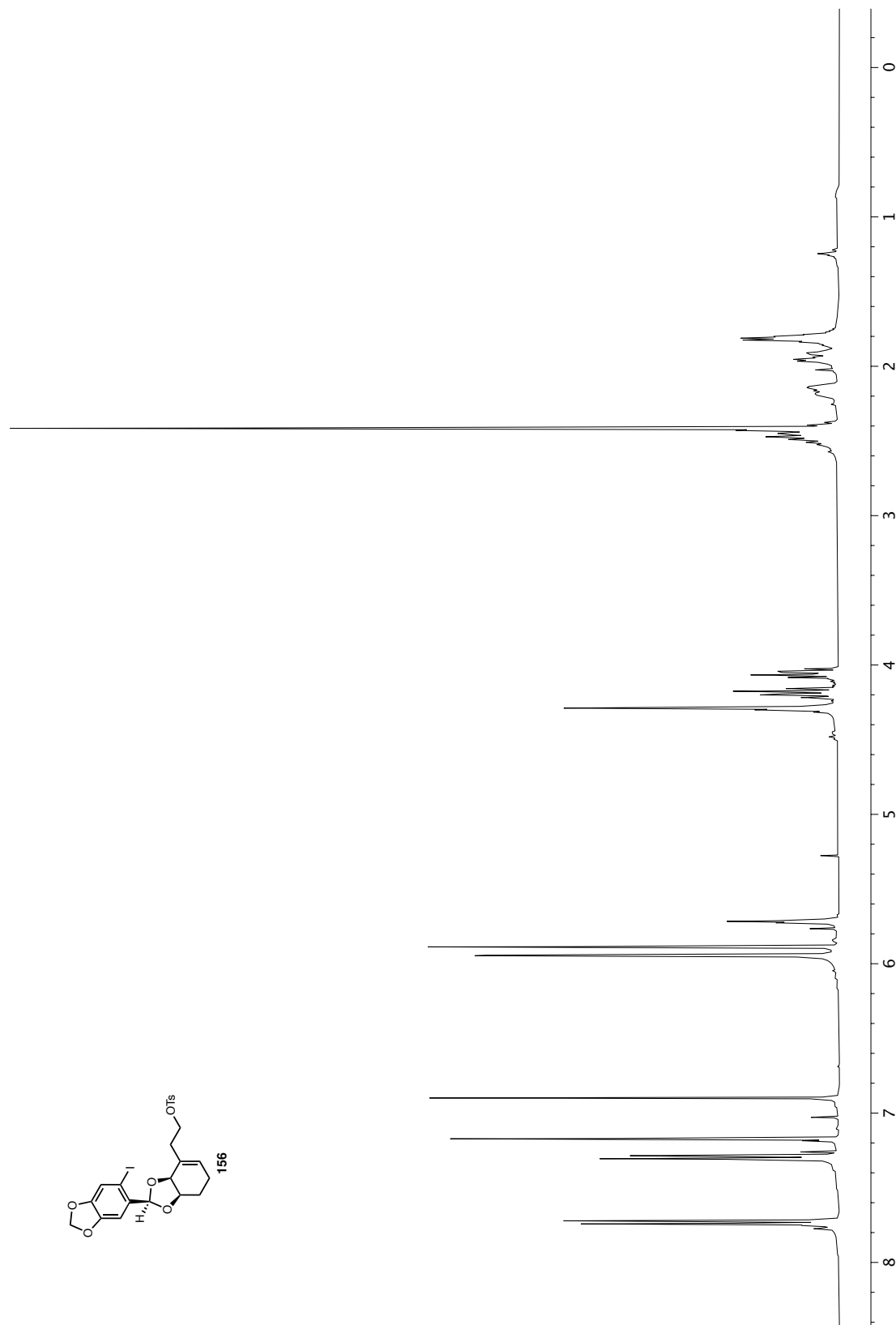
Figure A1.3 ^{1}H NMR (400 MHz, CDCl$_3$) of compound **156.**
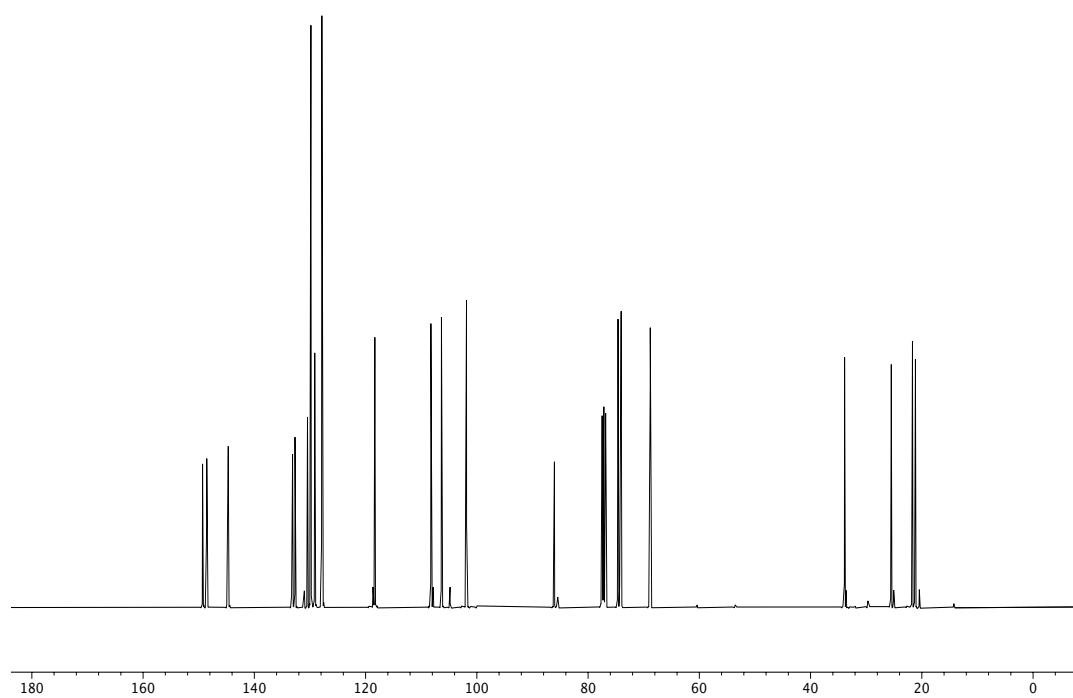
Figure A1.4 ^{13}C NMR (101 MHz, CDCl$_3$) of Compound **156**.
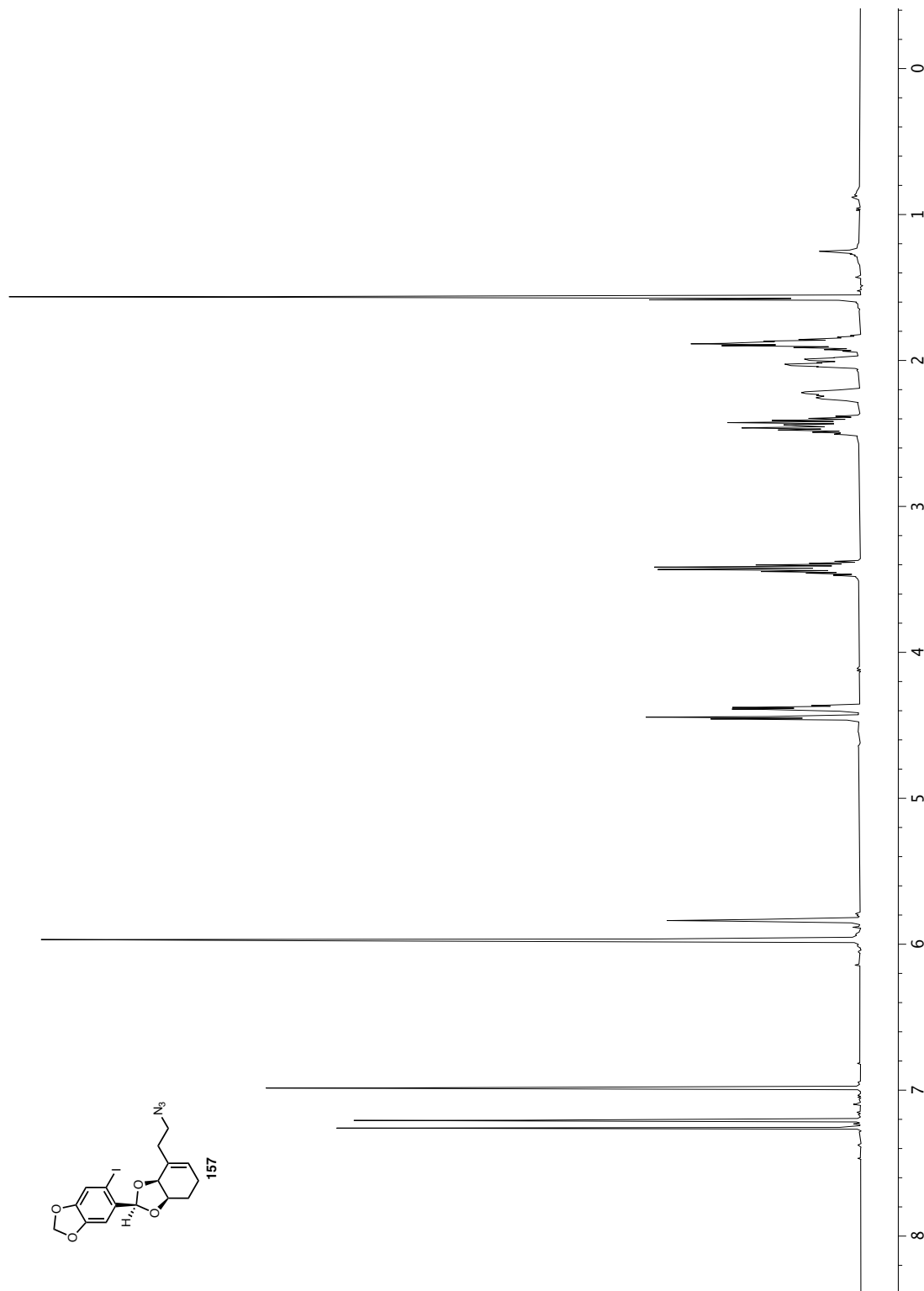
Figure A1.5 ^{1}H NMR (400 MHz, CDCl$_3$) of compound **157**.
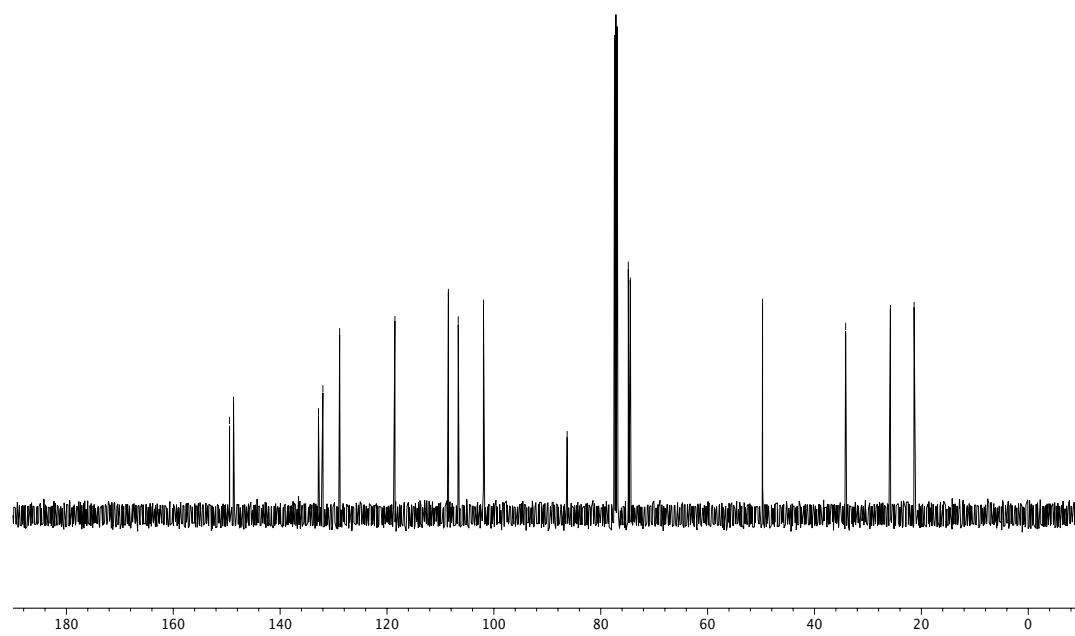
Figure A1.6 ¹³C NMR (101 MHz, CDCl₃) of Compound **157**.

Figure A1.7 ^{1}H NMR (400 MHz, CDCl$_3$) of compound **S1.**
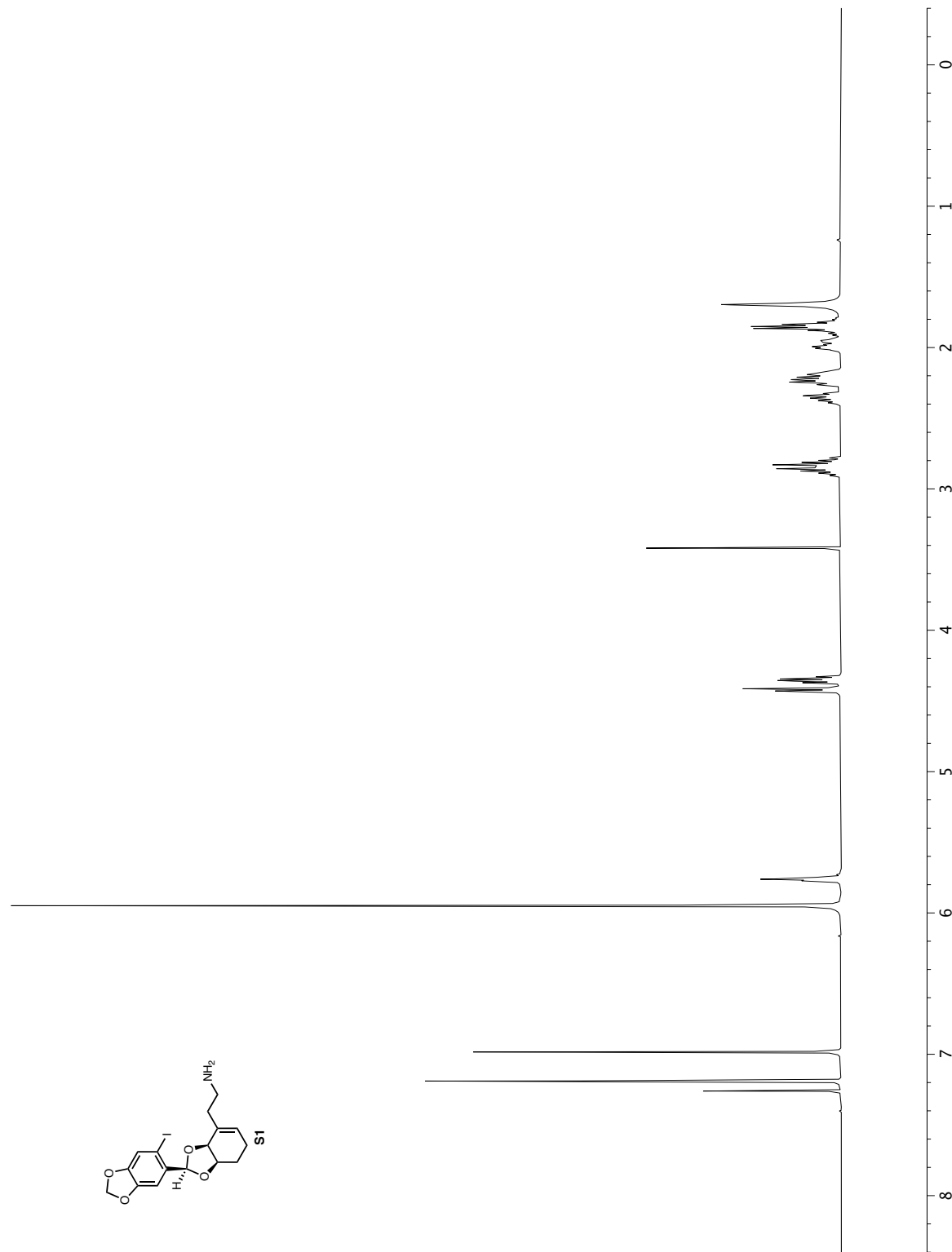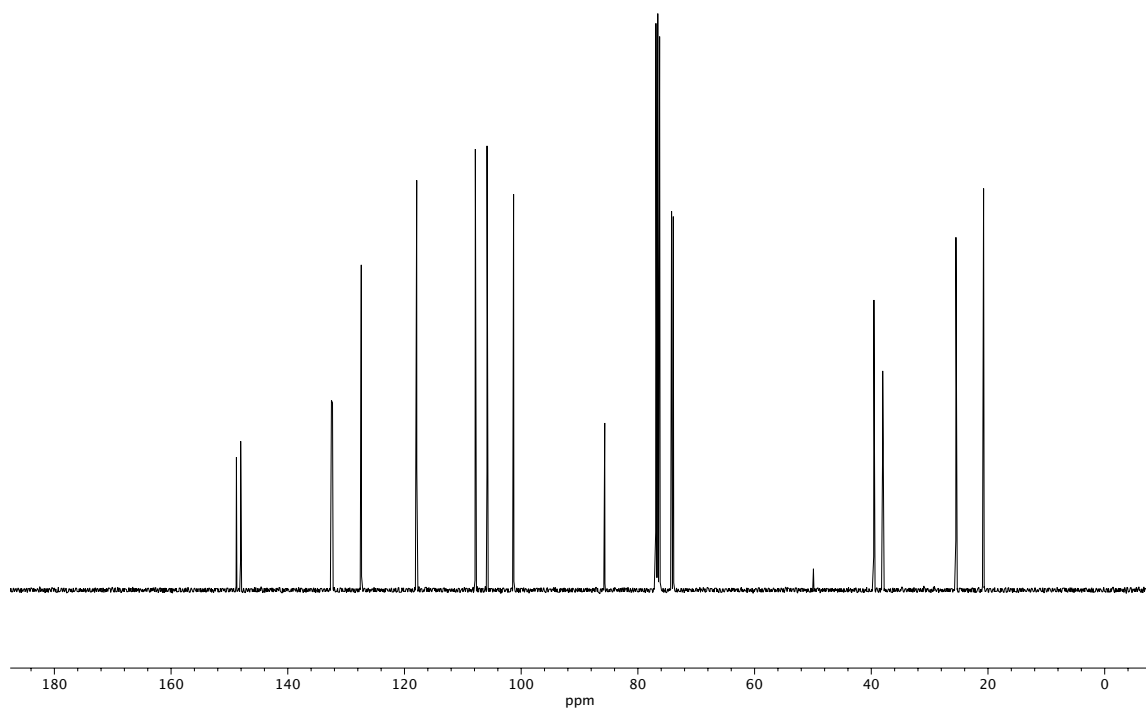
Figure A1.8 ^{13}C NMR (101 MHz, CDCl$_3$) of Compound **S1**.

Figure A1.9 ^{1}H NMR (400 MHz, CDCl$_3$) of compound **S2.**
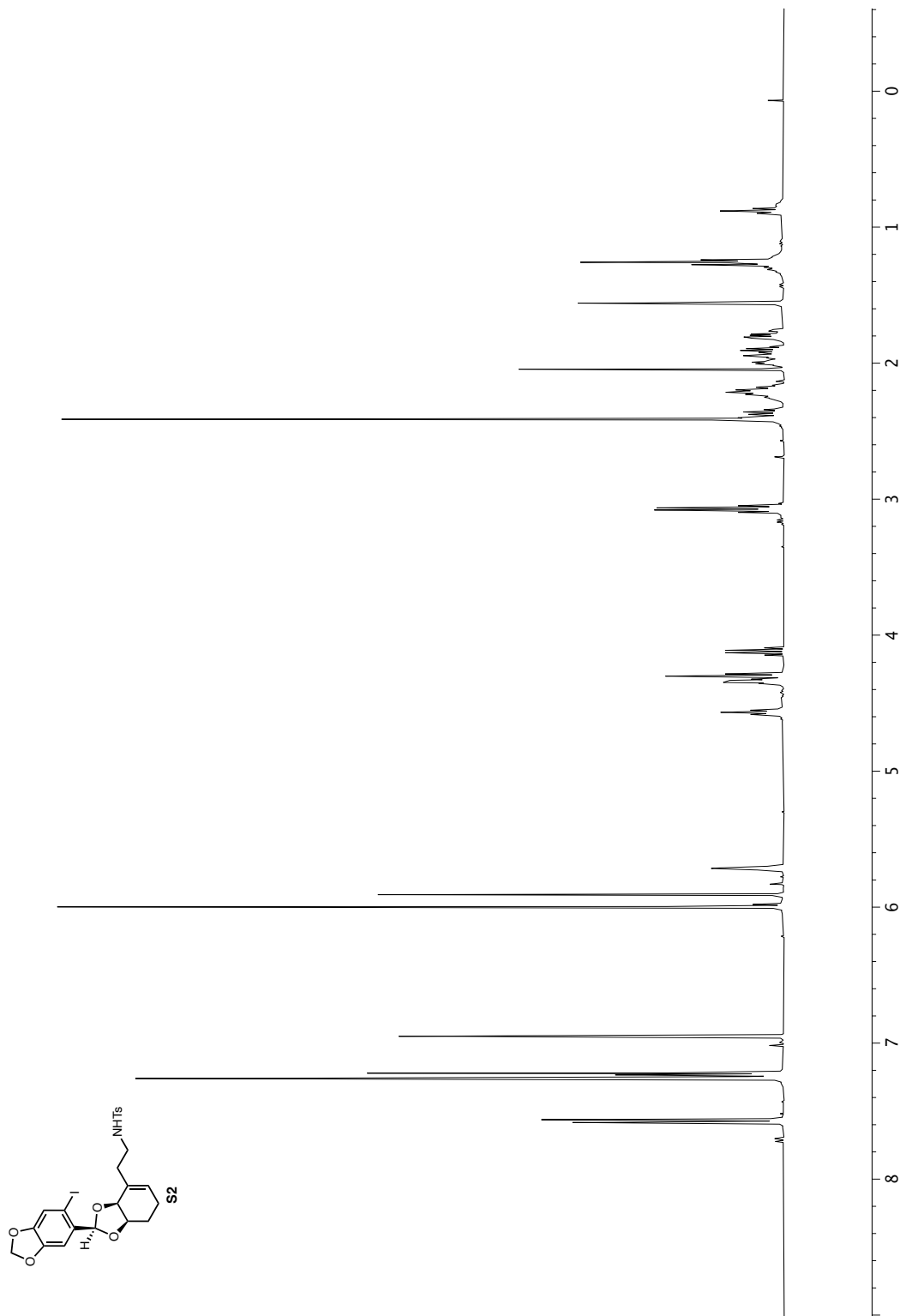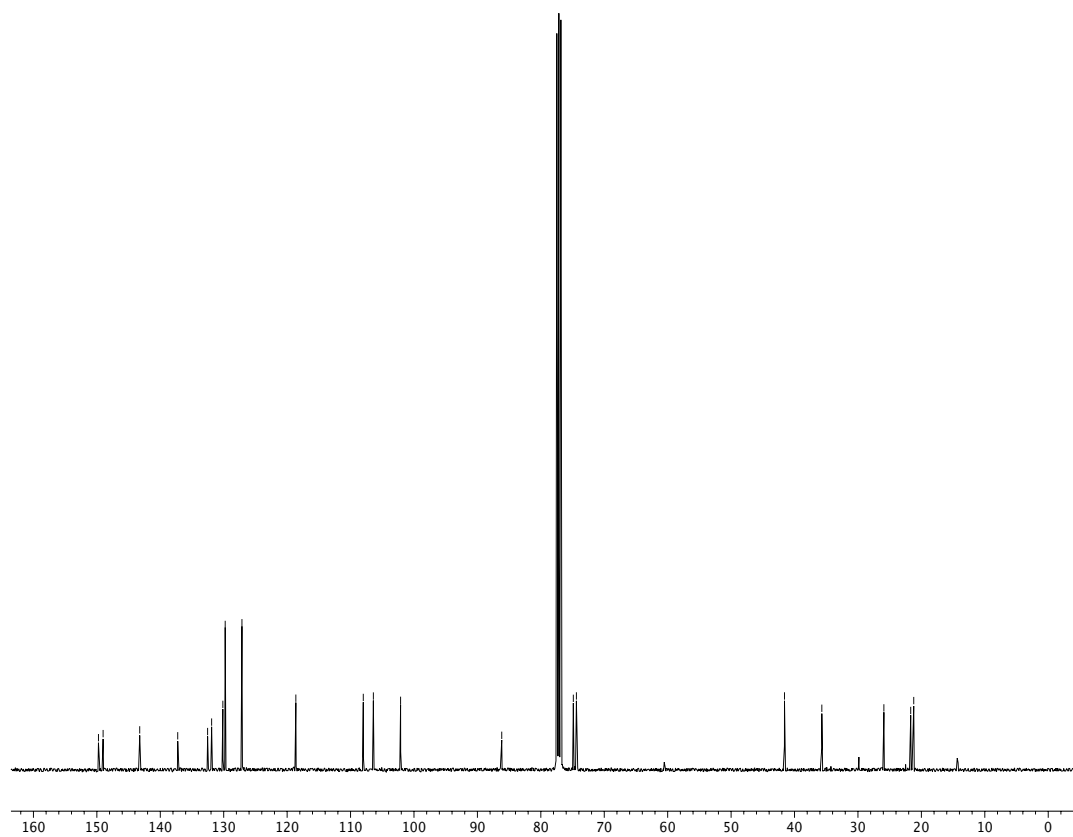
Figure A1.10 ^{13}C NMR (101 MHz, CDCl$_3$) of Compound **S2**.
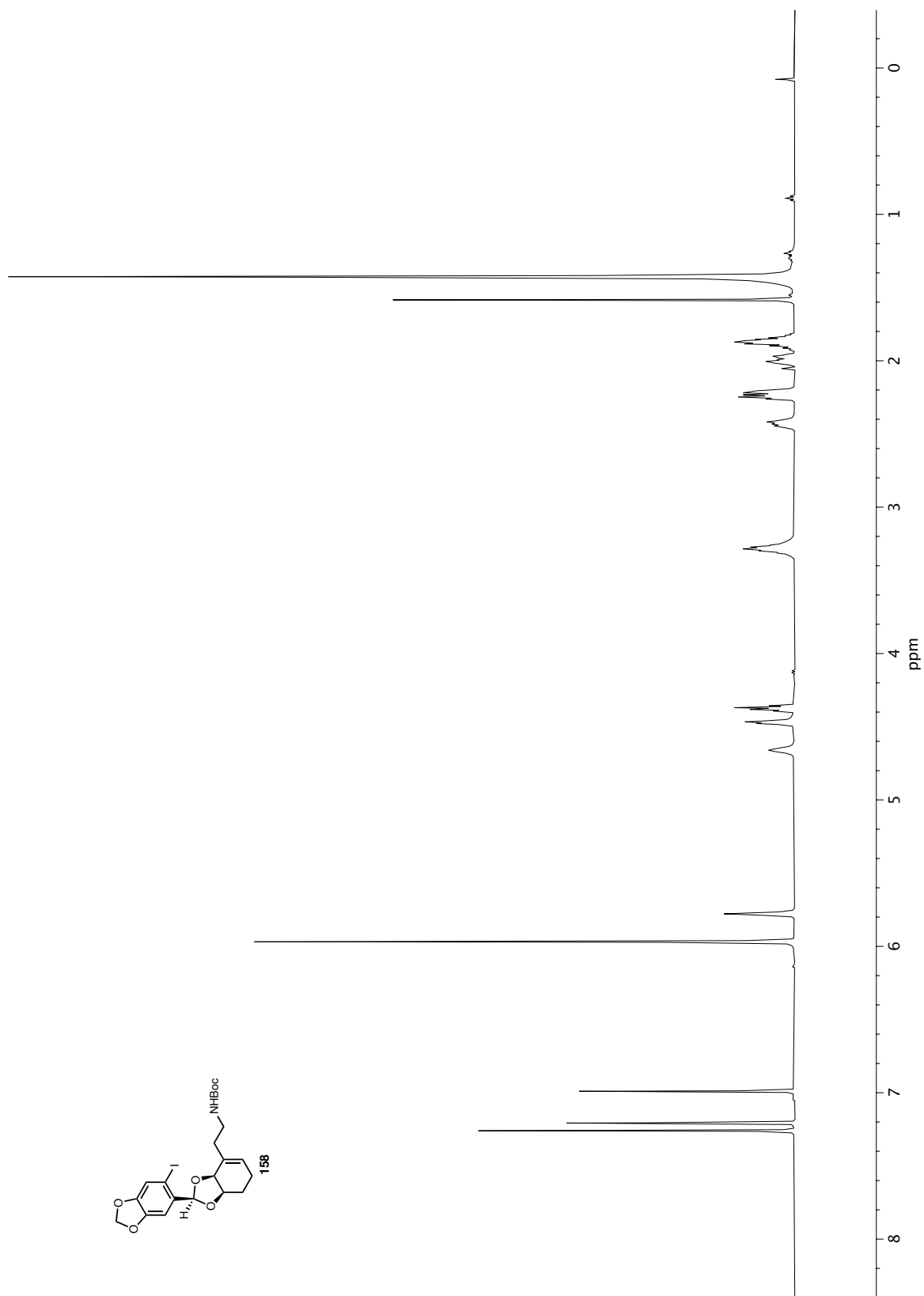
Figure A1.11 ^{1}H NMR (500 MHz, CDCl$_3$) of compound **158**.
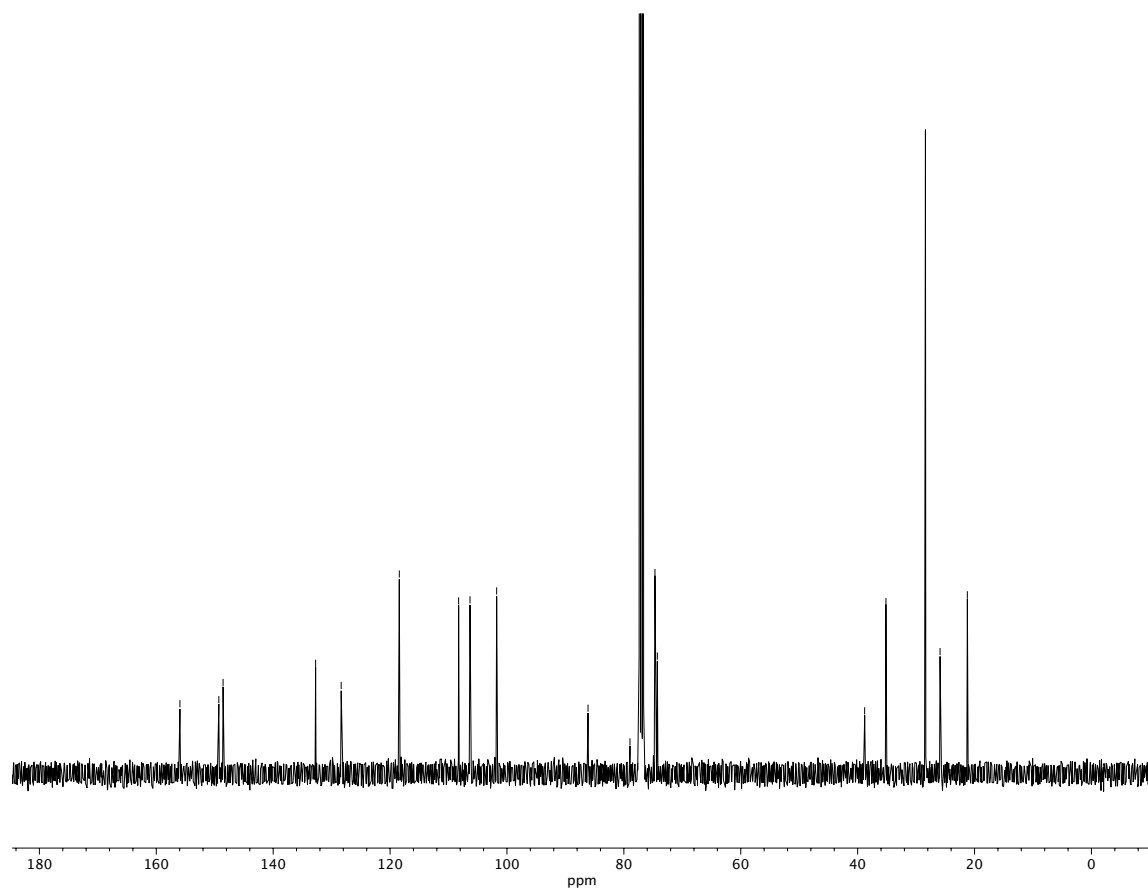
Figure A1.12 ¹³C NMR (101 MHz, CDCl₃) of Compound **158**.
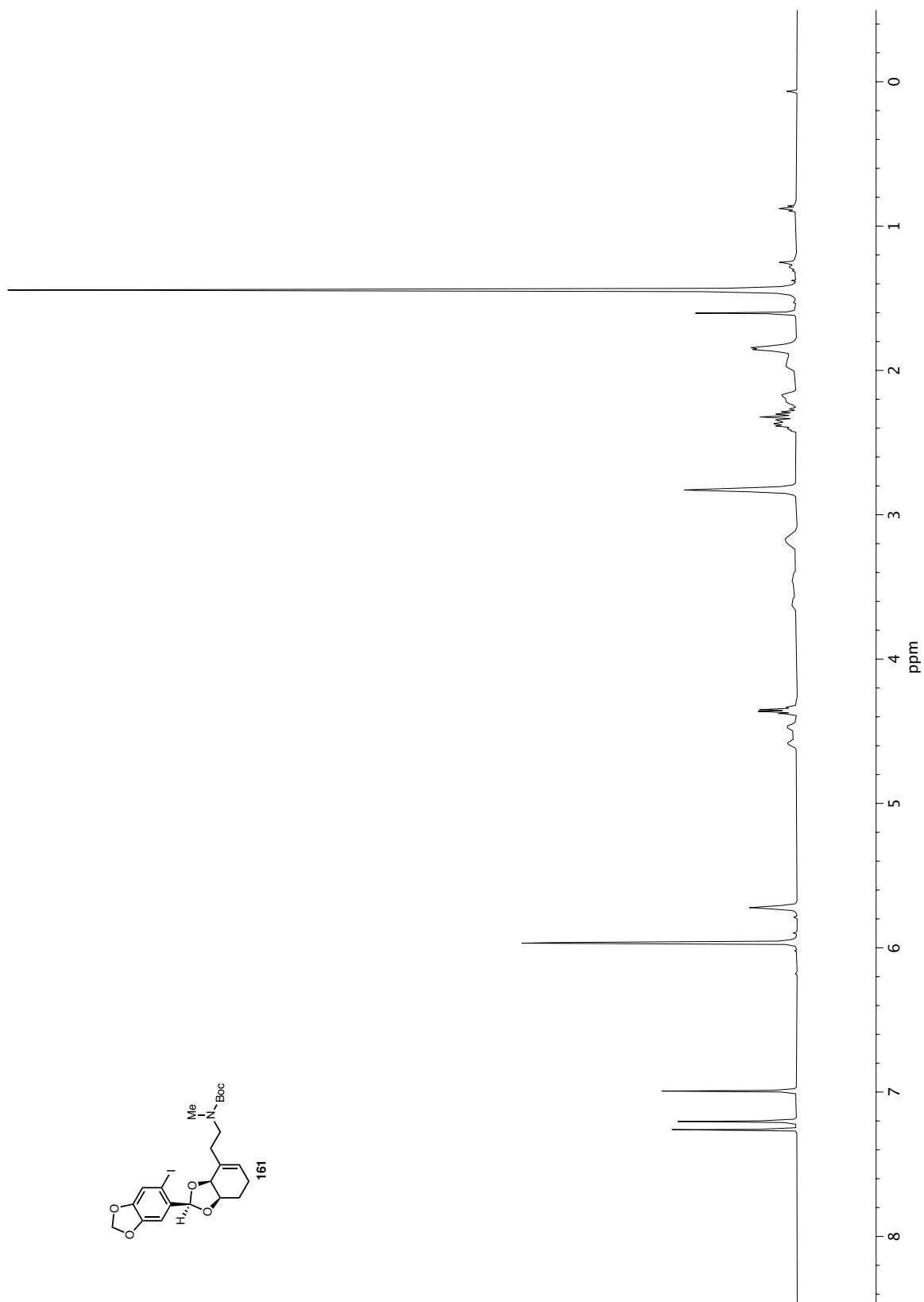
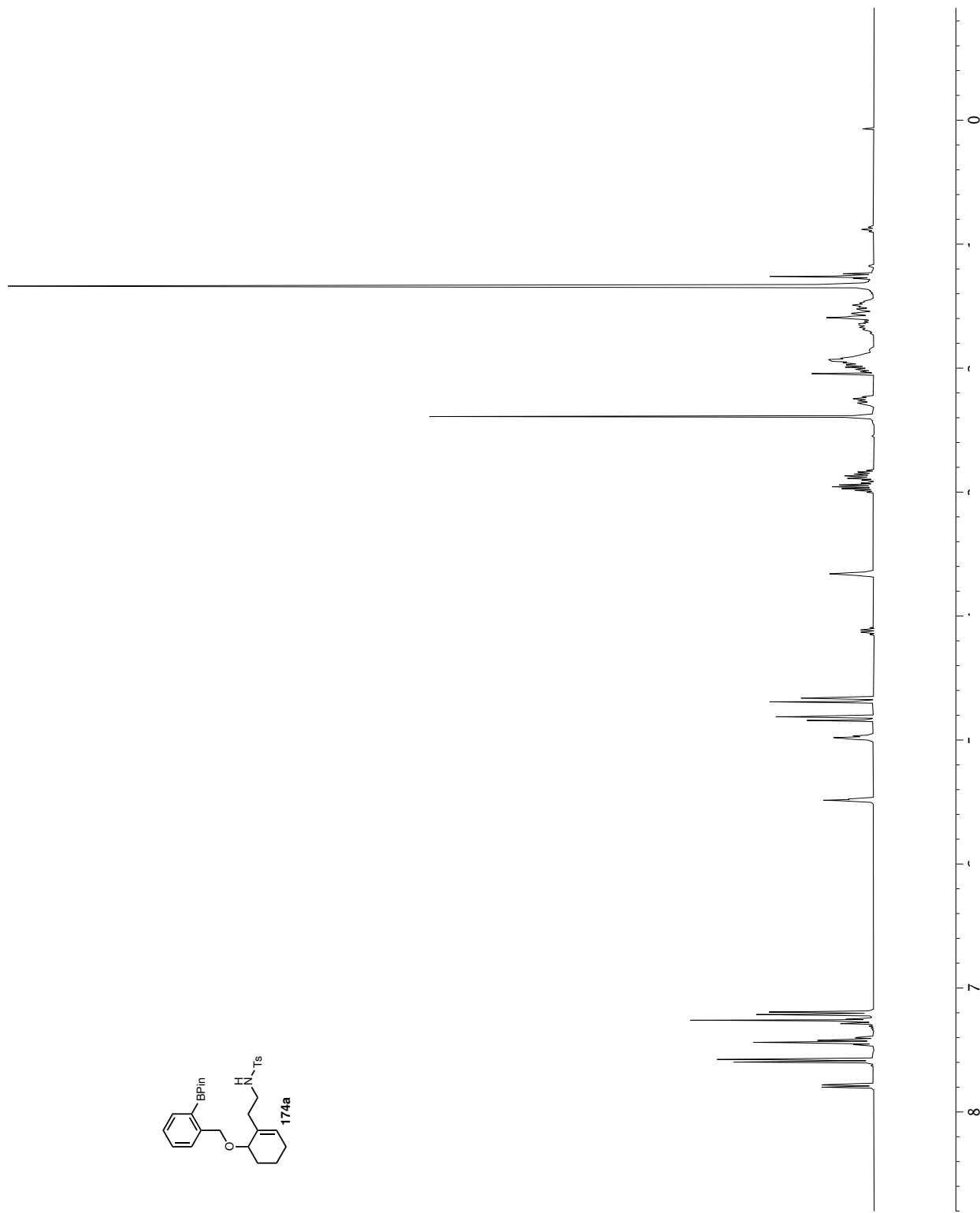***Figure A1.13*** ^{1}H NMR (400 MHz, CDCl$_3$) of compound **161.**
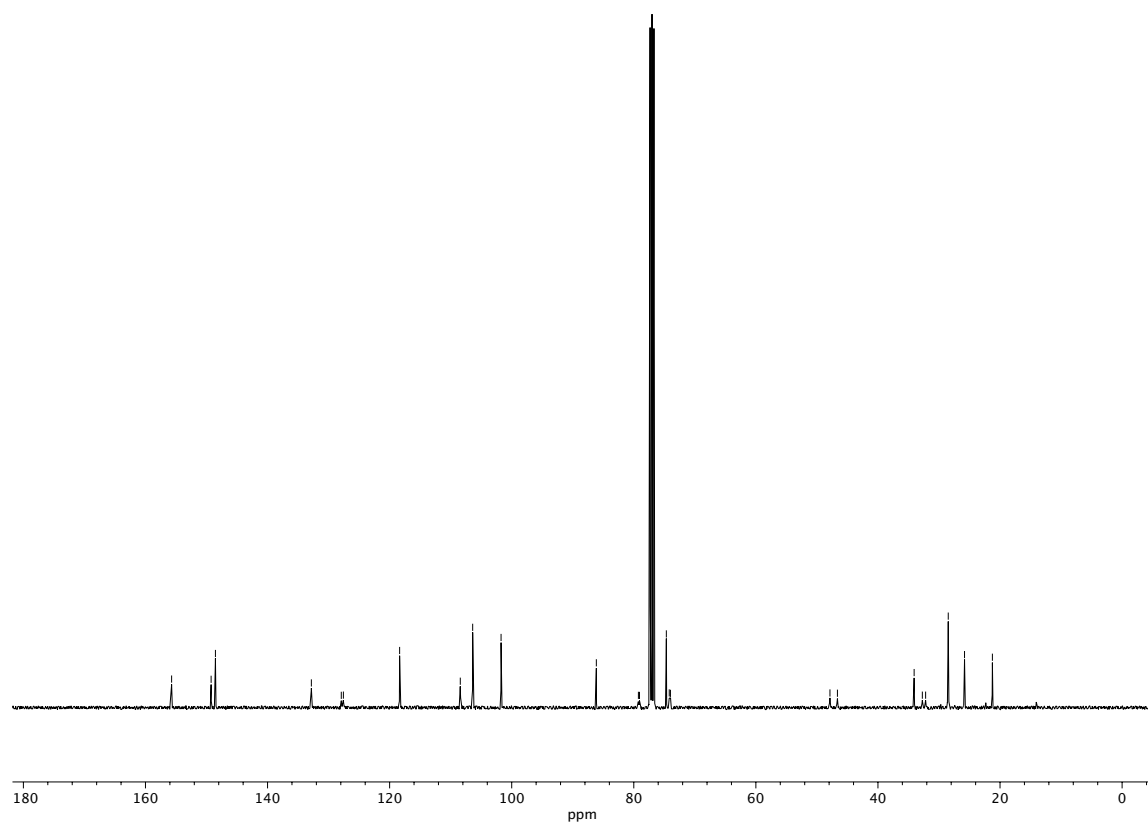
Figure A1.14 ^{13}C NMR (101 MHz, CDCl$_3$) of Compound **161**.

Figure A1.15 ^{1}H NMR (400 MHz, CDCl$_3$) of compound **150.**
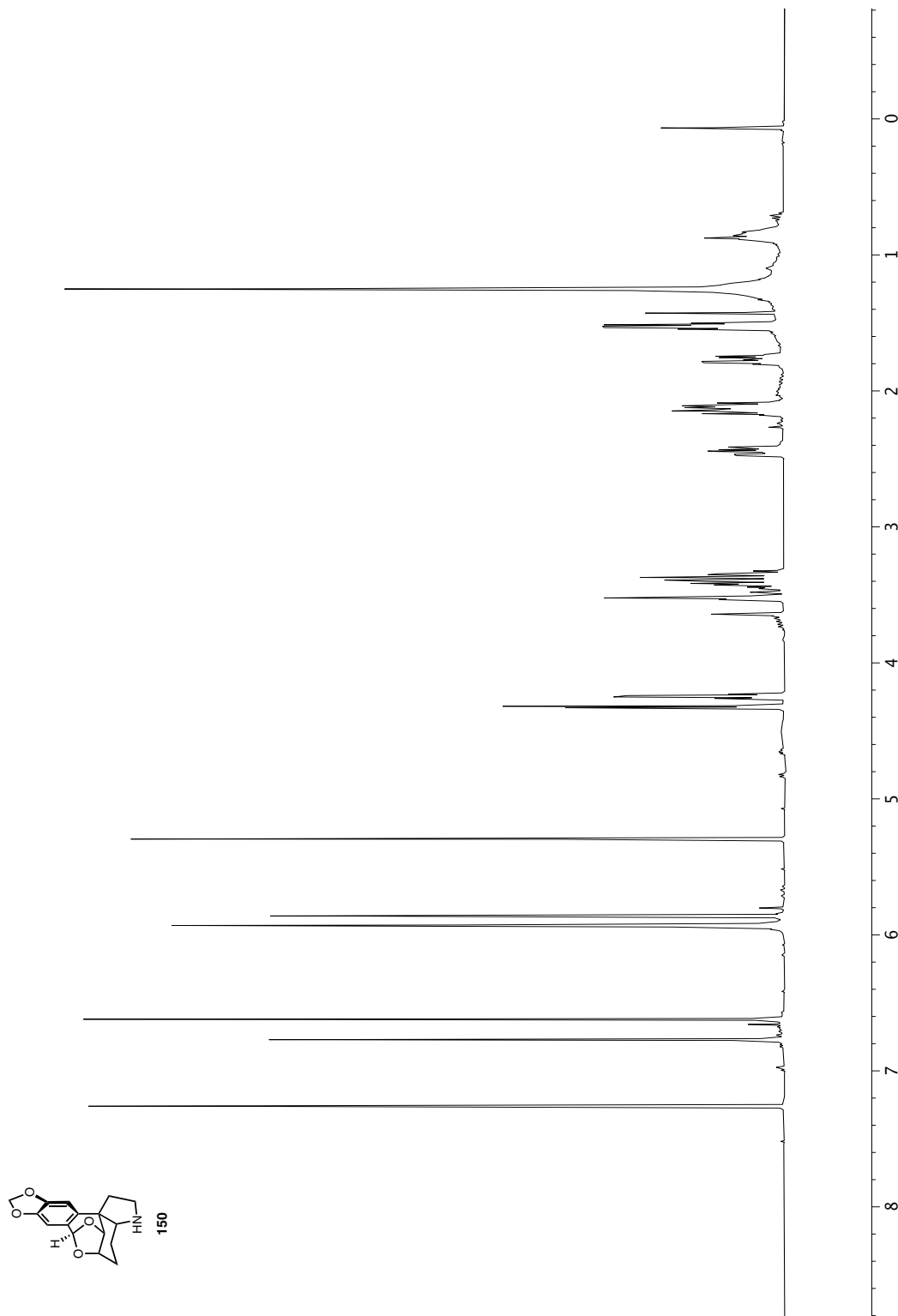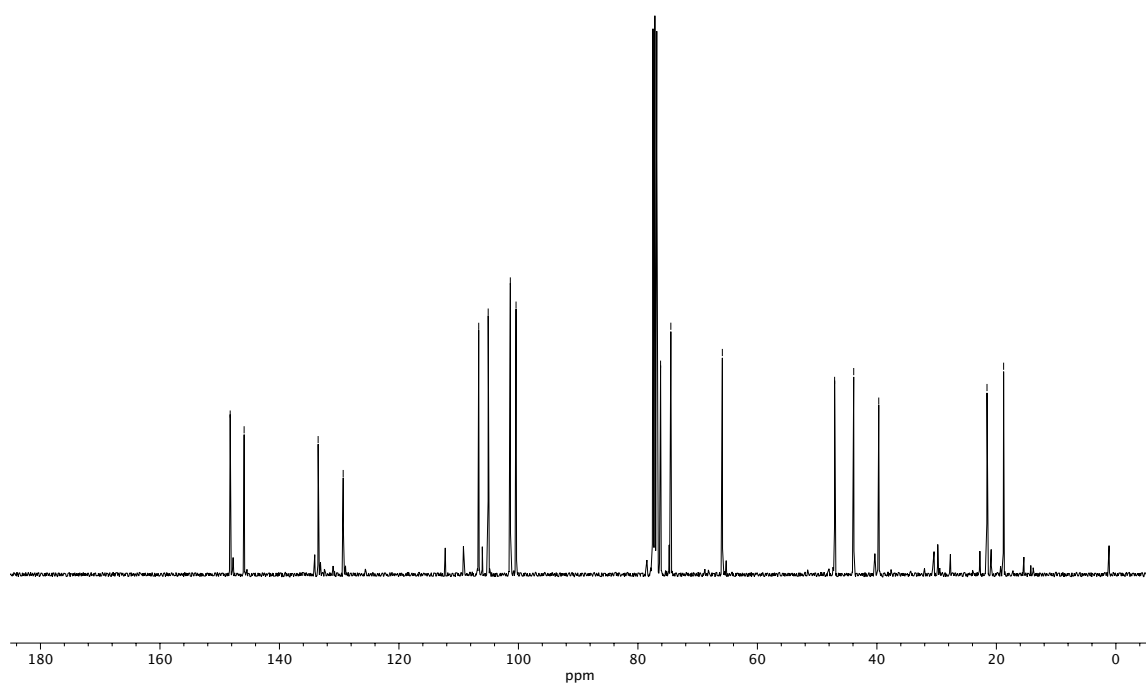
Figure A1.16 ^{13}C NMR (101 MHz, CDCl$_3$) of Compound **150**.
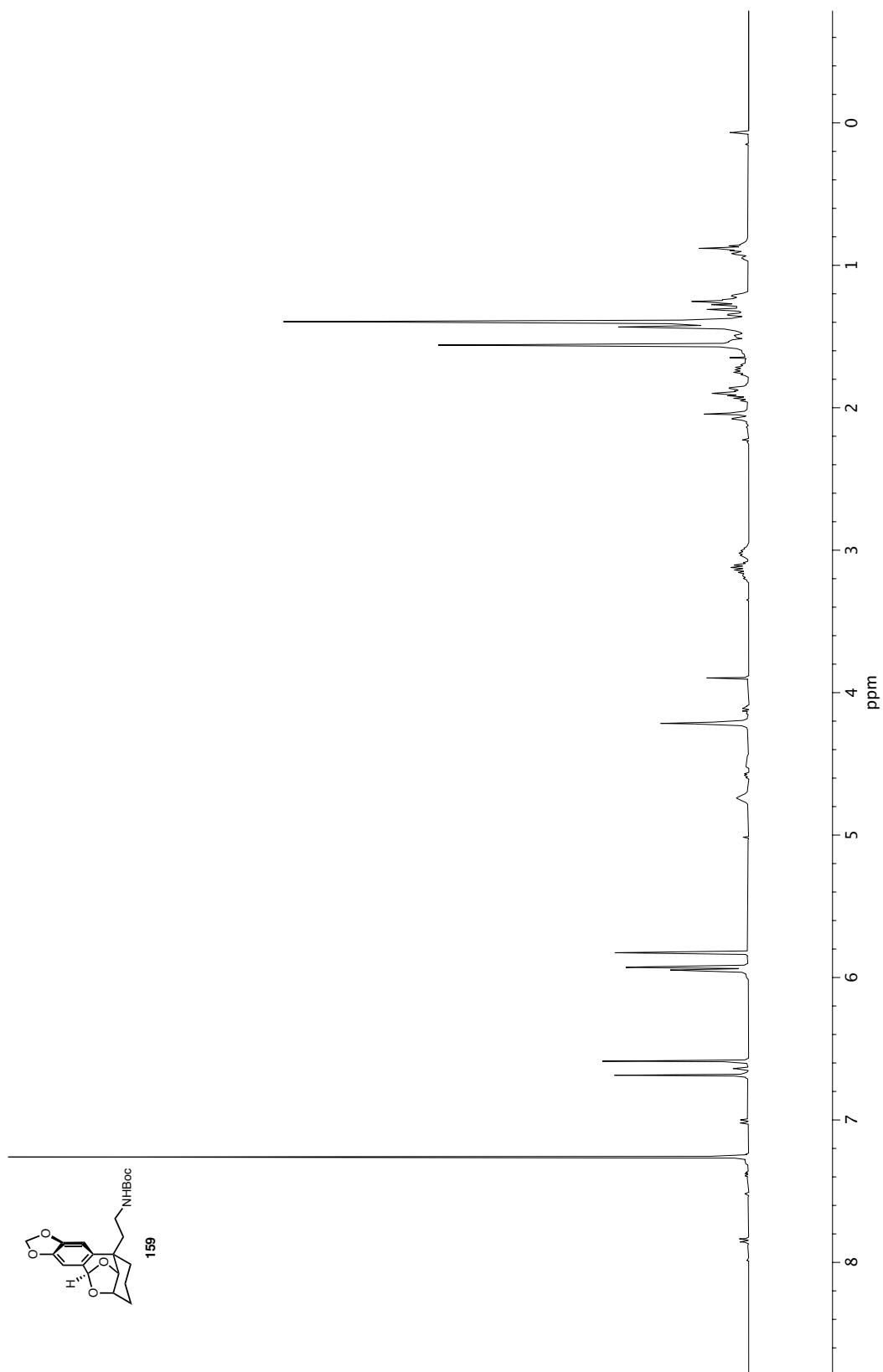
Figure A1.17 ^{1}H NMR (400 MHz, CDCl$_3$) of compound **159.**
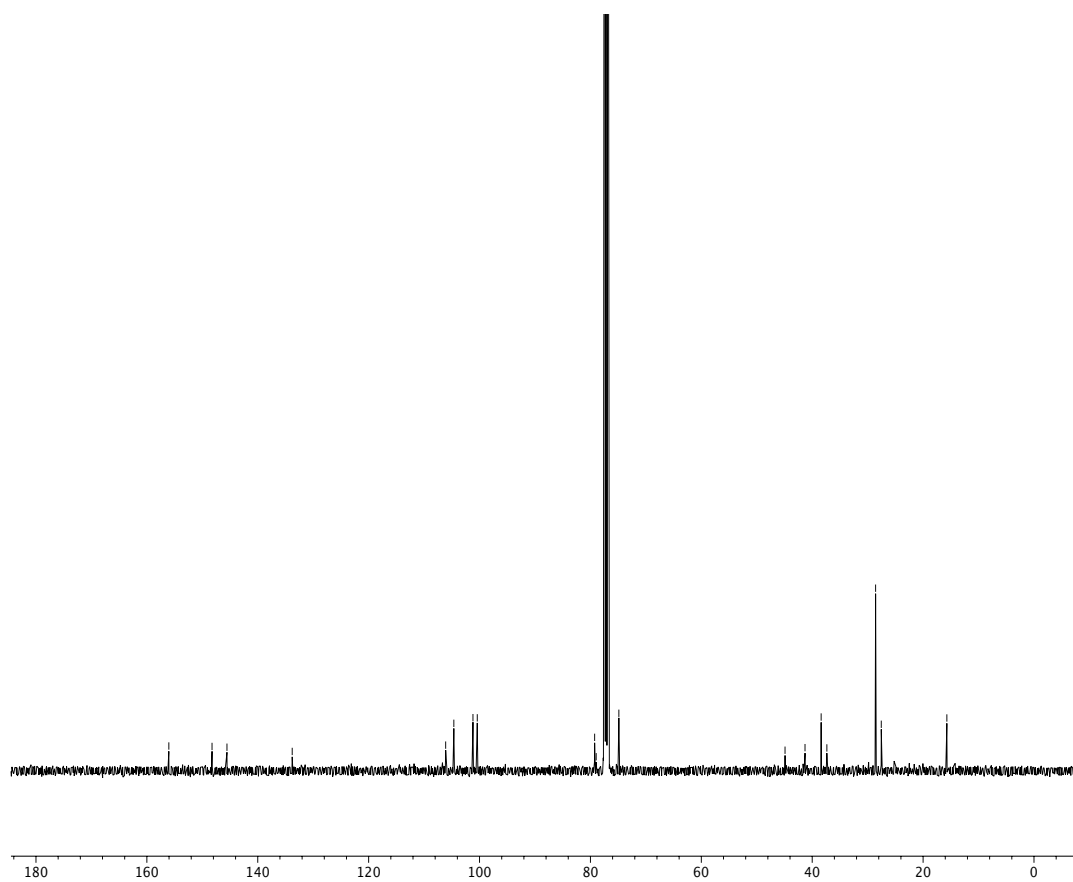
Figure A1.18 ^{13}C NMR (101 MHz, CDCl$_3$) of Compound **159**.
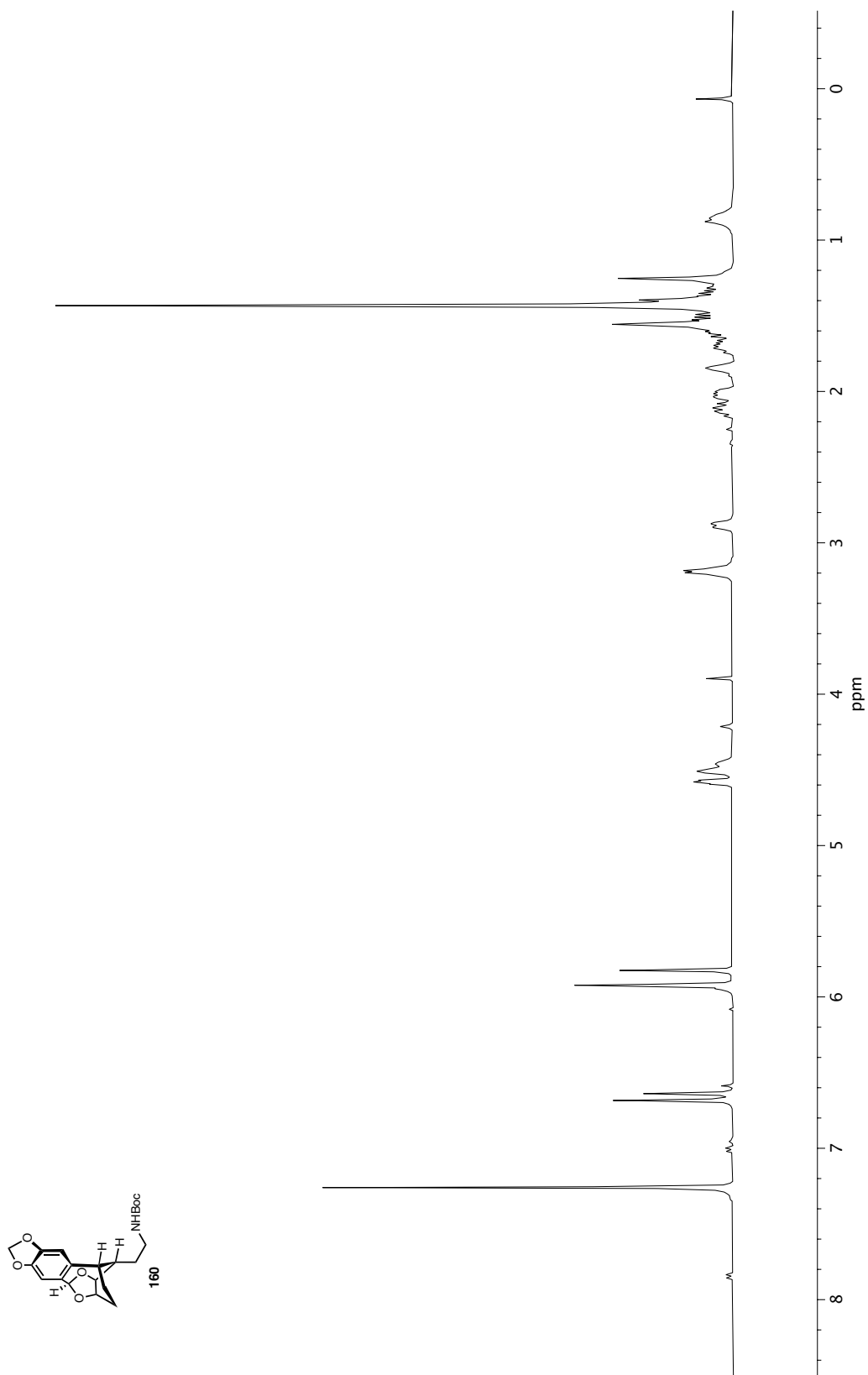
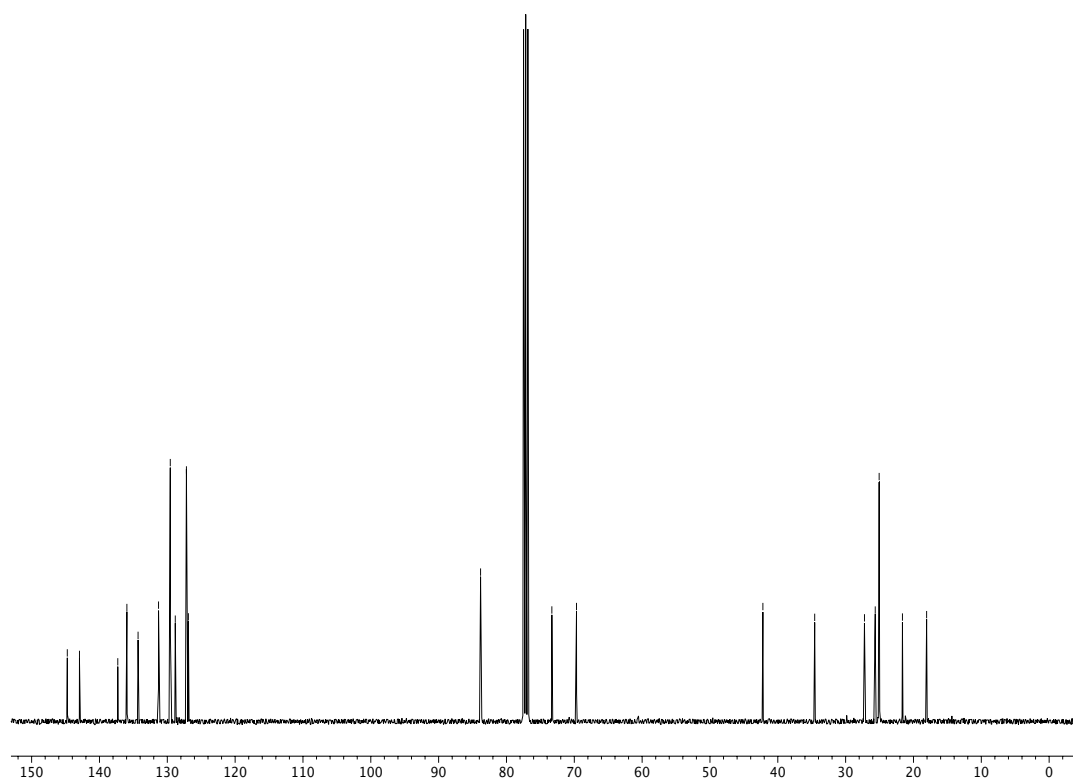**Figure A1.19** ¹H NMR (400 MHz, CDCl₃) of compound **160.**
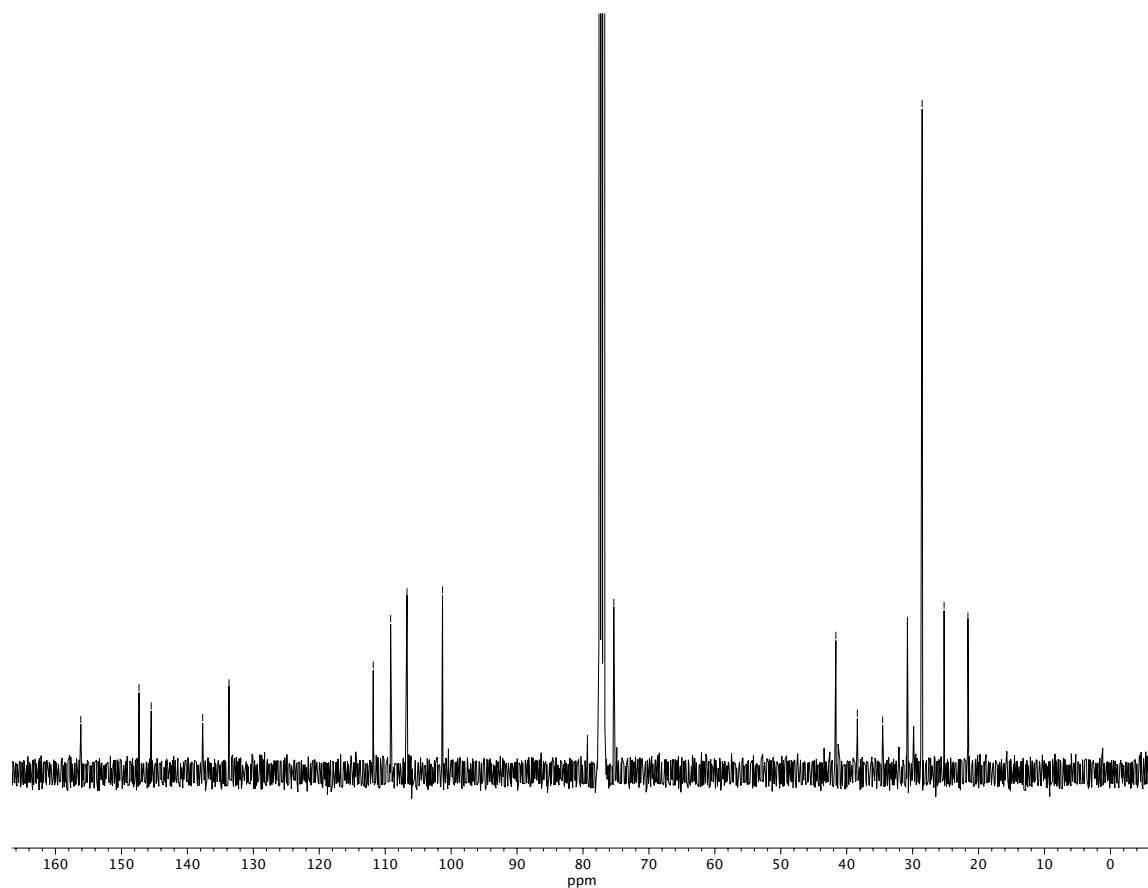
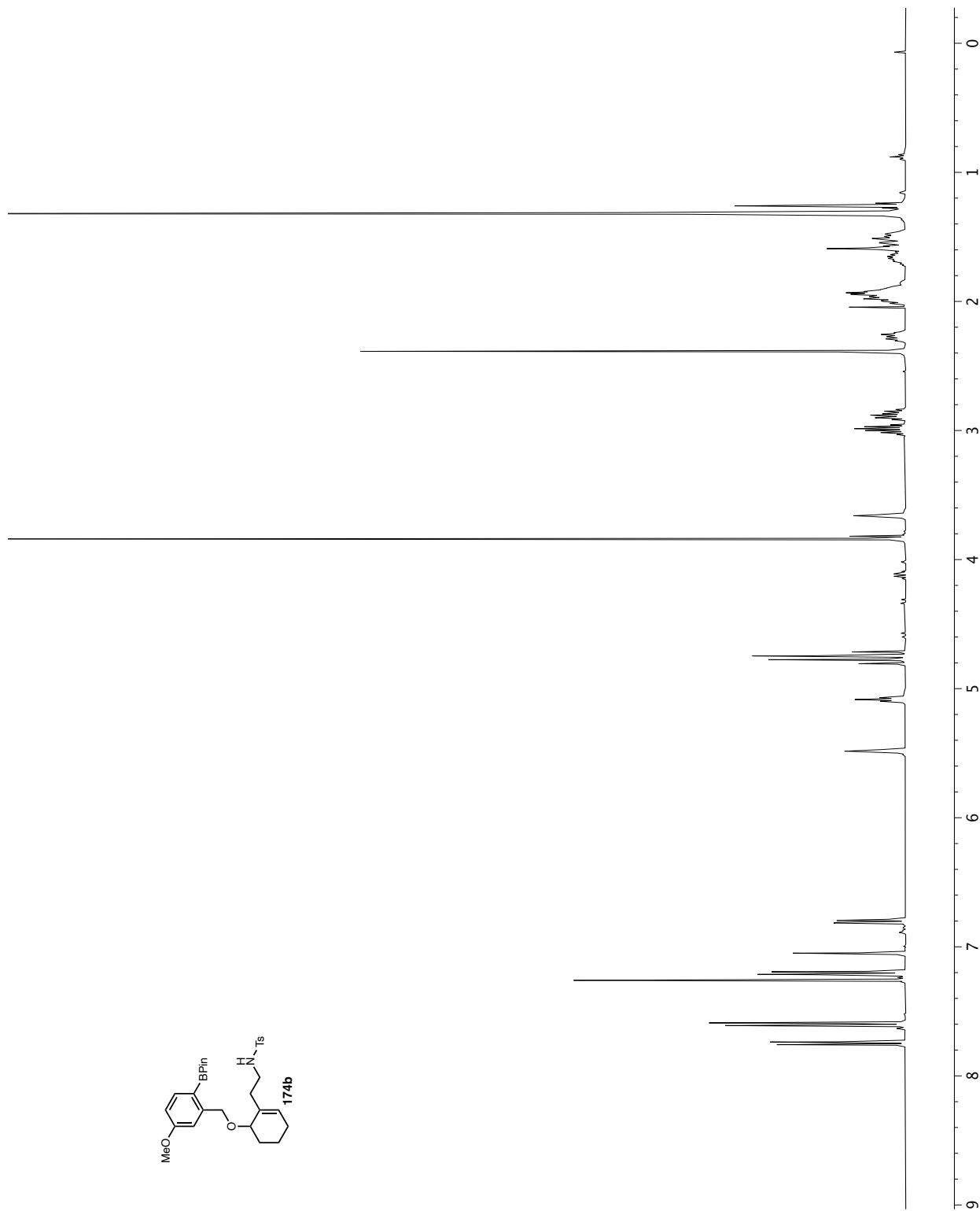***Figure A1.20*** ^{13}C NMR (101 MHz, CDCl$_3$) of Compound **160**.

Figure A1.21 ^{1}H NMR (400 MHz, CDCl$_3$) of compound **162.**
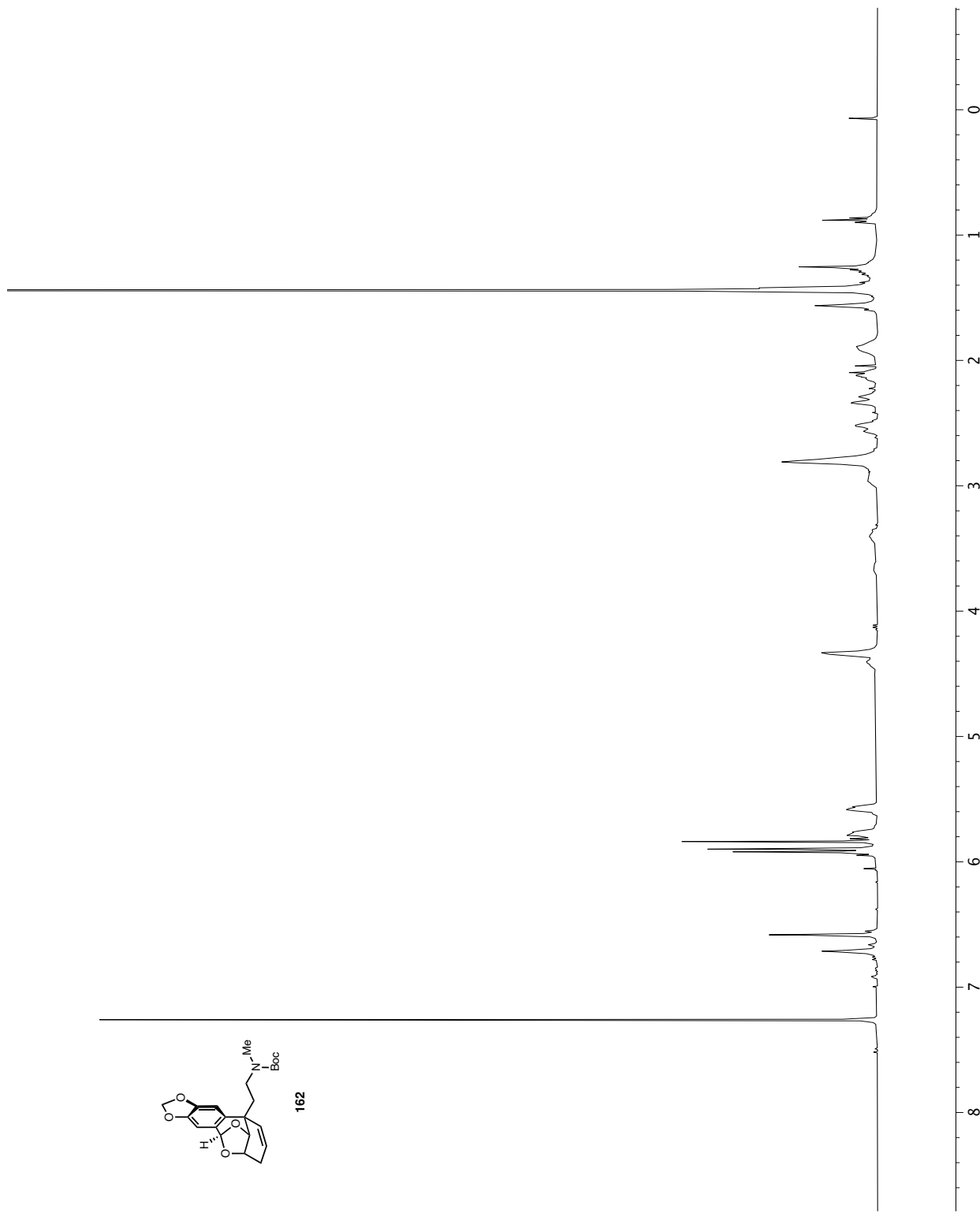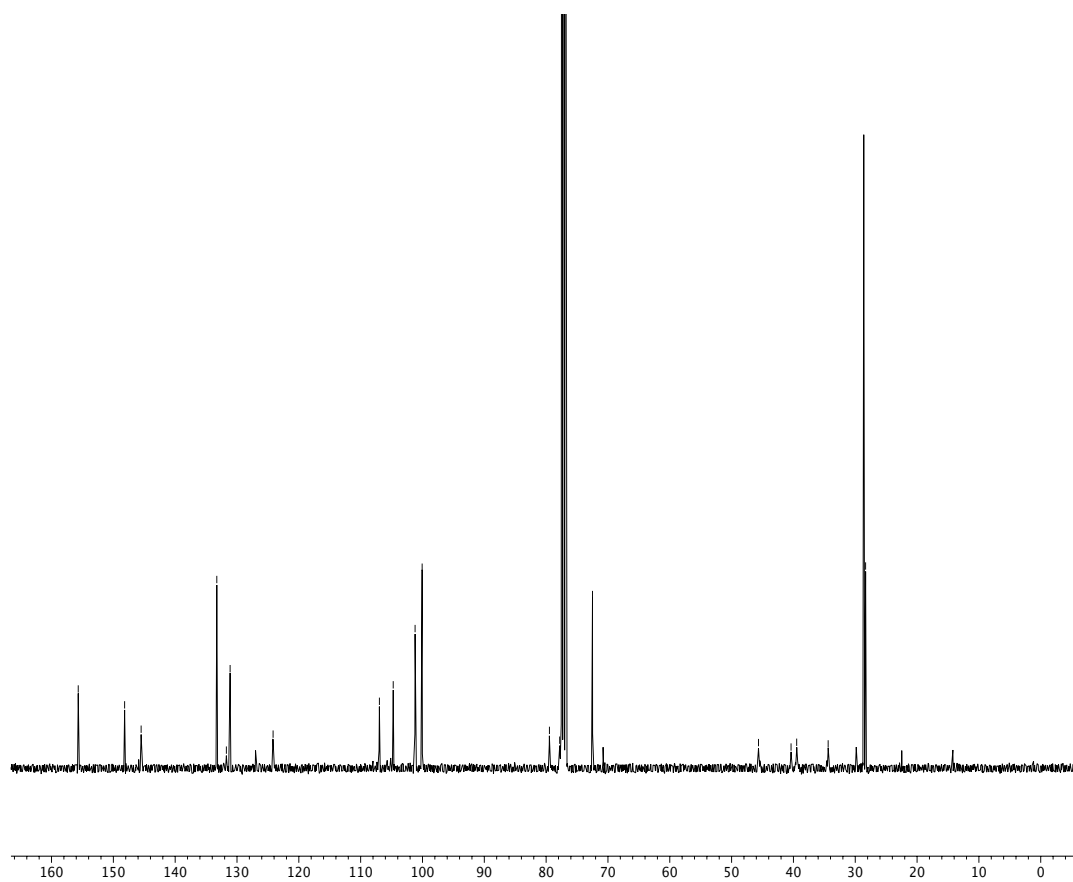
Figure A1.22 ^{13}C NMR (101 MHz, CDCl$_3$) of Compound **162**.
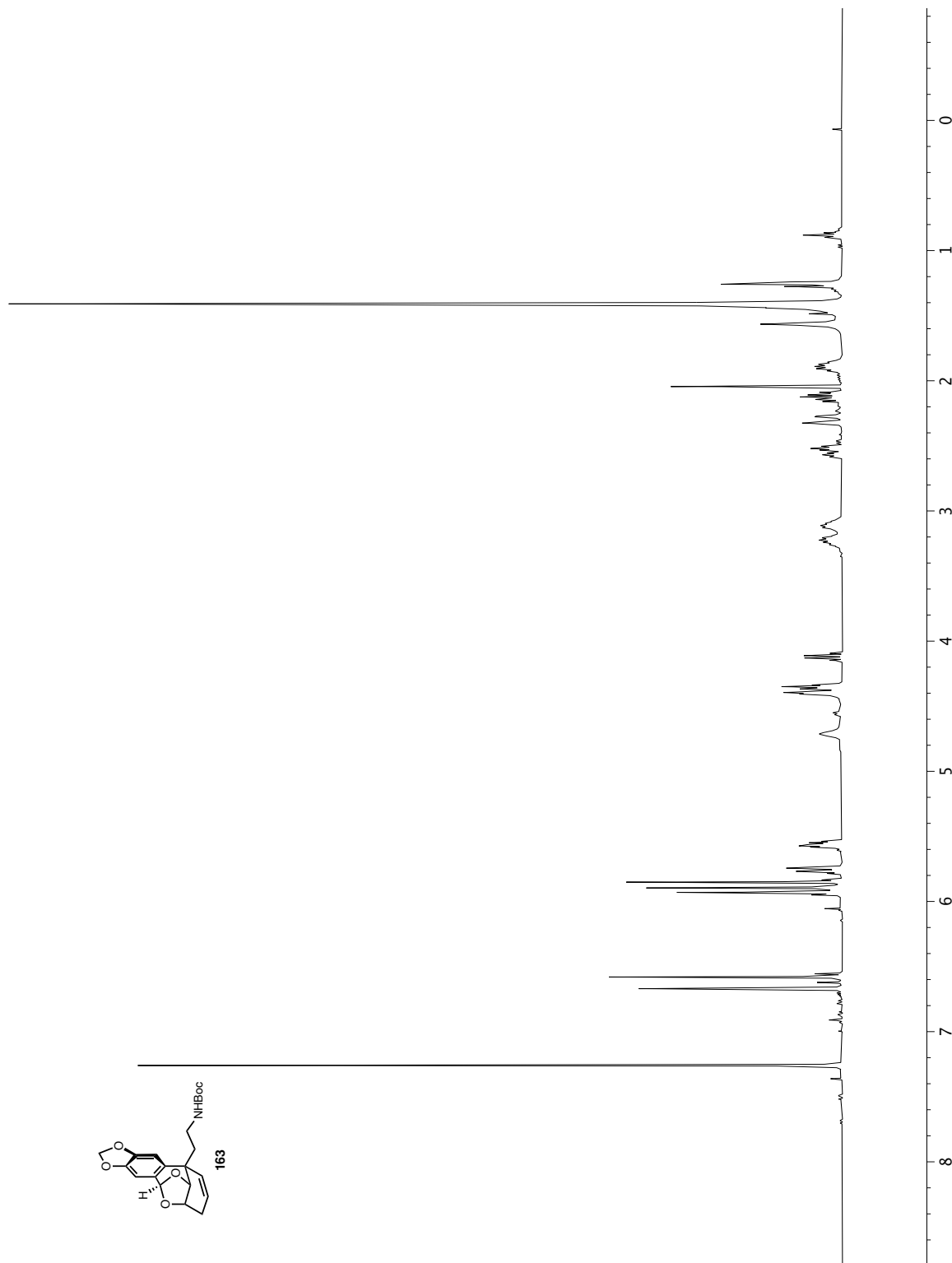
Figure A1.23 ^{1}H NMR (400 MHz, CDCl$_3$) of compound **163.**
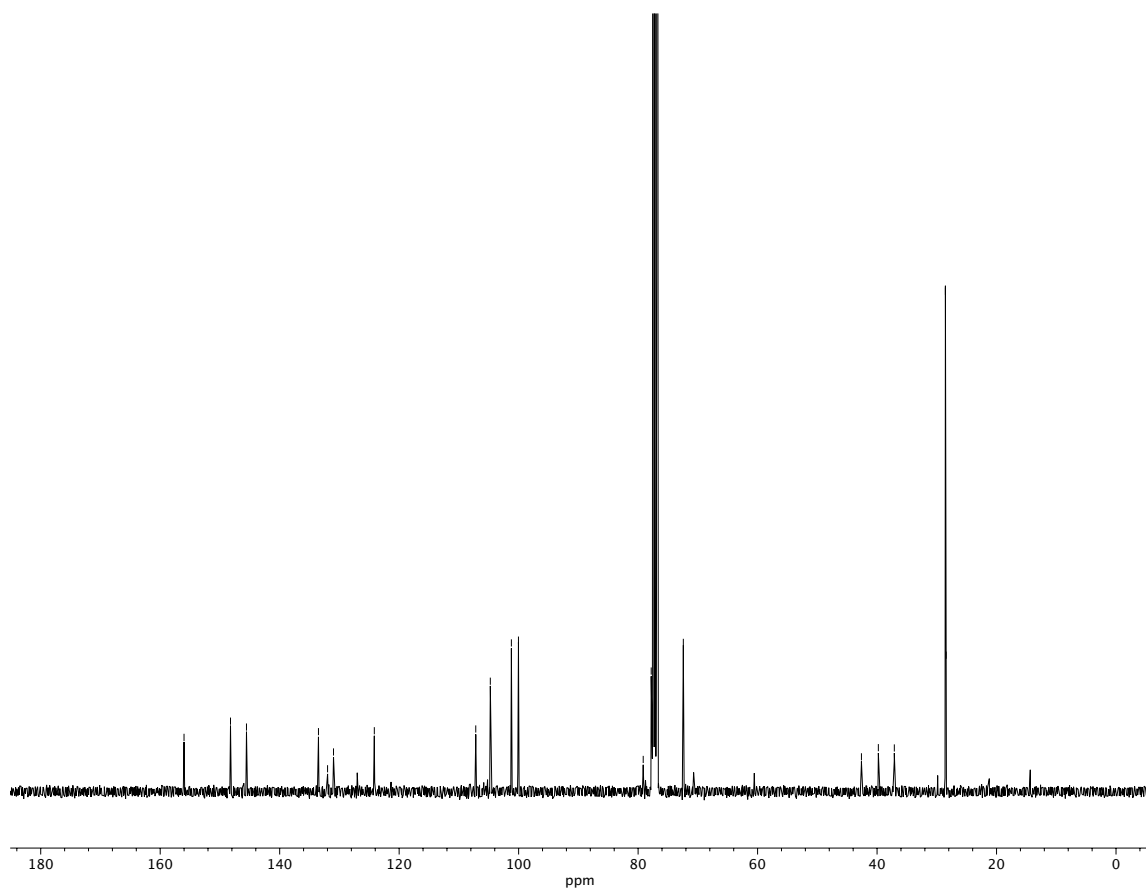
Figure A1.24 ^{13}C NMR (101 MHz, CDCl$_3$) of Compound **163**.
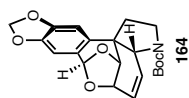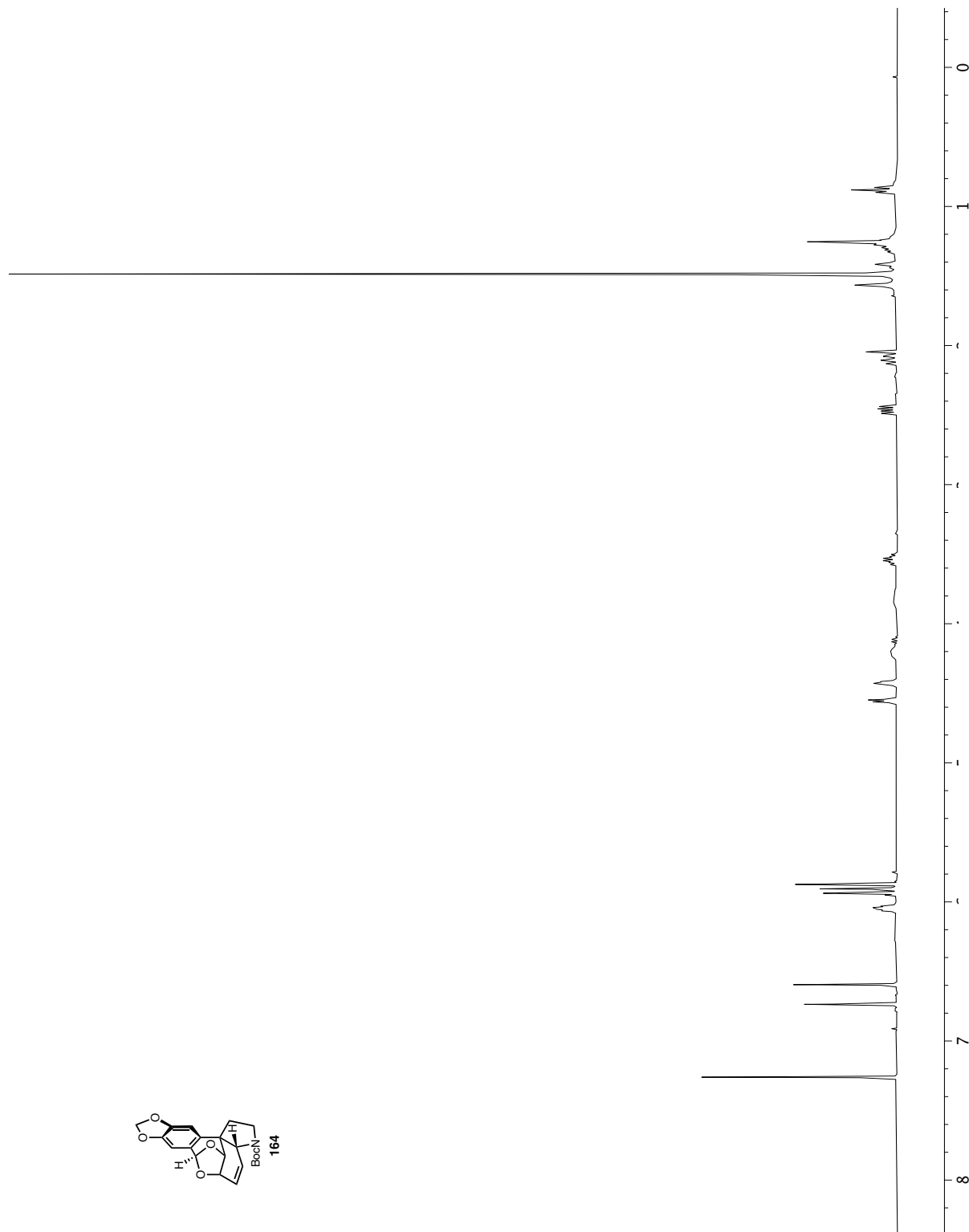
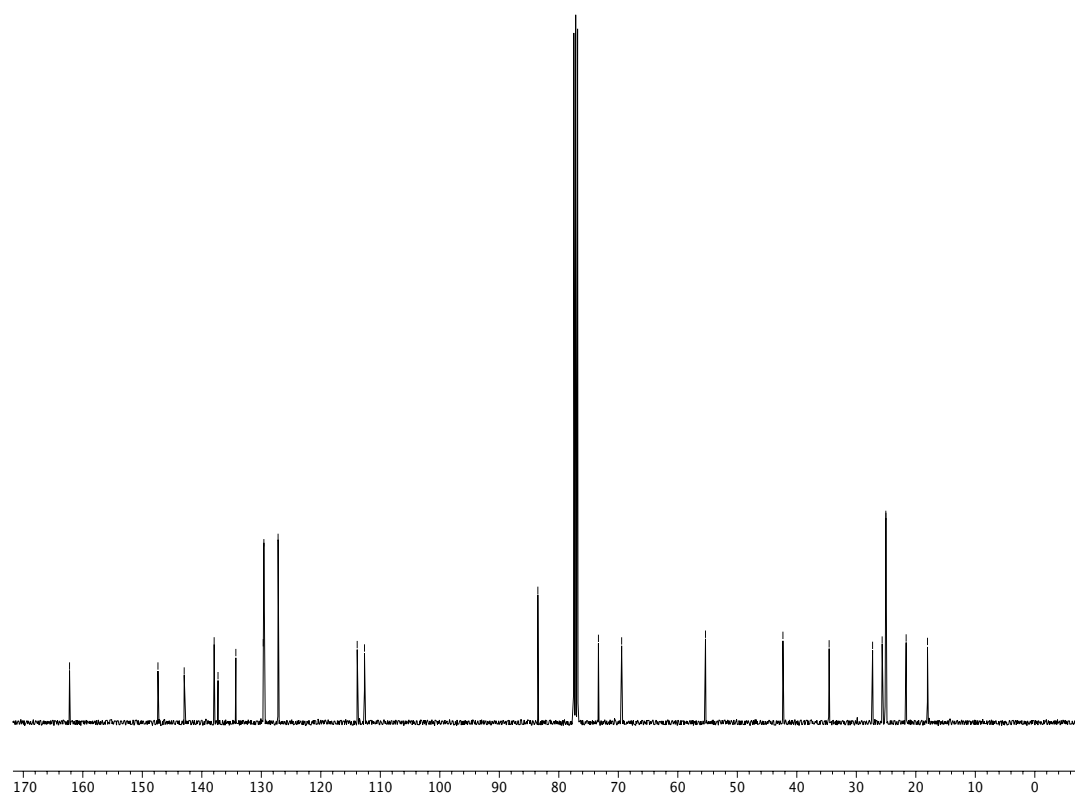***Figure A1.25*** ^{1}H NMR (400 MHz, CDCl$_3$) of compound **164.**
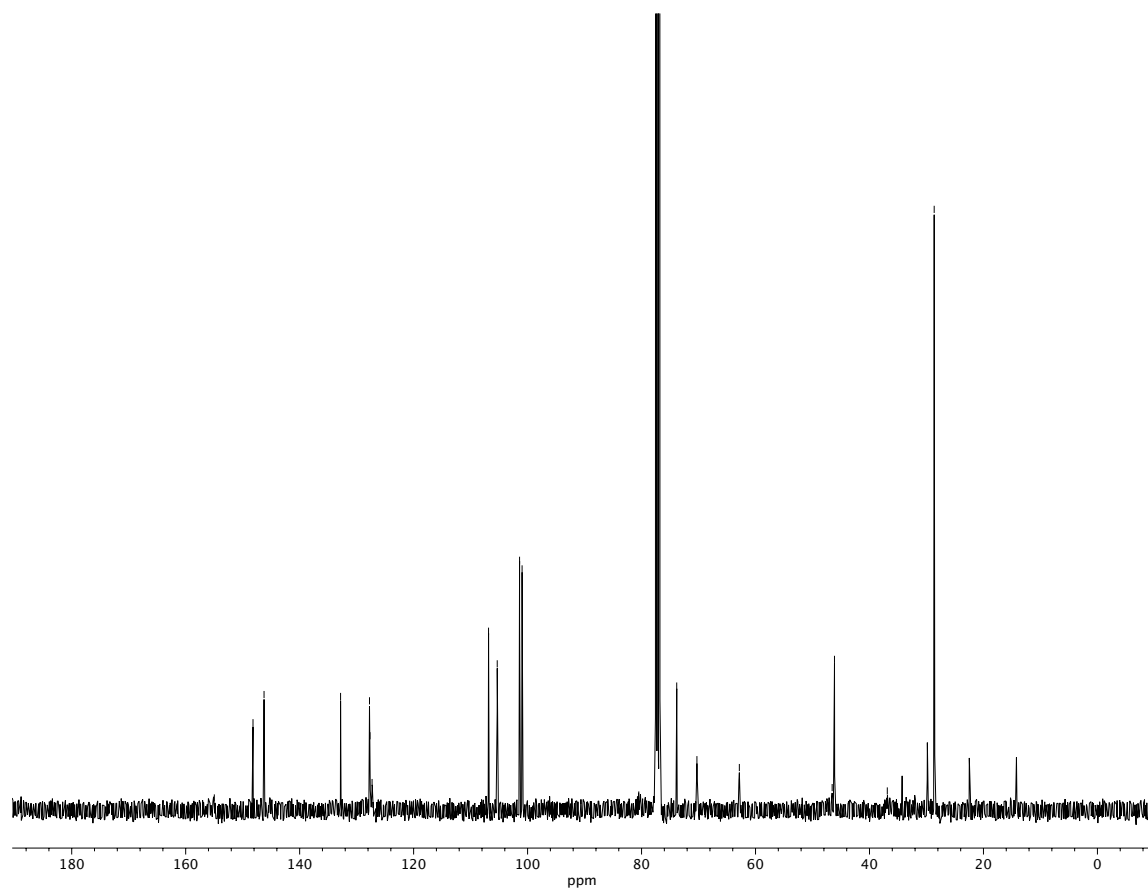
Figure A1.26 ^{13}C NMR (101 MHz, CDCl$_3$) of Compound **164**.
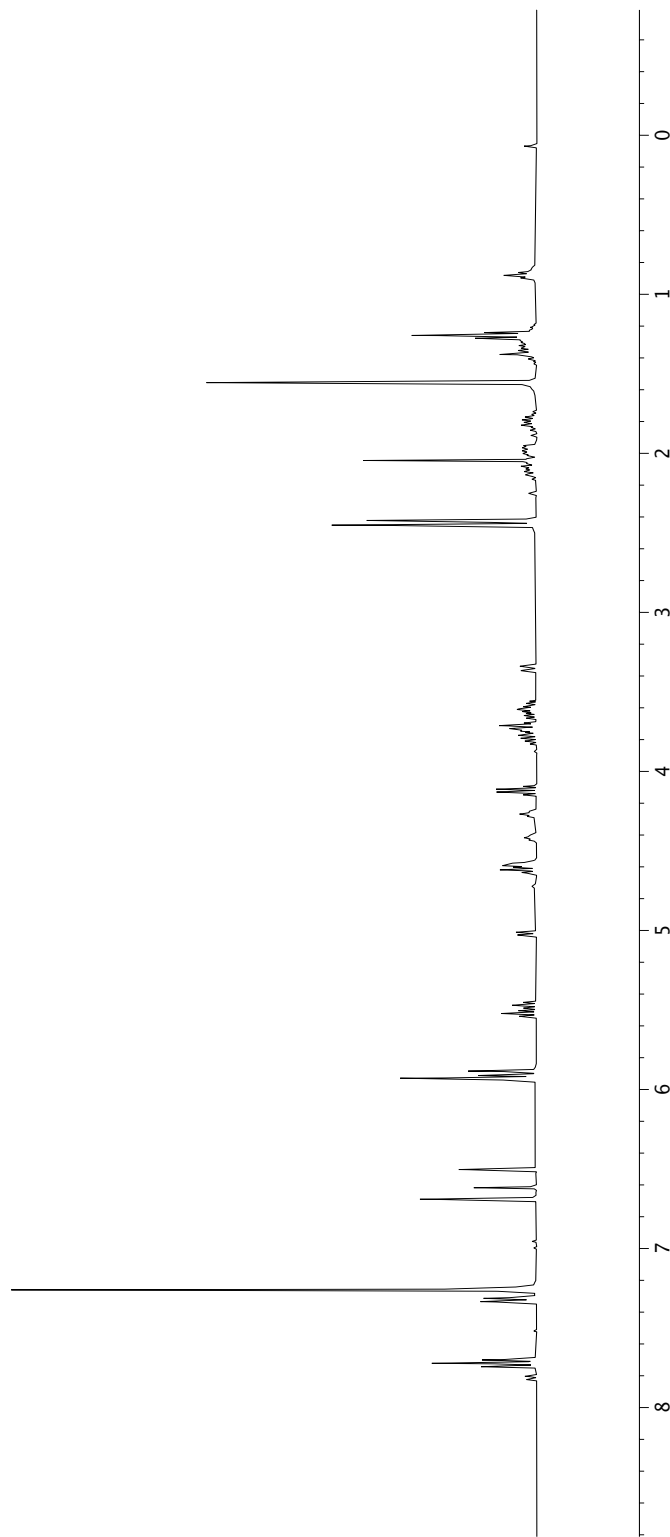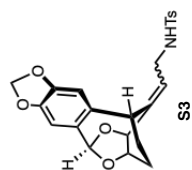
Figure A1.27 ^{1}H NMR (400 MHz, CDCl$_3$) of compound **S3.**
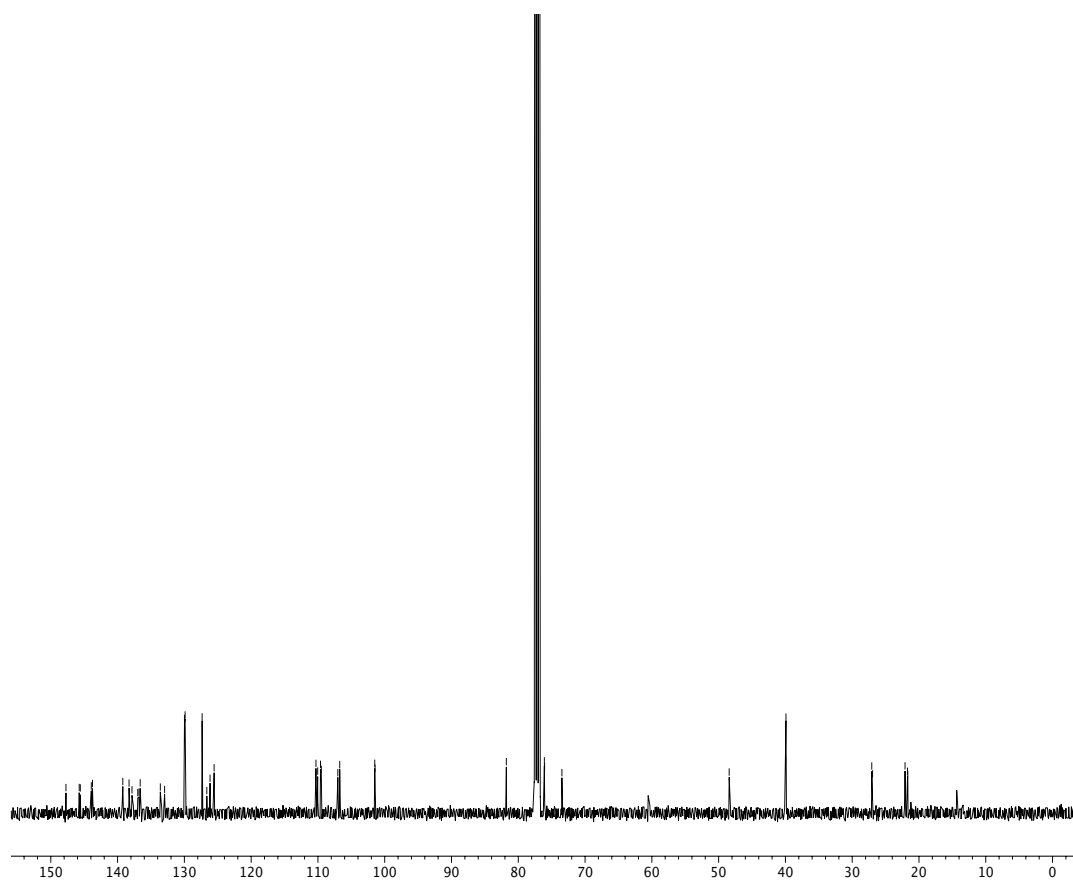
Figure A1.28 ^{13}C NMR (101 MHz, CDCl$_3$) of Compound **S3**.
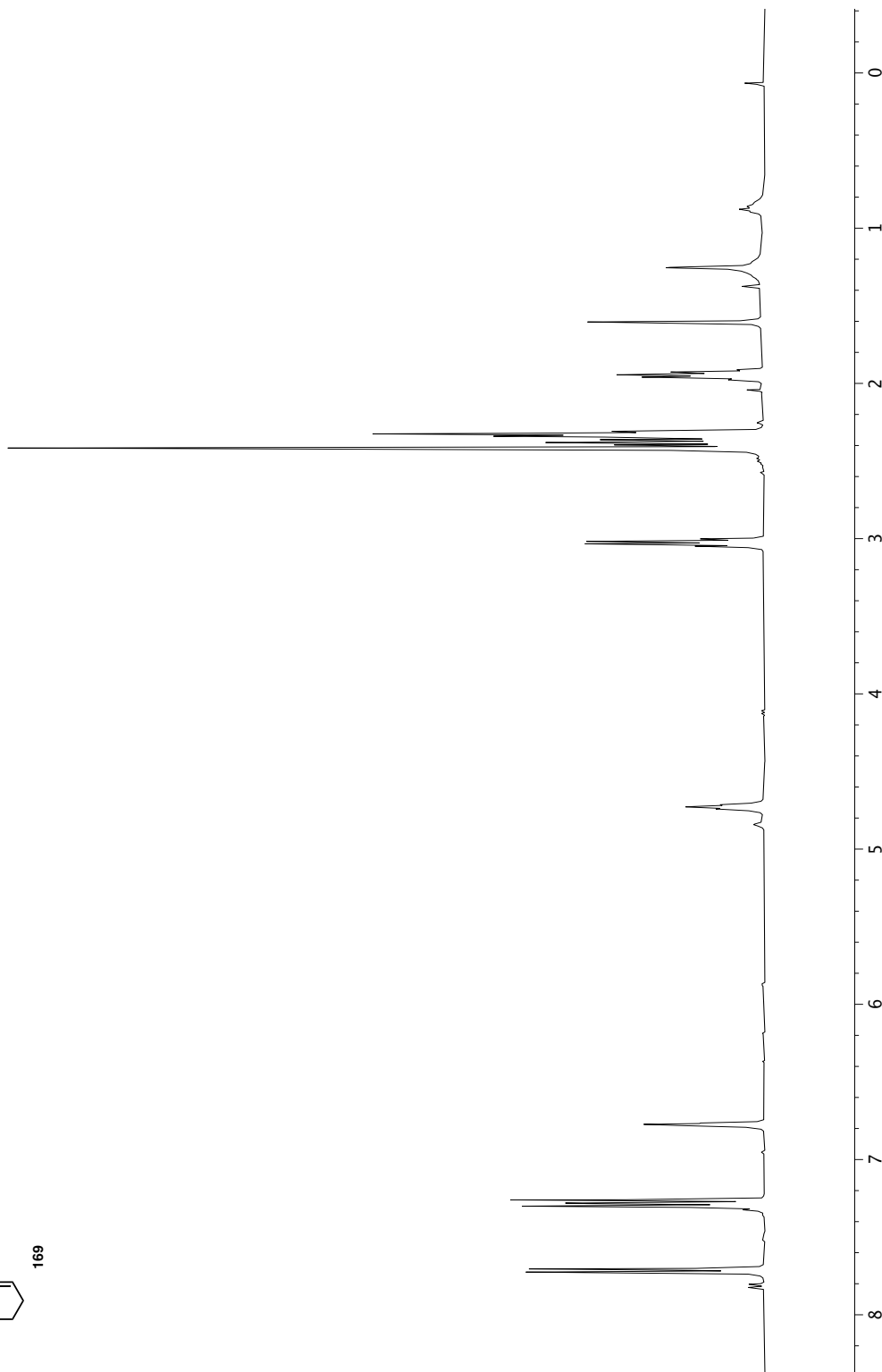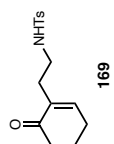
Figure A1.29 ¹H NMR (400 MHz, CDCl₃) of compound **169.**
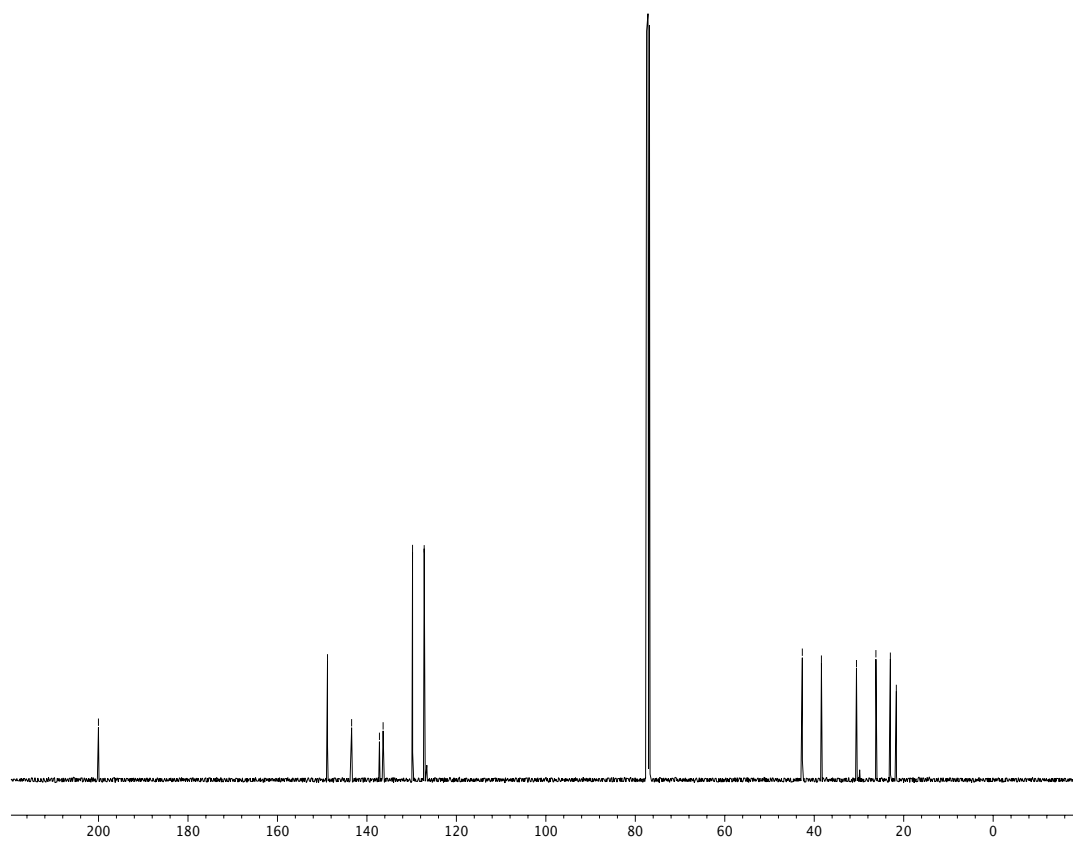
Figure A1.30 ^{13}C NMR (101 MHz, CDCl$_3$) of Compound **169**.
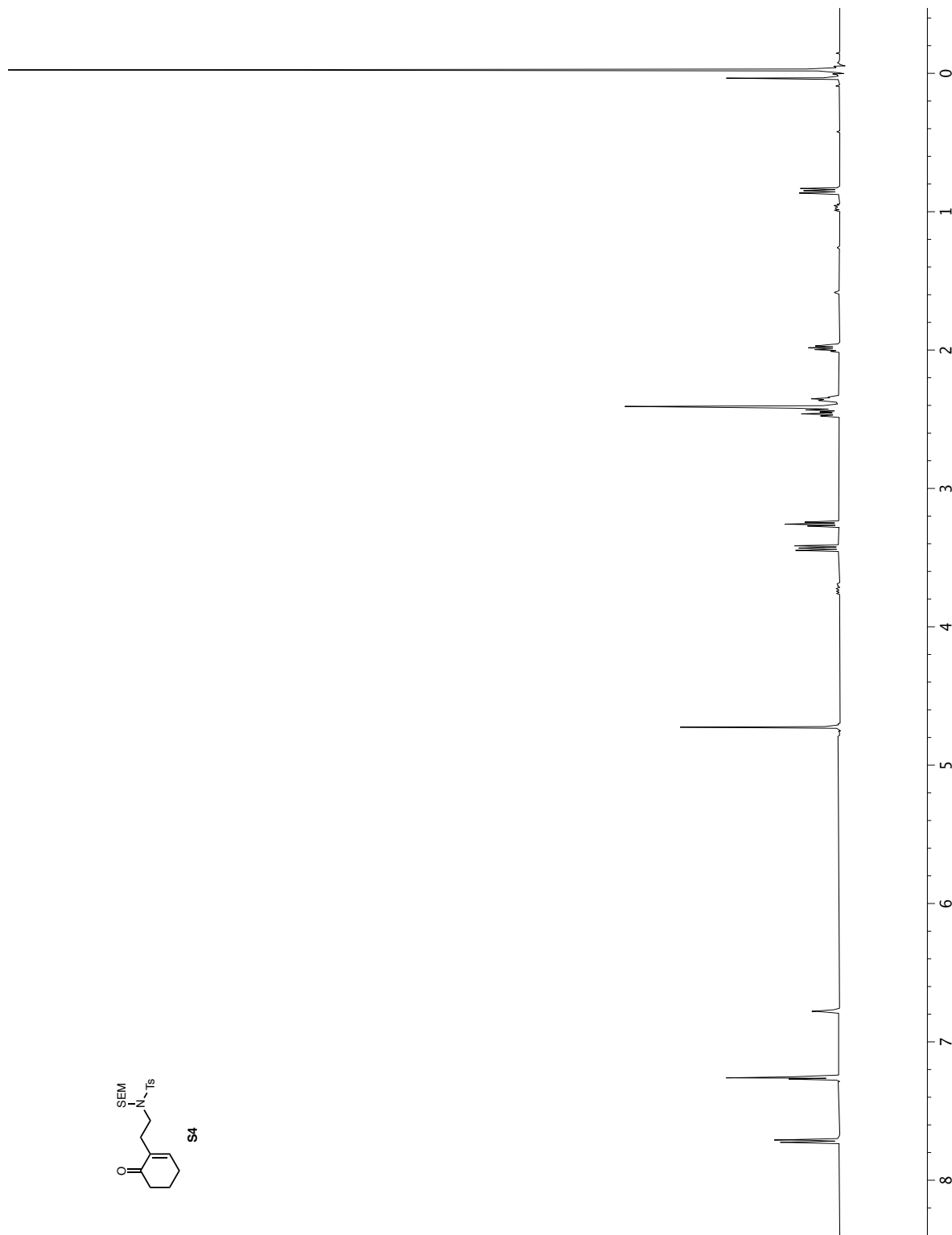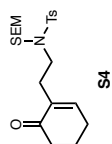
Figure A1.31 ^{1}H NMR (500 MHz, CDCl$_3$) of compound **S4.**
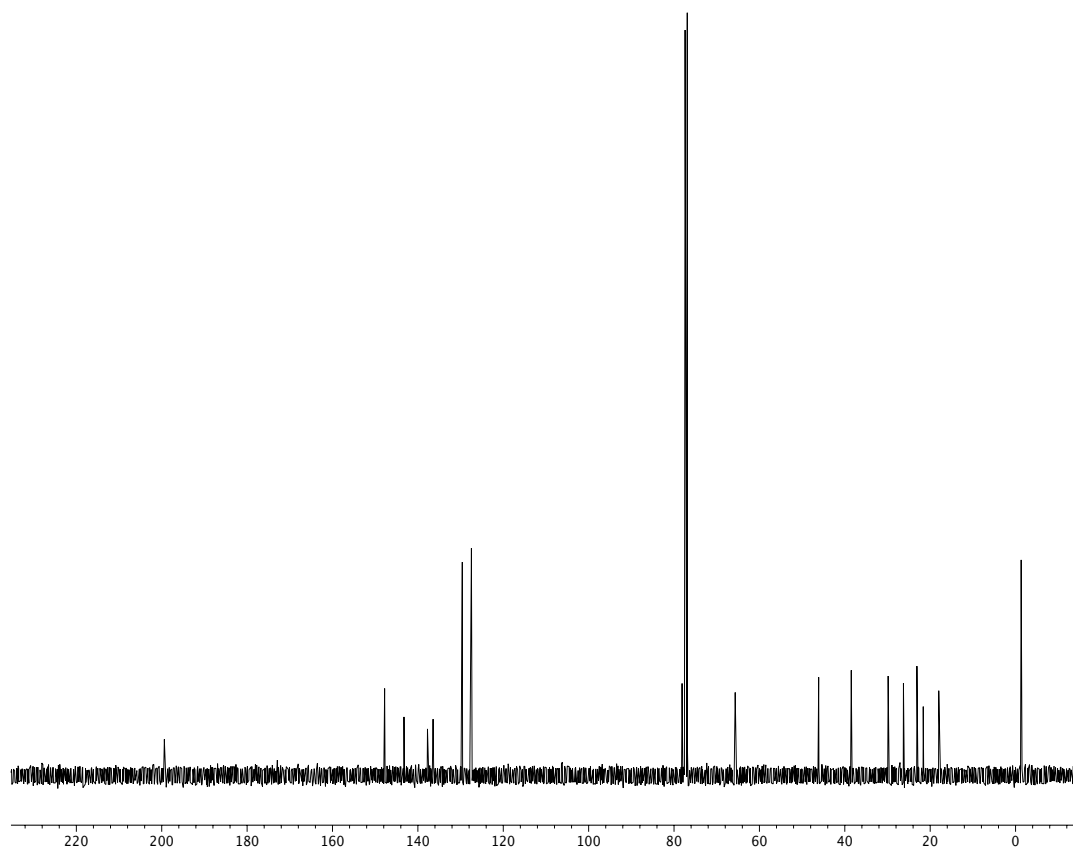
Figure A1.32 ^{13}C NMR (126 MHz, CDCl$_3$) of Compound **S4**.
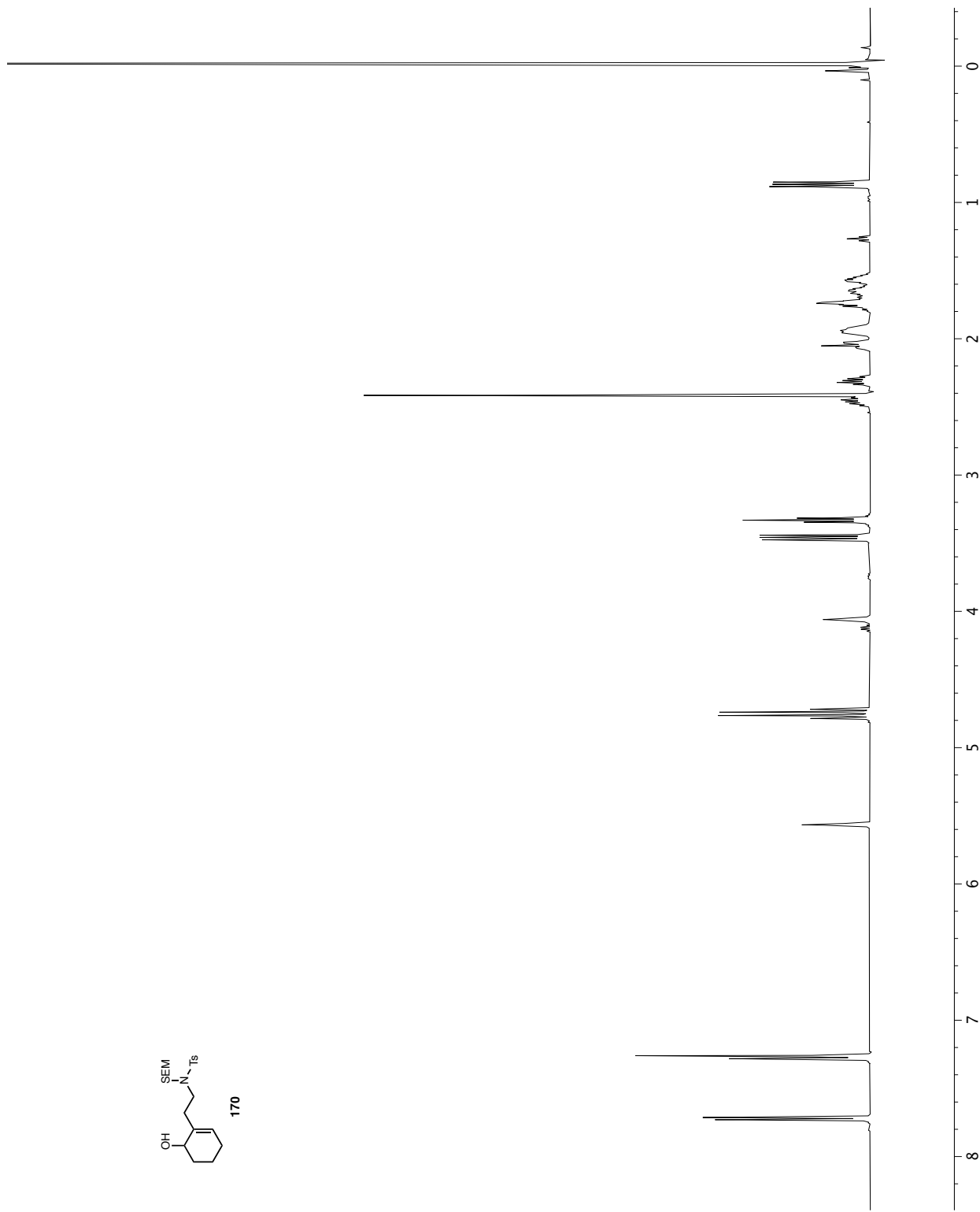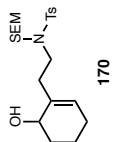
Figure A1.33 ^{1}H NMR (500 MHz, CDCl$_3$) of compound **170.**
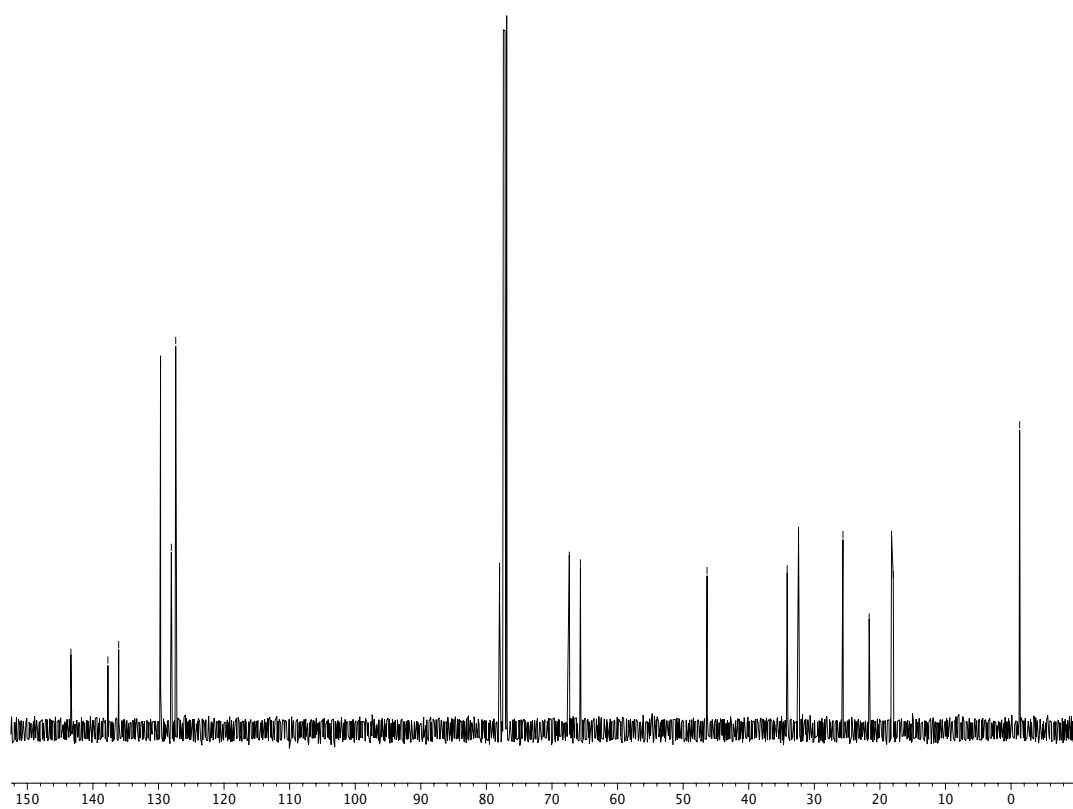
Figure A1.34 ^{13}C NMR (126 MHz, CDCl$_3$) of Compound **170**.
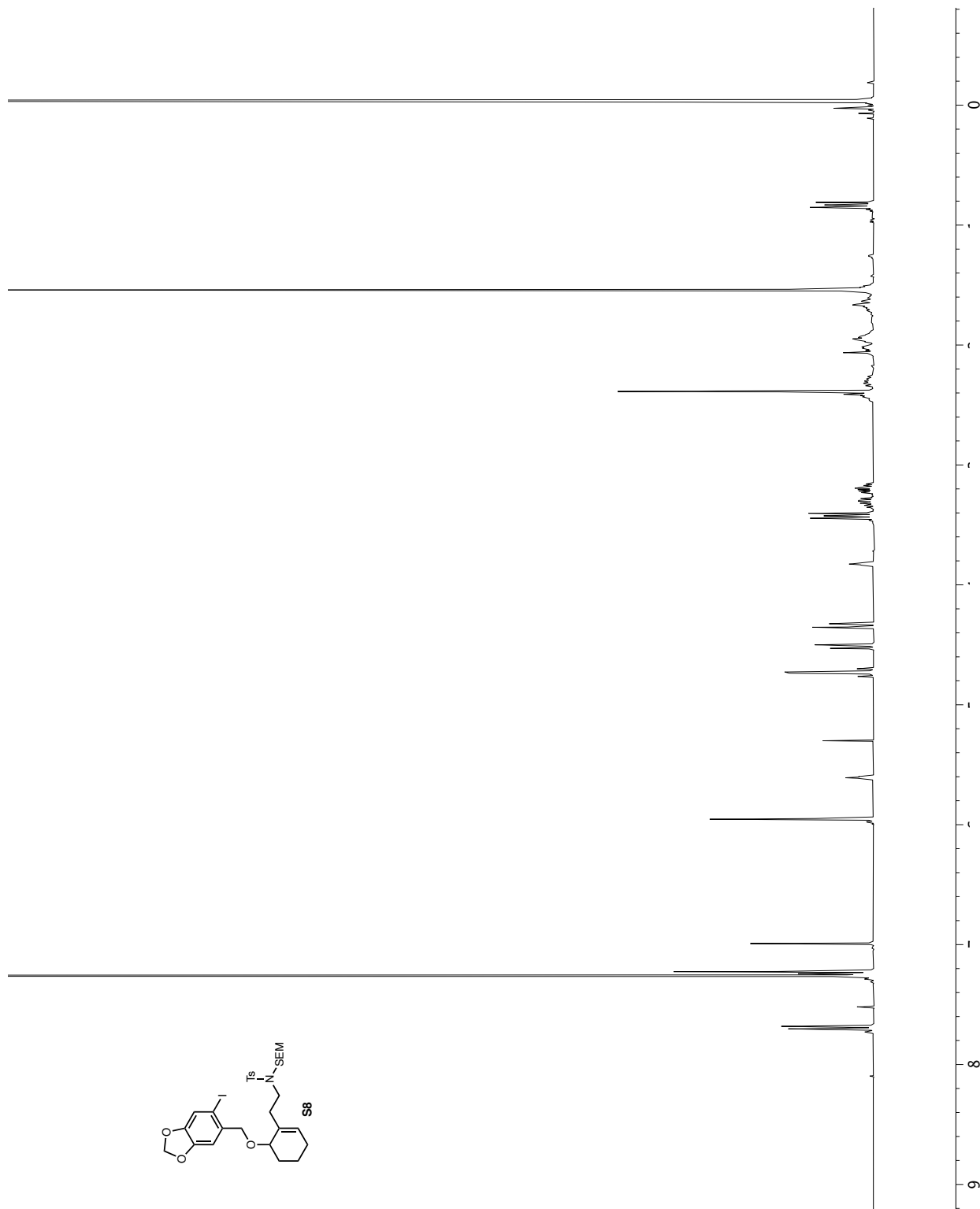
Figure A1.35 ^{1}H NMR (400 MHz, CDCl$_3$) of compound **S8.**
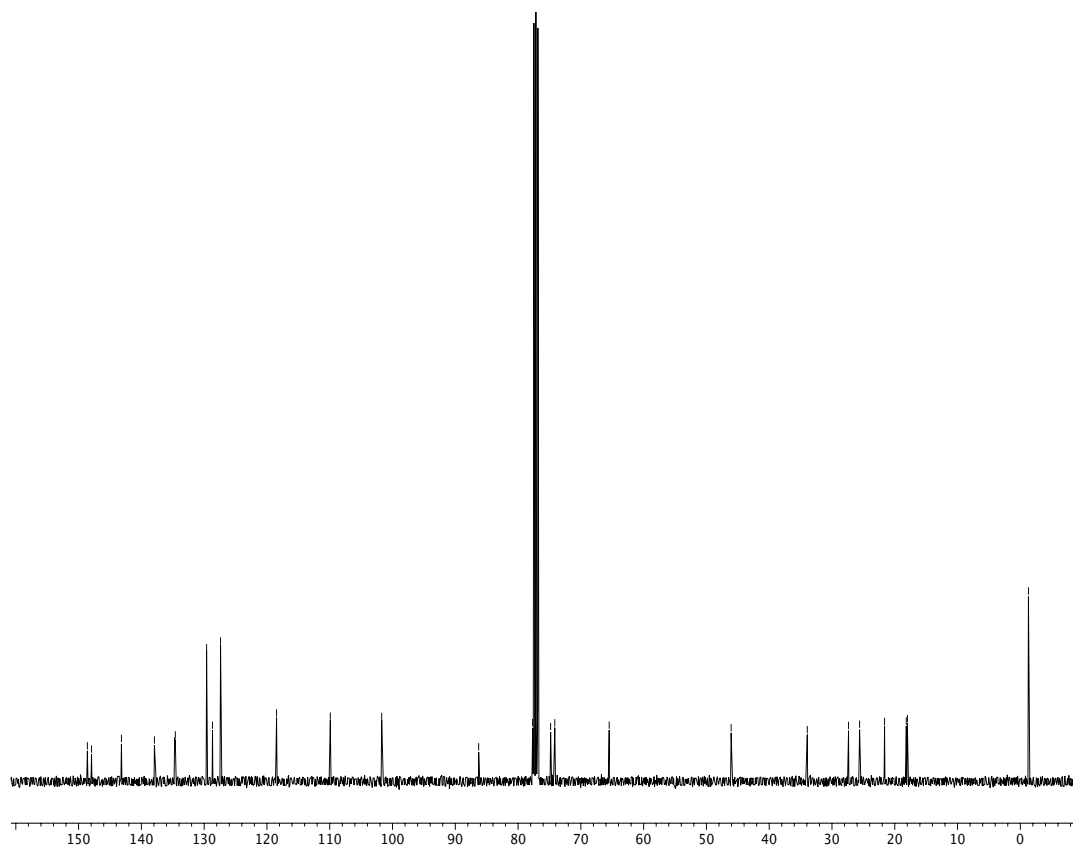
Figure A1.36 ^{13}C NMR (101 MHz, CDCl$_3$) of Compound **S8**.
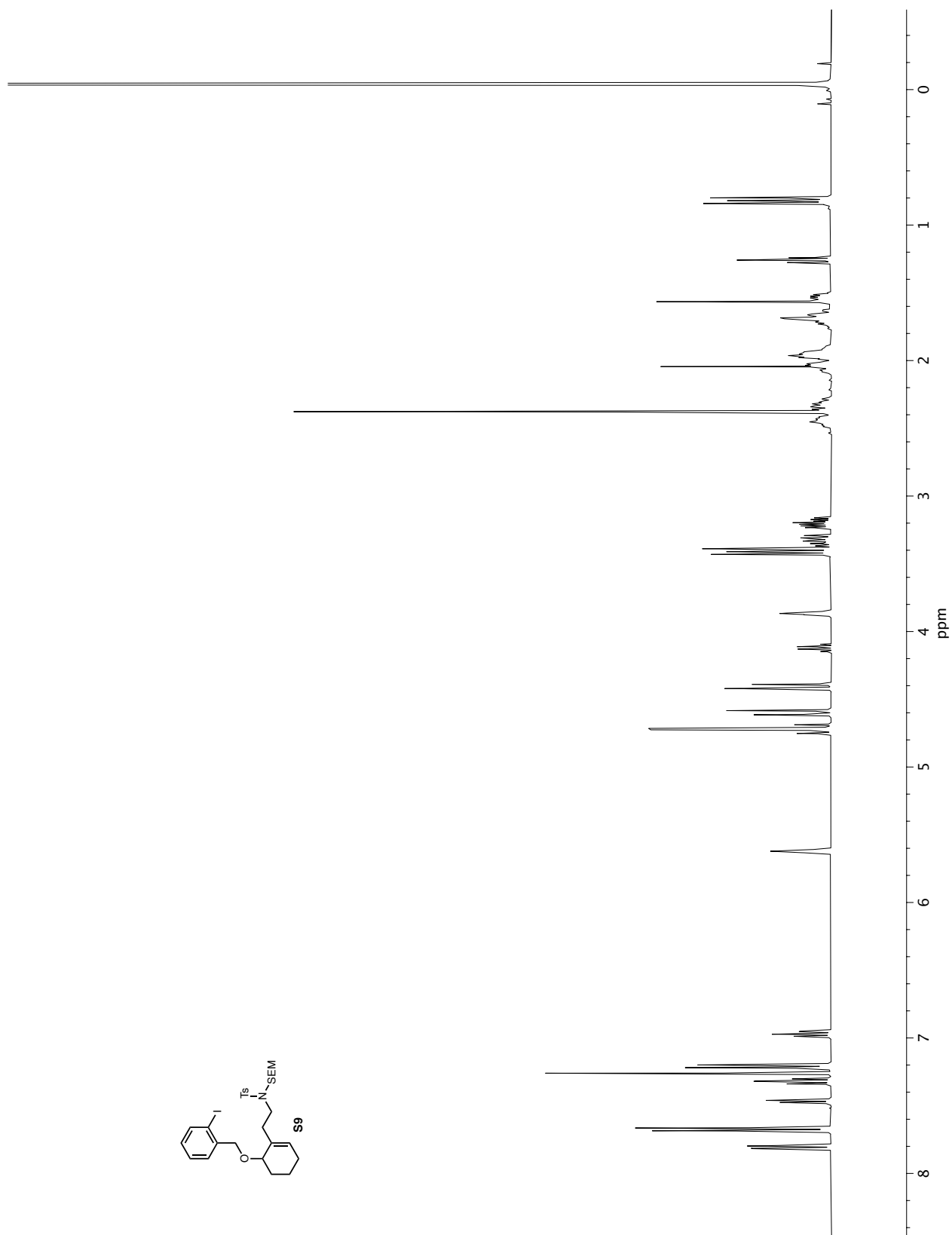
Figure A1.37 ^{1}H NMR (400 MHz, CDCl$_3$) of compound **S9**.
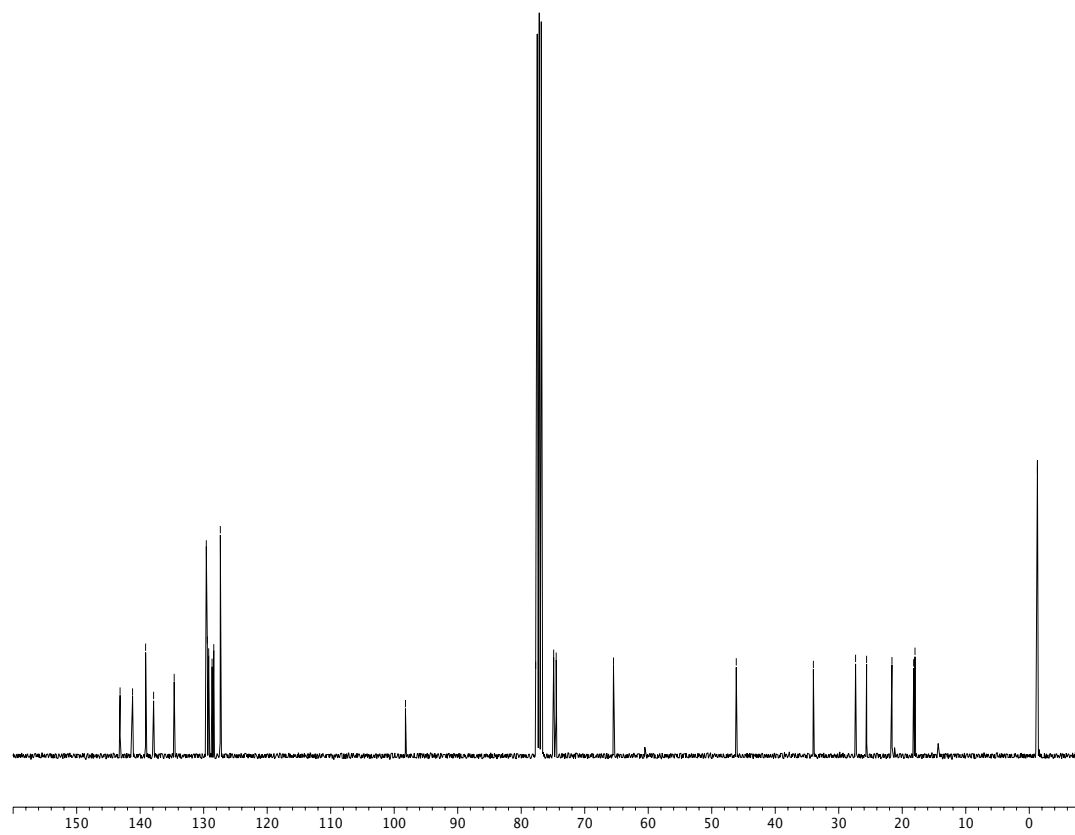
Figure A1.38 ^{13}C NMR (101 MHz, CDCl₃) of Compound **S9**.
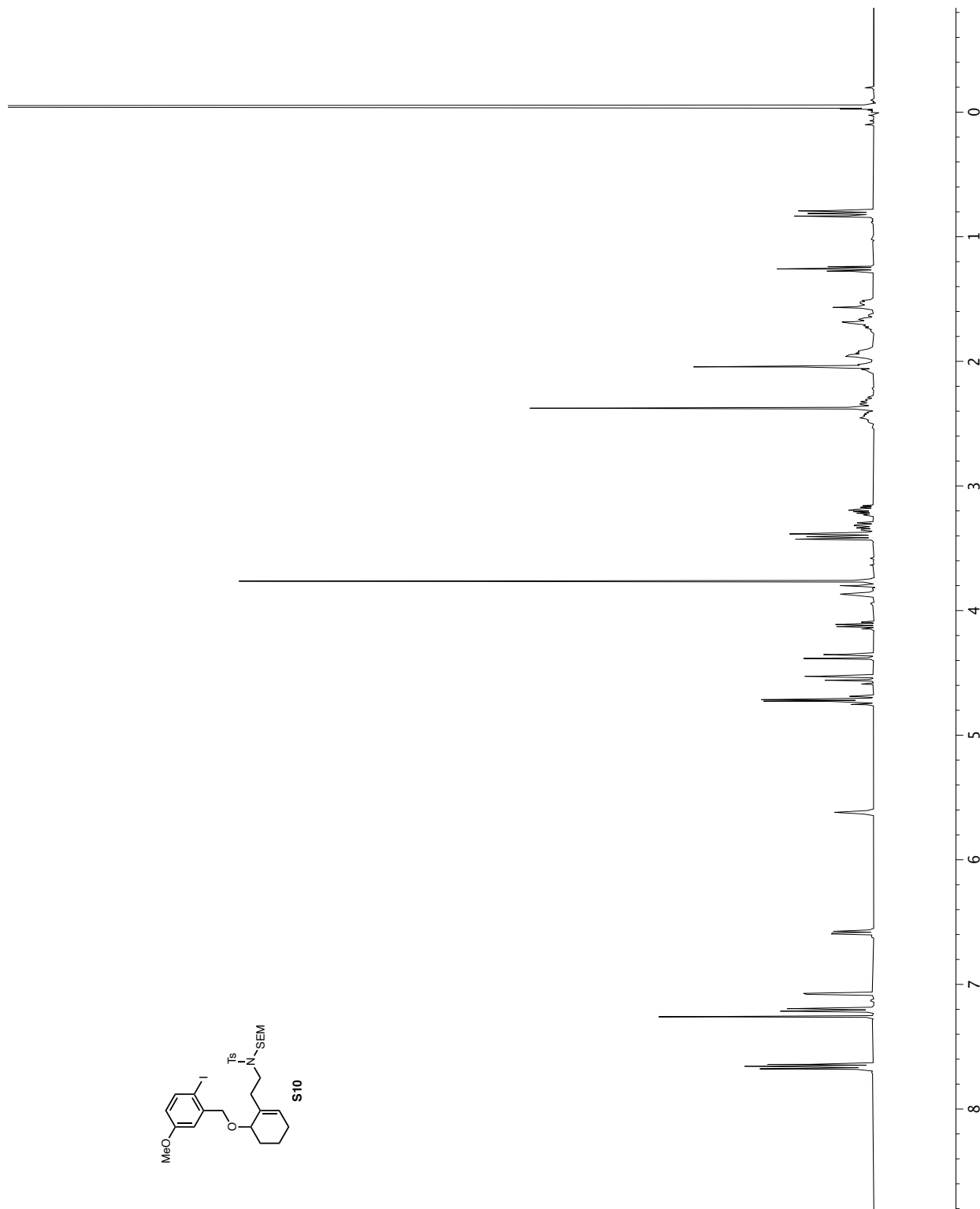
Figure A1.39 ^{1}H NMR (400 MHz, CDCl$_3$) of compound **S10.**

Figure A1.40 ^{13}C NMR (101 MHz, CDCl$_3$) of Compound **S10**.
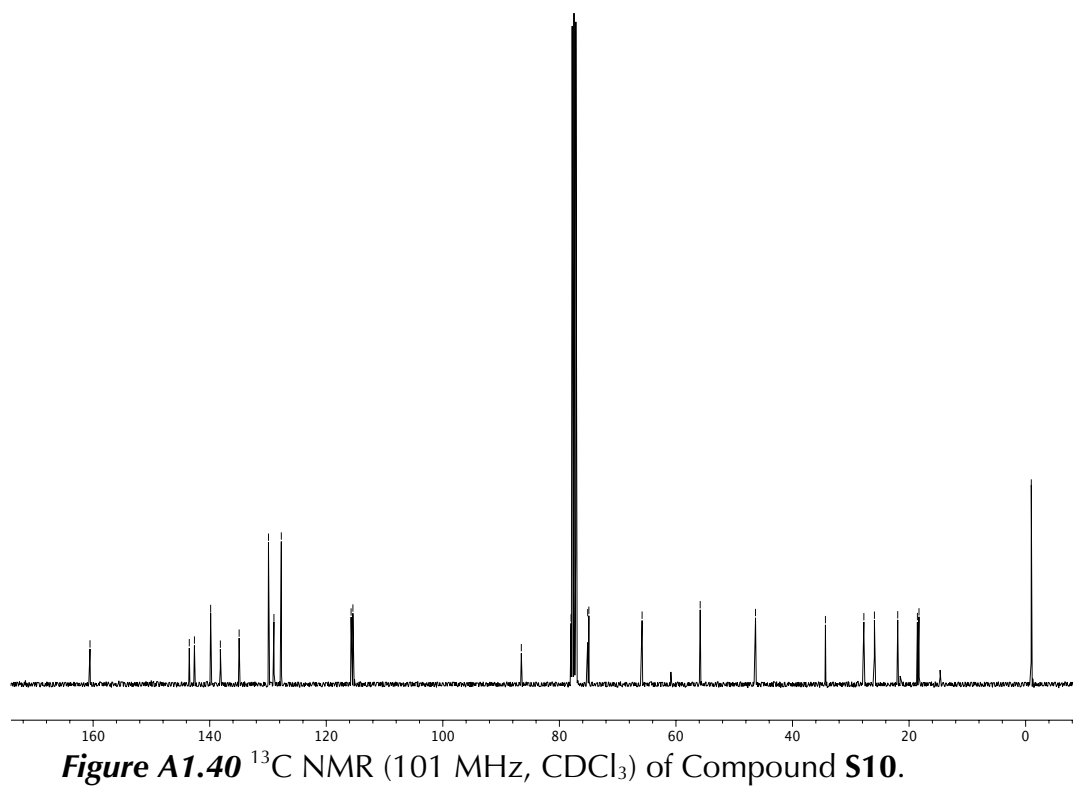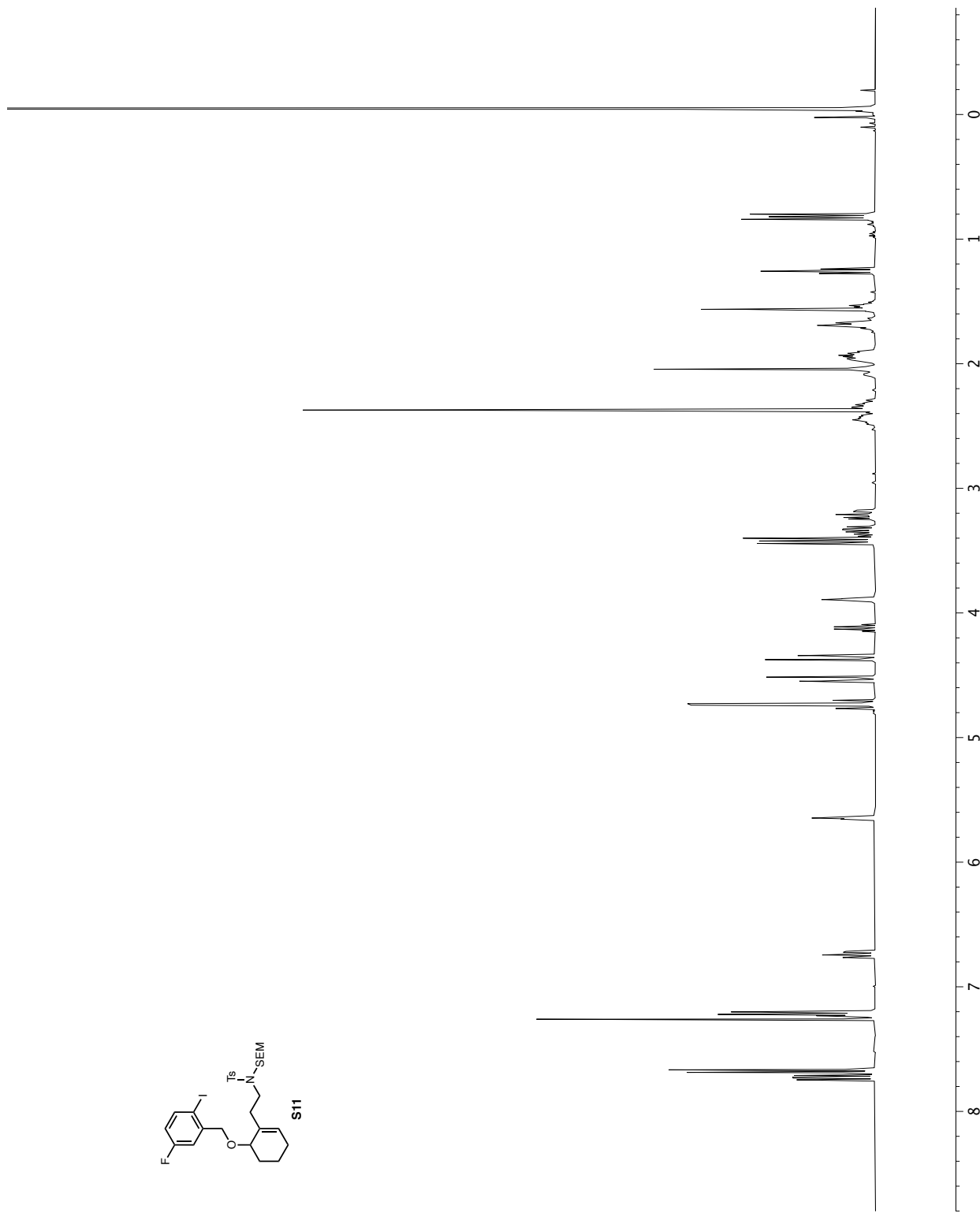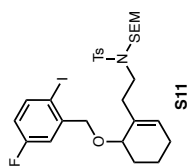
Figure A1.41 ^{1}H NMR (400 MHz, CDCl$_3$) of compound **S11.**

−115.9 −116.0 −116.1 −116.2 −116.3 −116.4 −116.5 −116.6 −116.7 −116.8 −116.9 −117.0 −117.1 −117.2 −117.3 −117.4 −117.5
ppm
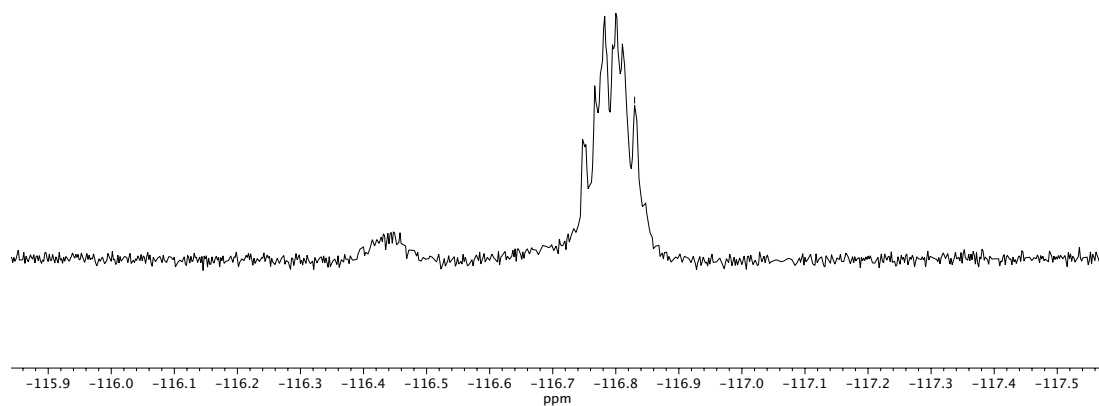
Figure A1.42 ^{19}F NMR (282 MHz, CDCl$_3$) of Compound **S11**.

160   140   120   100   80   60   40   20   0
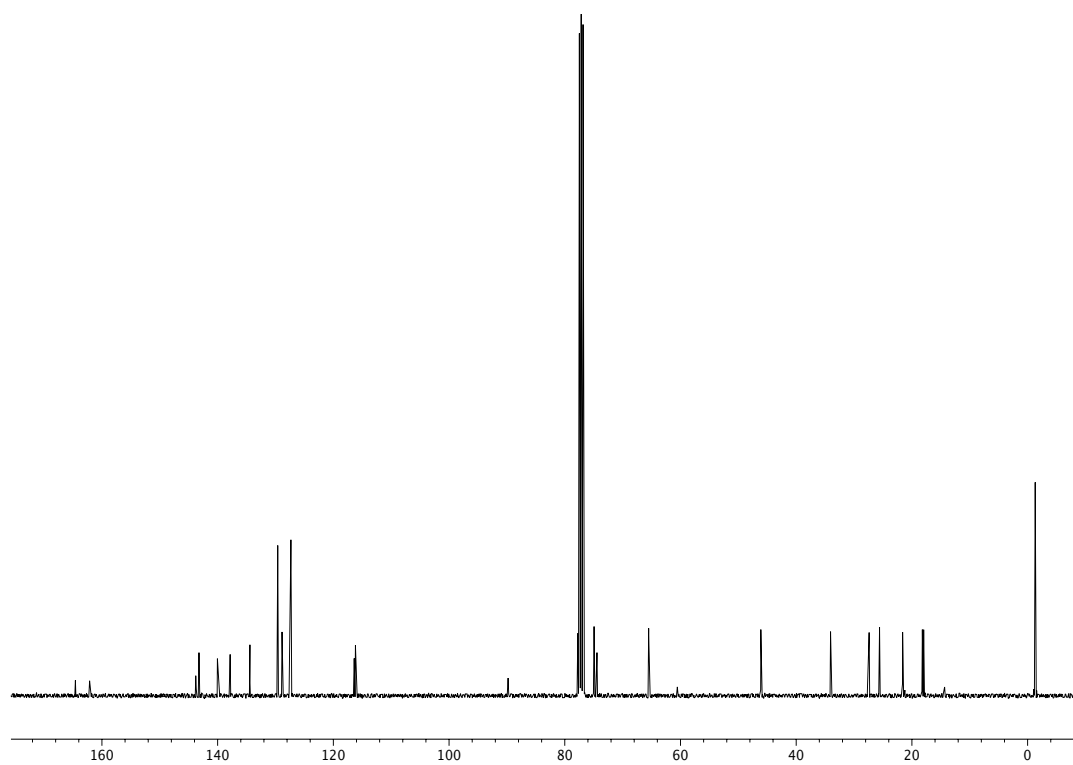
Figure A1.43 ^{13}C NMR (101 MHz, CDCl$_3$) of Compound **S11**.
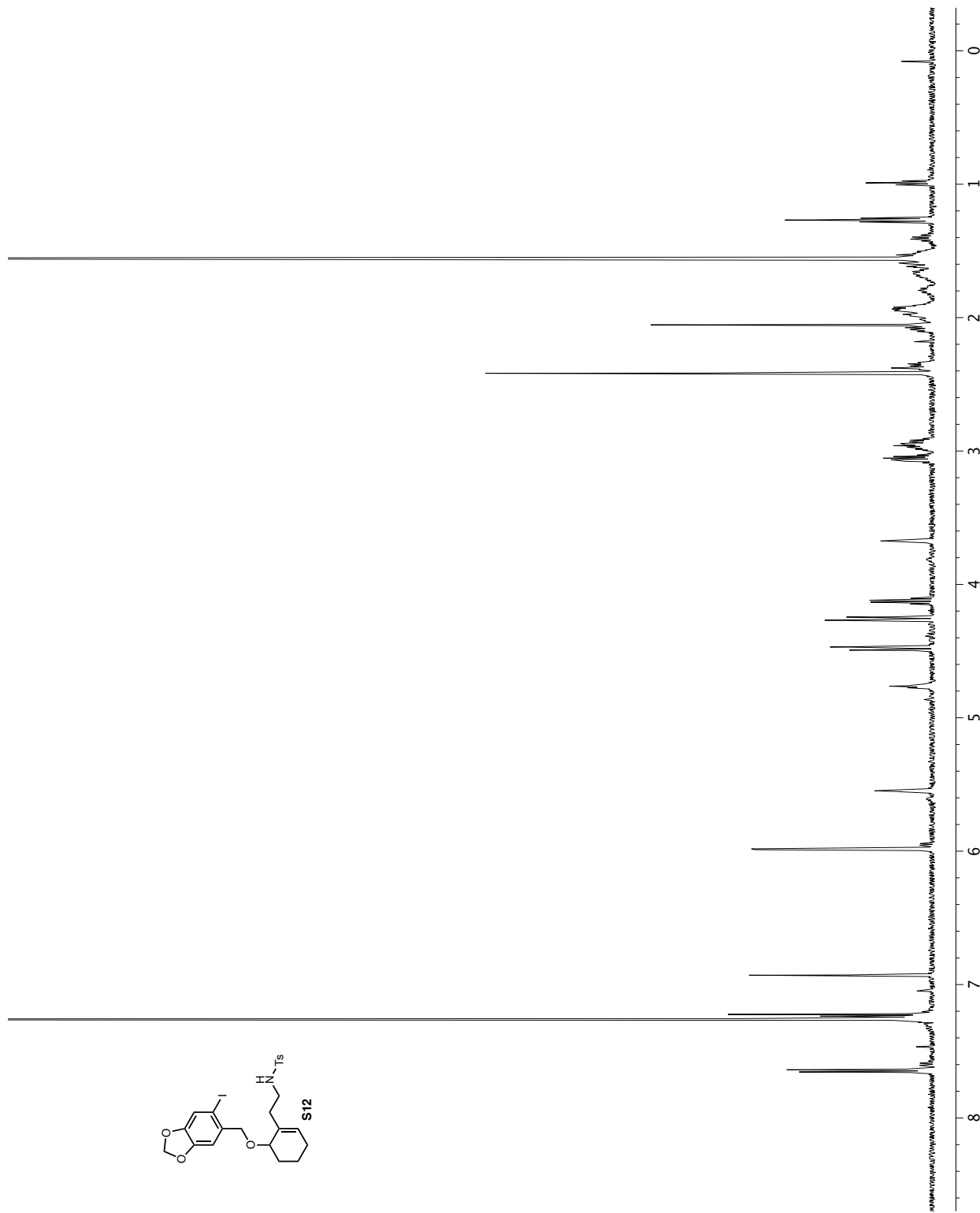
Figure A1.44 ^{1}H NMR (500 MHz, CDCl$_3$) of compound **S12**.
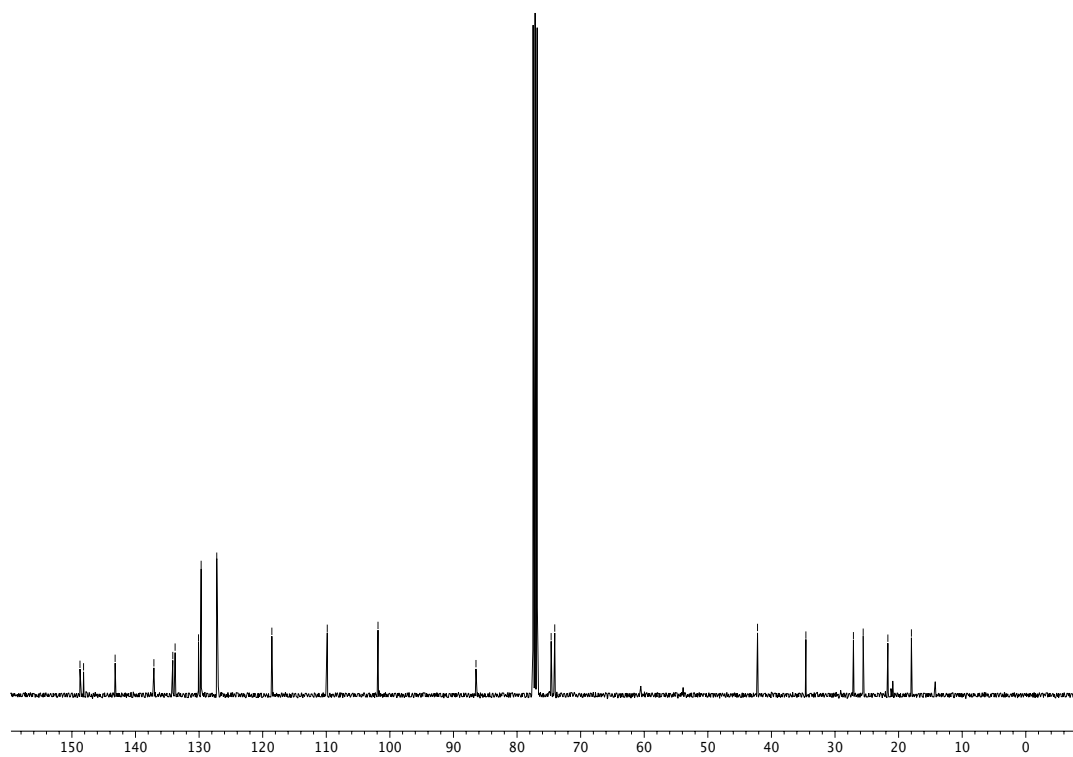
Figure A1.45 ^{13}C NMR (101 MHz, CDCl$_3$) of Compound **S12**.

Figure A1.46 ^{1}H NMR (400 MHz, CDCl$_3$) of compound **S13.**
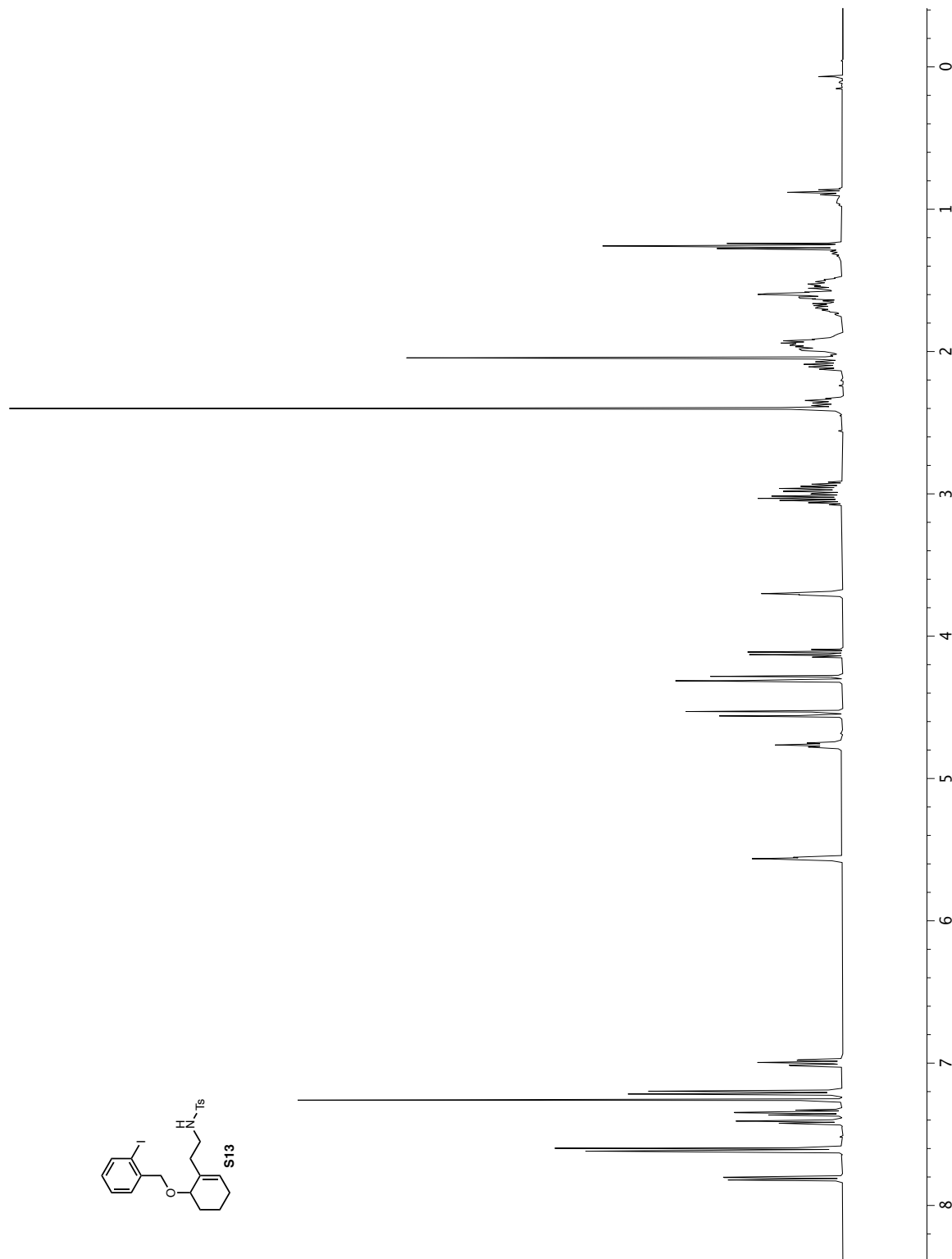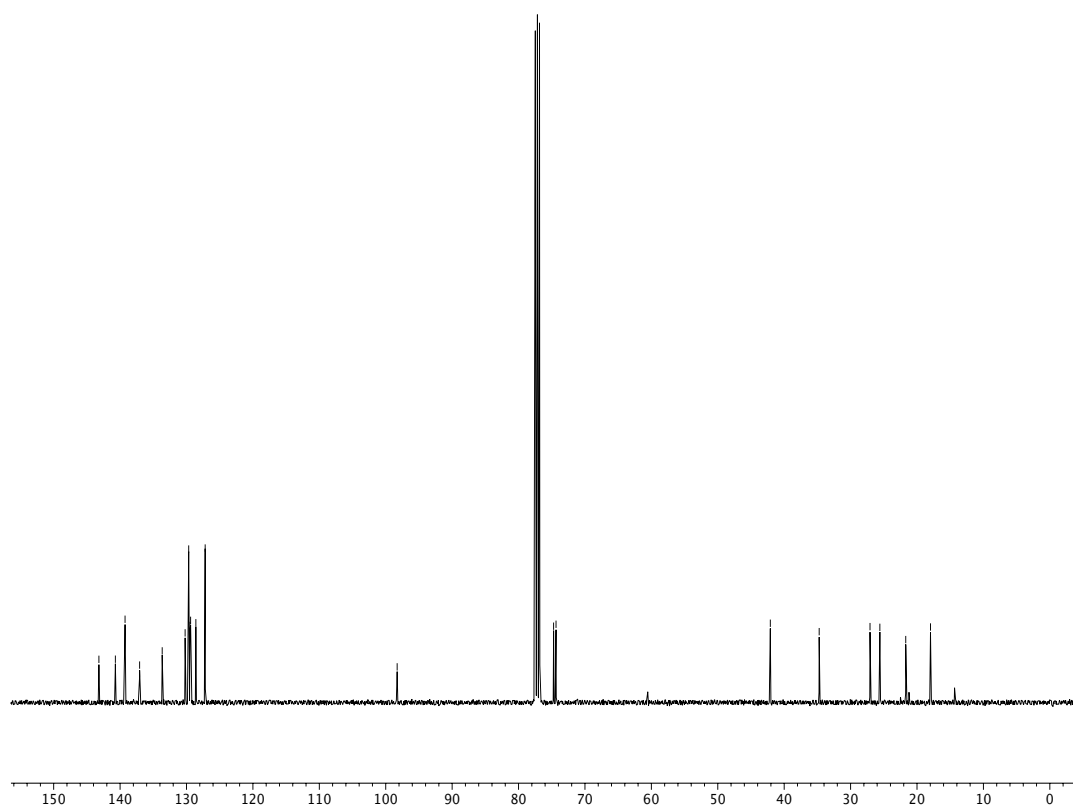
Figure A1.47 ^{13}C NMR (101 MHz, CDCl$_3$) of Compound **S13**.

Figure A1.48 ^{1}H NMR (400 MHz, CDCl$_3$) of compound **S14.**
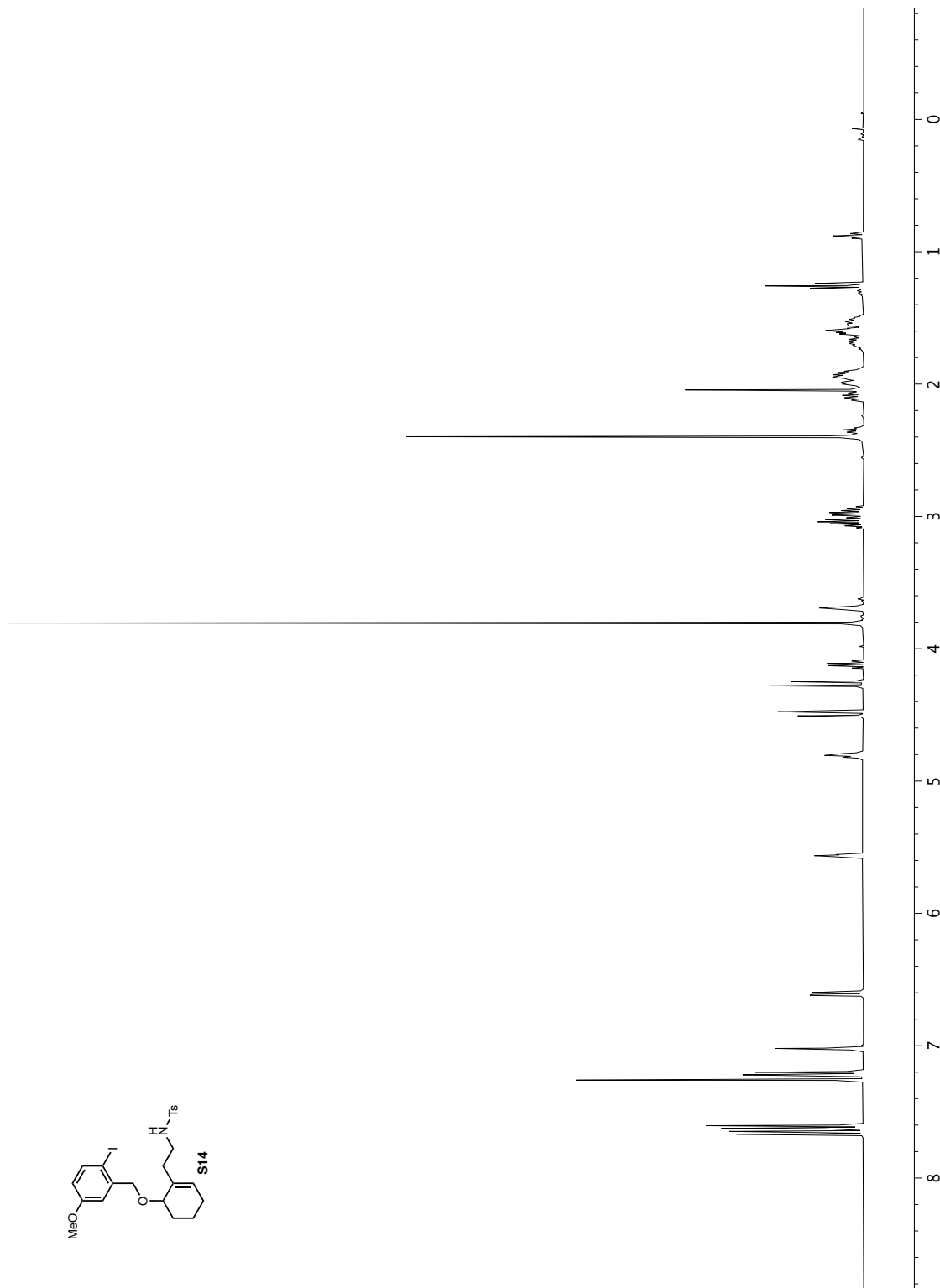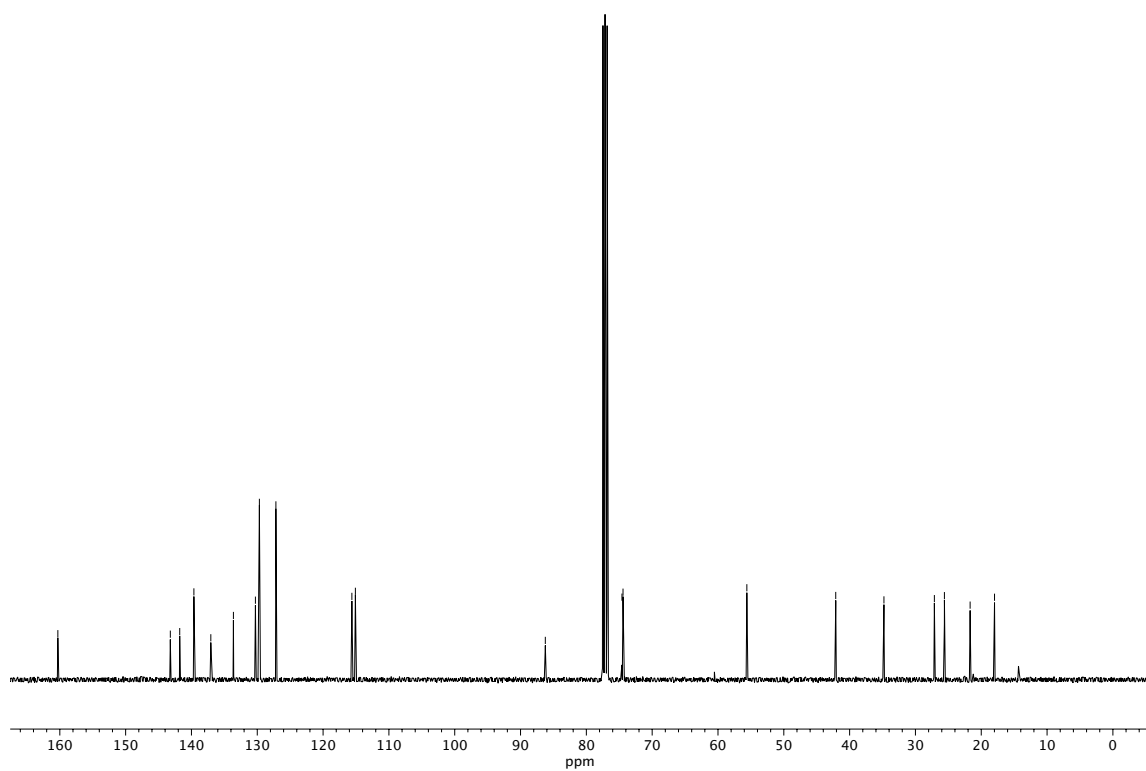
Figure A1.49 ^{13}C NMR (101 MHz, CDCl$_3$) of Compound **S14**.

Figure A1.50 ^{1}H NMR (400 MHz, CDCl$_3$) of compound **S15.**
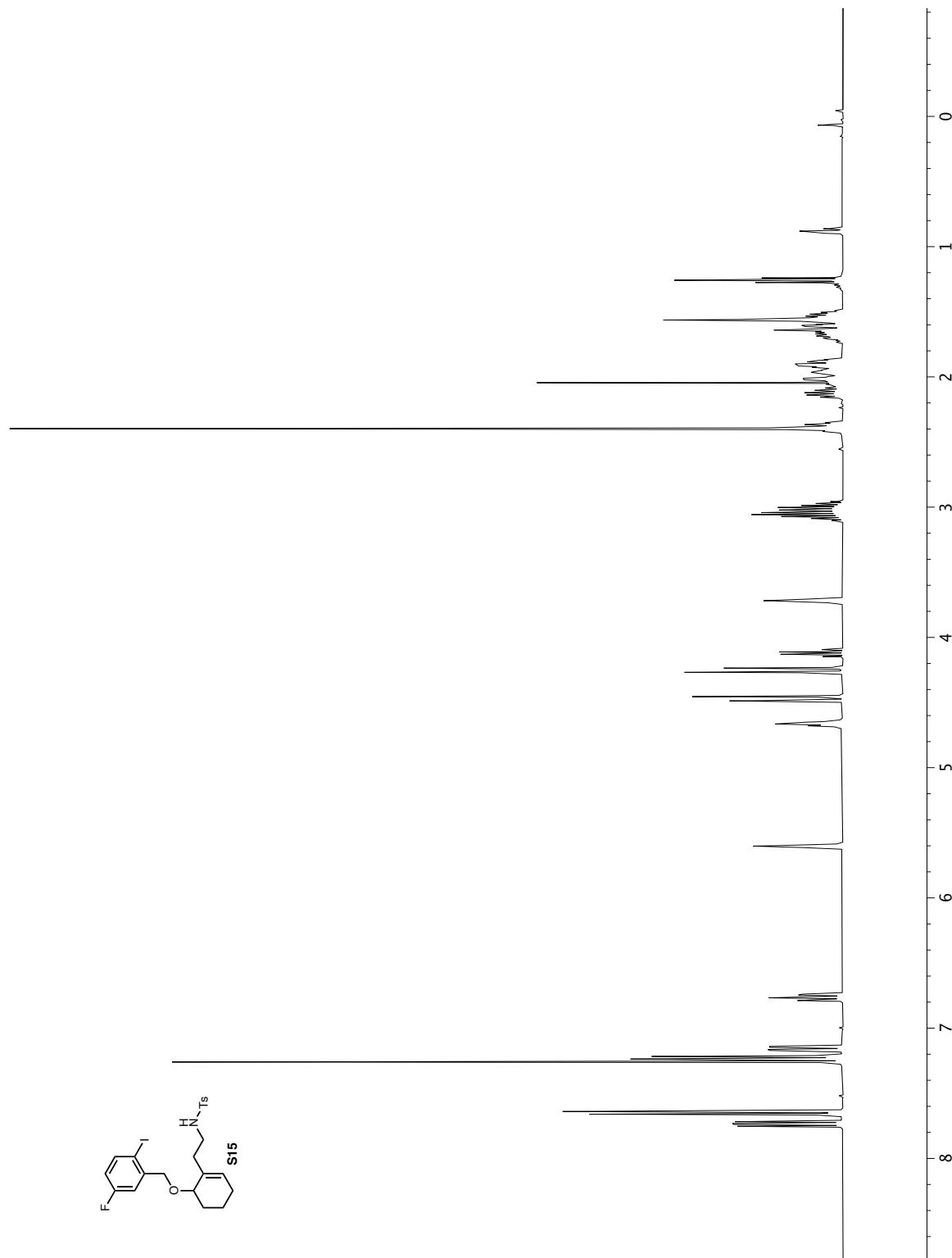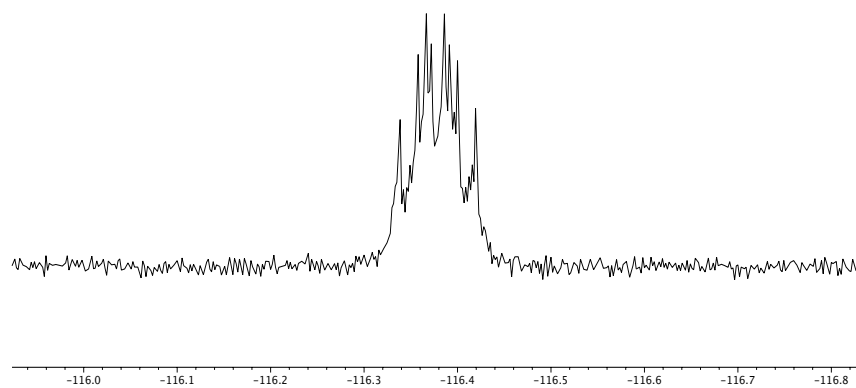
Figure A1.51 ^{19}F NMR (282 MHz, CDCl$_3$) of Compound **S15**.
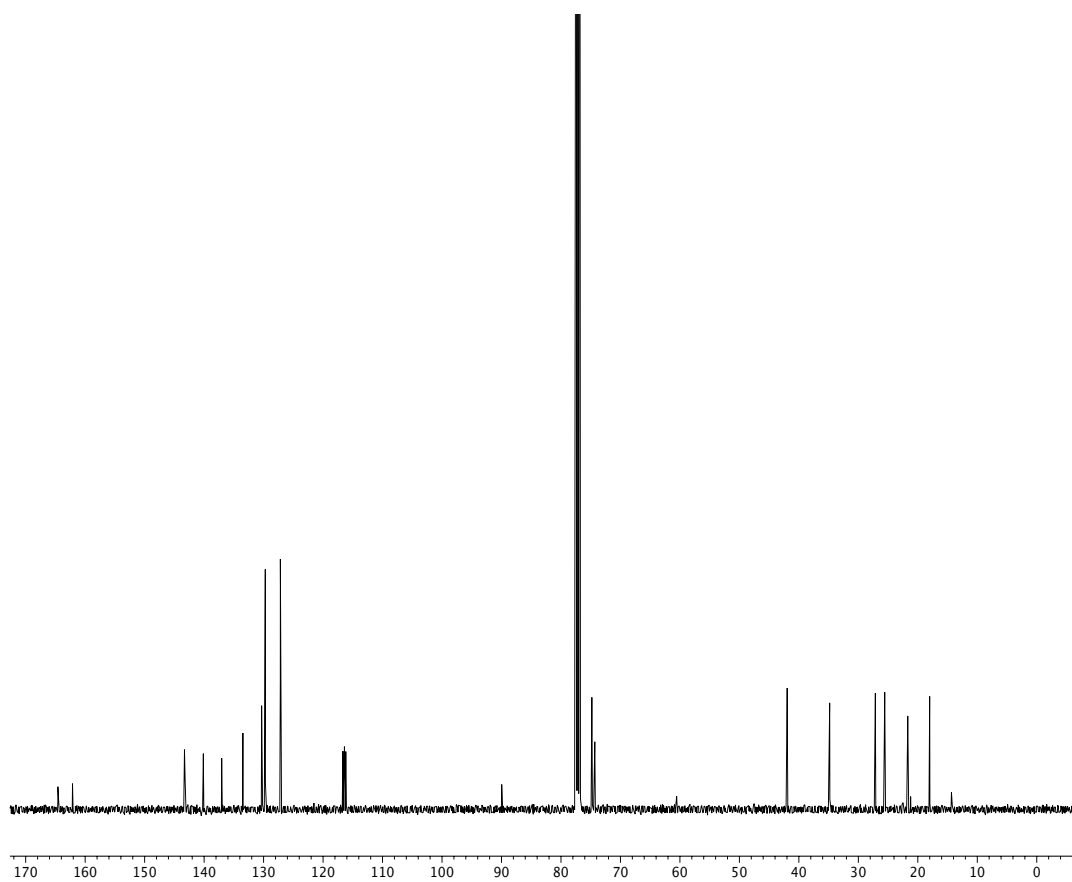
Figure A1.52 ^{13}C NMR (101 MHz, CDCl$_3$) of Compound **S15**.
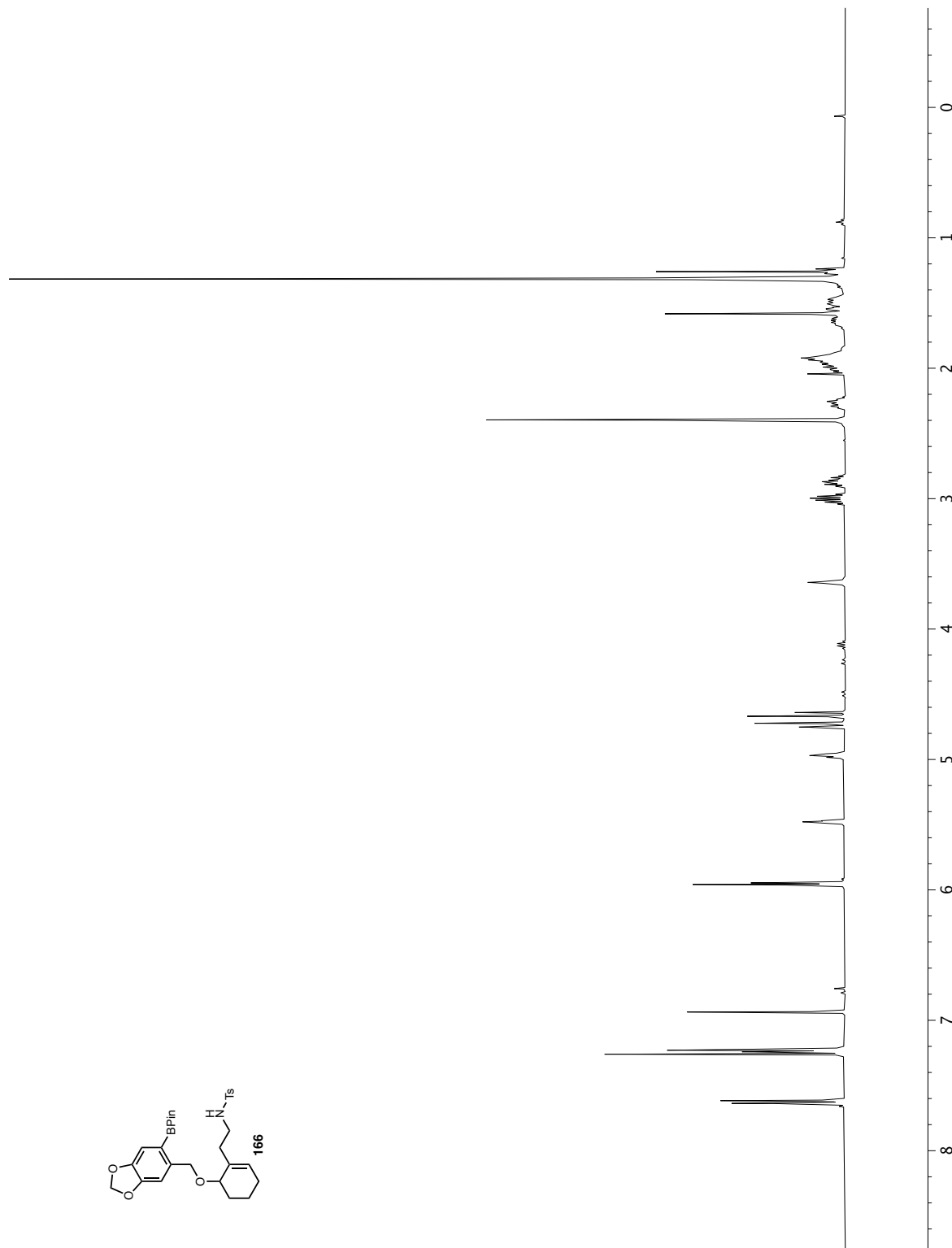
Figure A1.53 ^{1}H NMR (400 MHz, CDCl$_3$) of compound **166.**
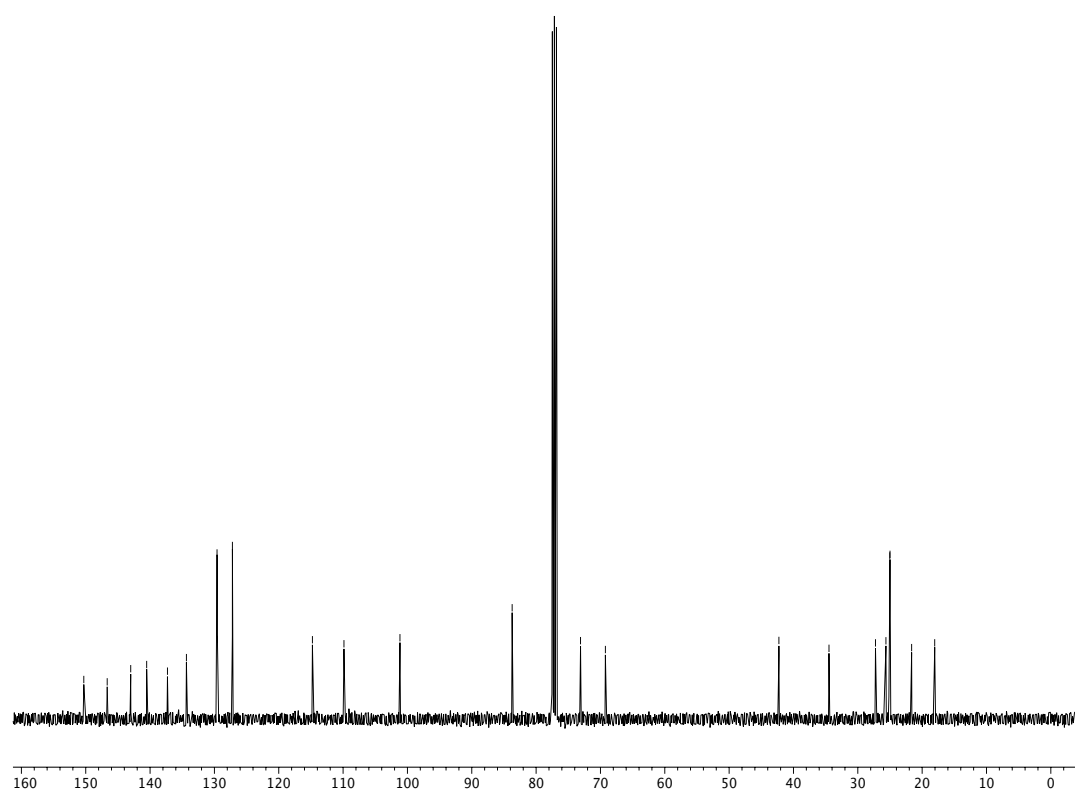
Figure A1.54 ^{13}C NMR (101 MHz, CDCl$_3$) of Compound **166**.

Figure A1.55 ^{1}H NMR (400 MHz, CDCl$_3$) of compound **174a.**

Figure A1.56 ^{13}C NMR (101 MHz, CDCl$_3$) of Compound **174a**.

Figure A1.57 ^{1}H NMR (400 MHz, CDCl$_3$) of compound **174b.**

Figure A1.58 ^{13}C NMR (101 MHz, CDCl$_3$) of Compound **174b**.
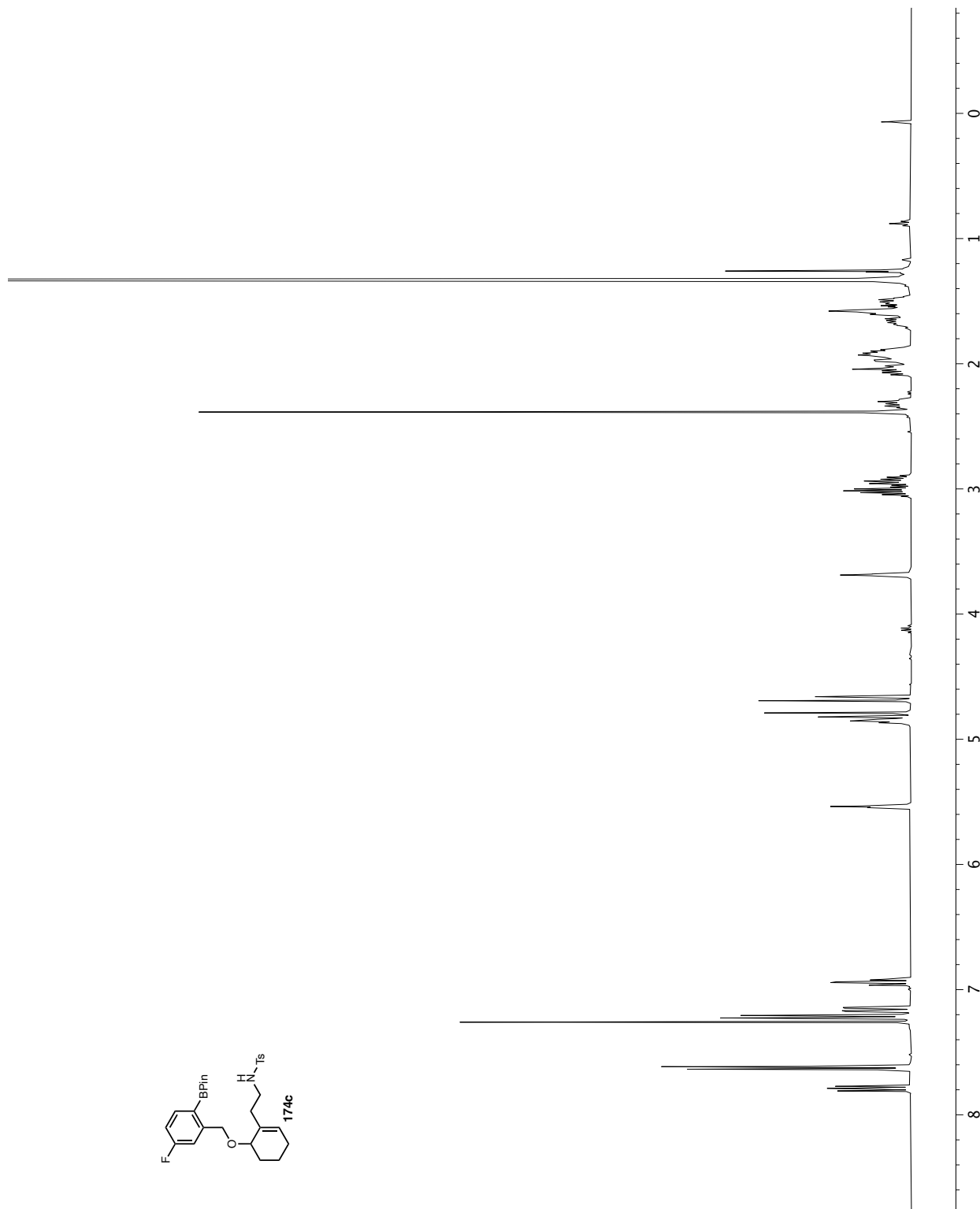
Figure A1.59 [^1]H NMR (400 MHz, CDCl$_3$) of compound **174c.**
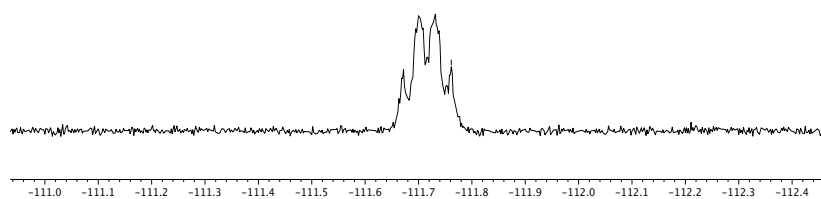
Figure A1.60 ^{19}F NMR (282 MHz, CDCl$_3$) of Compound **174c**.
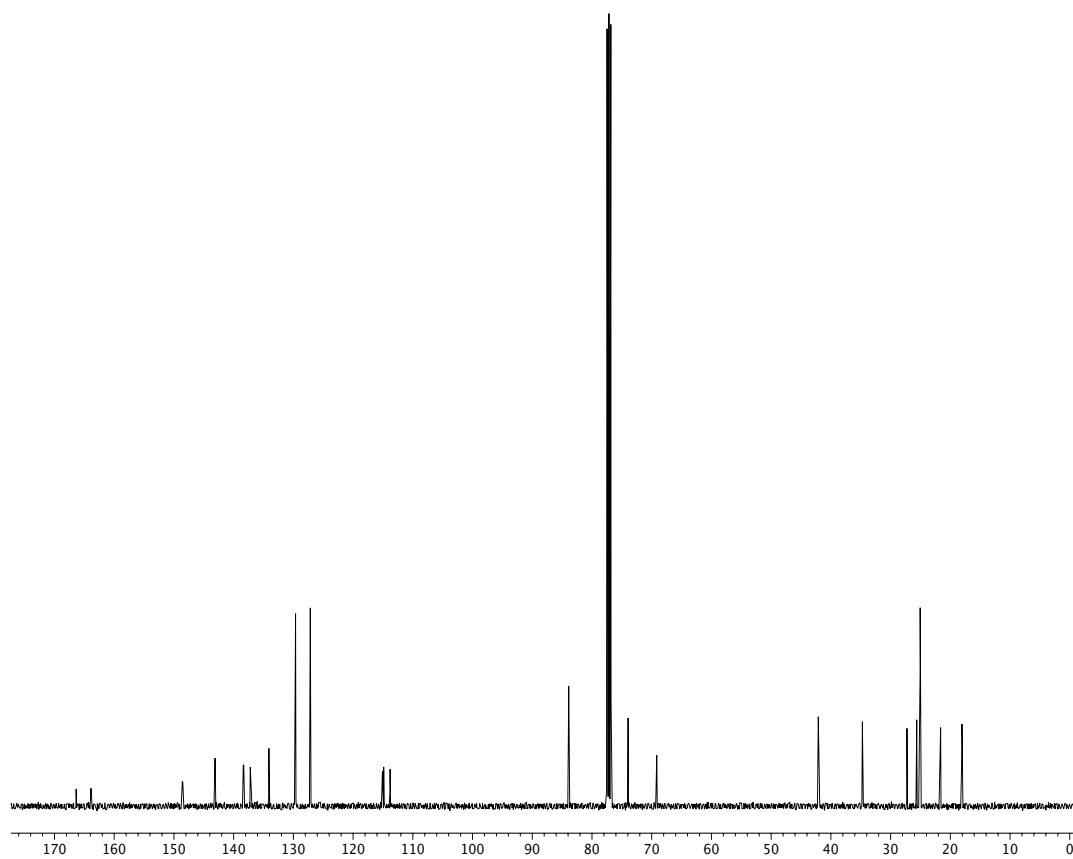
Figure A1.61 ^{13}C NMR (101 MHz, CDCl$_3$) of Compound **174c**.

Figure A1.62 ^{1}H NMR (400 MHz, CDCl$_3$) of compound **165.**

Figure A1.63 ¹³C NMR (101 MHz, CDCl₃) of Compound **165**.
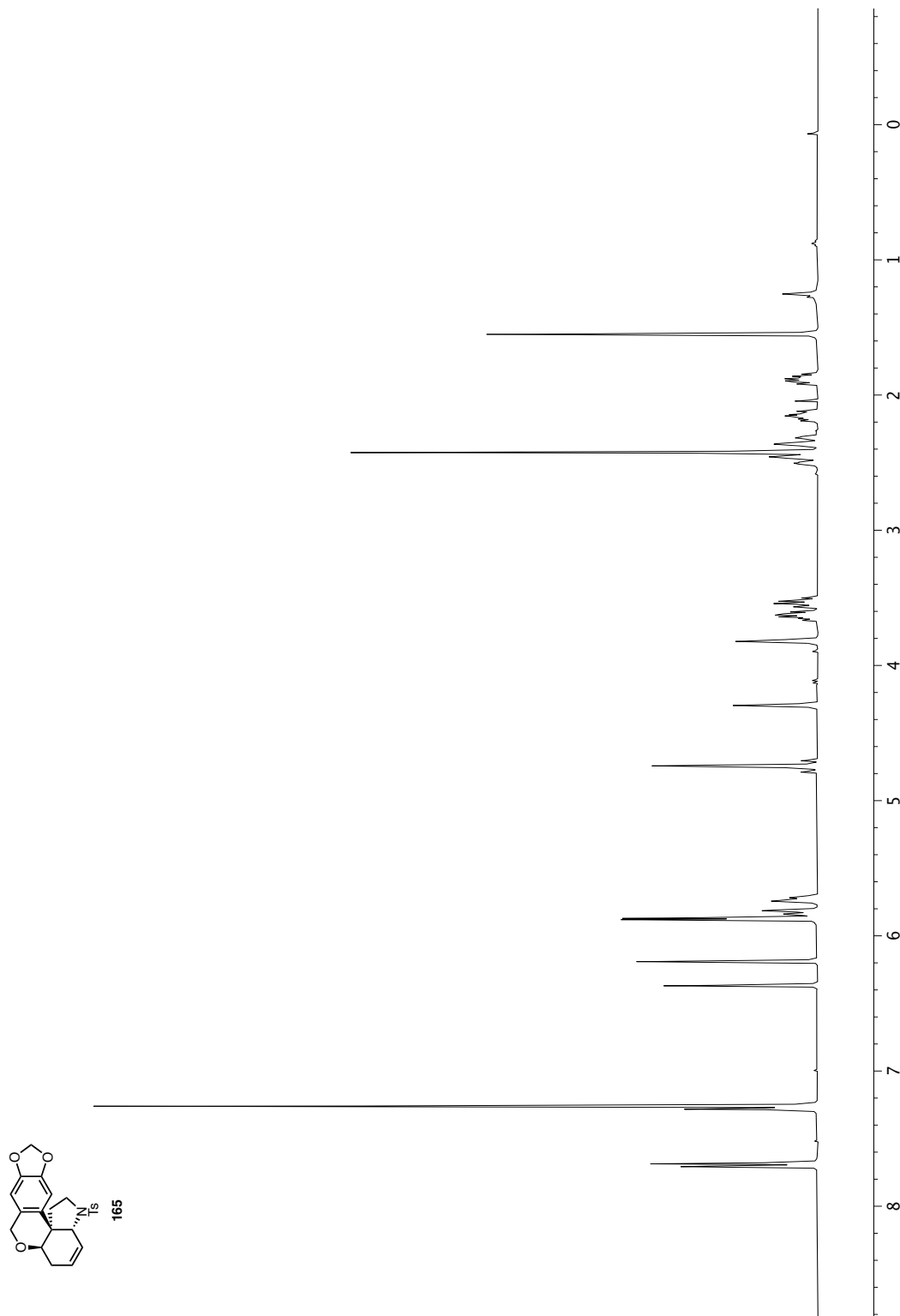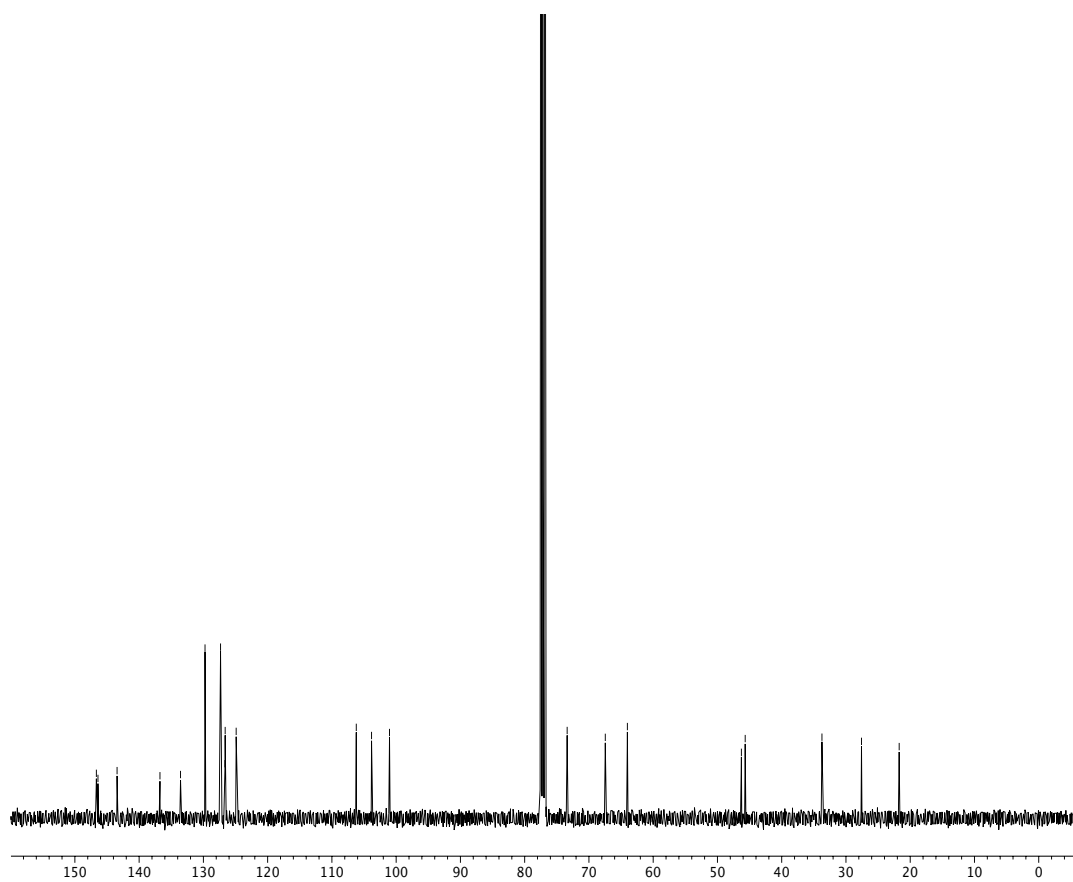
Figure A1.63 ^{13}C NMR (101 MHz, CDCl$_3$) of Compound **165**.
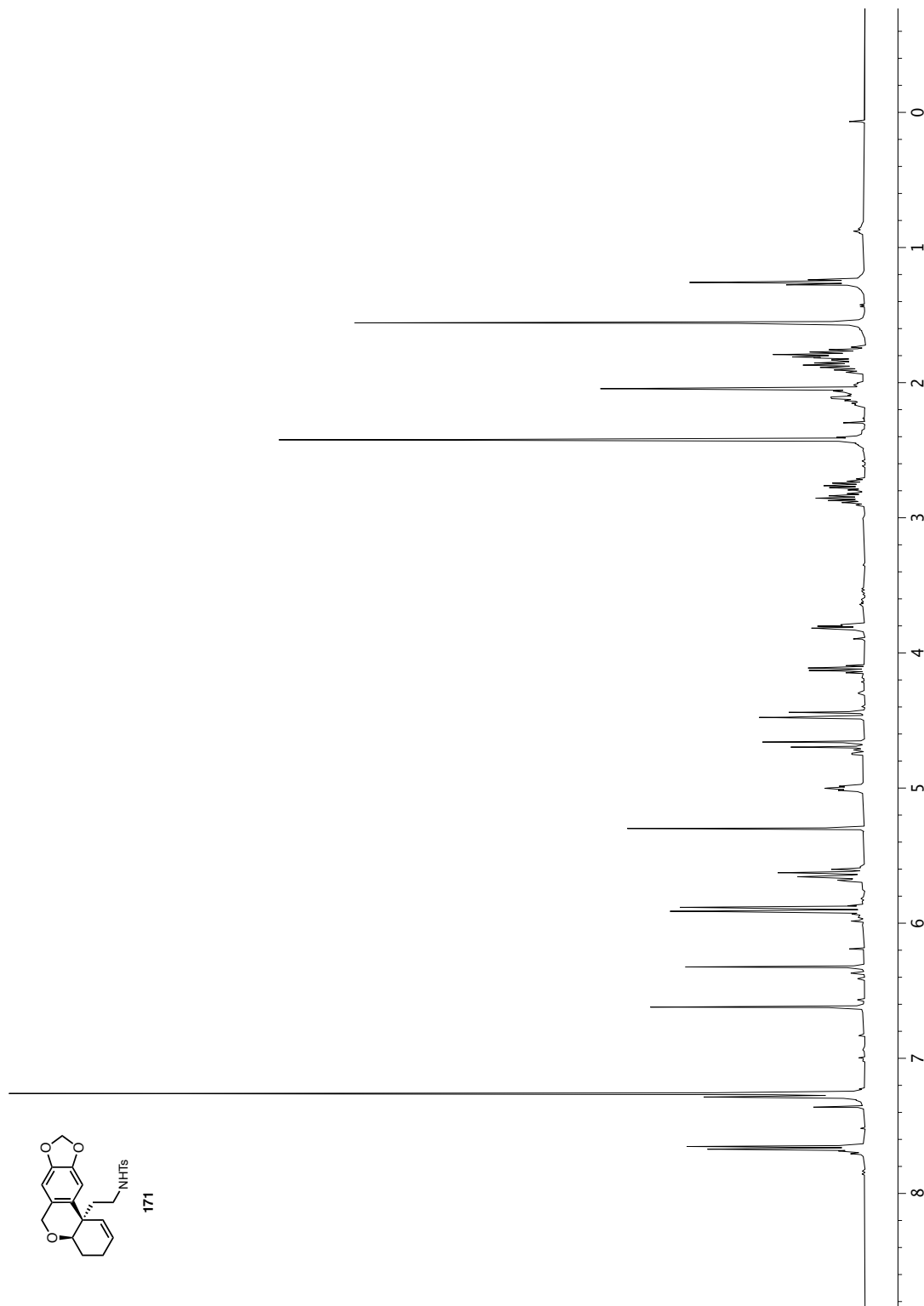
Figure A1.64 ^{1}H NMR (400 MHz, CDCl$_3$) of compound **171**.
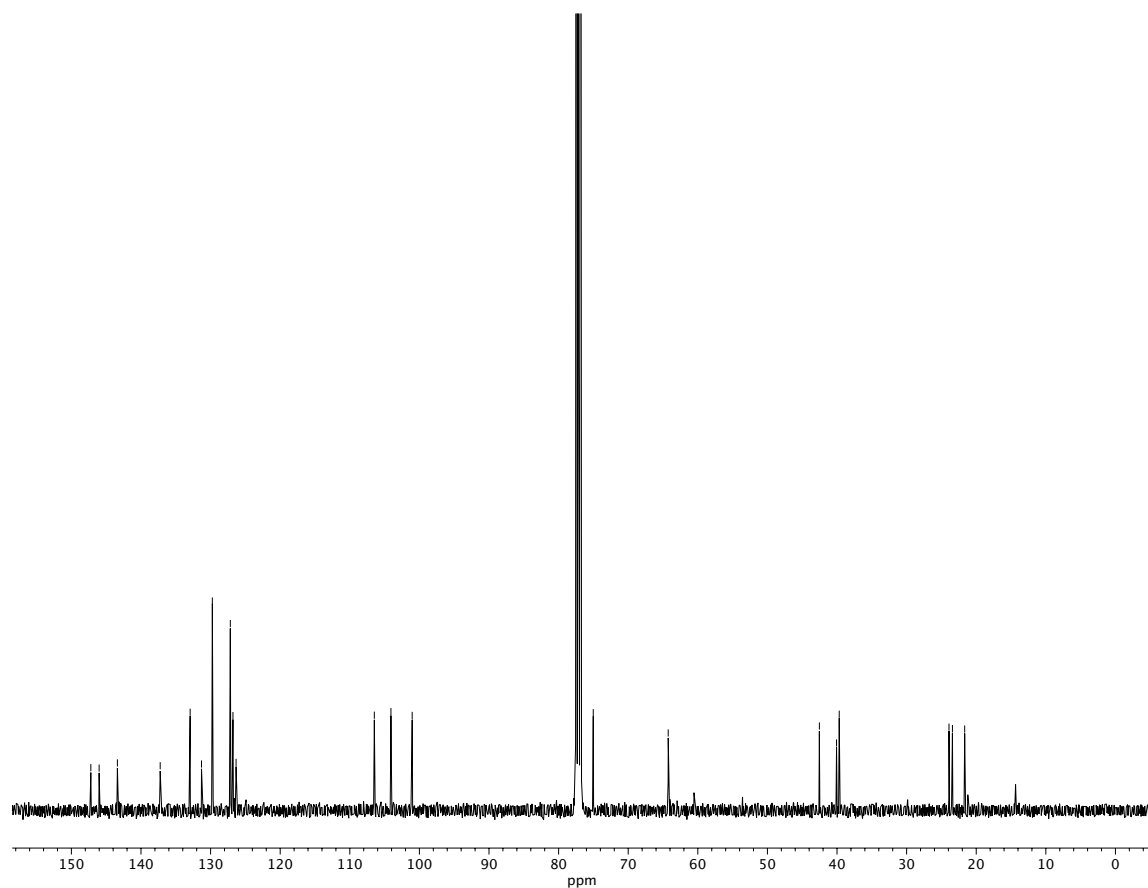
Figure A1.65 ^{13}C NMR (101 MHz, CDCl[3]) of Compound **171**.
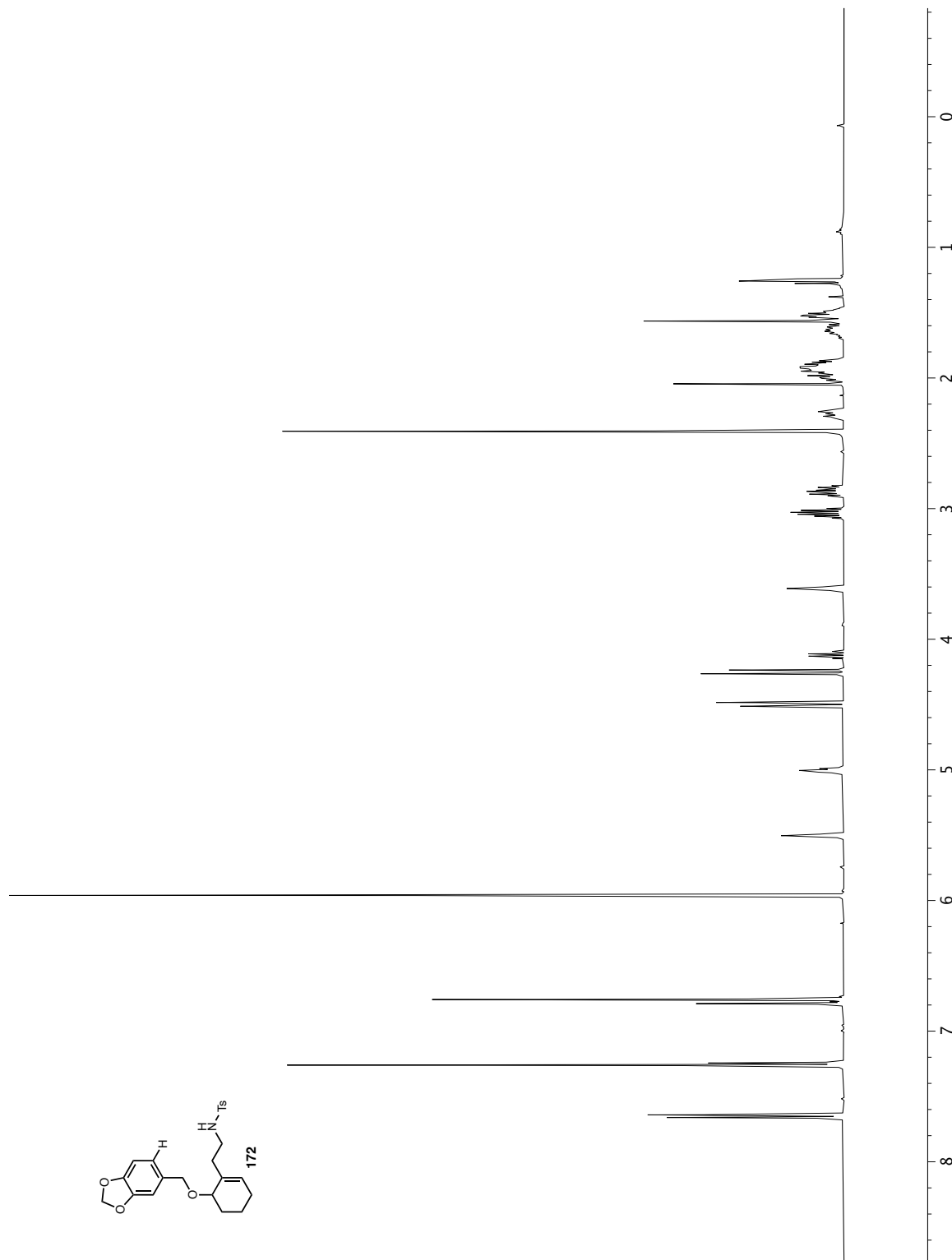
Figure A1.66 ^{1}H NMR (400 MHz, CDCl$_3$) of compound **172**.
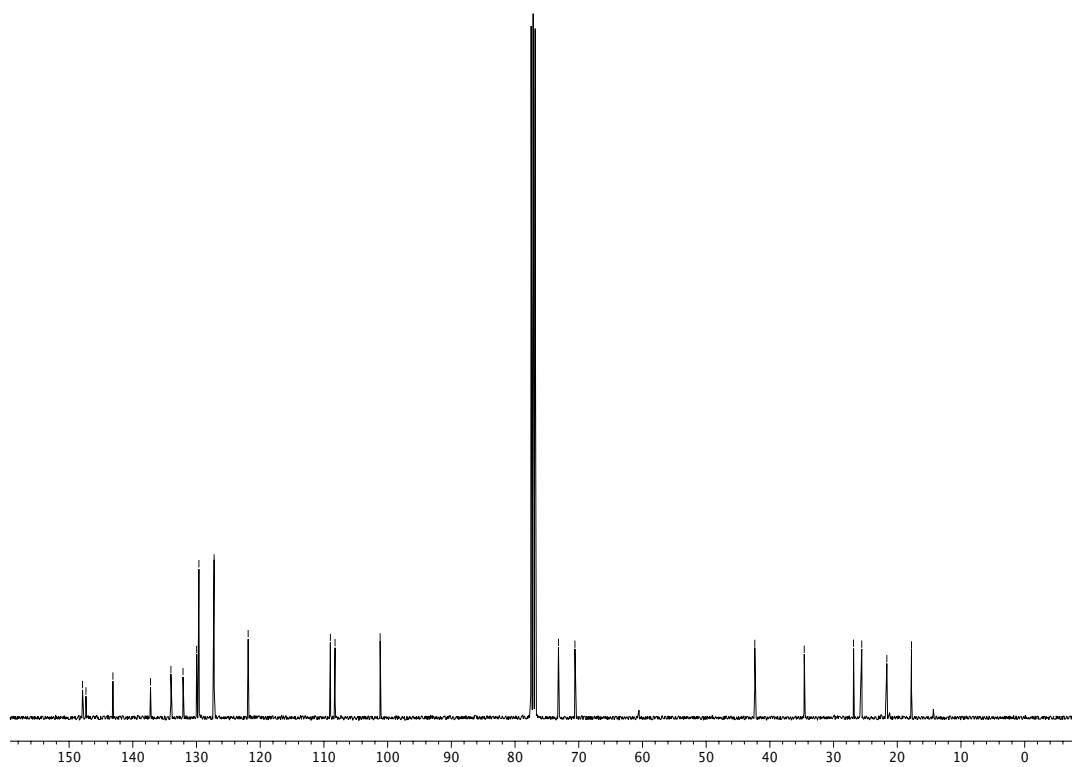
Figure A1.67 ^{13}C NMR (101 MHz, CDCl$_3$) of Compound **172**.

Figure A1.68 ^{1}H NMR (400 MHz, CDCl$_3$) of compound **173.**
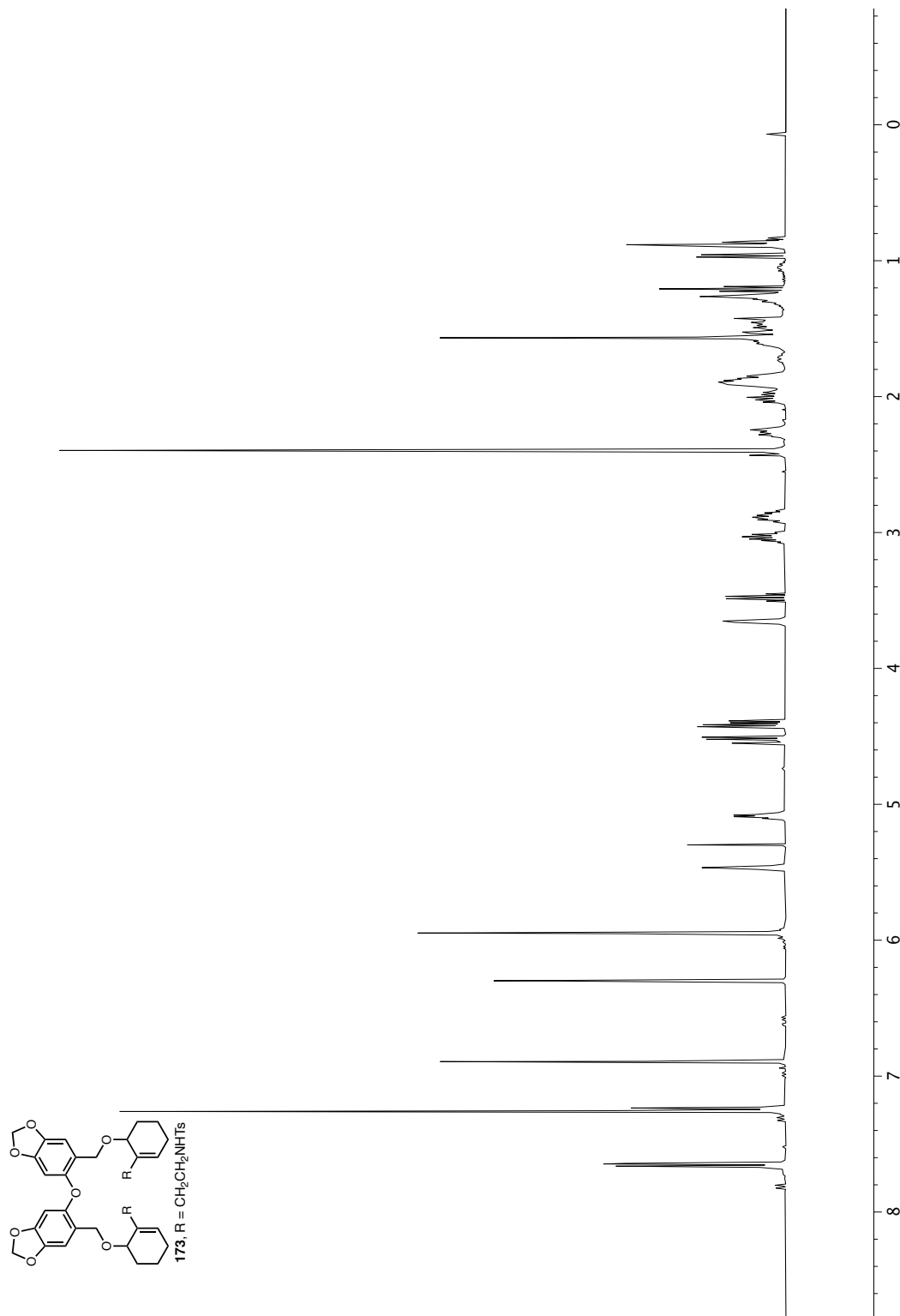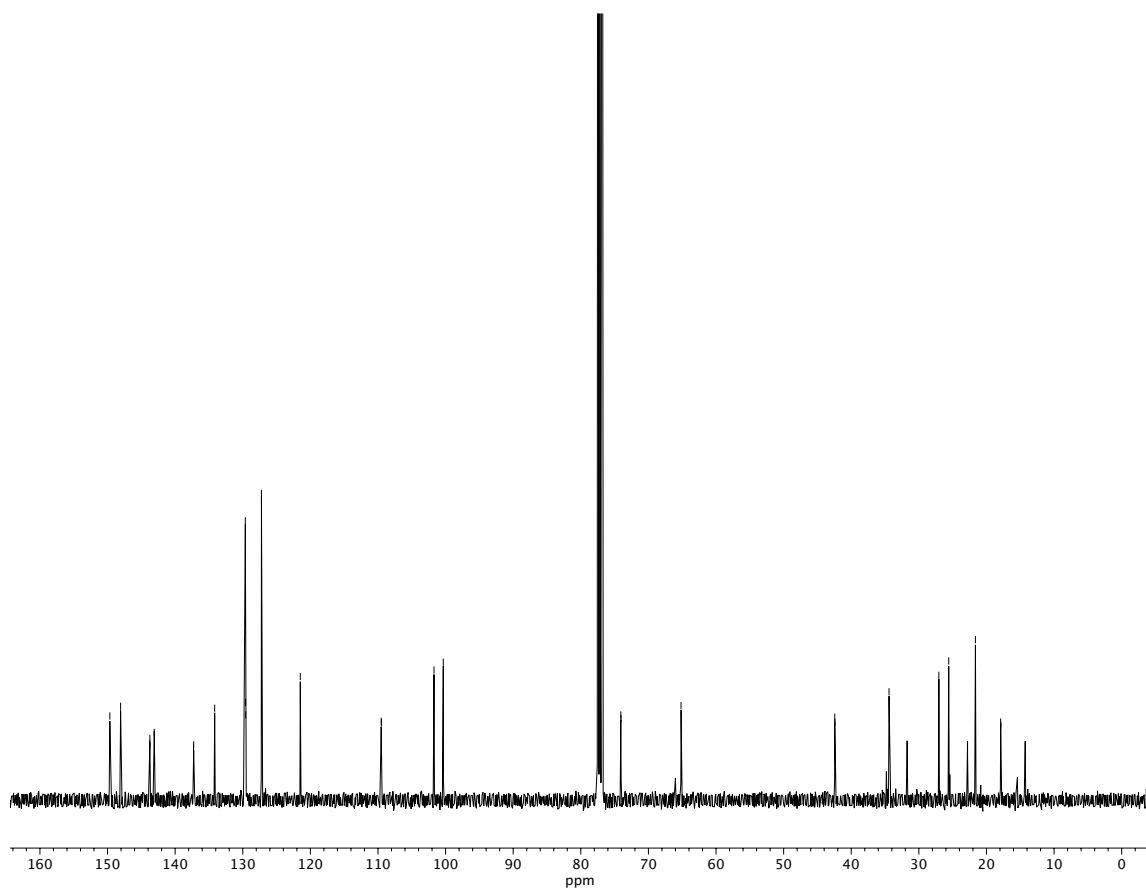
Figure A1.69 ^{13}C NMR (101 MHz, CDCl$_3$) of Compound **173**.

Figure A1.70 ^{1}H NMR (400 MHz, CDCl$_3$) of compound **175a.**
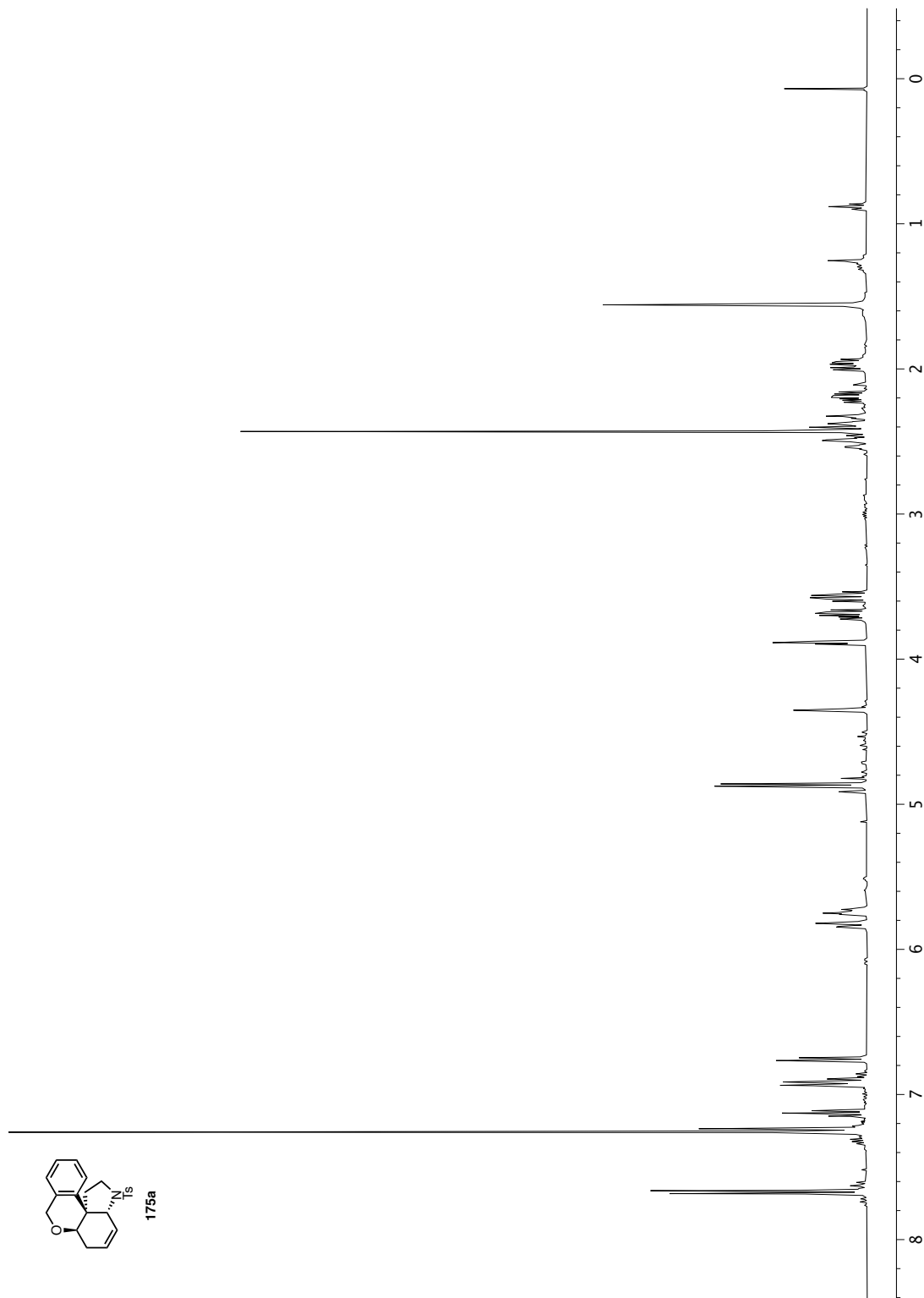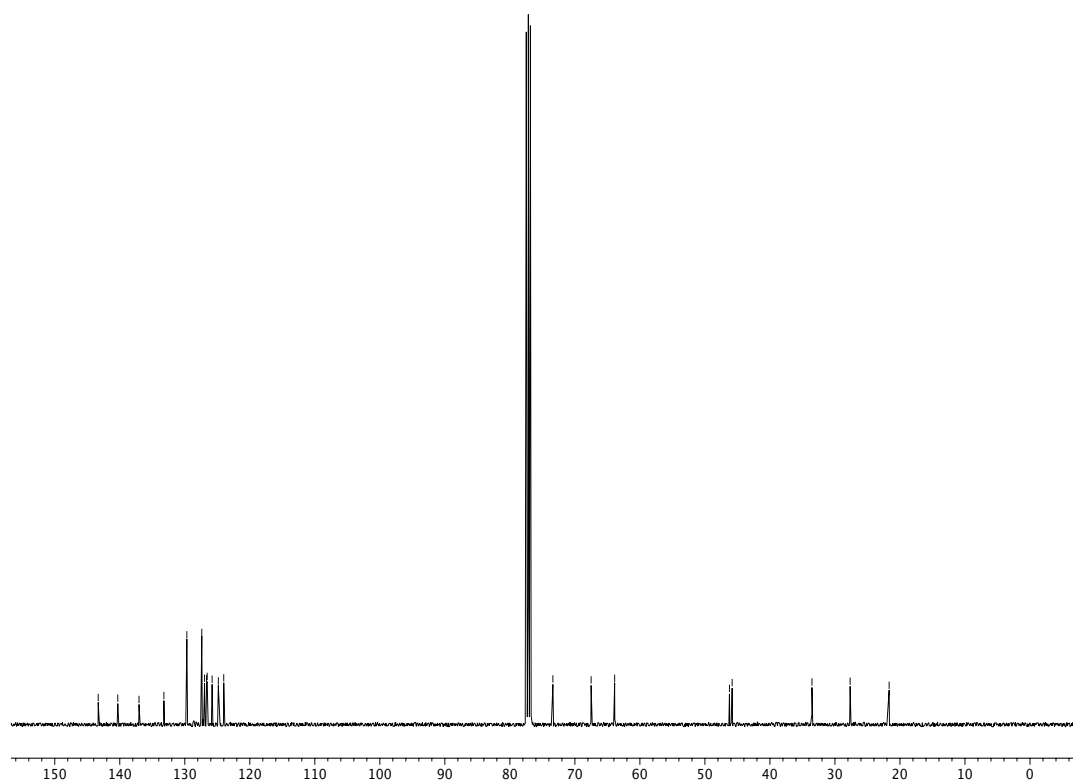
Figure A1.71 ^{13}C NMR (101 MHz, CDCl$_3$) of Compound **175a**.
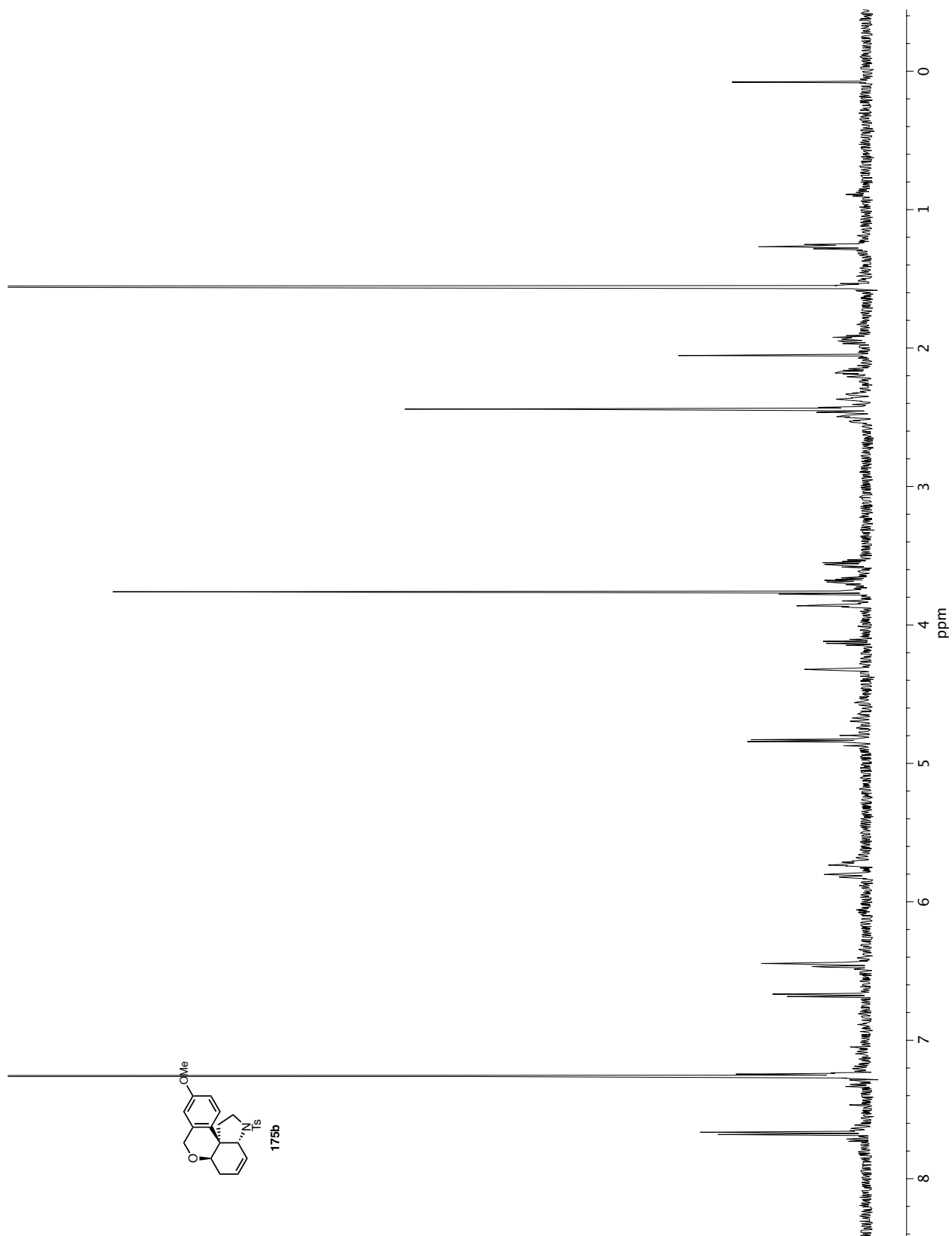
Figure A1.72 ^{1}H NMR (400 MHz, CDCl$_3$) of compound **175b.**
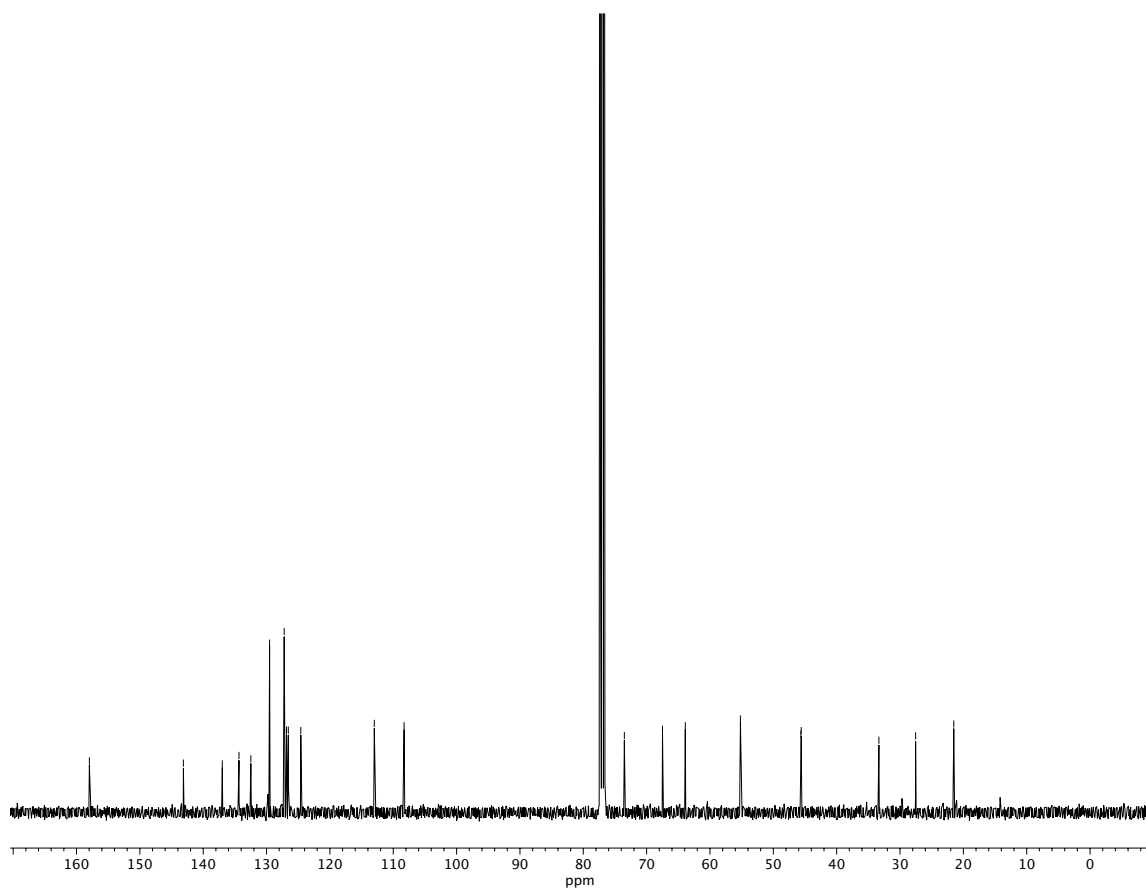
Figure A1.73 ^{13}C NMR (101 MHz, CDCl$_3$) of Compound **175b**.
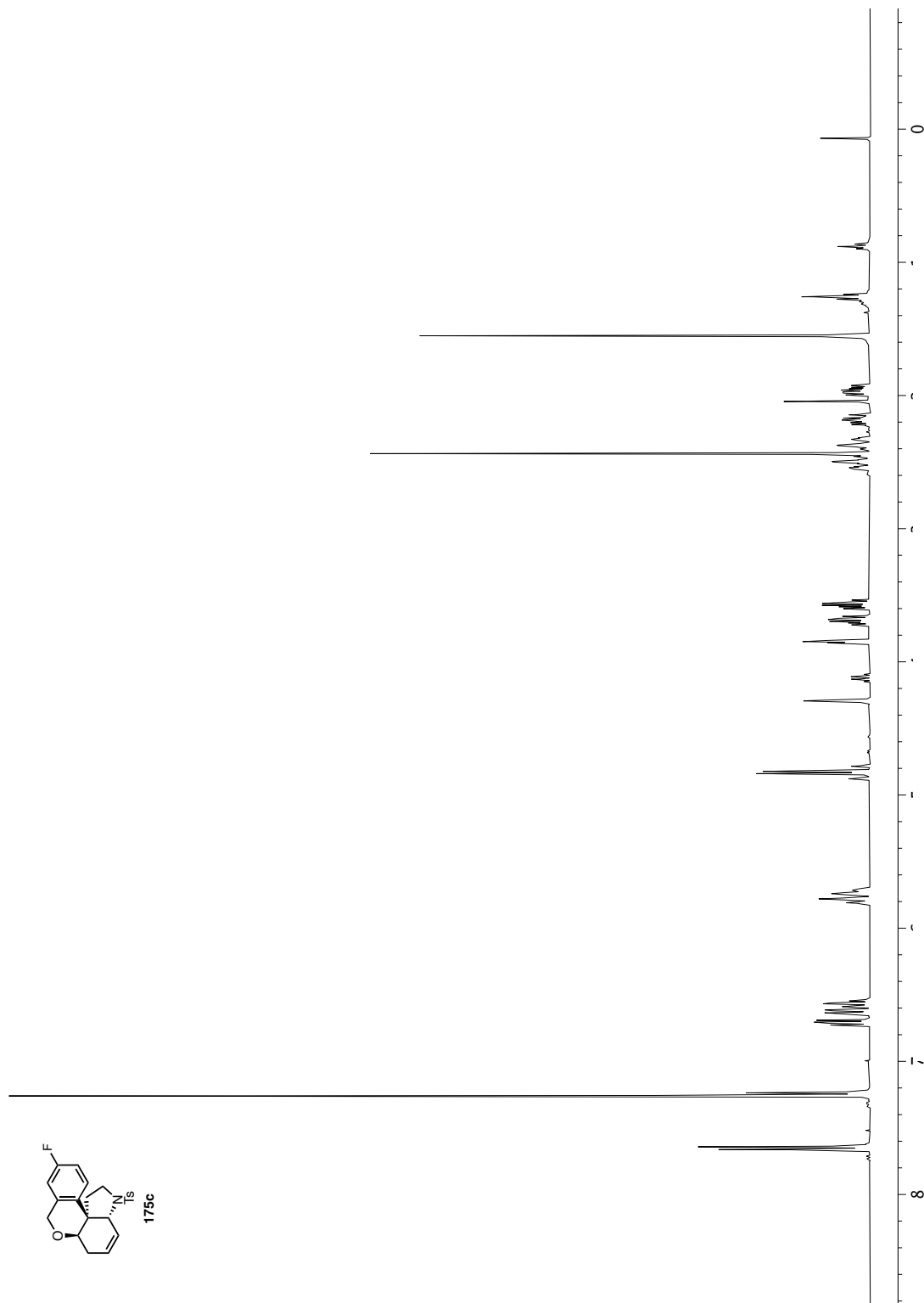
Figure A1.74 ¹H NMR (400 MHz, CDCl$_3$) of compound **175c.**
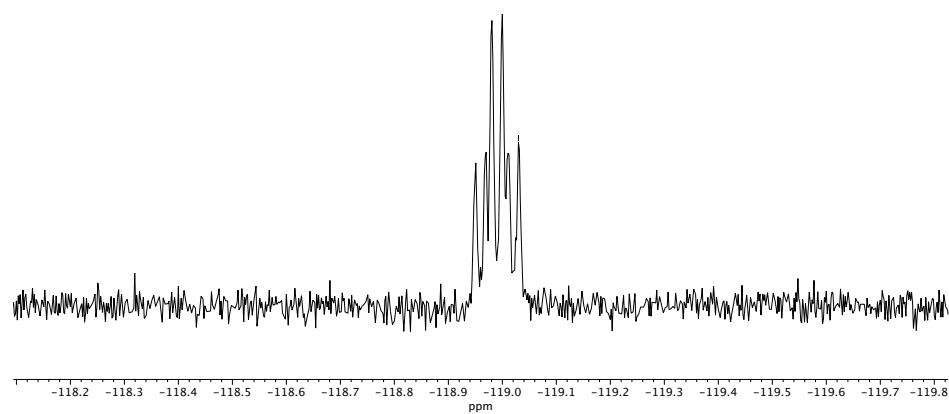
Figure A1.75 ^{19}F NMR (282 MHz, CDCl$_3$) of Compound **175c**.
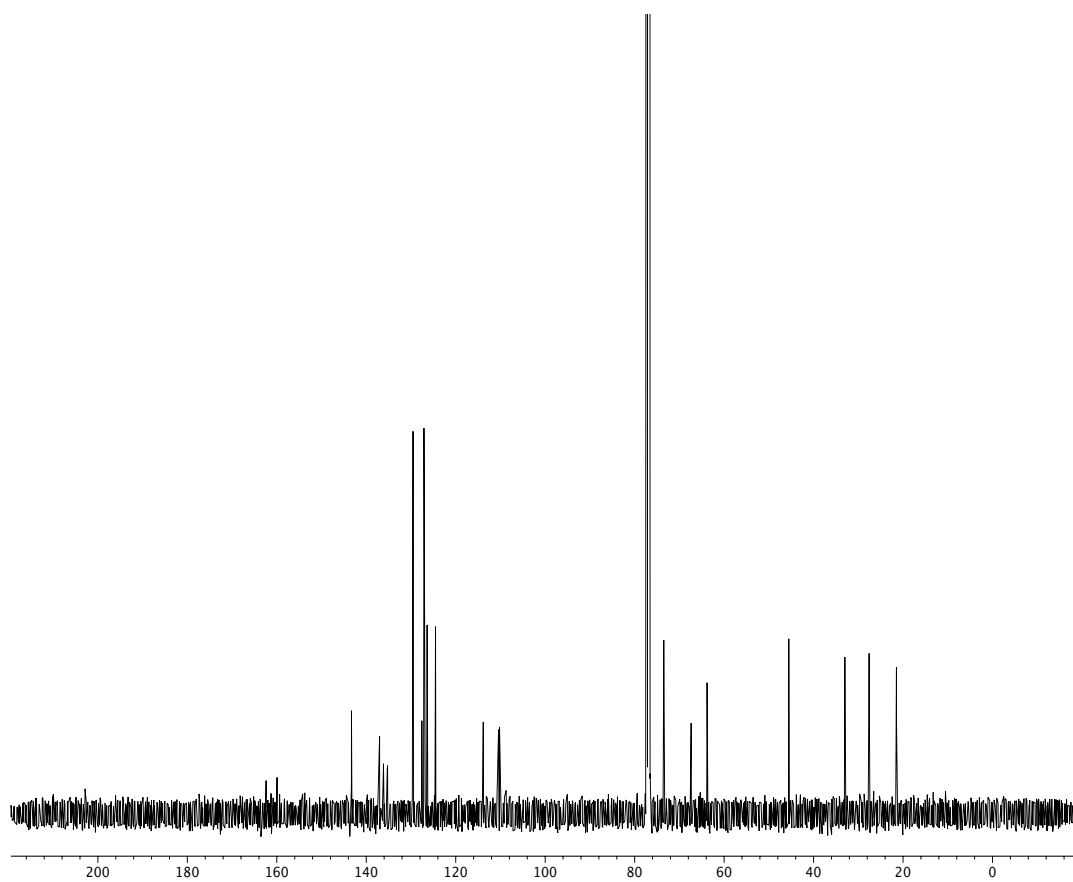
Figure A1.76 ^{13}C NMR (101 MHz, CDCl$_3$) of Compound **175c**.

CHAPTER 3

Enantioselective Nickel-Catalyzed α-Spirocyclization of Lactones

3.1 INTRODUCTION

Spirocyclic scaffolds frequently appear in molecules of interest to the chemical and biological communities (Figure 3.1A). Spironolactone (**176**), aptly named after its spirocyclic lactone core, is an FDA-approved drug for the treatment of hypertension and heart failure.[1] Spirocycles also comprise the backbones of chiral ligands, including *(R)*-SDP (**177**), which has been employed for enantioselective ketone hydrogenation.[2,3] Additionally, spirocyclic cores can be found in bioactive natural products such as exiguaquinol (**178**).[4,5] Despite the medicinal and synthetic utility of spirocycles, the enantioselective construction of these motifs remains a significant synthetic challenge, necessitating costly chiral separations and limiting their potential applications.[6]
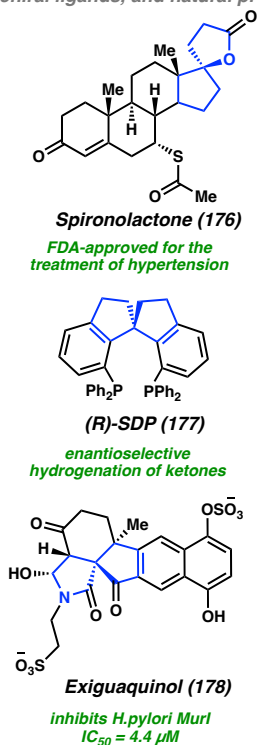
Methods for the asymmetric synthesis of spirocycles bearing a stereogenic quaternary center as the spiro atom are even less common, due to the added challenge of installing the all-carbon quaternary center enantioselectively.[7–10] In 2016, our laboratory disclosed a unique strategy for the enantioselective synthesis of all-carbon quaternary centers via a nickel-catalyzed C-acylation of lactams, furnishing β-keto lactam products (**181**) in up to
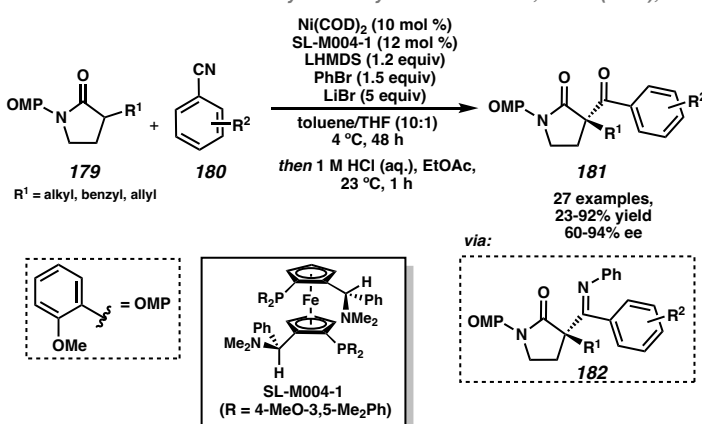
92% yield (Figure 3.1B).[11] Chiral Mandyphos ligand SL-M004-1 was employed in conjunction with Ni(COD)$_2$, imparting enantioselectivities as high as 94% ee. This reaction is thought to proceed through the addition of a metal enolate species to an aryl nitrile, giving rise to *N*-aryl imine products **182**. Subsequent hydrolysis of these species gives rise to the corresponding β-keto lactams (**181**).

Figure 3.1 *Spirocyclic motifs in molecules of synthetic interest, disclosure of a nickel-catalyzed C-acylation of lactams, and initial discovery of enantioselective lactone spirocyclization.*
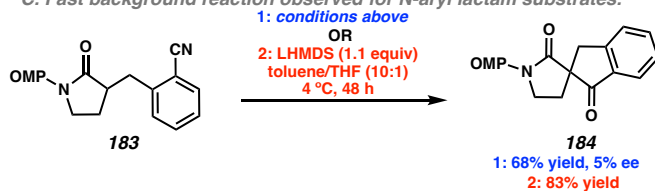

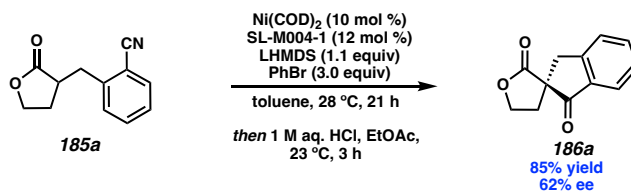A. Spirocycles are found in small molecule drugs, chiral ligands, and natural products.

Spironolactone (176)
FDA-approved for the treatment of hypertension

(R)-SDP (177)
enantioselective hydrogenation of ketones

Exiguaquinol (178)
inhibits H.pylori MurI
IC$_{50}$ = 4.4 μM

B. Enantioselective nickel-catalyzed C-acylation of lactams, Stoltz (2016), ref. 8

Ni(COD)$_2$ (10 mol %)
SL-M004-1 (12 mol %)
LHMDS (1.2 equiv)
PhBr (1.5 equiv)
LiBr (5 equiv)
toluene/THF (10:1)
4 °C, 48 h
then 1 M HCl (aq.), EtOAc, 23 °C, 1 h

179   180   181
R^1 = alkyl, benzyl, allyl

27 examples,
23-92% yield
60-94% ee

via:

= OMP

SL-M004-1
(R = 4-MeO-3,5-Me$_2$Ph)

182

C. Fast background reaction observed for N-aryl lactam substrates.[a]

1: *conditions above*
OR
2: LHMDS (1.1 equiv)
toluene/THF (10:1)
4 °C, 48 h

183   184
1: 68% yield, 5% ee
2: 83% yield

D. Reaction discovery: Nickel-catalyzed enantioselective spirocyclization of lactones.[a]

Ni(COD)$_2$ (10 mol %)
SL-M004-1 (12 mol %)
LHMDS (1.1 equiv)
PhBr (3.0 equiv)
toluene, 28 °C, 21 h
then 1 M aq. HCl, EtOAc, 23 °C, 3 h

185a   186a
85% yield
62% ee

3.2   RESULTS AND DISCUSSION

We recognized that an intramolecular version of this transformation using α-alkylated substrates, such as **183**, would give rise to spirocycles bearing an all-carbon quaternary center (Figure 3.1C). Subjecting **183** to the optimal conditions for the previously established intermolecular reaction gave spirocycle **184** in 68% yield, but in only 5% ee. We suspected that a base-promoted background reaction could be competing with the transition-metal catalyzed process for substrate **183**, explaining the low level of enantioselectivity. Indeed, when **8** was treated with a stoichiometric amount of LHMDS in the absence of the nickel catalyst, spirocycle **184** was formed in an 83% yield. The facile background reaction observed for **183** can be rationalized by the favorable kinetics of 5-membered ring formation.[12]

We surmised that altering the sterics and electronics of the enolate nucleophile could perhaps lower the rate of background reactivity and improve enantioselectivity. Specifically, we became interested in employing lactone nucleophiles, owing to their synthetic utility and prevalence in pharmaceutically relevant small molecules.[13] Moreover, on the basis of pKa,[14,15] and the weaker resonance donation of O vs. N, we predicted that a lactone enolate should be less nucleophilic than a lactam enolate, thereby slowing the rate of background reaction. To our delight, when α-substituted lactone **185a** was treated with LHMDS and PhBr in the presence of Ni(COD)$_2$ and Mandyphos ligand SL-M004-1, spirocyclic lactone **186a** was obtained in 85% yield and 62% ee (Figure 3.1D).

As suspected, when Ni(COD)$_2$ was omitted from the reaction, **186a** was observed in only 6% yield (Table 3.1, entry 1), indicating that the rate of base-promoted background reaction was much slower for lactone **185a** compared to more nucleophilic lactam **183**. Similarly, in the absence of PhBr, **186a** was formed in only 5% yield (entry 2), suggesting that the lactone α-spirocyclization was proceeding through a mechanistic framework similar to the previously described intermolecular lactam acylation. Indeed, the corresponding spirocyclic *N*-aryl imine product may be isolated prior to acid hydrolysis, if desired. (see Section 3.4: Experimental Section) The optimal reaction conditions for spirocyclization employed Ni(COD)$_2$ as the catalyst, Mandyphos ligand SL-M001-1 as the chiral ligand, LHMDS as the base, PhBr as the aryl halide, and TBME as the reaction solvent, affording **186a** in 90% yield and 83% ee (entry 3). When ligand SL-M009-1 was used in place of SL-M001-1, the reaction yield improved to 97%, but **186a** was formed with lower enantioselectivity (69% ee, entry 4). Interestingly, **186a** was obtained in 91% yield and 57% ee when diphosphine ligand *(S,S)*-BDPP was employed as the ligand (entry 5). Extensive investigation of additional chiral ligands was facilitated via an automated reaction setup (see Section 3.4: Experimental Section) but failed to improve the enantioselectivity of the reaction beyond 83% ee. When toluene was employed as the reaction solvent in place of TBME, **186a** was formed in 78% yield and 78% ee (entry 6). The addition of LiBr to the reaction mixture had no impact on reaction yield or enantioselectivity (entry 7). This contrasts with what was observed for the previously described lactam acylation, where the addition of LiBr led to a significant improvement in reaction yield and ee (Figure 1B). Finally, LHMDS was the optimal base in regard to enantioselectivity, with LiO′Bu

affording **186a** in 91% yield but only 72% ee (entry 8). We also probed the effect of varying

the sterics and electronics of the aryl halide component, but none of the other aryl halides

investigated led to greater reaction yield or enantioselectivity (see Supporting Information).

Air-stable nickel pre-catalysts such as Ni(COD)DQ were also investigated in this chemistry

but failed to afford **186a**.[16]

Table 3.1. *Reaction investigation*.

entry	deviation from optimal conditions	% yield[a]	% ee[b]
1	no Ni(COD)$_2$	6	-
2	no PhBr	5	-
3	none	90	83
4	SL-M009-1 instead of SL-M001-1	97	69
5	(S,S)-BDPP instead of SL-M001-1	91	57
6	toluene instead of TBME	78	78
7	5 equiv LiBr as additive	90	82
8	LiO^{t}Bu instead of LHMDS	91	72

[a]Yield was determined by HPLC relative to (4,4′)-di-*tert*-butylbiphenyl. [b] Enantiomeric excess was

determined via chiral SFC, and absolute stereochemistry was assigned in analogy to X-ray crystal

structures of **188b** and **188c**.

With the optimal conditions in hand, we began investigating the scope of the lactone α-

spirocyclization with respect to 5 and 6-membered ring formation (Table 3.2). We

evaluated the performance of the two best ligands, SL-M001-1, and SL-M009-1, for each

substrate. (see Supporting Information for detailed procedures for substrate synthesis).

Arene substitution *para* to the nitrile with an electron-donating methoxy group (**185b**)

resulted in lower yield but improved enantioselectivity with both SL-M001-1 (52% yield,

84% ee) and SL-M009-1 (67% yield, 83% ee) compared to electron-neutral substrate **185a**.

This effect of substitution on reaction yield may be due to the lower electrophilicity of the

aryl nitrile when an electron-donating group is introduced. Conversely, substitution *para*

to the nitrile with a slightly electron-withdrawing fluorine afforded **186c** with reduced

levels of enantioselectivity for both ligands employed. Finally, when substrate **185d** was

employed, 6-membered ring formation occurred in good yield but dramatically reduced

enantiomeric excess for both SL-M001-1 (81% yield, 50% ee) and SL-M009-1 (90% yield,

35% ee), suggesting that the mechanism of enantioinduction might be different for 6-

membered ring formation versus 5-membered ring formation. We aim to better understand

this phenomenon via computational investigation of the reaction mechanism, which is

currently underway.

Table 3.2. *Substrate scope of spirocyclization for 5 and 6-membered ring formation.*
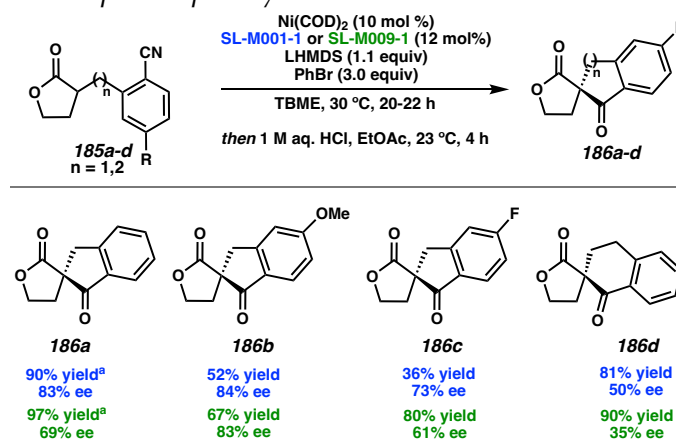
Next, we investigated the possibility of 7-membered ring formation within this reaction

manifold (Table 3.3). Medium-sized rings are prevalent in both pharmaceutical drugs and

natural products, but their preparation is often complicated by entropic factors and

transannular interactions.[17] Substrate **187a** was prepared from known α-allyl-γ-

butyrolactone and 2-vinylbenzonitrile in a facile two step sequence of olefin metathesis followed by hydrogenation (see Supporting Information). This synthetic sequence provided access to **187b – 187g** in good yields. When **187a** was subjected to the optimized conditions for spirocyclization at a slightly elevated temperature of 40 ºC, we were pleased to observe spirocycle **188a** in 54% yield and 78% ee for SL-M001-1 and 84% yield and 86% ee for SL-M009-1. This ligand performance is complementary to the trend observed for 5- and 6-membered ring formation. Notably, this reaction represents a fundamentally new approach to the formation of 7-membered carbocycles containing all-carbon quaternary centers.[18] Substitution of the arene with an electron-donating methoxy group *para* to the aryl nitrile (**188b**) resulted in improved reaction enantioselectivity but reduced yield for both ligands employed, in analogy to the trend observed for 5-membered ring formation. Spirocycle **188c**, containing a methyl group *para* to the aryl ketone, was obtained in good yield and enantioselectivity with both SL-M001-1 (57% yield, 90% ee) and SL-M009-1 (62% yield, 90% ee). When substrates **188d-188f** were surveyed, a strong electronic effect was noted. As the σ_p value of the substituent *para* to the nitrile increased from –F to –CO_2Et to –CF_3, the corresponding spirocyclic product was obtained with lower enantioselectivity.[19] Curious to see if background reactivity was responsible for this erosion of enantioselectivity, we treated **187f** with a stoichiometric amount of LHMDS in the absence of the nickel catalyst. Spirocycle **188f** was not observed under these conditions, suggesting that the lower levels of enantioselectivity observed for electron-poor substrates were not a result of competitive background reaction. We were pleased to find that the reaction was tolerant of an aryl chloride functional handle, with spirocycle **188g** obtained

in modest yield and enantioselectivity for both ligand systems employed. While other unidentified species were formed in these reactions, protodechlorination byproducts were not observed. Lastly, substrate **187h**, containing a *Z*-olefin embedded in the tether between the lactone and aryl nitrile, was evaluated. Unfortunately, low conversion was observed with this substrate, and spirocycle **188h** was isolated in low yield and enantioselectivity for both ligand systems tested. We posited that the rigidity in the tether imparted by the *Z*-olefin might affect the mechanism of C–C bond formation for this substrate, leading to lower yield and enantioselectivity. Nevertheless, the olefin functional handle remained intact under the reaction conditions.

Table 3.3. *Substrate scope for 7-membered ring formation.*
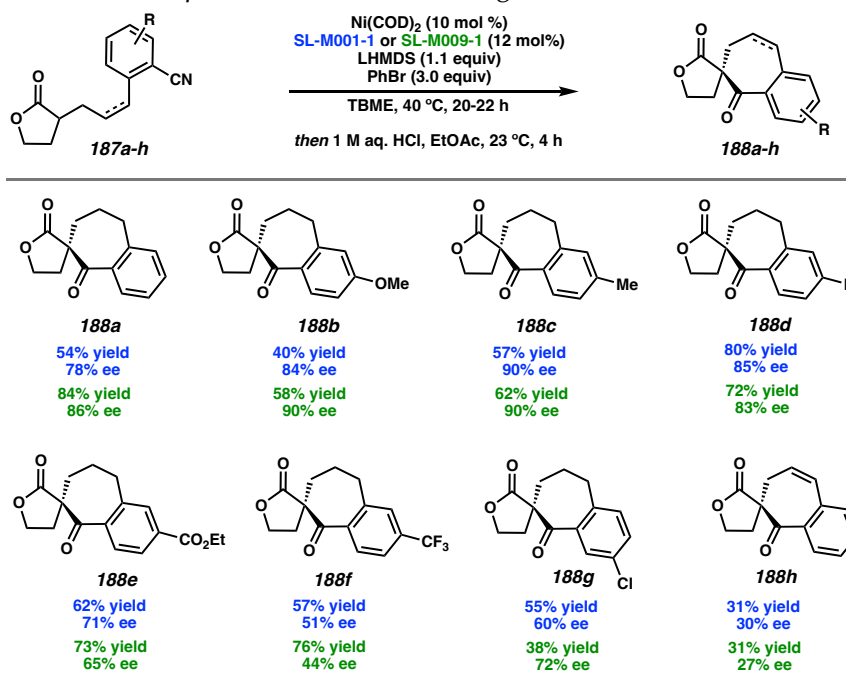
Finally, we investigated the impact of altering the enolate nucleophile on the spirocyclization (Scheme 1). When δ-valerolactone substrate **189** was subjected to the reaction conditions, employing SL-M009-1 as the ligand and toluene as the solvent,

spirocycle **190** was obtained in a low 27% yield with moderate enantioselectivity of 78%

ee. Undesired indanone byproduct **191** was also isolated in 46% yield. We hypothesized

that **191** was formed via ring opening and decarboxylation of spirocycle **190**. Previous

literature reports demonstrate that δ-valerolactone undergoes acid-promoted ring-opening

more readily than γ-butyrolactone, explaining why **190** was unstable to the conditions for

N-aryl imine hydrolysis.[20] This undesired reactivity was not observed for γ-butyrolactone

substrates. Lastly, we were pleased to find that α-alkylated tetralone substrate **192**

underwent spirocyclization in excellent yield and moderate enantioselectivity (91 % yield,

73% ee) when SL-M009-1 was employed as the ligand. A solvent mixture of 1:1

toluene/TBME provided better substrate solubility in this case.

Scheme 3.1 *Spirocyclization with other nucleophiles.*
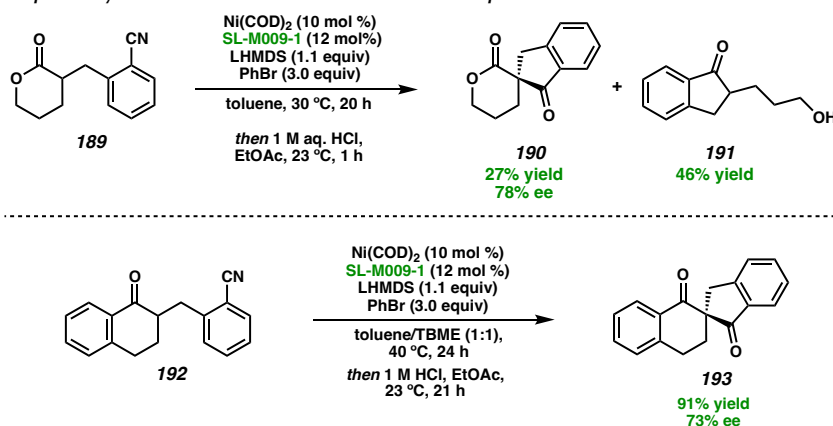
3.3 CONCLUSION

In summary, we have discovered a nickel-catalyzed enantioselective lactone α-

spirocyclization, affording 5-, 6-, and 7-membered spirocycles in good yield and

enantioselectivity. The reaction proceeds through an *N*-aryl imine intermediate, which is

hydrolyzed upon workup to provide enantioenrichced β-keto lactone products.

Interestingly, the reaction enantioselectivity was greatest for 7-membered ring formation (up to 90% ee), good for 5-membered ring formation (up to 84% ee) and moderate for 6-membered ring formation (up to 50% ee), suggesting mechanistic differences in the enantiodetermining steps across different ring sizes. During our investigation of substrate scope, we uncovered complementary ligand performance for many substrates by investigating both SL-M001-1 and SL-M009-1 as ligands on nickel. The spirocyclization was tolerant of multiple synthetically modular functional groups, including esters, aryl chlorides, and alkenes. Finally, the spirocyclization could be extended to tetralone nucleophiles, representing a potential avenue to expand this reaction manifold beyond lactone α-spirocyclization. Presently, we are investigating the free energy profile of the reaction to elucidate the elementary steps of the catalytic cycle and understand the origins of enantioselectivity. Ultimately, we aim to leverage computational insights on the reaction mechanism to tailor our catalyst and achieve higher levels of enantioselectivity with a broader scope of enolate nucleophiles.

3.4 EXPERIMENTAL SECTION

3.4.1 Materials and Methods

Unless otherwise stated, reactions were performed in flame-dried glassware under an argon or nitrogen atmosphere using dry, deoxygenated solvents. Solvents were dried by passage through an activated alumina column under argon. Reaction progress was monitored by thin-layer chromatography (TLC) or Agilent 1290 UHPLC-MS. TLC was performed using E. Merck silica gel 60 F254 precoated glass plates (0.25 mm) and

visualized by UV fluorescence quenching or $KMnO_4$ staining. Silicycle SiliaFlash® P60 Academic Silica gel (particle size 40–63 μm) was used for silica gel flash chromatography. ^{1}H NMR spectra were recorded on Varian Inova 500 MHz, Varian Inova 600 MHz, and Bruker 400 MHz spectrometers and are reported relative to residual $CHCl_3$ (δ 7.26 ppm). ^{13}C NMR spectra were recorded using a Bruker 400 MHz spectrometer (100 MHz) and are reported relative to residual $CHCl_3$ (δ 77.16 ppm) ^{19}F NMR spectra were recorded on a Varian Mercury 300 MHz spectrometer (282 MHz) or a Bruker 400 MHz spectrometer (376 MHz) and referenced to an external standard (hexafluorobenzene; ^{19}F NMR (282 MHz, $CDCl_3$) δ -161.64. Data for ^{1}H NMR are reported as follows: chemical shift (δ ppm), multiplicity, coupling constant (Hz), integration. Multiplicities are reported as follows: s = singlet, d = doublet, t = triplet, q = quartet, m = multiplet, br s = broad singlet. Data for ^{13}C NMR is reported in terms of chemical shifts (δ ppm). Some reported spectra include minor solvent impurities of water (δ 1.56 ppm), ethyl acetate (δ 4.12, 2.05, 1.26 ppm), methylene chloride (δ 5.30 ppm), acetone (δ 2.17 ppm), grease (δ 1.26, 0.86 ppm), and/or silicon grease (δ 0.07 ppm), which do not impact product assignments. IR spectra were obtained by use of a Perkin Elmer Spectrum BXII spectrometer using thin films deposited on NaCl plates and reported in frequency of absorption (cm^{-1}). Optical rotations were measured with a Jasco P-2000 polarimeter operating on the sodium D-line (589 nm), using a 100 mm path-length cell. Analytical SFC was performed with a Mettler SFC supercritical CO_2 analytical chromatography system utilizing Chiralpak (AD-H, AS-H or IC) or Chiralcel (OD-H, OJ-H, or OB-H) columns (4.6 mm x 25 cm) obtained from Daicel Chemical Industries, Ltd. High resolution mass spectra (HRMS) were obtained from the Caltech

Mass Spectral Facility using a JEOL JMS-600H High Resolution Mass Spectrometer in Field Ionization (FI) mode. The absolute configuration of **S41** was determined by X-ray crystallography and all other products are assigned by analogy. Reagents were purchased from commercial sources and used as received unless otherwise stated. Ni(COD)$_2$, SL-M001-1, SL-M009-1, and (S,S)-BDPP were purchased from Strem Chemicals. HG-II was gratuitously provided by Umicore.

3.4.2 Substrate Preparation

General Procedure A: LDA Alkylation for the Synthesis of Substrates 185a-c and 189
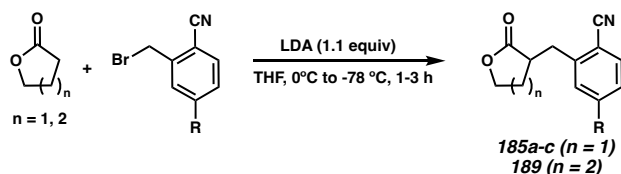
A round-bottom flask with a stir bar was flame-dried and cooled to room temperature under vacuum. The flask was backfilled with nitrogen, then diisopropylamine (1.1 equiv, freshly distilled over CaH) and 1/3 of the THF were added via syringe. The flask was cooled to 0 ºC in an ice bath, then *n*-BuLi (2.5 M in hexanes, 1.1 equiv) was added dropwise over 10 min. After stirring at 0 ºC for 20 min, the flask was cooled to -78 ºC, and a solution of the lactone (1 equiv) in 1/3 of the THF was added dropwise over 30 min. Lastly, a solution of benzyl bromide (1.2 equiv) was added dropwise over 30 minutes in the last 1/3 of the THF (0.43 M with respect to γ-butyrolactone) The reaction was stirred at -78 ºC until consumption of the lactone was observed by TLC. (1-3 hours depending on the substrate) The reaction was quenched at -78 ºC with sat. aq. NH$_4$Cl, diluted with EtOAc (1 x reaction volume), then immediately warmed to room temperature. The reaction was transferred to

a separatory funnel and the aqueous phase was extracted with EtOAc (2 x reaction volume). The combined organics were washed with brine (1 x reaction volume), dried over Na_2SO_4, and concentrated. The crude reaction was purified via silica gel flash column chromatography.
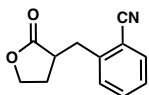

185a

Compound **185a** was prepared via General Procedure A from γ-butyrolactone (1 equiv, 25 mmol, 1.9 mL) and 2-cyanobenzyl bromide (1.2 equiv, 30 mmol, 5.88 g) with a reaction time of 3 h. The residue was purified by silica gel flash column chromatography (30% EtOAc/Hexanes) and then recrystallized (4:9 EtOAc/Hexanes, 130 mL) to afford **185a** as a fluffy white solid (2.02 g, 40% yield)

^{1}H NMR (600 MHz, CDCl_3) δ 7.65 (dd, J = 7.8, 1.4 Hz, 1H), 7.56 (td, J = 7.6, 1.4 Hz, 1H), 7.43 (d, J = 7.8 Hz, 1H), 7.36 (td, J = 7.6, 1.2 Hz, 1H), 4.31 (td, J = 8.8, 2.5 Hz, 1H), 4.17 (td, J = 9.5, 6.5 Hz, 1H), 3.42 (dd, J = 14.2, 5.3 Hz, 1H), 3.08 (dd, J = 14.2, 8.5 Hz, 1H), 2.95 (dtd, J = 11.0, 8.5, 5.3 Hz, 1H), 2.31 (dddd, J = 12.8, 8.8, 6.5, 2.4 Hz, 1H), 2.05 (dtd, J = 12.7, 10.3, 8.4 Hz, 1H).

^{13}C NMR (101 MHz, CDCl_3) δ 177.82, 142.45, 133.36, 133.07, 130.46, 127.62, 118.09, 113.04, 66.61, 40.90, 34.22, 28.10.

IR (NaCl, Thin Film) 2912, 2224, 1769, 1599, 1487, 1450, 1376, 1310, 1260, 1206, 1187, 1154, 1109, 1021, 957, 916, 765 cm^{-1}.

HRMS(FI) *m/z*: [M + •]⁺: Calculated for $C_{12}H_{11}NO_2$: 201.07898, Found: 201.07857.

S16
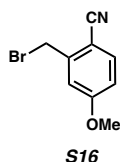
Compound **S16** was prepared in 2 steps from commercially available 4-bromo-2-methylbenzonitrile according to a published procedure. Spectral data matched those reported in the literature.[21]
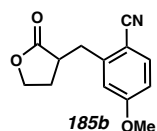
185b

Compound **185b** was prepared via General Procedure A from γ-butyrolactone (1 equiv, 0.83 mmol, 63 µL) and benzyl bromide **S1** (1.2 equiv, 1.0 mmol, 225.4 mg) with a reaction time of 1 h. The residue was purified by silica gel flash column chromatography (35% EtOAc/Hexanes) afford **185b** as a white solid (116.4 mg, 61% yield)

¹H NMR (400 MHz, CDCl₃) δ 7.57 (d, *J* = 8.6 Hz, 1H), 6.92 (d, *J* = 2.5 Hz, 1H), 6.85 (dd, *J* = 8.6, 2.5 Hz, 1H), 4.41 – 4.27 (m, 1H), 4.18 (ddd, *J* = 10.0, 9.1, 6.5 Hz, 1H), 3.85 (s, 3H), 3.37 (dd, *J* = 14.0, 5.2 Hz, 1H), 3.07 (dd, *J* = 14.1, 8.1 Hz, 1H), 2.94 (dtd, *J* = 10.9, 8.3, 5.2 Hz, 1H), 2.33 (dddd, *J* = 12.7, 8.7, 6.4, 2.5 Hz, 1H), 2.06 (dddd, *J* = 14.8, 12.7, 10.0, 8.4 Hz, 1H).

¹³C NMR (101 MHz, CDCl₃) δ 177.94, 163.23, 144.62, 134.71, 118.59, 115.84, 113.66, 104.67, 66.67, 55.76, 40.98, 34.28, 28.01.

IR (NaCl, Thin Film) 3060, 2941, 2915, 2884, 2218, 1768, 1605, 1567, 1494, 1462, 1455, 1431, 1375, 1293, 1249, 1209, 1153, 1110, 1072, 1022, 959, 921, 885, 823, 732, 698 cm⁻¹

HRMS(FI) *m/z*: [M + •]⁺ Calculated for $C_{13}H_{13}NO_3$: 231.08954; Found: 231.08824.
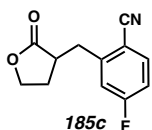
Compound **185c** was prepared via General Procedure A from γ-butyrolactone (1 equiv, 0.5 mmol, 38 μL) and 2-(bromomethyl)-4-fluorobenzonitrile (1.2 equiv, 0.6 mmol, 128 mg) with a reaction time of 2.5 h. The residue was purified by silica gel flash column chromatography (30% EtOAc/Hexanes) afford **185c** as a white solid (70.6 mg, 64% yield).

¹H NMR (400 MHz, CDCl₃) δ 7.67 (dd, *J* = 8.6, 5.5 Hz, 1H), 7.17 (dd, *J* = 9.1, 2.5 Hz, 1H), 7.13 – 7.03 (m, 1H), 4.35 (td, *J* = 8.8, 2.3 Hz, 1H), 4.19 (ddd, *J* = 10.2, 9.2, 6.4 Hz, 1H), 3.40 (dd, *J* = 14.2, 5.5 Hz, 1H), 3.09 (dd, *J* = 14.2, 8.1 Hz, 1H), 2.95 (dtd, *J* = 11.1, 8.3, 5.5 Hz, 1H), 2.35 (dddd, *J* = 12.7, 8.6, 6.4, 2.3 Hz, 1H), 2.05 (dddd, *J* = 12.7, 11.1, 10.2, 8.5 Hz, 1H).

¹³C NMR (101 MHz, CDCl₃) δ 177.48, 166.48, 163.92, 145.91, 145.82, 135.42, 135.32, 118.14, 117.92, 117.39, 115.62, 115.39, 109.21, 109.17, 66.59, 40.68, 34.23, 34.21, 28.17.

IR (NaCl, Thin Film) 2911, 2226, 1766, 1607, 1584, 1493, 1376, 1346, 1279, 1243, 1211, 1171, 1153, 1022, 985, 961, 825, 682 cm⁻¹.

HRMS(FI) *m/z*: [M + •]⁺: Calculated for $C_{12}H_{10}NO_2F$: 219.06959, Found: 219.06929.
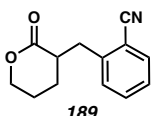
Compound **189** was prepared via General Procedure A from δ-valerolactone (1 equiv, 15 mmol, 1.39 mL) and 2-cyanobenzyl bromide (1.2 equiv, 18 mmol, 3.53 g) with a reaction time of 2 h. The residue was purified by silica gel flash column chromatography (35% EtOAc/Hexanes) afford **189** as a white solid (2.25 g, 80% yield)

¹H NMR (400 MHz, CDCl₃) δ 7.63 (dd, J = 7.7, 1.4 Hz, 1H), 7.54 (td, J = 7.6, 1.4 Hz, 1H), 7.47 (dd, J = 8.0, 1.3 Hz, 1H), 7.34 (td, J = 7.6, 1.3 Hz, 1H), 4.38 – 4.24 (m, 2H), 3.49 (dd, J = 14.0, 5.8 Hz, 1H), 3.03 (dd, J = 14.1, 7.8 Hz, 1H), 2.91 – 2.79 (m, 1H), 2.08 – 1.80 (m, 3H), 1.63 (ddt, J = 12.6, 11.1, 7.1 Hz, 1H).

¹³C NMR (101 MHz, CDCl₃) δ 173.49, 143.38, 133.12, 132.96, 130.89, 127.33, 118.27, 113.08, 68.45, 41.23, 35.56, 24.41, 22.02.
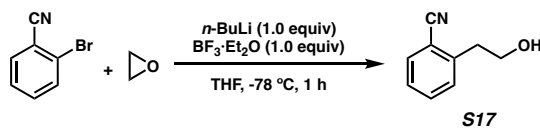
IR (NaCl, Thin Film) 3448, 3066, 2952, 2874, 2223, 1768, 1731, 1599, 1573, 1485, 1449, 1401, 1351, 1267, 1212, 1155, 1084, 983, 969, 902, 827, 766, 738, 624 cm⁻¹.

HRMS(FI) *m/z*: [M + •]⁺: Calculated for $C_{13}H_{13}NO_2$: 215.09436, Found: 215.09429.

Alkylation/Decarboxylative Protonation Sequence for the Synthesis of 185d
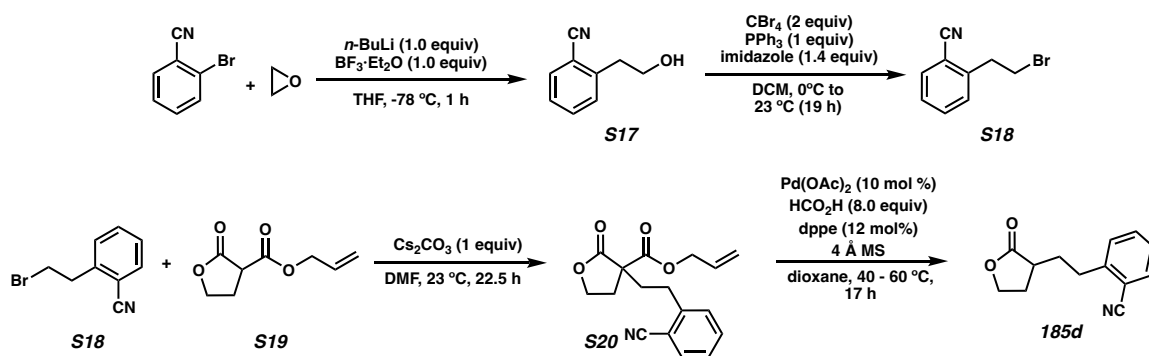
Preparation of Alcohol **S17**

A 250 RBF with stir bar was flame-dried and cooled under vacuum. The flask was opened, charged with 2-bromobenzonitrile as a solid (1 equiv, 12.5 mmol, 2.28 g), and then evacuated and purged with nitrogen 3x. THF (0.19 M, 67 mL) was added via cannula and

the solution was cooled to -78 °C. Next, *n*-BuLi (2.5 M in hexanes, 1 equiv, 12.5 mmol, 5 mL) was added dropwise over 10 minutes and the reaction was stirred at -78 °C for 15 minutes. Ethylene oxide (advertised as 2.5 – 3.3 M in THF, assumed 2.5 M, 2 equiv, 25 mmol, 10 mL) was added dropwise over 10 minutes, followed by BF$_3$•Et$_2$O (added quickly via syringe, 1 equiv, 12.5 mmol, 1.54 mL). The reaction was stirred at -78 °C for 1 hour, after which 2-bromobenzonitrile was observed to be fully consumed by TLC. The reaction was quenched at -78 °C by adding sat. NH$_4$Cl (50 mL) and EtOAc (40 mL), warmed to room temperature, and stirred at room temperature overnight. (CAUTION- ethylene oxide is a highly carcinogenic and volatile reagent, bp ~ 11 °C at 1 atm. Care should be exercised in handling and quenching this reaction.) The reaction mixture was transferred to a separatory funnel, the layers were separated, and the aqueous layer was extracted with EtOAc (3 x 50 mL). The combined organics were washed with brine, dried over Na$_2$SO$_4$, and concentrated. The residue was purified via column chromatography to afford **S17** as an off-white oil (1.02 g, 55% yield).

^{1}H NMR (500 MHz, CDCl$_3$) δ 7.68 (dd, *J* = 7.7, 1.4 Hz, 1H), 7.57 (td, *J* = 7.7, 1.4 Hz, 1H), 7.44 (dd, *J* = 7.8, 1.1 Hz, 1H), 7.37 (td, *J* = 7.6, 1.2 Hz, 1H), 3.99 (t, *J* = 6.5 Hz, 2H), 3.15 (t, *J* = 6.5 Hz, 2H).

^{13}C NMR (101 MHz, CDCl$_3$) δ 142.85, 133.04, 132.93, 130.50, 127.17, 118.24, 112.98, 62.75, 37.89.

IR (NaCl, Thin Film) 3434, 3068, 2952, 2881, 2224, 1599, 1486, 1449, 1210, 1165, 1099, 1048, 950, 761, 720 cm^{-1}.

HRMS(FI) *m/z*: [M + •]$^+$ Calculated for C$_9$H$_9$NO: 147.06841, Found: 147.06816.

Preparation of Bromide S18
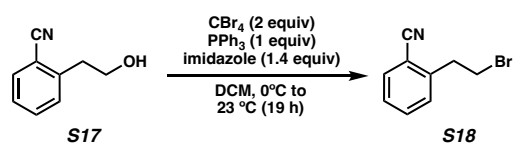
A 100 mL RBF with stir bar was charged with a solution of alcohol in DCM (0.3 M, 23.1 mL). The solution was cooled to 0 ºC, and then imidazole (1.4 equiv, 9.72 mmol, 662 mg) was added. Next, CBr$_4$ (2 equiv, 13.9 mmol, 4.6 g) was added, followed by PPh$_3$ (1 equiv, 6.93 mmol, 1.82 g), which was added slowly in 3 portions. The reaction was warmed to 23 ºC and stirred for 19 h. Upon consumption of the alcohol starting material, the reaction was quenched with sat. aq. NH$_4$Cl (1 x 25 mL and diluted with DCM (25 mL). The reaction was transferred to a separatory funnel, and the layers were separated. The aqueous layer was extracted with DCM (2 x 25 mL), and the combined organic layers were washed with water (1 x 25 mL) and brine, then dried over Na$_2$SO$_4$. The residue was purified via silica gel flash chromatography (5% EtOAc/Hexanes) to afford **S18** as a white solid (988 mg, 68% yield).

^{1}H NMR (400 MHz, CDCl$_3$) δ 7.66 (ddt, *J* = 7.7, 1.3, 0.7 Hz, 1H), 7.57 (td, *J* = 7.7, 1.4 Hz, 1H), 7.44 – 7.33 (m, 2H), 3.66 (t, *J* = 7.1 Hz, 2H), 3.41 (t, *J* = 7.1 Hz, 2H).

^{13}C NMR (101 MHz, CDCl$_3$) δ 142.51, 133.21, 133.01, 130.43, 127.76, 117.78, 112.74, 37.50, 31.40.

IR (NaCl, Thin Film) 3068, 2967, 2224, 1599, 1574, 1487, 1450, 1434, 1306, 1286, 1263, 1219, 1185, 1164, 11135, 1085, 1040, 1003, 956, 924, 895, 865, 765, 649 cm^{-1}

HRMS(FI) *m/z*: [M + •]$^+$: Calculated for C$_9$H$_8$NBr: 208.98401; Found: 208.98346

Preparation of Carboxy Lactone S19
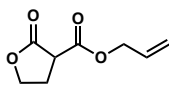
S19

A 250 mL RBF with a stir bar was flame-dried and cooled under vacuum. The flask was backfilled with N_2, opened, charged with NaH (65% wt, 2.5 equiv, 17.5 mmol, 700 mg), then evacuated and purged with N_2 3x. Next, 1/2 of the THF (29 mL) was added and the reaction was cooled to 0 ºC in an ice bath. A solution of γ-butyrolactone (1 equiv, 7 mmol, 0.53 mL) in the remaining 1/2 of the THF (29 mL) was added dropwise. The reaction was warmed to 23º C and diallyl carbonate (1.5 equiv), 10.5 mmol, 1.51 mL) was added quickly via syringe. The reaction was stirred at 23 ºC for 17 hours until the lactone was consumed. The reaction was quenched with sat. aq. NH_4Cl (1x 25 mL), transferred to a separatory funnel, and extracted with EtOAc (2 x 50 mL). The combined organics were washed with brine, dried over Na_2SO_4, and concentrated under vacuum. The residue was purified via silica gel flash column chromatography (30% EtOAc/hexanes to 50% EtOAc/hexanes) to give **S19** as a clear oil (884.5 mg, 71% yield). Spectral data matched those reported in the literature.[22]

Preparation of Carboxy lactone **S20**
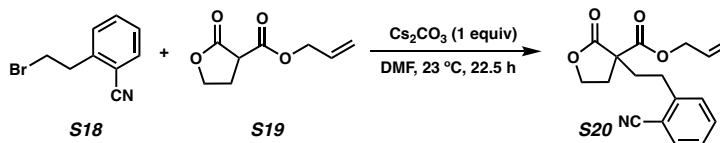
A 25 mL RBF with a stir bar was flame-dried and cooled under vacuum. The flask was backfilled with N_2, opened and charged with Cs_2CO_3 (1 equiv, 1.3 mmol, 423.6 mg). The flask was sealed, then evacuated and purged with nitrogen 3x. Then, a solution of **S19** (1 equiv, 1.3 mmol, 216.7 mg) in dry DMF (2.3 mL) was added, and the reaction was stirred

at 23 ºC for 30 min. Finally, bromide **S18** (1.8 equiv, 2.34 mmol, 491.6 mg was added as

a solution in the remaining dry DMF (2.3 mL, total concentration 0.28 M in **S19**) and the

reaction was stirred at 23 ºC for 22.5 hours. The reaction was quenched with water (1 x 10

mL), transferred to a separatory funnel, and extracted with EtOAc (3 x 15 mL). The

combined organics were washed with brine, dried over Na_2SO_4, and concentrated under

vacuum. The residue was purified via silica gel flash column chromatography (7.5%

EtOAc/toluene) to afford **S20** as a clear oil (248.6 mg, 64% yield).

^{1}H NMR (400 MHz, CDCl$_3$) δ 7.62 (dd, *J* = 7.7, 1.4 Hz, 1H), 7.54 (td, *J* = 7.7, 1.4 Hz,

1H), 7.41 – 7.28 (m, 2H), 5.93 (ddt, *J* = 17.2, 10.4, 5.8 Hz, 1H), 5.43 – 5.24 (m, 2H), 4.70

(dt, *J* = 5.8, 1.4 Hz, 2H), 4.46 – 4.39 (m, 2H), 2.97 (td, *J* = 12.9, 5.0 Hz, 1H), 2.92 – 2.76

(m, 2H), 2.53 – 2.38 (m, 2H), 2.07 (ddd, *J* = 13.9, 12.4, 4.8 Hz, 1H).

^{13}C NMR (101 MHz, CDCl$_3$) δ 174.35, 168.86, 144.60, 133.28, 132.98, 131.17, 129.91,

127.25, 119.64, 117.97, 112.37, 66.96, 66.56, 54.08, 35.40, 31.86, 30.04.

IR (NaCl, Thin Film) 3069, 2919, 2223, 1774, 1735, 1598, 1485, 1450, 1376, 1251, 1212,

1169, 1119, 1029, 954, 765 cm^{-1}

HRMS(FI) *m/z*: [M + •]$^+$ Calculated for $C_{17}H_{17}NO_4$: 299.11576; Found: 299.11472

Preparation of Substrate 185d
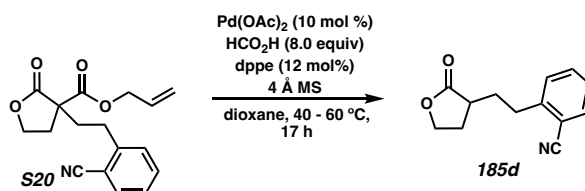
A 100 mL RBF equipped with a stir bar (capped with a 24/40 septa) was charged with 4 Å

molecular sieves (2.4 x mass substrate) and flame-dried under vacuum 3 x. The flask was

cooled under vacuum and then filled with nitrogen. The septum was secured onto the flask with electrical tape and pumped into the glovebox. Inside the glovebox, the flask was opened and charged with Pd(OAc)$_2$ (0.1 equiv, 0.07 mmol, 15.7 mg) and dppe (0.12 equiv, 0.088 mmol, 35.1 mg), sealed with a septum, and removed from the glovebox. Freshly dried 1,4-dioxane (18 mL) was added via syringe, and the reaction was heated to 40 ºC under nitrogen for 30 min. To the resulting green solution was added neat HCO$_2$H (8 equiv, 5.6 mmol, 0.21 mL), and the immediately **S20** (1 equiv, 0.7 mmol, 209.5 mg) was added as a solution in the remaining 1,4-dioxane (5 mL, total concentration in **S20** of 0.03 M). The reaction was heated to 60 ºC and stirred for 17 hours until **S20** was fully consumed by TLC. The reaction was cooled to room temperature, filtered through a short SiO$_2$ plug, concentrated under reduced pressure and loaded directly onto a silica gel column (30% EtOAc/hx) to afford **185d** as a clear oil (129.4 mg, 86% yield).

^{1}H NMR (400 MHz, CDCl$_3$) δ 7.62 (dd, J = 7.7, 1.4 Hz, 1H), 7.54 (td, J = 7.7, 1.4 Hz, 1H), 7.44 – 7.36 (m, 1H), 7.32 (td, J = 7.6, 1.2 Hz, 1H), 5.29 (s, 0H), 4.43 – 4.34 (m, 1H), 4.21 (td, J = 9.5, 6.4 Hz, 1H), 4.11 (q, J = 7.2 Hz, 0H), 2.98 (dd, J = 8.9, 7.1 Hz, 2H), 2.62 – 2.44 (m, 2H), 2.31 – 2.17 (m, 1H), 2.15 – 1.99 (m, 1H), 1.84 (dtd, J = 13.7, 8.7, 7.3 Hz, 1H).

^{13}C NMR (101 MHz, CDCl$_3$) δ 178.95, 145.01, 133.22, 133.01, 129.78, 127.12, 118.11, 112.46, 66.67, 38.75, 32.13, 31.67, 28.82.

IR (NaCl, Thin Film) 3513, 3064, 2923, 2868, 2222, 1766, 1649, 1598, 1573, 1485, 1450, 1375, 1300, 1168, 1111, 1062, 1024, 966, 936, 767, 703, 667, 624 cm^{-1}

HRMS(FI) *m/z*: [M + •]$^+$ Calculated for C$_{13}$H$_{13}$NO$_2$: 215.09463; Found: 215.09365

Suzuki Coupling/Olefin Metathesis/Hydrogenation Sequence for the Synthesis of Substrates 187a-g

**General Procedure B: Suzuki Coupling for the Synthesis of S21-S25**
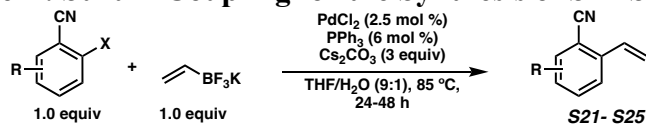
(Adapted from a published procedure)[23]

A 100 mL Schlenk tube was charged with aryl halide (1 equiv), potassium vinyltrifluoroborate (1 equiv), cesium carbonate (3 equiv), palladium dichloride (0.02 equiv), and triphenylphosphine (0.06 equiv) as solids. The tube was evacuated and purged with nitrogen 3x, then THF and H_2O were added via syringe (9:1 THF/H_2O, 0.5 M in aryl halide). The vessel was sealed and heated to 85 ºC for 20-48 h, depending on the aryl halide employed. The reaction was cooled to room temperature, opened to air, and diluted with H_2O (1 x 20 mL). The reaction was transferred to a separatory funnel and extracted with Et_2O (3 x 25 mL). The combined organics were washed with brine, dried over Na_2SO_4, and concentrated under vacuum. The residue was purified via silica gel flash column chromatography.
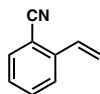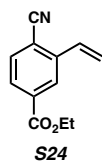

Compound **S21** was prepared via general procedure B from 2-bromobenzonitrile (1 equiv, 10 mmol, 1.82 g) and potassium vinyltrifluoroborate (1 equiv, 10 mmol, 1.34 g). The reaction was stirred for 46 hours, and **S21** was purified by silica gel flash chromatography (1-10% EtOAc/Hexanes) to afford **S21** as a clear oil (1.06 g, 76% yield). Spectral data matched those reported in the literature.[23]
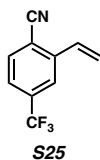
S22
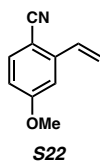
Compound **S22** was prepared via general procedure B from 2-bromo-4-methoxybenzonitrile (1 equiv, 4 mmol, 848 mg) and potassium vinyltrifluoroborate (1 equiv, 4 mmol, 536 mg). The reaction was stirred for 21 hours, and **S22** was purified by silica gel flash chromatography (1-10% EtOAc/Hexanes) to afford **S22** as a white solid (320.6 mg, 50% yield).

^{1}H NMR (400 MHz, CDCl$_3$) δ 7.56 (d, J = 8.7 Hz, 1H), 7.12 (d, J = 2.5 Hz, 1H), 7.04 (dd, J = 17.4, 11.0 Hz, 1H), 6.86 (dd, J = 8.6, 2.5 Hz, 1H), 5.92 (dd, J = 17.4, 0.6 Hz, 1H), 5.53 (dd, J = 10.9, 0.6 Hz, 1H), 3.88 (s, 3H).

^{13}C NMR (101 MHz, CDCl$_3$) δ 162.96, 142.79, 134.75, 133.16, 119.03, 118.34, 114.34, 110.69, 103.37, 55.70.

IR (NaCl, Thin Film) 3091, 3014, 2943, 2840, 2218, 1600, 1561, 1491, 1463, 1429, 1313, 1299, 1287, 1244, 1200, 1169, 1103, 1085, 1024, 986, 924, 874, 822, 683 cm^{-1}

HRMS(FI) *m/z*: [M + •]$^{+}$ Calculated for C$_{10}$H$_9$NO: 159.06841, Found: 159.06639.

S23
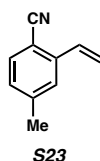
Compound **S23** was prepared via general procedure B from 2-bromo-4-methylbenzonitrile (1 equiv, 5.1 mmol, 1.0 g) and potassium vinyltrifluoroborate (1 equiv, 5.10 mmol, 683 mg). The reaction was stirred for 20 hours, and **S23** was purified via silica gel flash chromatography (0-5% EtOAc/Hexanes) to afford **S23** as a white solid (171 mg, 23% yield).

¹H NMR (400 MHz, CDCl₃) δ 7.55 – 7.44 (m, 2H), 7.15 (ddd, *J* = 7.9, 1.7, 0.8 Hz, 1H), 7.04 (dd, *J* = 17.4, 11.0 Hz, 1H), 5.93 (dd, *J* = 17.4, 0.7 Hz, 1H), 5.51 (dd, *J* = 11.0, 0.7 Hz, 1H), 2.42 (s, 3H).

¹³C NMR (101 MHz, CDCl₃) δ 143.67, 140.64, 133.14, 132.95, 129.06, 126.18, 118.69, 118.25, 108.41, 22.03.

IR (NaCl, Thin Film) 3093, 3017, 2988, 2957, 2922, 2223, 1603, 1560, 1486, 1455, 1421, 1379, 1314, 1291, 1231, 1162, 1038, 986, 925, 818, 778, 761, 650 cm⁻¹

HRMS(FI) *m/z*: [M + •]⁺ Calculated for C₁₀H₉N: 143.07350, Found: 143.07328

Compound **S24** was prepared via general procedure B from ethyl 3-bromo-4-cyanobenzoate (1 equiv, 1.18 mmol, 300 mg) and potassium vinyltrifluoroborate (1 equiv, 1.18 mmol, 158 mg). The reaction was stirred for 45 hours, and **S24** was purified via silica gel flash chromatography (10 % Et₂O/Hexanes) to afford **S24** as a white solid (207 mg, 87% yield).

¹H NMR (400 MHz, CDCl₃) δ 8.32 (d, *J* = 1.6 Hz, 1H), 7.98 (dd, *J* = 8.1, 1.6 Hz, 1H), 7.70 (dd, *J* = 8.1, 0.5 Hz, 1H), 7.10 (dd, *J* = 17.4, 11.0 Hz, 1H), 6.07 (d, *J* = 17.4 Hz, 1H), 5.63 (d, *J* = 11.1 Hz, 1H), 4.42 (q, *J* = 7.1 Hz, 2H), 1.42 (t, *J* = 7.1 Hz, 3H).

¹³C NMR (101 MHz, CDCl₃) δ 165.19, 141.10, 134.46, 133.13, 132.29, 128.59, 126.59, 120.38, 117.21, 114.80, 62.01, 14.40.

IR (NaCl, Thin Film) 2992, 2226, 1720, 1420, 1389, 1365, 1296, 1286, 1265, 1203, 1133, 1114, 1087, 1055, 1025, 993, 952, 929, 850, 759, 734 cm⁻¹

HRMS(FI) *m/z***:** [M + •]$^+$ Calculated for C$_{12}$H$_{11}$NO$_2$: 201.07898, Found: 201.07850

S25

Compound **S25** was prepared via general procedure B from 3-bromo-4-trifluoromethylbenzonitrile (1 equiv, 7.5 mmol, 1.87 g) and potassium vinyltrifluoroborate (1 equiv, 7.5 mmol, 1.0 g). The reaction was stirred for 48 hours, and **S25** was purified via silica gel flash chromatography (20% DCM/Hexanes) to afford **S25** as a white solid (925 mg, 63% yield).

^{1}H NMR (600 MHz, CDCl$_3$) δ 7.91 (s, 1H), 7.77 (d, *J* = 8.1 Hz, 1H), 7.60 (dd, *J* = 8.1, 1.7 Hz, 1H), 7.11 (dd, *J* = 17.4, 11.0 Hz, 1H), 6.05 (d, *J* = 17.4 Hz, 1H), 5.68 (d, *J* = 11.0 Hz, 1H).

^{13}C NMR (101 MHz, CDCl$_3$) δ 141.58, 134.66 (q, J = 33.2 Hz), 133.56, 131.82, 124.56 (q, *J* = 3.6 Hz), 122.97 (q, *J* = 273.2 Hz), 122.46 (q, *J* = 3.8 Hz). 121.01, 116.52, 114.38.

IR (**NaCl, Thin Film**) 3087, 2938, 2231, 1768, 1721, 1681, 1634, 1571, 1488, 1428, 1385, 1328, 1290, 1273, 1205, 1171, 1137, 1107, 1079, 1043, 984, 932, 904, 885, 836, 740, 690 cm^{-1}

HRMS(FI) *m/z***:** [M + •]$^+$ Calculated for C$_{10}$H$_6$NF$_3$: 197.04523, Found: 197.04431

Preparation of Styrene S26
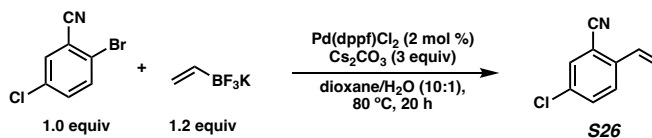
A 100 mL RBF equipped with a stir bar was charged with 2-bromo-5-chlorobenzonitrile (1 equiv, 5 mmol, 1.0823 g), potassium vinyltrifluoroborate (1.2 equiv, 6 mmol, 803.4 mg),

Cs$_2$CO$_3$ (3 equiv, 15 mmol, 4.8873 g), 1,4-dioxane (45.45 mL), and H$_2$O (4.55 mL) (0.1 M

total in aryl bromide). The solution was sparged with N$_2$ for 15 min then charged with

Pd(dppf)Cl$_2$ (0.02 equiv, 0.1 mmol, 73.2 mg). The flask was sealed, vacuum degassed 3 x

with N$_2$ then heated to 80 ºC with stirring. After reaction completion was noted via NMR

(20 h) the reaction was cooled to room temperature and concentrated in vacuo to remove

1,4-dioxane. The aqueous mixture was transferred to a separatory funnel and diluted with

EtOAc (50 mL) and sat. aq. NH$_4$Cl (50 mL). The layers were separated, and the aqueous

layer was extracted with EtOAc (2 x 50 mL). The combined organics were washed with

brine, dried over Na$_2$SO$_4$, and concentrated under vacuum. The residue was purified via

silica gel flash column chromatography (5% EtOAc/Hexanes) to afford **S26** as a white

solid (712.5 mg, 87% yield).

^{1}H NMR (400 MHz, CDCl$_3$) δ 7.62 (d, J = 6.2 Hz, 1H), 7.60 (s, 1H), 7.56 – 7.49 (m, 1H),

7.03 (ddd, J = 17.4, 11.1, 0.7 Hz, 1H), 5.94 (d, J = 17.4 Hz, 1H), 5.57 (d, J = 11.0 Hz, 1H).

^{13}C NMR (101 MHz, CDCl$_3$) δ 139.33, 133.93, 133.31, 132.49, 132.02, 126.90, 119.73,

116.63, 112.61.

IR (NaCl, Thin Film) 3611, 3072, 2358, 2224, 1479, 1463, 1418, 1314, 1265, 1212, 1177,

1119, 1087, 1028, 984, 927, 877, 859, 832, 813

HRMS(FI) *m/z*: [M + •]$^+$ Calculated for C$_9$H$_6$NCl: 163.01888, Found: 163.01847.

Preparation of Styrene S27
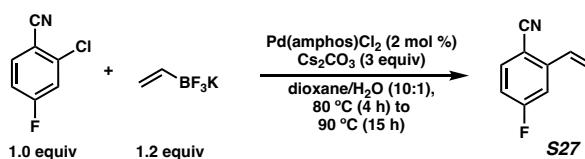
A 250 mL RBF equipped with a stir bar was charged with 1,4-dioxane (120 mL) and H_2O (12 mL). The solution was sparged with N_2 while stirring and the flask was charged sequentially with 2-chloro-4-fluorobenzonitrile (1 equiv, 15 mmol, 2.33 g), potassium vinyltrifluoroborate (1.2 equiv, 18 mmol, 2.41 g), and Cs_2CO_3 (3 equiv, 45 mmol, 14.66 g). The resulting suspension was sparged for an additional 15 min then charged with Bis(di-tert-butyl(4-dimethylaminophenyl)phosphine)dichloropalladium(II) (0.02 equiv, 0.3 mmol, 212.4 mg) The flask was sealed, vacuum degassed three times, then heated to 80 °C and stirred under N_2 for 4 hours. After 4 hours, the reaction was heated to 90 °C and stirred for an additional 15 hours. The reaction was cooled to ambient temperature and concentrated in vacuo to remove 1,4-dioxane. The aqueous mixture was transferred to a separatory funnel and diluted with EtOAc (100 mL) and sat. aq. NH_4Cl (100 mL). The layers were separated, and the aqueous layer was extracted with EtOAc (2 x 100 mL). The combined organics were washed with brine, dried over $MgSO_4$, and concentrated under vacuum. The residue was purified via silica gel flash column chromatography (2.5% EtOAc/Hexanes) to afford **S27** as a white solid (2.038 g, 92% yield).

¹H NMR (400 MHz, CDCl₃) δ 7.64 (dd, *J* = 8.6, 5.5 Hz, 1H), 7.35 (dd, *J* = 9.7, 2.5 Hz, 1H), 7.11 – 6.99 (m, 2H), 5.95 (d, *J* = 17.3 Hz, 1H), 5.61 (d, *J* = 11.0 Hz, 1H).

¹³C NMR (101 MHz, CDCl₃) δ 165.28 (d, J = 255.7) , 143.93 (d, *J* = 8.8 Hz), 135.39 (d, *J* = 9.5 Hz), 132.23 (d, *J* = 2.0 Hz), 120.39, 117.21, 115.97 (d, *J* = 23.1 Hz), 112.70 (d, *J* = 23.5 Hz), 107.48 (d, *J* = 3.1 Hz).

**¹⁹F NMR (376 MHz, CDCl₃)** δ -102.65 – -102.77 (m).

IR (NaCl, Thin Film) 3405, 3096, 3074, 3020, 2224, 1886, 1605, 1484, 1432, 1318, 1276, 1232, 1180, 1158, 1084, 1060, 984, 940, 893, 817, 7563, 691 cm⁻¹

**HRMS(FI)** *m/z*: [M + •]⁺ Calculated for C_9H_6NF: 147.04843, Found: 147.04816

General Procedure C: Olefin Metathesis for the Preparation of S29 – S35
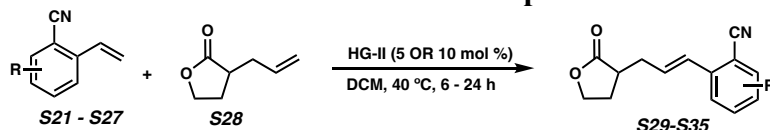
A two-necked round-bottom flask with a stir bar was flame-dried, fitted with an oven-dried reflux condenser, and cooled to room temperature under vacuum. The flask was backfilled with nitrogen, then styrene (3.0 equiv) and α-allyl-γ-butyrolactone **S28** (1.0 equiv) were added as solutions in dry dichloromethane (total concentration 0.05 M in **S28**). Subsequently, HG-II (0.05 equiv or 0.10 equiv depending on the styrene employed) was quickly added to the flask. The reaction mixture was stirred at 40 °C for 6 - 24 h depending on the substrate (until consumption of **S28** observed by TLC) then allowed to cool to ambient temperature. The crude reaction was concentrated under reduced pressure and the resulting residue was purified via silica gel flash column chromatography.
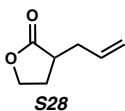
Compound **S28** was prepared according to a published procedure.[24] Spectral data was in accordance with those reported in the literature.
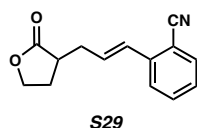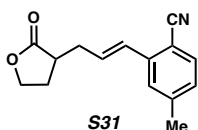

Prepared from styrene **S29** (484 mg, 3.75 mmol, 3 equiv) and lactone **S28** (0.158 mg, 1.25 mmol, 1 equiv) according to General Procedure B with a reaction time of 6 h. The crude

reaction was purified via flash column chromatography (35% EtOAc/hx) to afford **S29** as a clear oil (157.7 mg, 56% yield).

¹H NMR (400 MHz, CDCl₃) δ 7.65 – 7.58 (m, 2H), 7.53 (dddd, J = 8.1, 7.4, 1.3, 0.5 Hz, 1H), 7.32 (td, J = 7.6, 1.3 Hz, 1H), 6.83 (dd, J = 15.7, 1.6 Hz, 1H), 6.48 – 6.35 (m, 1H), 4.37 (td, J = 8.8, 2.8 Hz, 1H), 4.24 (ddd, J = 9.6, 9.1, 6.8 Hz, 1H), 2.87 – 2.72 (m, 2H), 2.63 – 2.50 (m, 1H), 2.44 (dddd, J = 12.7, 8.6, 6.8, 2.8 Hz, 1H), 2.16 – 2.00 (m, 1H).

¹³C NMR (101 MHz, CDCl₃) δ 178.57, 140.36, 133.07, 132.93, 131.84, 128.99, 127.74, 125.89, 118.10, 110.84, 66.75, 39.07, 33.72, 28.09.

IR (NaCl, thin film) 3516, 3066, 2989, 2911, 2221, 1769, 1650, 1596, 1566, 1479, 1453, 1372, 1296, 1280, 1202, 1154, 1112, 1021, 968, 915, 769, 705 cm⁻¹.

**HRMS(FI) *m/z*: [M + •]⁺** Calculated for C₁₄H₁₃NO₂: 227.09463, Found: 227.09429
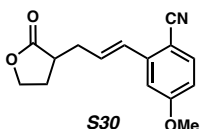
Prepared from styrene **S22** (320.6 mg, 2.01 mmol, 3 equiv) and lactone **S28** (84.7 mg, 0.671 mmol, 1 equiv) according to General Procedure B with a reaction time of 17 h. The crude reaction was purified via flash column chromatography (30% EtOAc/Hexanes) to afford **S30** as a white solid (61.8 mg, 36% yield).

¹H NMR (400 MHz, CDCl₃) δ 7.54 (dd, J = 8.7, 0.9 Hz, 1H), 7.04 (d, J = 2.5 Hz, 1H), 6.89 – 6.69 (m, 2H), 6.39 (dt, J = 15.6, 7.0 Hz, 1H), 4.38 (td, J = 8.9, 2.8 Hz, 1H), 4.24 (td, J = 9.4, 6.8 Hz, 1H), 3.87 (d, J = 0.8 Hz, 3H), 2.79 (tdd, J = 13.1, 7.0, 3.3 Hz, 2H), 2.62 – 2.50 (m, 1H), 2.44 (dddd, J = 9.4, 8.1, 6.7, 2.7 Hz, 1H), 2.15 – 2.00 (m, 1H).

¹³C NMR (101 MHz, CDCl₃) δ 178.60, 163.0, 142.35, 134.75, 131.78, 129.16, 118.5, 114.14, 110.91, 102.93, 66.78, 55.76, 39.07, 33.66, 28.08

IR (NaCl, thin film) 3521, 2976, 2943, 2914, 2596, 2217, 1769, 1760, 1650, 1600, 1562, 1493, 1486, 1299, 1244, 1157, 1025, 969, 827, 821 cm⁻¹.

HRMS(FI) *m/z*: [M + •]⁺ Calculated for C₁₅H₁₅NO₃: 257.10519, Found: 257.10486

Prepared from styrene **S23** (139.7 mg, 0.976 mmol, 3 equiv) and lactone **S28** (41 mg, 0.325 mmol, 1 equiv) according to General Procedure B with a reaction time of 21 h. The crude reaction was purified via flash column chromatography (33% EtOAc/Hexanes) to afford **S31** as a white solid (43.4 mg, 55% yield).

¹H NMR (600 MHz, CDCl₃) δ 7.56 (d, *J* = 8.5 Hz, 0H), 7.50 (d, *J* = 7.9 Hz, 1H), 7.40 (dd, *J* = 1.6, 0.8 Hz, 1H), 7.12 (ddd, *J* = 7.9, 1.7, 0.8 Hz, 1H), 6.80 (dt, *J* = 16.0, 1.5 Hz, 1H), 6.74 (d, *J* = 11.5 Hz, 0H), 6.39 (dt, *J* = 15.8, 7.1 Hz, 1H), 5.89 (dt, *J* = 11.5, 7.4 Hz, 0H), 4.37 (td, *J* = 8.8, 2.8 Hz, 1H), 4.32 (td, *J* = 8.9, 2.6 Hz, 0H), 4.24 (td, *J* = 9.4, 6.8 Hz, 1H), 2.79 (dtt, *J* = 10.4, 8.5, 4.9 Hz, 2H), 2.60 – 2.51 (m, 1H), 2.47 – 2.41 (m, 1H), 2.41 (s, 3H), 2.08 (dtd, *J* = 12.7, 9.9, 8.6 Hz, 1H).

¹³C NMR (101 MHz, CDCl₃) δ 178.64, 143.78, 140.42, 132.95, 131.37, 129.14, 128.73, 126.49, 118.43, 107.98, 66.78, 39.11, 33.69, 28.06, 22.01.

IR (NaCl, thin film) 2912, 2220, 1776, 1766, 1605, 1487, 1454, 1374, 1295, 1202, 1184, 1155, 1023, 968, 820 cm⁻¹.

HRMS(FI) *m/z*: [M + •]⁺ Calculated for C₁₅H₁₅NO₂: 241.11028, Found: 241.11023
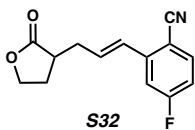
Prepared from styrene **S27** (882.9 mg, 6.0 mmol, 3 equiv) and lactone **S28** (252.3 mg, 2.0 mmol, 1 equiv) according to General Procedure B. The crude reaction was purified via flash column chromatography (30% EtOAc/hx) to afford **S32** as a tan solid (387.4 mg, 79% yield).

1H NMR (400 MHz, CDCl3) δ 7.63 (dd, J = 8.6, 5.5 Hz, 1H), 7.29 (dd, J = 9.7, 2.5 Hz, 1H), 7.03 (ddd, J = 8.7, 7.7, 2.5 Hz, 1H), 6.81 (dt, J = 15.8, 1.6 Hz, 1H), 6.44 (dt, J = 15.8, 7.1 Hz, 1H), 4.39 (td, J = 8.9, 2.7 Hz, 1H), 4.24 (td, J = 9.5, 6.7 Hz, 1H), 2.88 – 2.72 (m, 2H), 2.63 – 2.50 (m, 1H), 2.50 – 2.40 (m, 1H), 2.14 – 1.98 (m, 1H).

13C NMR (101 MHz, CDCl3) δ 178.38, 165.26 (d, J = 255.4 Hz), 143.46 (d, J = 9.1 Hz), 135.41 (d, J = 9.6 Hz), 133.36, 128.16 (d, J = 2.5 Hz), 117.42, 115.63 (d, J = 23.0 Hz), 113.00 (d, J = 23.3 Hz), 107.02, 66.73, 39.01, 33.68, 28.19.

19F NMR (376 MHz, CDCl3) δ -102.50 (td, J = 8.6, 5.6 Hz).

IR (NaCl, thin film) 2911, 2223, 1759, 1603, 1573, 1481, 1426, 1374, 1276, 1233, 1153, 1020, 975, 827, 693 cm^{-1}.

HRMS(FI) *m/z*: [M + •]$^+$ Calculated for $C_{14}H_{12}NO_2F$: 245.08521, Found: 245.08476
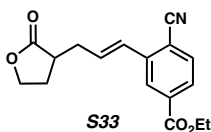
Prepared from styrene **S24** (151 mg, 0.750 mmol, 3 equiv) and lactone **S28** (31.5 mg, 0.250 mmol, 1 equiv) according to General Procedure B with a reaction time of 18.5 h. The crude
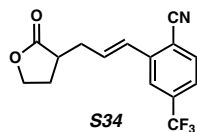
reaction was purified via flash column chromatography (33% EtOAc/Hexanes) to afford

S33 as a white solid (43.6 mg, 58% yield).

^{1}H NMR (400 MHz, CDCl$_3$) δ 8.24 (d, *J* = 1.6 Hz, 1H), 7.95 (dd, *J* = 8.1, 1.6 Hz, 1H),

7.68 (d, *J* = 8.1 Hz, 1H), 6.85 (dt, *J* = 15.6, 1.4 Hz, 1H), 6.52 (dt, *J* = 15.8, 7.1 Hz, 1H),

4.47 – 4.35 (m, 3H), 4.24 (ddd, *J* = 9.8, 9.1, 6.7 Hz, 1H), 2.91 – 2.73 (m, 2H), 2.62 – 2.51

(m, 1H), 2.46 (dddd, *J* = 12.7, 8.7, 6.7, 2.7 Hz, 1H), 2.08 (dtd, *J* = 12.7, 10.0, 8.5 Hz, 1H),

1.42 (t, *J* = 7.1 Hz, 3H).

^{13}C NMR (101 MHz, CDCl$_3$) δ 178.43, 165.16, 140.63, 134.49, 133.23, 133.14, 128.25,

128.22, 126.78, 117.38, 114.34, 66.72, 62.03, 39.03, 33.81, 28.17, 14.40

IR (NaCl, thin film) 2984, 2909, 2224, 1769, 1722, 1651, 1561, 1479, 1453, 1416, 1371,

1299, 1290, 1257, 1206, 1155, 1022, 970, 856, 765 cm^{-1}.

HRMS(FI) *m/z*: [M + •]$^+$ Calculated for C$_{17}$H$_{17}$NO$_4$: 299.11576, Found: 299.11590

Prepared from styrene **S25** (900 mg, 4.56 mmol, 3 equiv) and lactone **S13** (191.7 mg, 1.52

mmol, 1 equiv) according to General Procedure B with a reaction time of 13 h. The crude

reaction was purified via flash column chromatography (30% EtOAc/Hexanes) to afford

S34 as a white solid (262.6 mg, 59% yield).

^{1}H NMR (400 MHz, CDCl$_3$) δ 7.88 – 7.82 (m, 1H), 7.75 (d, *J* = 8.1 Hz, 1H), 7.57 (dd, *J*

= 8.2, 1.7 Hz, 1H), 6.87 (dt, *J* = 16.0, 1.4 Hz, 1H), 6.53 (dt, *J* = 15.8, 7.1 Hz, 1H), 4.40 (td,

J = 8.9, 2.6 Hz, 1H), 4.25 (td, *J* = 9.5, 6.7 Hz, 1H), 2.93 – 2.74 (m, 2H), 2.58 (dtd, *J* = 13.8,

7.6, 1.4 Hz, 1H), 2.47 (dddd, J = 12.7, 9.0, 6.7, 2.6 Hz, 1H), 2.08 (dtd, J = 12.7, 10.0, 7.6 Hz, 1H).

^{13}C NMR (101 MHz, CDCl$_3$) δ 178.32, 141.27, 135.31 – 134.30 (q, J = 33.0 Hz), 134.16, 133.71, 127.87, 124.29 (q, J = 3.7 Hz), 127.24 – 119.10 (q, J = 272.1), 123.08 – 122.62 (q, J = 3.7 Hz), 116.85, 114.05, 66.72, 38.99, 33.78, 28.23.

^{19}F NMR (282 MHz, CDCl$_3$) δ –63.55

IR (NaCl, thin film) 2913, 2230, 1774, 1423, 1377, 1329, 1208, 1166, 1130, 1073, 1024, 971, 916, 848 cm^{-1}.

HRMS(FI) *m/z*: [M + •]$^+$ Calculated for C$_{15}$H$_{12}$NO$_2$F$_3$: 295.08201, Found: 295.08017

S35
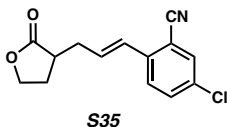
Prepared from styrene **S26** (490.8 mg, 3.0 mmol, 3 equiv) and lactone **S28** (126.2 mg, 1.0 mmol, 1 equiv) according to General Procedure B with a reaction time of 12 h. The crude reaction was purified via flash column chromatography (40% EtOAc/hx) to afford **S35** as a tan solid (237.8 mg, 91% yield).

^{1}H NMR (400 MHz, CDCl$_3$) δ 7.59 (d, J = 2.2 Hz, 1H), 7.55 (d, J = 8.6 Hz, 1H), 7.50 (dd, J = 8.6, 2.2 Hz, 1H), 6.78 (dt, J = 15.7, 1.5 Hz, 1H), 6.42 (dt, J = 15.8, 7.0 Hz, 1H), 5.95 (dt, J = 11.6, 7.3 Hz, 0H), 4.38 (td, J = 8.9, 2.7 Hz, 1H), 2.86 – 2.72 (m, 2H), 2.62 – 2.50 (m, 1H), 2.44 (dddd, J = 12.7, 8.5, 6.7, 2.8 Hz, 1H), 2.06 (dtd, J = 12.4, 10.0, 8.6 Hz, 1H).

^{13}C NMR (101 MHz, CDCl$_3$) δ 178.45, 138.90, 133.53, 133.36, 132.61, 132.47, 127.98, 127.21, 116.82, 112.13, 66.74, 39.04, 33.73, 28.15.

IR (NaCl, thin film) 3518, 3067, 2986, 2912, 2226, 1759, 1651, 1592, 1470, 1395, 1376, 1264, 1210, 1154, 1120, 1023, 971, 875, 705 cm^{-1}.

HRMS(FI) *m/z*: [M + •]$^+$ Calculated for C$_{14}$H$_{12}$NO$_2$Cl: 261.05566, Found: 261.05514

General Procedure D: Hydrogenation to Afford 187a-g
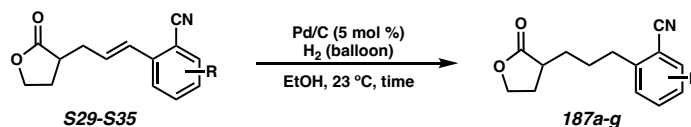
A round bottom flask equipped with a stir bar was charged with Pd/C (0.05 equiv) and alkene (1 equiv) in absolute EtOH (0.06 M). The vessel was sealed and vigorously sparged with a balloon of H$_2$ for 5 min. The reaction was stirred for 5 min to 3 hours depending on the substrate employed, until consumption of alkene was observed by LC/MS. The reaction was filtered through a short pad of celite, eluting with EtOAc. The residue was concentrated under reduced pressure and purified via flash column chromatography to afford **187a-g**.
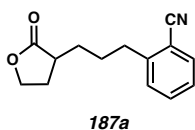
Compound **187a** was prepared via general procedure D from alkene **S29** (1 equiv, 0.62 mmol, 141.25 mg). The reaction was complete in 5 minutes, and **187a** was purified via silica gel flash chromatography (35% EtOAc/Hexanes) to afford **187a** as a clear oil (120.7 mg, 85% yield).

^{1}H NMR (400 MHz, CDCl$_3$) δ 7.62 (dd, *J* = 7.7, 1.4 Hz, 1H), 7.52 (td, *J* = 7.7, 1.4 Hz, 1H), 7.38 – 7.27 (m, 2H), 4.35 (td, *J* = 8.8, 2.8 Hz, 1H), 4.20 (td, *J* = 9.4, 6.7 Hz, 1H), 2.97

– 2.80 (m, 2H), 2.58 (dtd, J = 10.1, 8.8, 5.1 Hz, 1H), 2.50 – 2.38 (m, 1H), 2.06 – 1.89 (m, 2H), 1.89 – 1.72 (m, 2H), 1.62 – 1.48 (m, 1H).

¹³C NMR (101 MHz, CDCl₃) δ 179.28, 145.82, 133.01, 129.76, 126.84, 118.22, 112.36, 66.65, 39.09, 34.36, 29.95, 28.77, 28.61.

IR (NaCl, Thin Film) 3510, 3064, 2943, 2864, 22231769, 1599, 1573, 1485, 1454, 1376, 1293, 1180, 1150, 1021, 966, 941, 882, 828, 818, 762, 737, 702, 666, 614 cm⁻¹.

HRMS(FI) *m/z*: [M + •]⁺ Calculated for C₁₄H₁₅NO₂: 229.11028, Found: 229.10978.
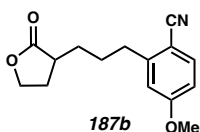
Compound **187b** was prepared via general procedure D from alkene **S30** (1 equiv, 0.62 mmol, 141.25 mg). The reaction was complete in 5 minutes, and **187b** was purified via silica gel flash chromatography (35% EtOAc/Hexanes) to afford **187b** as a clear oil (120.7 mg, 85% yield).

¹H NMR (400 MHz, CDCl₃) δ 7.58 – 7.50 (m, 1H), 6.80 (d, J = 8.1 Hz, 2H), 4.35 (td, J = 8.8, 2.8 Hz, 1H), 4.20 (ddd, J = 9.6, 9.1, 6.7 Hz, 1H), 3.85 (s, 3H), 2.92 – 2.75 (m, 2H), 2.58 (dtd, J = 10.2, 8.8, 5.1 Hz, 1H), 2.44 (dddd, J = 12.5, 8.7, 6.7, 2.8 Hz, 1H), 2.07 – 1.90 (m, 2H), 1.89 – 1.70 (m, 2H), 1.62 – 1.46 (m, 2H).

¹³C NMR (101 MHz, CDCl₃) δ 179.32, 163.06, 148.00, 134.73, 118.68, 115.32, 112.55, 104.04, 66.66, 55.67, 39.00, 34.53, 29.91, 28.76, 28.44.

IR (NaCl, Thin Film) 3517, 2932, 2864, 2217, 1769, 1605, 1567, 1495, 1463, 1455, 1374, 1311, 1291, 1248, 1179, 1171, 1147, 1109, 1023, 966, 941, 878, 815, 609 cm⁻¹

HRMS(FI) *m/z*: [M + •]⁺ Calculated for C₁₅H₁₇NO₃: 259.12084, Found: 259.11933
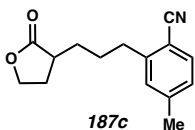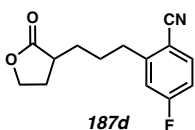
Compound **187c** was prepared via general procedure D from alkene **S31** (1 equiv, 0.717 mmol, 173.1 mg). The reaction was complete in 5 minutes, and **187c** was purified via silica gel flash chromatography (35% EtOAc/Hexanes) to afford **187c** as a clear oil (127.8 mg, 73% yield).

^{1}H NMR (400 MHz, CDCl$_3$) δ 7.49 (d, *J* = 7.8 Hz, 1H), 7.16 – 7.06 (m, 2H), 4.34 (td, *J* = 8.8, 2.8 Hz, 1H), 4.19 (td, *J* = 9.4, 6.7 Hz, 1H), 2.93 – 2.72 (m, 2H), 2.57 (dtd, *J* = 10.1, 8.8, 5.0 Hz, 1H), 2.44 (dddd, *J* = 12.6, 8.8, 6.7, 2.9 Hz, 1H), 2.39 (s, 3H), 2.04 – 1.88 (m, 2H), 1.87 – 1.69 (m, 2H), 1.54 (dtd, *J* = 13.3, 9.0, 5.4 Hz, 1H).

^{13}C NMR (101 MHz, CDCl$_3$) δ 179.25, 145.69, 143.94, 132.88, 130.52, 127.60, 118.56, 109.25, 66.66, 39.10, 34.29, 29.97, 28.76, 28.64, 21.94.

IR (NaCl, Thin Film) 3731, 3523, 2940, 2864, 2333, 2221, 1769, 1610, 1568, 1486, 1462, 1454, 1377, 1358, 1291, 1180, 1148, 1025, 967, 940, 822, 703 cm^{-1}

HRMS(FI) *m/z*: [M + •]$^+$ Calculated for C$_{15}$H$_{17}$NO$_2$: 243.12593, Found: 243.12584

Compound **187d** was prepared via General Procedure D from alkene **S32** (1 equiv, 1 mmol, 245.25 mg). The reaction was carried out in MeOH instead of EtOH (0.1 M). The reaction was complete in 5 minutes, and **187d** was purified via silica gel flash chromatography (30% EtOAc/Hexanes) to afford **187d** as an off-white solid (241.1 mg, 98% yield).

^{1}H NMR (400 MHz, CDCl$_3$) δ 7.65 (dd, *J* = 8.5, 5.5 Hz, 1H), 7.11 – 6.99 (m, 2H), 4.38 (td, *J* = 8.8, 2.7 Hz, 1H), 4.23 (ddd, *J* = 9.7, 9.1, 6.7 Hz, 1H), 2.99 – 2.82 (m, 2H), 2.60

(dtd, *J* = 10.2, 8.7, 5.2 Hz, 1H), 2.47 (dddd, *J* = 12.5, 8.8, 6.7, 2.8 Hz, 1H), 2.06 – 1.92 (m, 2H), 1.92 – 1.75 (m, 2H), 1.66 – 1.52 (m, 1H).

¹³C NMR (101 MHz, CDCl₃) δ 179.00, 166.34, 163.79, 149.20, 149.11, 135.23, 135.14, 117.38, 117.07, 116.85, 114.63, 114.40, 108.41, 108.38, 66.50, 38.93, 34.23, 34.22, 29.78, 28.67, 28.18.

¹⁹F NMR (376 MHz, CDCl₃) δ -102.35 – -102.46 (m).

IR (NaCl, Thin Film) 3523, 2934, 2868, 2225, 1769, 1608, 1583, 1488, 1468, 1461, 1454, 1422, 1375, 1280, 1241, 1218, 1175, 1152, 1107, 1024, 956, 947, 886, 875, 829, 822, 688, 634 cm⁻¹

HRMS(FI) *m/z*: [M + •]⁺ Calculated for $C_{14}H_{14}NO_2F$: 247.10086, Found: 247.10039
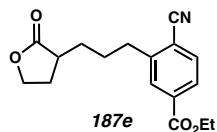
Compound **187e** was prepared via General Procedure D from alkene **S33** (1 equiv, 0.34 mmol, 102 mg). The reaction was performed in MeOH instead of EtOH (0.14 M)The reaction was complete in 3 h, and **187e** was purified via silica gel flash chromatography (35% EtOAc/Hexanes) to afford **187e** as a white solid (79.9 mg, 78% yield).

¹H NMR (400 MHz, CDCl₃) δ 8.01 – 7.92 (m, 2H), 7.69 (d, *J* = 8.0 Hz, 1H), 4.42 (t, *J* = 7.1 Hz, 2H), 4.38 – 4.32 (m, 1H), 4.20 (ddd, *J* = 9.7, 9.0, 6.7 Hz, 1H), 3.02 – 2.85 (m, 2H), 2.58 (dtd, *J* = 10.3, 8.8, 5.1 Hz, 1H), 2.45 (dddd, *J* = 12.5, 9.0, 6.7, 2.7 Hz, 1H), 2.06 – 1.91 (m, 2H), 1.91 – 1.74 (m, 2H), 1.64 – 1.50 (m, 1H), 1.42 (t, *J* = 7.1 Hz, 3H).

¹³C NMR (101 MHz, CDCl₃) δ 179.15, 165.26, 146.17, 134.53, 133.05, 130.49, 127.71, 117.47, 116.25, 66.63, 61.95, 39.10, 34.35, 30.00, 28.79, 28.59, 14.41.

IR (NaCl, Thin Film) 3516, 2985, 2938, 2226, 1769, 1727, 1608, 1567, 1462, 1454, 1415, 1371, 1296, 1270, 1262, 1207, 1178, 1149, 1105, 1024, 969, 942, 861, 818, 768, 737 cm^{-1}

HRMS(FI) *m/z*: [M + •]$^+$ Calculated for C$_{17}$H$_{19}$NO$_4$: 301.13141, Found: 301.13117
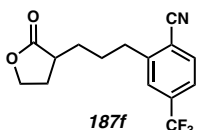
187f

Compound **187f** was prepared via General Procedure D from alkene **S34** (1 equiv, 0.887 mmol, 262.6 mg). The reaction was performed in 7:1 EtOH/EtOAc instead of EtOH (0.06 M). The reaction was complete in 30 min, and **187f** was purified via silica gel flash chromatography (35% EtOAc/Hexanes) to afford **187f** as a white solid (158.7 mg, 60% yield).

^{1}H NMR (400 MHz, CDCl$_3$) δ 7.76 (dt, *J* = 8.0, 0.8 Hz, 1H), 7.63 – 7.54 (m, 2H), 4.36 (td, *J* = 8.8, 2.7 Hz, 1H), 4.21 (ddd, *J* = 9.9, 9.1, 6.7 Hz, 1H), 3.04 – 2.87 (m, 2H), 2.59 (dtd, *J* = 10.4, 8.7, 5.2 Hz, 1H), 2.45 (dddd, *J* = 12.6, 8.9, 6.6, 2.7 Hz, 1H), 2.06 – 1.73 (m, 4H), 1.67 – 1.59 (m, 1H).

^{13}C NMR (101 MHz, CDCl$_3$) δ 179.06, 146.99, 134.80 (q, *J* = 33.2 Hz), 133.56, 127.28 – 119.12 (q, *J* = 272.4 Hz) , 126.48 (q, *J* = 3.7 Hz), 123.82 (q, *J* = 3.7 Hz), 116.91, 116.00, 66.62, 39.04, 34.43, 30.00, 28.79, 28.51.

^{19}F NMR (282 MHz, CDCl$_3$) δ -63.43.

IR (NaCl, Thin Film) 3506, 3088, 2926, 2869, 2229, 1769, 1702, 1483, 1461, 1421, 1376, 1331, 1285, 1209, 1171, 1132, 1093, 1077, 1024, 968, 941, 904, 840, 734, 723, 705, 682, 667, 623 cm^{-1}.

HRMS(FI) *m/z*: [M + •]$^+$ Calculated for C$_{15}$H$_{14}$NO$_2$F$_3$: 297.09766, Found: 297.09618.
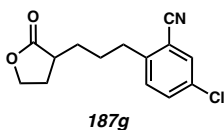
187g

Compound **187g** was prepared via General Procedure D from alkene **S35** (1 equiv, 0.887 mmol, 262.6 mg). The reaction was performed in MeOH instead of EtOH (0.1 M). The reaction was complete in 15 min, and **XXg** was purified via reverse phase chromatography (C18 reverse phase silica gel), eluting with 10-100% MeCN/H$_2$O (0.1% TFA to afford **187g** as an off-white solid (56.1 mg, 39% yield).

^{1}H NMR (400 MHz, CDCl$_3$) δ 7.59 (d, *J* = 2.2 Hz, 1H), 7.49 (dd, *J* = 8.4, 2.3 Hz, 1H), 7.28 (d, *J* = 8.4 Hz, 1H), 4.35 (td, *J* = 8.8, 2.7 Hz, 1H), 4.20 (td, *J* = 9.4, 6.6 Hz, 1H), 2.94 – 2.78 (m, 2H), 2.57 (dtd, *J* = 10.2, 8.7, 5.2 Hz, 1H), 2.44 (dddd, *J* = 12.5, 9.0, 6.6, 2.8 Hz, 1H), 2.02 – 1.87 (m, 2H), 1.87 – 1.70 (m, 2H), 1.61 – 1.49 (m, 1H).

^{13}C NMR (101 MHz, CDCl$_3$) δ 179.16, 144.33, 133.40, 132.69, 132.47, 131.13, 116.93, 113.87, 66.64, 39.06, 33.85, 29.89, 28.78, 28.49.

IR (NaCl, Thin Film) 3750, 3523, 3069, 2937, 2865, 2227, 1759, 1715, 1595, 1563, 1485, 1463, 1455, 1395, 1377, 1338, 1264, 1210, 1179, 1150, 1126, 1088, 1024, 972, 940, 899, 874, 838, 709, 641 cm^{-1}.

HRMS(FI) *m/z*: [M + •]$^+$ Calculated for C$_{14}$H$_{14}$NO$_2$Cl: 263.07131, Found: 263.07090.

Synthesis of Z Olefin Substrate 187h: Sonogashira/Lindlar Reduction Sequence

Preparation of S37: Sonogashira Coupling
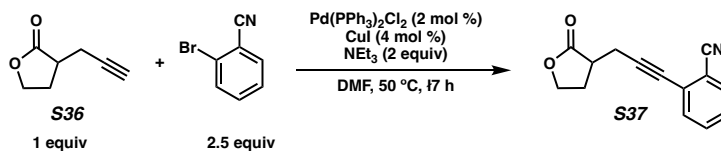
A 50 mL RBF equipped with a stir bar was flame-dried and cooled under vacuum. The flask was opened and charged with **S36** (1 equiv, 3 mmol, 372.4 mg), 2-bromobenzonitrile (2.5 equiv, 7.5 mmol, 1.365 g), and toluene (~ 20 mL). The solution was concentrated in vacuo to dry reagents. The flask was then placed under a N_2 atmosphere. A second 50 mL RBF equipped with a stir bar was flame-dried, cooled under vacuum, and backfilled with N_2. The flask was charged with Pd(PPh$_3$)$_2$Cl$_2$ (0.02 equiv, 0.06 mmol, 42.1 mg), CuI (0.04 equiv, 0.12 mmol, 22.9 mg), and 1/2 of the dry DMF (10 mL). The flask was sealed, and the solution was sparged with N_2 for 15 min. The other flask was charged with 10 mL dry DMF and sparged with N_2 for 15 min. The solution containing **S36** and 2-bromobenzonitrile was transferred to the catalyst solution via syringe. The reaction was stirred at 50 °C under N_2 for 17 h. Then, the reaction was cooled to 23 °C, diluted with EtOAc (25 mL), filtered through a pad of celite, and concentrated in vacuo. The residue was purified by silica gel flash column chromatography (30% EtOAc/Hexanes) to afford **S37** as a tan solid (580.3 mg, 86% yield).

¹H NMR (400 MHz, CDCl₃) δ 7.63 (d, *J* = 7.6 Hz, 1H), 7.58 – 7.47 (m, 2H), 7.45 – 7.35 (m, 1H), 4.48 (td, *J* = 8.9, 2.3 Hz, 1H), 4.27 (dddd, *J* = 10.1, 9.3, 6.8, 1.0 Hz, 1H), 3.02 (dd, *J* = 16.8, 4.1 Hz, 1H), 2.97 – 2.87 (m, 1H), 2.82 (dd, *J* = 16.6, 7.7 Hz, 1H), 2.65 (dddd, *J* = 12.8, 8.8, 6.7, 2.3 Hz, 1H), 2.51 – 2.35 (m, 1H).

¹³C NMR (101 MHz, CDCl₃) δ 177.69, 132.64, 132.58, 132.49, 128.38, 127.28, 117.89, 115.60, 93.14, 79.29, 66.95, 38.78, 27.92, 20.92.

IR (NaCl, Thin Film) 3522, 3039, 2986, 2913, 2229, 1769, 1592, 1564, 1482, 1455, 1445, 1378, 1346, 1303, 1212, 1170, 1158, 1100, 1022, 960, 887, 764 cm⁻¹
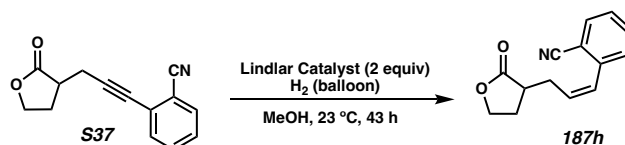
HRMS(FI) *m/z***:** $[M + \bullet]^+$ Calculated for $C_{14}H_{11}NO$: 225.07898, Found: 225.07855

Preparation of **S36**

S36
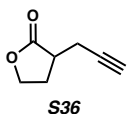
Compound **S36** was prepared according to a published procedure.[25] Spectral data were in accordance with those described in the literature.

Preparation of **187h**: Lindlar Reduction

S37   **187h**

A 50 mL 2-necked RBF equipped with a stir bar was charged with **S37** (1 equiv, 1.5 mmol) Lindlar's catalyst (1 equiv, 1.5 mmol, 337.9 mg) followed by MeOH (15 mL, 0.1 M). The vessel was sealed, evacuated and backfilled with N_2 (x 6), then evacuated and backfilled with H_2 6 x. The heterogeneous mixture was vigorously stirred under a balloon of H_2 at 23 ºC for 24 hours. After this time, an additional portion of Lindlar's catalyst (1 equiv, 1.5 mmol, 337.9 mg) was added. The vessel was sealed, evacuated, backfilled with H_2 (x 6), and stirred for an additional 19 h. The reaction was filtered through a short pad of celite, eluting with MeOH (2 x 10 mL), and the filtrate was concentrated under reduced pressure. The residue was purified sequentially via silica gel flash column chromatography then via preparative scale HPLC with C_{18} silica (30% MeCN/H_2O) to afford **187h** (165.2 mg, 48% yield).

^{1}H NMR (400 MHz, CDCl$_3$) δ 7.68 (ddd, *J* = 7.8, 1.4, 0.6 Hz, 1H), 7.58 (td, *J* = 7.7, 1.4 Hz, 1H), 7.43 – 7.32 (m, 2H), 6.78 (dt, *J* = 11.6, 1.9 Hz, 1H), 5.92 (dt, *J* = 11.6, 7.4 Hz,

1H), 4.33 (td, J = 8.9, 2.6 Hz, 1H), 4.19 (ddd, J = 10.0, 9.1, 6.7 Hz, 1H), 2.80 (dddd, J =

14.9, 6.9, 4.7, 1.9 Hz, 1H), 2.68 (dtd, J = 10.5, 8.8, 4.7 Hz, 1H), 2.49 – 2.35 (m, 2H), 1.91

(dddd, J = 12.7, 10.5, 9.9, 8.6 Hz, 1H).

^{13}C NMR (101 MHz, CDCl$_3$) δ 178.41, 140.39, 132.92, 132.59, 132.23, 129.56, 128.17,

127.57, 117.84, 112.27, 66.57, 39.14, 29.09, 28.20.

IR (NaCl, Thin Film) 3519, 3067, 2989, 2910, 2223, 1769, 1650, 1595, 1566, 1479, 1446,

1402, 1374, 1341, 1309, 1211, 1160, 1024, 955, 921, 844, 825, 777, 761, 702, 680 cm^{-1}.

HRMS(FI) *m/z*: [M + •]$^+$ Calculated for C$_{14}$H$_{13}$NO$_2$: 227.09463, Found: 227.09428.

Preparation of Tetralone Substrate 192: Alkylation/Decarboxylative Protonation Sequence

Preparation of S39: Alkylation of β-Keto Ester S38
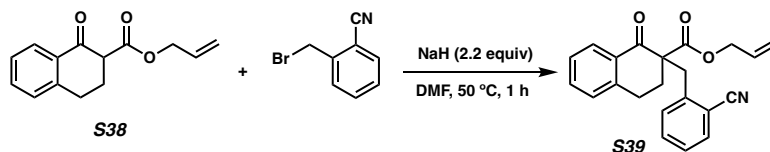
A 2-necked 25 mL RBF equipped with a stir bar was flame-dried and cooled under vacuum.

The flask was backfilled with N$_2$ and charged with a solution of **S38** in DMF (1 equiv, 1.13

mmol, 261.2 mg), then NaH (2.2 equiv, 2.49 mmol, 99.6 mg) was added portionwise. The

reaction was stirred under N$_2$ at 23 ºC for 30 min, then 2-cyanobenzyl bromide (1.5 equiv,

1.70 mmol, 333.3 mg) was added as a solid and the reaction was heated to 50 ºC for 1 hour

until **S23** was consumed. The reaction was cooled to ambient temperature, diluted with

H$_2$O (1 x 10 mL) and EtOAc (1 x 10 mL) and transferred to a separatory funnel. The

aqueous layer was extracted with EtOAc (3 x 10 mL) and the combined organic layers

were washed with H$_2$O (3 x 10 mL) then brine, dried over Na$_2$SO$_4$, and concentrated under

reduced pressure. The residue was purified via silica gel flash column chromatography (10%

EtOAc/Hexanes) to afford **S39** as a clear oil (292.0 mg, 75% yield).

¹H NMR (400 MHz, CDCl₃) δ 8.08 (dd, *J* = 7.9, 1.5 Hz, 1H), 7.62 (ddd, *J* = 7.7, 1.5, 0.6

Hz, 1H), 7.51 – 7.38 (m, 3H), 7.31 (td, *J* = 7.5, 1.4 Hz, 2H), 7.17 (d, *J* = 7.7 Hz, 1H), 5.76

(ddt, *J* = 17.6, 10.2, 5.5 Hz, 1H), 5.18 – 5.08 (m, 2H), 4.65 – 4.50 (m, 2H), 3.75 – 3.61 (m,

2H), 3.09 (ddd, *J* = 17.2, 12.2, 4.7 Hz, 1H), 2.87 (ddd, *J* = 17.5, 4.9, 3.0 Hz, 1H), 2.62 (ddd,

J = 13.6, 4.7, 3.0 Hz, 1H), 2.07 (ddd, *J* = 13.6, 12.2, 4.9 Hz, 1H).

¹³C NMR (101 MHz, CDCl₃) δ 194.04, 170.38, 143.17, 140.82, 133.85, 132.98, 132.69,

132.24, 131.82, 131.27, 128.90, 128.32, 127.52, 126.96, 118.70, 118.60, 114.69, 66.22,

59.09, 37.98, 30.67, 26.15.

IR (NaCl, Thin Film) 3067, 3027, 2933, 2223, 1730, 1688, 1649, 1599, 1485, 1450,

1356, 1294, 1260, 1233, 1180, 1123, 1101, 1065, 976, 935, 834, 802, 763, 746, 671 cm⁻¹

HRMS(FI) *m/z*: [M + •]⁺ Calculated for C₂₂H₁₉NO₃: 345.13649, Found: 345.13600
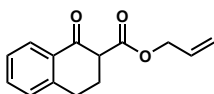
S38

Compound **S38** was prepared according to a published procedure.[26] Spectral data

matched those reported in the literature.

Preparation of Tetralone Substrate 192: Decarboxylative Protonation of S39
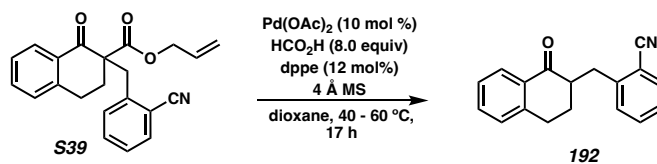
A 100 mL RBF with stir bar (capped with a 24/40 septa) was charged with 4 Å molecular

sieves (2.4 x mass substrate) and flame-dried under vacuum 3 x. The vial was cooled under

vacuum and then filled with nitrogen. The septa was secured onto the flask with electrical tape and pumped into the glovebox. Inside the glovebox, the flask was opened and charged with Pd(OAc)$_2$ (0.1 equiv, 0.093 mmol, 20.1 mg) and dppe (0.12 equiv, 0.116 mmol, 46.2 mg), sealed with a septa, and removed from the glovebox. Freshly dried 1,4-dioxane (31 mL) was added via syringe, and the reaction was heated to 40 ºC under nitrogen for 30 minutes. To the resulting green solution was added neat HCO$_2$H (8 equiv, 7.44 mmol, 0.28 mL), and the immediately **S39** (1 equiv, 0.93 mmol, 320.2 mg) was added as a solution in the remaining 1,4-dioxane (5 mL, total concentration in **S39** of 0.03 M). The reaction was heated to 60 ºC and stirred for 17 hours until **S39** was fully consumed by TLC. The reaction was cooled to room temperature, filtered through a short SiO$_2$ plug, concentrated under reduced pressure and loaded directly onto a silica gel column (20% EtOAc/hx) to afford **192** as a white solid (180.9 mg, 74% yield).

¹H NMR (400 MHz, CDCl₃) δ 8.05 (dd, *J* = 7.9, 1.5 Hz, 1H), 7.64 (dd, *J* = 7.7, 1.4 Hz, 1H), 7.58 – 7.39 (m, 3H), 7.32 (tt, *J* = 7.5, 1.6 Hz, 2H), 7.25 – 7.20 (m, 1H), 3.66 (dd, *J* = 14.0, 5.1 Hz, 1H), 3.07 – 2.95 (m, 3H), 2.94 – 2.82 (m, 1H), 2.14 (dq, *J* = 13.0, 4.3 Hz, 1H), 1.92 (tt, *J* = 12.9, 8.1 Hz, 1H).

¹³C NMR (101 MHz, CDCl₃) δ 198.55, 144.62, 143.99, 133.61, 132.98, 132.93, 132.43, 130.77, 128.88, 127.71, 126.95, 126.85, 118.40, 113.26, 49.31, 34.54, 29.03, 28.37.

IR (NaCl, Thin Film) 2938, 2222, 1680, 1598, 1482, 1452, 1291, 1222, 933, 758, 738 cm^{-1}

HRMS(FI) *m/z*: [M + •]$^+$ Calculated for C$_{18}$H$_{15}$NO: 261.11536, Found: 261.11508

Preparation of Lactam Substrate 183
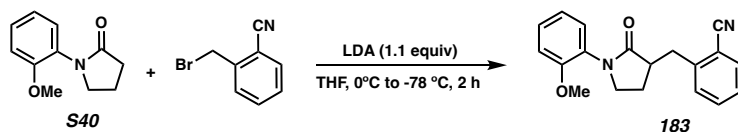
A 100 mL round-bottom flask with a stir bar was flame-dried and cooled to room temperature under vacuum. The flask was backfilled with nitrogen, then diisopropylamine (1.1 equiv, 11 mmol, 1.54 mL) and 1/3 of the THF (11 mL) were added via syringe. The flask was cooled to 0 ºC in an ice bath, then *n*-BuLi (2.5 M in hexanes, 1.1 equiv, 11 mmol, 4.4 mL) was added dropwise over ten minutes. After stirring at 0 ºC for 20 minutes, the flask was cooled to -78 ºC, and a solution of **S40** (1 equiv, 10 mmol, 1.91 g) in 1/3 of the THF (11 mL) was added dropwise over 30 minutes. Lastly, a solution of 2-cyanobenzyl bromide (1.2 equiv, 12 mmol, 2.35 g) was added dropwise over 30 minutes in the last 1/3 of the THF (11 mL, 0.3 M in **S40**) The reaction was stirred at -78 ºC for 2 hours, until consumption of **S40** was observed by TLC. The reaction was quenched at -78 ºC with sat. aq. NH$_4$Cl (30 mL), diluted with EtOAc (1 x 30 mL), then immediately warmed to ambient temperature. The reaction was transferred to a separatory funnel and the aqueous phase was extracted with EtOAc (2 x 30 mL). The combined organics were washed with brine, dried over Na$_2$SO$_4$, and concentrated. The crude reaction was purified via silica gel flash column chromatography (40-50% EtOAc/Hexanes) to give a white solid which was recrystallized from 1:4 EtOAc/Hexanes (300 mL) to afford pure **183** as a fluffy white solid (1.41 g, 46% yield).

¹H NMR (400 MHz, CDCl₃) δ 7.68 – 7.61 (m, 1H), 7.59 – 7.48 (m, 2H), 7.38 – 7.27 (m, 2H), 7.25 – 7.21 (m, 1H), 7.02 – 6.92 (m, 2H), 3.82 (s, 3H), 3.73 – 3.55 (m, 2H), 3.46 (dd,

J = 14.1, 5.0 Hz, 1H), 3.16 (dd, J = 14.1, 8.7 Hz, 1H), 3.04 – 2.92 (m, 1H), 2.22 (dddd, J

= 12.6, 8.4, 7.2, 3.4 Hz, 1H), 1.95 (ddt, J = 12.6, 9.3, 8.4 Hz, 1H).

^{13}C NMR (101 MHz, CDCl$_3$) δ 175.18, 154.91, 143.92, 133.09, 132.87, 130.59, 128.87,

128.68, 127.29, 127.09, 120.99, 118.49, 113.26, 112.14, 55.73, 48.07, 43.77, 35.08, 25.22.

IR (NaCl, Thin Film) 3384, 3064, 2940, 2900, 2880, 2837, 2222, 1695, 1595, 1503, 1486,

1460, 1525, 1407, 1302, 1278, 1253, 1183, 1161, 1122, 1104, 1045, 1024, 893, 765, 759

cm^{-1}

HRMS(FI) *m/z*: [M + •]$^{+}$ Calculated for C$_{19}$H$_{18}$N$_2$O$_2$: 306.13683, Found: 306.13659

3.4.3 Spirocyclization of Lactam 183
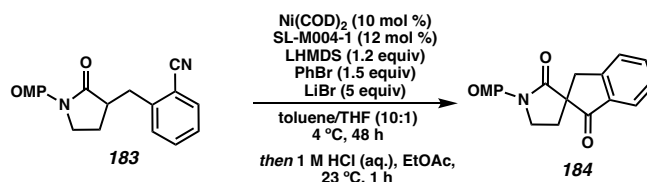
The reaction was setup according to the literature procedure on a 0.2 mmol scale.[11] The

reaction yield was determined by ^{1}H NMR relative to 1,3,5-trimethoxybenzene as an

internal standard (68% yield).

^{1}H NMR (400 MHz, CDCl$_3$) δ 7.77 (dt, J = 7.7, 1.0 Hz, 1H), 7.62 (td, J = 7.4, 1.2 Hz,

1H), 7.50 (dt, J = 7.6, 0.9 Hz, 1H), 7.44 – 7.36 (m, 1H), 7.36 – 7.27 (m, 2H), 7.02 – 6.92

(m, 2H), 4.08 (ddd, J = 9.3, 8.4, 7.5 Hz, 1H), 3.92 – 3.80 (m, 5H), 3.07 (d, J = 17.1 Hz,

1H), 2.64 (ddd, J = 12.6, 7.5, 2.8 Hz, 1H), 2.35 (dt, J = 12.6, 8.6 Hz, 1H).

¹³C NMR (101 MHz, CDCl₃) δ 204.87, 173.12, 154.98, 153.95, 135.39, 135.25, 128.94, 128.90, 127.83, 127.28, 126.55, 124.74, 121.10, 112.21, 58.90, 55.90, 47.45, 38.06, 31.02.

IR (NaCl, Thin Film) 3384, 3052, 2925, 2853, 2839, 1713, 1693, 1582, 1605, 1597, 1504, 1463, 1455, 1408, 1308, 12798, 1255, 1209, 1184, 1153, 1122, 1102, 1090, 1043, 1024, 995, 979, 918, 909, 882, 872, 806, 786, 750 cm^{-1}
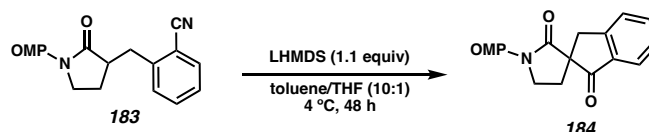
HRMS(FI) *m/z*: [M + •]$^{+}$ Calculated for $C_{19}H_{17}N_2O_3$: 307.12084, Found: 307.12200

SFC Conditions: 35% IPA, 2.5 mL/min, Chiralcel OD-H column, λ = 210 nm, t_R (min): major = 2.810, minor = 6.464
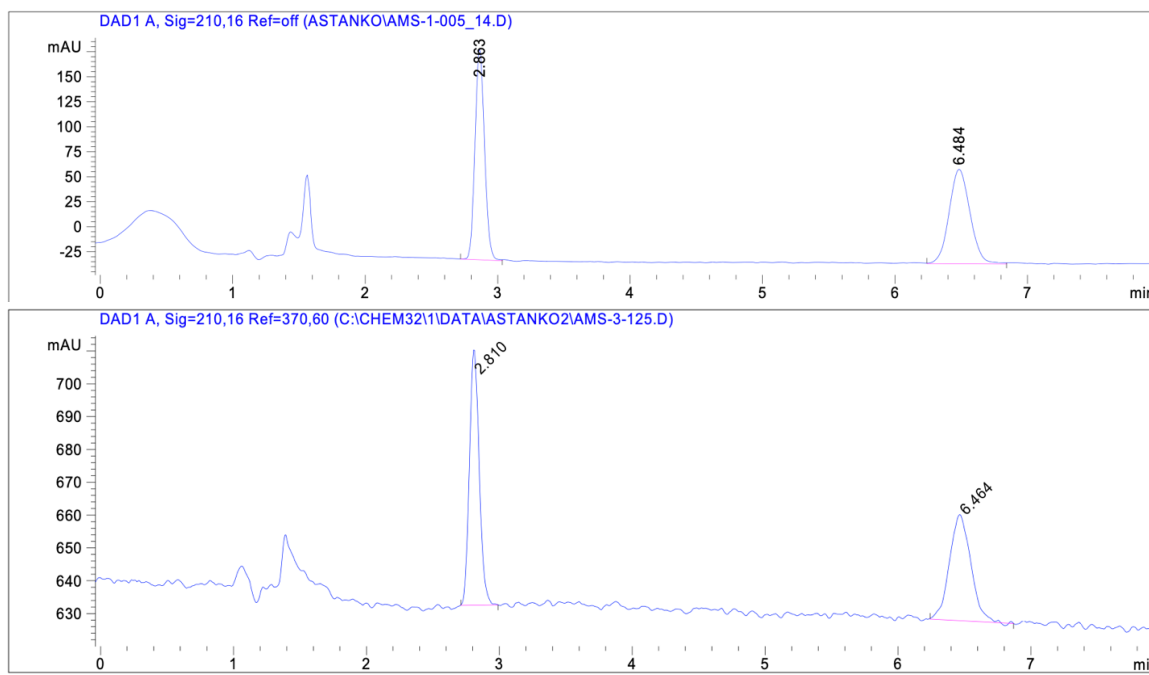
Peak #	RetTime [min]	Type	Width [min]	Area [mAU*s]	Height [mAU]	Area %
1	2.810	BB	0.0844	399.52484	77.20418	52.5985
2	6.464	BB	0.1822	360.04947	32.27435	47.4015

Background Reaction Promoted by LHMDS

A 1 dram vial with a stir bar was flame-dried and pumped into a nitrogen-filled glovebox.

The vial was charged with **183** (1 equiv, 0.05 mmol, 15.32 mg). Then, 0.55 mL of a 10:1

mixture of toluene/THF was added via syringe. The solution was chilled to 4 ºC, then

LHMDS (1.1 equiv, 0.055 mmol, 9.2 mg) was added and the resulting yellow solution

was stirred at 4 ºC for 48 h. The yield of **184** was determined to be 83% by ^{1}H NMR

relative to 1,3,5-trimethoxybenzene as an internal standard.

3.4.4 General Procedure for Spirocyclization: Optimization Scale (Procedure

Employed for Experiments in Table 2)
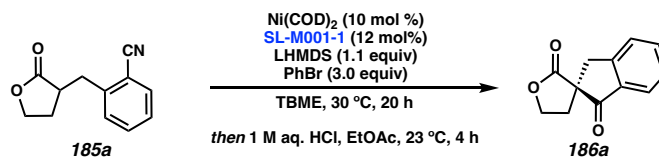
In a nitrogen-filled glovebox, a 1 dram vial was charged with a stir bar, Ni(COD)$_2$ (10

mol %, 0.006 mmol, 1.7 mg) as a solid, SL-M001-1 (12 mol%, 0.0072 mmol, 5.9 mg), and

half of the TBME (200 μL). The vial was sealed with a Teflon-lined cap. A separate 1 dram

vial was charged with a stir bar, **185a** (1 equiv, 0.06 mmol, 12.1 mg), and LHMDS (1.1

equiv, 0.066 mmol, 11.0 mg) as solids. Then, the remaining TBME (200 μL) was added

via syringe. Lastly, PhBr (3 equiv, 0.3 mmol, 32 µL) was added via microsyringe, and the vial was sealed with a Teflon-lined cap. Both vials were stirred at 30 ºC for 3 minutes, and then the vial containing the orange Ni-ligand complex was added to the vial containing the enolate solution via glass pipet. The reaction vial was sealed with a Teflon lined cap and stirred inside the nitrogen-filled glovebox at 30 ºC for 20-24 hours. The reaction was then removed from the glovebox, opened to air, transferred to a 2 dram vial, and diluted with 1 mL of EtOAc. Next, 1 mL of 1 M aq. HCl was added, the reaction was capped, and the resulting biphasic solution was stirred vigorously for 4 hours. Then, the layers were separated, and the aqueous layer was extracted with EtOAc (2 x 0.5 mL). The combined organics were washed with sat. aq. $NaHCO_3$ (1 mL), brine (1 mL), dried over Na_2SO_4, and concentrated *in vacuo*. A solution of 4,4'-Di-*tert*-butylbiphenyl in acetonitrile was added to the crude reaction, and the reaction yield was determined via HPLC using a calibration curve. Enantiomeric excess was determined by analytical SFC.
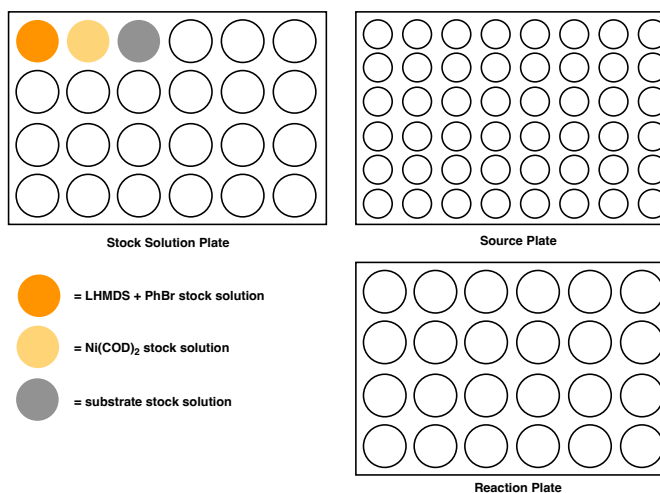
3.4.5 Additional Optimization Experiments

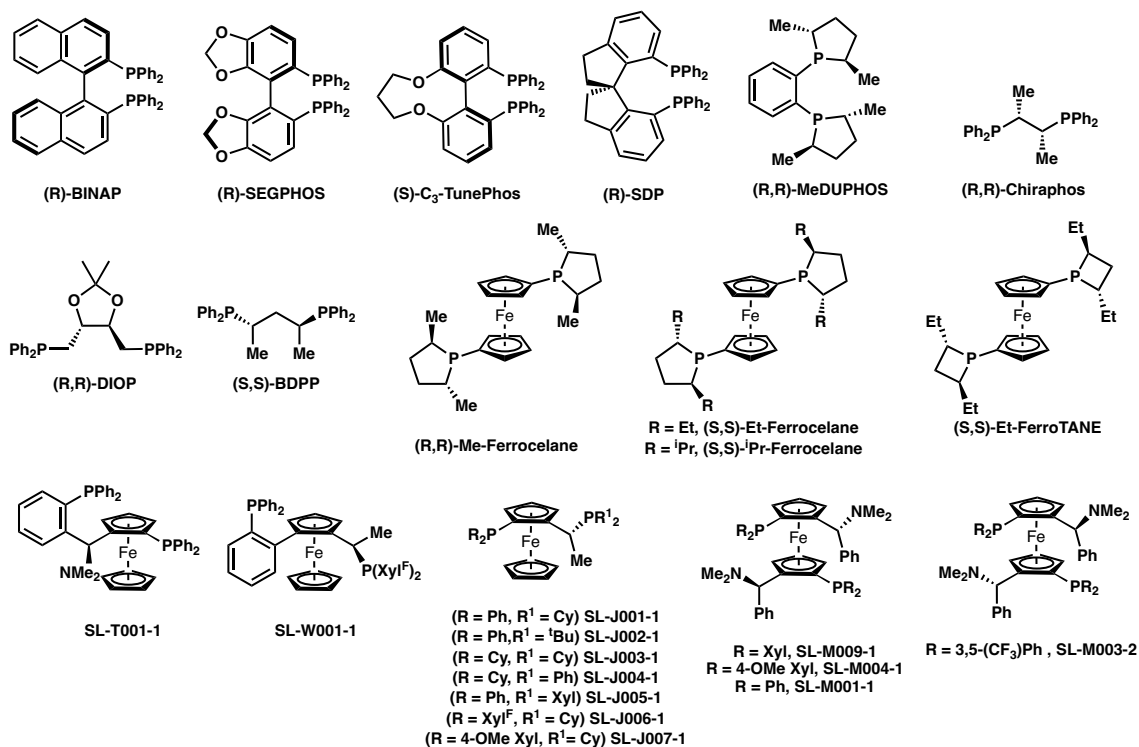**Aryl Halide Screening: (Setup Manually via General Procedure for Spirocyclization: Optimization Scale)**
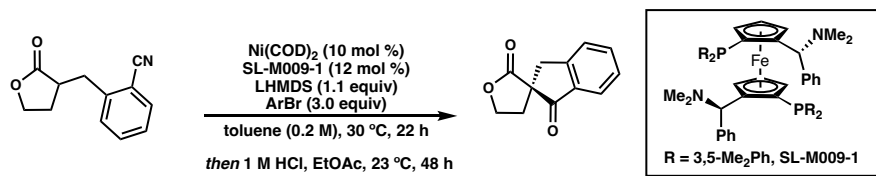
	entry	ArBr	% yield (HPLC)	% ee
	1	bromobenzene	82	80
neutral	2	2-bromotoluene	69	71
	3	3-bromotoluene	92	72
	4	2-bromoanisole	19	51
electron-rich	5	3-bromoanisole	75	76
	6	4-bromoanisole	99	75
	7	2-bromobenzotrifluoride	68	56
electron-poor	8	3-bromobenzotrifluoride	82	56
	9	4-bromobenzotrifluoride	58	53
	10	5-bromo-m-xylene	31	58
bulky	11	4-bromo-2,6-dimethylanisole	38	48
	12	4-tertbutylbromobenzene	20	4
	13	1-bromo-2-methyl-1-propene	37	21
misc.	14	2-bromonaphthalene	56	73
	15	3-bromoquinoline	19	27

Ligand Screening: Automated Reaction Setup

The following steps were performed using a custom-designed automated liquid handling system equipped with a gastight syringe (picture below).

Stock Solution Plate

Source Plate

= LHMDS + PhBr stock solution

= Ni(COD)₂ stock solution

= substrate stock solution

Reaction Plate

Ligand Screening:

(R)-BINAP   (R)-SEGPHOS   (S)-C$_3$-TunePhos   (R)-SDP   (R,R)-MeDUPHOS   (R,R)-Chiraphos

(R,R)-DIOP   (S,S)-BDPP   (R,R)-Me-Ferrocelane

R = Et, (S,S)-Et-Ferrocelane
R = ^{i}Pr, (S,S)-^{i}Pr-Ferrocelane

(S,S)-Et-FerroTANE

SL-T001-1   SL-W001-1

(R = Ph, R^1 = Cy) SL-J001-1
(R = Ph, R^1 = ^{t}Bu) SL-J002-1
(R = Cy, R^1 = Cy) SL-J003-1
(R = Cy, R^1 = Ph) SL-J004-1
(R = Ph, R^1 = Xyl) SL-J005-1
(R = Xyl^F, R^1 = Cy) SL-J006-1
(R = 4-OMe Xyl, R^1= Cy) SL-J007-1

R = Xyl, SL-M009-1
R = 4-OMe Xyl, SL-M004-1
R = Ph, SL-M001-1

R = 3,5-(CF$_3$)Ph , SL-M003-2

Ligands were weighed out by hand into 1 dram vials and placed in the reaction plate. The

source plate was filled with 1/2 dram high-recovery vials. Stock solutions of LHMDS +

PhBr, Ni(COD)$_2$, and substrate **185a** in toluene were prepared and placed in the stock

solution plate.

Command 1: Dispense 75 µL LHMDS and PhBr into source plate.

Command 2: Dispense 150 µL Ni(COD)$_2$ into reaction plate.

Command 3: Dispense 75 µL into source plate.

Command 4: Draw up solution from source plate and dispense into corresponding vial in

the reaction plate.

The reactions were manually capped, and the reaction plate was placed in a stirring module

and tumble stirred at 200 rpm for 20 hours. The reaction plate was removed from the

glovebox and each vial was diluted with 1 mL EtOAc and 1 mL aq. HCl and stirred at 23

ºC for 4 hours. The layers were separated, the organic layer was concentrated down and a

Ni(COD)$_2$ (10 mol %)
ligand (12 mol %)
LHMDS (1.1 equiv)
PhBr (3 equiv)

tol (0.16 M), 30 ºC, 22.5 h

then 1 M HCl, EtOAc, o/n
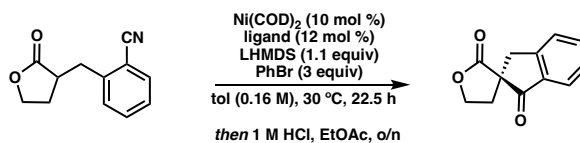
BINAP & Friends

entry	ligand	% yield (HPLC)	% ee
1	(R)-BINAP	91	37
2	(R)-SEGPHOS	44	35
3	(S)-C3-TunePhos	36	-38
4	(R)-SDP	31	-8

Other *C$_2$* - symmetric diphosphines

entry	ligand	% yield (HPLC)	% ee
5	(R,R)-MeDuPhos	27	14
6	(R,R)-ChiraPhos	11	-10
7	(R,R)-DIOP	77	-20
8	(S,S)-BDPP	96	44

Misc. Ferrocene backbone Diphosphines

entry	ligand	% yield (HPLC)	% ee
9	SL-T001-1	84	6
10	SL-W001-1	83	-10

Ferrocelane/FerroTANE Ligands

entry	ligand	% yield (HPLC)	% ee
11	(2R,5R)-Me-Ferrocelane	91	-26
12	(2S,5S)-Et-Ferrocelane	68	-26
13	(2S,5S)-^{i}Pr-Ferrocelane	17*	14
14	(2S,4S)-Et-FerroTANE	68	-24

Mandyphos ligands

entry	ligand	% yield (HPLC)	% ee
15	SL-M003-2	25	4
16	SL-M004-1	90	55
17	SL-M009-1	49	61
18	SL-M001-1	78	78

Josiphos ligands

entry	ligand	% yield (HPLC)	% ee
19	SL-J001-1	84	12
20	SL-J002-1	92	8
21	SL-J003-1	38	-6
22	SL-J004-1	51	-8
23	SL-J005-1	60	3
24	SL-J006-1	85	23
25	SL-J007-1	45	10

solution of 4,4'-Di-*tert* butylbiphenyl in acetonitrile was added to the crude reaction, and

the reaction yield was determined via HPLC using a calibration curve.

3.4.6 General Procedure for Spirocyclization: Isolation Scale
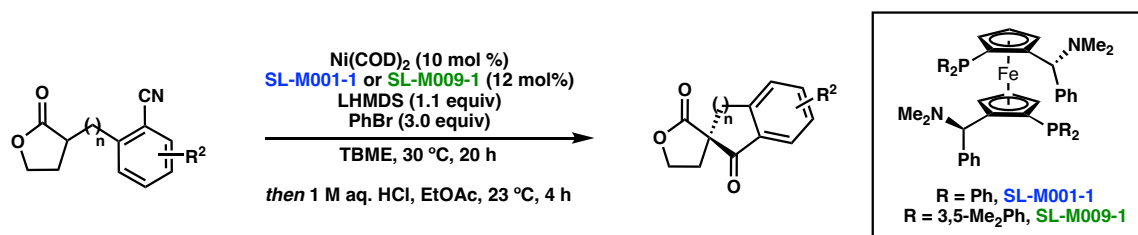
In a nitrogen-filled glovebox, a 1 dram vial was charged with a stir bar, Ni(COD)$_2$ (10

mol %, 0.01 mmol, 2.8 mg) as a solid, ligand (12 mol%, 0.012 mmol), and half of the

TBME (333 μL). The vial was sealed with a Teflon-lined cap. A separate 1 dram vial was

charged with a stir bar, substrate (1 equiv, 0.1 mmol)*, and ¼ of the TBME (167 μL).

LHMDS (1.1 equiv, 0.11 mmol, 18.4 mg) was added to the vial containing the substrate (1

equiv, 0.1 mmol) as a solution in the remaining ¼ of the TBME (167 μL). Lastly, PhBr (3

equiv, 0.3 mmol, 32 μL) was added via microsyringe and the vial was sealed with a Teflon-

lined cap. Both vials were stirred at 30 ºC for 3 minutes, and then the vial containing the

orange Ni-ligand complex was added to the vial containing the enolate solution via glass

pipet. The reaction vial was sealed with a Teflon lined cap and stirred inside the nitrogen-

filled glovebox at 30 ºC (5,6-membered rings) or 40 ºC (7-membered rings) for 20-24 hours.

The reaction was then removed from the glovebox, opened to air, transferred to a 2 dram

vial, and diluted with 2 mL of EtOAc. Next, 2 mL of 1 M aq. HCl was added, the reaction

was capped, and the resulting biphasic solution was stirred vigorously for 4 hours. Then,

the layers were separated, and the aqueous layer was extracted with EtOAc (2 x 1 mL).

The combined organics were washed with sat. aq. NaHCO$_3$ (1 mL), brine (1 mL), dried

over Na₂SO₄, and concentrated *in vacuo*. The residue was purified via flash column chromatography.

*solid substrates were added via spatula, and oils were added via stock solution in TBME.

Spectroscopic Data for Enantioenriched Spirocycles

(*R*)-4,5-dihydro-2*H*-spiro[furan-3,2'-indene]-1',2(3'*H*)-dione (186a)
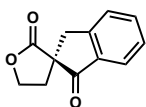
186a

¹H NMR (400 MHz, CDCl₃) δ 7.77 (d, *J* = 7.7 Hz, 1H), 7.66 (td, *J* = 7.5, 1.2 Hz, 1H), 7.51 (dt, *J* = 7.7, 1.0 Hz, 1H), 7.47 – 7.39 (m, 1H), 4.75 (td, *J* = 9.1, 7.1 Hz, 1H), 4.47 (td, *J* = 8.7, 3.0 Hz, 1H), 3.76 (d, *J* = 17.2 Hz, 1H), 3.12 (d, *J* = 17.2 Hz, 1H), 2.75 (ddd, *J* = 12.8, 7.1, 3.0 Hz, 1H), 2.46 (dt, *J* = 12.8, 9.0 Hz, 1H).

¹³C NMR (101 MHz, CDCl₃) δ 201.89, 175.79, 153.11, 136.02, 134.31, 128.36, 126.55, 125.15, 66.62, 56.73, 37.82, 33.71.

IR (NaCl, Thin Film) 3408, 2954, 2920, 2855, 1759, 1747, 1704, 1698, 1682, 1604, 1463, 1427, 1375, 1304, 1283, 1193, 1141, 1045, 1023, 990, 965, 917, 891, 781, 769, 756, 741, 724, 668 cm⁻¹

HRMS(FI) *m/z*: [M + •]⁺ Calculated for C₁₂H₁₀O₃: 202.06299, Found: 202.06196

[α]$_d^{23}$ = -91.6908 (*c* = 1.20, CHCl₃) (83% ee, with SL-M001-1)

**SFC Conditions:** 15% IPA, 2.5 mL/min, Chiralcel AD-H , λ = 254 nm, t$_R$ (min): major = 3.594, minor = 3.896

Racemic Reaction SFC Trace:
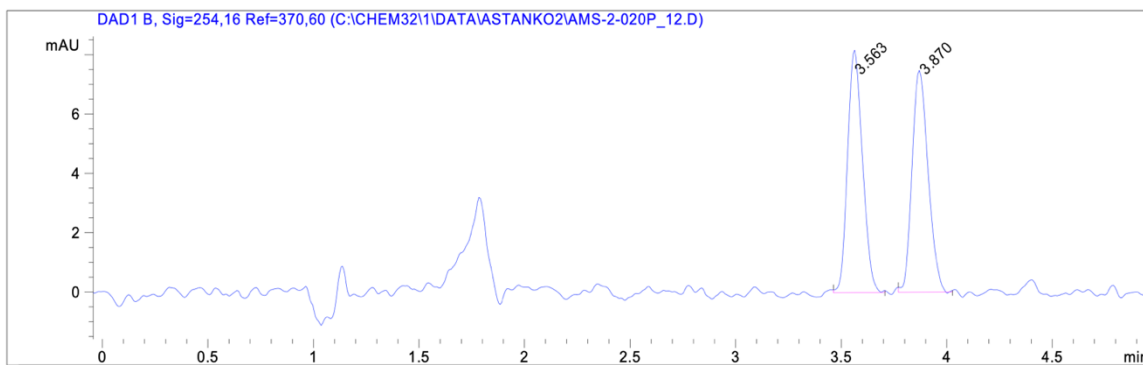
Ligand: SL-M001-1 (83% ee)
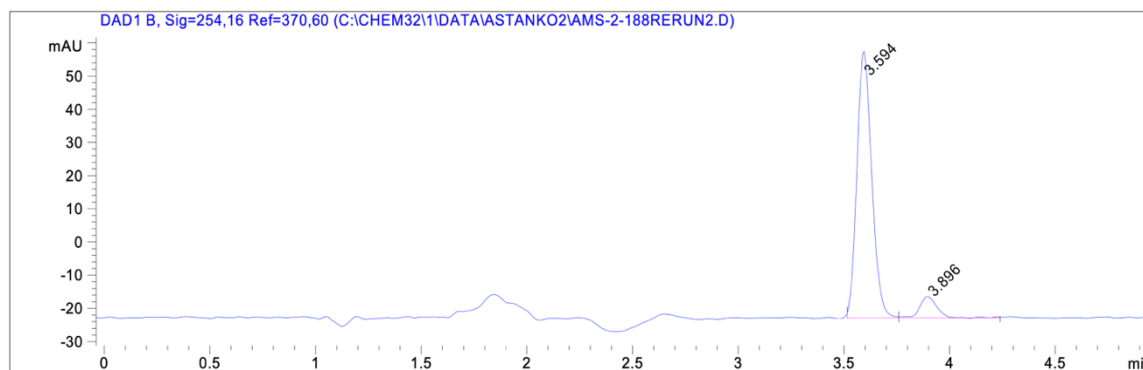
Peak #	RetTime [min]	Type	Width [min]	Area [mAU*s]	Height [mAU]	Area %
1	3.594	BB	0.0775	392.11343	79.54290	91.3891
2	3.896	BB	0.0872	36.94589	6.41641	8.6109

Ligand: SL-M009-1 (69% ee)
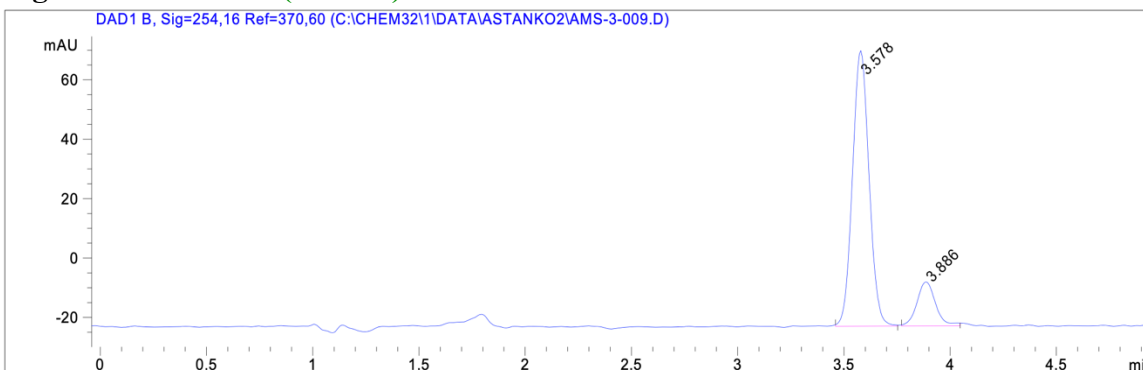
Peak #	RetTime [min]	Type	Width [min]	Area [mAU*s]	Height [mAU]	Area %
1	3.578	BB	0.0852	502.68723	92.82005	84.6862
2	3.886	BB	0.0934	90.90060	14.85968	15.3138

(*R*)-5'-methoxy-4,5-dihydro-2*H*-spiro[furan-3,2'-indene]-1',2(3'*H*)-dione (186b)
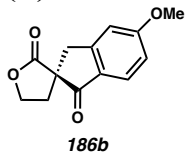
Prepared via "General Procedure for Spirocyclization: Isolation Scale". The residue was purified via flash column chromatography (10% EtOAc/toluene) to afford **186b** as a yellow oil.

With **SL-M001-1**: 12.1 mg, 52% yield

With **SL-M009-1**: 15.5 mg, 67% yield

^{1}H NMR (400 MHz, CDCl$_3$) δ 7.62 (d, *J* = 8.5 Hz, 1H), 6.92 – 6.81 (m, 2H), 4.68 (td, *J* = 9.0, 7.2 Hz, 1H), 4.38 (td, *J* = 8.8, 2.9 Hz, 1H), 3.83 (s, 3H), 3.62 (d, *J* = 17.2 Hz, 1H), 2.98 (d, *J* = 17.2 Hz, 1H), 2.67 (ddd, *J* = 12.8, 7.1, 2.9 Hz, 1H), 2.37 (dt, *J* = 12.8, 9.1 Hz, 1H).
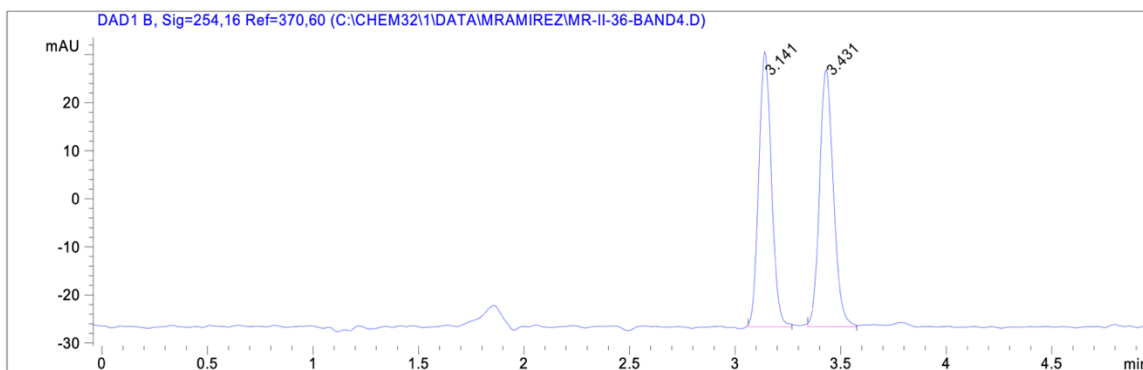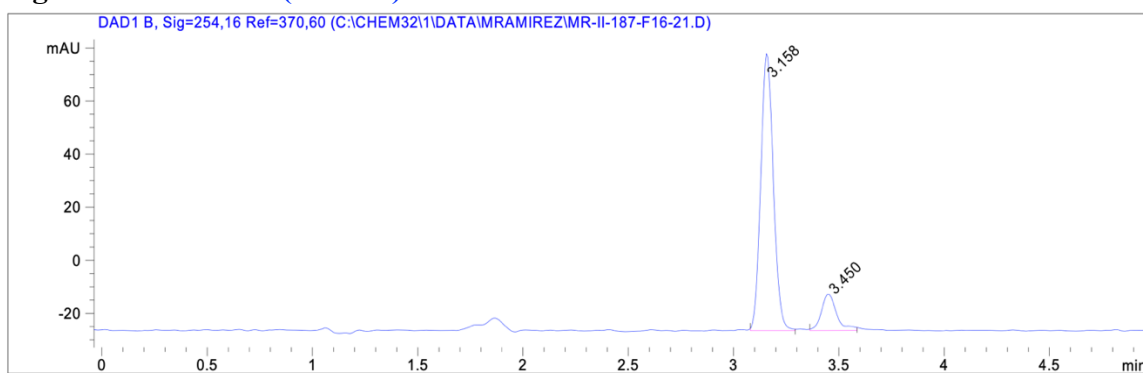
^{13}C NMR (101 MHz, CDCl$_3$) δ 199.82, 176.20, 166.38, 156.18, 127.36, 126.81, 116.55, 109.61, 66.65, 60.67, 56.91, 55.94, 37.75, 33.68.

IR (NaCl, Thin Film) 3059, 2979, 2942, 2918, 2843, 1789, 1634, 1599, 1488, 1453, 1427, 1375, 1340, 1308, 1271, 1221, 1179, 1132, 1184, 1025, 988, 96, 927, 910, 877, 848, 819, 777, 736, 700, 665 cm^{-1}

HRMS(FI) *m/z*: [M + •]$^+$ Calculated for C$_{13}$H$_{12}$O$_4$: 232.07356, Found: 232.07305

[α]$_d^{23}$ = -199.8078 (*c* = 0.9, CHCl$_3$) (84% ee, with SL-M001-1)

SFC Conditions: 20% IPA, 2.5 mL/min, Chiralcel AD-H , λ = 254 nm, t$_R$ (min): major = 3.594, minor = 3.896

**Racemic Reaction SFC Trace:**
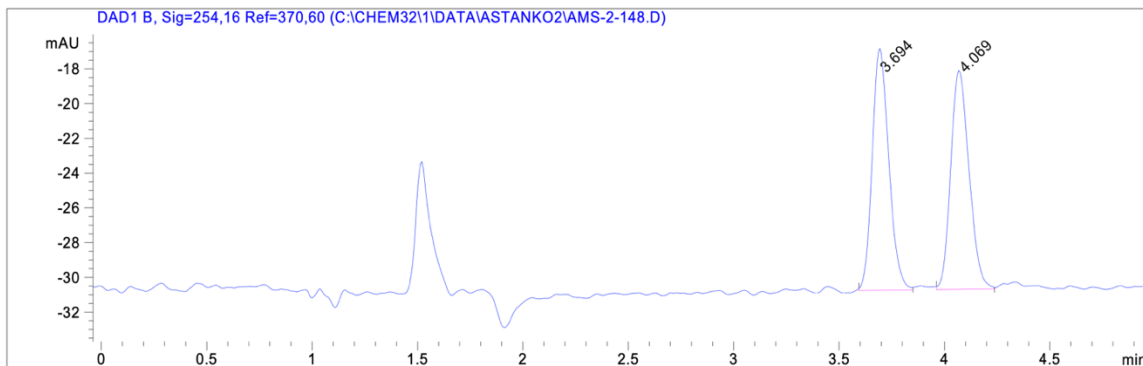
Ligand: SL-M001-1 (84% ee)
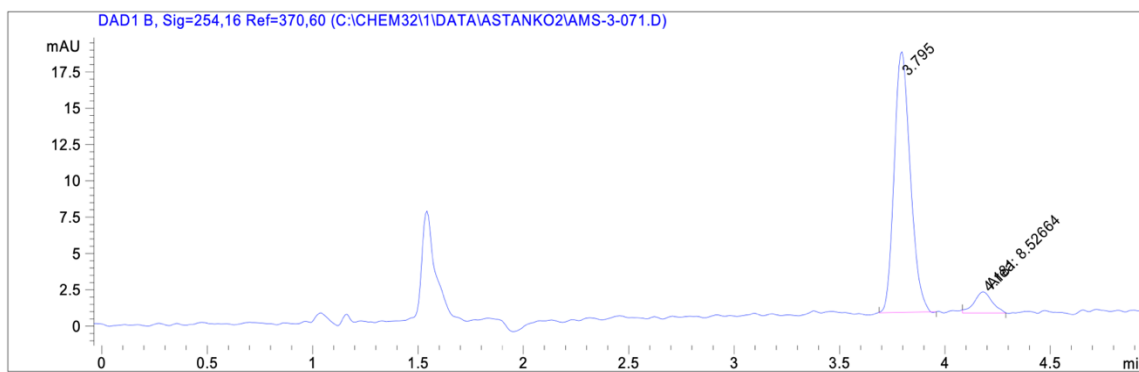
Peak #	RetTime [min]	Type	Width [min]	Area [mAU*s]	Height [mAU]	Area %
1	3.795	BB	0.0866	95.48299	17.80623	91.8021
2	4.181	MM	0.0973	8.52664	1.45980	8.1979

Ligand: SL-M001-1 (83% ee)
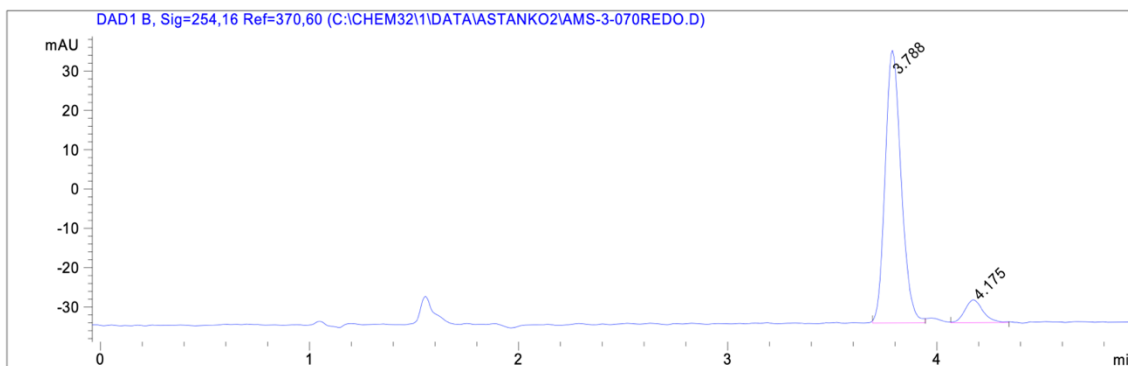
Peak #	RetTime [min]	Type	Width [min]	Area [mAU*s]	Height [mAU]	Area %
1	3.788	BB	0.0824	368.97717	69.02843	91.3628
2	4.175	BB	0.0946	34.88214	5.76245	8.6372

(*R*)-5'-fluoro-4,5-dihydro-2*H*-spiro[furan-3,2'-indene]-1',2(3'*H*)-dione (186c)
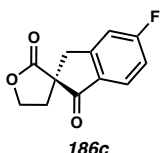
Prepared via "General Procedure for Spirocyclization: Isolation Scale". The residue was purified via flash column chromatography (10% EtOAc/toluene) to afford **186c** as a white solid.

With **SL-M001-1**: 8.0 mg, 36% yield

With **SL-M009-1**: 17.7 mg, 80% yield

^{1}H NMR (400 MHz, CDCl$_3$) δ 7.72 (dd, *J* = 8.4, 5.2 Hz, 1H), 7.15 – 7.03 (m, 2H), 4.69 (ddd, *J* = 9.4, 8.8, 7.1 Hz, 1H), 4.41 (td, *J* = 8.8, 2.8 Hz, 1H), 3.67 (d, *J* = 17.4 Hz, 1H), 3.04 (d, *J* = 17.4 Hz, 1H), 2.69 (ddd, *J* = 12.8, 7.1, 2.9 Hz, 1H), 2.39 (dt, *J* = 12.8, 9.1 Hz, 1H).

^{13}C NMR (101 MHz, CDCl$_3$) δ 199.93, 175.49, 169.26, 166.69, 156.07, 155.97, 130.70, 130.69, 127.60, 127.50, 117.00, 116.76, 113.49, 113.26, 66.65, 57.07, 37.56, 33.57.

IR (NaCl, Thin Film) 2915, 1760, 1704, 1614, 1592, 1375, 1306, 1256, 1234, 1180, 1091, 1024, 991, 682 cm^{-1}

HRMS(FI) *m/z*: [M + •]$^+$ Calculated for C$_{12}$H$_{12}$O$_3$F: 220.05357, Found: 220.05320

[α]$_d^{23}$ = -33.1477 (*c* = 1.07, CHCl$_3$) (73% ee, with SL-M001-1)

**SFC Conditions:** 15% IPA, 2.5 mL/min, Chiralcel AD-H , λ = 254 nm, t$_R$ (min): major = 3.594, minor = 3.896

Racemic Reaction SFC Trace:

DAD1 B, Sig=254,16 Ref=370,60 (C:\CHEM32\1\DATA\MRAMIREZ\MR-II-36-BAND4.D)

Ligand: SL-M001-1 (73% ee)

DAD1 B, Sig=254,16 Ref=370,60 (C:\CHEM32\1\DATA\MRAMIREZ\MR-II-187-F16-21.D)

Peak #	RetTime [min]	Type	Width [min]	Area [mAU*s]	Height [mAU]	Area %
1	3.158	BB	0.0689	435.17227	103.75427	86.3326
2	3.450	BB	0.0788	68.89269	13.67562	13.6674

Ligand: SL-M001-1 (61% ee)

DAD1 B, Sig=254,16 Ref=370,60 (C:\CHEM32\1\DATA\MRAMIREZ\MR-II-188-F27-43.D)
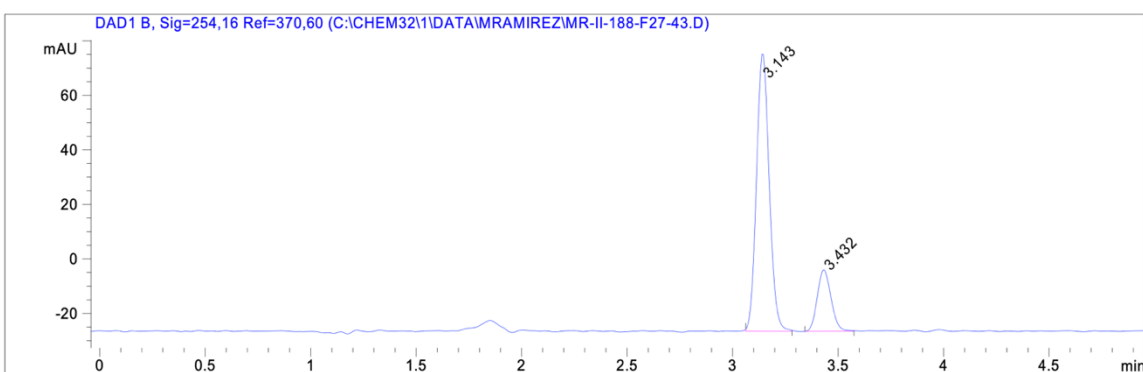
Peak #	RetTime [min]	Type	Width [min]	Area [mAU*s]	Height [mAU]	Area %
1	3.143	BB	0.0657	428.47272	100.60065	80.6942
2	3.432	BB	0.0731	102.51039	22.52154	19.3058

(*R*)-3',4,4',5-tetrahydro-1'*H*,2*H*-spiro[furan-3,2'-naphthalene]-1',2-dione (186d)
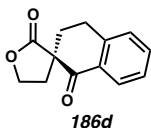
Prepared via "General Procedure for Spirocyclization: Isolation Scale". The residue was purified via flash column chromatography (10% EtOAc/toluene) to afford **186d** as a white solid.

With **SL-M001-1**: 17.5 mg, 81% yield

With **SL-M009-1**: 19.5 mg, 90% yield

^{1}H NMR (400 MHz, CDCl$_3$) δ 8.05 (dd, *J* = 7.9, 1.4 Hz, 1H), 7.53 (td, *J* = 7.5, 1.5 Hz, 1H), 7.35 (td, *J* = 7.6, 1.1 Hz, 1H), 7.28 (d, *J* = 7.8 Hz, 1H), 4.52 – 4.38 (m, 2H), 3.36 – 3.25 (m, 1H), 2.98 (ddd, *J* = 17.0, 9.4, 4.7 Hz, 1H), 2.74 (ddd, *J* = 13.0, 6.8, 3.9 Hz, 1H), 2.65 (ddd, *J* = 14.0, 9.4, 4.7 Hz, 1H), 2.28 (dt, *J* = 13.0, 8.6 Hz, 1H), 2.17 (ddd, *J* = 13.7, 6.5, 4.7 Hz, 1H).

^{13}C NMR (101 MHz, CDCl$_3$) δ 194.21, 175.91, 143.71, 134.50, 130.27, 128.97, 128.48, 127.30, 65.91, 54.74, 33.03, 31.35, 25.58.

IR (NaCl, Thin Film) 3530, 3332, 3064, 2933, 2867, 1769, 1673, 1600, 1480, 1454, 1434, 1375, 1356, 1339, 1320, 1297, 1231, 1210, 1183, 1157, 1114, 1057, 1030, 983, 973, 939, 906, 825, 800, 780, 746, 727, 697, 665, 644 cm^{-1}

HRMS(FI) *m/z*: [M + •]$^+$ Calculated for C$_{13}$H$_{12}$O$_3$:216.07864, Found: 216.07776

**[α]$_d^{23}$** = -56.3394 (*c* = 0.71, CHCl$_3$) (50% ee, with SL-M001-1)

SFC Conditions: 40% IPA, 2.5 mL/min, Chiralcel IC , λ = 254 nm, t$_R$ (min): major = 5.592, minor = 6.445

Racemic Reaction SFC Trace:

Ligand: **SL-M001-1 (50% ee)**
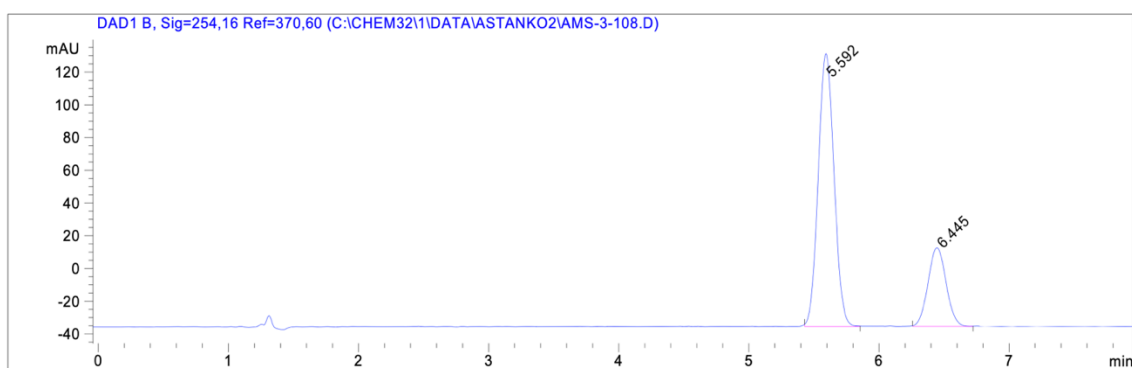
Peak #	RetTime [min]	Type	Width [min]	Area [mAU*s]	Height [mAU]	Area %
1	5.592	BB	0.1306	1406.28772	166.45354	75.2358
2	6.445	BB	0.1526	462.88586	47.95432	24.7642

Ligand: SL-M009-1 (35% ee)
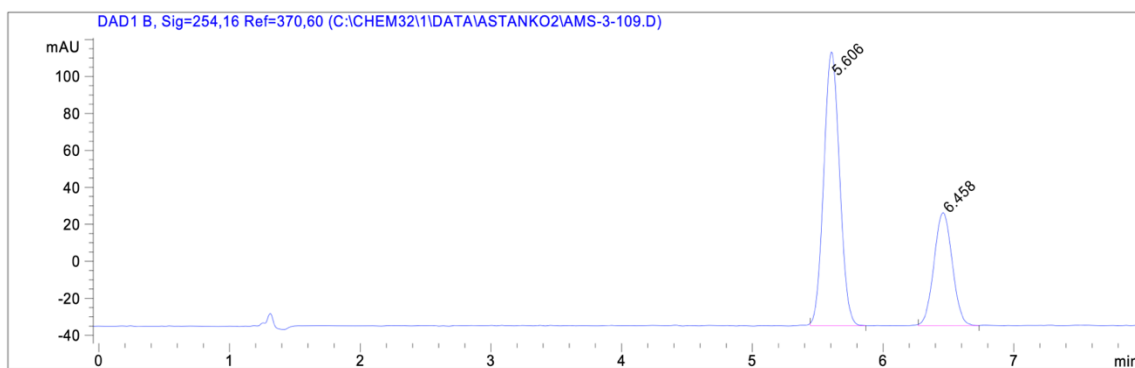
Peak #	RetTime [min]	Type	Width [min]	Area [mAU*s]	Height [mAU]	Area %
1	5.606	BB	0.1304	1247.08411	147.86218	67.7350
2	6.458	BB	0.1535	594.03723	61.08478	32.2650

(*R*)-4',5',8,9-tetrahydro-2'*H*-spiro[benzo[7]annulene-6,3'-furan]-2',5(7*H*)-dione (188a)
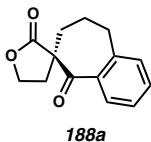
188a

Prepared via "General Procedure for Spirocyclization: Isolation Scale". The residue was purified via flash column chromatography (10% EtOAc/toluene) to afford **188a** as a white solid.

With **SL-M001-1**: 12.4 mg, 54% yield

With **SL-M009-1**: 23.3 mg, 84% yield

¹H NMR (600 MHz, CDCl₃) δ 7.50 – 7.42 (m, 2H), 7.32 (td, *J* = 7.5, 1.2 Hz, 1H), 7.17 (d, *J* = 7.1 Hz, 1H), 4.51 (dt, *J* = 8.8, 7.7 Hz, 1H), 4.39 (td, *J* = 8.6, 4.2 Hz, 1H), 2.95 (ddd, *J* = 14.6, 6.0, 4.6 Hz, 1H), 2.79 (ddd, *J* = 14.6, 10.3, 6.3 Hz, 1H), 2.71 (ddd, *J* = 12.9, 7.5, 4.2 Hz, 1H), 2.32 (dt, *J* = 12.9, 8.2 Hz, 1H), 2.26 (ddd, *J* = 14.7, 10.2, 5.8 Hz, 1H), 2.04 (ddtd, *J* = 14.2, 10.1, 5.9, 4.2 Hz, 1H), 1.97 – 1.89 (m, 1H), 1.86 (ddd, *J* = 14.6, 5.6, 4.2 Hz, 1H).

¹³C NMR (101 MHz, CDCl₃) δ 206.82, 176.47, 138.66, 137.97, 132.72, 128.99, 128.53, 127.30, 66.18, 57.89, 32.67, 31.98, 30.10, 22.11.

IR (NaCl, Thin Film) 2942, 2868, 1759, 1667, 1597, 1448, 1377, 1351, 1293, 1256, 1218, 1184, 1152, 1028, 958, 889, 765, 709 cm⁻¹

HRMS(FI) *m/z*: [M + •]⁺ Calculated for C₁₄H₁₄O₃: 230.09429, Found: 230.09380

[α]ᴅ²³ = -22.0581 (*c* = 0.74, CHCl₃) (86% ee, with SL-M009-1)

**SFC Conditions:** 15% IPA, 2.5 mL/min, Chiralcel AD-H , λ = 254 nm, tᴿ (min): major = 5.058, minor = 5.431

Racemic Reaction SFC Trace:

DAD1 B, Sig=254,16 Ref=370,60 (C:\CHEM32\1\DATA\ASTANKO2\AMS-3-075.D)

Ligand: SL-M001-1 (78% ee)

DAD1 B, Sig=254,16 Ref=370,60 (C:\CHEM32\1\DATA\ASTANKO2\AMS-3-076.D)

Peak #	RetTime [min]	Type	Width [min]	Area [mAU*s]	Height [mAU]	Area %
1	5.058	BB	0.1033	52.25823	7.69287	10.7509
2	5.431	BB	0.1120	433.82452	60.27815	89.2491

Ligand: SL-M009-1 (86% ee)

DAD1 B, Sig=254,16 Ref=370,60 (C:\CHEM32\1\DATA\ASTANKO2\AMS-2-240.D)
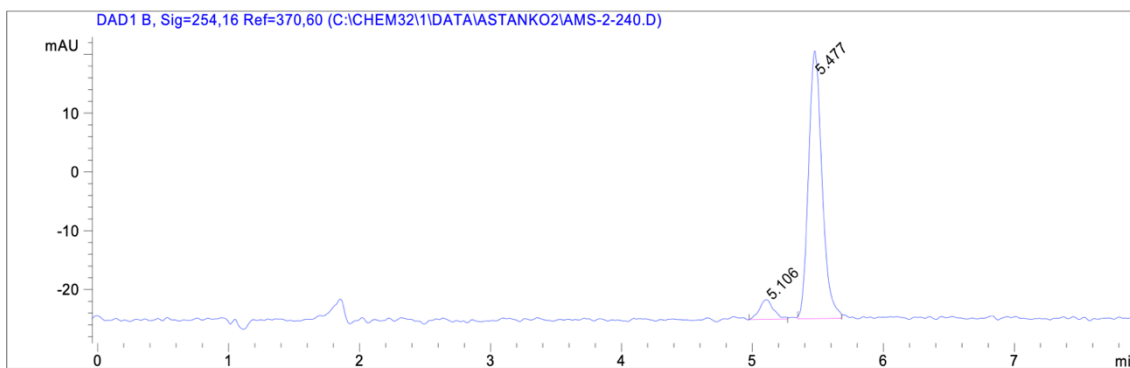
Peak #	RetTime [min]	Type	Width [min]	Area [mAU*s]	Height [mAU]	Area %
1	5.106	BB	0.1110	24.85866	3.33173	7.0396
2	5.477	BB	0.1084	328.26852	45.38785	92.9604

(*R*)-2-methoxy-4',5',8,9-tetrahydro-2'*H*-spiro[benzo[7]annulene-6,3'-furan]-2',5(7*H*)-dione (188b)
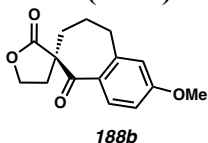
188b

Prepared via "General Procedure for Spirocyclization: Isolation Scale". The residue was purified via flash column chromatography (0-10% EtOAc/toluene) to afford **188b** as a white solid.

With **SL-M001-1**: 10.5 mg, 40% yield

With **SL-M009-1**: 14.5 mg, 58% yield

^{1}H NMR (400 MHz, CDCl3) δ 7.54 (d, *J* = 8.6 Hz, 1H), 6.82 (dd, *J* = 8.6, 2.5 Hz, 1H), 6.67 (d, *J* = 2.5 Hz, 1H), 4.50 (td, *J* = 8.5, 7.3 Hz, 1H), 4.39 (td, *J* = 8.6, 3.9 Hz, 1H), 3.85 (s, 3H), 2.91 (ddd, *J* = 14.6, 6.1, 4.5 Hz, 1H), 2.80 (ddd, *J* = 14.6, 10.4, 6.1 Hz, 1H), 2.69 (ddd, *J* = 12.9, 7.4, 3.9 Hz, 1H), 2.39 – 2.23 (m, 2H), 2.03 (tq, *J* = 11.3, 4.8 Hz, 1H), 1.98 – 1.89 (m, 1H), 1.89 – 1.80 (m, 1H).

^{13}C NMR (101 MHz, CDCl3) δ 204.86, 176.84, 163.16, 140.78, 131.45, 131.15, 114.73, 111.90, 65.93, 57.78, 55.44, 32.58, 32.47, 29.84, 22.03.

IR (NaCl, Thin Film) 3514, 2946, 2868, 1765, 1731, 1659, 1651, 1598, 1573, 1556, 1493, 1454, 1375, 1351, 1313, 1285, 1272, 1252, 1214, 1185, 1168, 1116, 1098, 1032, 995, 958, 914, 856, 825, 777, 673 cm^{-1}

HRMS(FI) *m/z*: [M + •]$^{+}$ Calculated for $C_{15}H_{16}O_4$: 260.10486, Found: 260.10464

[α]$_d^{23}$ = -15.1893 (*c* = 1.21, CHCl$_3$) (90% ee, with SL-M009-1)

**SFC Conditions:** 25% IPA, 2.5 mL/min, Chiralcel AD-H , λ = 254 nm, t$_R$ (min): major = 5.058, minor = 5.431

Racemic Reaction SFC Trace:
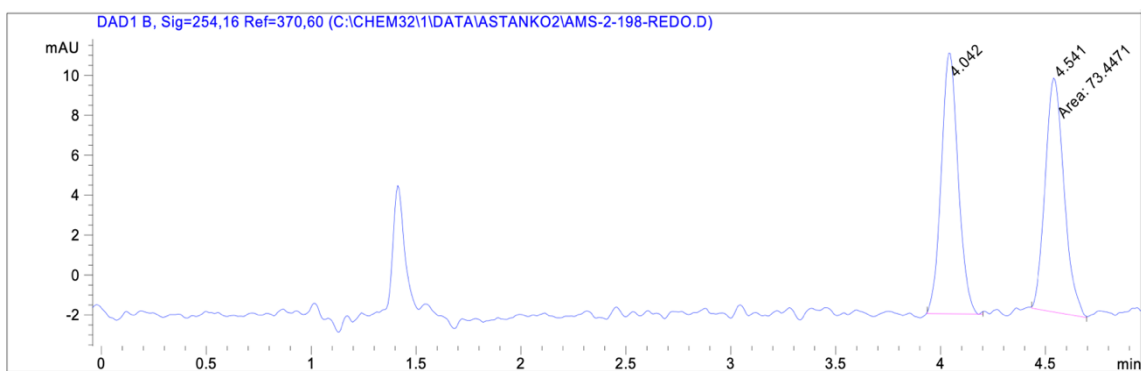
Ligand: SL-M001-1 (84% ee)
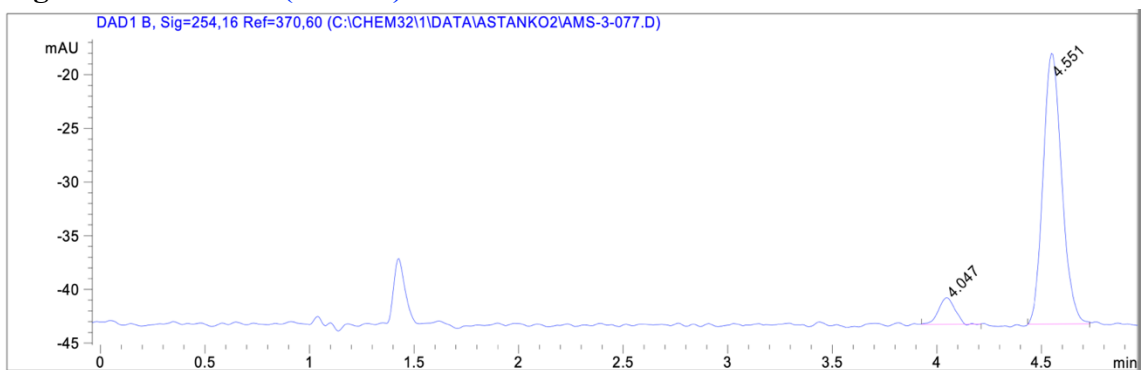
Peak #	RetTime [min]	Type	Width [min]	Area [mAU*s]	Height [mAU]	Area %
1	4.047	BB	0.0875	13.40620	2.46214	7.8637
2	4.551	BB	0.0968	157.07646	25.16463	92.1363

Ligand: SL-M009-1 (90% ee)
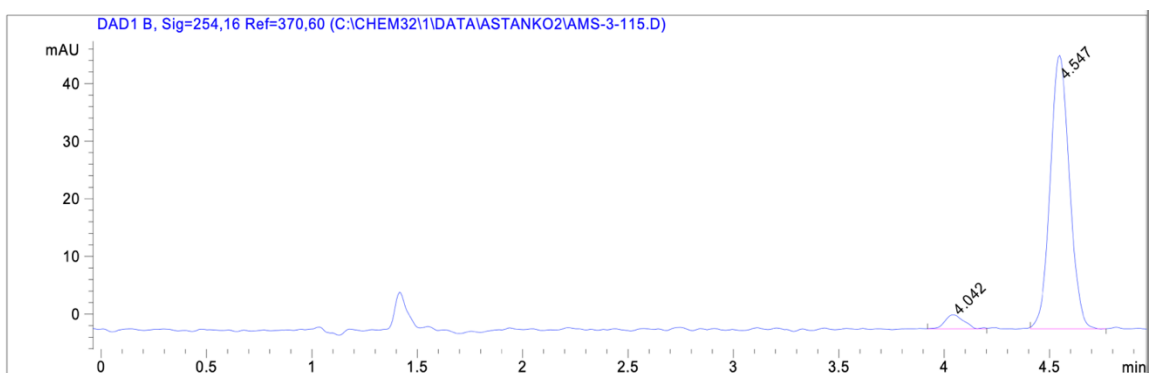
Peak #	RetTime [min]	Type	Width [min]	Area [mAU*s]	Height [mAU]	Area %
1	4.042	BB	0.0952	15.33959	2.44568	4.8399
2	4.547	BB	0.1001	301.59924	47.46842	95.1601

(*R*)-2-methyl-4',5',8,9-tetrahydro-2'*H*-spiro[benzo[7]annulene-6,3'-furan]-2',5(7*H*)-dione (188c)
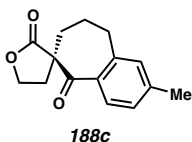
Prepared via "General Procedure for Spirocyclization: Isolation Scale". The residue was purified via flash column chromatography (10% EtOAc/toluene) to afford **188c** as a white solid.

With **SL-M001-1**: 13.8 mg, 57% yield

With **SL-M009-1**: 15.7 mg, 62% yield

^{1}H NMR (400 MHz, CDCl$_3$) δ 7.41 (d, *J* = 7.7 Hz, 1H), 7.12 (dd, *J* = 7.9, 1.6 Hz, 1H), 6.98 (s, 1H), 4.49 (q, *J* = 8.2 Hz, 1H), 4.38 (td, *J* = 8.6, 4.0 Hz, 1H), 2.90 (dt, *J* = 14.6, 5.3 Hz, 1H), 2.83 – 2.74 (m, 1H), 2.74 – 2.64 (m, 1H), 2.37 (s, 3H), 2.37 – 2.20 (m, 2H), 2.09 – 1.80 (m, 3H).

^{13}C NMR (101 MHz, CDCl$_3$) δ 206.29, 176.70, 143.45, 138.23, 135.92, 129.85, 128.98, 127.94, 66.10, 57.94, 32.71, 32.14, 30.12, 22.19, 21.63.

IR (NaCl, Thin Film) 3514, 2948, 2869, 1767, 1667, 1605, 1453, 1383, 1348, 1315, 1294, 1284, 1251, 1236, 1210, 1183, 1152, 1117, 1034, 1014, 1117, 1034, 1014, 990, 959, 918, 852, 828, 775, 703 cm^{-1}

HRMS(FI) *m/z*: [M + •]$^+$ Calculated for C$_{15}$H$_{16}$O$_4$: 244.10994, Found: 244.10963

[α]$_d^{23}$ = -19.8090 (*c* = 1.11, CHCl$_3$) (90% ee, with SL-M009-1)

**SFC Conditions:** 15% IPA, 2.5 mL/min, Chiralcel AD-H , λ = 254 nm, t$_R$ (min): major = 7.021, minor = 7.686

Racemic Reaction SFC Trace:

DAD1 B, Sig=254,16 Ref=370,60 (C:\CHEM32\1\DATA\ASTANKO2\AMS-3-120.D)

Ligand: SL-M001-1 (90% ee)

DAD1 B, Sig=254,16 Ref=370,60 (C:\CHEM32\1\DATA\ASTANKO2\AMS-3-118-DI.D)
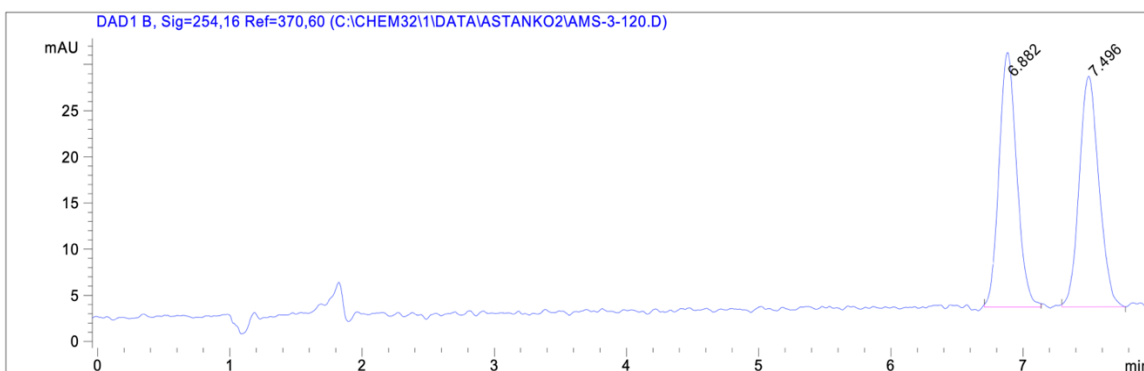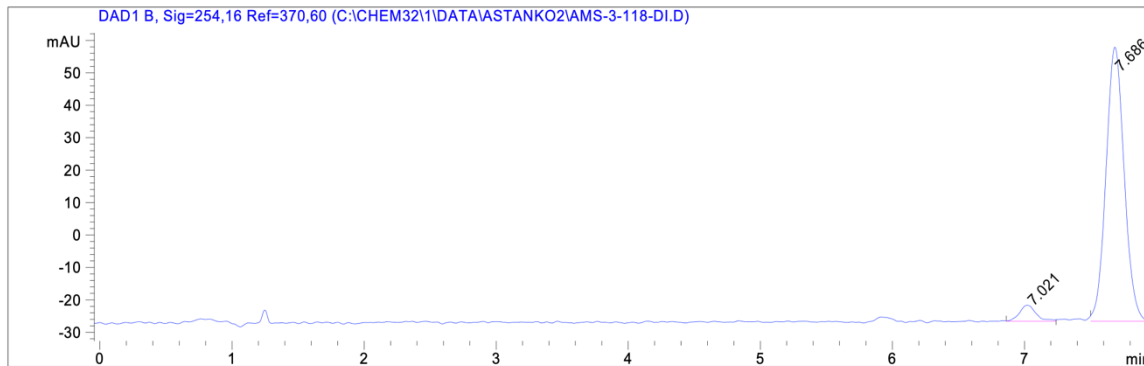
Peak #	RetTime [min]	Type	Width [min]	Area [mAU*s]	Height [mAU]	Area %
1	7.021	BB	0.1358	43.67125	4.91007	5.1132
2	7.686	BBA	0.1480	810.42255	84.41804	94.8868

Ligand: SL-M009-1 (90% ee)

DAD1 B, Sig=254,16 Ref=370,60 (C:\CHEM32\1\DATA\ASTANKO2\AMS-3-119-DI.D)
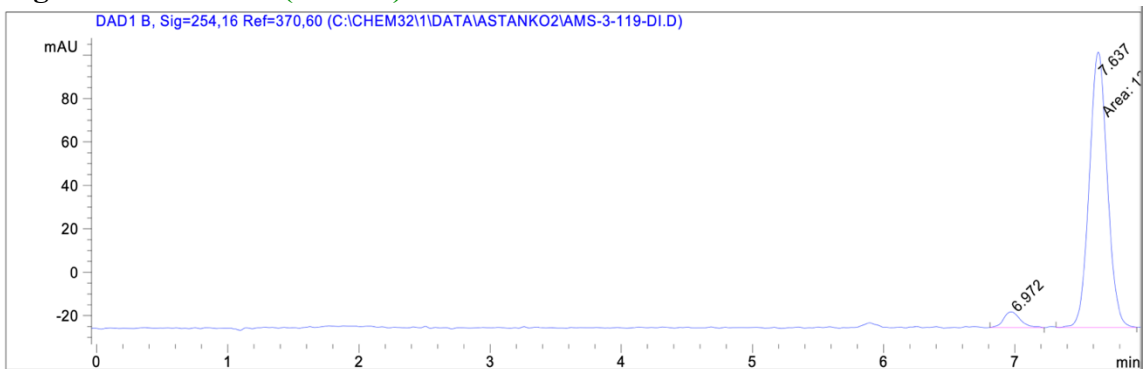
Peak #	RetTime [min]	Type	Width [min]	Area [mAU*s]	Height [mAU]	Area %
1	6.972	BB	0.1400	64.53312	7.23743	5.0621
2	7.637	MM	0.1587	1210.28711	127.14150	94.9379

(*R*)-2-fluoro-4',5',8,9-tetrahydro-2'*H*-spiro[benzo[7]annulene-6,3'-furan]-2',5(7*H*)-dione (188d)
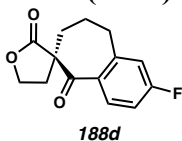
188d

Prepared via "General Procedure for Spirocyclization: Isolation Scale". The residue was purified via flash column chromatography (10% EtOAc/toluene) to afford **188d** as a white solid.

With **SL-M001-1**: 19.8 mg, 80% yield

With **SL-M009-1**: 17.8 mg, 72% yield

¹H NMR (400 MHz, CDCl₃) δ 7.51 (dd, *J* = 8.6, 5.7 Hz, 1H), 7.00 (td, *J* = 8.4, 2.5 Hz, 1H), 6.88 (dd, *J* = 9.1, 2.5 Hz, 1H), 4.51 (dt, *J* = 8.9, 7.8 Hz, 1H), 4.40 (td, *J* = 8.6, 4.3 Hz, 1H), 2.95 (ddd, *J* = 14.6, 6.1, 4.7 Hz, 1H), 2.86 – 2.76 (m, 1H), 2.76 – 2.66 (m, 1H), 2.38 – 2.19 (m, 2H), 2.12 – 2.01 (m, 1H), 2.01 – 1.82 (m, 2H).

¹³C NMR (101 MHz, CDCl₃) δ 205.28, 176.36, 166.56, 164.04, 141.31 (d, *J* = 8.6 Hz), 134.87 (d, *J* = 3.2 Hz), 131.44 (d, *J* = 9.4 Hz), 115.21 (dd, *J* = 172.5, 21.8 Hz), 66.15, 57.86, 32.66, 32.03, 29.93, 21.90.

IR (NaCl, Thin Film) 3518, 3068, 2946, 2870, 1765, 1710, 1672, 1606, 1586, 1486, 1454, 1376, 1352, 1294, 1274, 1242, 1209, 1184, 1169, 1160, 1107, 1095, 1076, 1030, 994, 964, 867, 828, 777, 703 cm⁻¹

HRMS(FI) *m/z*: [M + •]⁺ Calculated for C₁₄H₁₃O₃F: 248.08487, Found: 248.08436

[α]ₔ²³ = -22.5267 (*c* = 0.86, CHCl₃) (85% ee, with SL-M001-1)

SFC Conditions: 15% IPA, 2.5 mL/min, Chiralcel AD-H , λ = 254 nm, t$_R$ (min): major = 3.969, minor = 4.259

Racemic Reaction SFC Trace:
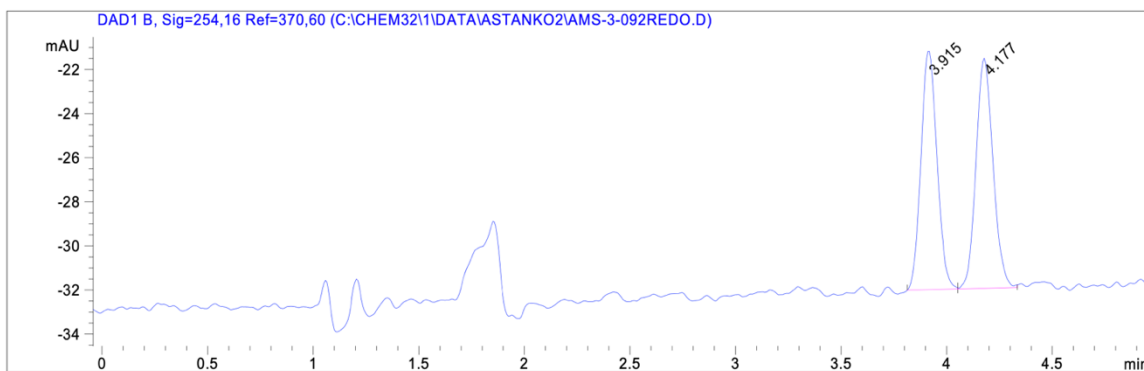
**Ligand: SL-M001-1 (85% ee)**
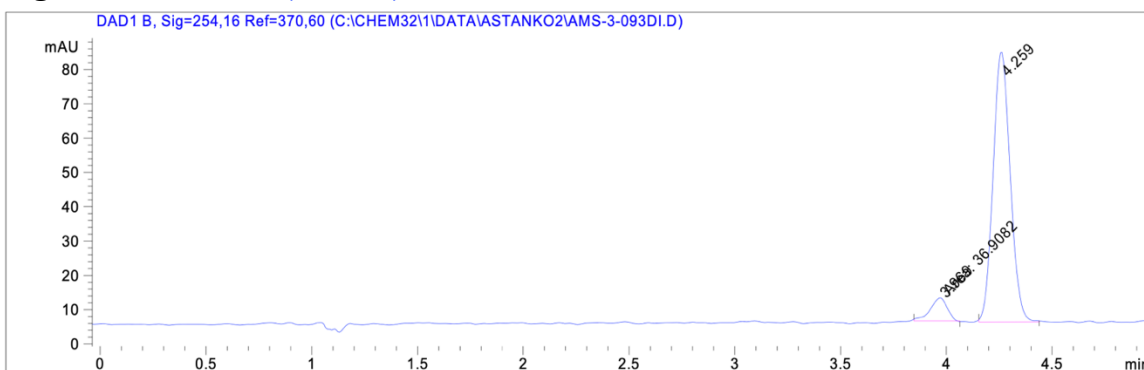
Peak #	RetTime [min]	Type	Width [min]	Area [mAU*s]	Height [mAU]	Area %
1	3.969	MM	0.0914	36.90817	6.73291	7.6830
2	4.259	BB	0.0901	443.48242	78.30865	92.3170

Ligand: SL-M009-1 (83% ee)
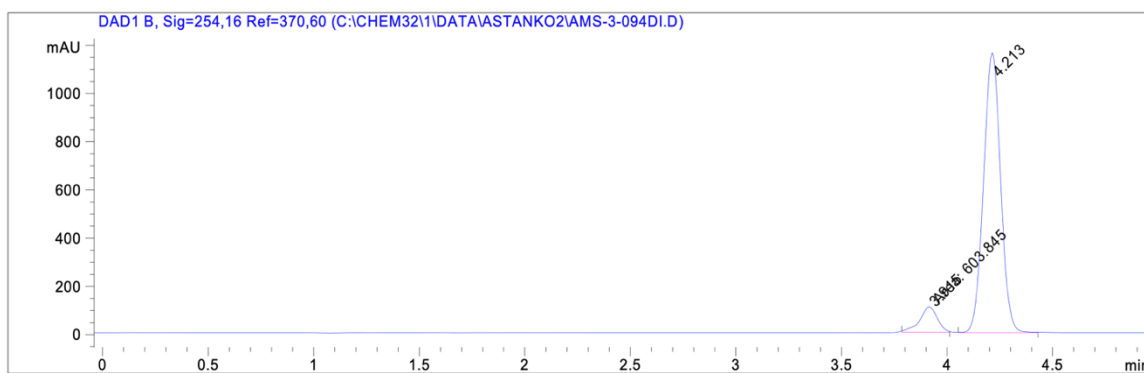
Peak #	RetTime [min]	Type	Width [min]	Area [mAU*s]	Height [mAU]	Area %
1	3.915	MM	0.0956	603.84479	105.25763	8.4873
2	4.213	VB	0.0897	6510.82715	1156.08105	91.5127

ethyl (*R*)-2',5-dioxo-4',5,5',7,8,9-hexahydro-2'*H*-spiro[benzo[7]annulene-6,3'-furan]-2-carboxylate (188e)
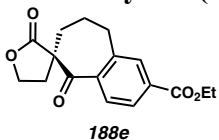
188e

Prepared via "General Procedure for Spirocyclization: Isolation Scale". The residue was

purified via flash column chromatography (10% EtOAc/toluene) to afford **188e** as a

white solid.

With **SL-M001-1**: 18.6 mg, 62% yield

With **SL-M009-1**: 22.2 mg, 73% yield

¹H NMR (600 MHz, CDCl₃) δ 7.97 (dd, *J* = 7.9, 1.6 Hz, 1H), 7.86 (d, *J* = 1.6 Hz, 1H),

7.50 (d, *J* = 7.9 Hz, 1H), 4.53 (dt, *J* = 8.9, 7.7 Hz, 1H), 4.44 – 4.36 (m, 3H), 3.03 (ddd, *J*

= 14.6, 6.1, 4.6 Hz, 1H), 2.81 (ddd, *J* = 14.6, 10.2, 6.3 Hz, 1H), 2.74 (ddd, *J* = 12.9, 7.7,

4.5 Hz, 1H), 2.32 (dt, *J* = 12.9, 8.1 Hz, 1H), 2.23 (ddd, *J* = 14.8, 10.1, 5.7 Hz, 1H), 2.12 –

2.05 (m, 1H), 1.94 (dddd, *J* = 16.0, 10.3, 8.2, 5.1 Hz, 1H), 1.87 (ddd, *J* = 14.7, 5.5, 4.4

Hz, 1H), 1.41 (t, *J* = 7.1 Hz, 3H).

¹³C NMR (101 MHz, CDCl₃) δ 206.43, 175.96, 165.88, 142.26, 137.93, 133.97, 130.03,

128.40, 66.23, 61.57, 57.88, 32.59, 31.70, 30.02, 21.90, 14.43.

IR (NaCl, Thin Film) 2934, 2866, 1764, 1417, 1681, 1567, 1453, 1416, 1369, 1352,

1288, 1254, 1214, 1184, 1153, 1108, 1026, 960, 919, 862, 752 cm⁻¹

HRMS(FI) *m/z*: [M + •]⁺ Calculated for $C_{17}H_{18}O_5$: 302.11542, Found: 302.11534

**[α]$_d^{23}$** = -37.2952 (*c* = 0.62, CHCl₃) (70% ee, with SL-M001-1)

SFC Conditions: 20% IPA, 2.5 mL/min, Chiralcel AD-H , λ = 254 nm, t$_R$ (min): major =

3.942, minor = 4.285

Racemic Reaction SFC Trace:
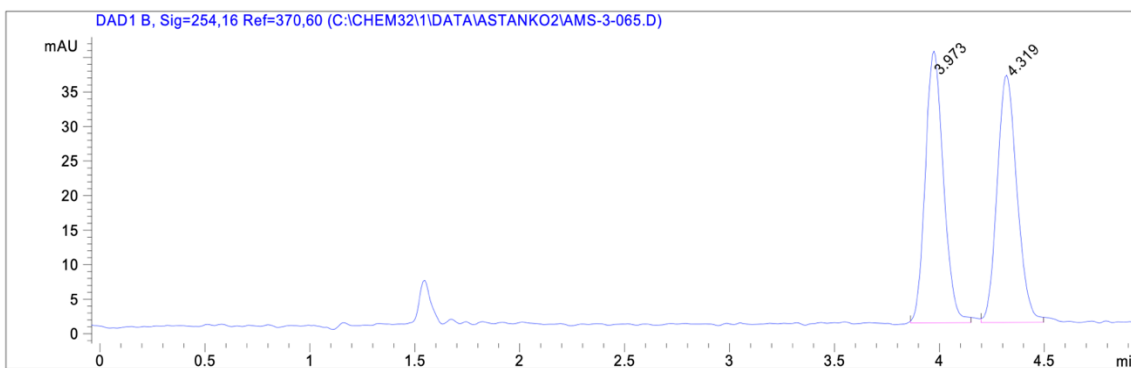
Ligand: SL-M001-1 (71% ee)
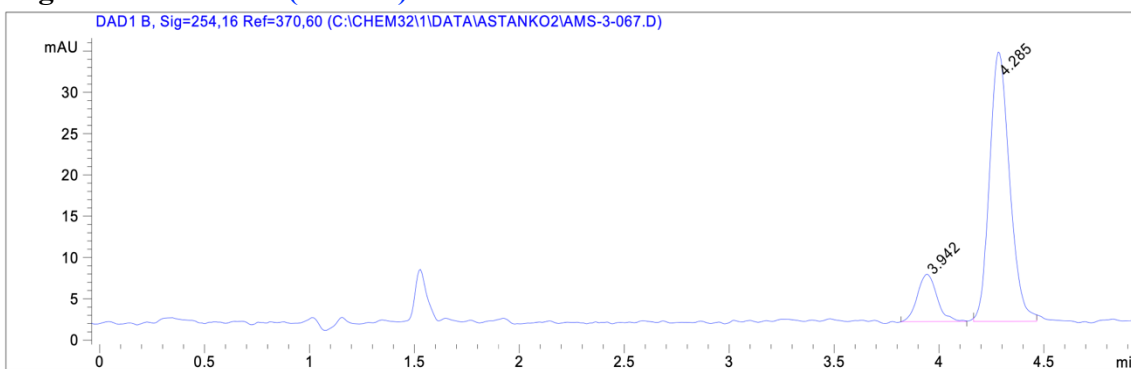
Peak #	RetTime [min]	Type	Width [min]	Area [mAU*s]	Height [mAU]	Area %
1	3.942	BB	0.1041	37.34255	5.72555	14.6502
2	4.285	BB	0.1019	217.55139	32.57594	85.3498

Ligand: SL-M009-1 (65% ee)
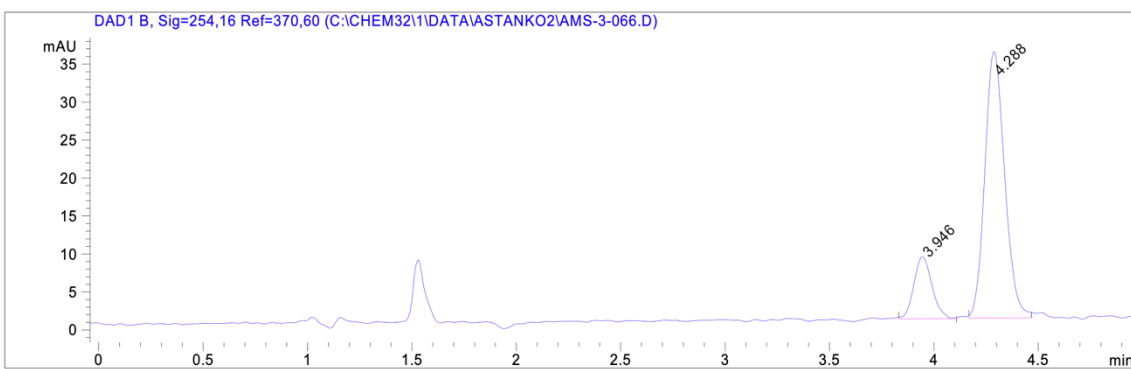
1	3.946	BB	0.0945	49.15547	8.13326	17.4600
2	4.288	BB	0.1013	232.37579	35.04961	82.5400

(*R*)-2-(trifluoromethyl)-4',5',8,9-tetrahydro-2'*H*-spiro[benzo[7]annulene-6,3'-furan]-2',5(7*H*)-dione (188f)
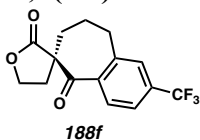
188f

Prepared via "General Procedure for Spirocyclization: Isolation Scale". The residue was purified via flash column chromatography (10% EtOAc/toluene) to afford **188f** as an off-white solid.

With **SL-M001-1**: 20.9 mg, 57% yield

With **SL-M009-1**: 22.7 mg, 76% yield

¹H NMR (400 MHz, CDCl₃) δ 7.63 – 7.53 (m, 2H), 7.49 – 7.42 (m, 1H), 4.54 (dt, *J* = 8.8, 7.6 Hz, 1H), 4.41 (ddd, *J* = 8.9, 8.3, 4.5 Hz, 1H), 3.10 – 2.99 (m, 1H), 2.89 – 2.71 (m, 2H), 2.37 – 2.19 (m, 2H), 2.16 – 2.02 (m, 1H), 2.02 – 1.84 (m, 2H).

¹³C NMR (101 MHz, CDCl₃) δ 205.89, 175.77, 141.72, 138.61, 133.94 (q, *J* = 32.4 Hz), 128.84, 125.88 (q, *J* = 3.5 Hz), 123.67 (d, *J* = 272.7 Hz), 124.27 (q, *J* = 4.0 Hz), 66.26, 57.89, 32.60, 31.78, 30.05, 21.83.

¹⁹F NMR (282 MHz, CDCl₃) δ -61.47.

IR (NaCl, Thin Film) 2949, 2869, 1764, 1685, 1455, 1422, 1376, 1331, 1279, 1254, 1218, 1167, 1126, 1073, 1030, 959, 900, 859, 841, 769, 736, 708 cm⁻¹

HRMS(FI) *m/z*: [M + •]⁺ Calculated for $C_{15}H_{13}O_3F_3$: 298.08168, Found: 298.08054

[α]$_d^{23}$ = -19.8407 (*c* = 1.18, CHCl₃) (51% ee, with SL-M001-1)

SFC Conditions: 10% IPA, 2.5 mL/min, Chiralcel AD-H , λ = 254 nm, t$_R$ (min): major = 3.281, minor = 3.485

Racemic Reaction SFC Trace:
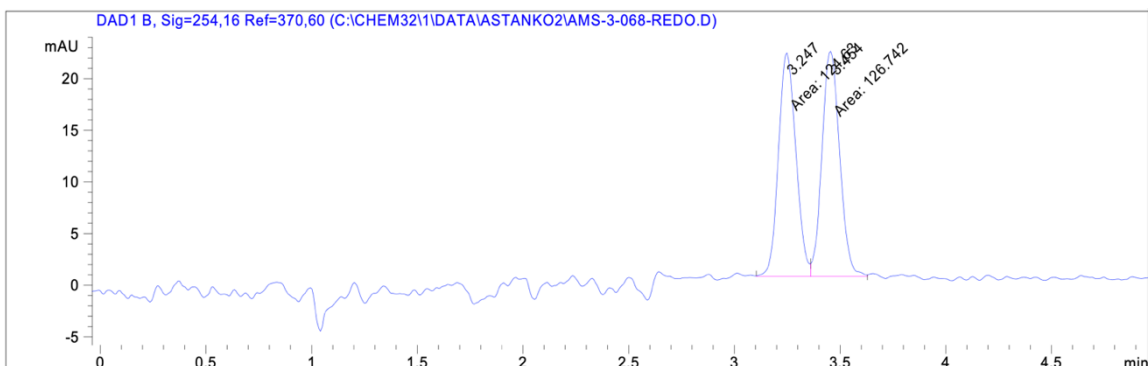
Ligand: SL-M001-1 (51% ee)
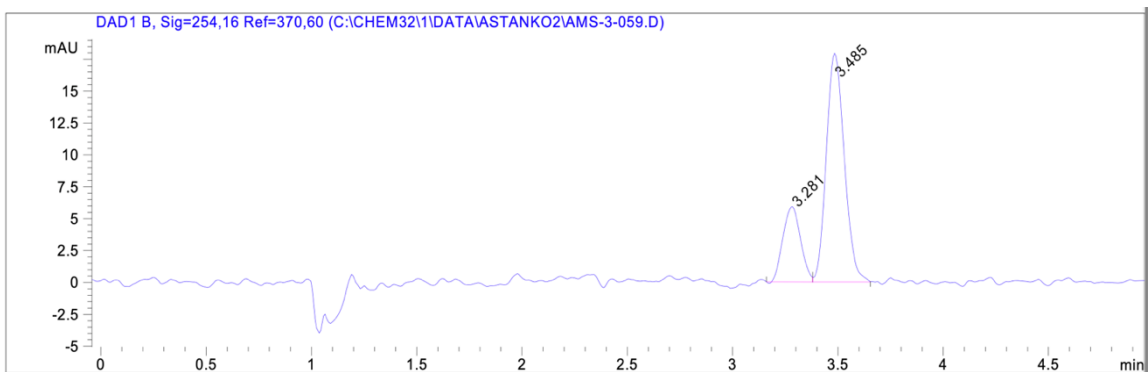
Peak #	RetTime [min]	Type	Width [min]	Area [mAU*s]	Height [mAU]	Area %
1	3.281	BV	0.0922	34.37086	5.87584	24.3245
2	3.485	VB	0.0937	106.93066	17.88833	75.6755

Ligand: SL-M009-1 (44% ee)
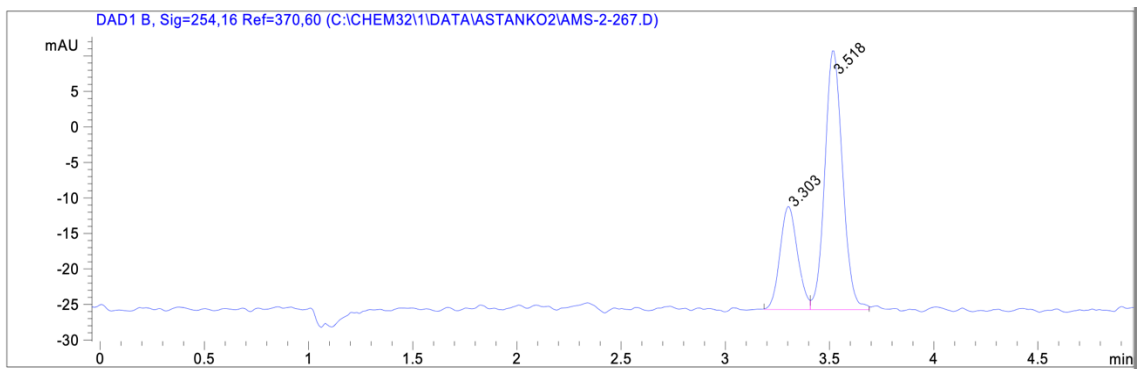
Peak #	RetTime [min]	Type	Width [min]	Area [mAU*s]	Height [mAU]	Area %
1	3.303	BV	0.0925	84.92978	14.45905	28.2082
2	3.518	VB	0.0932	216.15219	36.46727	71.7918

(*R*)-3-chloro-4',5',8,9-tetrahydro-2'*H*-spiro[benzo[7]annulene-6,3'-furan]-2',5(7*H*)-dione (188g)
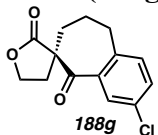
Prepared via "General Procedure for Spirocyclization: Isolation Scale". The residue was purified via flash column chromatography (10% EtOAc/toluene) to afford **188g** as an off-white solid.

With **SL-M001-1**: 14.2 mg, 55% yield

With **SL-M009-1**: 10.2 mg, 38% yield

¹H NMR (400 MHz, CDCl₃) δ 7.47 – 7.37 (m, 2H), 7.12 (d, *J* = 8.0 Hz, 1H), 4.51 (dt, *J* = 8.9, 7.7 Hz, 1H), 4.39 (td, *J* = 8.6, 4.4 Hz, 1H), 2.95 (dt, *J* = 14.8, 5.1 Hz, 1H), 2.83 – 2.67 (m, 2H), 2.38 – 2.17 (m, 2H), 2.12 – 1.97 (m, 1H), 1.98 – 1.81 (m, 2H).

¹³C NMR (101 MHz, CDCl₃) δ 205.33, 176.02, 139.87, 136.37, 133.27, 132.45, 130.51, 128.33, 66.17, 57.93, 32.74, 31.36, 30.07, 21.99.

IR (NaCl, Thin Film) 3061, 2919, 2852, 2774, 1769, 1681, 1592, 1479, 1454, 1401, 1377, 1352, 1301, 1285, 1253, 1216, 1193, 1167, 1153, 1121, 1103, 1075, 1030, 993, 971, 888, 837, 823, 732, 715, 639 cm^{-1}

HRMS(FI) *m/z*: [M + •]$^{+}$ Calculated for C$_{14}$H$_{13}$O$_3$Cl: 264.05532, Found: 264.05518

**[α]$_d^{23}$ = -14.7140** (*c* = 1.18, CHCl₃) (72% ee, with SL-M009-1)

SFC Conditions: 40% IPA, 2.5 mL/min, Chiralcel IC , λ = 254 nm, t$_R$ (min): major = 3.894, minor = 5.126

Racemic Reaction SFC Trace:
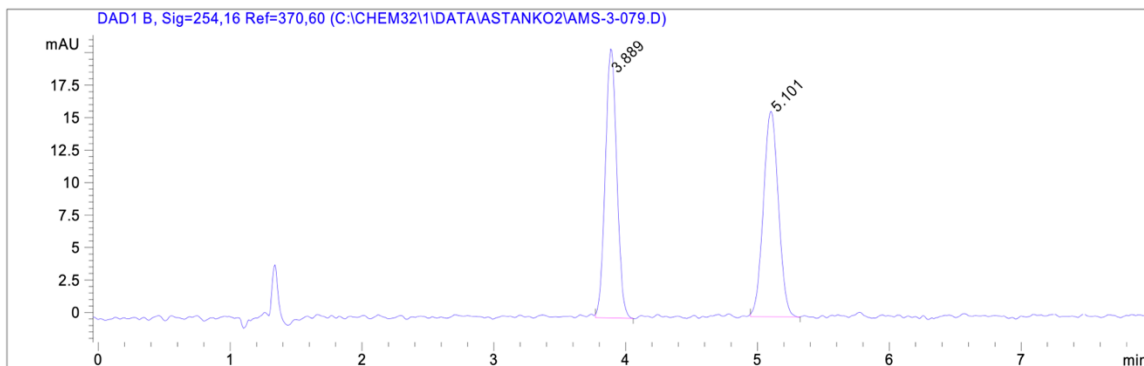
Ligand: SL-M001-1 (60% ee)
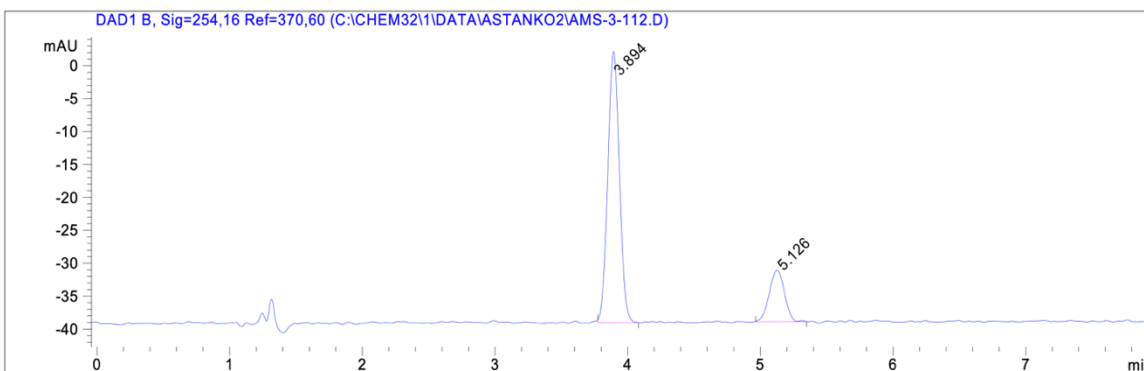
Peak #	RetTime [min]	Type	Width [min]	Area [mAU*s]	Height [mAU]	Area %
1	3.894	BB	0.0995	251.70132	41.08957	80.1797
2	5.126	BB	0.1249	62.22002	7.81212	19.8203

Ligand: SL-M009-1 (72% ee)
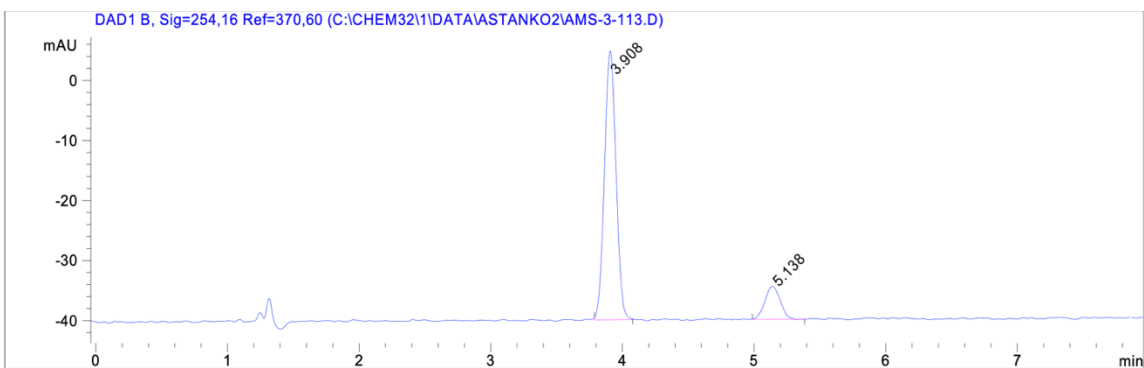
Peak #	RetTime [min]	Type	Width [min]	Area [mAU*s]	Height [mAU]	Area %
1	3.908	BB	0.0954	273.72900	44.70275	86.0707
2	5.138	BB	0.1296	44.29908	5.52047	13.9293

(*R*)-4',5'-dihydro-2'*H*-spiro[benzo[7]annulene-6,3'-furan]-2',5(7*H*)-dione (188h)
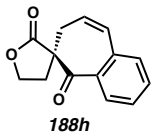
188h

Prepared via "General Procedure for Spirocyclization: Isolation Scale". The residue was purified via flash column chromatography (10% EtOAc/toluene) to afford **188h** as an off-white oil.

With **SL-M001-1**: 7.1 mg, 31% yield

With **SL-M009-1**: 7.1 mg, 31% yield

^{1}H NMR (400 MHz, CDCl$_3$) δ 7.99 (dd, *J* = 7.9, 1.4 Hz, 1H), 7.55 (td, *J* = 7.6, 1.5 Hz, 1H), 7.36 (td, *J* = 7.6, 1.3 Hz, 1H), 7.24 (d, *J* = 1.2 Hz, 0H), 6.60 (dd, *J* = 11.4, 2.6 Hz, 1H), 6.15 (ddd, *J* = 11.4, 8.0, 4.2 Hz, 1H), 4.35 (ddd, *J* = 9.2, 8.3, 2.2 Hz, 1H), 4.22 (ddd, *J* = 10.2, 9.1, 6.4 Hz, 1H), 3.12 (ddd, *J* = 17.0, 4.2, 2.6 Hz, 1H), 2.60 – 2.44 (m, 2H), 2.33 (ddd, *J* = 13.4, 10.2, 8.4 Hz, 1H).

^{13}C NMR (101 MHz, CDCl$_3$) δ 198.96, 175.64, 135.76, 133.83, 133.53, 132.49, 131.37, 131.35, 128.75, 128.01, 65.67, 60.71, 32.89, 31.13.

IR (NaCl, Thin Film) 2956, 2918, 2849, 1769, 1658, 1591, 1480, 1461, 1442, 1371, 1350, 1313, 1281, 1239, 1172, 1113, 1025, 973, 959, 929, 794, 782 cm^{-1}

HRMS(FI) *m/z*: [M + •]$^+$ Calculated C$_{14}$H$_{12}$O$_3$: 228.07864, Found: 228.07849

[α]$_d^{23}$ = -12.9574 (*c* = 0.68, CHCl$_3$) (31% ee, with SL-M001-1)

SFC Conditions: 40% IPA, 2.5 mL/min, Chiralcel IC , λ = 254 nm, t$_R$ (min): major = 7.429, minor = 8.418

Racemic Reaction SFC Trace:

DAD1 B, Sig=254,16 Ref=370,60 (C:\CHEM32\1\DATA\ASTANKO2\AMS-3-104-C1.D)

Ligand: SL-M001-1 (31% ee)

DAD1 B, Sig=254,16 Ref=370,60 (C:\CHEM32\1\DATA\ASTANKO2\AMS-3-105REDO.D)
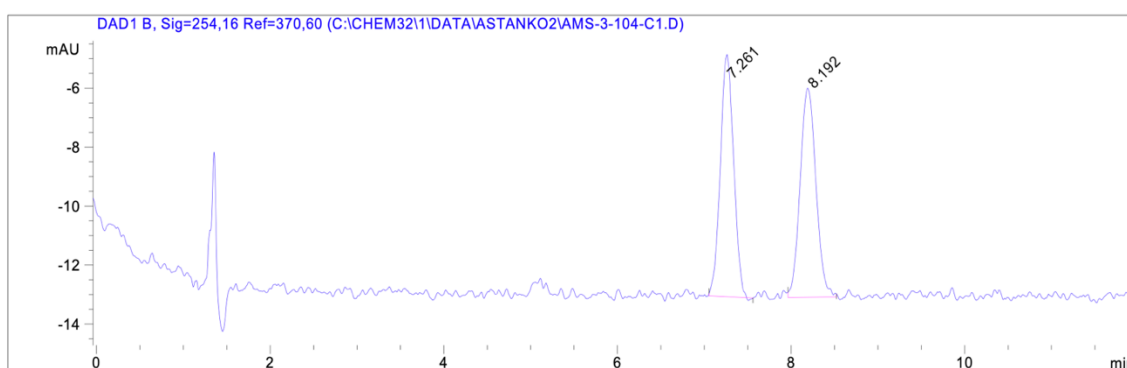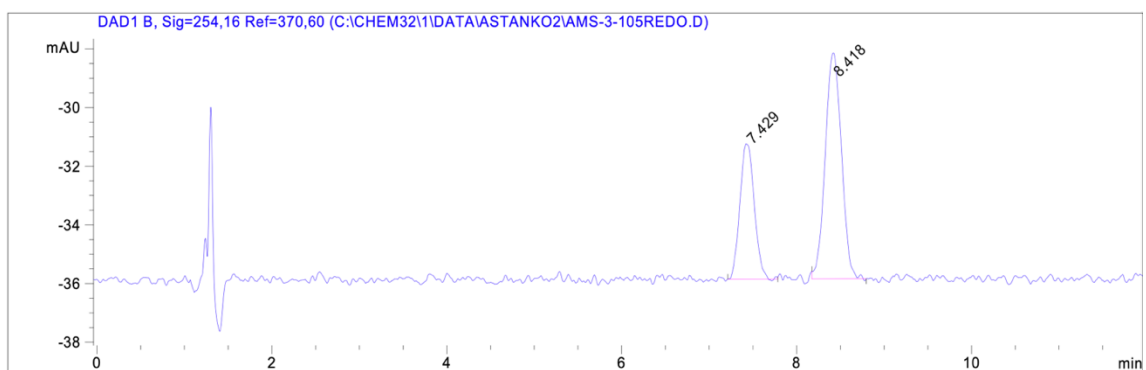
Peak #	RetTime [min]	Type	Width [min]	Area [mAU*s]	Height [mAU]	Area %
1	7.429	BB	0.1852	52.74116	4.61911	34.6593
2	8.418	BB	0.2065	99.42921	7.70936	65.3407

Ligand: SL-M009-1 (27% ee)

DAD1 B, Sig=254,16 Ref=370,60 (C:\CHEM32\1\DATA\ASTANKO2\AMS-3-106.D)
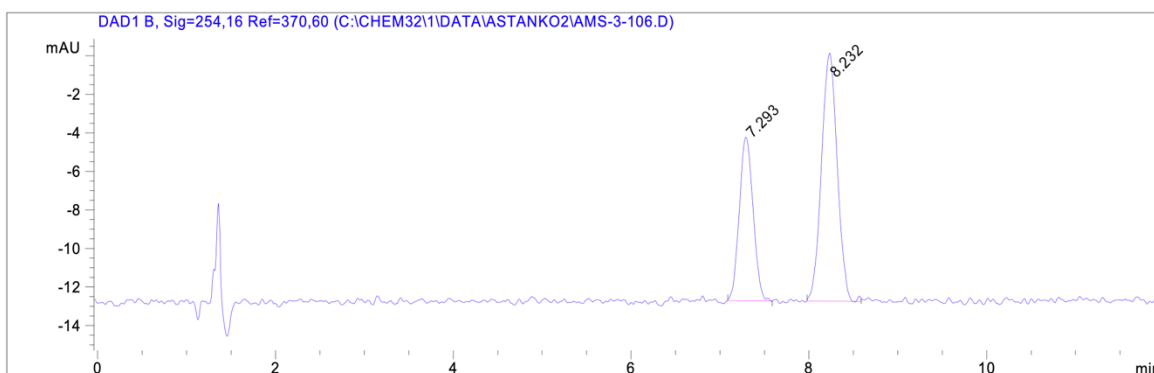
Peak #	RetTime [min]	Type	Width [min]	Area [mAU*s]	Height [mAU]	Area %
1	7.293	BB	0.1660	91.51656	8.47285	36.6210
2	8.232	BB	0.1958	158.38516	12.84905	63.3790

(*S*)-5',6'-dihydro-2'*H*,4'*H*-spiro[indene-2,3'-pyran]-1,2'(3*H*)-dione (190)
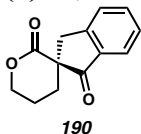
Prepared via "General Procedure for Spirocyclization: Isolation Scale" using SL-M009-1 as the ligand, but performed on a 0.06 mmol scale with toluene in place of TBME as the reaction solvent. The residue was purified via preparative scale TLC (50% EtOAc/Hexanes) to afford **190** as a white solid (3.5 mg, 27% yield) along with **191** as a yellow oil (5.2 mg, 46% yield).

^{1}H NMR (600 MHz, CDCl$_3$) δ 7.79 (d, *J* = 7.7 Hz, 1H), 7.64 (t, *J* = 7.5 Hz, 1H), 7.47 (d, *J* = 7.6 Hz, 1H), 7.42 (t, *J* = 7.5 Hz, 1H), 4.69 – 4.63 (m, 1H), 4.51 (dq, *J* = 11.6, 5.4 Hz, 1H), 3.05 (d, *J* = 16.8 Hz, 1H), 2.46 – 2.27 (m, 2H), 2.00 – 1.88 (m, 2H).

^{13}C NMR (101 MHz, CDCl$_3$) δ 203.00, 170.56, 152.82, 135.77, 134.28, 128.22, 126.49, 125.38, 71.00, 56.66, 41.86, 31.16, 20.58.

IR (NaCl, Thin Film) 2919, 2851, 1704, 1604, 1446, 1334, 1288, 1273, 1193, 1158, 1095, 980, 946, 799, 730, 679 cm^{-1}

HRMS(FI) *m/z*: [M + •]$^+$ Calculated for C$_{13}$H$_{12}$O$_3$: 216.07864, Found: 216.07826

[α]$_d^{23}$ = -35.4600 (*c* = 0.1, CHCl$_3$) (28% ee, with SL-M001-1)

SFC Conditions: 40% IPA, 2.5 mL/min, Chiralcel AD-H , λ = 254 nm, t$_R$ (min): major = 5.247, minor = 6.275

Racemic Reaction SFC Trace:
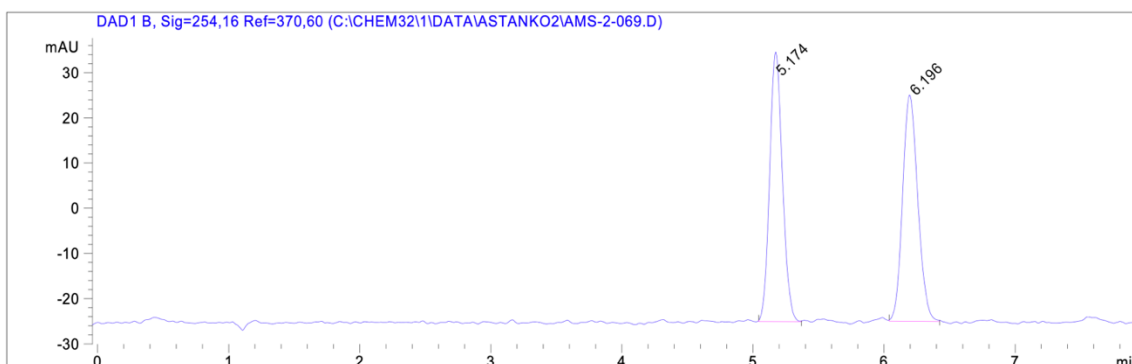
Ligand: SL-M009-1 (78% ee)

Peak #	RetTime [min]	Type	Width [min]	Area [mAU*s]	Height [mAU]	Area %
1	5.247	BB	0.1043	449.31207	65.29883	89.1182
2	6.275	BB	0.1169	54.86319	6.89300	10.8818
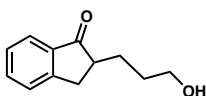
191

¹H NMR (400 MHz, CDCl₃) δ 7.75 (d, *J* = 7.6 Hz, 1H), 7.59 (td, *J* = 7.4, 1.3 Hz, 1H), 7.46 (dp, *J* = 7.7, 1.0 Hz, 1H), 7.42 – 7.34 (m, 1H), 3.69 (t, *J* = 6.4 Hz, 2H), 3.36 (dd, *J* = 17.1, 7.9 Hz, 1H), 2.84 (dd, *J* = 17.2, 4.0 Hz, 1H), 2.71 (dddd, *J* = 8.8, 7.9, 5.1, 4.0 Hz, 1H), 2.07 – 1.93 (m, 1H), 1.80 – 1.68 (m, 2H), 1.65 – 1.54 (m, 2H).

¹³C NMR (101 MHz, CDCl₃) δ 208.77, 153.48, 136.53, 134.62, 127.25, 126.38, 123.77, 62.45, 46.82, 32.75, 30.16, 27.43.

IR (NaCl, Thin Film) 3416, 3068, 3032, 2932, 2861, 1694, 1607, 1588, 1464, 1434, 1371, 1331, 1295, 1206, 1181, 1151, 1123, 1058, 1027, 1014, 852, 823, 752, 723 cm^{-1}

HRMS(FI) *m/z*: [M + •]$^+$ Calculated for $C_{12}H_{14}O_2$: 190.09938, Found: 190.09927

(*S*)-3',4'-dihydro-1'*H*-spiro[indene-2,2'-naphthalene]-1,1'(3*H*)-dione

193
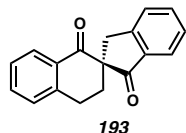
Prepared via "General Procedure for Spirocyclization: Isolation Scale" at 40 ºC with SL-M009-1 and 1:1 toluene/TBME in place of TBME. The residue was purified via flash column chromatography (10% EtOAc/Hexanes) to afford **193** as a white solid (23.8 mg, 91% yield).

^{1}H NMR (400 MHz, CDCl$_3$) δ 8.03 (dd, *J* = 7.9, 1.4 Hz, 1H), 7.75 (d, *J* = 7.7 Hz, 1H), 7.62 (td, *J* = 7.5, 1.2 Hz, 1H), 7.56 – 7.46 (m, 2H), 7.44 – 7.36 (m, 1H), 7.37 – 7.27 (m, 2H), 3.84 (d, *J* = 17.0 Hz, 1H), 3.49 (ddd, *J* = 17.0, 8.9, 4.9 Hz, 1H), 3.09 – 2.94 (m, 2H), 2.56 (ddd, *J* = 13.7, 6.8, 4.9 Hz, 1H), 2.31 (ddd, *J* = 13.7, 8.8, 4.9 Hz, 1H).

^{13}C NMR (101 MHz, CDCl$_3$) δ 204.22, 196.52, 153.05, 144.40, 135.38, 135.33, 133.98, 131.58, 128.94, 128.31, 127.95, 126.94, 126.59, 124.82, 61.22, 38.14, 32.34, 25.63.

Spectral data were in accordance with those reported in the literature for **193**.[27]

IR (NaCl, Thin Film) 2923, 1704, 1667, 1602, 1453, 1425, 1324, 1295, 1275, 1228, 1155, 1134, 1070, 965, 937, 888, 870, 801, 780, 756, 745 cm^{-1}

[α]$_d^{23}$ = -92.0347 (*c* = 0.72, CHCl$_3$) (73% ee, with SL-M009-1)

SFC Conditions: 30% IPA, 2.5 mL/min, Chiralcel AD-H , λ = 254 nm, t$_R$ (min): major = 3.675, minor = 4.570

Racemic Reaction SFC Trace:
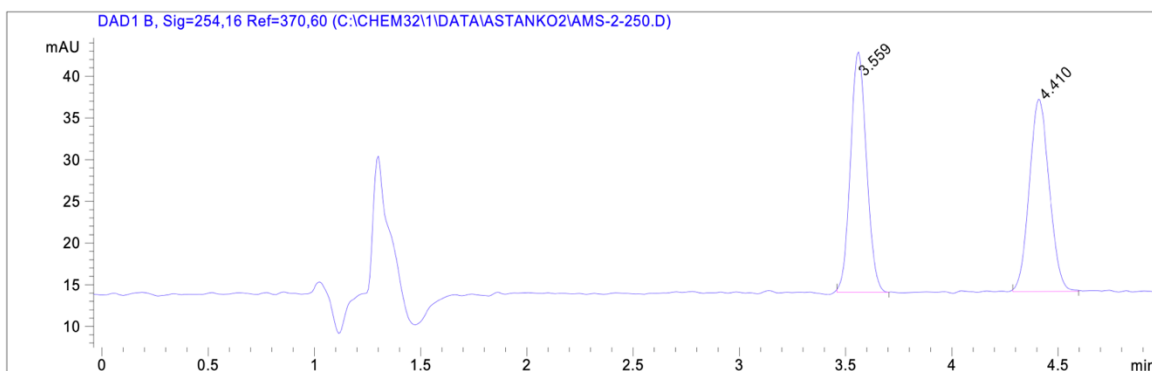
Ligand: SL-M009-1 (73% ee)
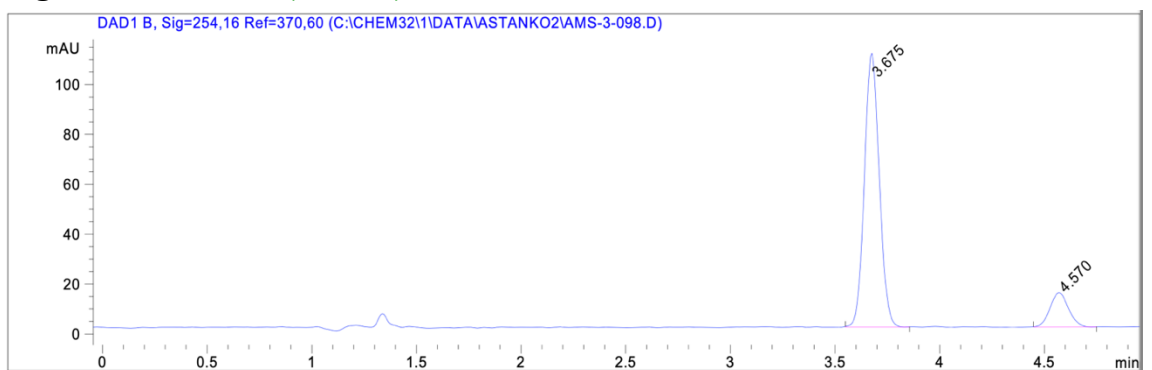
Peak #	RetTime [min]	Type	Width [min]	Area [mAU*s]	Height [mAU]	Area %
1	3.675	BB	0.0777	543.41553	109.82867	86.6345
2	4.570	BB	0.0970	83.83552	13.76704	13.3655

Isolation of *N*-Aryl Imine S41
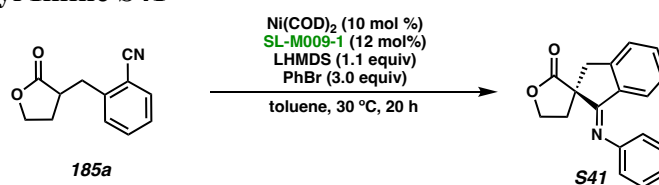
Compound **S41** was prepared following the "General Procedure for Spirocyclization: Isolation Scale", with SL-M009-1 as the ligand, and toluene was used in place of TBME. NO aqueous reaction quench was performed. Instead, the crude reaction was filtered through a short SiO₂ plug, eluting with EtOAc. The residue was purified by column chromatography (25% EtOAc/Hexanes) to afford **S41** as a yellow foam. (15.4 mg, 46% yield)

¹H NMR (600 MHz, CDCl₃) δ 7.40 – 7.33 (m, 4H), 7.15 (tt, *J* = 7.5, 1.2 Hz, 1H), 6.99 –

6.93 (m, 1H), 6.89 – 6.84 (m, 2H), 6.57 (d, *J* = 8.0 Hz, 1H), 4.79 (td, *J* = 8.8, 7.2 Hz, 1H),

4.46 (td, *J* = 8.6, 3.2 Hz, 1H), 3.73 (d, *J* = 16.8 Hz, 1H), 3.13 (d, *J* = 16.8 Hz, 1H), 2.92

(ddd, *J* = 12.7, 7.2, 3.2 Hz, 1H), 2.51 (dt, *J* = 12.8, 8.8 Hz, 1H).

¹³C NMR (101 MHz, CDCl₃) δ 178.42, 172.08, 150.74, 149.46, 132.62, 132.10, 129.65,

128.47, 127.14, 127.13, 126.33, 123.94, 118.29, (2 C's, overlapped), 66.57, 54.84, 39.57,

36.15.

IR (NaCl, Thin Film) 2925, 1764, 1654, 1591, 1485, 1467, 1447, 1375, 1301, 1285,

1220, 1207, 1171, 1157, 1095, 1069, 1054, 1027, 963, 912, 805, 771, 757, 711, 677 cm⁻¹

HRMS(FI) *m/z*: [M + •]⁺ Calculated for C18H15NO2: 277.11028, Found: 277.11003

3.4.7 X-Ray Structure Determination

X-Ray Structure Determination: Compound S41

X-ray coordinate of compound **S41**.
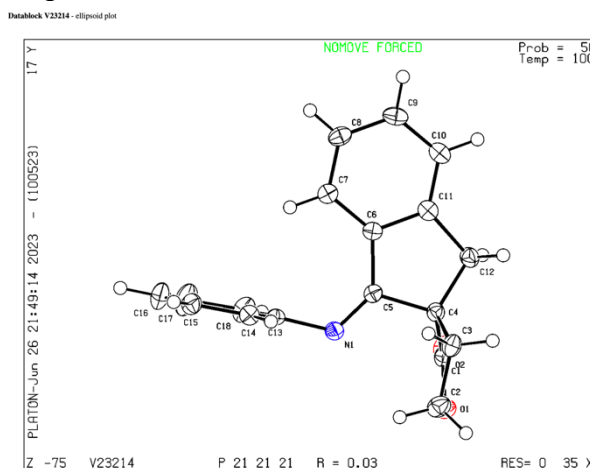
Low-temperature diffraction data (*φ*-and *ω*-scans) were collected on a Bruker AXS D8

VENTURE KAPPA diffractometer coupled to a PHOTON II CPAD detector with Cu *K*_α

radiation ($\lambda = 1.54178$ Å) from an IµS micro-source for the structure of compound V23214.

The structure was solved by direct methods using SHELXS[i] and refined against F^2 on all

data by full-matrix least squares with SHELXL-2019[ii] using established refinement

techniques.[iii] All non-hydrogen atoms were refined anisotropically. All hydrogen atoms

were included into the model at geometrically calculated positions and refined using a

riding model. The isotropic displacement parameters of all hydrogen atoms were fixed to

1.2 times the U value of the atoms they are linked to (1.5 times for methyl groups).

Compound V23214 crystallizes in the orthorhombic space group $P2_12_12_1$ with one

molecule in the asymmetric unit.

Crystal data and structure refinement for **S41**

Empirical formula	$C_{18} H_{15} NO_2$
Formula weight	277.31
Temperature	100(2) K
Wavelength	1.54178 Å
Crystal system	Orthorhombic
Space group	$P2_12_12_1$
Unit cell dimensions	$a = 8.4202(10)$ Å $\quad$ a= 90°.
	$b = 9.7385(14)$ Å $\quad$ b= 90°.
	$c = 17.3452(16)$ Å $\quad$ g = 90°.
Volume	1422.3(3) Å^3
Z	4
Density (calculated)	1.295 Mg/m^3
Absorption coefficient	0.677 mm^{-1}
F(000)	584
Crystal size	0.200 x 0.150 x 0.100 mm^3
Theta range for data collection	5.100 to 74.489°.

Index ranges	$-10<=h<=10, -12<=k<=12, -21<=l<=21$
Reflections collected	19589
Independent reflections	2899 [R(int) = 0.0515]
Completeness to theta = 67.679°	100.0 %
Absorption correction	Semi-empirical from equivalents
Max. and min. transmission	0.7538 and 0.6485
Refinement method	Full-matrix least-squares on F^2
Data / restraints / parameters	2899 / 0 / 190
Goodness-of-fit on F^2	1.057
Final R indices [I>2sigma(I)]	R1 = 0.0288, wR2 = 0.0665
R indices (all data)	R1 = 0.0317, wR2 = 0.0683
Absolute structure parameter	-0.04(11)
Extinction coefficient	n/a
Largest diff. peak and hole	0.168 and -0.138 e.$Å^{-3}$

Atomic coordinates (x 104) and equivalent isotropic displacement parameters (Å^2 x 10^3)

for **S41**. U(eq) is defined as one third of the trace of the orthogonalized U^{ij} tensor.

	x	y	z	U(eq)
O(1)	315(2)	897(1)	2882(1)	25(1)
C(1)	1464(2)	1725(2)	2612(1)	21(1)
O(2)	1281(2)	2429(1)	2053(1)	27(1)
C(2)	827(2)	217(2)	3587(1)	29(1)
C(3)	2629(2)	319(2)	3588(1)	24(1)
C(4)	2946(2)	1624(2)	3116(1)	19(1)
C(5)	3011(2)	2888(2)	3644(1)	18(1)
N(1)	1747(2)	3294(2)	3973(1)	21(1)
C(13)	1732(2)	4426(2)	4487(1)	19(1)
C(14)	2020(2)	4222(2)	5269(1)	22(1)
C(15)	1932(2)	5318(2)	5778(1)	24(1)
C(16)	1524(3)	6608(2)	5516(1)	32(1)
C(17)	1182(3)	6795(2)	4741(1)	39(1)
C(18)	1294(3)	5717(2)	4224(1)	29(1)
C(6)	4674(2)	3378(2)	3651(1)	19(1)
C(7)	5420(2)	4372(2)	4107(1)	21(1)
C(8)	7036(2)	4596(2)	4005(1)	24(1)
C(9)	7895(2)	3856(2)	3458(1)	25(1)
C(10)	7150(2)	2883(2)	2997(1)	23(1)
C(11)	5540(2)	2648(2)	3098(1)	21(1)
C(12)	4511(2)	1651(2)	2661(1)	24(1)

Table S3. Bond lengths [Å] and angles [°] for **S26**.

O(1)-C(1)	1.343(2)
O(1)-C(2)	1.457(2)
C(1)-O(2)	1.197(2)

C(1)-C(4)	1.527(2)
C(2)-C(3)	1.520(3)
C(2)-H(2A)	0.9900
C(2)-H(2B)	0.9900
C(3)-C(4)	1.536(2)
C(3)-H(3A)	0.9900
C(3)-H(3B)	0.9900
C(4)-C(5)	1.535(2)
C(4)-C(12)	1.537(2)
C(5)-N(1)	1.271(2)
C(5)-C(6)	1.480(2)
N(1)-C(13)	1.417(2)
C(13)-C(18)	1.388(3)
C(13)-C(14)	1.392(2)
C(14)-C(15)	1.387(3)
C(14)-H(14)	0.9500
C(15)-C(16)	1.380(3)
C(15)-H(15)	0.9500
C(16)-C(17)	1.388(3)
C(16)-H(16)	0.9500
C(17)-C(18)	1.383(3)
C(17)-H(17)	0.9500
C(18)-H(18)	0.9500
C(6)-C(7)	1.399(2)
C(6)-C(11)	1.399(3)
C(7)-C(8)	1.390(3)
C(7)-H(7)	0.9500
C(8)-C(9)	1.394(3)
C(8)-H(8)	0.9500
C(9)-C(10)	1.389(3)
C(9)-H(9)	0.9500
C(10)-C(11)	1.386(2)
C(10)-H(10)	0.9500

C(11)-C(12)	1.506(3)
C(12)-H(12A)	0.9900
C(12)-H(12B)	0.9900
C(1)-O(1)-C(2)	110.63(14)
O(2)-C(1)-O(1)	122.20(16)
O(2)-C(1)-C(4)	127.31(17)
O(1)-C(1)-C(4)	110.49(15)
O(1)-C(2)-C(3)	105.51(15)
O(1)-C(2)-H(2A)	110.6
C(3)-C(2)-H(2A)	110.6
O(1)-C(2)-H(2B)	110.6
C(3)-C(2)-H(2B)	110.6
H(2A)-C(2)-H(2B)	108.8
C(2)-C(3)-C(4)	103.09(15)
C(2)-C(3)-H(3A)	111.1
C(4)-C(3)-H(3A)	111.1
C(2)-C(3)-H(3B)	111.1
C(4)-C(3)-H(3B)	111.1
H(3A)-C(3)-H(3B)	109.1
C(1)-C(4)-C(5)	108.62(14)
C(1)-C(4)-C(3)	102.54(14)
C(5)-C(4)-C(3)	110.59(14)
C(1)-C(4)-C(12)	113.90(14)
C(5)-C(4)-C(12)	105.19(14)
C(3)-C(4)-C(12)	115.95(16)
N(1)-C(5)-C(6)	133.50(16)
N(1)-C(5)-C(4)	119.19(16)
C(6)-C(5)-C(4)	107.31(15)
C(5)-N(1)-C(13)	122.15(15)
C(18)-C(13)-C(14)	119.73(16)
C(18)-C(13)-N(1)	120.04(16)
C(14)-C(13)-N(1)	119.99(16)

C(15)-C(14)-C(13)	120.06(17)
C(15)-C(14)-H(14)	120.0
C(13)-C(14)-H(14)	120.0
C(16)-C(15)-C(14)	120.36(17)
C(16)-C(15)-H(15)	119.8
C(14)-C(15)-H(15)	119.8
C(15)-C(16)-C(17)	119.29(18)
C(15)-C(16)-H(16)	120.4
C(17)-C(16)-H(16)	120.4
C(18)-C(17)-C(16)	120.96(19)
C(18)-C(17)-H(17)	119.5
C(16)-C(17)-H(17)	119.5
C(17)-C(18)-C(13)	119.53(17)
C(17)-C(18)-H(18)	120.2
C(13)-C(18)-H(18)	120.2
C(7)-C(6)-C(11)	120.31(16)
C(7)-C(6)-C(5)	130.78(16)
C(11)-C(6)-C(5)	108.90(15)
C(8)-C(7)-C(6)	118.50(18)
C(8)-C(7)-H(7)	120.7
C(6)-C(7)-H(7)	120.7
C(7)-C(8)-C(9)	120.87(18)
C(7)-C(8)-H(8)	119.6
C(9)-C(8)-H(8)	119.6
C(10)-C(9)-C(8)	120.66(17)
C(10)-C(9)-H(9)	119.7
C(8)-C(9)-H(9)	119.7
C(11)-C(10)-C(9)	118.81(17)
C(11)-C(10)-H(10)	120.6
C(9)-C(10)-H(10)	120.6
C(10)-C(11)-C(6)	120.84(17)
C(10)-C(11)-C(12)	127.28(17)
C(6)-C(11)-C(12)	111.88(15)

C(11)-C(12)-C(4)	104.23(14)
C(11)-C(12)-H(12A)	110.9
C(4)-C(12)-H(12A)	110.9
C(11)-C(12)-H(12B)	110.9
C(4)-C(12)-H(12B)	110.9
H(12A)-C(12)-H(12B)	108.9

_____

Symmetry transformations used to generate equivalent atoms:

Anisotropic displacement parameters (Å² x 10³) for **S41**. The anisotropic
displacement factor exponent takes the form: $-2p^2 [h^2 a^{*2}U^{11} + ... + 2 h k a^* b^* U^{12}]$

	U^{11}	U^{22}	U^{33}	U^{23}	U^{13}	U^{12}
O(1)	22(1)	27(1)	27(1)	-2(1)	-3(1)	-2(1)
C(1)	22(1)	20(1)	20(1)	-6(1)	-1(1)	1(1)
O(2)	34(1)	27(1)	21(1)	0(1)	-6(1)	4(1)
C(2)	32(1)	27(1)	27(1)	3(1)	0(1)	-7(1)
C(3)	30(1)	21(1)	20(1)	0(1)	-3(1)	1(1)
C(4)	19(1)	21(1)	18(1)	-2(1)	-1(1)	1(1)
C(5)	20(1)	20(1)	14(1)	2(1)	-2(1)	-1(1)
N(1)	18(1)	24(1)	21(1)	-2(1)	-1(1)	0(1)
C(13)	15(1)	22(1)	20(1)	-2(1)	1(1)	-2(1)
C(14)	23(1)	22(1)	22(1)	1(1)	0(1)	1(1)
C(15)	29(1)	27(1)	17(1)	-2(1)	2(1)	-3(1)
C(16)	46(1)	23(1)	27(1)	-8(1)	1(1)	-1(1)
C(17)	62(2)	19(1)	35(1)	2(1)	-7(1)	4(1)
C(18)	40(1)	25(1)	21(1)	3(1)	-6(1)	-2(1)
C(6)	19(1)	20(1)	17(1)	4(1)	0(1)	0(1)
C(7)	22(1)	21(1)	20(1)	3(1)	-2(1)	0(1)
C(8)	23(1)	22(1)	27(1)	5(1)	-5(1)	-3(1)
C(9)	18(1)	29(1)	29(1)	9(1)	-1(1)	0(1)
C(10)	22(1)	27(1)	20(1)	5(1)	2(1)	4(1)
C(11)	22(1)	22(1)	18(1)	4(1)	-1(1)	2(1)
C(12)	22(1)	29(1)	19(1)	-4(1)	1(1)	1(1)

Hydrogen coordinates (x 10^4) and isotropic displacement parameters (Å^2x 10 ^{3}) for **S41**.

	x	y	z	U(eq)
H(2A)	486	-756	3589	34
H(2B)	375	680	4045	34
H(3A)	3116	-496	3342	28
H(3B)	3045	410	4120	28
H(14)	2278	3331	5454	26
H(15)	2154	5178	6309	29
H(16)	1477	7361	5864	39
H(17)	867	7676	4562	47
H(18)	1073	5860	3693	34
H(7)	4835	4881	4478	25
H(8)	7563	5263	4313	29
H(9)	9001	4018	3400	30
H(10)	7734	2387	2620	28
H(12A)	5004	728	2646	28
H(12B)	4333	1970	2126	28

Torsion angles [°] for **S41**.

_____

C(2)-O(1)-C(1)-O(2)	-177.02(17)
C(2)-O(1)-C(1)-C(4)	2.5(2)
C(1)-O(1)-C(2)-C(3)	-19.2(2)
O(1)-C(2)-C(3)-C(4)	27.33(19)
O(2)-C(1)-C(4)-C(5)	77.3(2)
O(1)-C(1)-C(4)-C(5)	-102.15(16)
O(2)-C(1)-C(4)-C(3)	-165.62(18)
O(1)-C(1)-C(4)-C(3)	14.92(18)
O(2)-C(1)-C(4)-C(12)	-39.6(2)
O(1)-C(1)-C(4)-C(12)	140.99(16)
C(2)-C(3)-C(4)-C(1)	-25.06(18)
C(2)-C(3)-C(4)-C(5)	90.60(18)
C(2)-C(3)-C(4)-C(12)	-149.79(16)
C(1)-C(4)-C(5)-N(1)	43.2(2)
C(3)-C(4)-C(5)-N(1)	-68.6(2)
C(12)-C(4)-C(5)-N(1)	165.55(15)
C(1)-C(4)-C(5)-C(6)	-137.06(15)
C(3)-C(4)-C(5)-C(6)	111.15(16)
C(12)-C(4)-C(5)-C(6)	-14.75(18)
C(6)-C(5)-N(1)-C(13)	-1.7(3)
C(4)-C(5)-N(1)-C(13)	177.93(15)
C(5)-N(1)-C(13)-C(18)	97.1(2)
C(5)-N(1)-C(13)-C(14)	-88.5(2)
C(18)-C(13)-C(14)-C(15)	-2.5(3)
N(1)-C(13)-C(14)-C(15)	-176.97(17)
C(13)-C(14)-C(15)-C(16)	1.5(3)
C(14)-C(15)-C(16)-C(17)	0.8(3)
C(15)-C(16)-C(17)-C(18)	-2.0(4)
C(16)-C(17)-C(18)-C(13)	0.9(4)
C(14)-C(13)-C(18)-C(17)	1.3(3)
N(1)-C(13)-C(18)-C(17)	175.8(2)

N(1)-C(5)-C(6)-C(7)	8.8(3)
C(4)-C(5)-C(6)-C(7)	-170.81(17)
N(1)-C(5)-C(6)-C(11)	-172.14(18)
C(4)-C(5)-C(6)-C(11)	8.22(18)
C(11)-C(6)-C(7)-C(8)	-1.1(3)
C(5)-C(6)-C(7)-C(8)	177.89(17)
C(6)-C(7)-C(8)-C(9)	0.4(3)
C(7)-C(8)-C(9)-C(10)	0.5(3)
C(8)-C(9)-C(10)-C(11)	-0.8(3)
C(9)-C(10)-C(11)-C(6)	0.2(3)
C(9)-C(10)-C(11)-C(12)	179.75(18)
C(7)-C(6)-C(11)-C(10)	0.8(3)
C(5)-C(6)-C(11)-C(10)	-178.39(16)
C(7)-C(6)-C(11)-C(12)	-178.88(16)
C(5)-C(6)-C(11)-C(12)	2.0(2)
C(10)-C(11)-C(12)-C(4)	169.22(17)
C(6)-C(11)-C(12)-C(4)	-11.2(2)
C(1)-C(4)-C(12)-C(11)	134.16(16)
C(5)-C(4)-C(12)-C(11)	15.33(18)
C(3)-C(4)-C(12)-C(11)	-107.18(17)

_____

Symmetry transformations used to generate equivalent atoms:

X-Ray Structure Determination: Compound 188b

X-ray coordinate of **188b**.
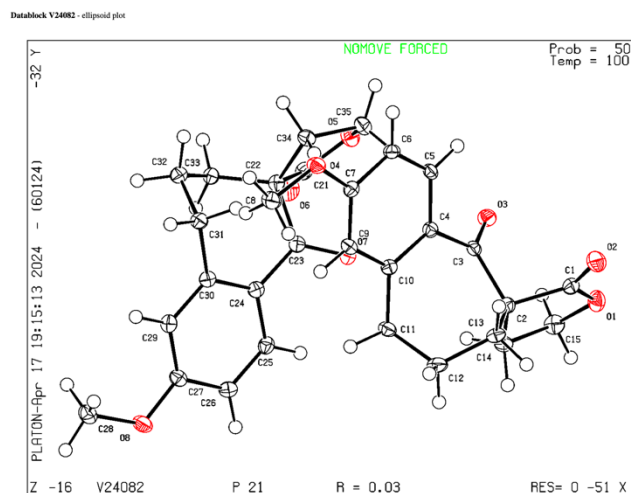
Low-temperature diffraction data (ϕ-and ω-scans) were collected on a Bruker AXS D8 VENTURE KAPPA diffractometer coupled to a PHOTON II CPAD detector with Cu K_α radiation ($\lambda = 1.54178$ Å) from an IμS micro-source for the structure of compound V24082. The structure was solved by direct methods using SHELXS[i] and refined against F^2 on all data by full-matrix least squares with SHELXL-2019[ii] using established refinement techniques.[iii] All non-hydrogen atoms were refined anisotropically. All hydrogen atoms were included into the model at geometrically calculated positions and refined using a riding model. The isotropic displacement parameters of all hydrogen atoms were fixed to 1.2 times the U value of the atoms they are linked to (1.5 times for methyl groups). Compound **188b** crystallizes in the monoclinic space group $P2_1$ with one molecule in the asymmetric unit.

Crystal data and structure refinement for **188b**.

Identification code	V24082
Empirical formula	C15 H16 O4
Formula weight	260.28
Temperature	100(2) K
Wavelength	1.54178 Å
Crystal system	Monoclinic
Space group	P2$_1$
Unit cell dimensions	a = 8.4789(9) Å a= 90°.
	b = 10.7304(9) Å b= 102.577(7)°.
	c = 13.9179(11) Å g = 90°.
Volume	1235.9(2) Å^3
Z	4
Density (calculated)	1.399 Mg/m^3
Absorption coefficient	0.833 mm^{-1}
F(000)	552
Crystal size	0.300 x 0.200 x 0.200 mm^3
Theta range for data collection	3.253 to 74.518°.
Index ranges	-10<=h<=9, -13<=k<=13, -16<=l<=17
Reflections collected	27571
Independent reflections	5037 [R(int) = 0.0380]
Completeness to theta = 67.679°	100.0 %
Absorption correction	Semi-empirical from equivalents
Max. and min. transmission	0.7538 and 0.6329
Refinement method	Full-matrix least-squares on F^2
Data / restraints / parameters	5037 / 1 / 345
Goodness-of-fit on F^2	1.027
Final R indices [I>2sigma(I)]	R1 = 0.0275, wR2 = 0.0706
R indices (all data)	R1 = 0.0282, wR2 = 0.0709
Absolute structure parameter	-0.02(7)
Extinction coefficient	n/a
Largest diff. peak and hole	0.178 and -0.183 e.Å^{-3}

Atomic coordinates (x 10^4) and equivalent isotropic displacement parameters (Å^2x 10^3) for **188b**. U(eq) is defined as one third of the trace of the orthogonalized U^{ij} tensor.

	x	y	z	U(eq)
C(1)	12956(2)	5769(2)	9952(1)	17(1)
O(1)	14128(2)	4949(1)	9898(1)	21(1)
O(2)	13245(2)	6814(1)	10248(1)	24(1)
C(2)	11270(2)	5190(2)	9598(1)	13(1)
C(3)	10646(2)	5783(2)	8574(1)	13(1)
O(3)	11507(1)	5741(1)	7978(1)	18(1)
C(4)	9095(2)	6486(2)	8360(1)	14(1)
C(5)	9059(2)	7622(2)	7854(1)	14(1)
C(6)	7666(2)	8330(2)	7646(1)	14(1)
C(7)	6271(2)	7899(2)	7920(1)	14(1)
O(4)	4983(2)	8674(1)	7700(1)	18(1)
C(8)	3478(2)	8266(2)	7903(2)	21(1)
C(9)	6274(2)	6739(2)	8384(1)	15(1)
C(10)	7691(2)	6038(2)	8618(1)	14(1)
C(11)	7711(2)	4788(2)	9118(1)	16(1)
C(12)	8634(2)	4817(2)	10198(1)	19(1)
C(13)	10260(2)	5492(2)	10357(1)	15(1)
C(14)	11676(2)	3800(2)	9511(1)	16(1)
C(15)	13435(2)	3807(2)	9413(1)	21(1)
C(21)	7963(2)	4268(2)	4940(1)	17(1)
O(5)	9174(2)	5098(1)	5016(1)	21(1)
O(6)	8013(2)	3258(1)	4575(1)	25(1)
C(22)	6570(2)	4800(2)	5364(1)	14(1)
C(23)	6784(2)	4161(2)	6378(1)	14(1)
O(7)	8151(2)	4110(1)	6894(1)	19(1)
C(24)	5413(2)	3523(2)	6680(1)	14(1)
C(25)	5766(2)	2416(2)	7216(1)	16(1)
C(26)	4561(2)	1703(2)	7462(1)	17(1)

C(27)	2957(2)	2102(2)	7172(1)	16(1)
O(8)	1852(2)	1316(1)	7426(1)	21(1)
C(28)	179(2)	1589(2)	7062(2)	22(1)
C(29)	2587(2)	3236(2)	6685(1)	15(1)
C(30)	3810(2)	3958(2)	6440(1)	14(1)
C(31)	3429(2)	5216(2)	5960(1)	16(1)
C(32)	3499(2)	5214(2)	4865(1)	18(1)
C(33)	4963(2)	4525(2)	4645(1)	16(1)
C(34)	7026(2)	6191(2)	5480(1)	16(1)
C(35)	8853(2)	6191(2)	5566(1)	19(1)

Bond lengths [Å] and angles [°] for **188b**.

C(1)-O(2)	1.201(2)
C(1)-O(1)	1.342(2)
C(1)-C(2)	1.538(2)
O(1)-C(15)	1.459(2)
C(2)-C(13)	1.533(2)
C(2)-C(14)	1.541(2)
C(2)-C(3)	1.546(2)
C(3)-O(3)	1.220(2)
C(3)-C(4)	1.488(2)
C(4)-C(10)	1.401(2)
C(4)-C(5)	1.405(2)
C(5)-C(6)	1.381(2)
C(5)-H(5)	0.9500
C(6)-C(7)	1.398(2)
C(6)-H(6)	0.9500
C(7)-O(4)	1.354(2)
C(7)-C(9)	1.402(2)
O(4)-C(8)	1.434(2)
C(8)-H(8A)	0.9800
C(8)-H(8B)	0.9800

C(8)-H(8C)	0.9800
C(9)-C(10)	1.395(2)
C(9)-H(9)	0.9500
C(10)-C(11)	1.510(2)
C(11)-C(12)	1.536(2)
C(11)-H(11A)	0.9900
C(11)-H(11B)	0.9900
C(12)-C(13)	1.530(2)
C(12)-H(12A)	0.9900
C(12)-H(12B)	0.9900
C(13)-H(13A)	0.9900
C(13)-H(13B)	0.9900
C(14)-C(15)	1.528(2)
C(14)-H(14A)	0.9900
C(14)-H(14B)	0.9900
C(15)-H(15A)	0.9900
C(15)-H(15B)	0.9900
C(21)-O(6)	1.200(2)
C(21)-O(5)	1.347(2)
C(21)-C(22)	1.541(2)
O(5)-C(35)	1.458(2)
C(22)-C(33)	1.533(2)
C(22)-C(34)	1.542(2)
C(22)-C(23)	1.543(2)
C(23)-O(7)	1.224(2)
C(23)-C(24)	1.487(2)
C(24)-C(25)	1.400(2)
C(24)-C(30)	1.406(2)
C(25)-C(26)	1.378(3)
C(25)-H(25)	0.9500
C(26)-C(27)	1.399(2)
C(26)-H(26)	0.9500
C(27)-O(8)	1.363(2)

C(27)-C(29)	1.395(3)
O(8)-C(28)	1.429(2)
C(28)-H(28A)	0.9800
C(28)-H(28B)	0.9800
C(28)-H(28C)	0.9800
C(29)-C(30)	1.396(2)
C(29)-H(29)	0.9500
C(30)-C(31)	1.510(2)
C(31)-C(32)	1.539(2)
C(31)-H(31A)	0.9900
C(31)-H(31B)	0.9900
C(32)-C(33)	1.532(2)
C(32)-H(32A)	0.9900
C(32)-H(32B)	0.9900
C(33)-H(33A)	0.9900
C(33)-H(33B)	0.9900
C(34)-C(35)	1.528(2)
C(34)-H(34A)	0.9900
C(34)-H(34B)	0.9900
C(35)-H(35A)	0.9900
C(35)-H(35B)	0.9900
O(2)-C(1)-O(1)	122.21(16)
O(2)-C(1)-C(2)	126.41(16)
O(1)-C(1)-C(2)	111.39(15)
C(1)-O(1)-C(15)	110.38(14)
C(13)-C(2)-C(1)	108.27(14)
C(13)-C(2)-C(14)	115.23(14)
C(1)-C(2)-C(14)	102.06(13)
C(13)-C(2)-C(3)	114.68(14)
C(1)-C(2)-C(3)	103.70(13)
C(14)-C(2)-C(3)	111.36(14)
O(3)-C(3)-C(4)	121.13(15)

O(3)-C(3)-C(2)	118.41(15)
C(4)-C(3)-C(2)	120.24(14)
C(10)-C(4)-C(5)	119.96(15)
C(10)-C(4)-C(3)	122.53(15)
C(5)-C(4)-C(3)	117.49(14)
C(6)-C(5)-C(4)	120.42(15)
C(6)-C(5)-H(5)	119.8
C(4)-C(5)-H(5)	119.8
C(5)-C(6)-C(7)	119.79(16)
C(5)-C(6)-H(6)	120.1
C(7)-C(6)-H(6)	120.1
O(4)-C(7)-C(6)	115.06(15)
O(4)-C(7)-C(9)	124.76(15)
C(6)-C(7)-C(9)	120.18(16)
C(7)-O(4)-C(8)	118.41(14)
O(4)-C(8)-H(8A)	109.5
O(4)-C(8)-H(8B)	109.5
H(8A)-C(8)-H(8B)	109.5
O(4)-C(8)-H(8C)	109.5
H(8A)-C(8)-H(8C)	109.5
H(8B)-C(8)-H(8C)	109.5
C(10)-C(9)-C(7)	120.05(15)
C(10)-C(9)-H(9)	120.0
C(7)-C(9)-H(9)	120.0
C(9)-C(10)-C(4)	119.50(15)
C(9)-C(10)-C(11)	120.57(15)
C(4)-C(10)-C(11)	119.90(15)
C(10)-C(11)-C(12)	112.65(14)
C(10)-C(11)-H(11A)	109.1
C(12)-C(11)-H(11A)	109.1
C(10)-C(11)-H(11B)	109.1
C(12)-C(11)-H(11B)	109.1
H(11A)-C(11)-H(11B)	107.8

C(13)-C(12)-C(11)	113.76(14)
C(13)-C(12)-H(12A)	108.8
C(11)-C(12)-H(12A)	108.8
C(13)-C(12)-H(12B)	108.8
C(11)-C(12)-H(12B)	108.8
H(12A)-C(12)-H(12B)	107.7
C(12)-C(13)-C(2)	114.91(14)
C(12)-C(13)-H(13A)	108.5
C(2)-C(13)-H(13A)	108.5
C(12)-C(13)-H(13B)	108.5
C(2)-C(13)-H(13B)	108.5
H(13A)-C(13)-H(13B)	107.5
C(15)-C(14)-C(2)	103.92(14)
C(15)-C(14)-H(14A)	111.0
C(2)-C(14)-H(14A)	111.0
C(15)-C(14)-H(14B)	111.0
C(2)-C(14)-H(14B)	111.0
H(14A)-C(14)-H(14B)	109.0
O(1)-C(15)-C(14)	105.38(14)
O(1)-C(15)-H(15A)	110.7
C(14)-C(15)-H(15A)	110.7
O(1)-C(15)-H(15B)	110.7
C(14)-C(15)-H(15B)	110.7
H(15A)-C(15)-H(15B)	108.8
O(6)-C(21)-O(5)	122.24(16)
O(6)-C(21)-C(22)	126.68(16)
O(5)-C(21)-C(22)	111.08(15)
C(21)-O(5)-C(35)	110.33(13)
C(33)-C(22)-C(21)	108.92(14)
C(33)-C(22)-C(34)	114.93(14)
C(21)-C(22)-C(34)	101.71(13)
C(33)-C(22)-C(23)	115.02(14)
C(21)-C(22)-C(23)	103.81(13)

C(34)-C(22)-C(23)	110.93(14)
O(7)-C(23)-C(24)	120.82(16)
O(7)-C(23)-C(22)	117.65(15)
C(24)-C(23)-C(22)	121.28(14)
C(25)-C(24)-C(30)	119.47(15)
C(25)-C(24)-C(23)	116.84(15)
C(30)-C(24)-C(23)	123.68(16)
C(26)-C(25)-C(24)	121.26(16)
C(26)-C(25)-H(25)	119.4
C(24)-C(25)-H(25)	119.4
C(25)-C(26)-C(27)	119.09(16)
C(25)-C(26)-H(26)	120.5
C(27)-C(26)-H(26)	120.5
O(8)-C(27)-C(29)	124.80(16)
O(8)-C(27)-C(26)	114.63(16)
C(29)-C(27)-C(26)	120.56(16)
C(27)-O(8)-C(28)	117.83(14)
O(8)-C(28)-H(28A)	109.5
O(8)-C(28)-H(28B)	109.5
H(28A)-C(28)-H(28B)	109.5
O(8)-C(28)-H(28C)	109.5
H(28A)-C(28)-H(28C)	109.5
H(28B)-C(28)-H(28C)	109.5
C(27)-C(29)-C(30)	120.17(15)
C(27)-C(29)-H(29)	119.9
C(30)-C(29)-H(29)	119.9
C(29)-C(30)-C(24)	119.26(16)
C(29)-C(30)-C(31)	120.36(15)
C(24)-C(30)-C(31)	120.32(15)
C(30)-C(31)-C(32)	112.70(14)
C(30)-C(31)-H(31A)	109.1
C(32)-C(31)-H(31A)	109.1
C(30)-C(31)-H(31B)	109.1

C(32)-C(31)-H(31B)	109.1
H(31A)-C(31)-H(31B)	107.8
C(33)-C(32)-C(31)	113.97(14)
C(33)-C(32)-H(32A)	108.8
C(31)-C(32)-H(32A)	108.8
C(33)-C(32)-H(32B)	108.8
C(31)-C(32)-H(32B)	108.8
H(32A)-C(32)-H(32B)	107.7
C(32)-C(33)-C(22)	114.85(14)
C(32)-C(33)-H(33A)	108.6
C(22)-C(33)-H(33A)	108.6
C(32)-C(33)-H(33B)	108.6
C(22)-C(33)-H(33B)	108.6
H(33A)-C(33)-H(33B)	107.5
C(35)-C(34)-C(22)	103.61(14)
C(35)-C(34)-H(34A)	111.0
C(22)-C(34)-H(34A)	111.0
C(35)-C(34)-H(34B)	111.0
C(22)-C(34)-H(34B)	111.0
H(34A)-C(34)-H(34B)	109.0
O(5)-C(35)-C(34)	105.11(13)
O(5)-C(35)-H(35A)	110.7
C(34)-C(35)-H(35A)	110.7
O(5)-C(35)-H(35B)	110.7
C(34)-C(35)-H(35B)	110.7
H(35A)-C(35)-H(35B)	108.8

Symmetry transformations used to generate equivalent atoms:

Anisotropic displacement parameters $(Å^2 x\ 10^3)$ for **188b**. The anisotropic displacement factor exponent takes the form: $-2p^2[\ h^2\ a^{*2}U^{11} + ... + 2\ h\ k\ a^*\ b^*\ U^{12}\ ]$

	U^{11}	U^{22}	U^{33}	U^{23}	U^{13}	U^{12}

C(1)	16(1)	21(1)	14(1)	2(1)	2(1)	-1(1)
O(1)	14(1)	26(1)	23(1)	-1(1)	4(1)	1(1)
O(2)	27(1)	20(1)	23(1)	-3(1)	2(1)	-7(1)
C(2)	12(1)	13(1)	14(1)	0(1)	3(1)	0(1)
C(3)	13(1)	12(1)	14(1)	-1(1)	3(1)	-3(1)
O(3)	16(1)	21(1)	17(1)	2(1)	7(1)	2(1)
C(4)	14(1)	14(1)	13(1)	0(1)	3(1)	0(1)
C(5)	12(1)	16(1)	13(1)	-1(1)	4(1)	-4(1)
C(6)	18(1)	12(1)	13(1)	2(1)	2(1)	-1(1)
C(7)	14(1)	14(1)	13(1)	-1(1)	2(1)	1(1)
O(4)	15(1)	16(1)	24(1)	6(1)	6(1)	2(1)
C(8)	15(1)	20(1)	28(1)	6(1)	7(1)	3(1)
C(9)	15(1)	14(1)	16(1)	0(1)	5(1)	-2(1)
C(10)	15(1)	15(1)	13(1)	1(1)	3(1)	0(1)
C(11)	14(1)	15(1)	22(1)	5(1)	7(1)	1(1)
C(12)	19(1)	20(1)	20(1)	7(1)	9(1)	4(1)
C(13)	19(1)	15(1)	13(1)	2(1)	6(1)	4(1)
C(14)	19(1)	12(1)	17(1)	1(1)	5(1)	1(1)
C(15)	21(1)	20(1)	22(1)	0(1)	7(1)	4(1)
C(21)	16(1)	20(1)	16(1)	0(1)	4(1)	2(1)
O(5)	17(1)	24(1)	22(1)	-2(1)	8(1)	-2(1)
O(6)	27(1)	21(1)	30(1)	-7(1)	9(1)	5(1)
C(22)	14(1)	14(1)	15(1)	-1(1)	4(1)	1(1)
C(23)	15(1)	11(1)	16(1)	-1(1)	3(1)	2(1)
O(7)	15(1)	20(1)	20(1)	3(1)	0(1)	0(1)
C(24)	17(1)	13(1)	14(1)	-2(1)	3(1)	0(1)
C(25)	14(1)	16(1)	17(1)	0(1)	2(1)	2(1)
C(26)	20(1)	14(1)	17(1)	2(1)	4(1)	1(1)
C(27)	17(1)	15(1)	16(1)	-1(1)	6(1)	-2(1)
O(8)	17(1)	19(1)	29(1)	6(1)	8(1)	-1(1)
C(28)	16(1)	23(1)	26(1)	2(1)	7(1)	-3(1)
C(29)	14(1)	16(1)	16(1)	-2(1)	4(1)	1(1)

C(30)	16(1)	13(1)	12(1)	-2(1)	4(1)	1(1)
C(31)	14(1)	13(1)	19(1)	2(1)	4(1)	3(1)
C(32)	16(1)	18(1)	18(1)	4(1)	3(1)	1(1)
C(33)	16(1)	17(1)	14(1)	0(1)	2(1)	-2(1)
C(34)	18(1)	14(1)	18(1)	0(1)	5(1)	-1(1)
C(35)	18(1)	18(1)	21(1)	-1(1)	4(1)	-4(1)

Hydrogen coordinates (x 10^4) and isotropic displacement parameters ($Å^2$x 10 ^{3}) for **188b**.

	x	y	z	U(eq)
H(5)	10000	7906	7654	16
H(6)	7656	9108	7319	17
H(8A)	3127	7502	7532	31
H(8B)	2660	8916	7707	31
H(8C)	3619	8100	8609	31
H(9)	5310	6430	8541	18
H(11A)	8218	4165	8756	20
H(11B)	6584	4519	9090	20
H(12A)	7953	5233	10596	23
H(12B)	8822	3950	10439	23
H(13A)	10899	5277	11020	19
H(13B)	10059	6401	10346	19
H(14A)	11555	3334	10105	19
H(14B)	10967	3419	8925	19
H(15A)	14015	3067	9737	25
H(15B)	13499	3808	8711	25
H(25)	6858	2151	7414	19
H(26)	4816	951	7822	20
H(28A)	-84	2385	7335	32
H(28B)	-479	925	7259	32
H(28C)	-47	1644	6342	32
H(29)	1499	3517	6520	18
H(31A)	4209	5836	6313	19
H(31B)	2334	5474	6022	19
H(32A)	2502	4821	4481	21
H(32B)	3520	6087	4638	21
H(33A)	5072	4749	3973	19

H(33B)	4754	3617	4652	19
H(34A)	6469	6676	4900	20
H(34B)	6746	6545	6079	20
H(35A)	9200	6962	5280	22
H(35B)	9432	6131	6264	22

Torsion angles [°] for **188b**

O(2)-C(1)-O(1)-C(15)	-173.69(17)
C(2)-C(1)-O(1)-C(15)	6.61(19)
O(2)-C(1)-C(2)-C(13)	-47.4(2)
O(1)-C(1)-C(2)-C(13)	132.27(15)
O(2)-C(1)-C(2)-C(14)	-169.39(17)
O(1)-C(1)-C(2)-C(14)	10.29(18)
O(2)-C(1)-C(2)-C(3)	74.8(2)
O(1)-C(1)-C(2)-C(3)	-105.52(16)
C(13)-C(2)-C(3)-O(3)	169.34(15)
C(1)-C(2)-C(3)-O(3)	51.49(19)
C(14)-C(2)-C(3)-O(3)	-57.6(2)
C(13)-C(2)-C(3)-C(4)	-5.3(2)
C(1)-C(2)-C(3)-C(4)	-123.13(16)
C(14)-C(2)-C(3)-C(4)	127.83(16)
O(3)-C(3)-C(4)-C(10)	139.84(18)
C(2)-C(3)-C(4)-C(10)	-45.7(2)
O(3)-C(3)-C(4)-C(5)	-38.3(2)
C(2)-C(3)-C(4)-C(5)	136.15(16)
C(10)-C(4)-C(5)-C(6)	2.8(2)
C(3)-C(4)-C(5)-C(6)	-178.97(15)
C(4)-C(5)-C(6)-C(7)	-1.5(3)
C(5)-C(6)-C(7)-O(4)	178.70(15)
C(5)-C(6)-C(7)-C(9)	-1.4(3)
C(6)-C(7)-O(4)-C(8)	176.28(15)
C(9)-C(7)-O(4)-C(8)	-3.6(3)

O(4)-C(7)-C(9)-C(10)	-177.05(16)
C(6)-C(7)-C(9)-C(10)	3.1(2)
C(7)-C(9)-C(10)-C(4)	-1.8(2)
C(7)-C(9)-C(10)-C(11)	179.97(15)
C(5)-C(4)-C(10)-C(9)	-1.2(2)
C(3)-C(4)-C(10)-C(9)	-179.27(15)
C(5)-C(4)-C(10)-C(11)	177.12(15)
C(3)-C(4)-C(10)-C(11)	-1.0(2)
C(9)-C(10)-C(11)-C(12)	-108.37(18)
C(4)-C(10)-C(11)-C(12)	73.4(2)
C(10)-C(11)-C(12)-C(13)	-45.7(2)
C(11)-C(12)-C(13)-C(2)	-43.1(2)
C(1)-C(2)-C(13)-C(12)	-171.09(14)
C(14)-C(2)-C(13)-C(12)	-57.59(19)
C(3)-C(2)-C(13)-C(12)	73.68(19)
C(13)-C(2)-C(14)-C(15)	-138.90(15)
C(1)-C(2)-C(14)-C(15)	-21.83(17)
C(3)-C(2)-C(14)-C(15)	88.27(16)
C(1)-O(1)-C(15)-C(14)	-21.06(19)
C(2)-C(14)-C(15)-O(1)	26.39(17)
O(6)-C(21)-O(5)-C(35)	-174.80(17)
C(22)-C(21)-O(5)-C(35)	5.72(19)
O(6)-C(21)-C(22)-C(33)	-45.2(2)
O(5)-C(21)-C(22)-C(33)	134.24(15)
O(6)-C(21)-C(22)-C(34)	-166.95(18)
O(5)-C(21)-C(22)-C(34)	12.50(18)
O(6)-C(21)-C(22)-C(23)	77.8(2)
O(5)-C(21)-C(22)-C(23)	-102.76(15)
C(33)-C(22)-C(23)-O(7)	163.83(15)
C(21)-C(22)-C(23)-O(7)	44.9(2)
C(34)-C(22)-C(23)-O(7)	-63.6(2)
C(33)-C(22)-C(23)-C(24)	-10.4(2)
C(21)-C(22)-C(23)-C(24)	-129.32(16)

C(34)-C(22)-C(23)-C(24)	122.15(16)
O(7)-C(23)-C(24)-C(25)	-32.4(2)
C(22)-C(23)-C(24)-C(25)	141.69(16)
O(7)-C(23)-C(24)-C(30)	148.95(17)
C(22)-C(23)-C(24)-C(30)	-37.0(2)
C(30)-C(24)-C(25)-C(26)	4.0(3)
C(23)-C(24)-C(25)-C(26)	-174.74(16)
C(24)-C(25)-C(26)-C(27)	-0.3(3)
C(25)-C(26)-C(27)-O(8)	178.22(16)
C(25)-C(26)-C(27)-C(29)	-3.2(3)
C(29)-C(27)-O(8)-C(28)	8.3(3)
C(26)-C(27)-O(8)-C(28)	-173.19(15)
O(8)-C(27)-C(29)-C(30)	-178.51(17)
C(26)-C(27)-C(29)-C(30)	3.0(3)
C(27)-C(29)-C(30)-C(24)	0.6(2)
C(27)-C(29)-C(30)-C(31)	-176.81(15)
C(25)-C(24)-C(30)-C(29)	-4.1(2)
C(23)-C(24)-C(30)-C(29)	174.56(16)
C(25)-C(24)-C(30)-C(31)	173.36(15)
C(23)-C(24)-C(30)-C(31)	-8.0(2)
C(29)-C(30)-C(31)-C(32)	-107.41(18)
C(24)-C(30)-C(31)-C(32)	75.2(2)
C(30)-C(31)-C(32)-C(33)	-44.1(2)
C(31)-C(32)-C(33)-C(22)	-43.9(2)
C(21)-C(22)-C(33)-C(32)	-168.54(14)
C(34)-C(22)-C(33)-C(32)	-55.2(2)
C(23)-C(22)-C(33)-C(32)	75.46(19)
C(33)-C(22)-C(34)-C(35)	-141.88(14)
C(21)-C(22)-C(34)-C(35)	-24.40(16)
C(23)-C(22)-C(34)-C(35)	85.50(16)
C(21)-O(5)-C(35)-C(34)	-21.92(18)
C(22)-C(34)-C(35)-O(5)	28.62(17)

Symmetry transformations used to generate equivalent atoms:

X-Ray Structure Determination: Compound 188c
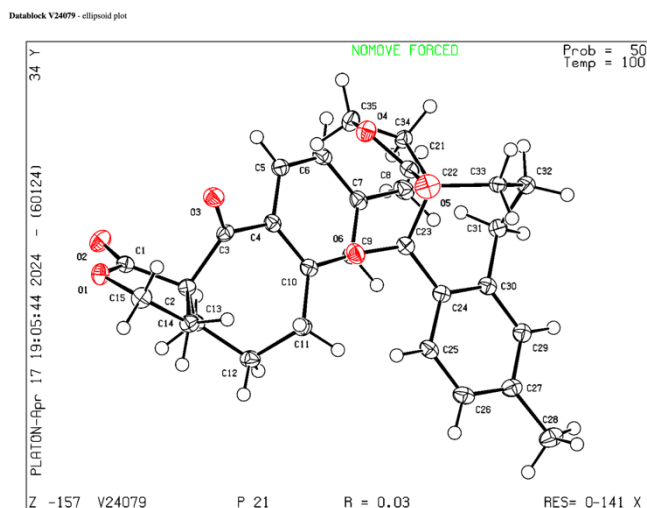
Low-temperature diffraction data (ϕ-and ω-scans) were collected on a Bruker AXS D8 VENTURE KAPPA diffractometer coupled to a PHOTON II CPAD detector with Cu K_α radiation ($\lambda = 1.54178$ Å) from an IμS micro-source for the structure of compound V24079. The structure was solved by direct methods using SHELXS and refined against F^2 on all data by full-matrix least squares with SHELXL-2019 using established refinement techniques. All non-hydrogen atoms were refined anisotropically. All hydrogen atoms were included into the model at geometrically calculated positions and refined using a riding model. The isotropic displacement parameters of all hydrogen atoms were fixed to 1.2 times the U value of the atoms they are linked to (1.5 times for methyl groups). Compound **188c** crystallizes in the monoclinic space group $P2_1$ with two molecules in the asymmetric unit.

Crystal data and structure refinement for **188c**.

Identification code	V24079
Empirical formula	C15 H16 O3
Formula weight	244.28
Temperature	100(2) K
Wavelength	1.54178 Å
Crystal system	Monoclinic
Space group	P2$_1$
Unit cell dimensions	a = 8.2548(9) Å α= 90°.
	b = 13.6753(6) Å β= 90.362(7)°.
	c = 10.8014(8) Å γ = 90°.
Volume	1219.31(17) Å^3
Z	4
Density (calculated)	1.331 Mg/m^3
Absorption coefficient	0.745 mm^{-1}
F(000)	520
Crystal size	0.200 x 0.200 x 0.200 mm^3
Theta range for data collection	4.093 to 75.115°.
Index ranges	-10<=h<=10, -17<=k<=17, -13<=l<=13
Reflections collected	28637
Independent reflections	4973 [R(int) = 0.0471]
Completeness to theta = 67.679°	100.0 %
Absorption correction	Semi-empirical from equivalents
Max. and min. transmission	0.7538 and 0.6520
Refinement method	Full-matrix least-squares on F^2
Data / restraints / parameters	4973 / 1 / 327
Goodness-of-fit on F^2	1.028
Final R indices [I>2sigma(I)]	R1 = 0.0291, wR2 = 0.0717
R indices (all data)	R1 = 0.0331, wR2 = 0.0728
Absolute structure parameter	-0.11(6)
Extinction coefficient	n/a
Largest diff. peak and hole	0.208 and -0.170 e.Å^{-3}

Atomic coordinates (x 10^4) and equivalent isotropic displacement parameters (Å^2x 10^3) for **188c**. U(eq) is defined as one third of the trace of the orthogonalized U^{ij} tensor.

	x	y	z	U(eq)
O(4)	7579(2)	7432(1)	7689(1)	22(1)
O(1)	10760(2)	2494(1)	7340(1)	21(1)
O(6)	5821(2)	5637(1)	6512(1)	22(1)
O(5)	6494(2)	7976(1)	5923(1)	27(1)
O(2)	9683(2)	2024(1)	9131(1)	25(1)
O(3)	8855(2)	4358(1)	8378(1)	23(1)
C(23)	4601(2)	6124(1)	6674(2)	16(1)
C(3)	7708(2)	3806(1)	8273(2)	16(1)
C(21)	6343(2)	7552(2)	6889(2)	18(1)
C(24)	3021(2)	5837(1)	6102(2)	16(1)
C(7)	3220(2)	4452(1)	10108(2)	18(1)
C(10)	4634(2)	3819(1)	8298(2)	17(1)
C(1)	9524(2)	2406(2)	8135(2)	18(1)
C(5)	6152(2)	4475(1)	10040(2)	17(1)
C(11)	4579(2)	3383(2)	7019(2)	18(1)
C(4)	6124(2)	4031(1)	8874(2)	16(1)
C(13)	6587(2)	2078(2)	7766(2)	17(1)
C(25)	3080(3)	5334(1)	4969(2)	19(1)
C(30)	1512(2)	6059(1)	6621(2)	17(1)
C(9)	3216(2)	4044(2)	8923(2)	18(1)
C(22)	4775(2)	7098(1)	7390(2)	15(1)
C(26)	1669(3)	5118(2)	4328(2)	21(1)
C(6)	4716(3)	4671(2)	10659(2)	20(1)
C(29)	104(2)	5842(1)	5949(2)	19(1)
C(31)	1401(2)	6497(2)	7898(2)	18(1)
C(34)	5235(2)	6916(2)	8763(2)	17(1)
C(2)	7952(2)	2826(2)	7584(2)	16(1)
C(15)	10275(2)	3062(2)	6262(2)	22(1)
C(12)	5045(2)	2295(2)	7018(2)	20(1)

C(32)	1843(2)	7587(2)	7924(2)	21(1)
C(35)	7081(2)	6840(2)	8739(2)	21(1)
C(27)	159(3)	5393(2)	4787(2)	20(1)
C(8)	1643(3)	4640(2)	10760(2)	23(1)
C(33)	3374(2)	7821(2)	7189(2)	18(1)
C(14)	8427(2)	2992(2)	6219(2)	19(1)
C(28)	-1370(3)	5204(2)	4057(2)	26(1)

Bond lengths [Å] and angles [°] for **188c**.

O(4)-C(21)	1.343(2)
O(4)-C(35)	1.456(2)
O(1)-C(1)	1.342(2)
O(1)-C(15)	1.455(3)
O(6)-C(23)	1.221(2)
O(5)-C(21)	1.200(3)
O(2)-C(1)	1.203(3)
O(3)-C(3)	1.215(2)
C(23)-C(24)	1.492(3)
C(23)-C(22)	1.547(3)
C(3)-C(4)	1.496(3)
C(3)-C(2)	1.547(3)
C(21)-C(22)	1.537(3)
C(24)-C(30)	1.403(3)
C(24)-C(25)	1.405(3)
C(7)-C(9)	1.396(3)
C(7)-C(6)	1.399(3)
C(7)-C(8)	1.506(3)
C(10)-C(9)	1.389(3)
C(10)-C(4)	1.405(3)
C(10)-C(11)	1.506(3)
C(1)-C(2)	1.536(3)
C(5)-C(6)	1.390(3)

C(5)-C(4)	1.399(3)
C(5)-H(5)	0.9500
C(11)-C(12)	1.537(3)
C(11)-H(11A)	0.9900
C(11)-H(11B)	0.9900
C(13)-C(12)	1.533(3)
C(13)-C(2)	1.535(3)
C(13)-H(13A)	0.9900
C(13)-H(13B)	0.9900
C(25)-C(26)	1.384(3)
C(25)-H(25)	0.9500
C(30)-C(29)	1.398(3)
C(30)-C(31)	1.507(3)
C(9)-H(9)	0.9500
C(22)-C(33)	1.536(3)
C(22)-C(34)	1.549(3)
C(26)-C(27)	1.396(3)
C(26)-H(26)	0.9500
C(6)-H(6)	0.9500
C(29)-C(27)	1.399(3)
C(29)-H(29)	0.9500
C(31)-C(32)	1.534(3)
C(31)-H(31A)	0.9900
C(31)-H(31B)	0.9900
C(34)-C(35)	1.528(3)
C(34)-H(34A)	0.9900
C(34)-H(34B)	0.9900
C(2)-C(14)	1.545(3)
C(15)-C(14)	1.528(3)
C(15)-H(15A)	0.9900
C(15)-H(15B)	0.9900
C(12)-H(12A)	0.9900
C(12)-H(12B)	0.9900

C(32)-C(33)	1.531(3)
C(32)-H(32A)	0.9900
C(32)-H(32B)	0.9900
C(35)-H(35A)	0.9900
C(35)-H(35B)	0.9900
C(27)-C(28)	1.506(3)
C(8)-H(8A)	0.9800
C(8)-H(8B)	0.9800
C(8)-H(8C)	0.9800
C(33)-H(33A)	0.9900
C(33)-H(33B)	0.9900
C(14)-H(14A)	0.9900
C(14)-H(14B)	0.9900
C(28)-H(28A)	0.9800
C(28)-H(28B)	0.9800
C(28)-H(28C)	0.9800
C(21)-O(4)-C(35)	110.64(14)
C(1)-O(1)-C(15)	110.66(15)
O(6)-C(23)-C(24)	121.12(18)
O(6)-C(23)-C(22)	117.84(17)
C(24)-C(23)-C(22)	120.80(16)
O(3)-C(3)-C(4)	120.94(18)
O(3)-C(3)-C(2)	118.66(17)
C(4)-C(3)-C(2)	120.26(16)
O(5)-C(21)-O(4)	122.37(18)
O(5)-C(21)-C(22)	126.39(18)
O(4)-C(21)-C(22)	111.23(16)
C(30)-C(24)-C(25)	119.33(18)
C(30)-C(24)-C(23)	123.62(17)
C(25)-C(24)-C(23)	117.03(17)
C(9)-C(7)-C(6)	118.11(18)
C(9)-C(7)-C(8)	119.97(18)

C(6)-C(7)-C(8)	121.92(18)
C(9)-C(10)-C(4)	118.48(18)
C(9)-C(10)-C(11)	120.89(18)
C(4)-C(10)-C(11)	120.61(17)
O(2)-C(1)-O(1)	122.11(17)
O(2)-C(1)-C(2)	126.60(18)
O(1)-C(1)-C(2)	111.27(16)
C(6)-C(5)-C(4)	120.46(18)
C(6)-C(5)-H(5)	119.8
C(4)-C(5)-H(5)	119.8
C(10)-C(11)-C(12)	112.17(17)
C(10)-C(11)-H(11A)	109.2
C(12)-C(11)-H(11A)	109.2
C(10)-C(11)-H(11B)	109.2
C(12)-C(11)-H(11B)	109.2
H(11A)-C(11)-H(11B)	107.9
C(5)-C(4)-C(10)	119.84(18)
C(5)-C(4)-C(3)	118.08(17)
C(10)-C(4)-C(3)	122.07(17)
C(12)-C(13)-C(2)	114.24(16)
C(12)-C(13)-H(13A)	108.7
C(2)-C(13)-H(13A)	108.7
C(12)-C(13)-H(13B)	108.7
C(2)-C(13)-H(13B)	108.7
H(13A)-C(13)-H(13B)	107.6
C(26)-C(25)-C(24)	120.50(19)
C(26)-C(25)-H(25)	119.8
C(24)-C(25)-H(25)	119.8
C(29)-C(30)-C(24)	118.96(18)
C(29)-C(30)-C(31)	120.30(17)
C(24)-C(30)-C(31)	120.72(17)
C(10)-C(9)-C(7)	122.49(18)
C(10)-C(9)-H(9)	118.8

C(7)-C(9)-H(9)	118.8
C(33)-C(22)-C(21)	109.00(16)
C(33)-C(22)-C(23)	114.60(15)
C(21)-C(22)-C(23)	104.32(15)
C(33)-C(22)-C(34)	114.74(15)
C(21)-C(22)-C(34)	101.59(15)
C(23)-C(22)-C(34)	111.19(16)
C(25)-C(26)-C(27)	120.97(19)
C(25)-C(26)-H(26)	119.5
C(27)-C(26)-H(26)	119.5
C(5)-C(6)-C(7)	120.54(18)
C(5)-C(6)-H(6)	119.7
C(7)-C(6)-H(6)	119.7
C(30)-C(29)-C(27)	121.86(19)
C(30)-C(29)-H(29)	119.1
C(27)-C(29)-H(29)	119.1
C(30)-C(31)-C(32)	112.77(17)
C(30)-C(31)-H(31A)	109.0
C(32)-C(31)-H(31A)	109.0
C(30)-C(31)-H(31B)	109.0
C(32)-C(31)-H(31B)	109.0
H(31A)-C(31)-H(31B)	107.8
C(35)-C(34)-C(22)	103.48(15)
C(35)-C(34)-H(34A)	111.1
C(22)-C(34)-H(34A)	111.1
C(35)-C(34)-H(34B)	111.1
C(22)-C(34)-H(34B)	111.1
H(34A)-C(34)-H(34B)	109.0
C(13)-C(2)-C(1)	108.69(16)
C(13)-C(2)-C(14)	114.32(16)
C(1)-C(2)-C(14)	101.87(15)
C(13)-C(2)-C(3)	114.68(15)
C(1)-C(2)-C(3)	104.41(15)

C(14)-C(2)-C(3)	111.51(16)
O(1)-C(15)-C(14)	105.10(15)
O(1)-C(15)-H(15A)	110.7
C(14)-C(15)-H(15A)	110.7
O(1)-C(15)-H(15B)	110.7
C(14)-C(15)-H(15B)	110.7
H(15A)-C(15)-H(15B)	108.8
C(13)-C(12)-C(11)	113.26(16)
C(13)-C(12)-H(12A)	108.9
C(11)-C(12)-H(12A)	108.9
C(13)-C(12)-H(12B)	108.9
C(11)-C(12)-H(12B)	108.9
H(12A)-C(12)-H(12B)	107.7
C(33)-C(32)-C(31)	113.02(16)
C(33)-C(32)-H(32A)	109.0
C(31)-C(32)-H(32A)	109.0
C(33)-C(32)-H(32B)	109.0
C(31)-C(32)-H(32B)	109.0
H(32A)-C(32)-H(32B)	107.8
O(4)-C(35)-C(34)	105.16(15)
O(4)-C(35)-H(35A)	110.7
C(34)-C(35)-H(35A)	110.7
O(4)-C(35)-H(35B)	110.7
C(34)-C(35)-H(35B)	110.7
H(35A)-C(35)-H(35B)	108.8
C(26)-C(27)-C(29)	118.12(19)
C(26)-C(27)-C(28)	120.95(19)
C(29)-C(27)-C(28)	120.9(2)
C(7)-C(8)-H(8A)	109.5
C(7)-C(8)-H(8B)	109.5
H(8A)-C(8)-H(8B)	109.5
C(7)-C(8)-H(8C)	109.5
H(8A)-C(8)-H(8C)	109.5

H(8B)-C(8)-H(8C)	109.5
C(32)-C(33)-C(22)	114.56(16)
C(32)-C(33)-H(33A)	108.6
C(22)-C(33)-H(33A)	108.6
C(32)-C(33)-H(33B)	108.6
C(22)-C(33)-H(33B)	108.6
H(33A)-C(33)-H(33B)	107.6
C(15)-C(14)-C(2)	103.86(15)
C(15)-C(14)-H(14A)	111.0
C(2)-C(14)-H(14A)	111.0
C(15)-C(14)-H(14B)	111.0
C(2)-C(14)-H(14B)	111.0
H(14A)-C(14)-H(14B)	109.0
C(27)-C(28)-H(28A)	109.5
C(27)-C(28)-H(28B)	109.5
H(28A)-C(28)-H(28B)	109.5
C(27)-C(28)-H(28C)	109.5
H(28A)-C(28)-H(28C)	109.5
H(28B)-C(28)-H(28C)	109.5

Symmetry transformations used to generate equivalent atoms:

Anisotropic displacement parameters ($Å^2$x 10^3) for compound **188c**. The anisotropic displacement factor exponent takes the form: $-2p^2[h^2 a^{*2}U^{11} + ... + 2 h k a^* b^* U^{12}]$

	U^{11}	U^{22}	U^{33}	U^{23}	U^{13}	U^{12}
O(4)	16(1)	23(1)	25(1)	2(1)	1(1)	-3(1)
O(1)	16(1)	23(1)	23(1)	2(1)	2(1)	2(1)
O(6)	19(1)	21(1)	26(1)	-3(1)	3(1)	2(1)
O(5)	30(1)	28(1)	23(1)	7(1)	5(1)	-6(1)
O(2)	26(1)	29(1)	21(1)	6(1)	-4(1)	0(1)

O(3)	19(1)	22(1)	28(1)	-4(1)	1(1)	-3(1)
C(23)	18(1)	17(1)	13(1)	2(1)	4(1)	-1(1)
C(3)	17(1)	17(1)	15(1)	2(1)	-2(1)	-1(1)
C(21)	20(1)	15(1)	20(1)	-2(1)	2(1)	-1(1)
C(24)	21(1)	14(1)	14(1)	1(1)	1(1)	-1(1)
C(7)	22(1)	14(1)	18(1)	2(1)	2(1)	2(1)
C(10)	20(1)	14(1)	16(1)	2(1)	1(1)	-1(1)
C(1)	18(1)	16(1)	20(1)	-2(1)	-1(1)	-1(1)
C(5)	22(1)	13(1)	17(1)	1(1)	-3(1)	0(1)
C(11)	16(1)	24(1)	15(1)	-3(1)	0(1)	0(1)
C(4)	19(1)	14(1)	16(1)	2(1)	1(1)	1(1)
C(13)	19(1)	15(1)	16(1)	-1(1)	3(1)	-2(1)
C(25)	24(1)	16(1)	16(1)	-1(1)	3(1)	1(1)
C(30)	20(1)	14(1)	17(1)	2(1)	1(1)	-2(1)
C(9)	18(1)	17(1)	18(1)	0(1)	-1(1)	0(1)
C(22)	16(1)	17(1)	13(1)	1(1)	1(1)	-2(1)
C(26)	29(1)	18(1)	16(1)	-1(1)	1(1)	-2(1)
C(6)	29(1)	16(1)	14(1)	0(1)	-1(1)	2(1)
C(29)	19(1)	17(1)	21(1)	2(1)	1(1)	-1(1)
C(31)	15(1)	22(1)	17(1)	-2(1)	3(1)	-1(1)
C(34)	18(1)	20(1)	14(1)	1(1)	0(1)	1(1)
C(2)	17(1)	17(1)	14(1)	1(1)	1(1)	0(1)
C(15)	20(1)	27(1)	18(1)	2(1)	4(1)	-1(1)
C(12)	18(1)	22(1)	20(1)	-4(1)	1(1)	-3(1)
C(32)	18(1)	24(1)	20(1)	-4(1)	-1(1)	2(1)
C(35)	19(1)	25(1)	20(1)	3(1)	-2(1)	2(1)
C(27)	26(1)	15(1)	20(1)	3(1)	-4(1)	-5(1)
C(8)	27(1)	24(1)	18(1)	-3(1)	4(1)	3(1)
C(33)	22(1)	16(1)	15(1)	-2(1)	-2(1)	1(1)
C(14)	19(1)	22(1)	15(1)	0(1)	1(1)	-1(1)
C(28)	28(1)	26(1)	25(1)	2(1)	-6(1)	-7(1)

Hydrogen coordinates (x 10^4) and isotropic displacement parameters (Å^2x 10^3)

for compound **188c**.

	x	y	z	U(eq)
H(5)	7159	4644	10413	21
H(11A)	5331	3748	6477	22
H(11B)	3472	3457	6673	22
H(13A)	6992	1423	7531	20
H(13B)	6309	2056	8656	20
H(25)	4096	5142	4641	22
H(9)	2206	3916	8530	21
H(26)	1728	4776	3563	25
H(6)	4751	4955	11461	23
H(29)	-918	6005	6292	23
H(31A)	2139	6138	8463	22
H(31B)	283	6415	8208	22
H(34A)	4881	7466	9293	21
H(34B)	4742	6303	9071	21
H(15A)	10753	2787	5500	26
H(15B)	10625	3751	6349	26
H(12A)	4139	1911	7365	24
H(12B)	5206	2079	6153	24
H(32A)	927	7969	7579	25
H(32B)	2005	7793	8794	25
H(35A)	7559	7094	9518	26
H(35B)	7425	6152	8630	26
H(8A)	765	4686	10147	34
H(8B)	1717	5255	11223	34
H(8C)	1420	4102	11333	34
H(33A)	3750	8484	7422	21
H(33B)	3094	7834	6297	21
H(14A)	8072	2437	5694	22

H(14B)	7943	3603	5894	22
H(28A)	-1487	5702	3410	39
H(28B)	-2304	5233	4611	39
H(28C)	-1312	4555	3675	39

Torsion angles [°] for compound **188c**.

C(35)-O(4)-C(21)-O(5)	-176.3(2)
C(35)-O(4)-C(21)-C(22)	4.6(2)
O(6)-C(23)-C(24)-C(30)	151.25(19)
C(22)-C(23)-C(24)-C(30)	-34.5(3)
O(6)-C(23)-C(24)-C(25)	-30.1(3)
C(22)-C(23)-C(24)-C(25)	144.22(18)
C(15)-O(1)-C(1)-O(2)	-174.64(19)
C(15)-O(1)-C(1)-C(2)	6.8(2)
C(9)-C(10)-C(11)-C(12)	-107.1(2)
C(4)-C(10)-C(11)-C(12)	74.7(2)
C(6)-C(5)-C(4)-C(10)	2.7(3)
C(6)-C(5)-C(4)-C(3)	-177.85(17)
C(9)-C(10)-C(4)-C(5)	-1.1(3)
C(11)-C(10)-C(4)-C(5)	177.19(18)
C(9)-C(10)-C(4)-C(3)	179.49(18)
C(11)-C(10)-C(4)-C(3)	-2.2(3)
O(3)-C(3)-C(4)-C(5)	-37.1(3)
C(2)-C(3)-C(4)-C(5)	138.54(18)
O(3)-C(3)-C(4)-C(10)	142.3(2)
C(2)-C(3)-C(4)-C(10)	-42.1(3)
C(30)-C(24)-C(25)-C(26)	4.3(3)
C(23)-C(24)-C(25)-C(26)	-174.40(18)
C(25)-C(24)-C(30)-C(29)	-5.0(3)
C(23)-C(24)-C(30)-C(29)	173.69(18)
C(25)-C(24)-C(30)-C(31)	173.22(18)
C(23)-C(24)-C(30)-C(31)	-8.1(3)
C(4)-C(10)-C(9)-C(7)	-1.4(3)

C(11)-C(10)-C(9)-C(7)	-179.74(19)
C(6)-C(7)-C(9)-C(10)	2.3(3)
C(8)-C(7)-C(9)-C(10)	-177.39(19)
O(5)-C(21)-C(22)-C(33)	-44.3(3)
O(4)-C(21)-C(22)-C(33)	134.69(16)
O(5)-C(21)-C(22)-C(23)	78.5(2)
O(4)-C(21)-C(22)-C(23)	-102.47(17)
O(5)-C(21)-C(22)-C(34)	-165.8(2)
O(4)-C(21)-C(22)-C(34)	13.2(2)
O(6)-C(23)-C(22)-C(33)	160.42(17)
C(24)-C(23)-C(22)-C(33)	-14.1(2)
O(6)-C(23)-C(22)-C(21)	41.3(2)
C(24)-C(23)-C(22)-C(21)	-133.16(17)
O(6)-C(23)-C(22)-C(34)	-67.4(2)
C(24)-C(23)-C(22)-C(34)	118.10(18)
C(24)-C(25)-C(26)-C(27)	0.1(3)
C(4)-C(5)-C(6)-C(7)	-1.8(3)
C(9)-C(7)-C(6)-C(5)	-0.6(3)
C(8)-C(7)-C(6)-C(5)	179.04(19)
C(24)-C(30)-C(29)-C(27)	1.3(3)
C(31)-C(30)-C(29)-C(27)	-176.89(18)
C(29)-C(30)-C(31)-C(32)	-105.8(2)
C(24)-C(30)-C(31)-C(32)	76.0(2)
C(33)-C(22)-C(34)-C(35)	-141.82(17)
C(21)-C(22)-C(34)-C(35)	-24.4(2)
C(23)-C(22)-C(34)-C(35)	86.09(18)
C(12)-C(13)-C(2)-C(1)	-167.25(15)
C(12)-C(13)-C(2)-C(14)	-54.2(2)
C(12)-C(13)-C(2)-C(3)	76.4(2)
O(2)-C(1)-C(2)-C(13)	-46.9(3)
O(1)-C(1)-C(2)-C(13)	131.63(16)
O(2)-C(1)-C(2)-C(14)	-167.9(2)
O(1)-C(1)-C(2)-C(14)	10.6(2)

O(2)-C(1)-C(2)-C(3)	75.9(2)
O(1)-C(1)-C(2)-C(3)	-105.54(17)
O(3)-C(3)-C(2)-C(13)	165.89(17)
C(4)-C(3)-C(2)-C(13)	-9.8(2)
O(3)-C(3)-C(2)-C(1)	47.1(2)
C(4)-C(3)-C(2)-C(1)	-128.65(18)
O(3)-C(3)-C(2)-C(14)	-62.2(2)
C(4)-C(3)-C(2)-C(14)	122.11(18)
C(1)-O(1)-C(15)-C(14)	-21.6(2)
C(2)-C(13)-C(12)-C(11)	-42.0(2)
C(10)-C(11)-C(12)-C(13)	-47.3(2)
C(30)-C(31)-C(32)-C(33)	-45.3(2)
C(21)-O(4)-C(35)-C(34)	-20.9(2)
C(22)-C(34)-C(35)-O(4)	28.0(2)
C(25)-C(26)-C(27)-C(29)	-3.7(3)
C(25)-C(26)-C(27)-C(28)	176.72(19)
C(30)-C(29)-C(27)-C(26)	3.0(3)
C(30)-C(29)-C(27)-C(28)	-177.41(19)
C(31)-C(32)-C(33)-C(22)	-43.6(2)
C(21)-C(22)-C(33)-C(32)	-165.36(16)
C(23)-C(22)-C(33)-C(32)	78.2(2)
C(34)-C(22)-C(33)-C(32)	-52.2(2)
O(1)-C(15)-C(14)-C(2)	27.1(2)
C(13)-C(2)-C(14)-C(15)	-139.45(17)
C(1)-C(2)-C(14)-C(15)	-22.4(2)
C(3)-C(2)-C(14)-C(15)	88.43(19)

Symmetry transformations used to generate equivalent atoms:

3.5   REFERENCES

(1)   Hiesinger, K.; Dar'in, D.; Proschak, E.; Krasavin, M. Spirocyclic Scaffolds in Medicinal Chemistry. *J. Med. Chem.* **2021**, *64* (1), 150–183.

(2)   Xie, J.-H.; Wang, L.-X.; Fu, Y.; Zhu, S.-F.; Fan, B.-M.; Duan, H.-F.; Zhou, Q.-L. Synthesis of Spiro Diphosphines and Their Application in Asymmetric Hydrogenation of Ketones. *J. Am. Chem. Soc.* **2003**, *125* (15), 4404–4405.

(3)   Xie, J.-H.; Liu, S.; Huo, X.-H.; Cheng, X.; Duan, H.-F.; Fan, B.-M.; Wang, L.-X.; Zhou, Q.-L. RuII-SDP-Complex-Catalyzed Asymmetric Hydrogenation of Ketones. Effect of the Alkali Metal Cation in the Reaction. *J. Org. Chem.* **2005**, *70* (8), 2967–2973.

(4)   de Almeida Leone, P.; Carroll, A. R.; Towerzey, L.; King, G.; McArdle, B. M.; Kern, G.; Fisher, S.; Hooper, J. N. A.; Quinn, R. J. Exiguaquinol: A Novel Pentacyclic Hydroquinone from Neopetrosia Exigua That Inhibits Helicobacter Pylori MurI. *Org. Lett.* **2008**, *10* (12), 2585–2588.

(5)   Schwarzwalder, G. M.; Scott, D. R.; Vanderwal, C. D. A Synthesis of Exiguaquinol Dessulfate. *Chemistry – A European Journal* **2016**, *22* (50), 17953–17957.

(6)   Ding, A.; Meazza, M.; Guo, H.; Yang, J. W.; Rios, R. New Development in the Enantioselective Synthesis of Spiro Compounds. *Chem. Soc. Rev.* **2018**, *47* (15), 5946–5996.

(7)   Quasdorf, K. W.; Overman, L. E. Catalytic Enantioselective Synthesis of Quaternary Carbon Stereocentres. *Nature* **2014**, *516* (7530), 181–191.

(8)   Inanaga, K.; Wollenburg, M.; Bachman, S.; Hafeman, N. J.; Stoltz, B. M. Catalytic

Enantioselective Synthesis of Carbocyclic and Heterocyclic Spiranes via a

Decarboxylative Aldol Cyclization. *Chem. Sci.* **2020**, *11* (28), 7390–7395.

(9)   Rahemtulla, B. F.; Clark, H. F.; Smith, M. D. Catalytic Enantioselective Synthesis

of C1- and C2-Symmetric Spirobiindanones through Counterion-Directed Enolate

C-Acylation. *Angewandte Chemie International Edition* **2016**, *55* (42), 13180–

13183.

(10) Xu, P.-W.; Yu, J.-S.; Chen, C.; Cao, Z.-Y.; Zhou, F.; Zhou, J. Catalytic

Enantioselective Construction of Spiro Quaternary Carbon Stereocenters. *ACS*

Catal. **2019**, *9* (3), 1820–1882.

(11) Hayashi, M.; Bachman, S.; Hashimoto, S.; Eichman, C. C.; Stoltz, B. M. Ni-

Catalyzed Enantioselective C-Acylation of α-Substituted Lactams. *J. Am. Chem.*

Soc. **2016**, *138* (29), 8997–9000.

(12) Casadei, M. A.; Galli, C.; Mandolini, L. Ring-Closure Reactions. 22. Kinetics of

Cyclization of Diethyl (.Omega.-Bromoalkyl)Malonates in the Range of 4- to 21-

Membered Rings. Role of Ring Strain. *J. Am. Chem. Soc.* **1984**, *106* (4), 1051–

1056.

(13) Ren, Y.; Kinghorn, A. D. Development of Potential Antitumor Agents from the

Scaffolds of Plant-Derived Terpenoid Lactones. *J. Med. Chem.* **2020**, *63* (24),

15410–15448.

(14) Bordwell, F. G.; Fried, H. E. Acidities of the Hydrogen-Carbon Protons in

Carboxylic Esters, Amides, and Nitriles. *J. Org. Chem.* **1981**, *46* (22), 4327–4331.

(15) Arnett, E. M.; Harrelson, J. A. Jr. Ion Pairing and Reactivity of Enolate Anions. 7. A Spectacular Example of the Importance of Rotational Barriers: The Ionization of Meldrum's Acid. *J. Am. Chem. Soc.* **1987**, *109* (3), 809–812.

(16) Tran, V. T.; Li, Z.-Q.; Apolinar, O.; Derosa, J.; Joannou, M. V.; Wisniewski, S. R.; Eastgate, M. D.; Engle, K. M. Ni(COD)(DQ): An Air-Stable 18-Electron Nickel(0)–Olefin Precatalyst. *Angewandte Chemie International Edition* **2020**, *59* (19), 7409–7413.

(17) Illuminati, G.; Mandolini, L. Ring Closure Reactions of Bifunctional Chain Molecules. *Acc. Chem. Res.* **1981**, *14* (4), 95–102.

(18) Yet, L. Metal-Mediated Synthesis of Medium-Sized Rings. *Chem. Rev.* **2000**, *100* (8), 2963–3008.

(19) Hansch, Corwin.; Leo, A.; Taft, R. W. A Survey of Hammett Substituent Constants and Resonance and Field Parameters. *Chem. Rev.* **1991**, *91* (2), 165–195.

(20) Houk, K. N.; Jabbari, A.; Hall, H. K.; Alemán, C. Why δ-Valerolactone Polymerizes and γ-Butyrolactone Does Not. *J. Org. Chem.* **2008**, *73* (7), 2674–2678.

(21) John, J.; Thomas, J.; Parekh, N.; Dehaen, W. Tandem Organocatalyzed Knoevenagel Condensation/1,3-Dipolar Cycloaddition towards Highly Functionalized Fused 1,2,3-Triazoles. *European Journal of Organic Chemistry* **2015**, *2015* (22), 4922–4930.

(22) Duchemin, N.; Buccafusca, R.; Daumas, M.; Ferey, V.; Arseniyadis, S. A Unified Strategy for the Synthesis of Difluoromethyl- and Vinylfluoride-Containing Scaffolds. *Org. Lett.* **2019**, *21* (20), 8205–8210.

(23) Molander, G. A.; Brown, A. R. Suzuki−Miyaura Cross-Coupling Reactions of Potassium Vinyltrifluoroborate with Aryl and Heteroaryl Electrophiles. *J. Org. Chem.* **2006**, *71* (26), 9681–9686.

(24) Johnston, D.; McCusker, C. F.; Muir, K.; Procter, D. J. Samarium(II)-Mediated 4-Exo-Trig Cyclisations of Unsaturated Aldehydes. A Stereoselective Approach to Functionalised Cyclobutanols. *J. Chem. Soc., Perkin Trans. 1* **2000**, No. 5, 681–695.

(25) Bunders, C.; Cavanagh, J.; Melander, C. Flustramine Inspired Synthesis and Biological Evaluation of Pyrroloindoline Triazole Amides as Novel Inhibitors of Bacterial Biofilms. *Org. Biomol. Chem.* **2011**, *9* (15), 5476–5481.

(26) James, J.; Akula, R.; Guiry, P. J. Pd-Catalyzed Decarboxylative Asymmetric Protonation (DAP) Using Chiral PHOX Ligands vs. Chiral Ligand-Free Conditions Employing (1R,2S)(–)-Ephedrine – A Comparison Study. *European Journal of Organic Chemistry* **2019**, *2019* (13), 2421–2427.

(27) Qiu, B.; Xu, D.; Sun, Q.; Miao, C.; Lee, Y.-M.; Li, X.-X.; Nam, W.; Sun, W. Highly Enantioselective Oxidation of Spirocyclic Hydrocarbons by Bioinspired Manganese Catalysts and Hydrogen Peroxide. *ACS Catal.* **2018**, *8* (3), 2479–2487.

(28) Sheldrick, G. M. Phase Annealing in SHELX-90: Direct Methods for Larger Structures. *Acta Cryst A* **1990**, *46* (6), 467–473.

(29) Sheldrick, G. M. Crystal Structure Refinement with SHELXL. *Acta Cryst C* **2015**, *71* (1), 3–8.

(30) Müller, P. Practical Suggestions for Better Crystal Structures. *Crystallography Reviews* **2009**, *15* (1), 57–83.

APPENDIX 2

Spectra Relevant to Chapter 3: Enantioselective Nickel-Catalyzed α-

Spirocyclization of Lactones
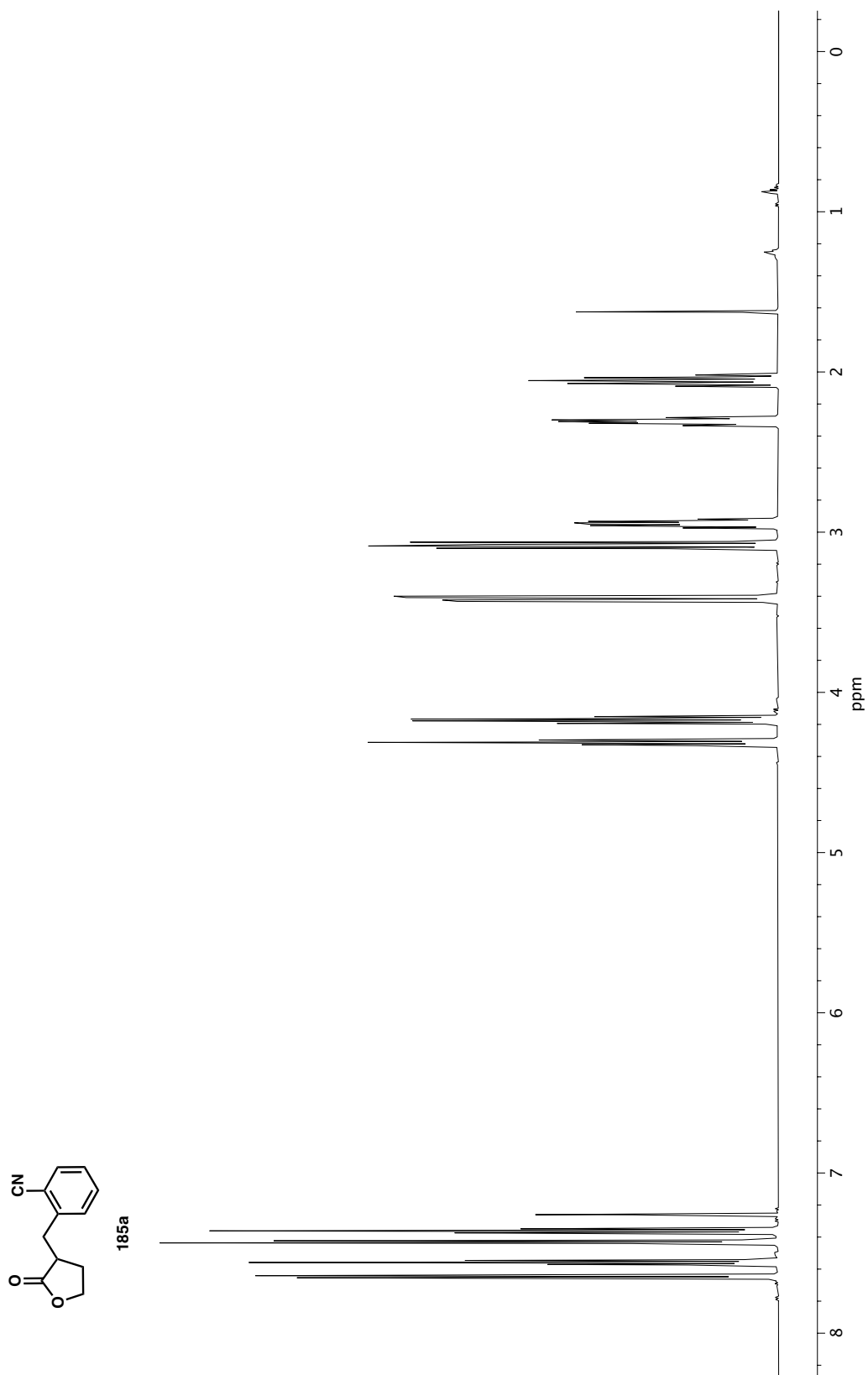
Figure A2.1 ^{1}H NMR (400 MHz, CDCl$_3$) of compound **185a**.
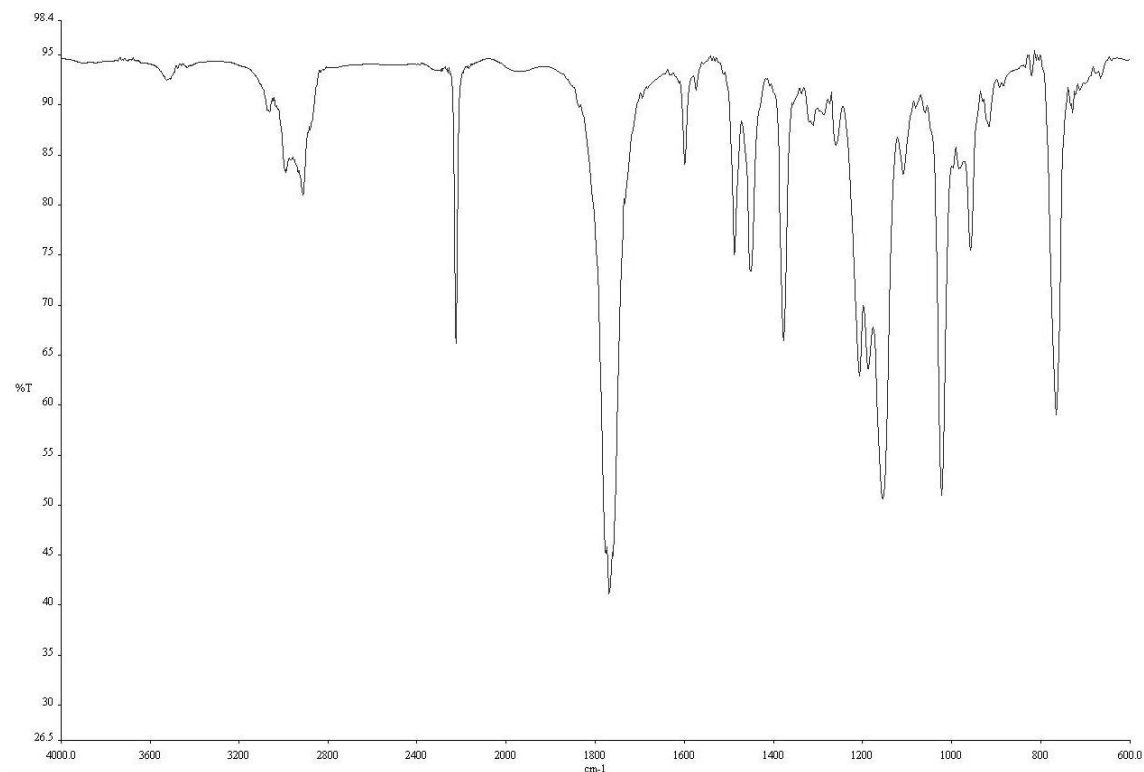
Figure A2.2 IR (NaCl, Thin Film) of compound **185a**.
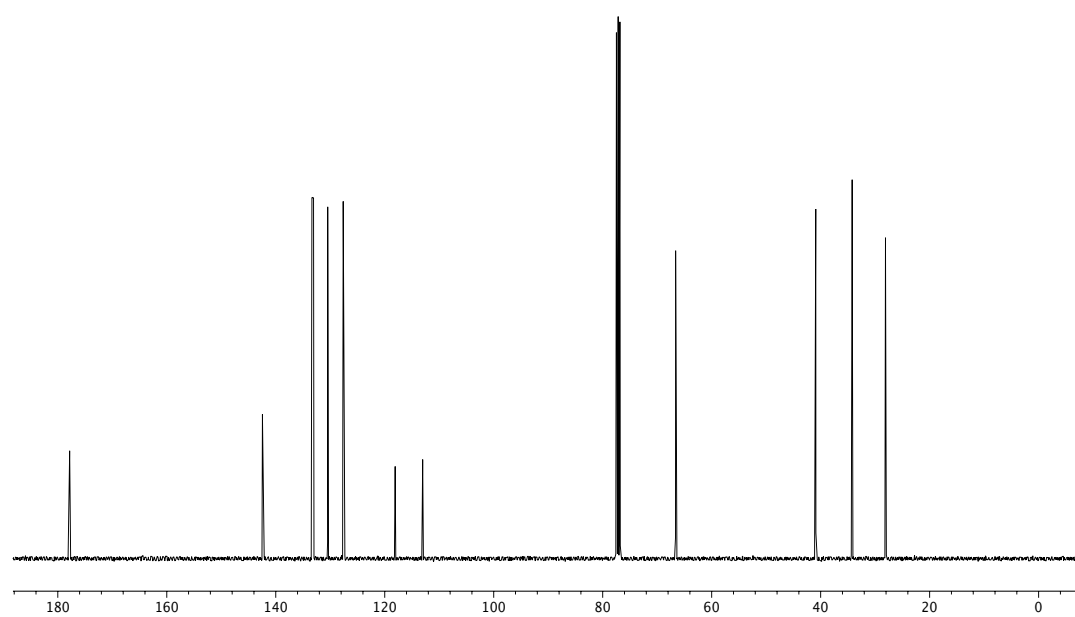
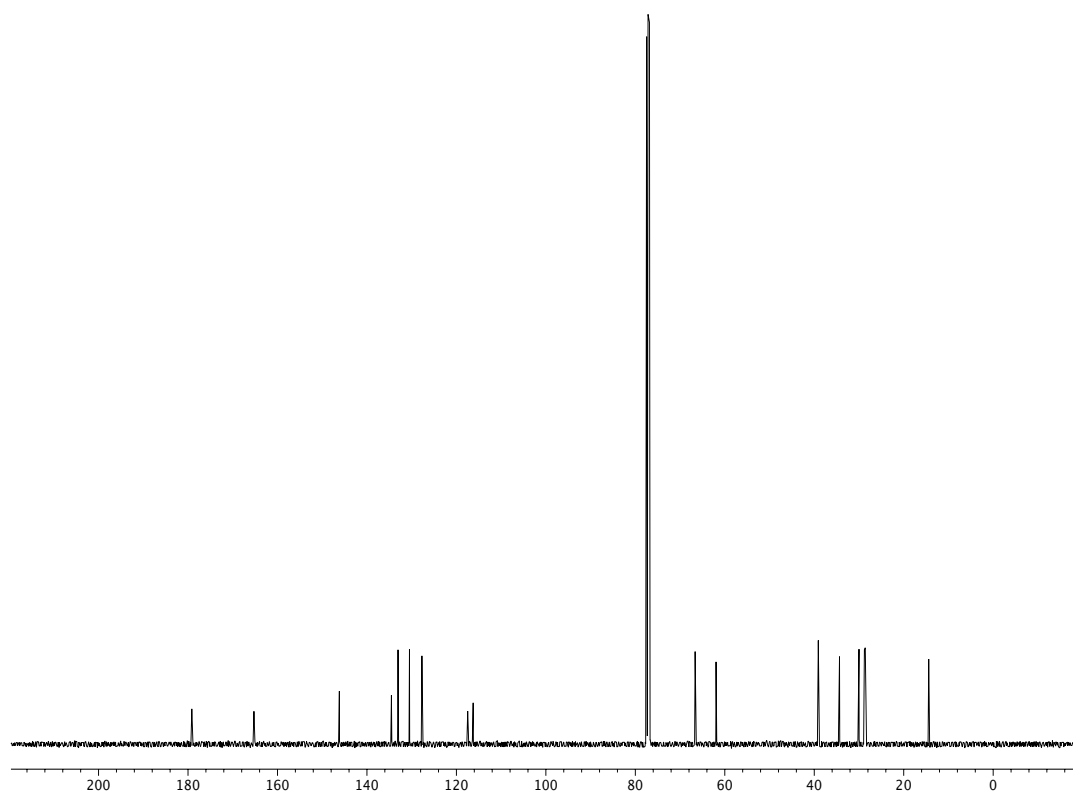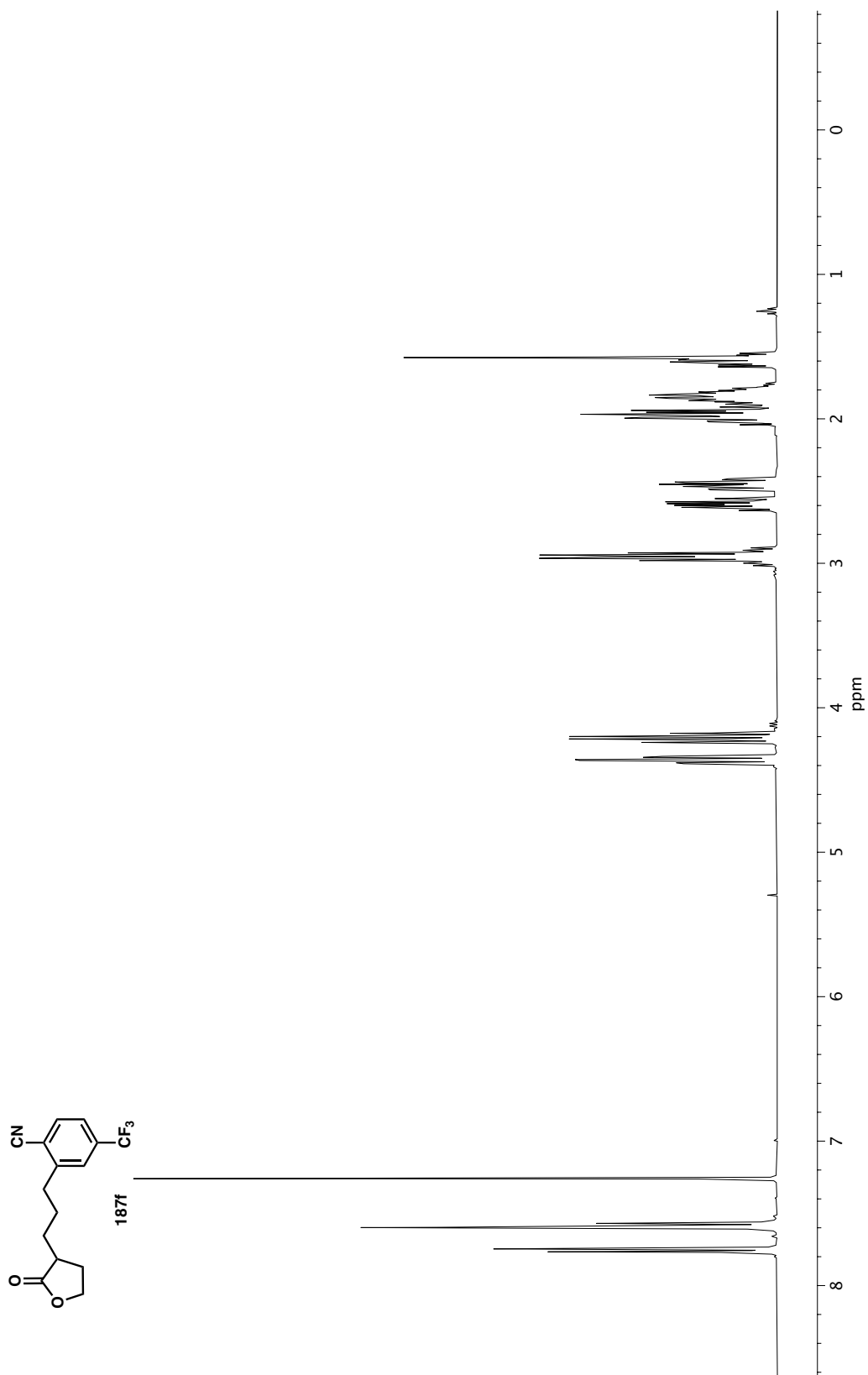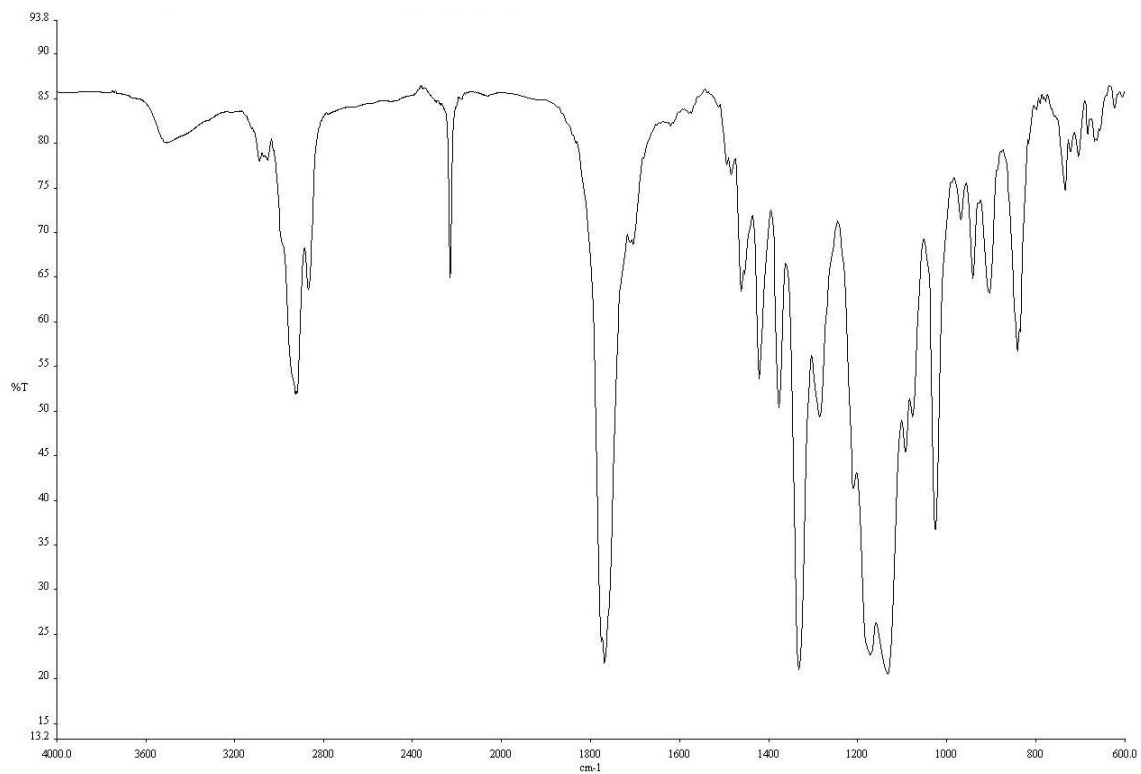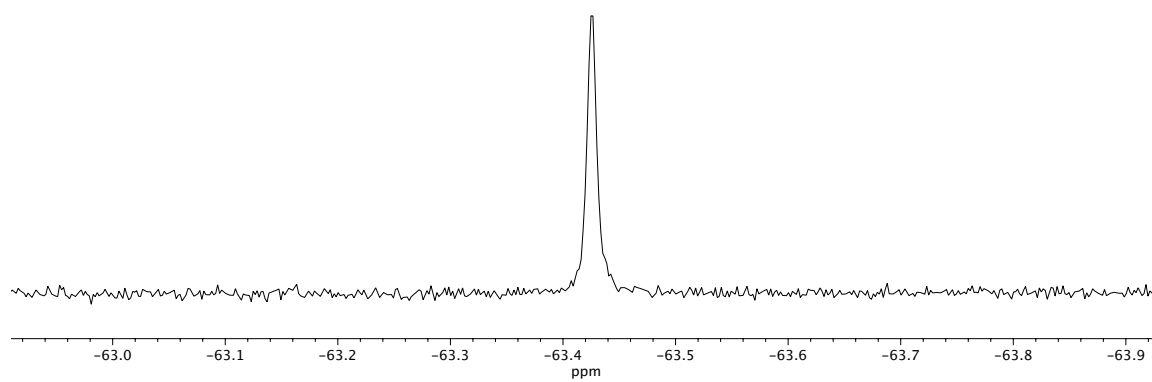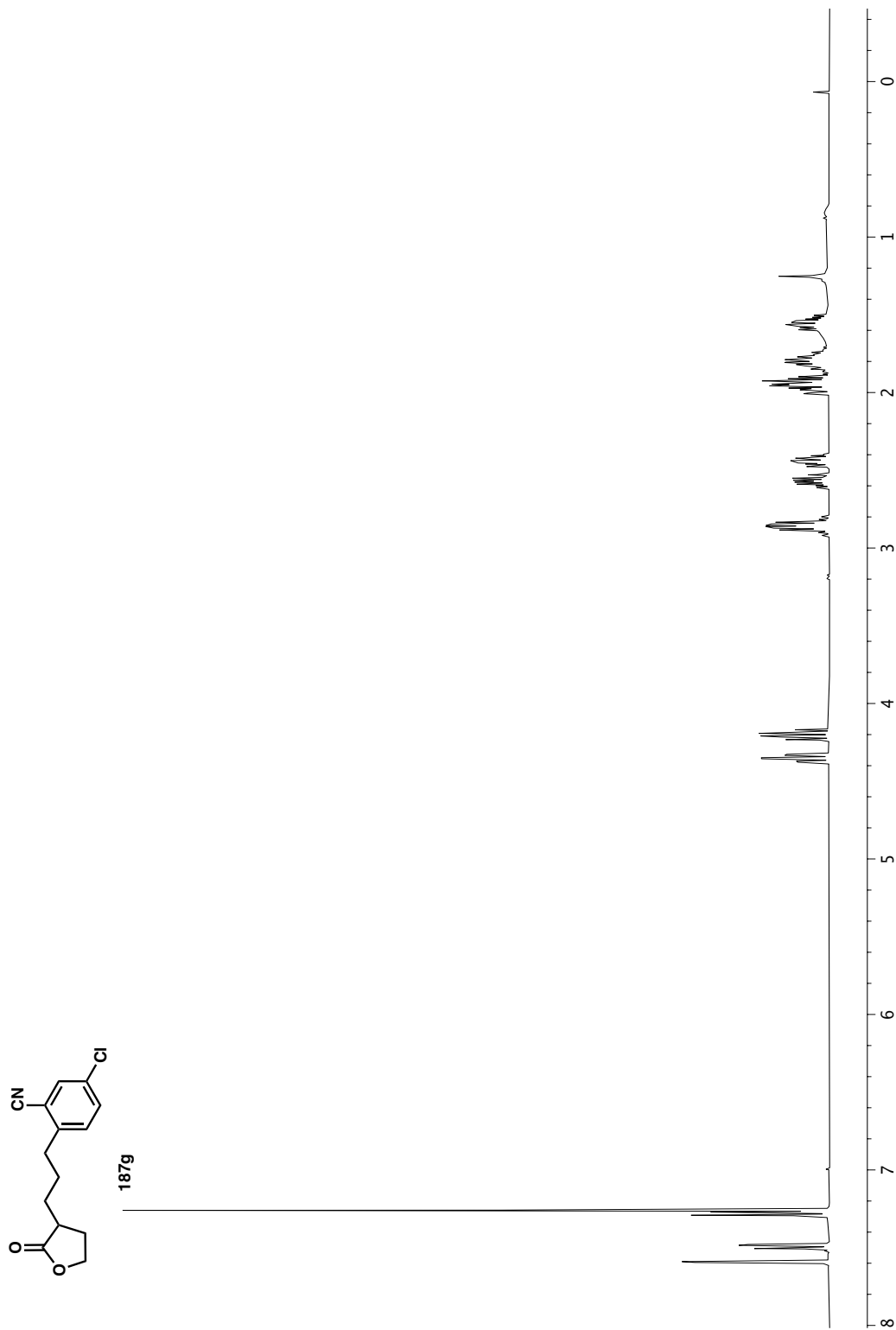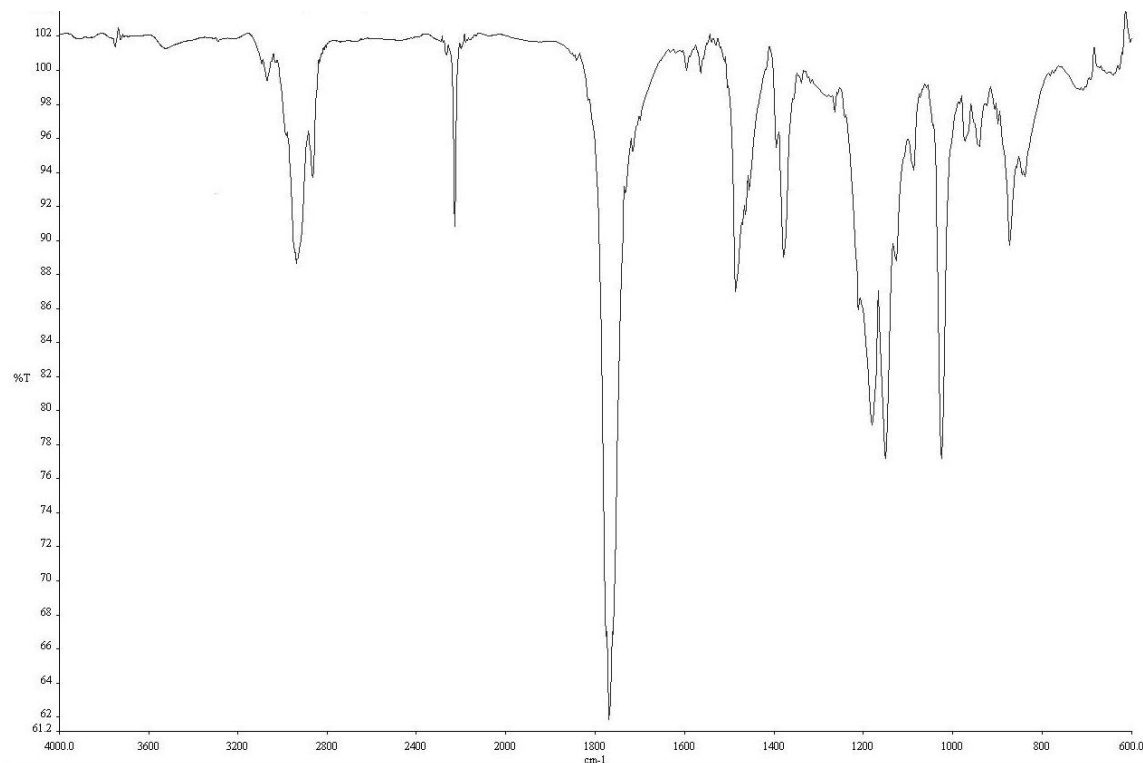*Figure A2.3* ^{13}C NMR (101 MHz, CDCl$_3$) of compound **185a**.
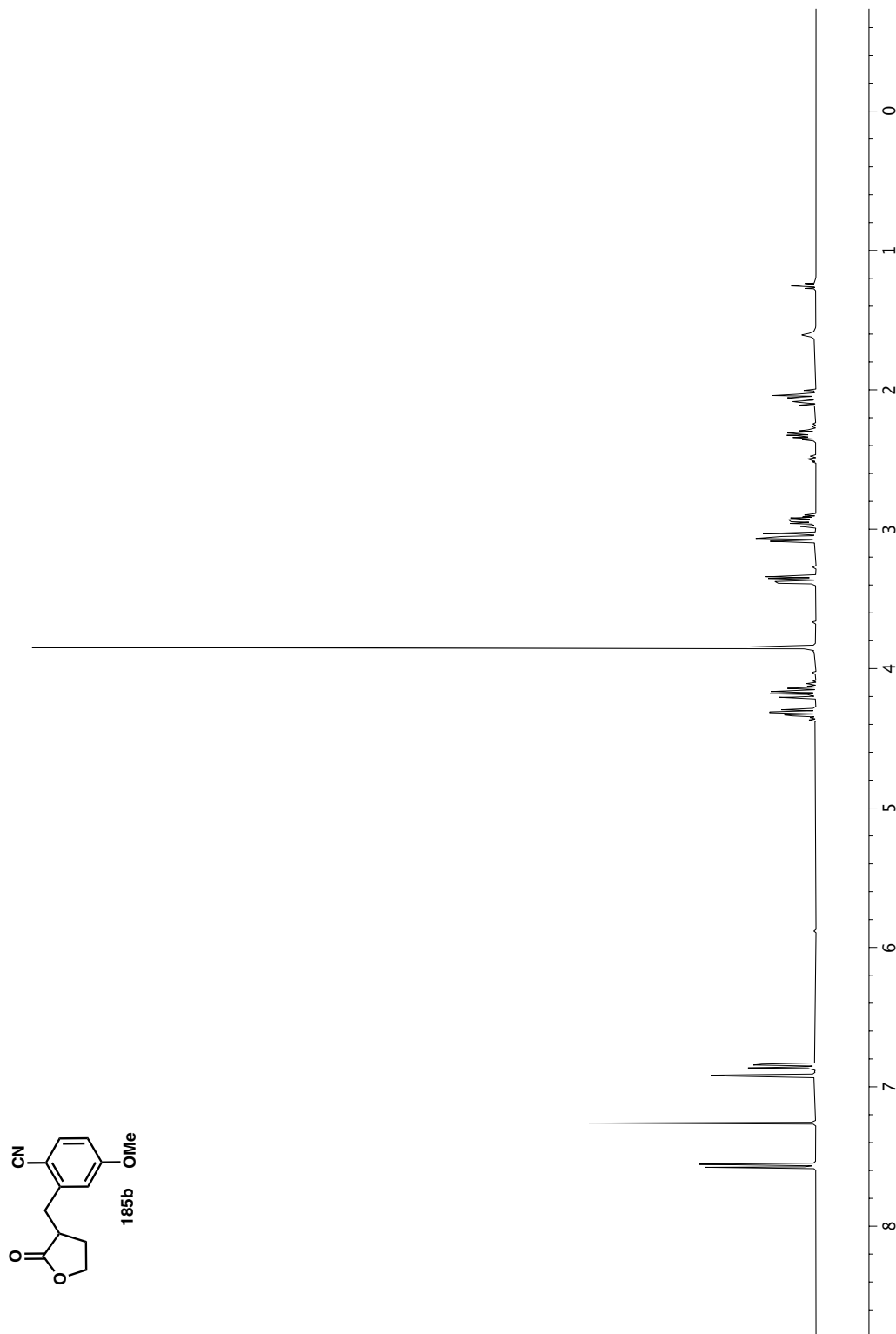
Figure A2.4 ^{1}H NMR (400 MHz, CDCl$_3$) of compound **185b.**
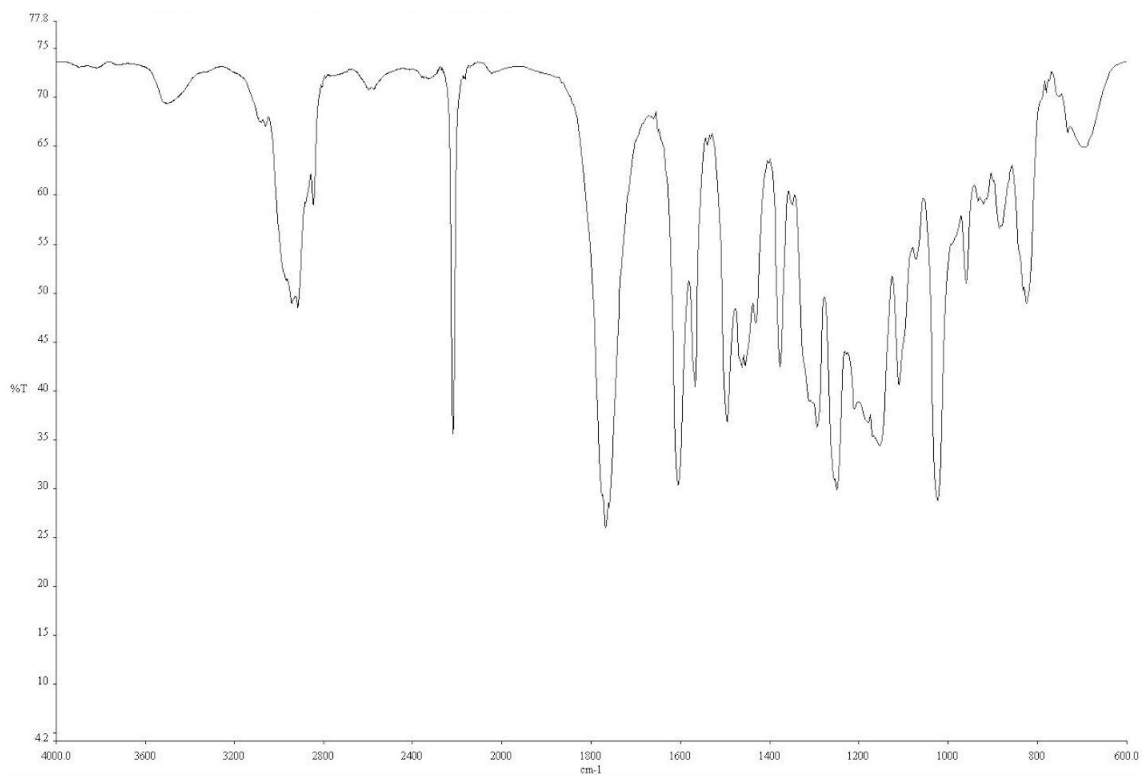
Figure A2.5 IR (NaCl, Thin Film) of compound **185b**.
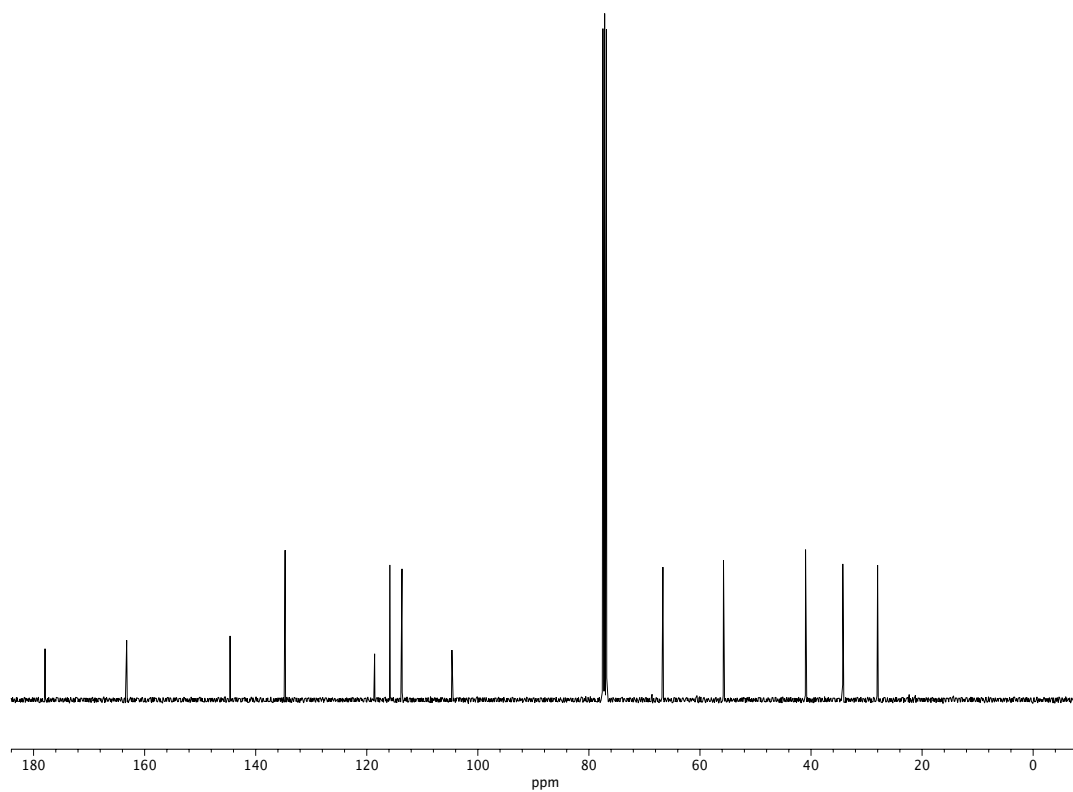
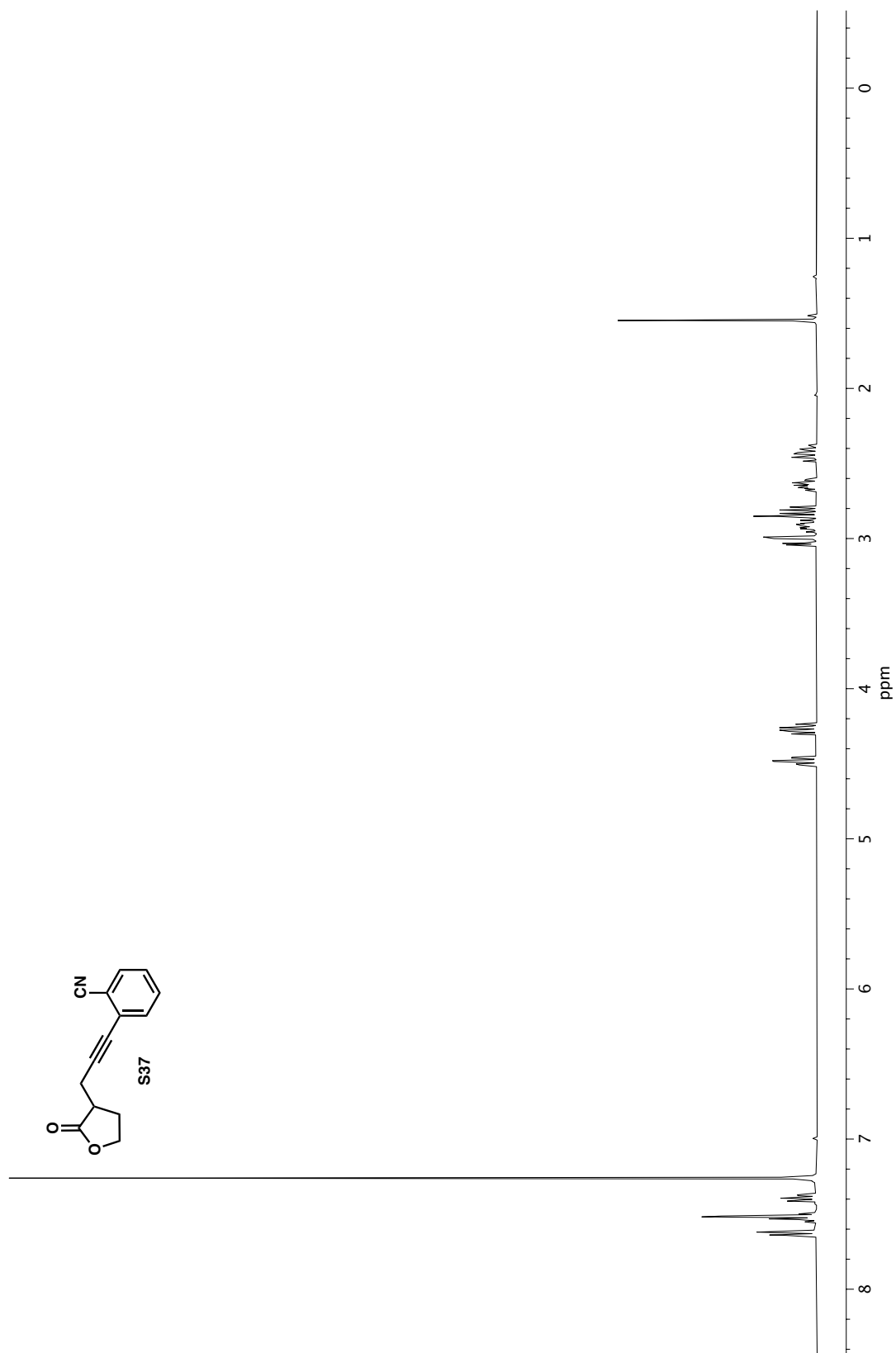***Figure A2.6*** ^{13}C NMR (101 MHz, CDCl$_3$) of compound **185b**.
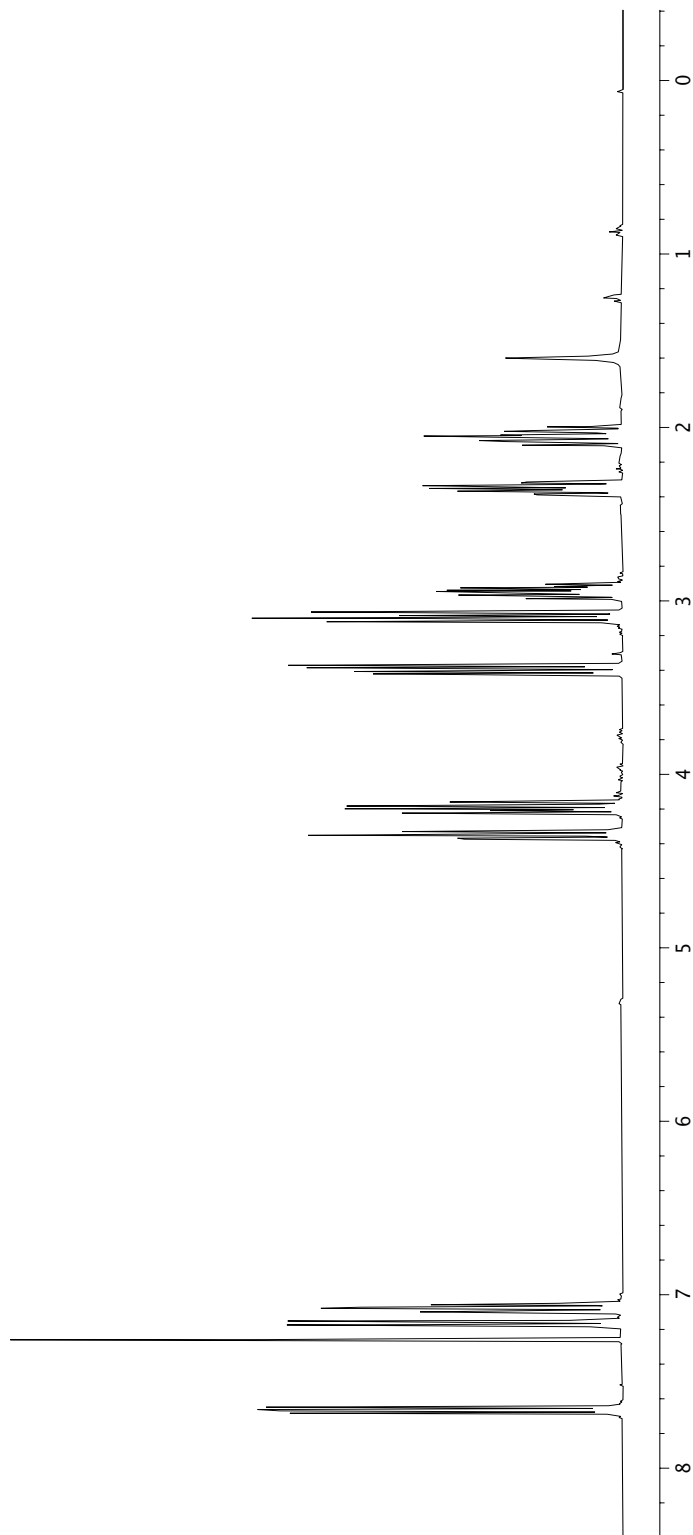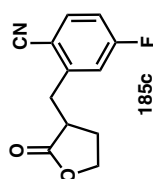
Figure A2.7 ¹H NMR (400 MHz, CDCl₃) of compound **185c.**
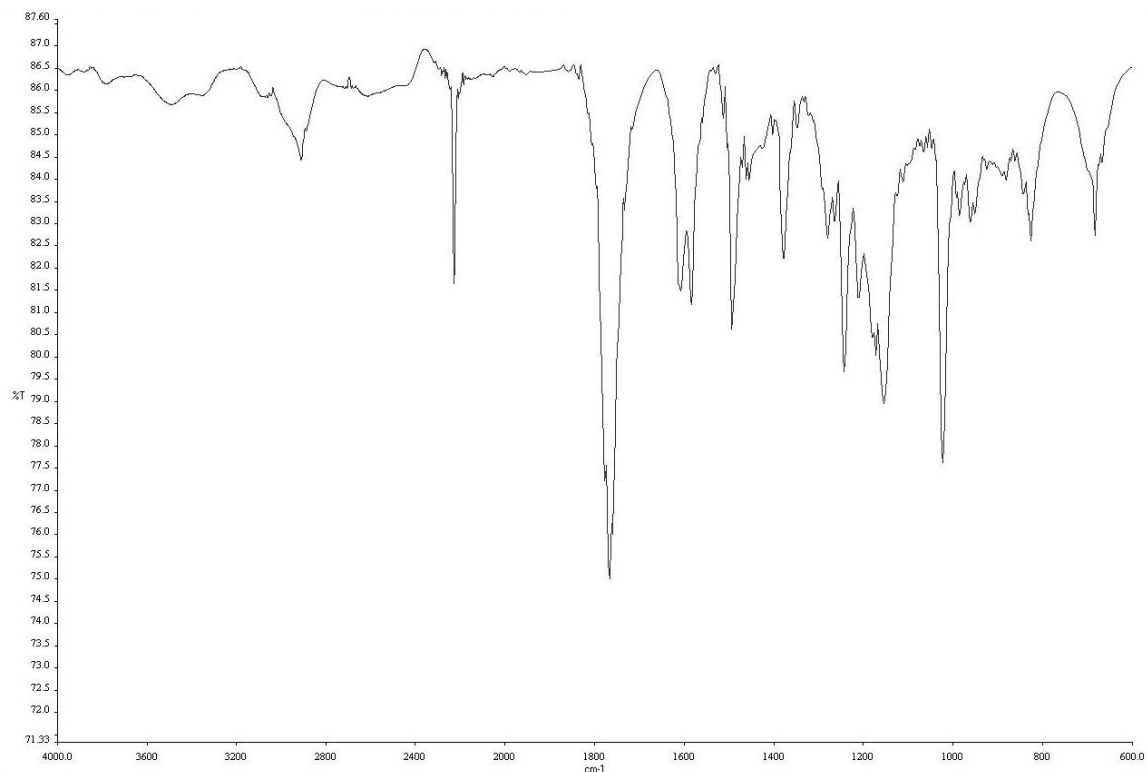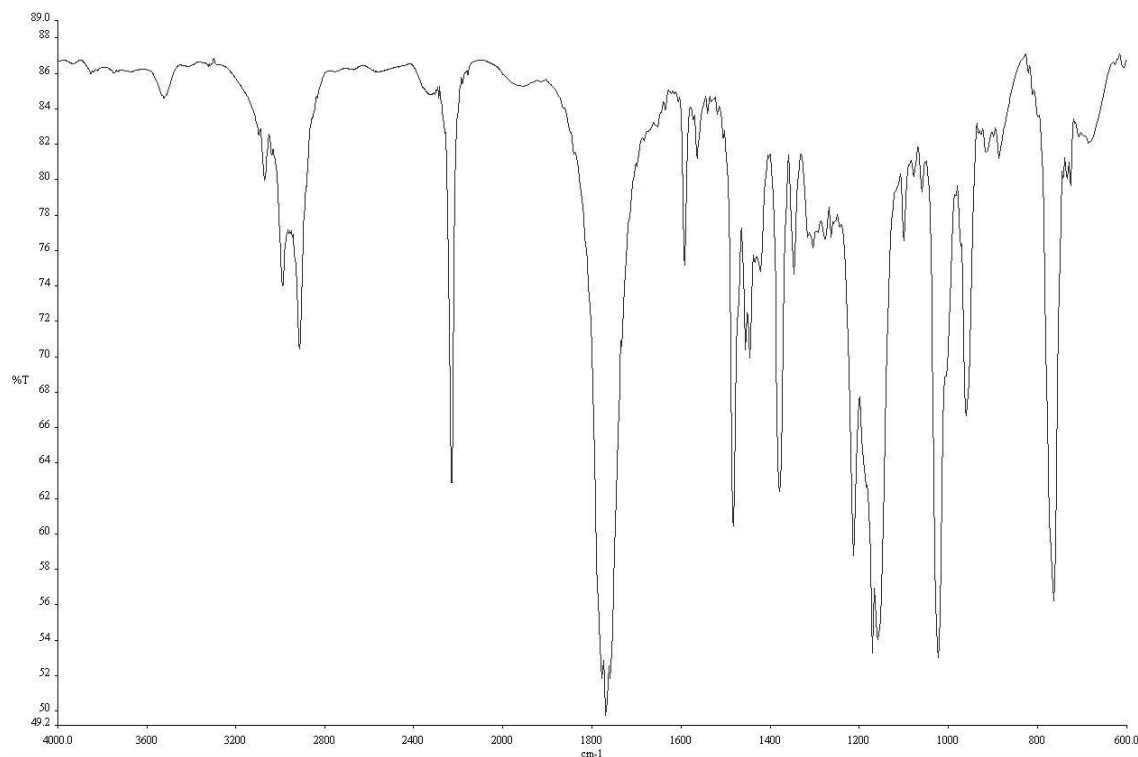
Figure A2.8 IR (NaCl, Thin Film) of compound **185c**.
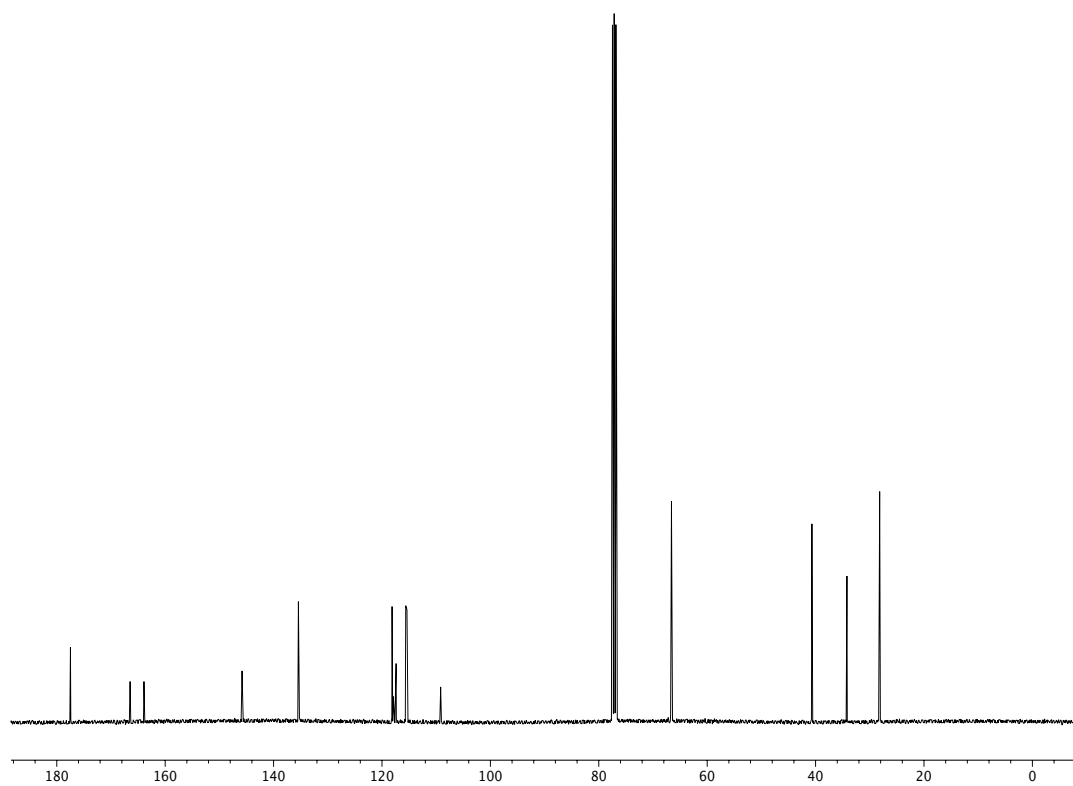
Figure A2.9 ^{13}C NMR (101 MHz, CDCl$_3$) of compound **185c**.
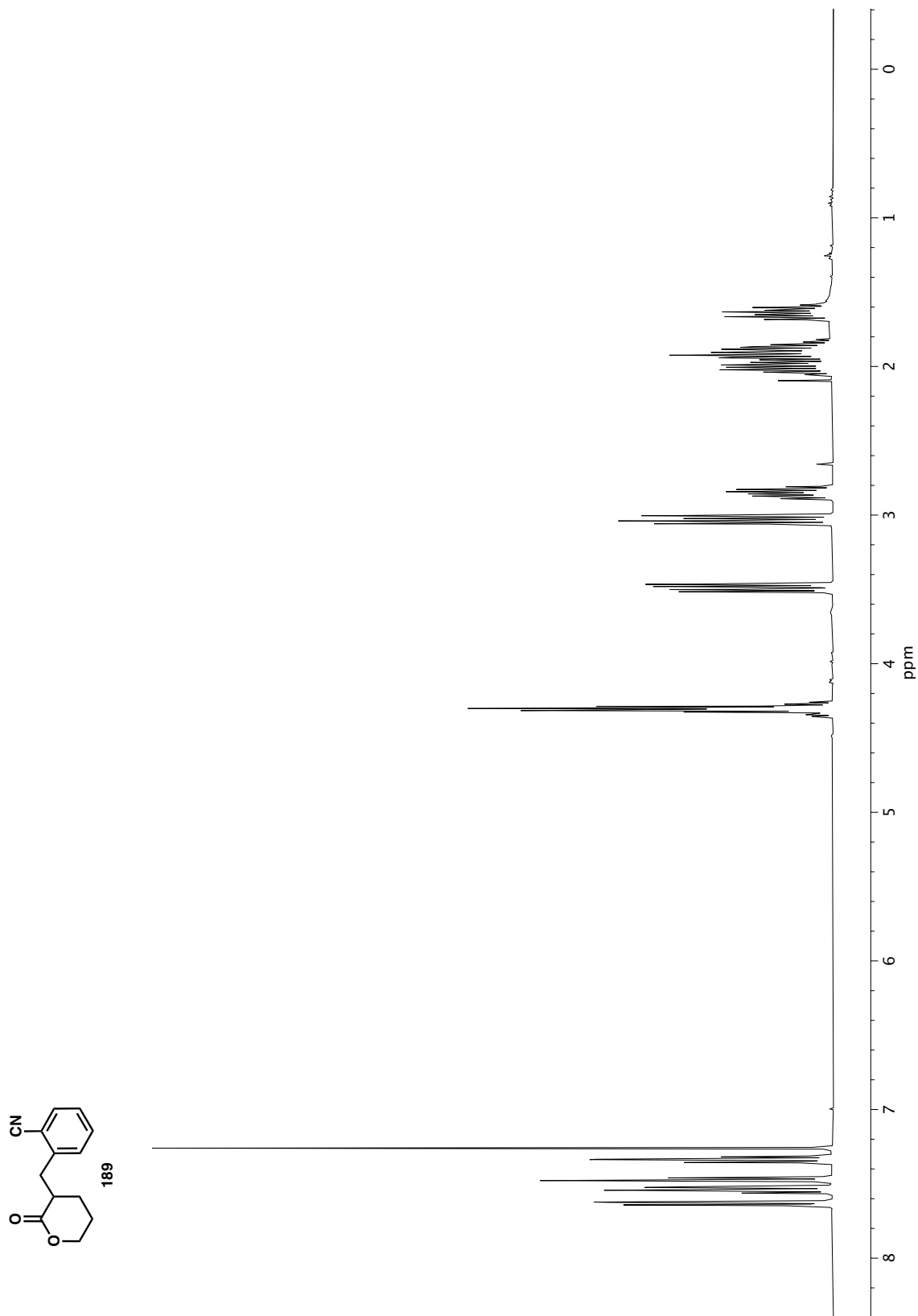
Figure A2.10 ¹H NMR (400 MHz, CDCl₃) of compound **189.**
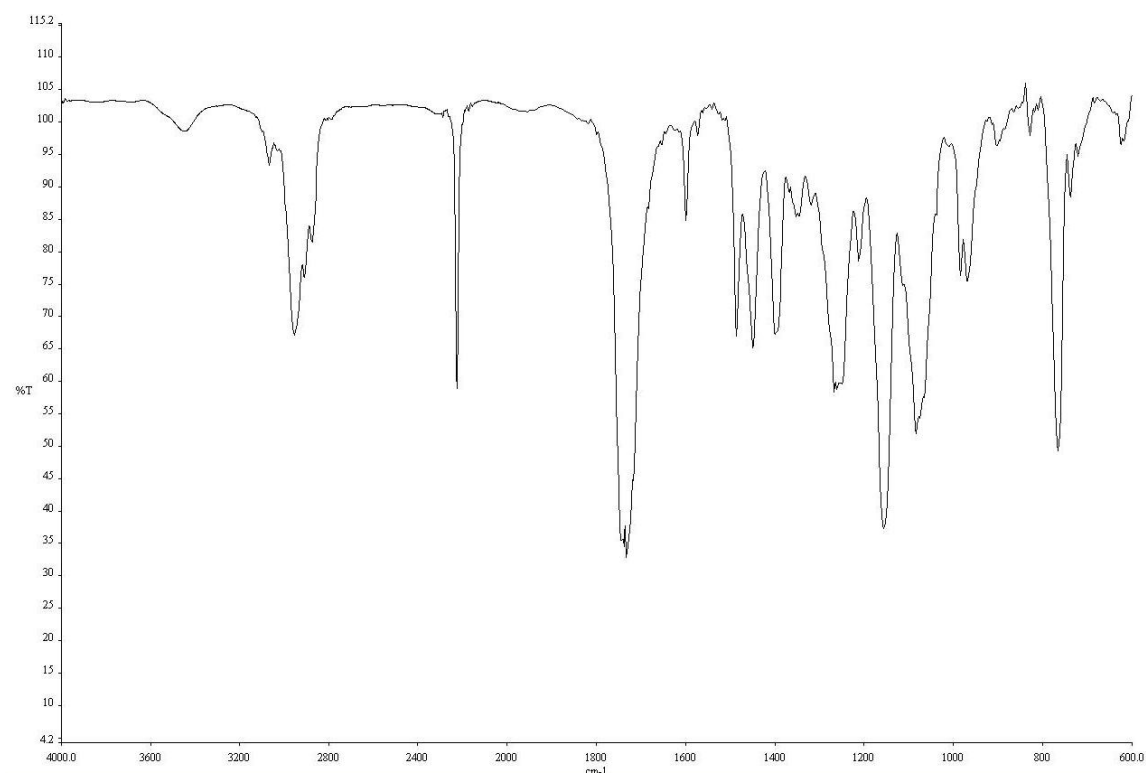
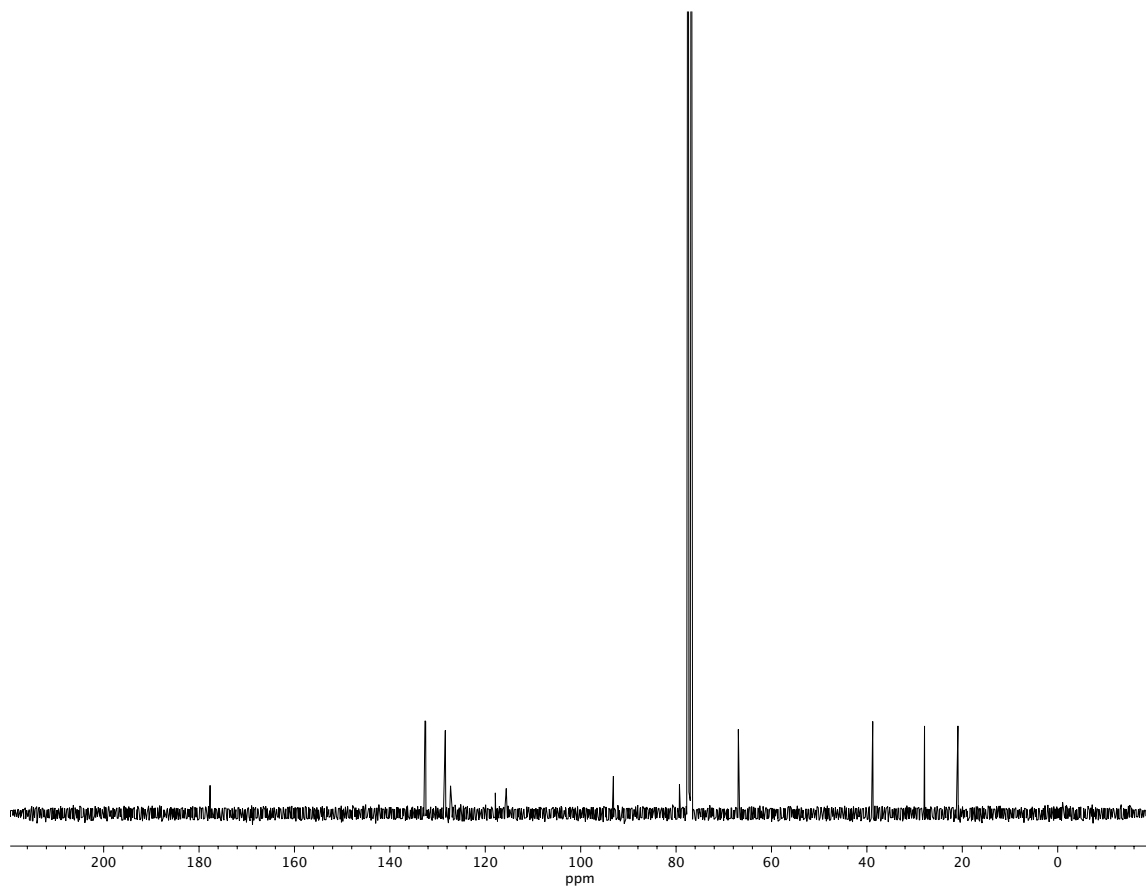***Figure A2.11*** IR (NaCl, Thin Film) of compound **189**.
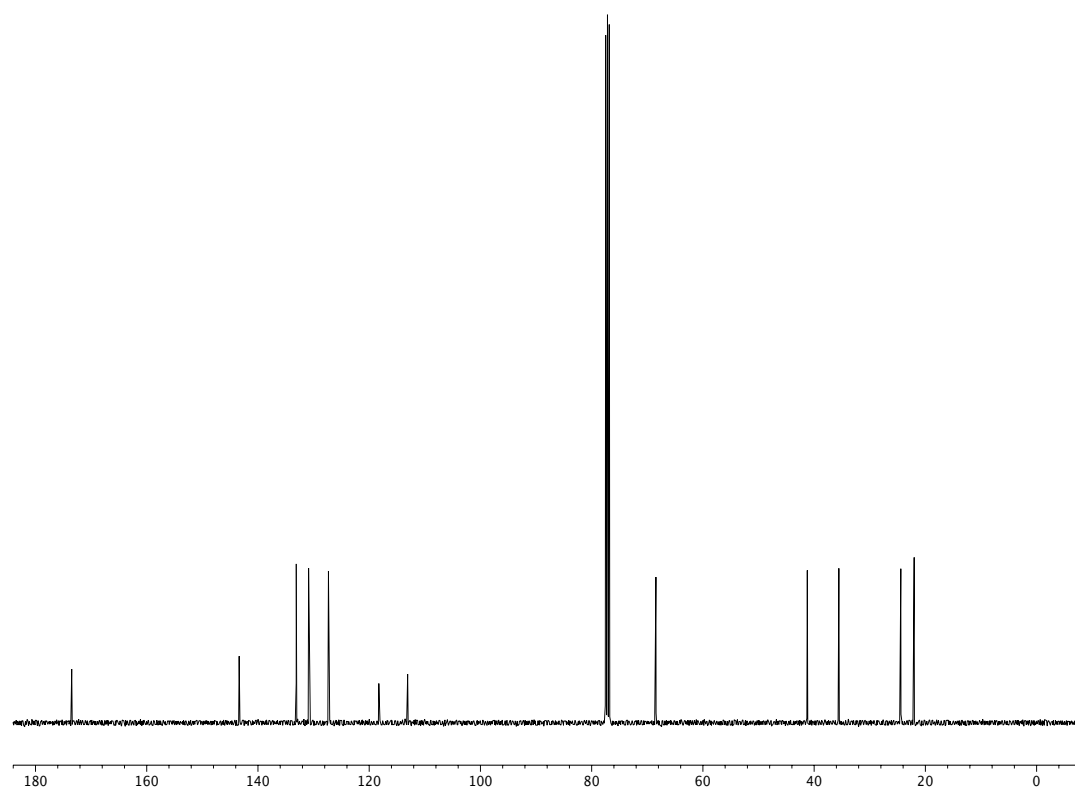
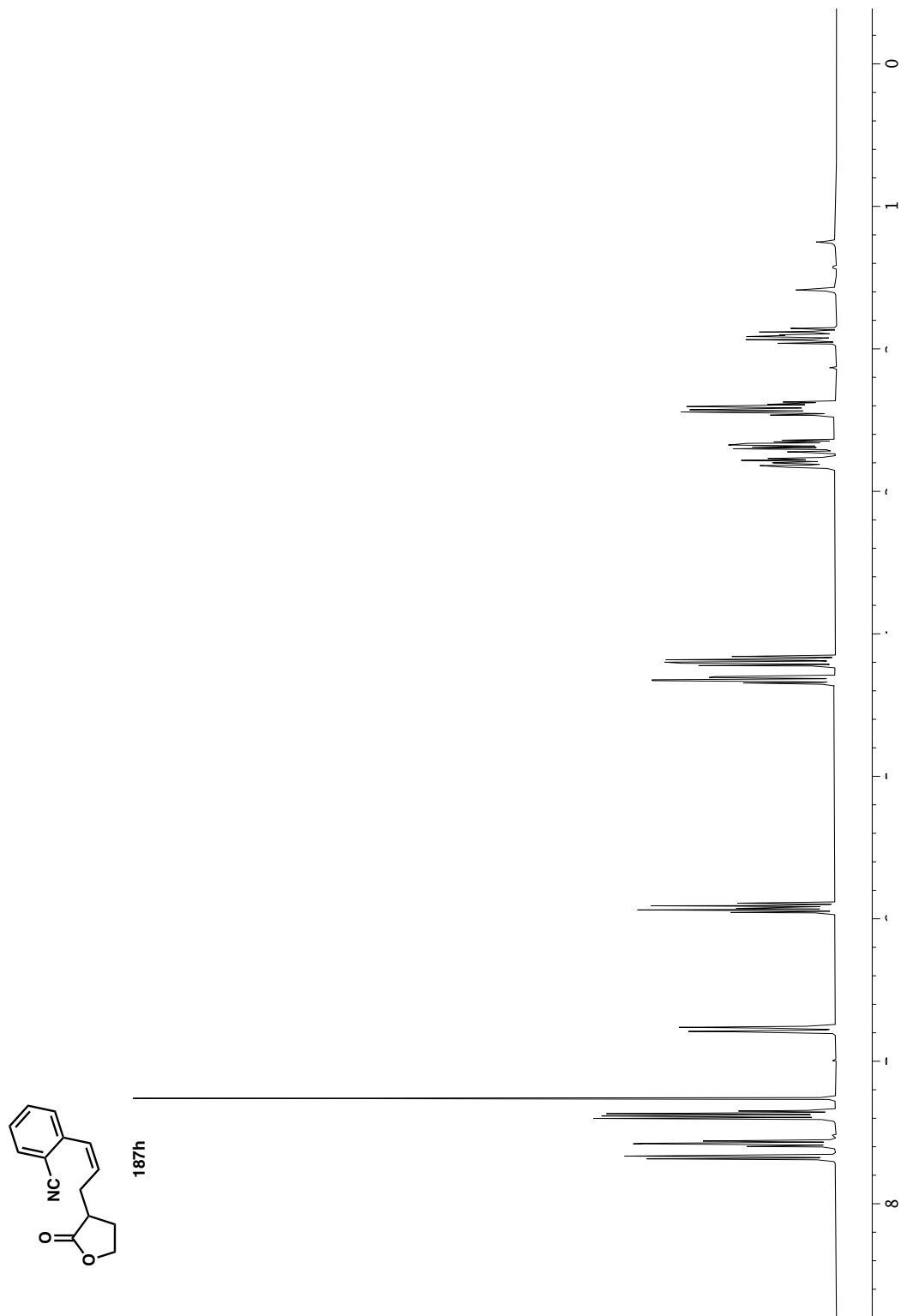***Figure A2.12*** ^{13}C NMR (101 MHz, CDCl$_3$) of compound **189**.

Figure A2.13 ^{1}H NMR (500 MHz, CDCl$_3$) of compound **S17**.
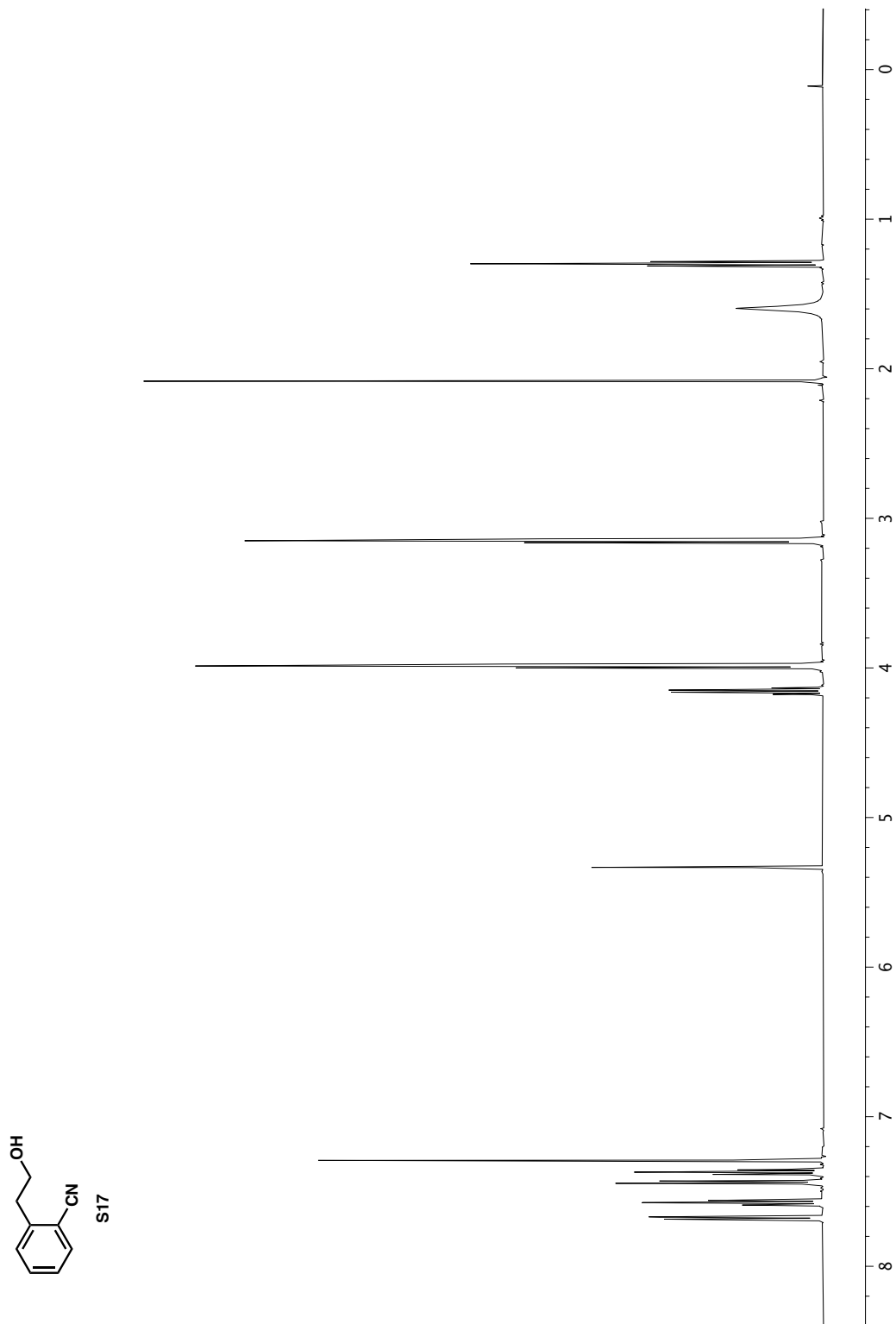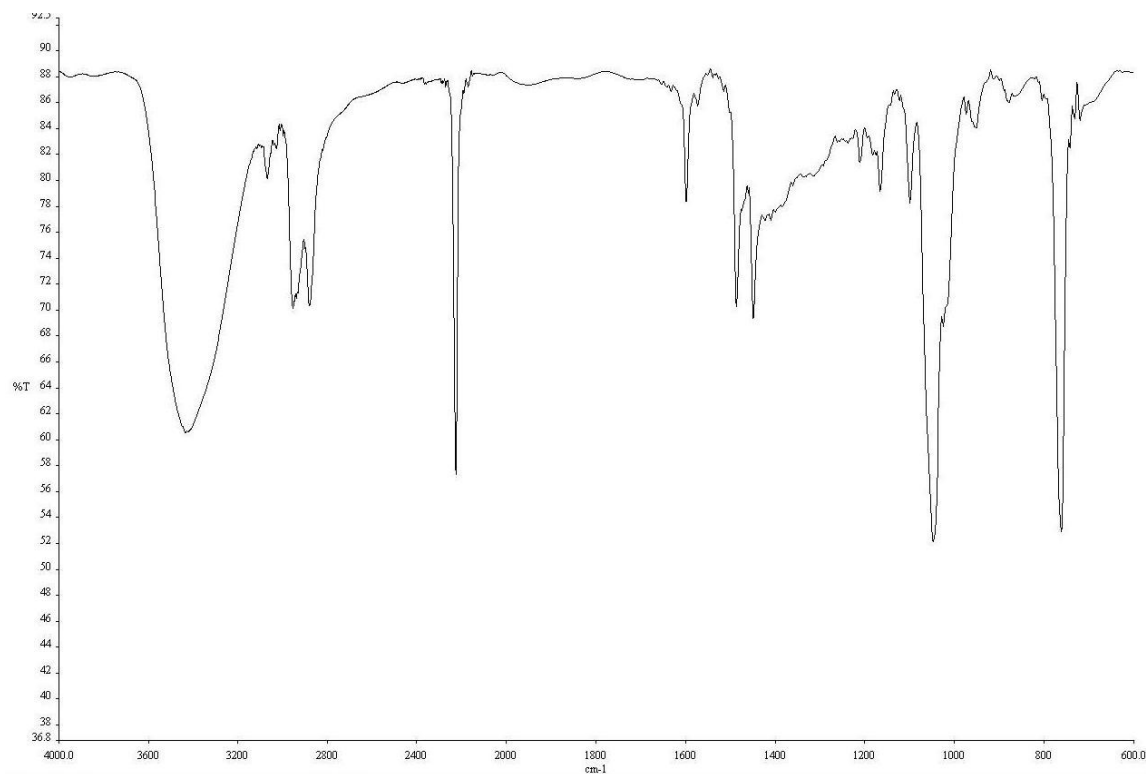
Figure A2.14 IR (NaCl, Thin Film) of compound **S17**.
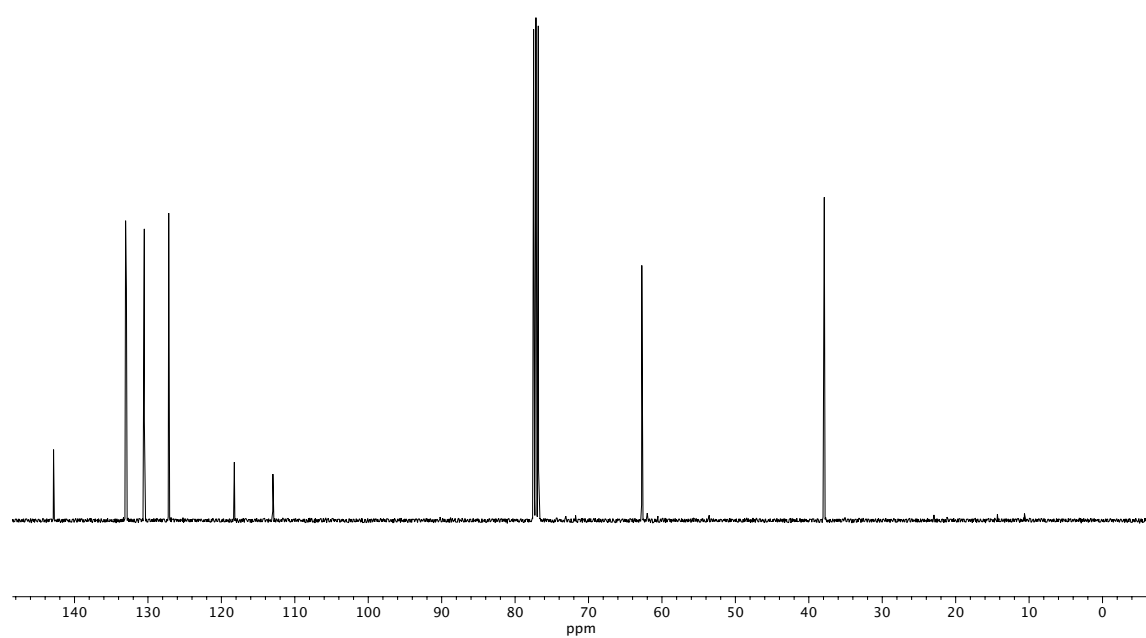
Figure A2.15 ^{13}C NMR (101 MHz, CDCl$_3$) of compound **S17**.
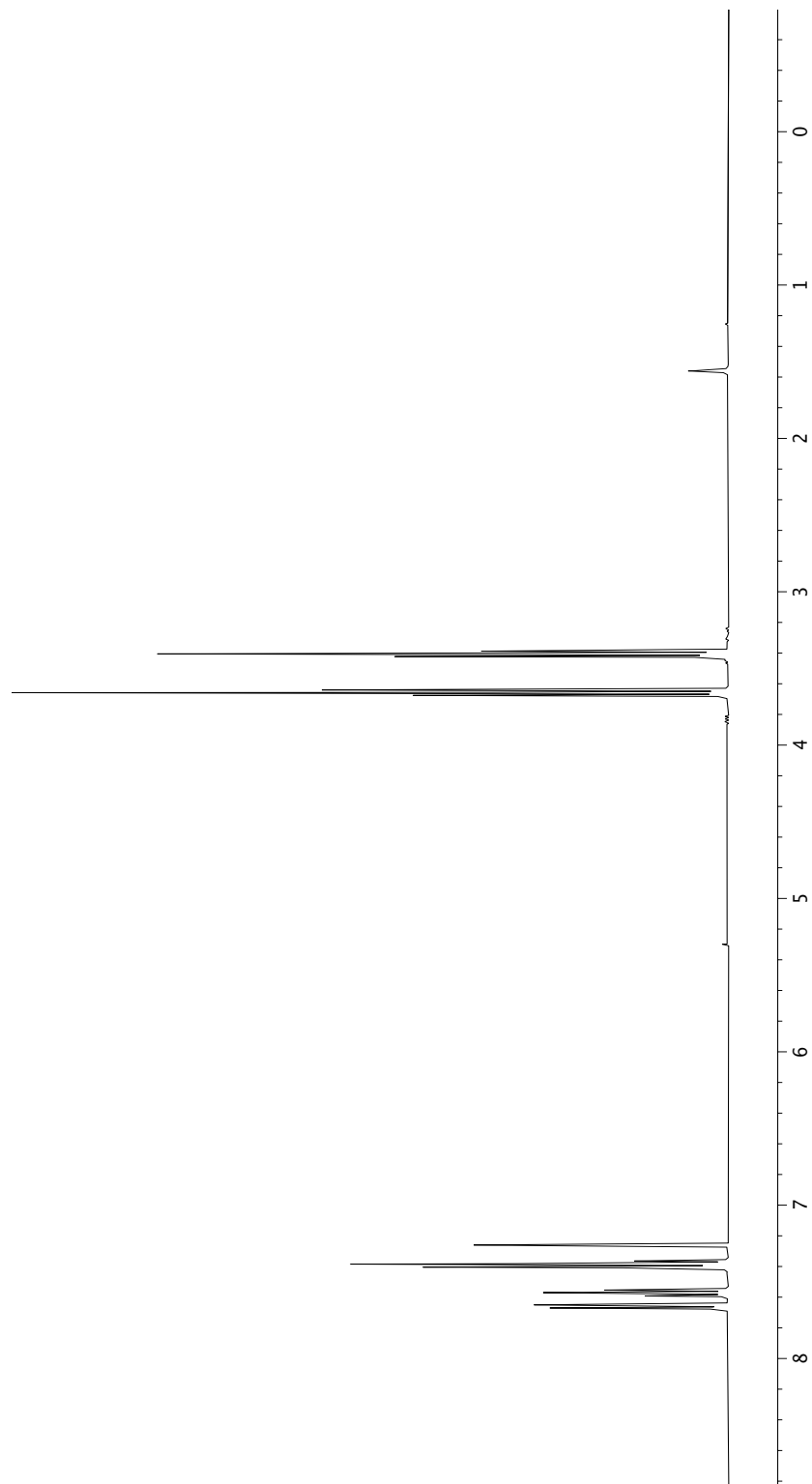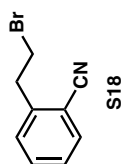
Figure A2.16 ¹H NMR (400 MHz, CDCl₃) of compound **S18.**
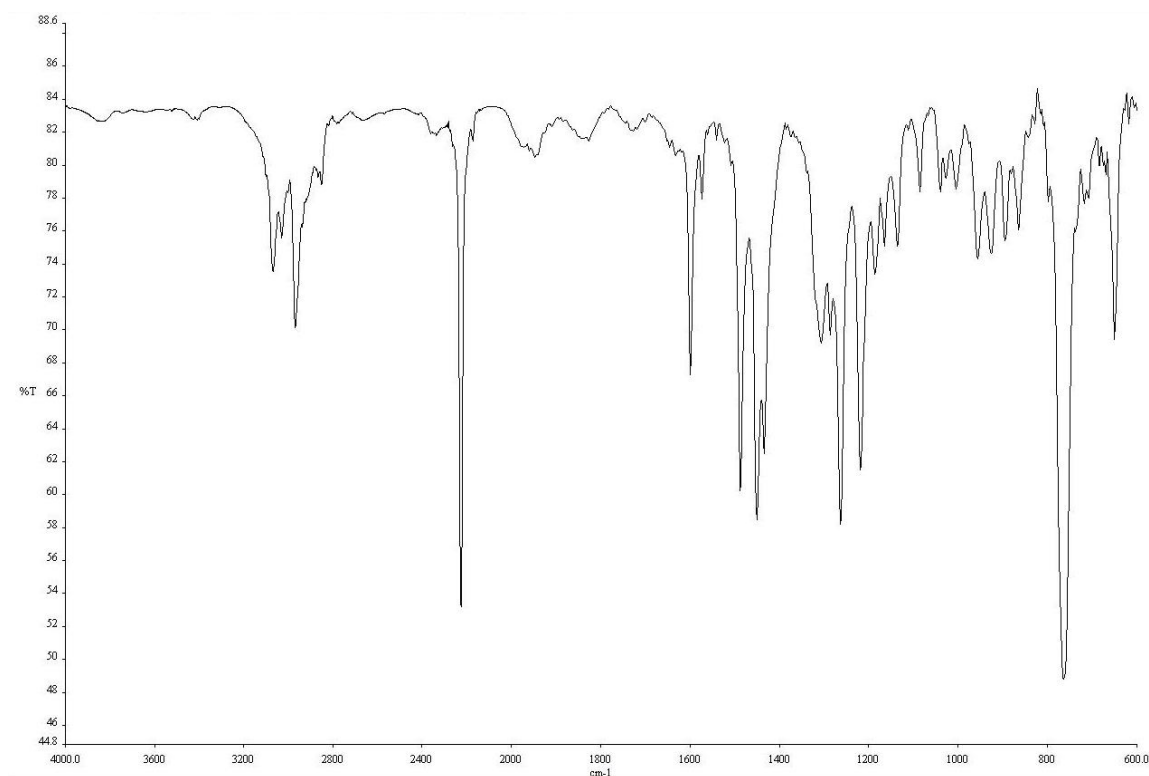
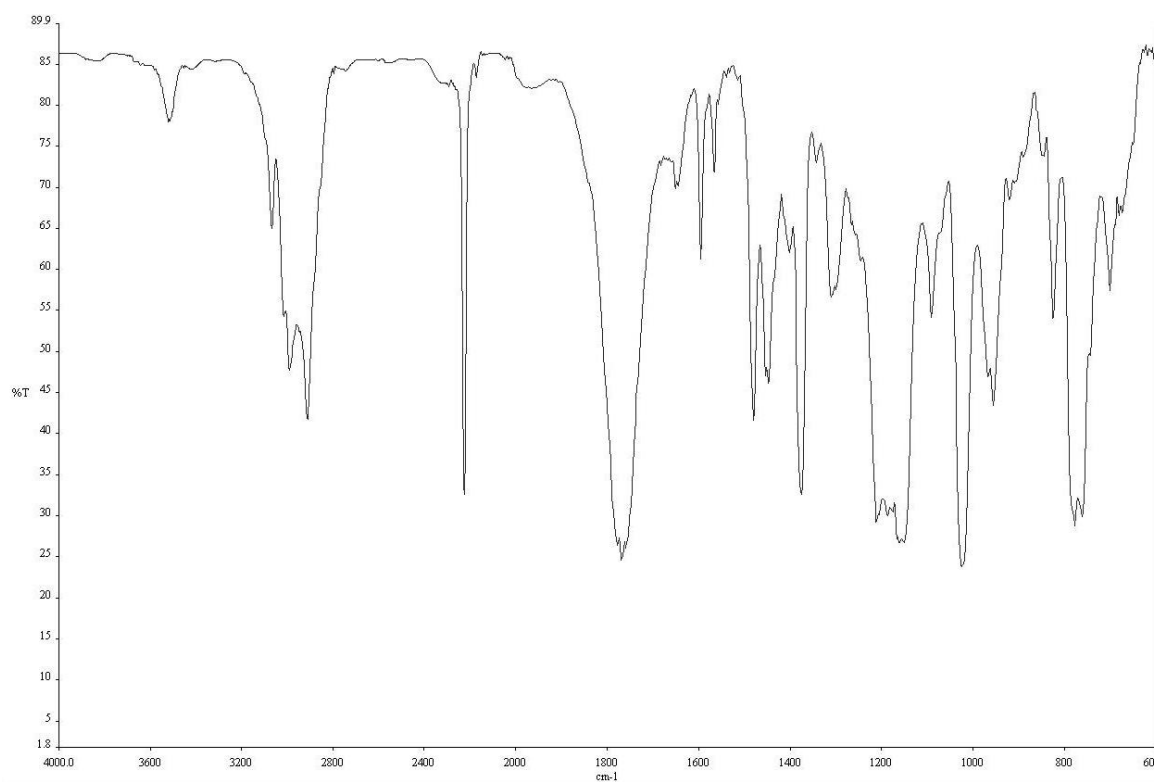***Figure A2.17*** IR (NaCl, Thin Film) of compound **S18**.
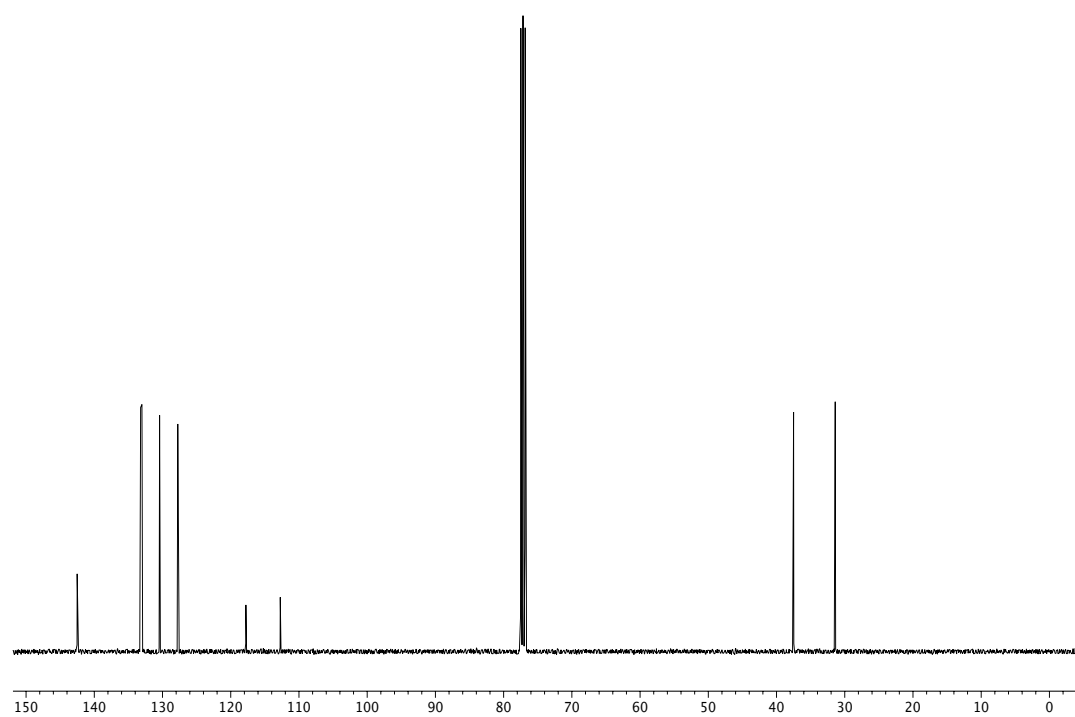
Figure A2.18 ¹³C NMR (101 MHz, CDCl₃) of compound **S18**.

Figure A2.19 ^{1}H NMR (400 MHz, CDCl$_3$) of compound **S20.**
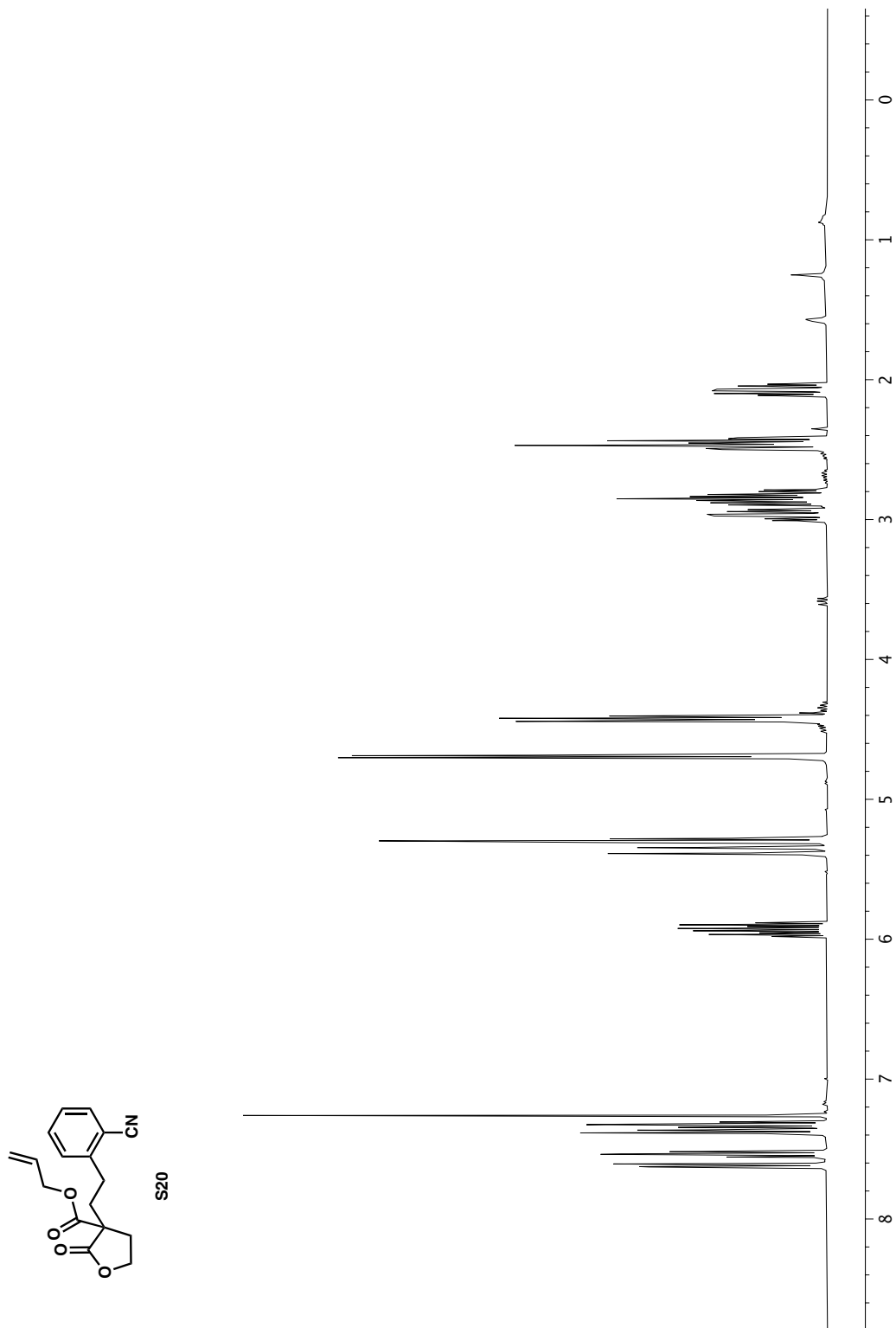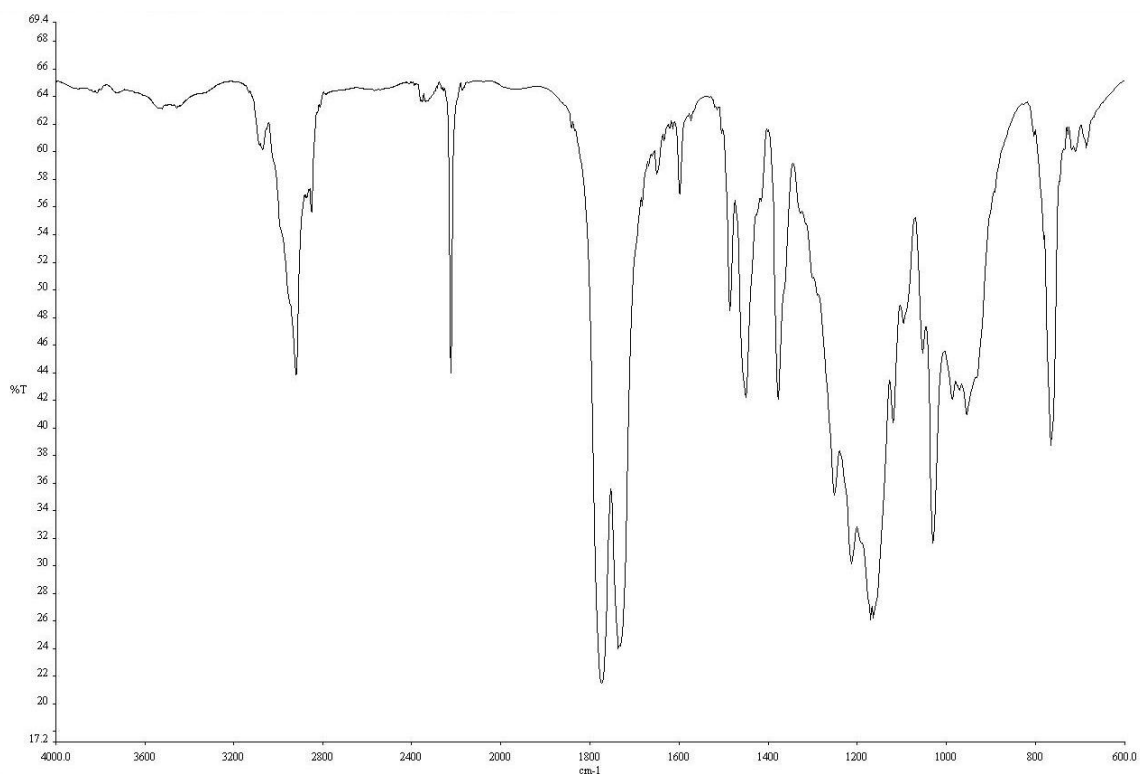
Figure A2.20 IR (NaCl, Thin Film) of compound **S20**.
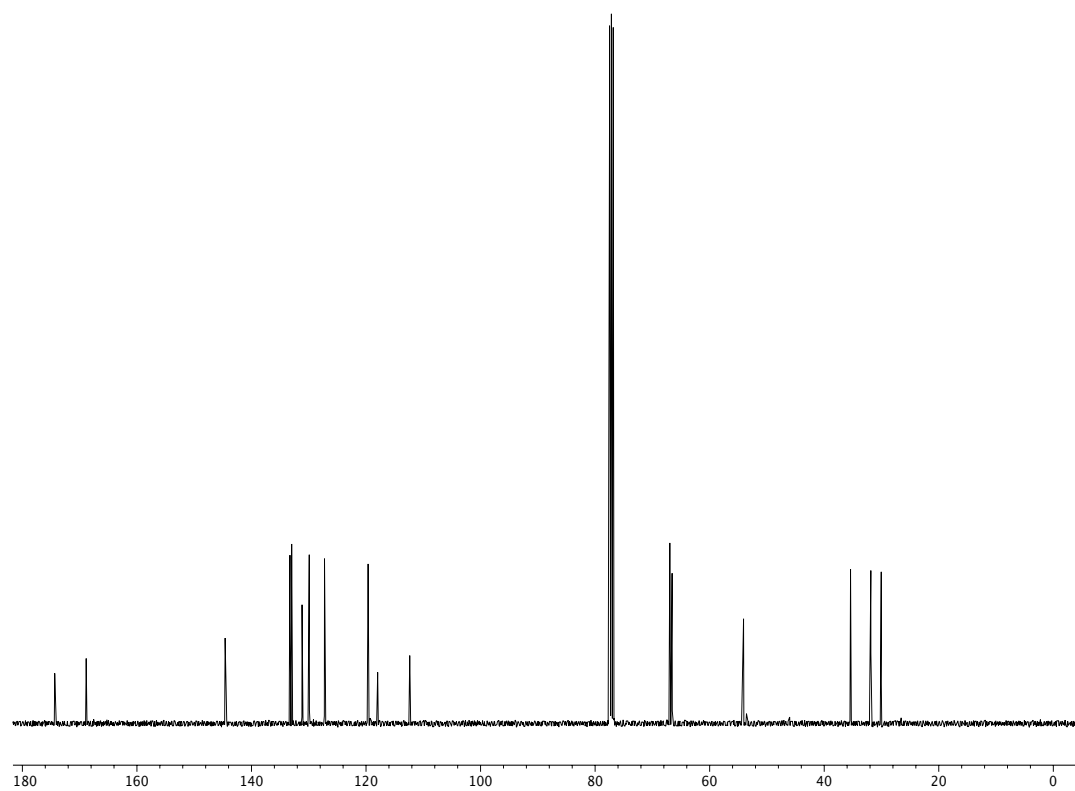
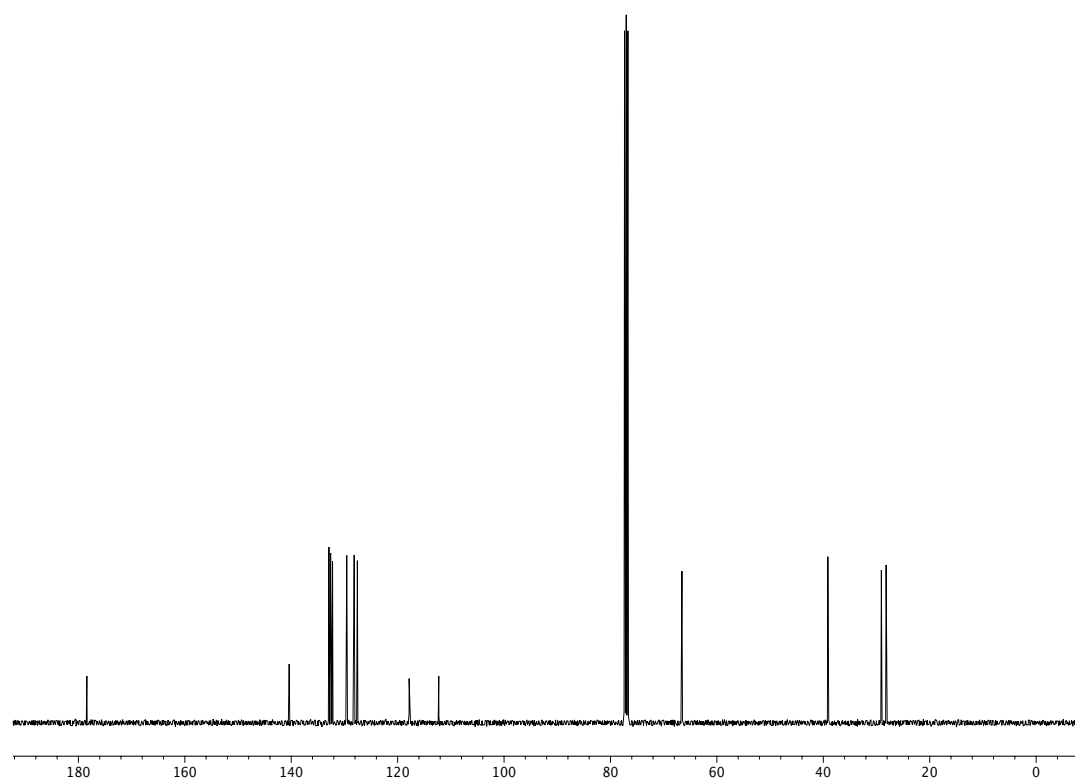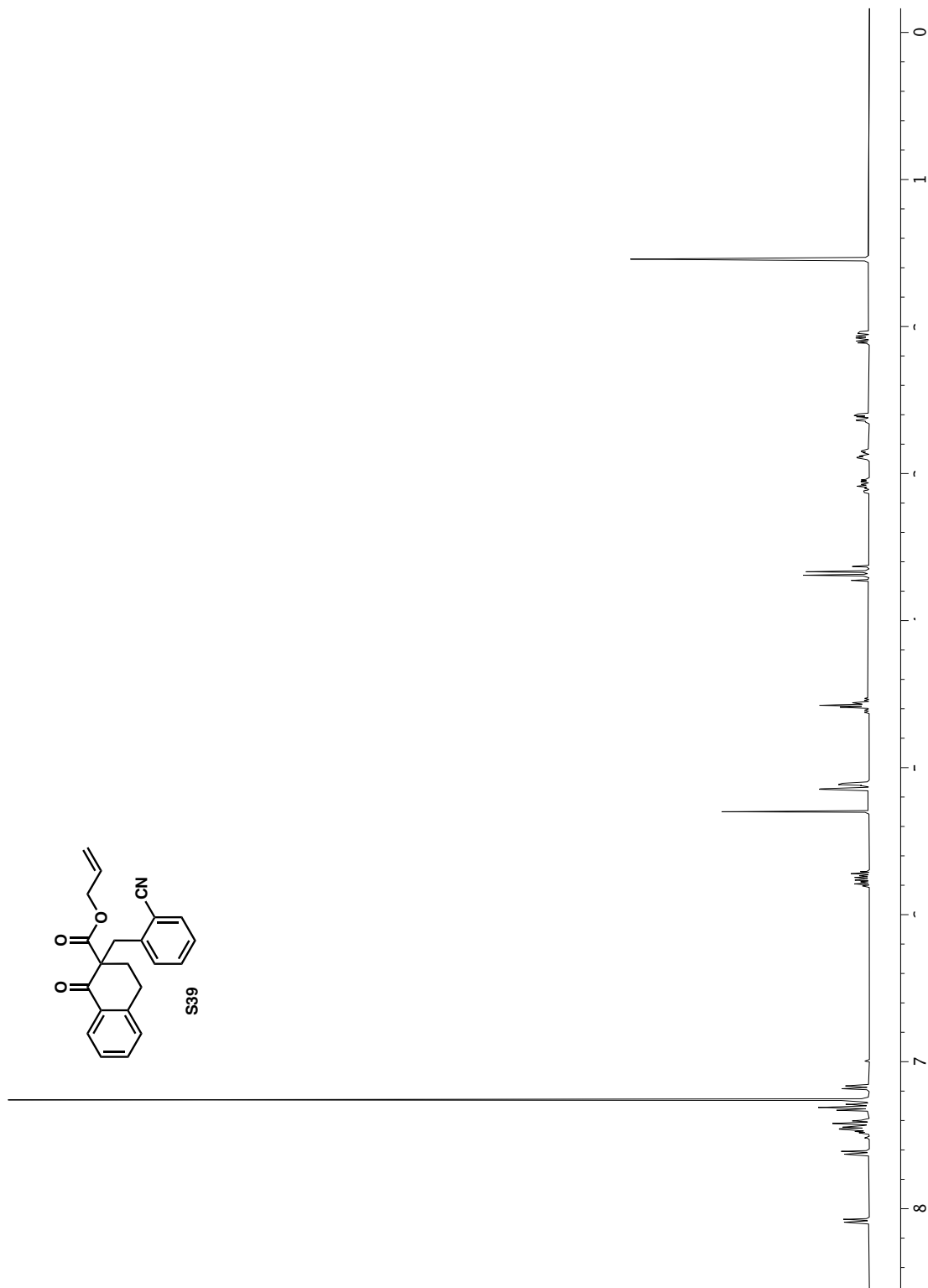***Figure A2.21*** ^{13}C NMR (101 MHz, CDCl$_3$) of compound **S20**.
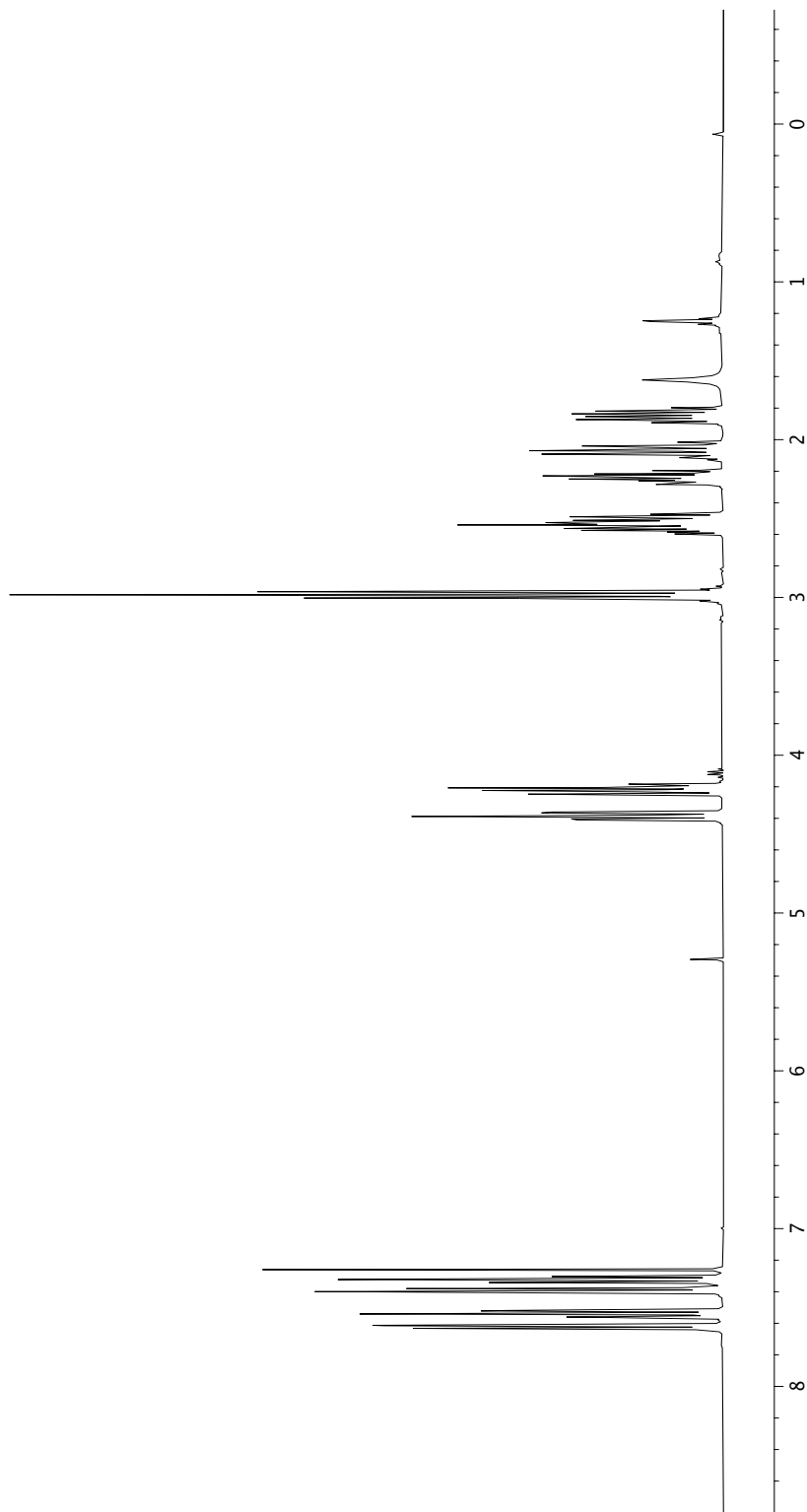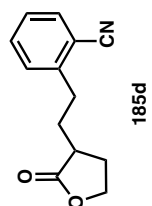
Figure A2.22 ¹H NMR (400 MHz, CDCl₃) of compound **185d.**
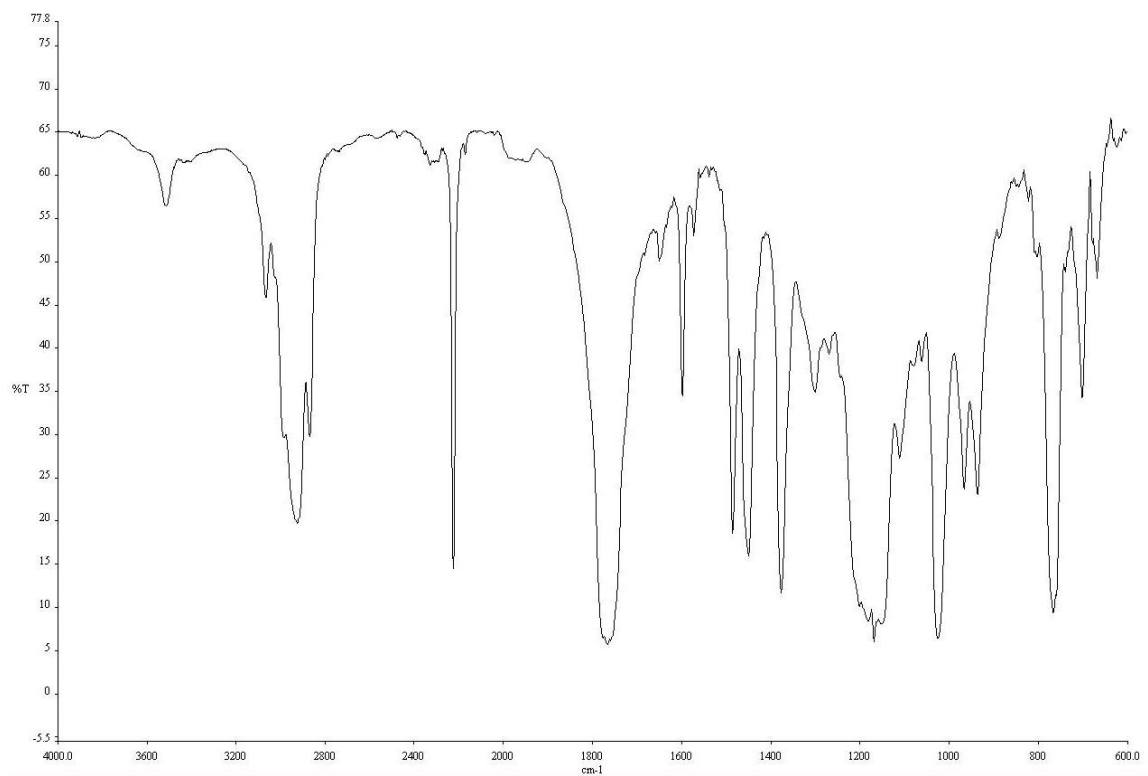
Figure A2.23 IR (NaCl, Thin Film) of compound **185d**.
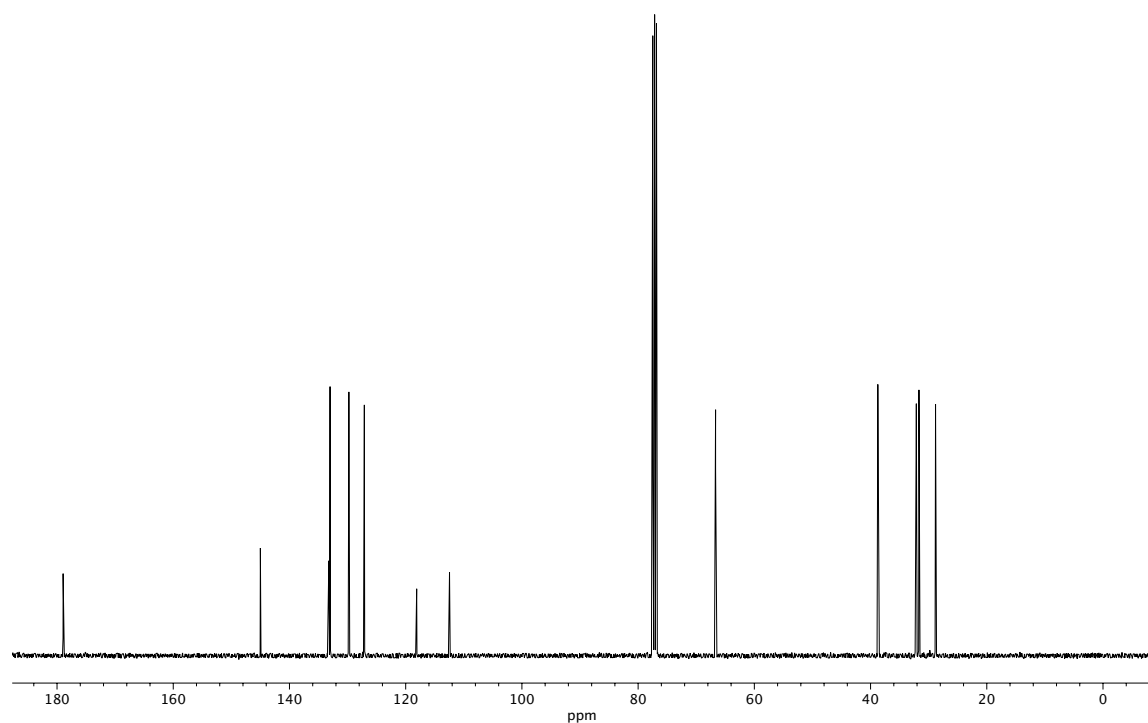
Figure A2.24 ^{13}C NMR (101 MHz, CDCl$_3$) of compound **185d**.
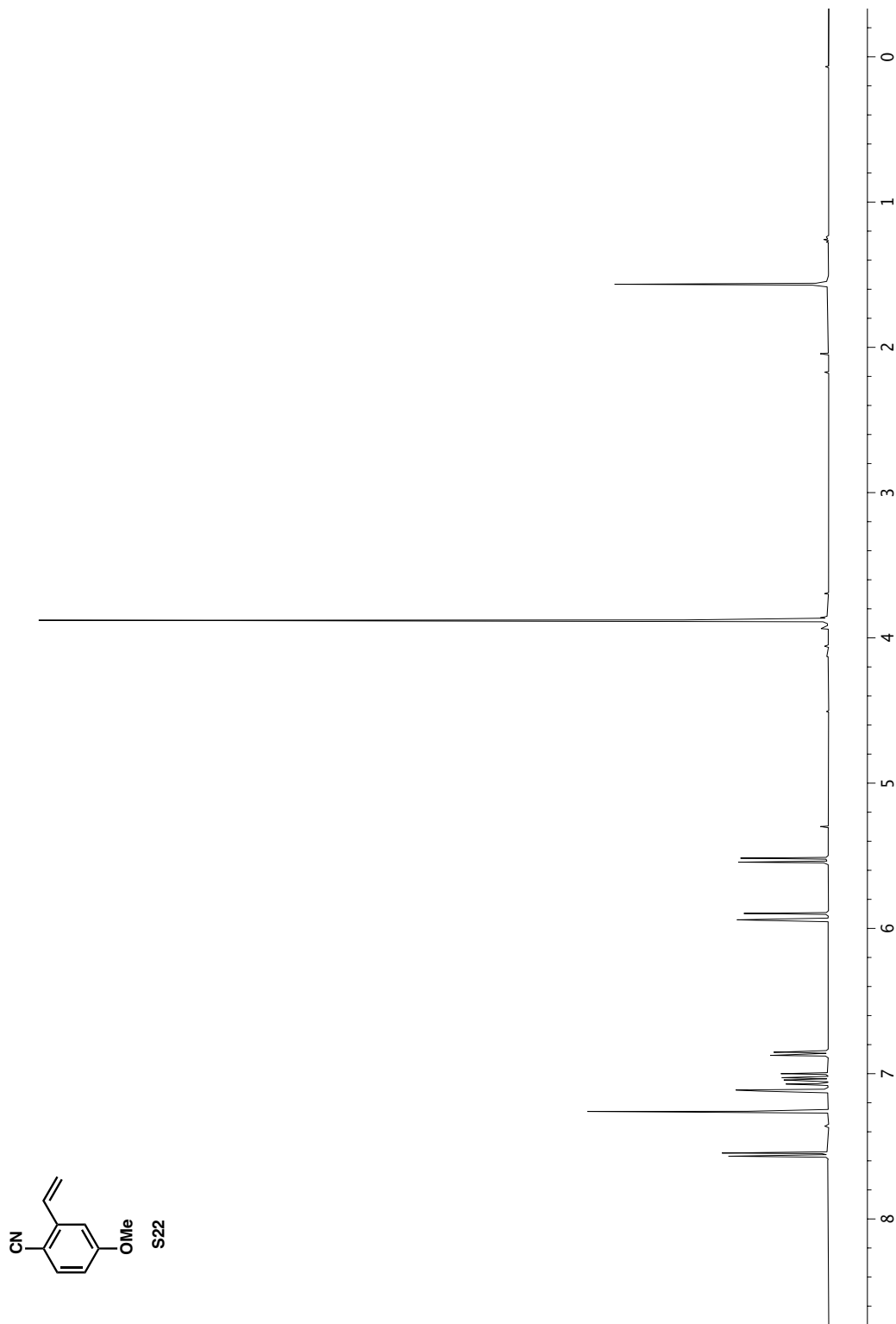
Figure A2.25 ^{1}H NMR (400 MHz, CDCl$_3$) of compound **S22.**
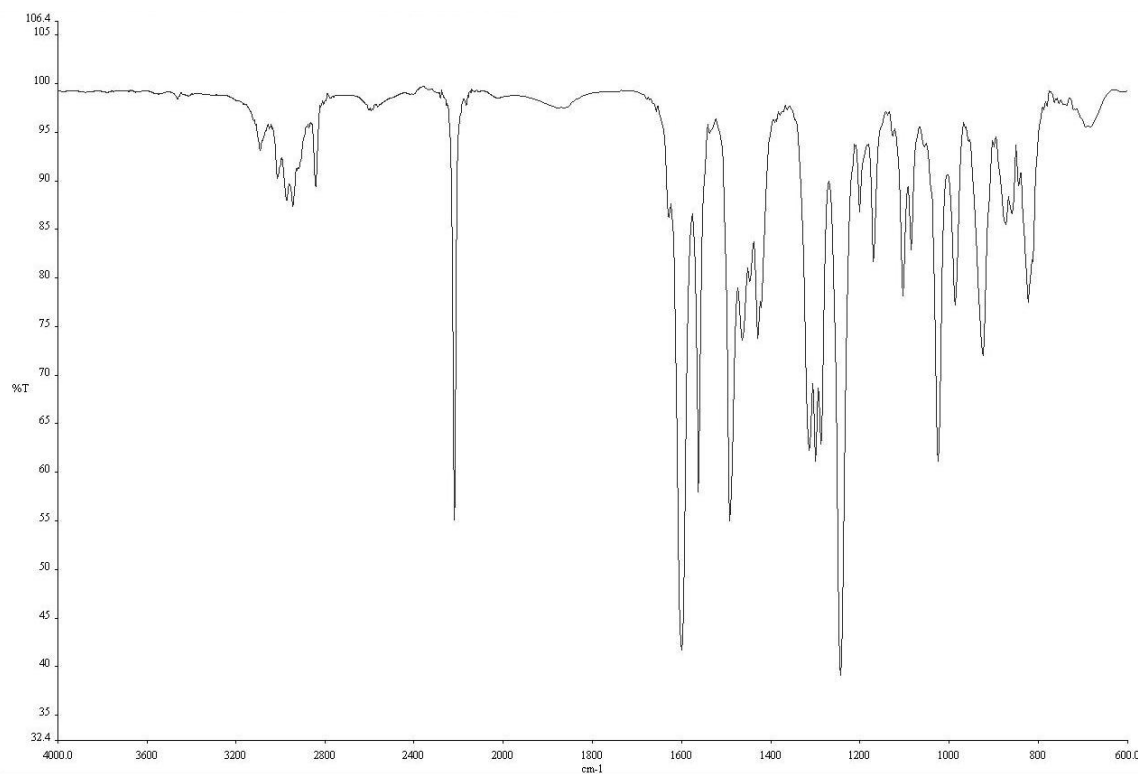
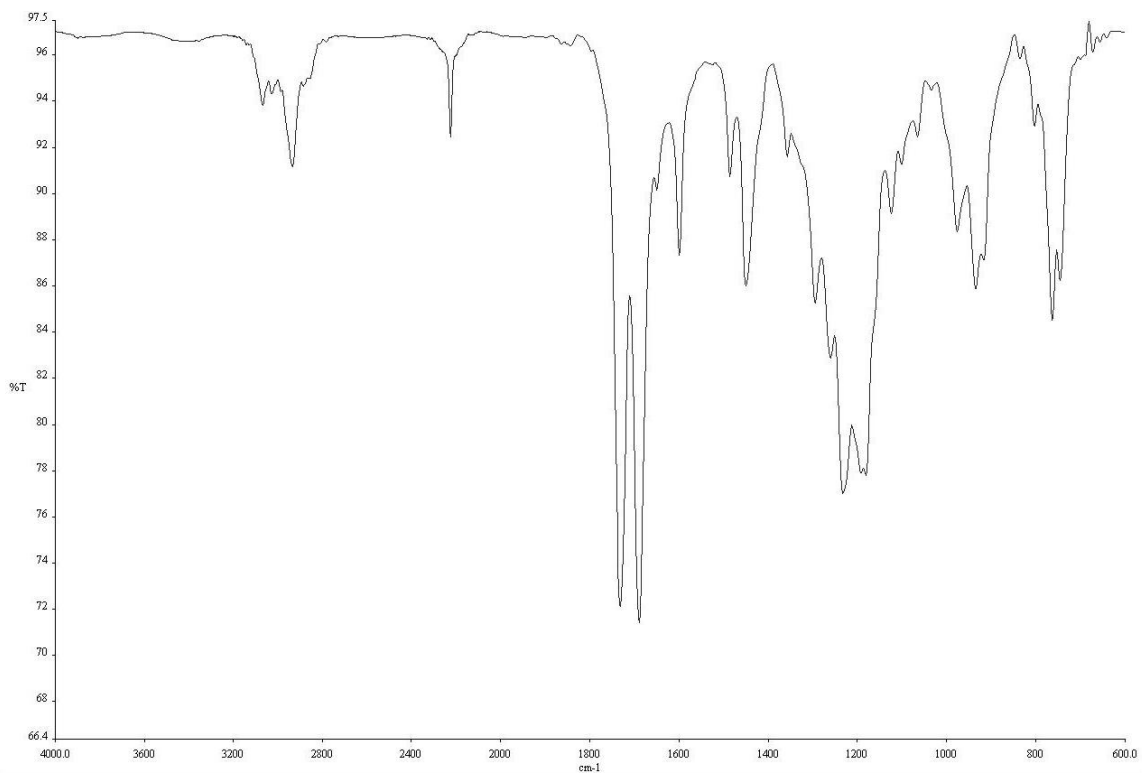***Figure A2.26*** IR (NaCl, Thin Film) of compound **S22**.
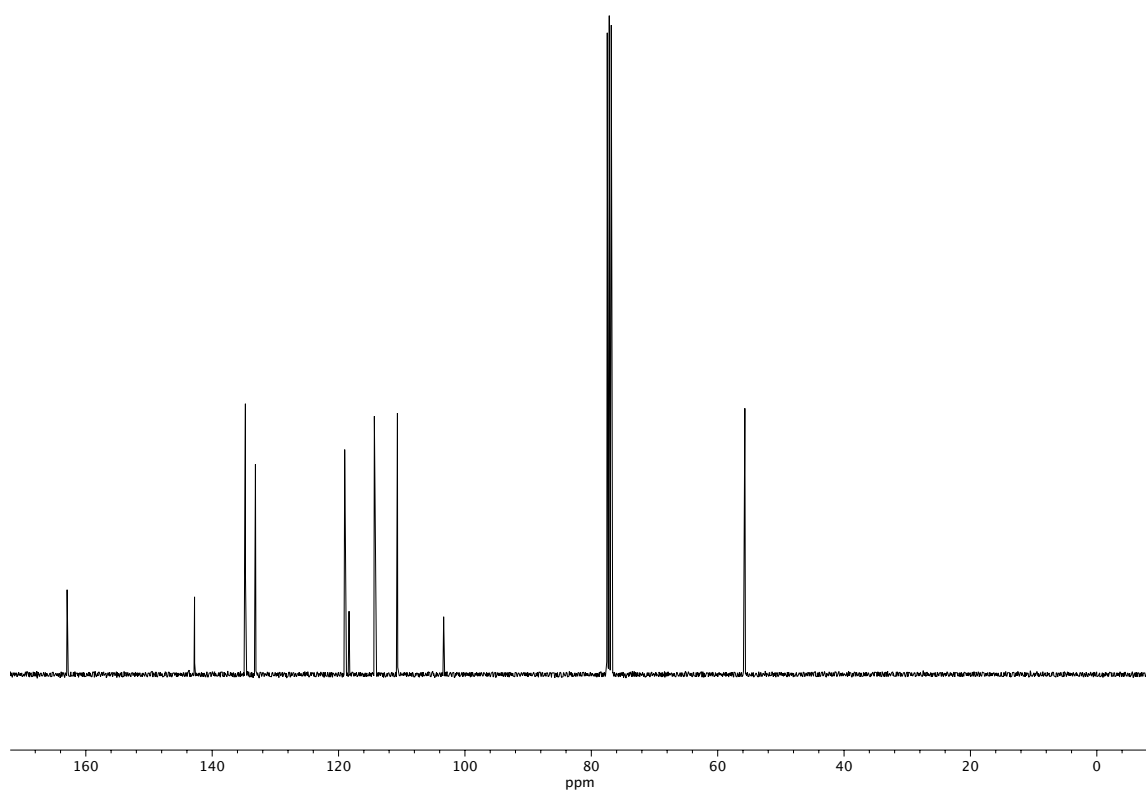
Figure A2.27 ¹³C NMR (101 MHz, CDCl₃) of compound **S22**.
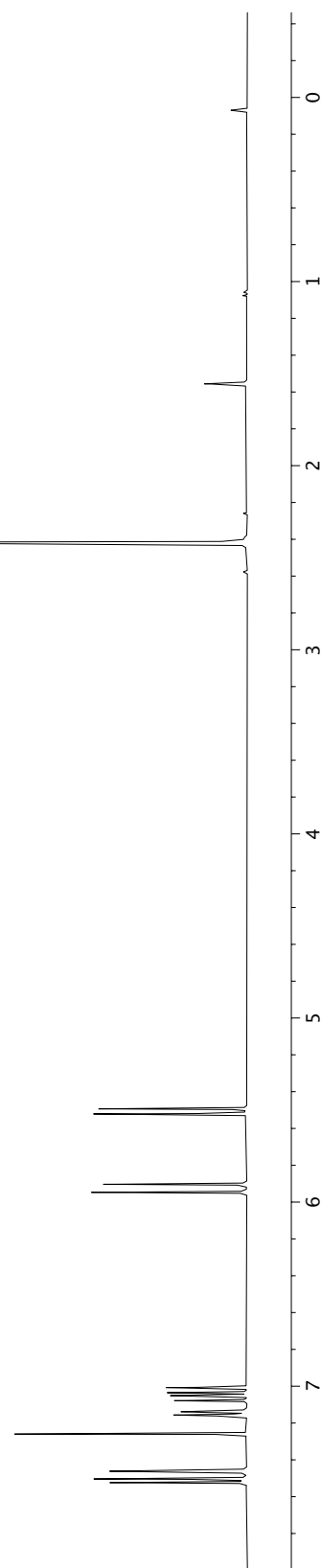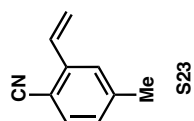
Figure A2.28 ^{1}H NMR (400 MHz, CDCl$_3$) of compound **S23.**
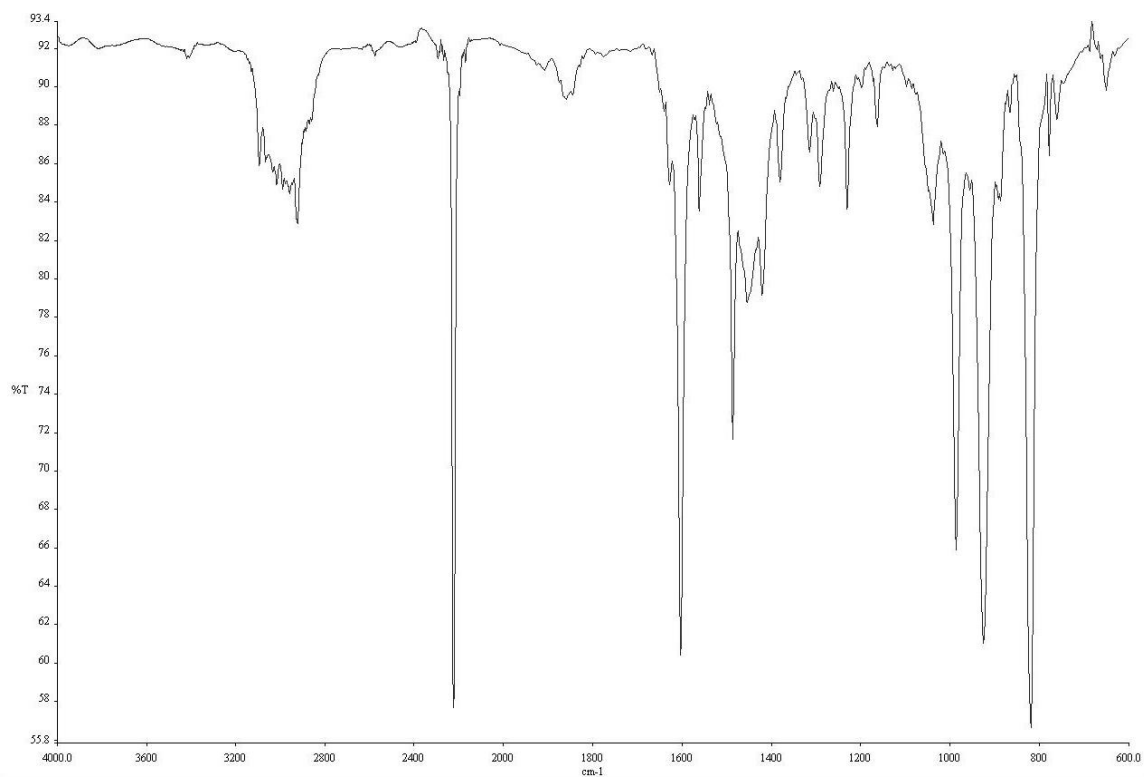
Figure A2.29 IR (NaCl, Thin Film) of compound **S23**.
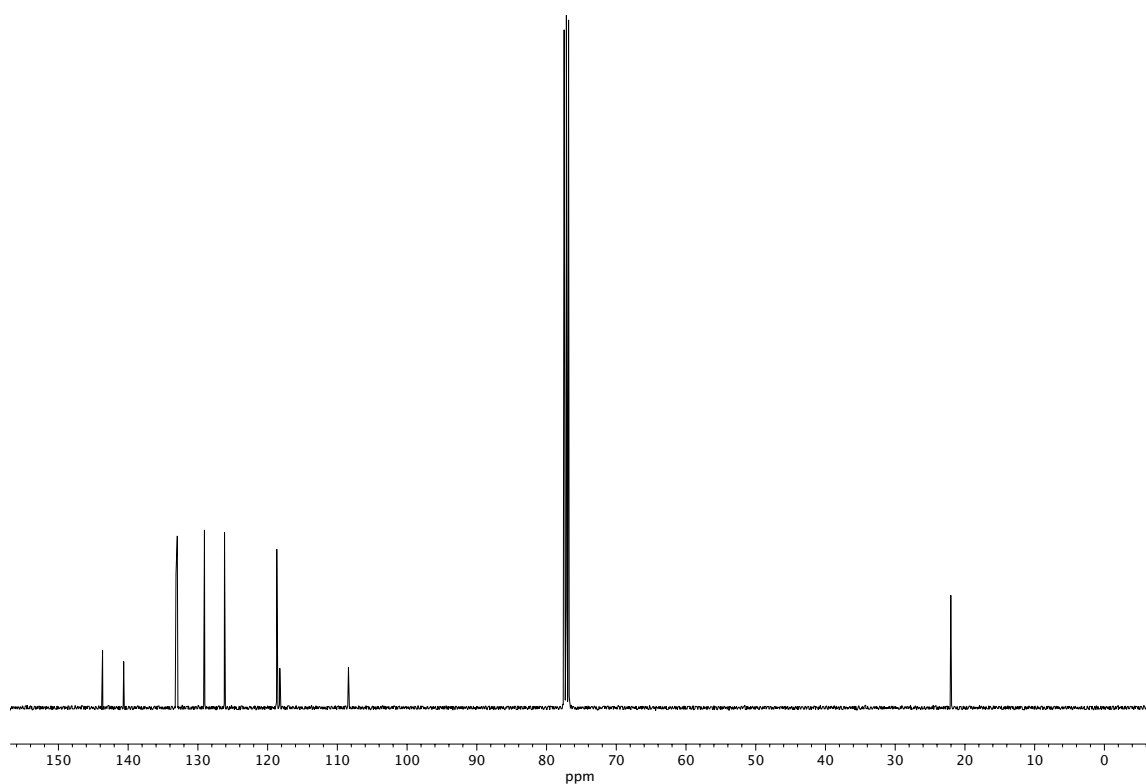
Figure A2.30 ^{13}C NMR (101 MHz, CDCl$_3$) of compound **S23**.
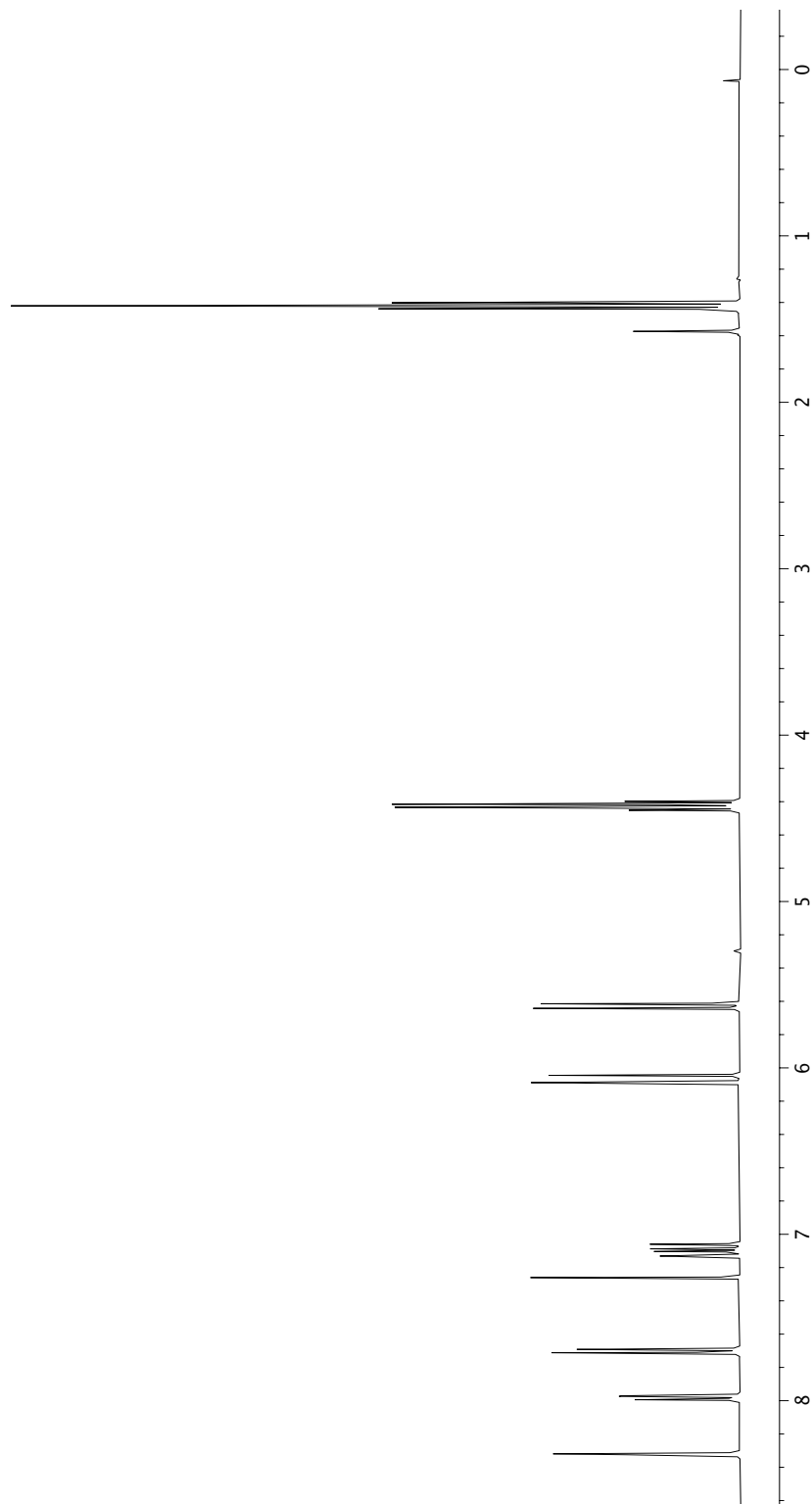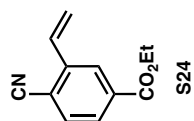
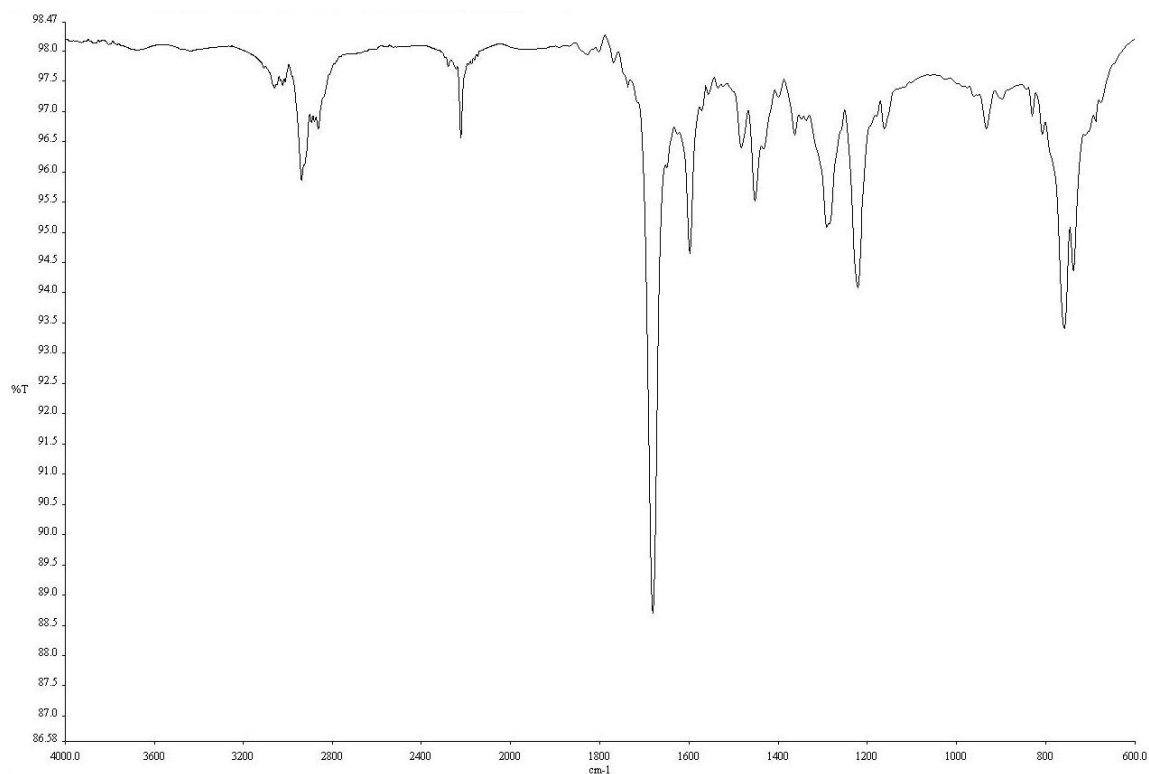***Figure A2.31*** ^{1}H NMR (400 MHz, CDCl$_3$) of compound **S24.**
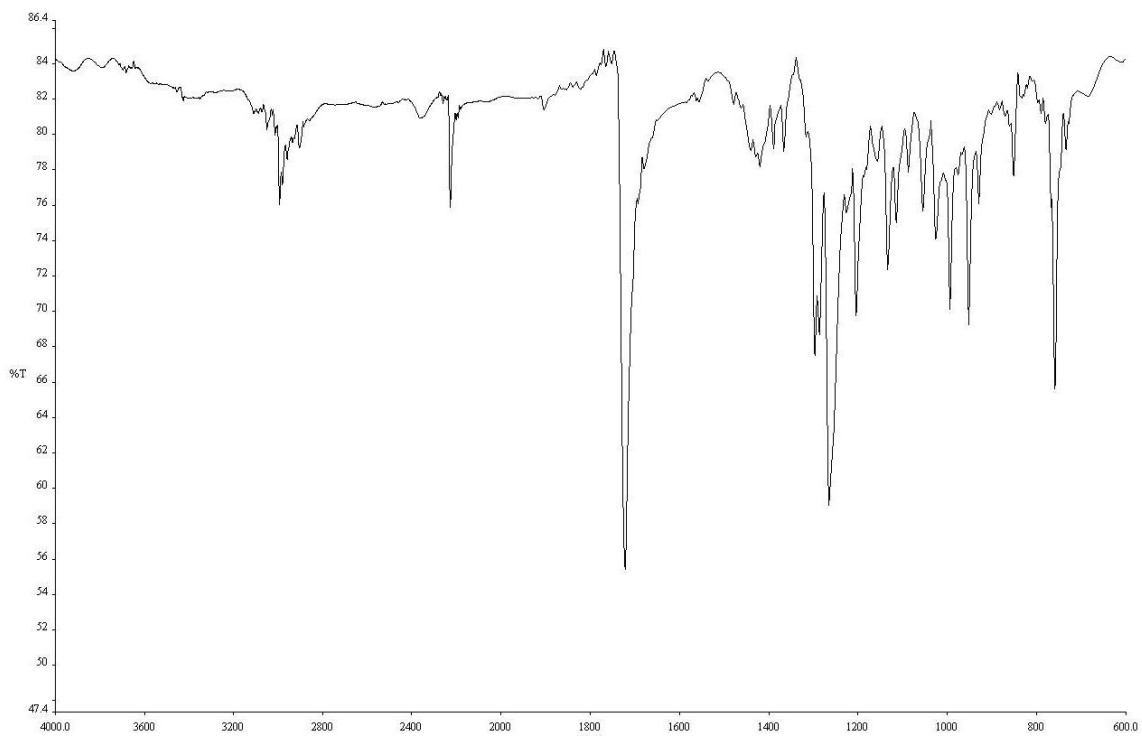
Figure A2.32 IR (NaCl, Thin Film) of compound **S24**.
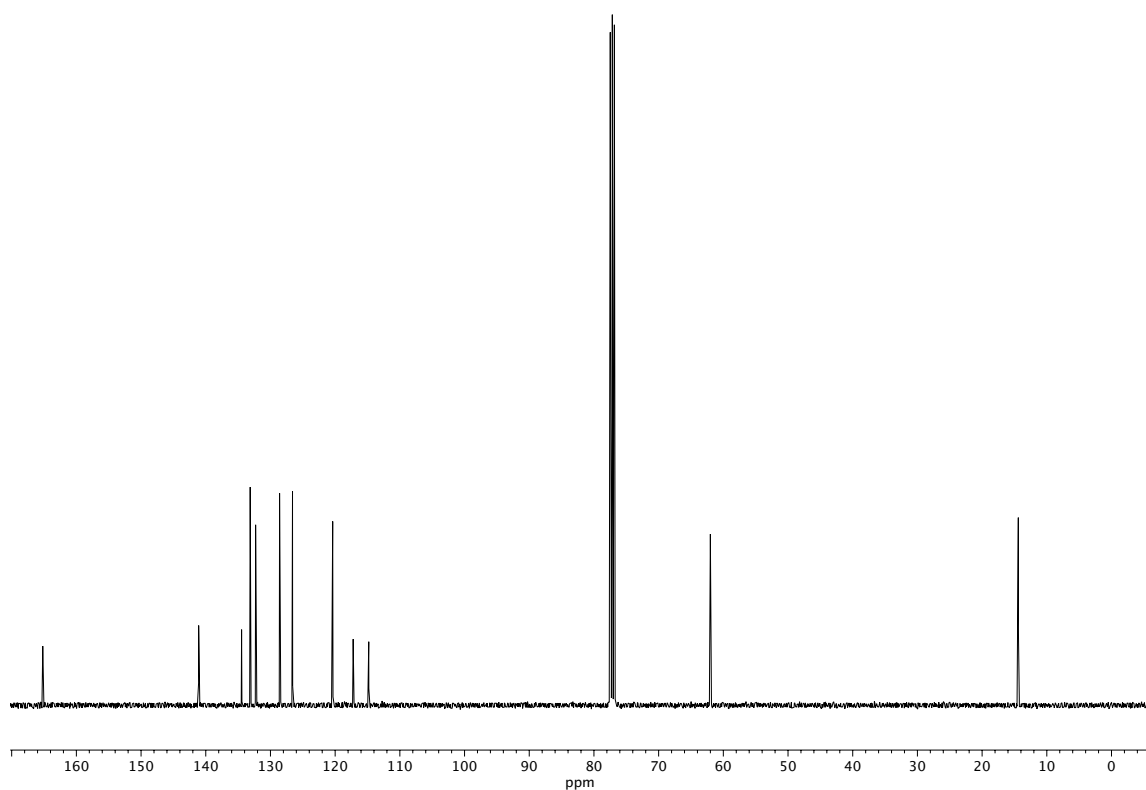
Figure A2.33 ¹³C NMR (101 MHz, CDCl₃) of compound **S24**.
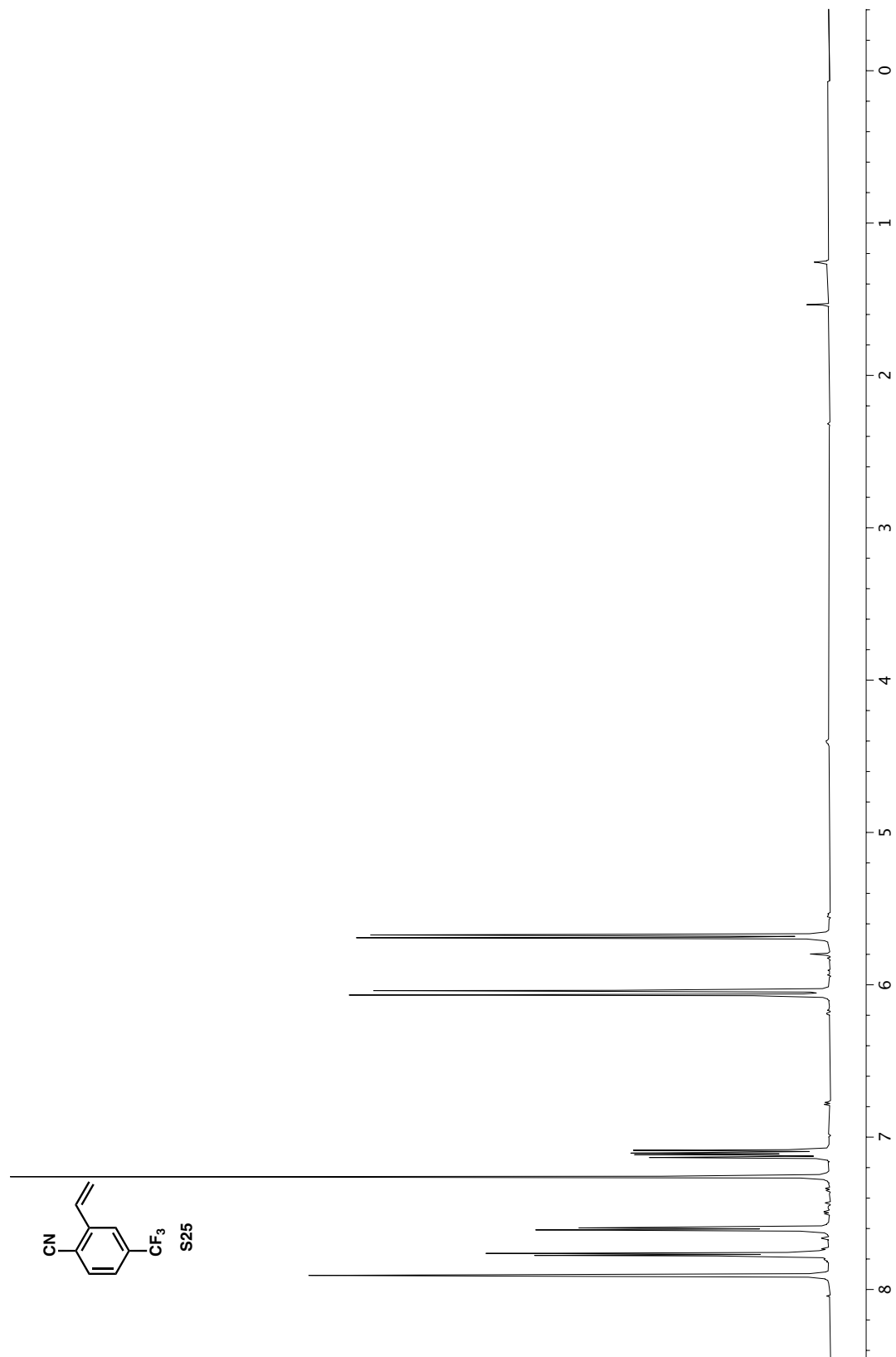
Figure A2.34 ¹H NMR (400 MHz, CDCl₃) of compound **S25.**
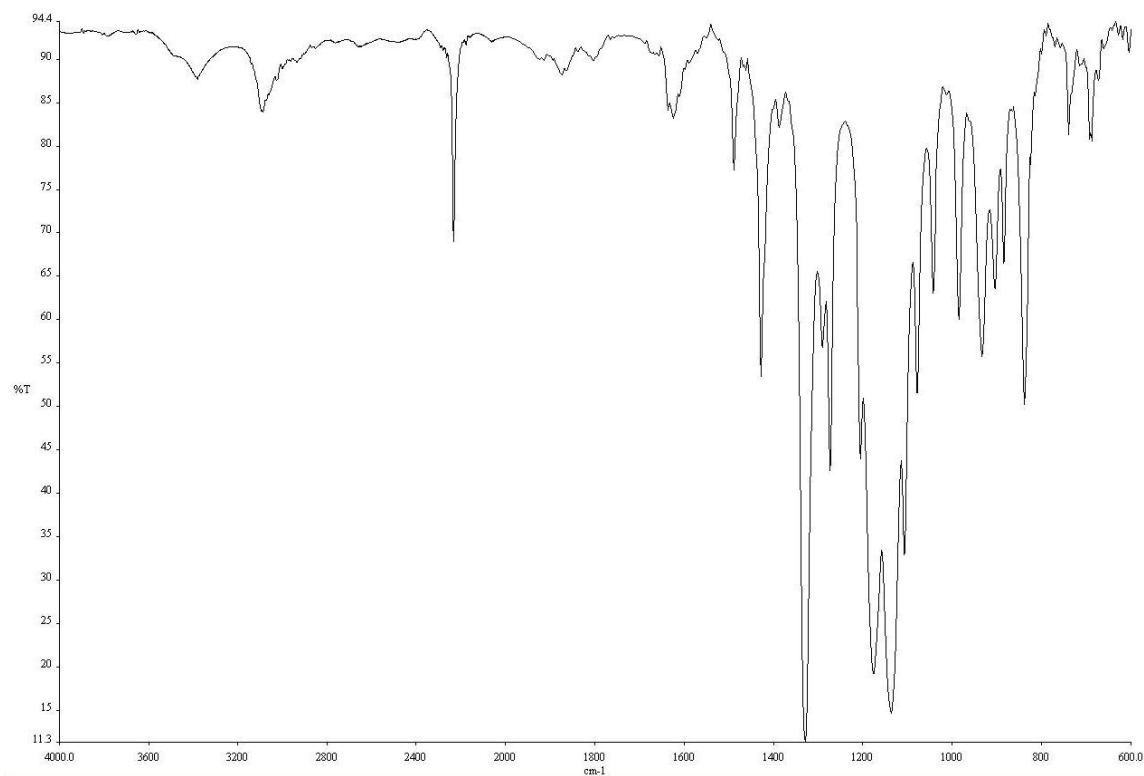
Figure A2.35 IR (NaCl, Thin Film) of compound **S25**.
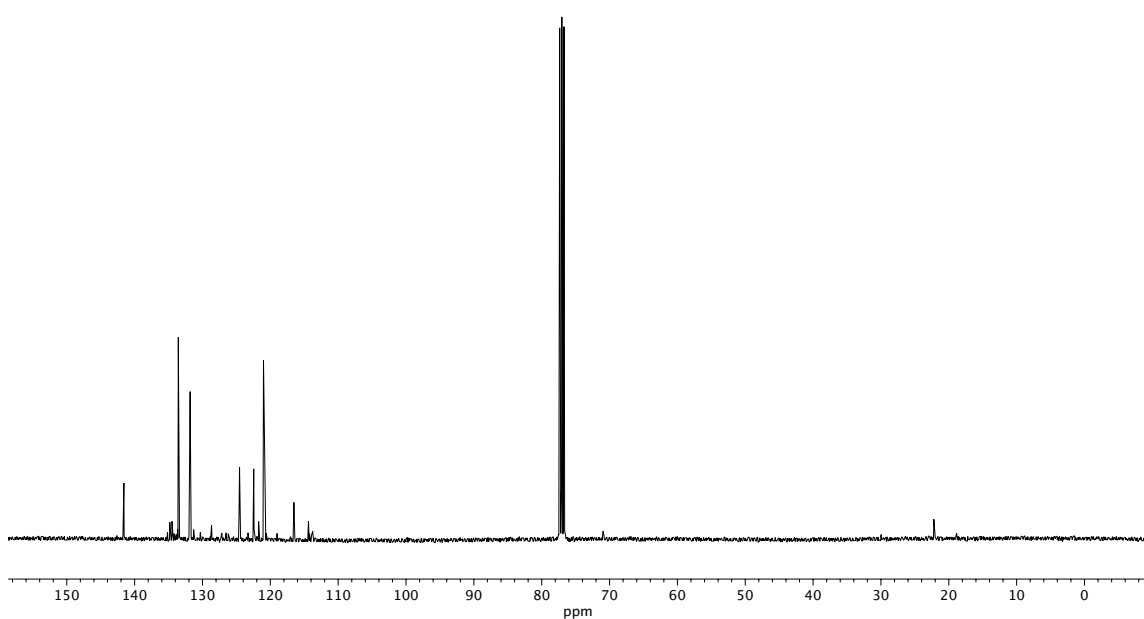
Figure A2.36 ^{13}C NMR (101 MHz, CDCl$_3$) of compound **S25**.
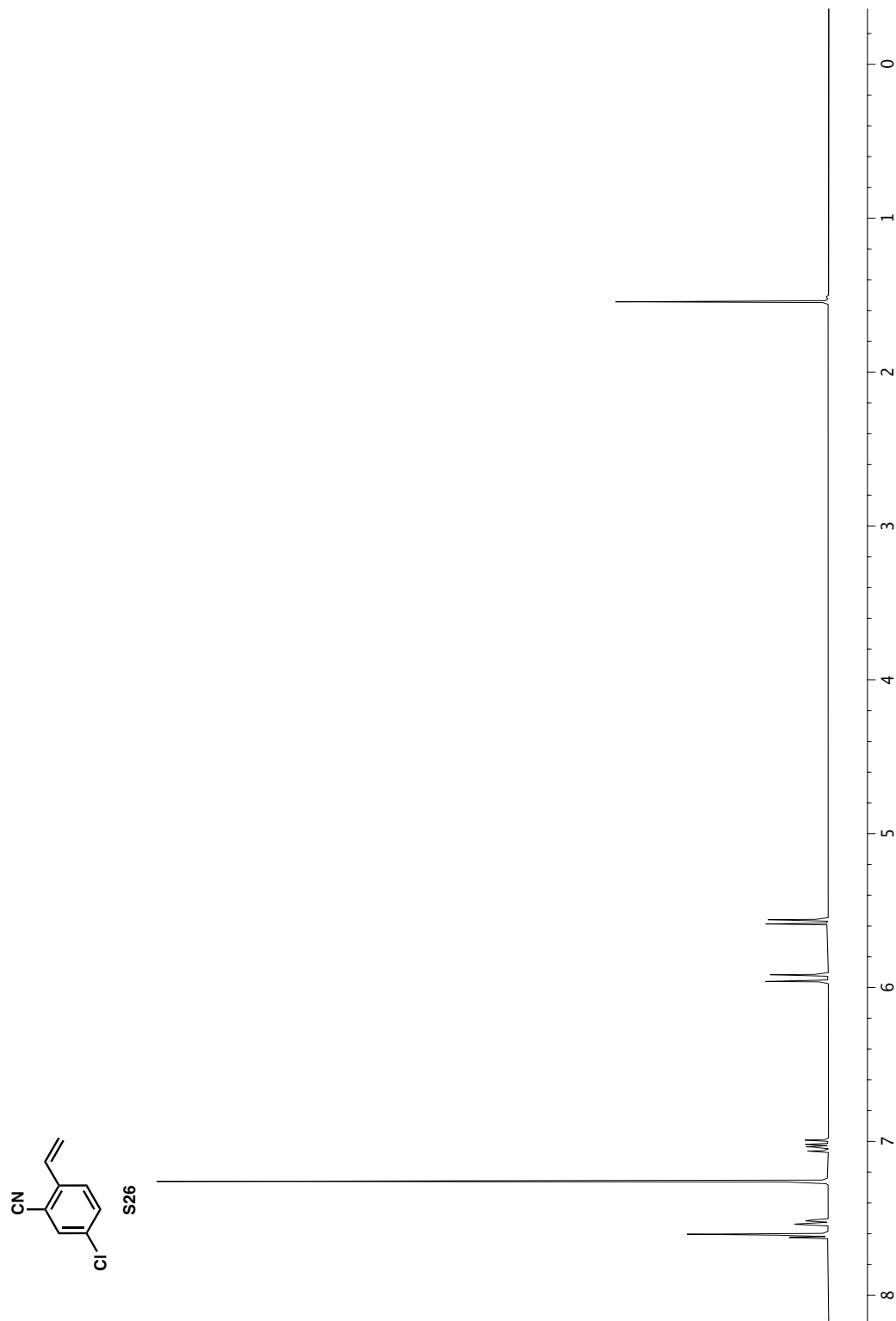
Figure A2.37 ^{1}H NMR (400 MHz, CDCl$_3$) of compound **S26.**
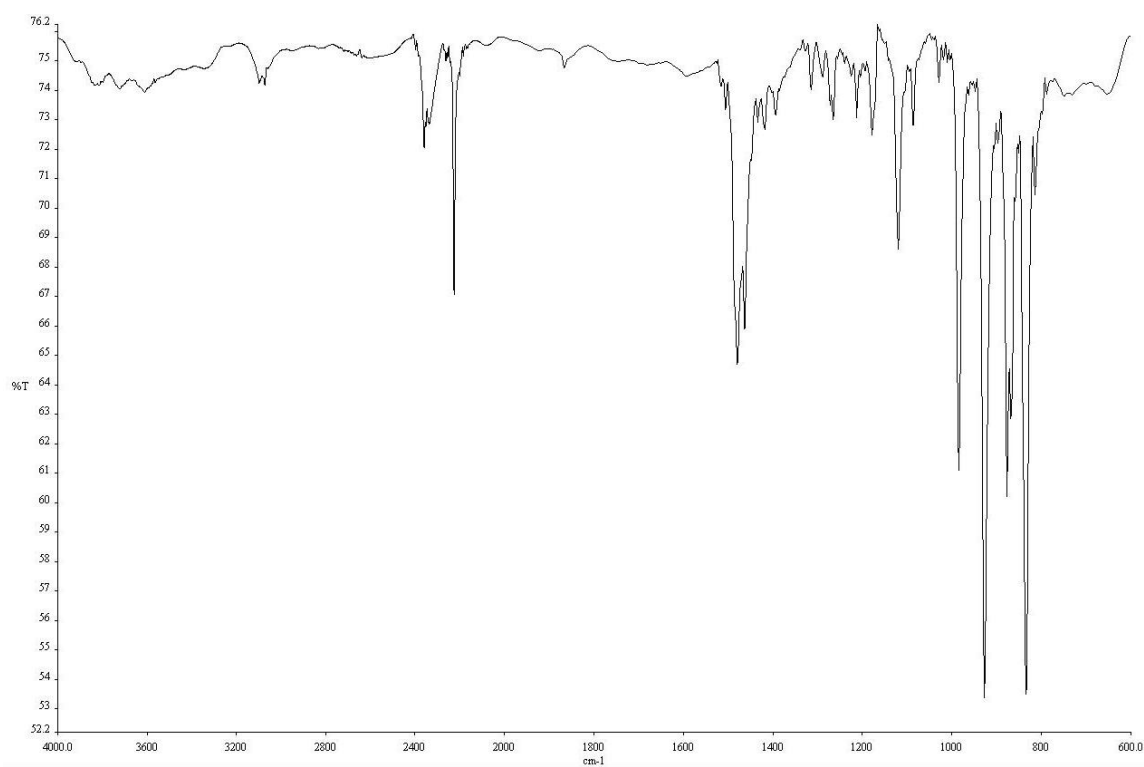
Figure A2.38 IR (NaCl, Thin Film) of compound **S26**.
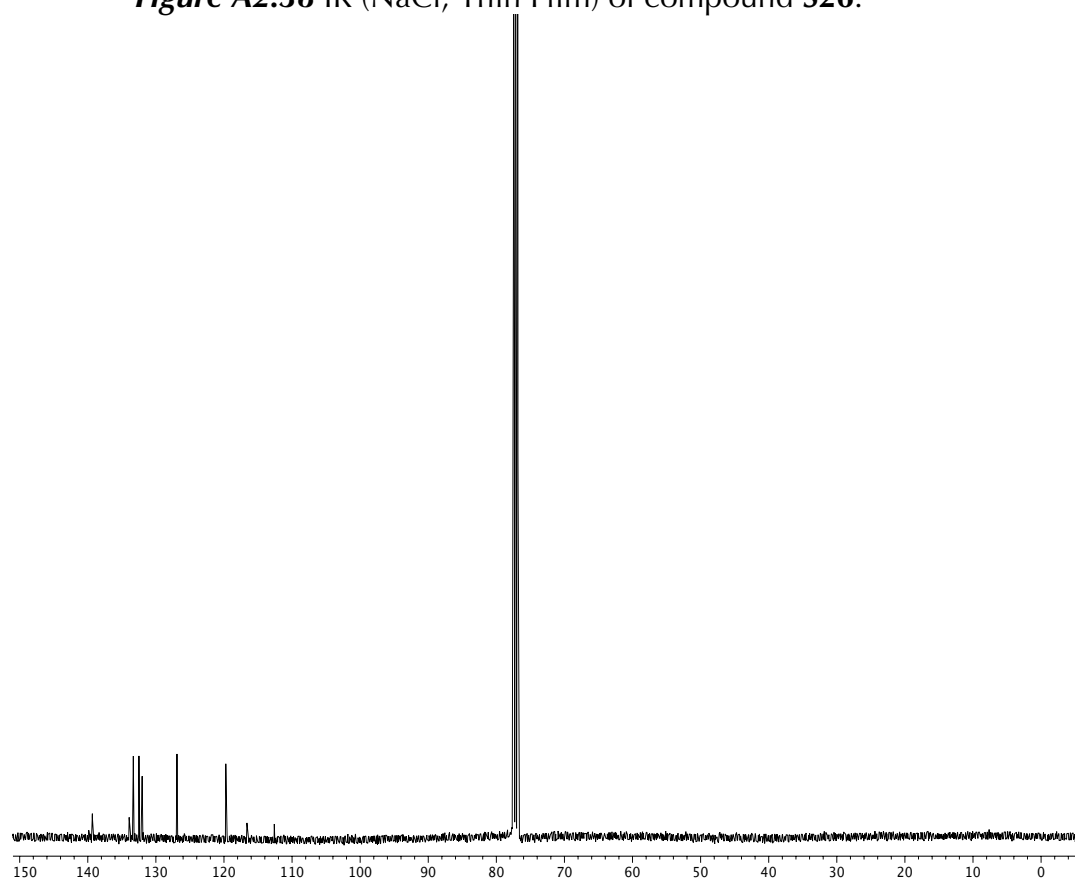
Figure A2.39 ^{13}C NMR (101 MHz, CDCl$_3$) of compound **S26**.
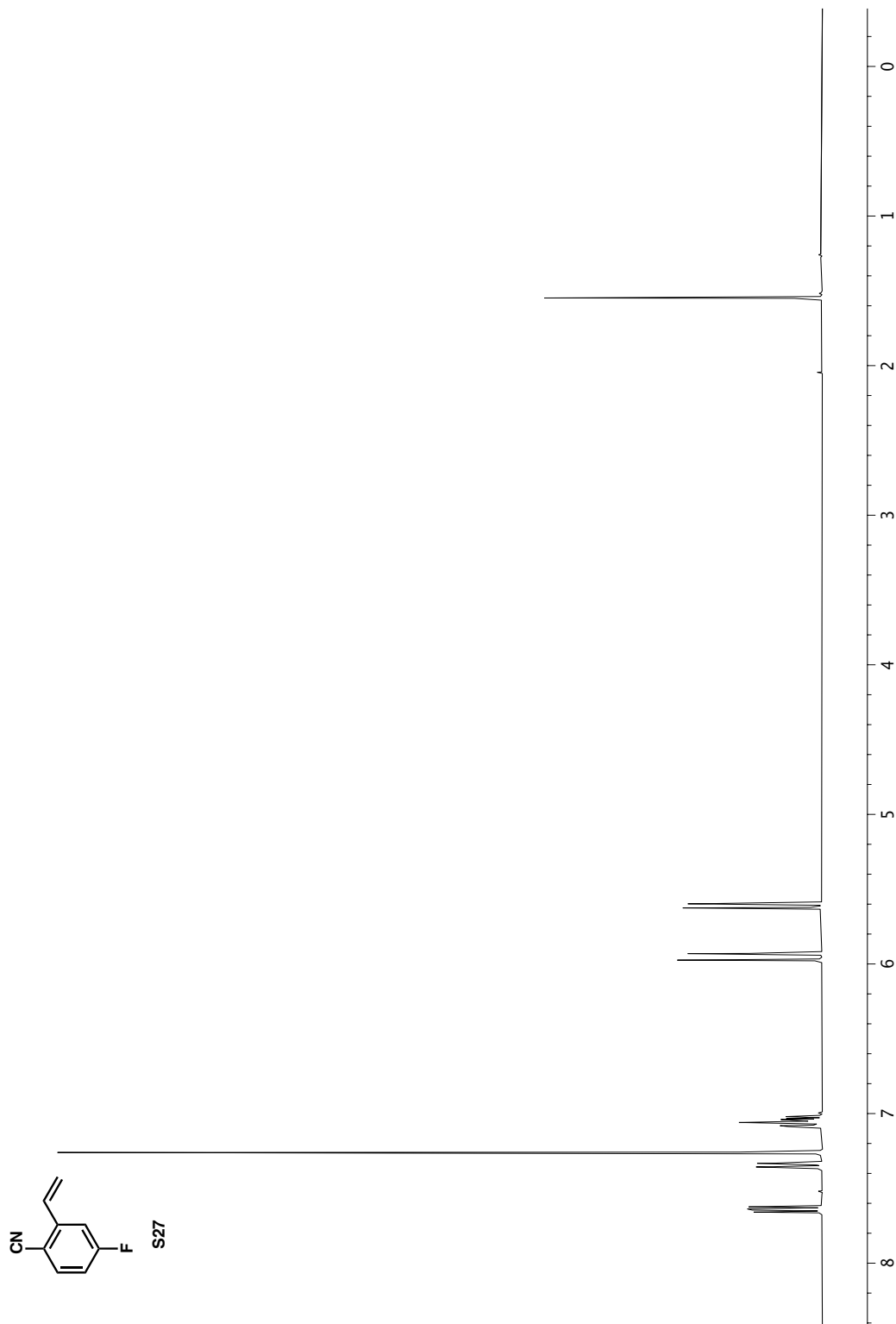
Figure A2.40 ¹H NMR (400 MHz, CDCl₃) of compound **S27.**
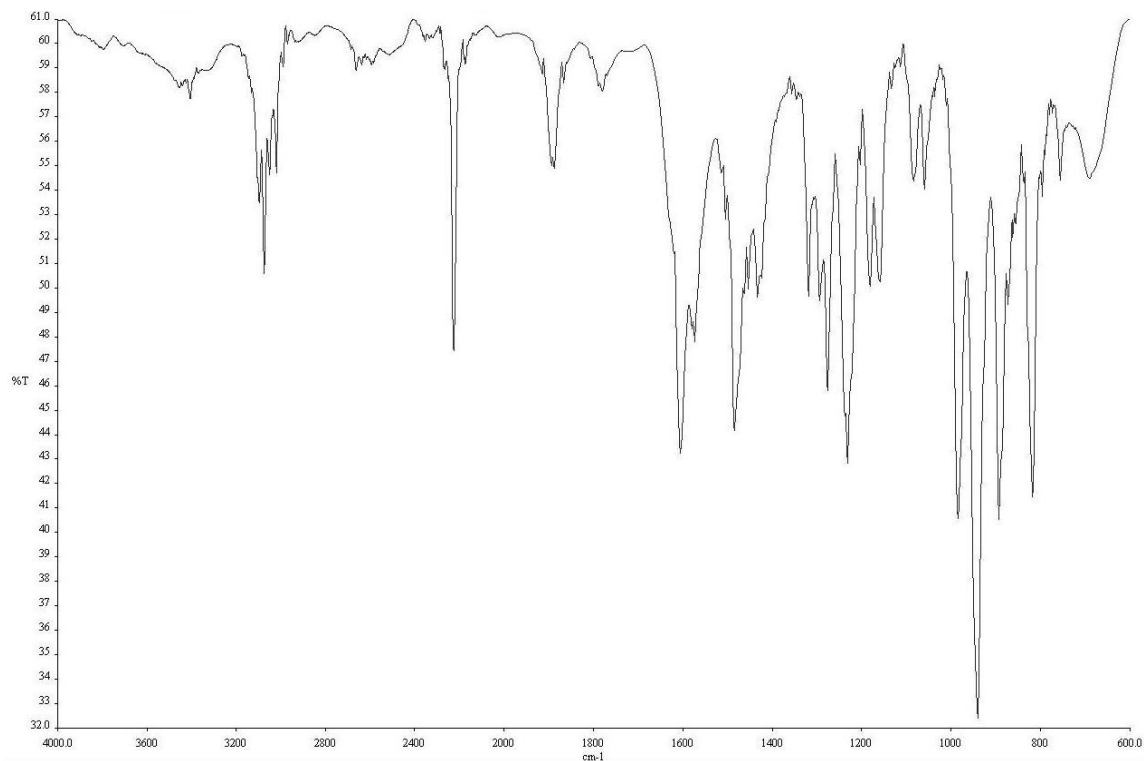
Figure A2.41 IR (NaCl, Thin Film) of compound **S27**.
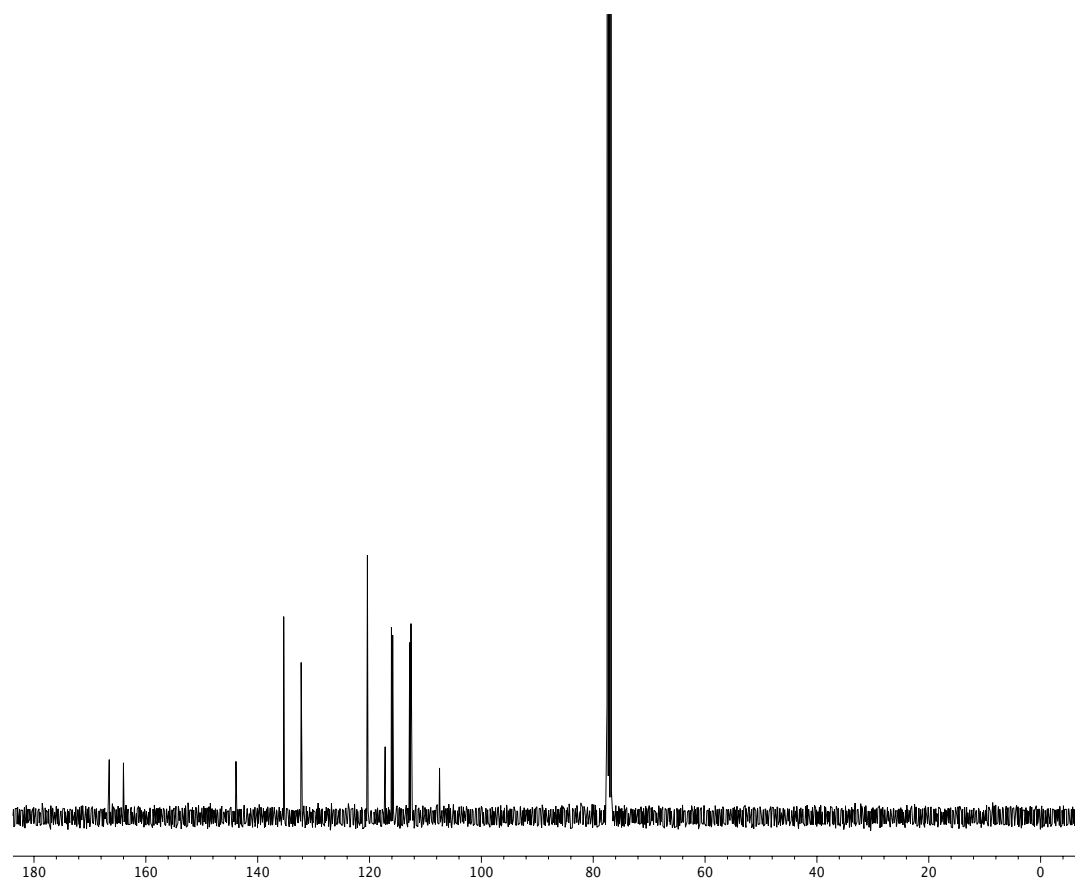
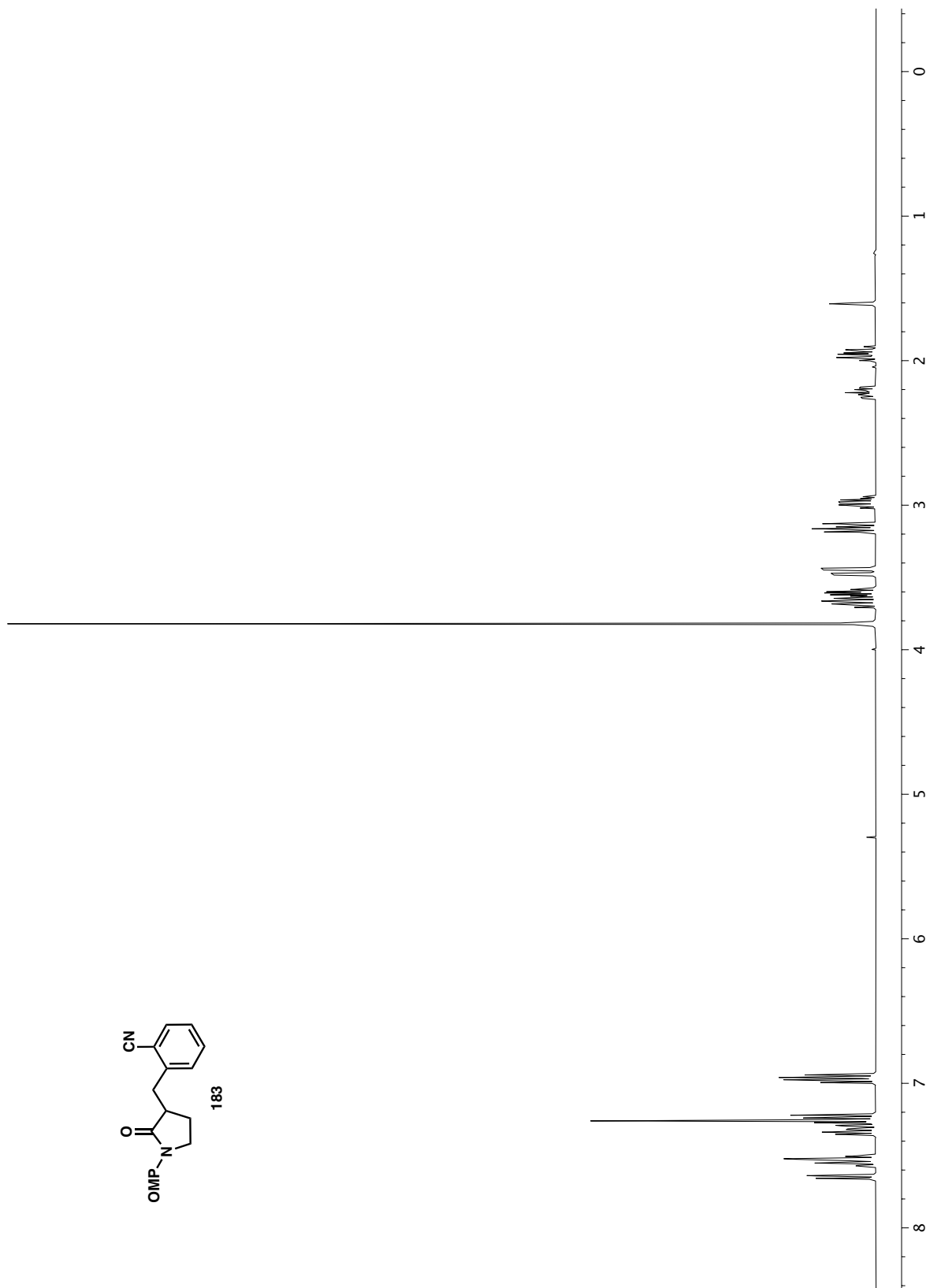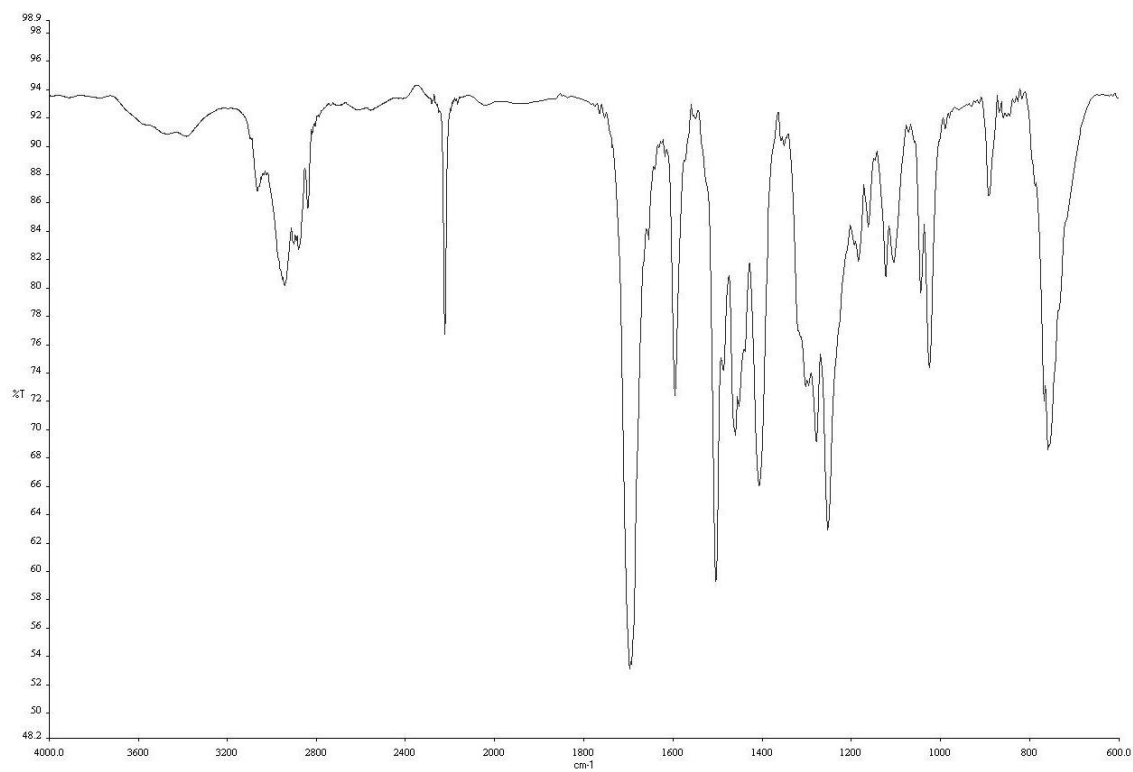**Figure A2.42** ^{13}C NMR (101 MHz, CDCl$_3$) of compound **S27**.
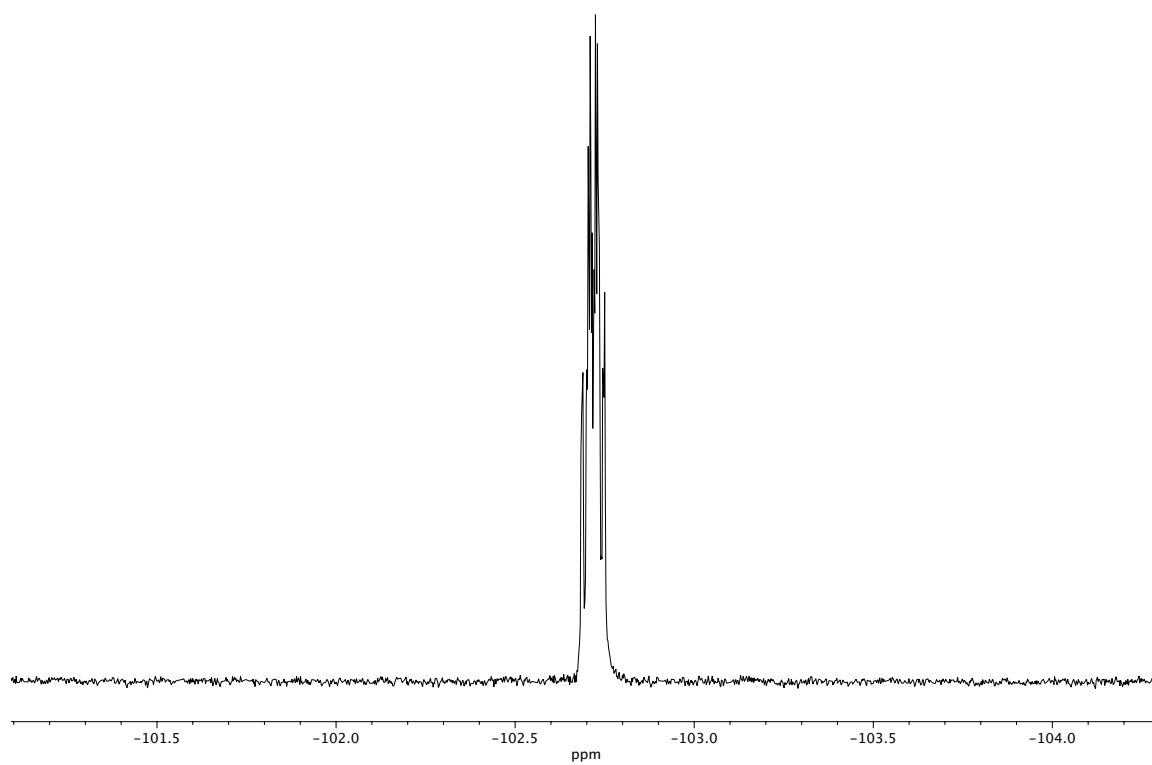
Figure A2.43 ^{19}F NMR (376 MHz, CDCl$_3$) of compound **S27**.
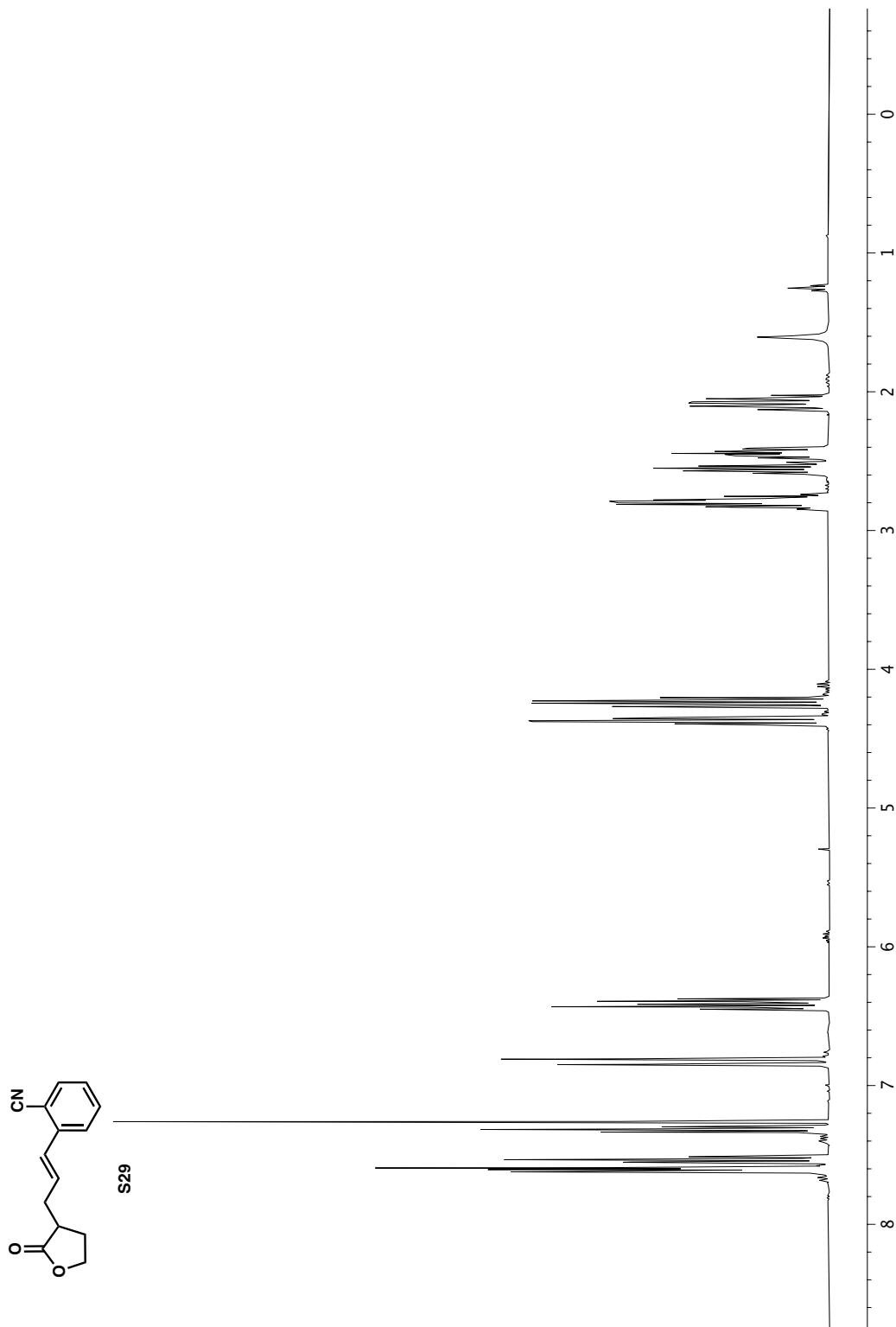
Figure A2.44 ^{1}H NMR (400 MHz, CDCl$_3$) of compound **S29.**
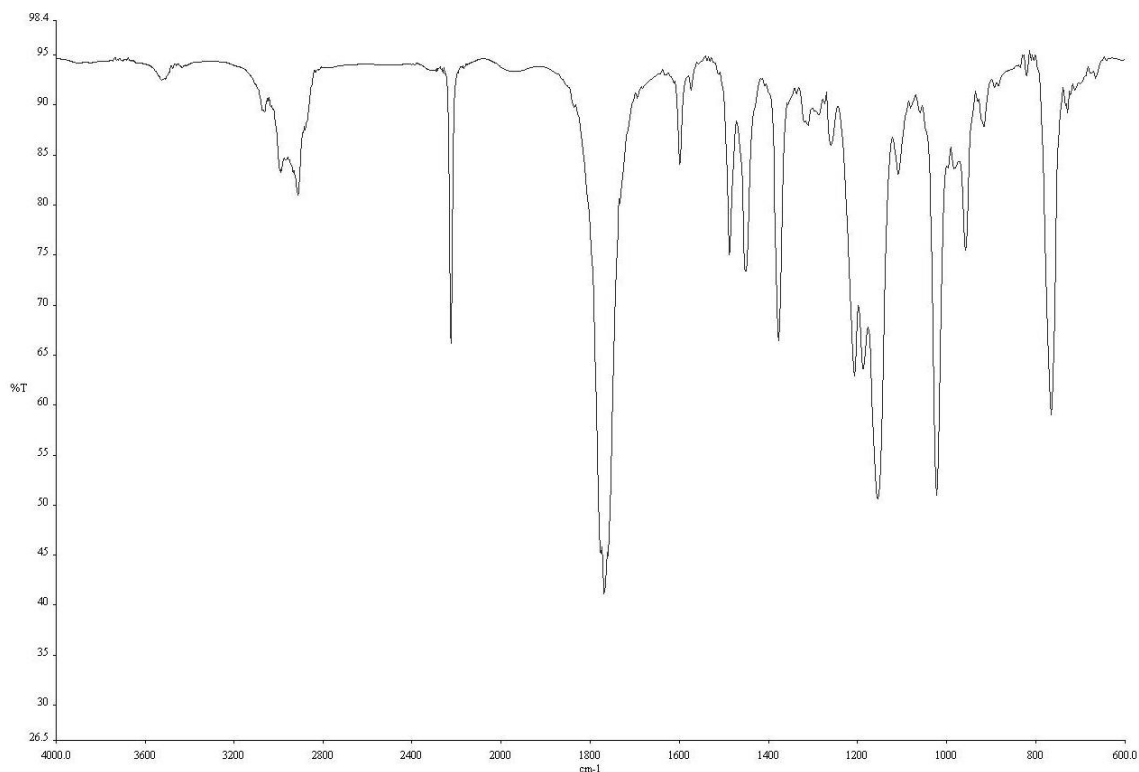
Figure A2.45 IR (NaCl, Thin Film) of compound **S29**.
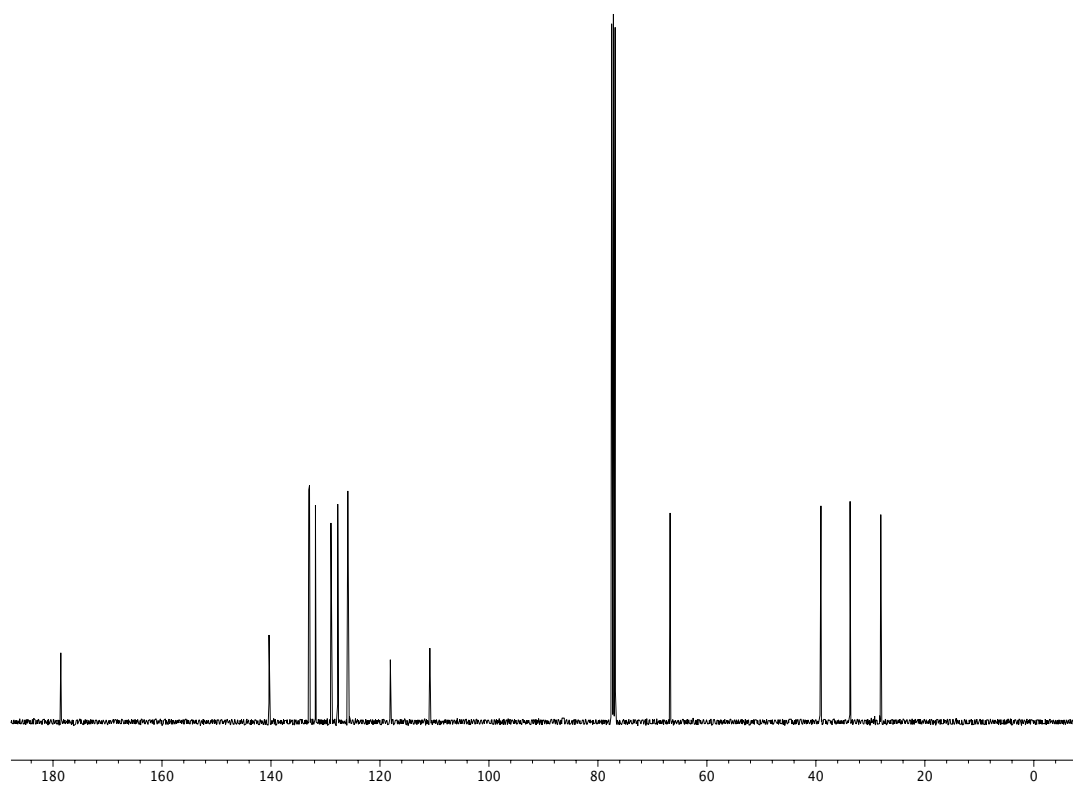
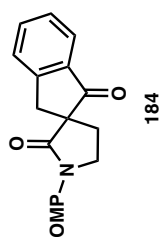***Figure A2.46*** ^{13}C NMR (101 MHz, CDCl$_3$) of compound **S29**.
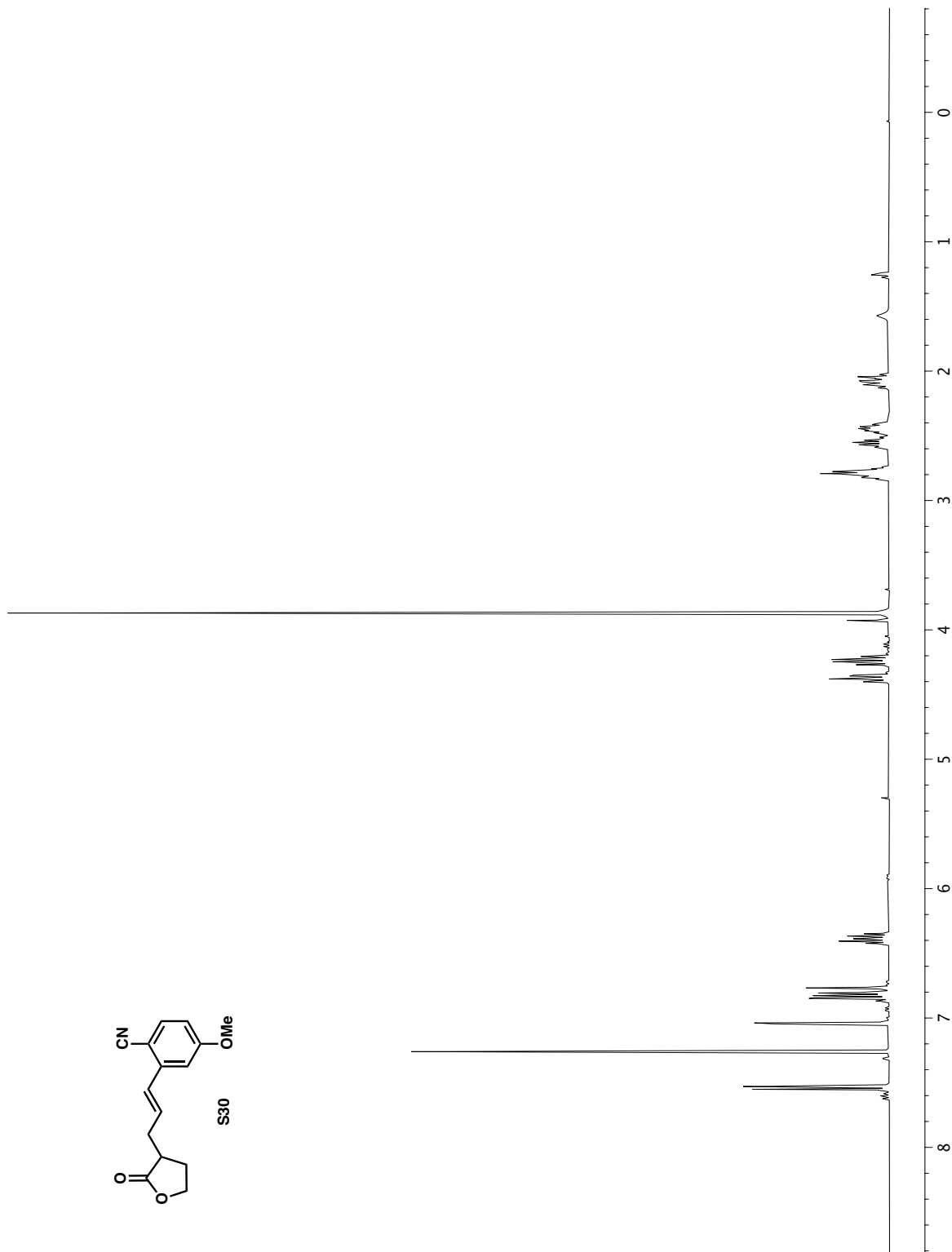
Figure A2.47 ^{1}H NMR (400 MHz, CDCl$_3$) of compound **S30.**
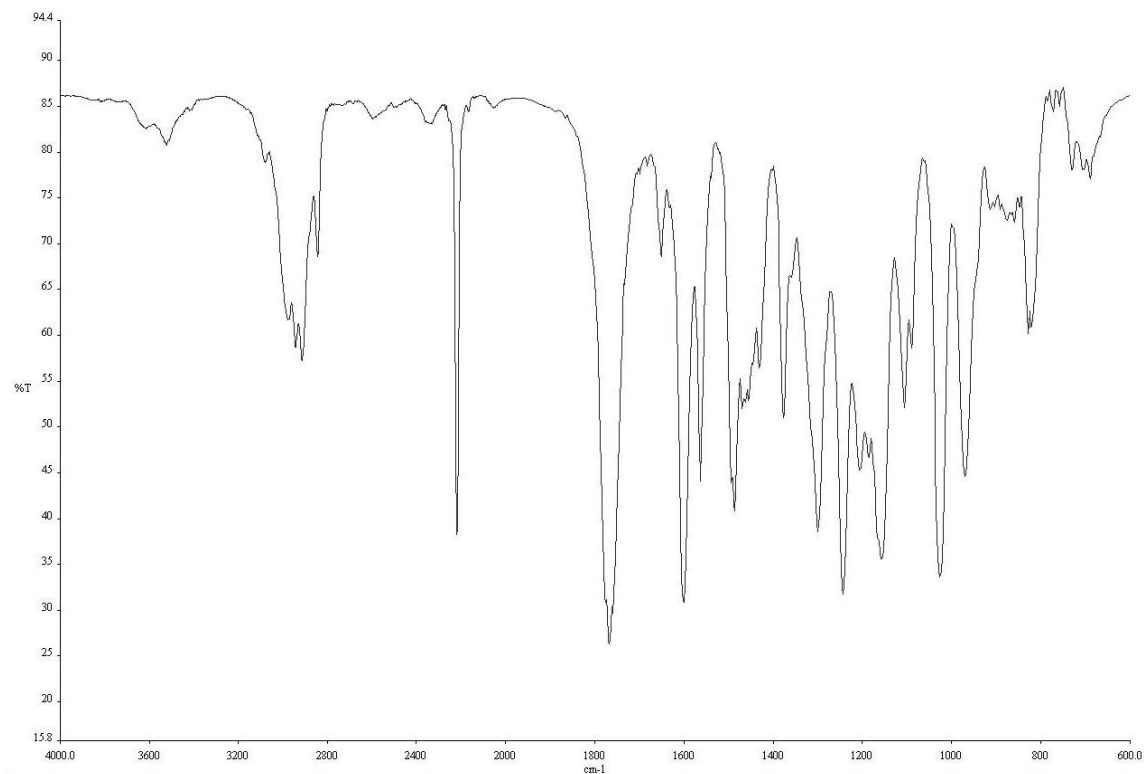
Figure A2.48 IR (NaCl, Thin Film) of compound **S30**.
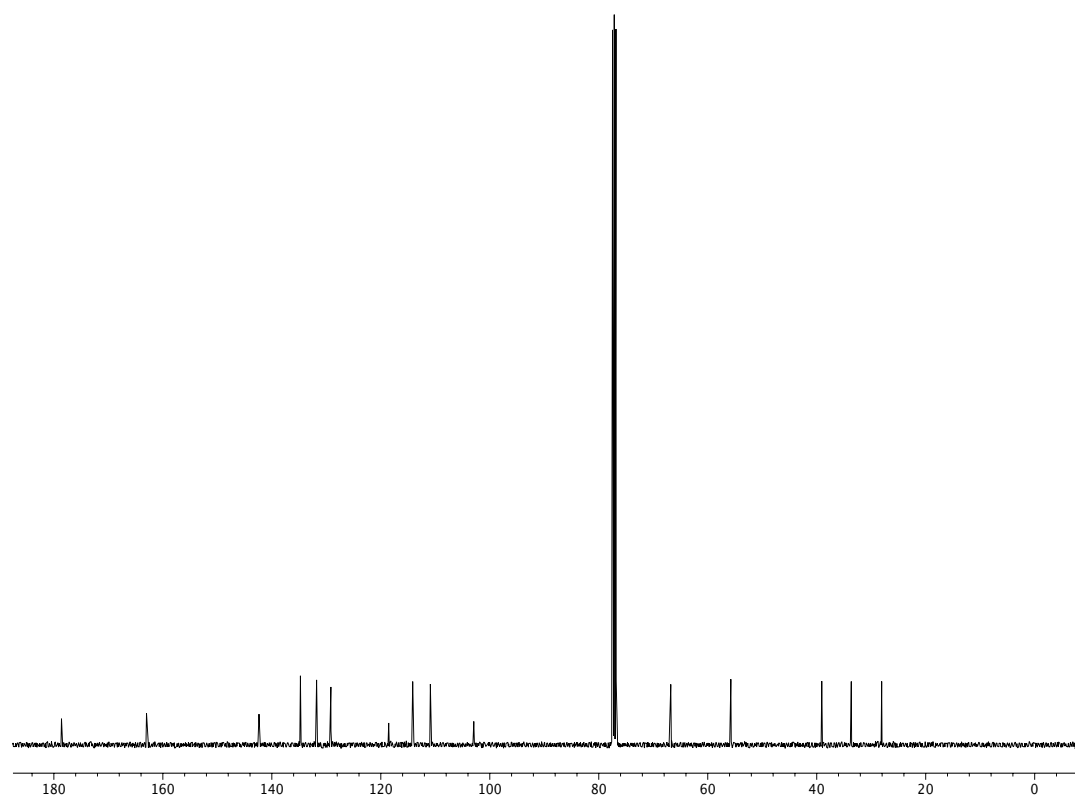
Figure A2.49 ^{13}C NMR (101 MHz, CDCl$_3$) of compound **S30**.
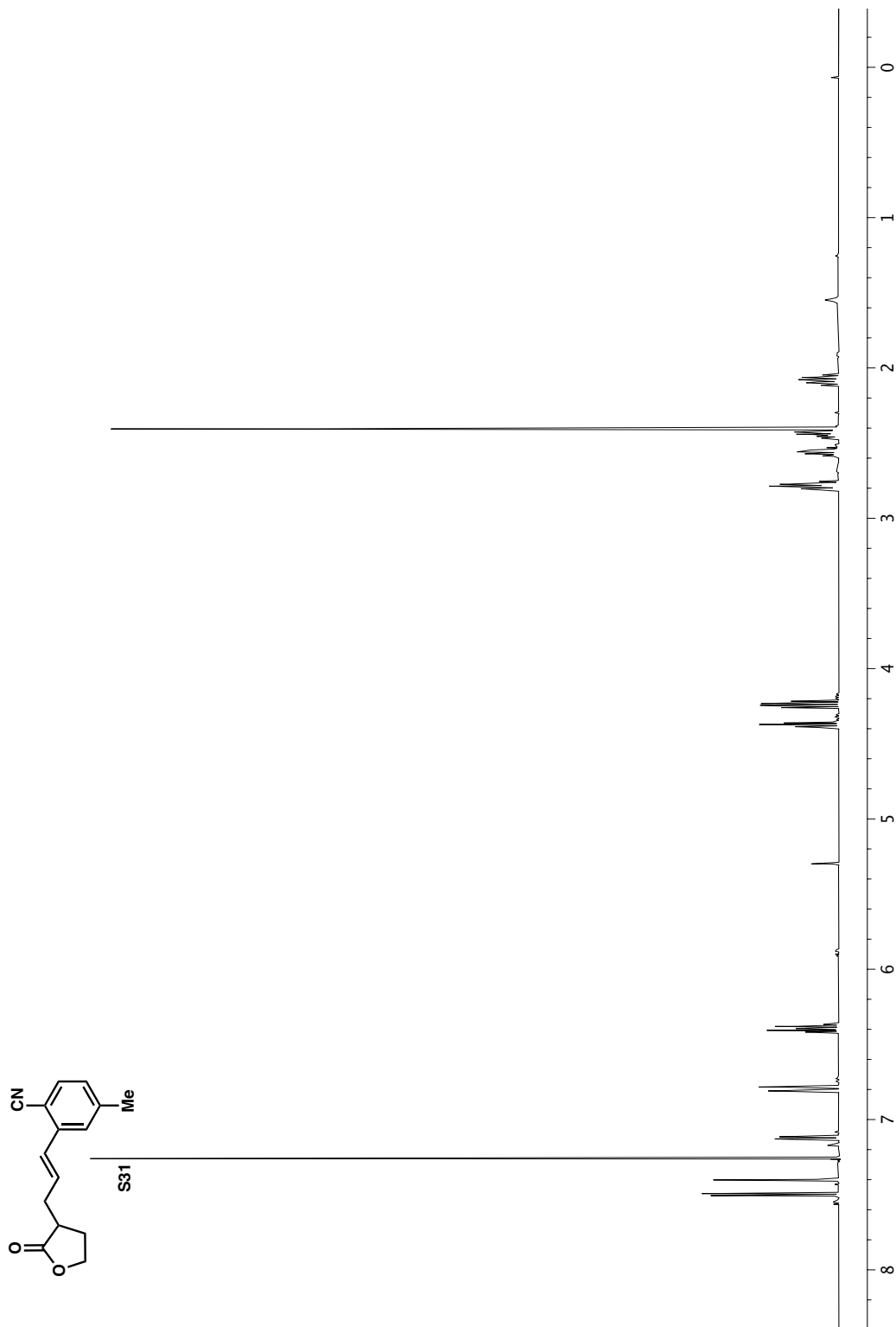
Figure A2.50 ^{1}H NMR (400 MHz, CDCl$_3$) of compound **S31.**
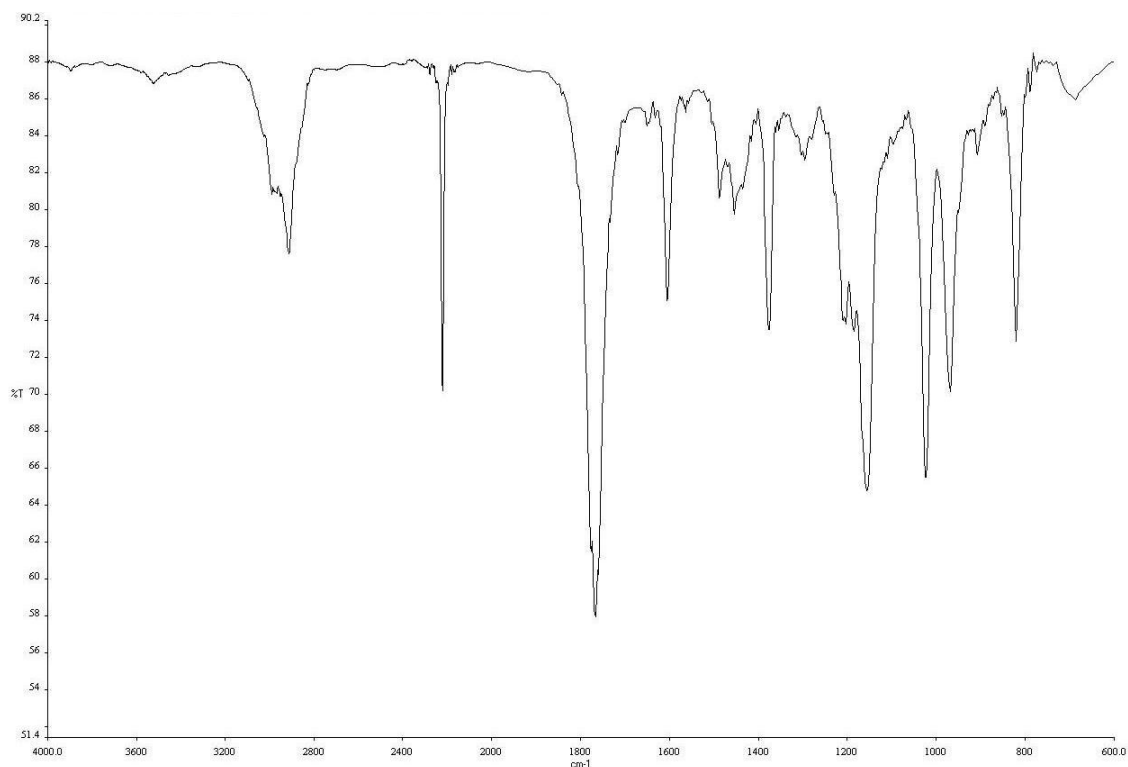
Figure A2.51 IR (NaCl, Thin Film) of compound **S31**.
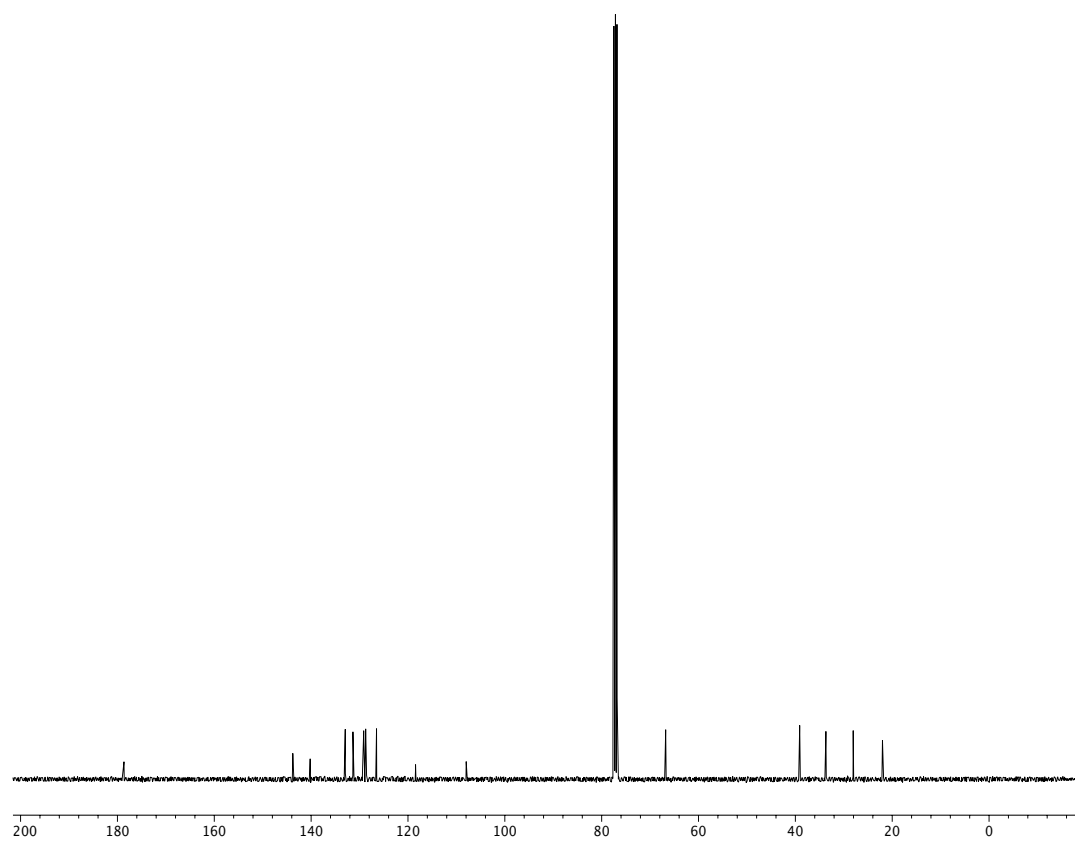
Figure A2.52 ^{13}C NMR (101 MHz, CDCl$_3$) of compound **S31**.
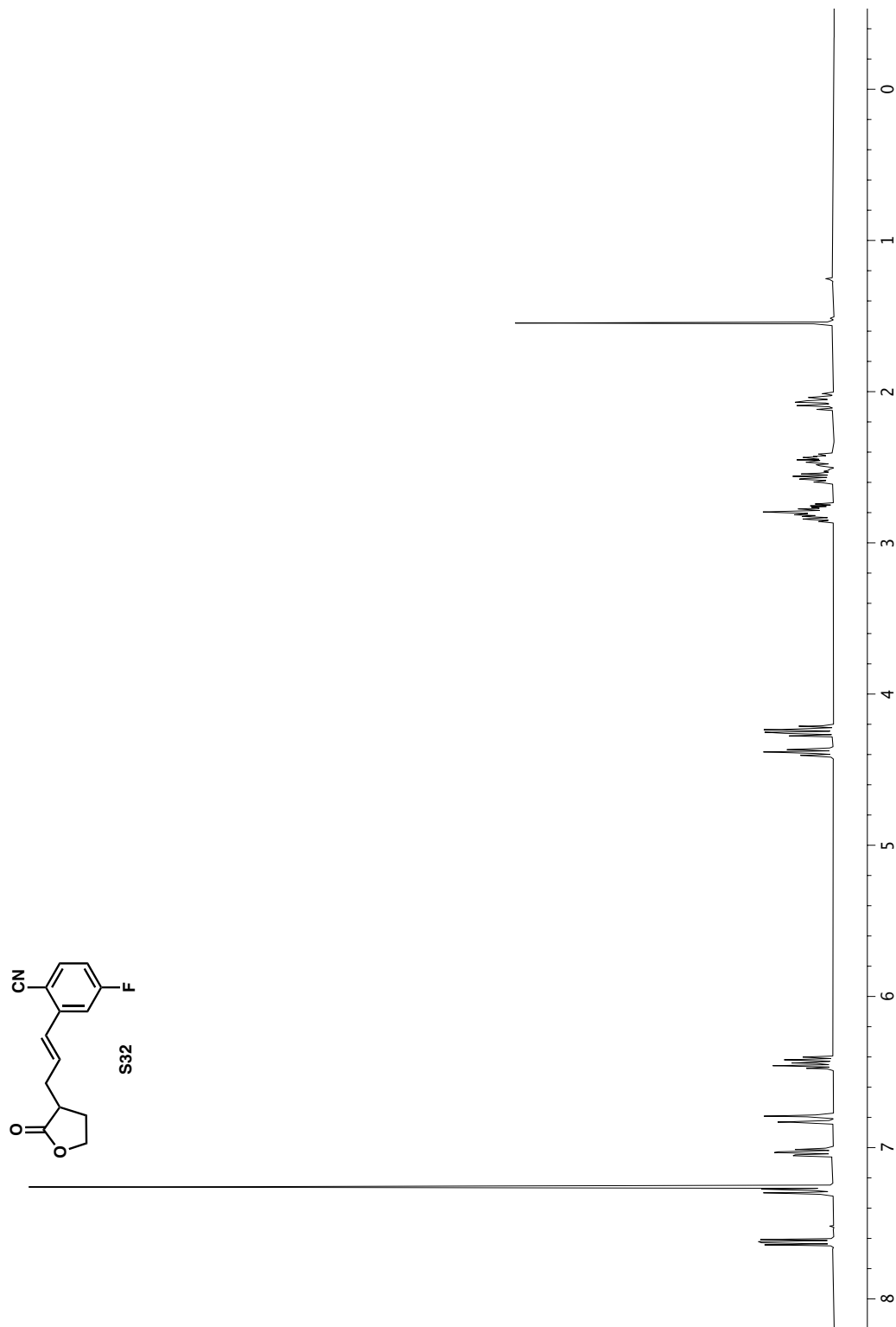
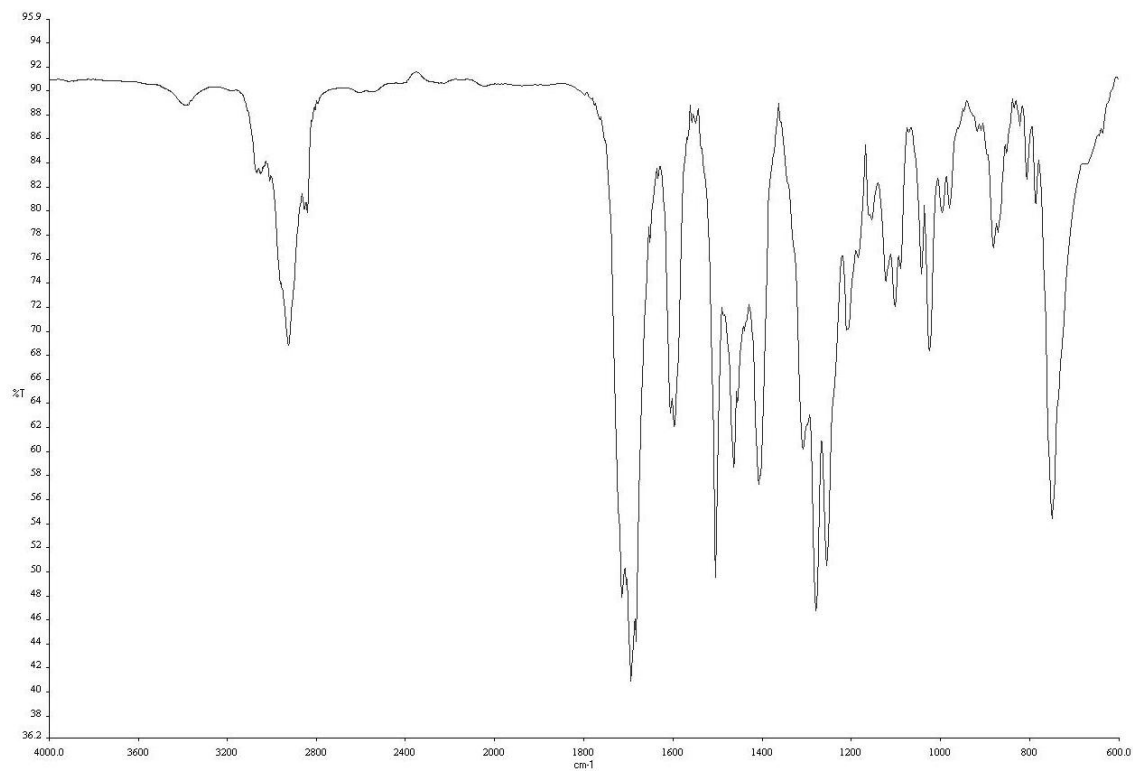***Figure A2.53*** ^{1}H NMR (400 MHz, CDCl$_3$) of compound **S32.**
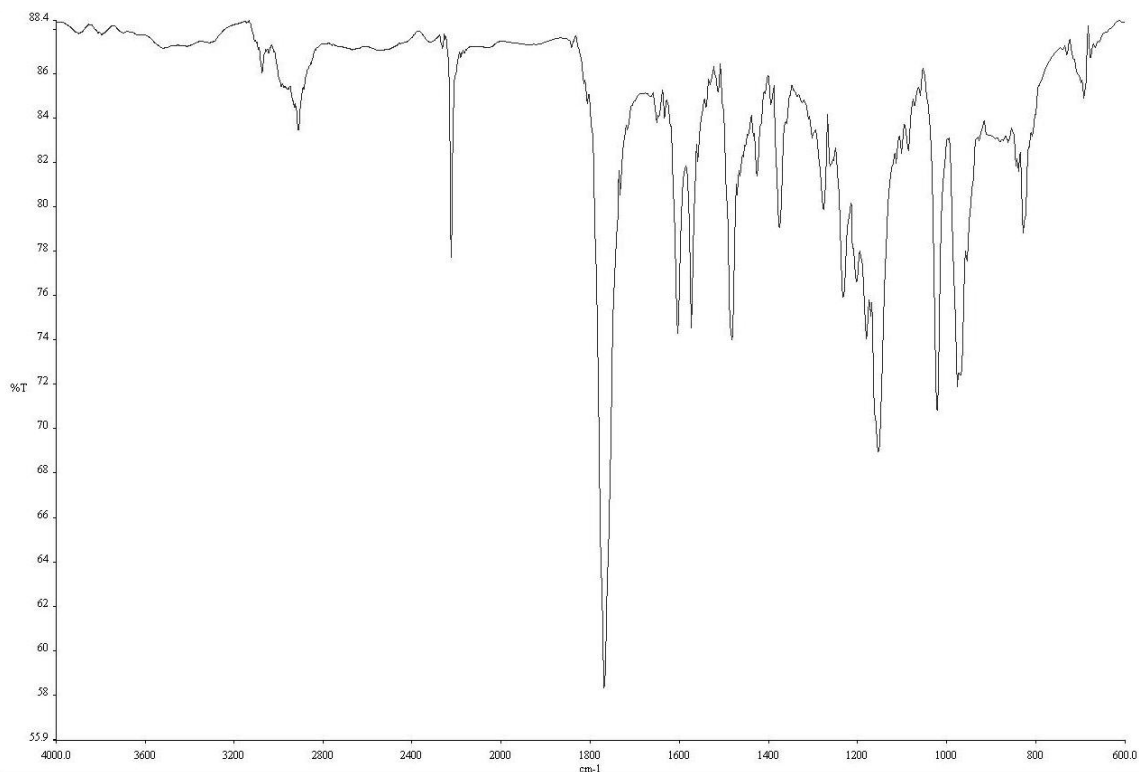
Figure A2.54 IR (NaCl, Thin Film) of compound **S32**.
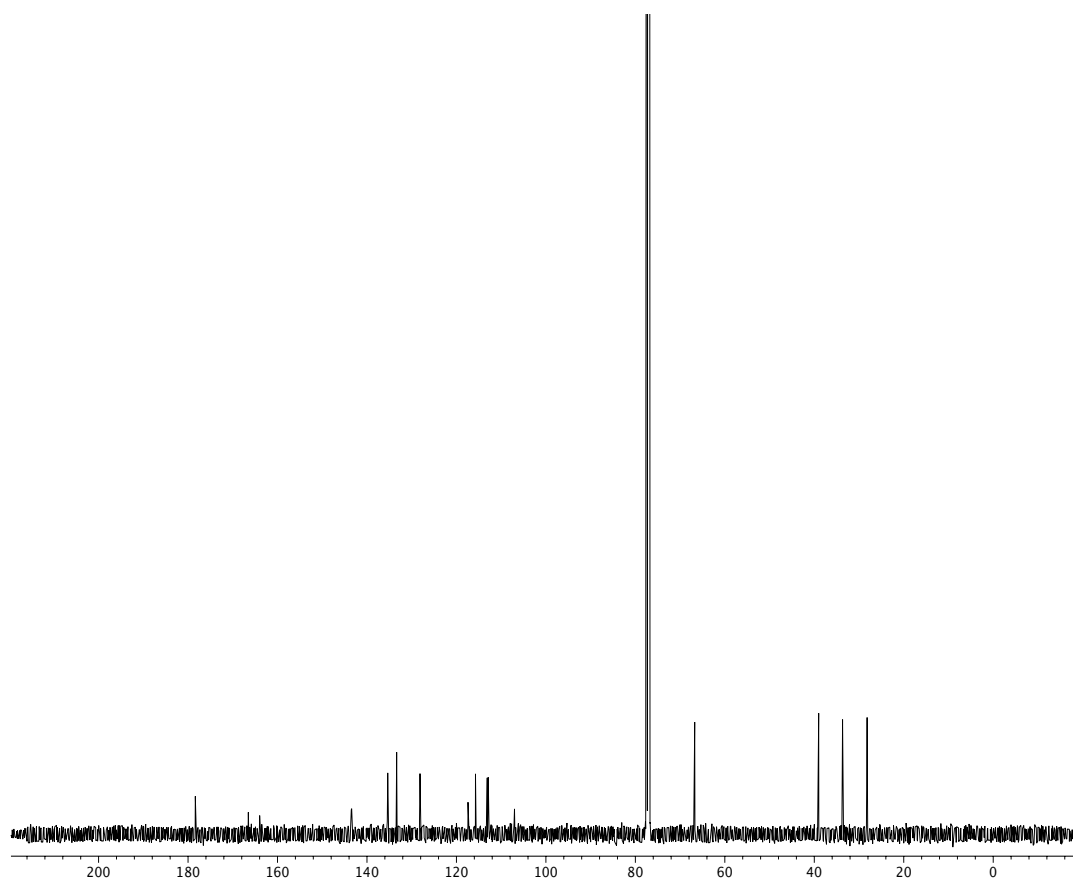
Figure A2.55 ^{13}C NMR (101 MHz, CDCl$_3$) of compound **S32**.
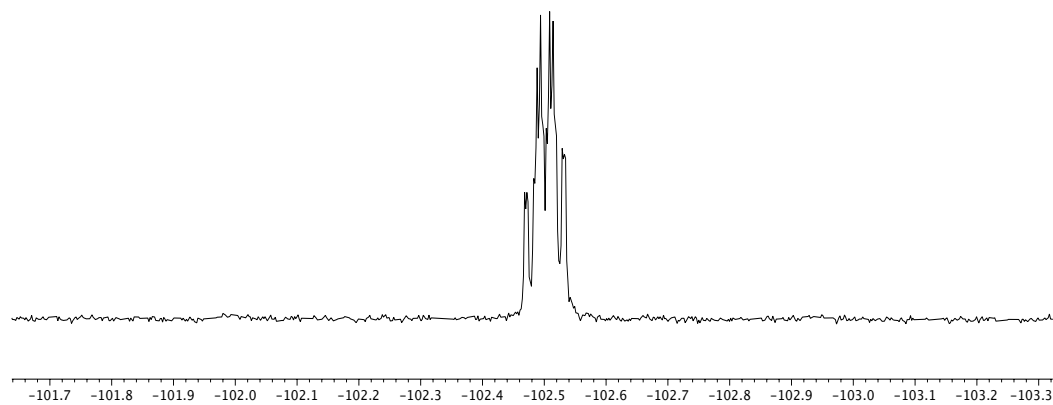
Figure A2.56 ^{19}F NMR (376 MHz, CDCl$_3$) of compound **S32**.
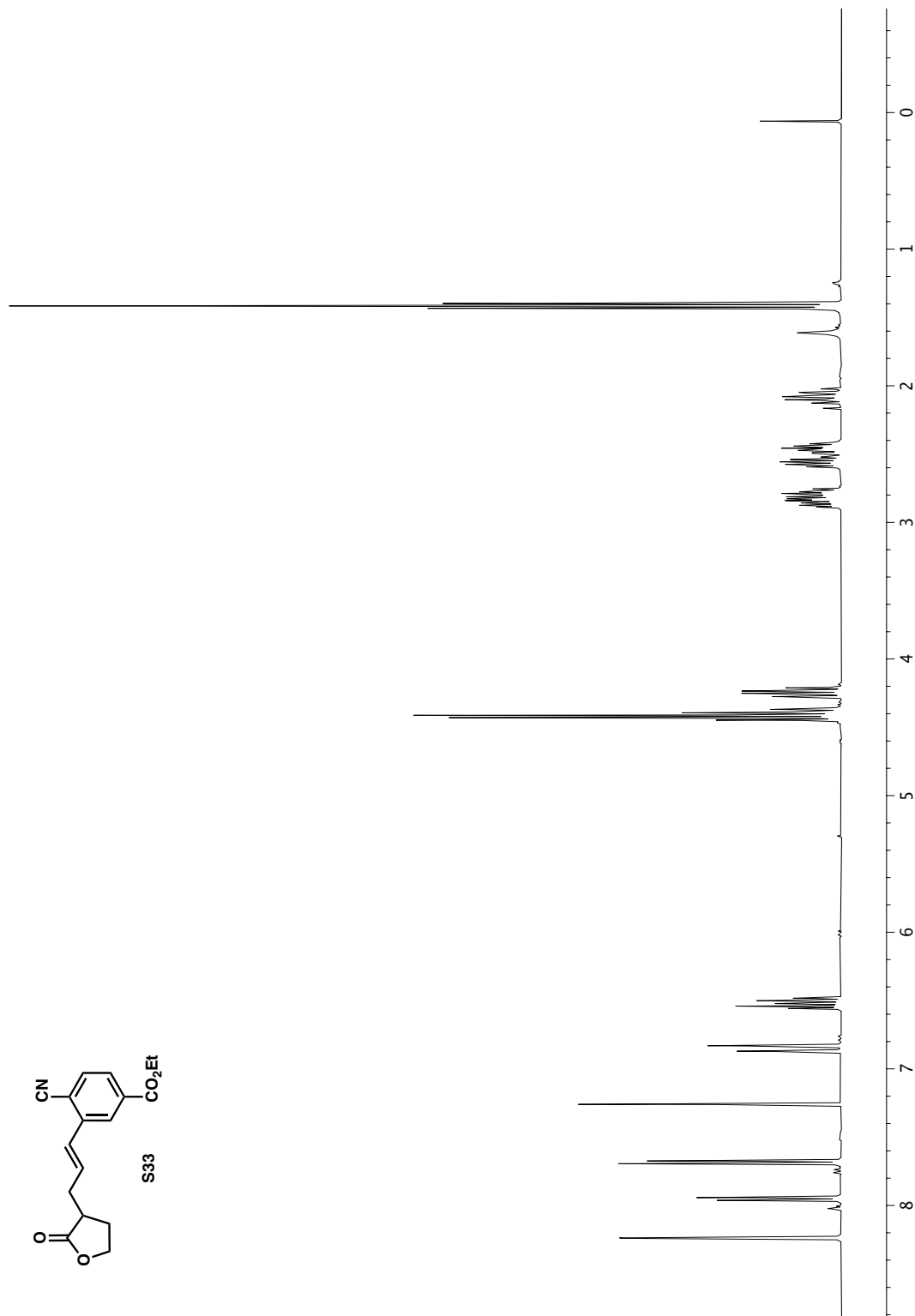
Figure A2.57 ^{1}H NMR (400 MHz, CDCl$_3$) of compound **S33.**
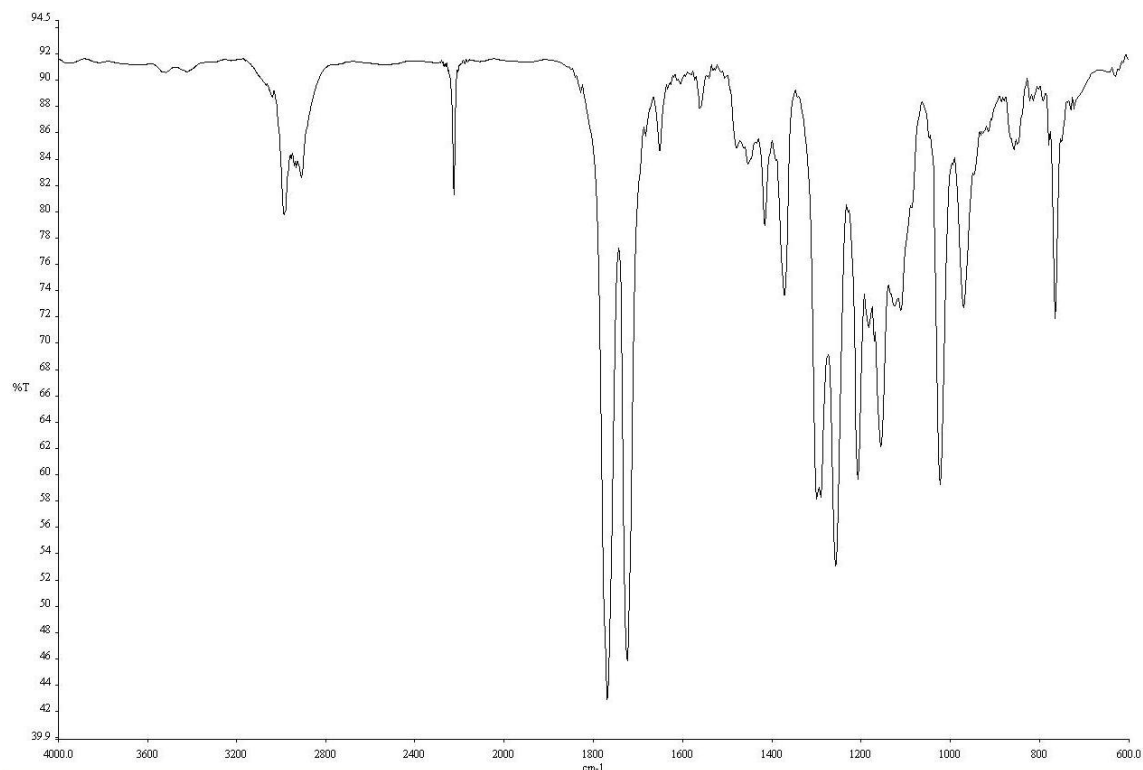
Figure A2.58 IR (NaCl, Thin Film) of compound **S33**.
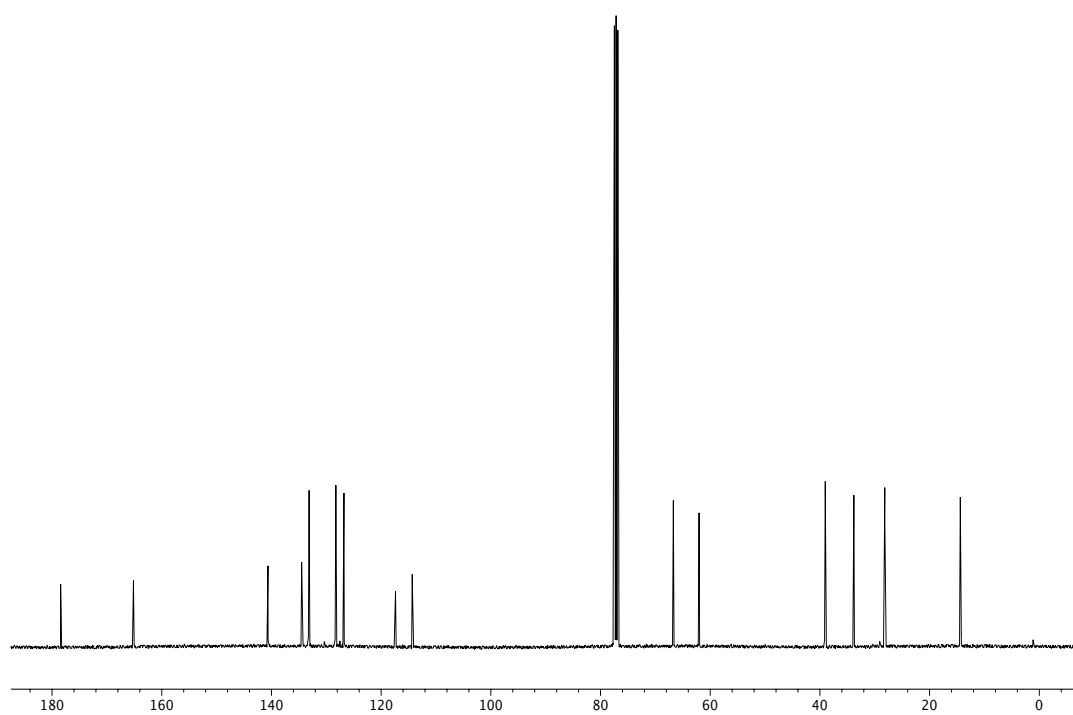
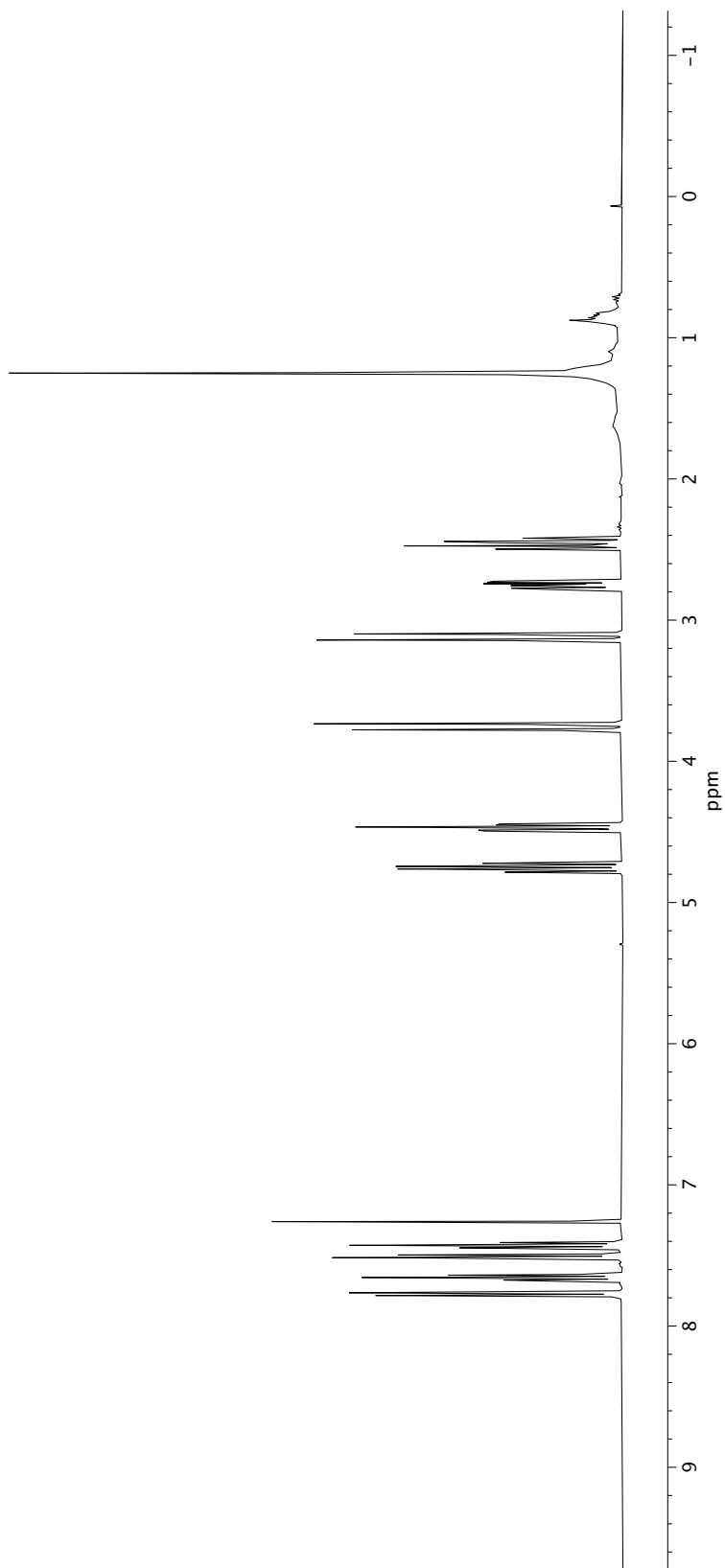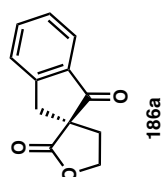*Figure A2.59* ^{13}C NMR (101 MHz, CDCl$_3$) of compound **S33**.
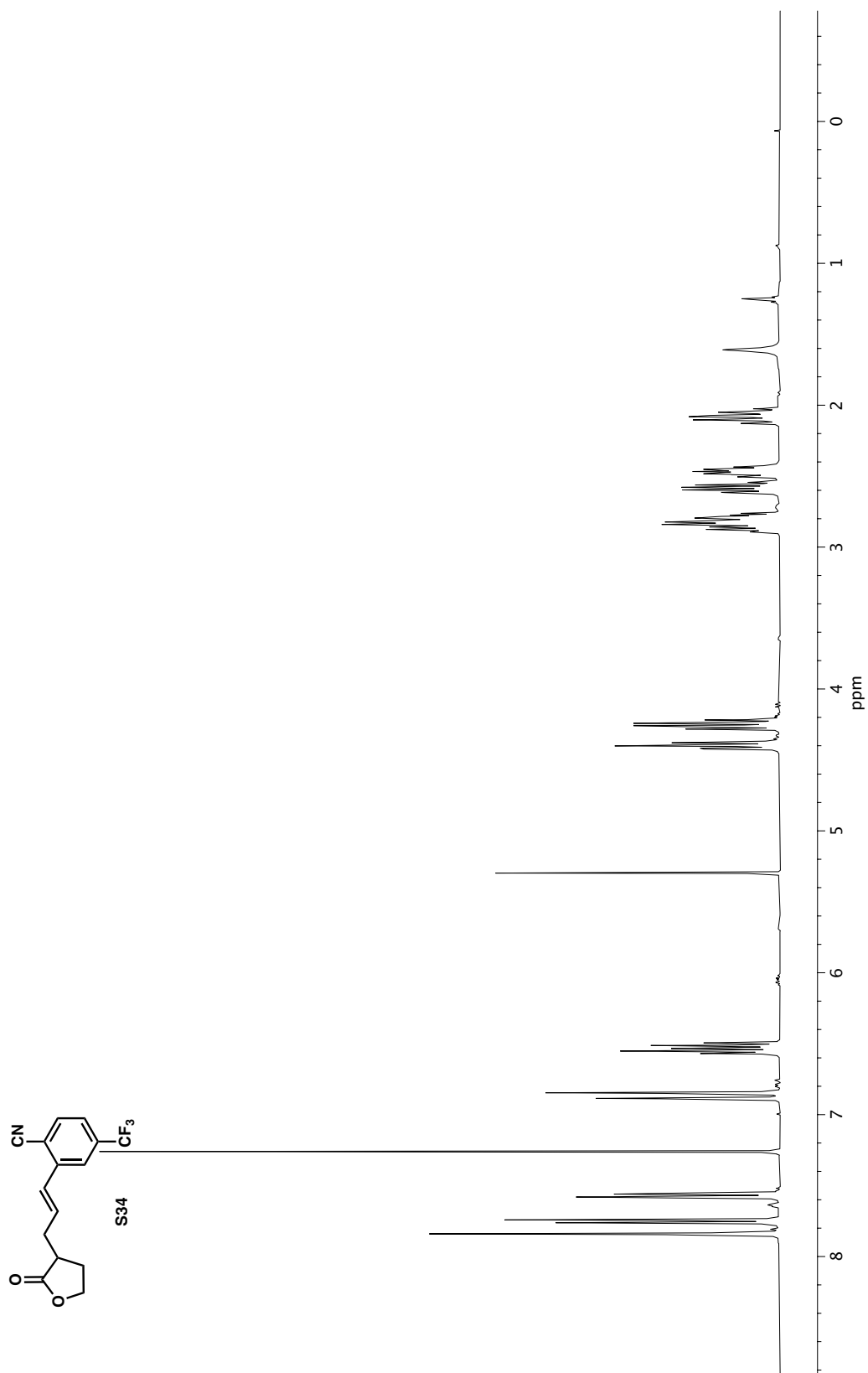
Figure A2.60 ^{1}H NMR (400 MHz, CDCl$_3$) of compound **S34.**
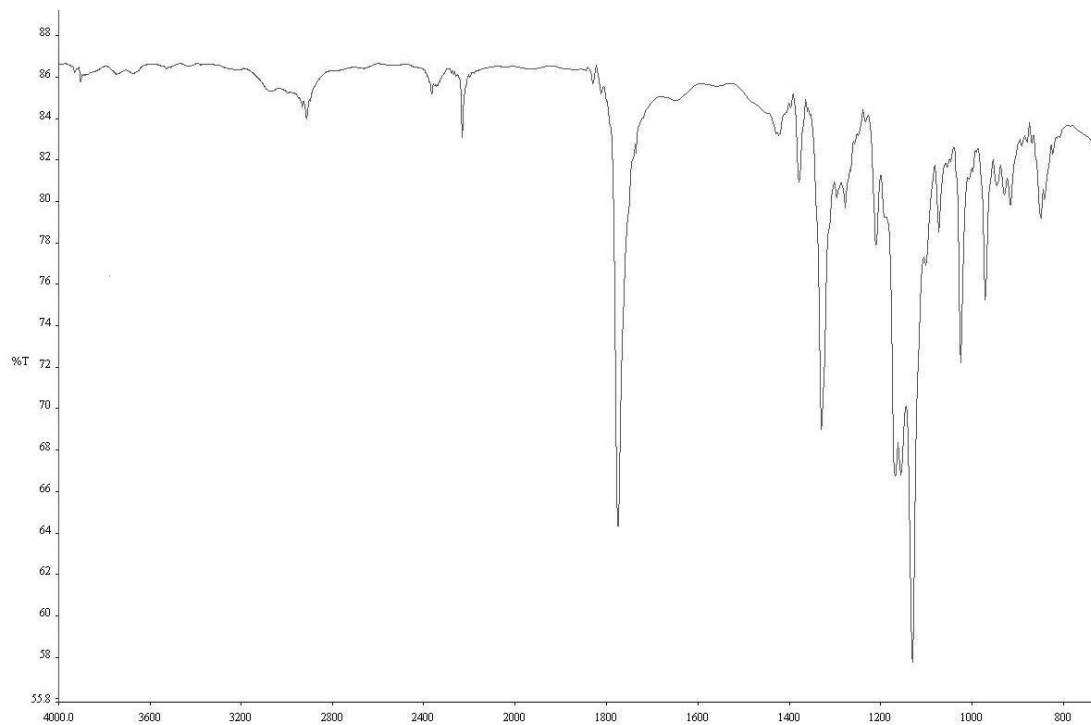
Figure A2.61 IR (NaCl, Thin Film) of compound **S34**.
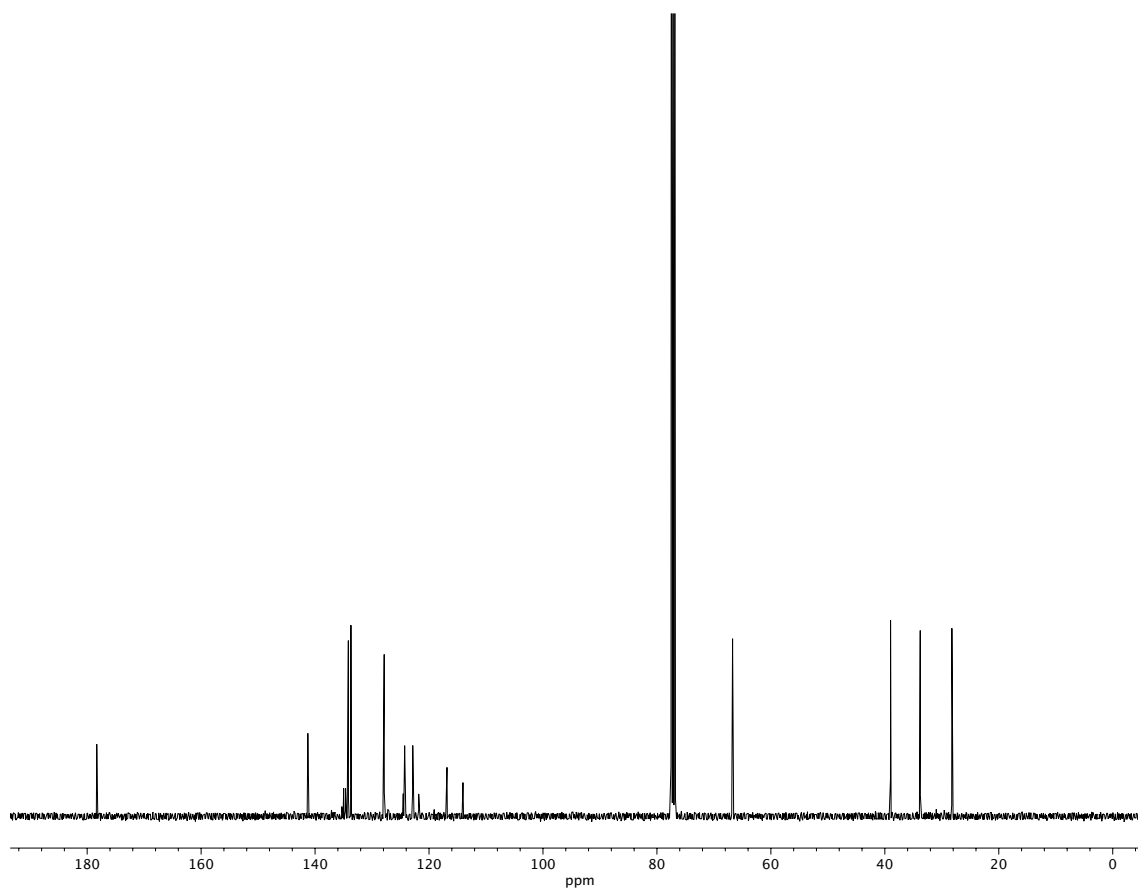
Figure A2.62 ^{13}C NMR (101 MHz, CDCl$_3$) of compound **S34**.
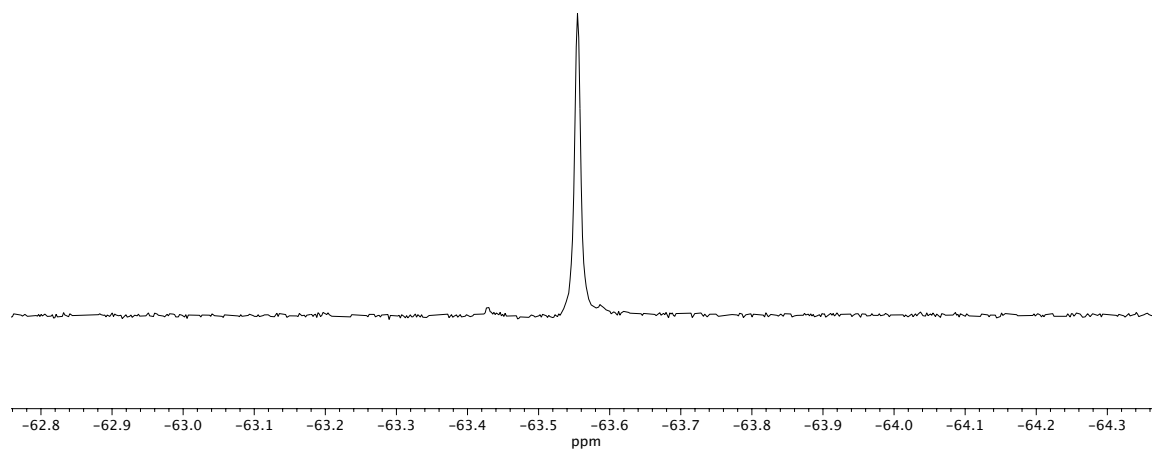
Figure A2.63 ^{19}F NMR (376 MHz, CDCl$_3$) of compound **S34**.
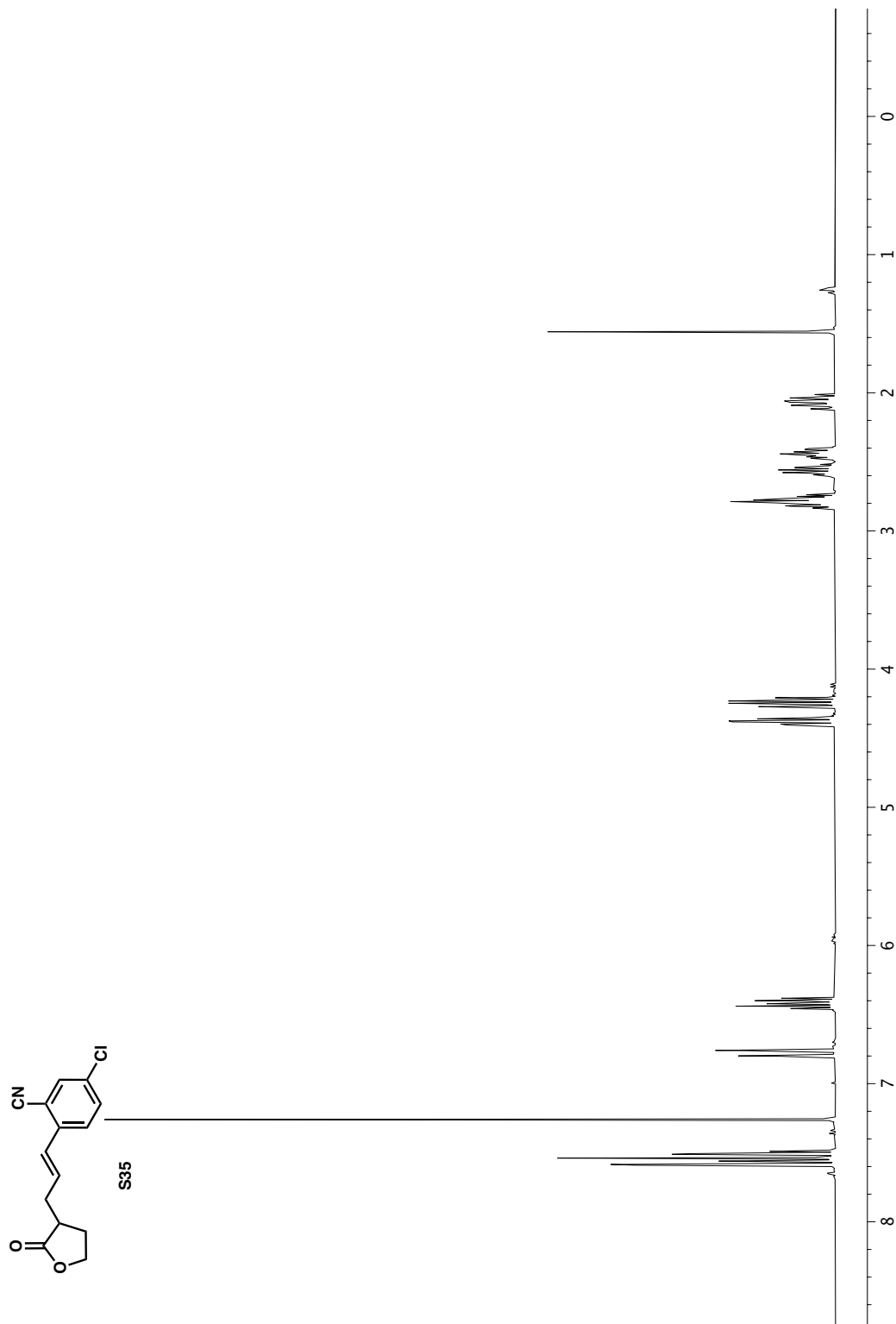
Figure A2.64 ^{1}H NMR (400 MHz, CDCl$_3$) of compound **S35**.
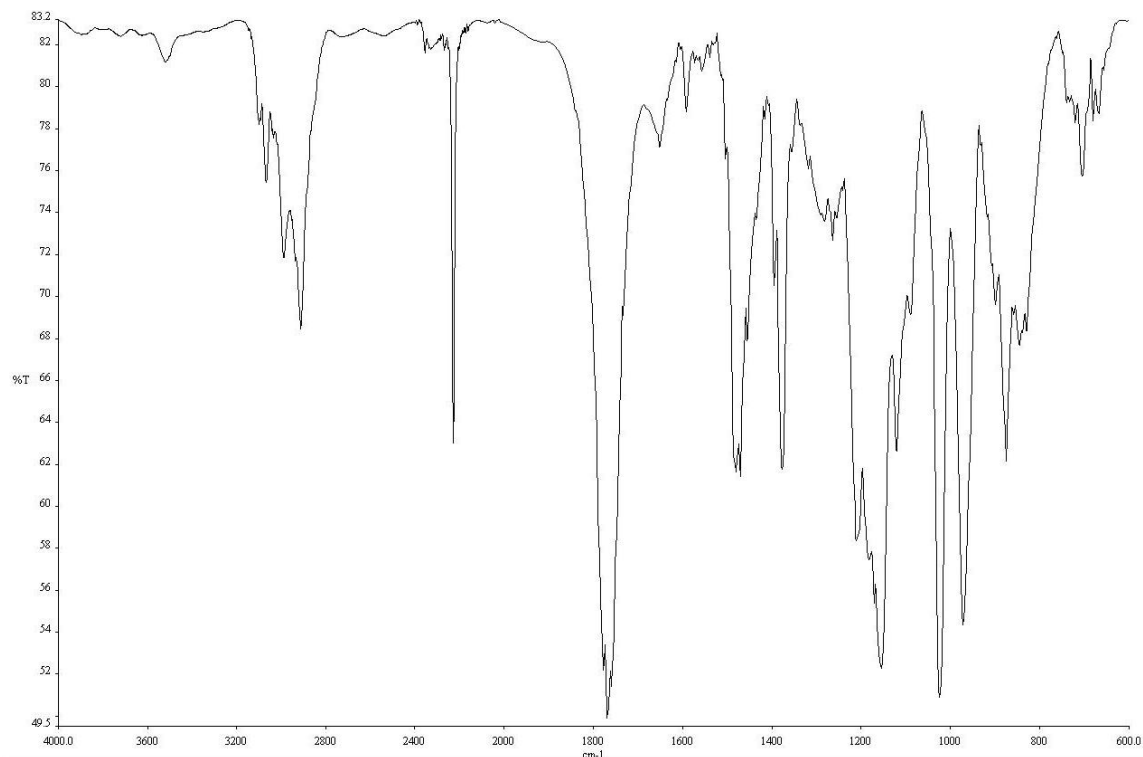
Figure A2.65 IR (NaCl, Thin Film) of compound **S35**.
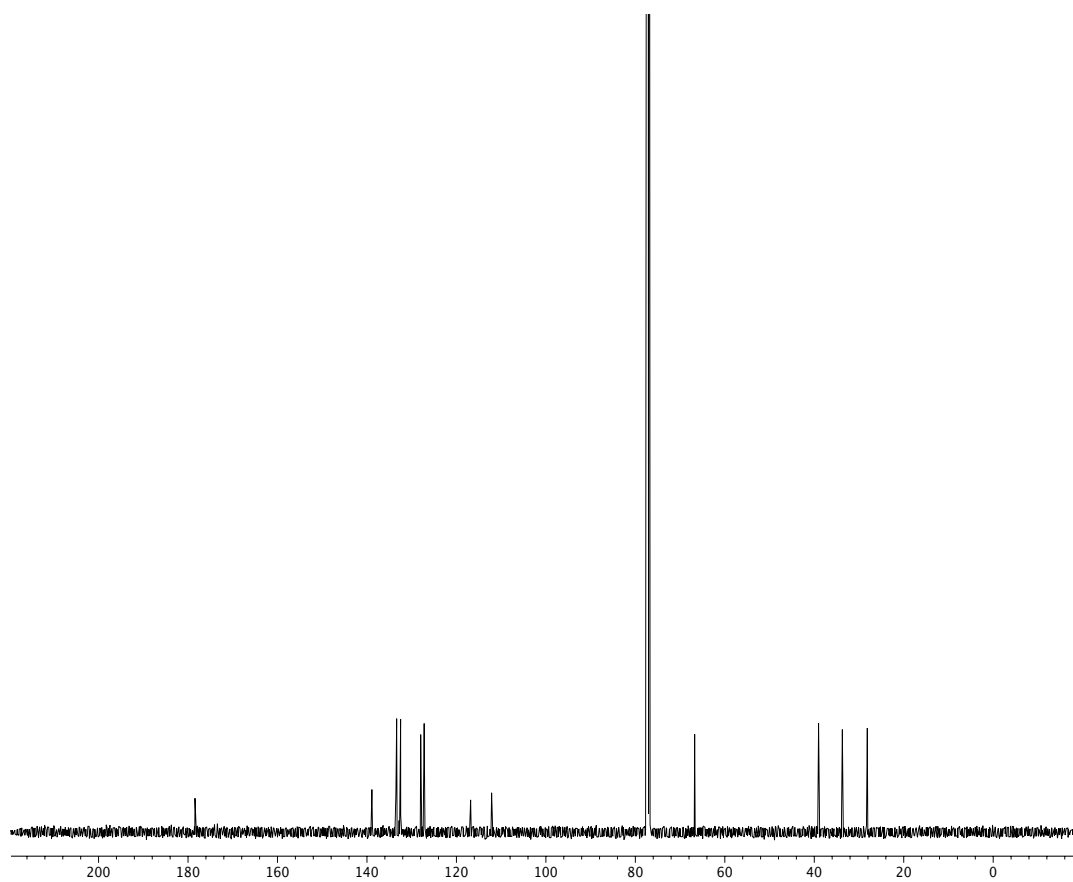
Figure A2.66 ^{13}C NMR (101 MHz, CDCl$_3$) of compound **S35**.
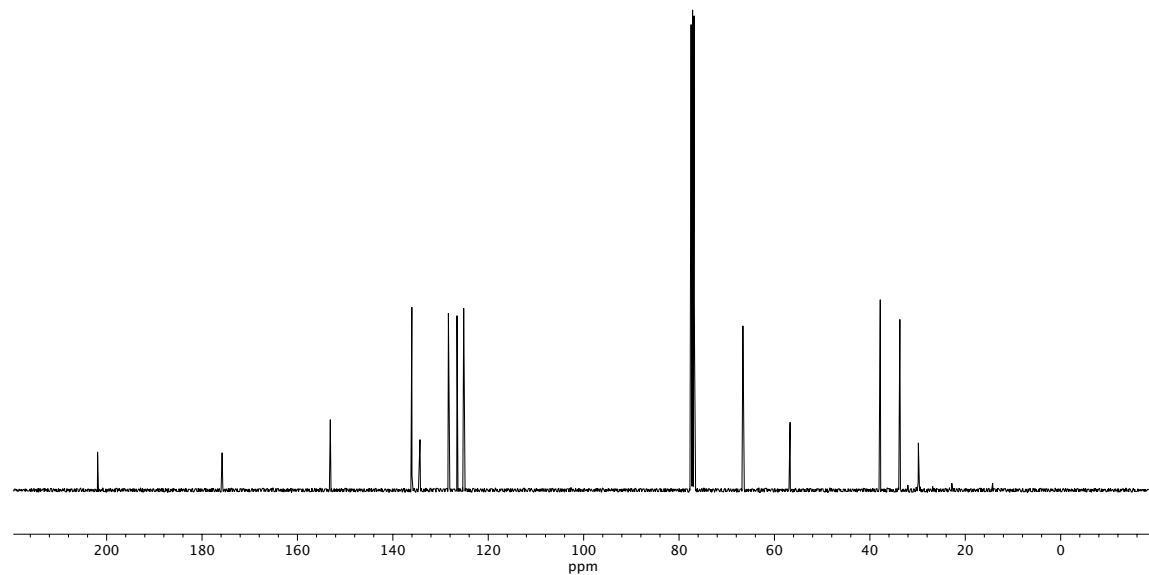
Figure A2.67 ^{1}H NMR (400 MHz, CDCl$_3$) of compound **187a**.
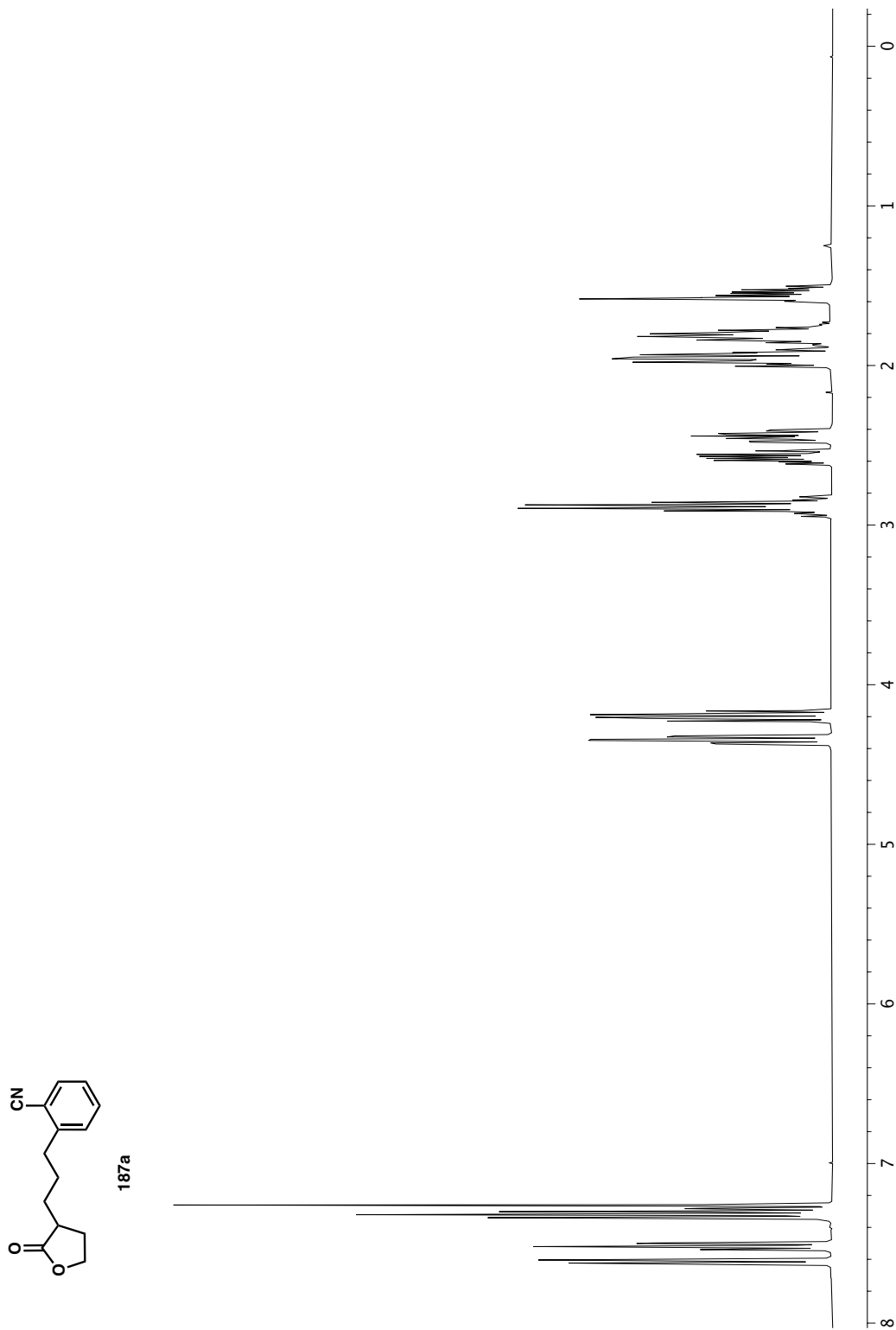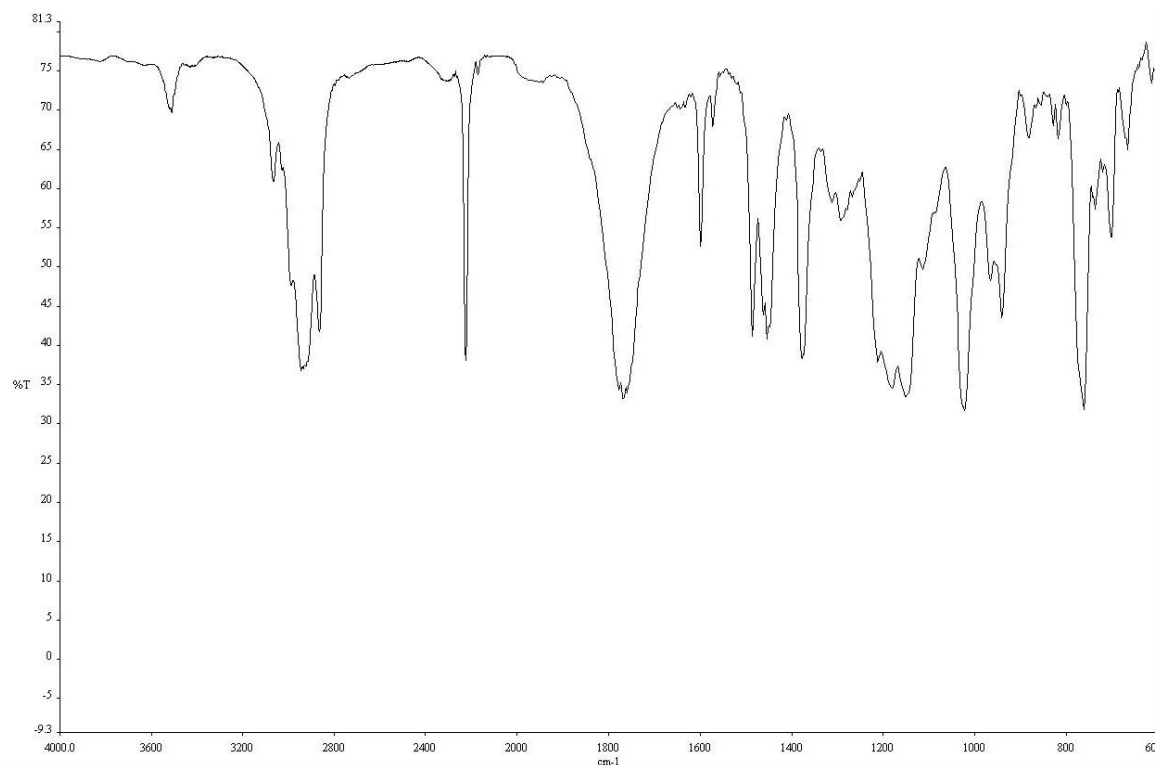
Figure A2.68 IR (NaCl, Thin Film) of compound **187a**.
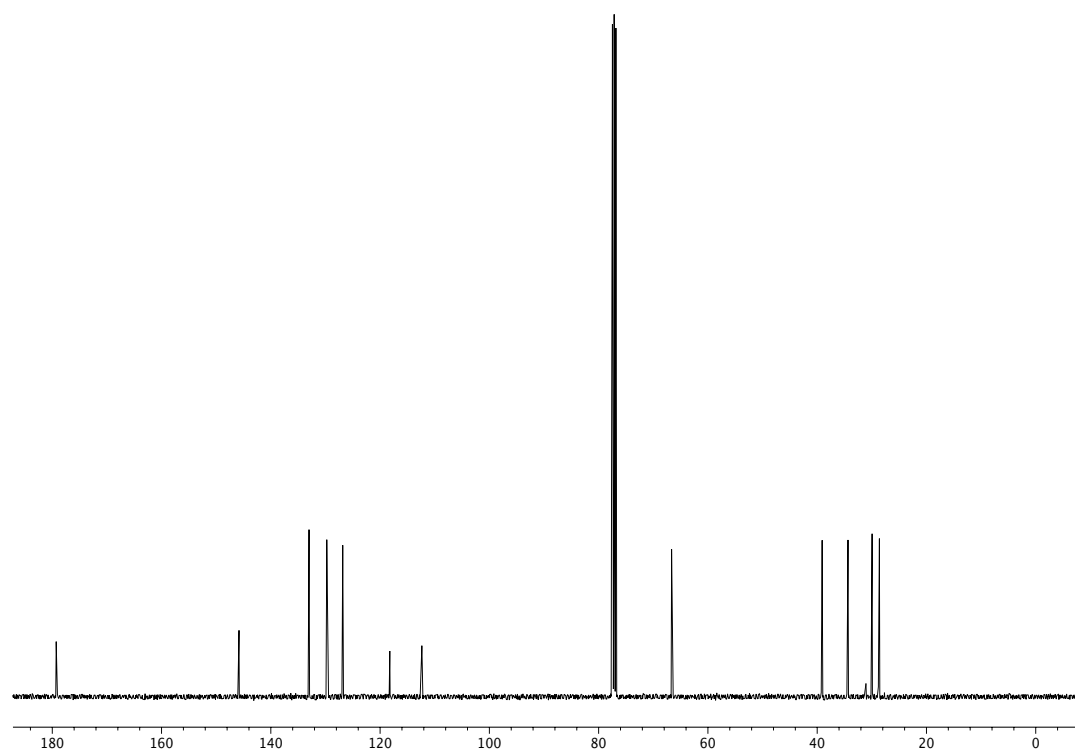
Figure A2.69 ^{13}C NMR (101 MHz, CDCl$_3$) of compound **187a**.

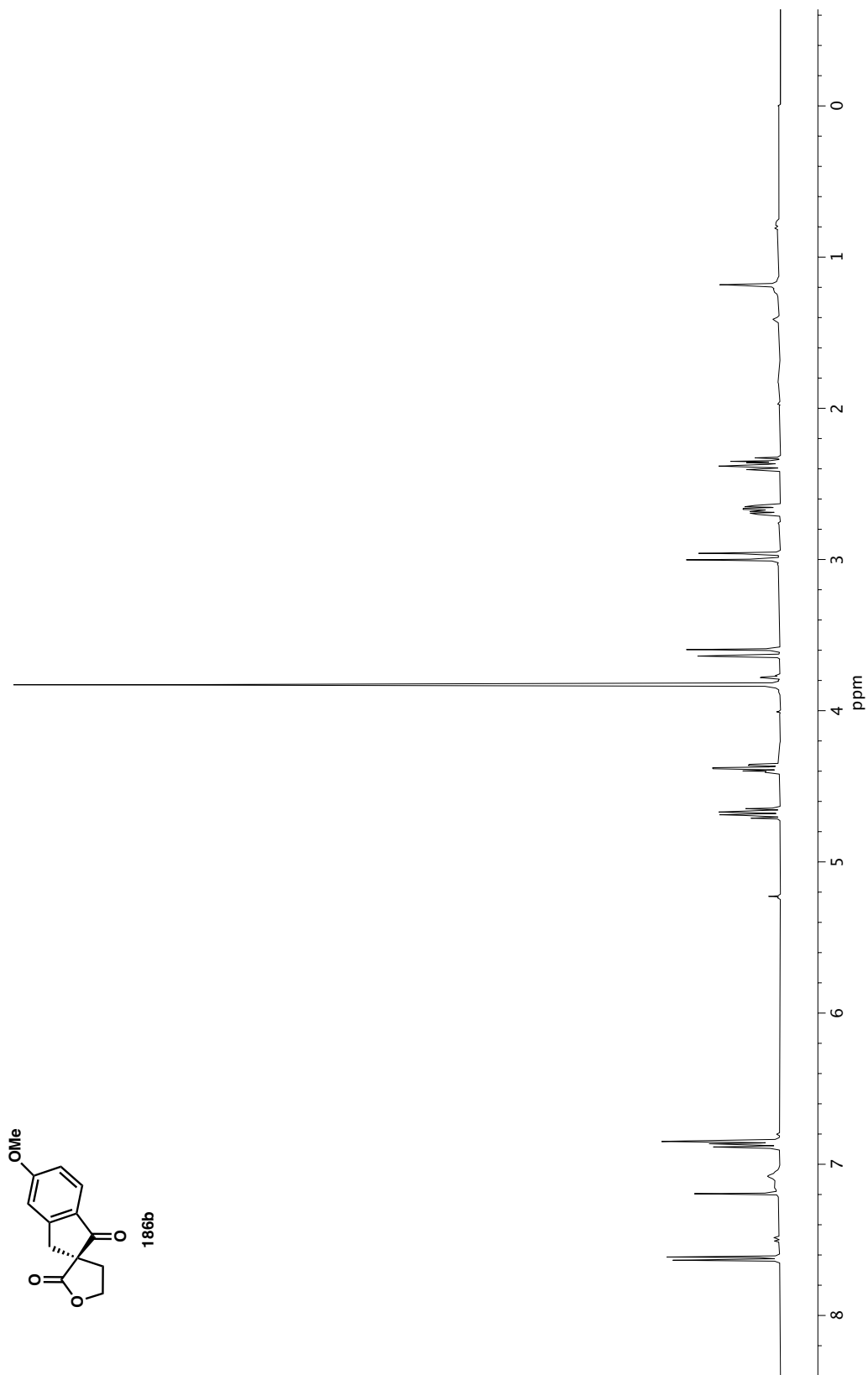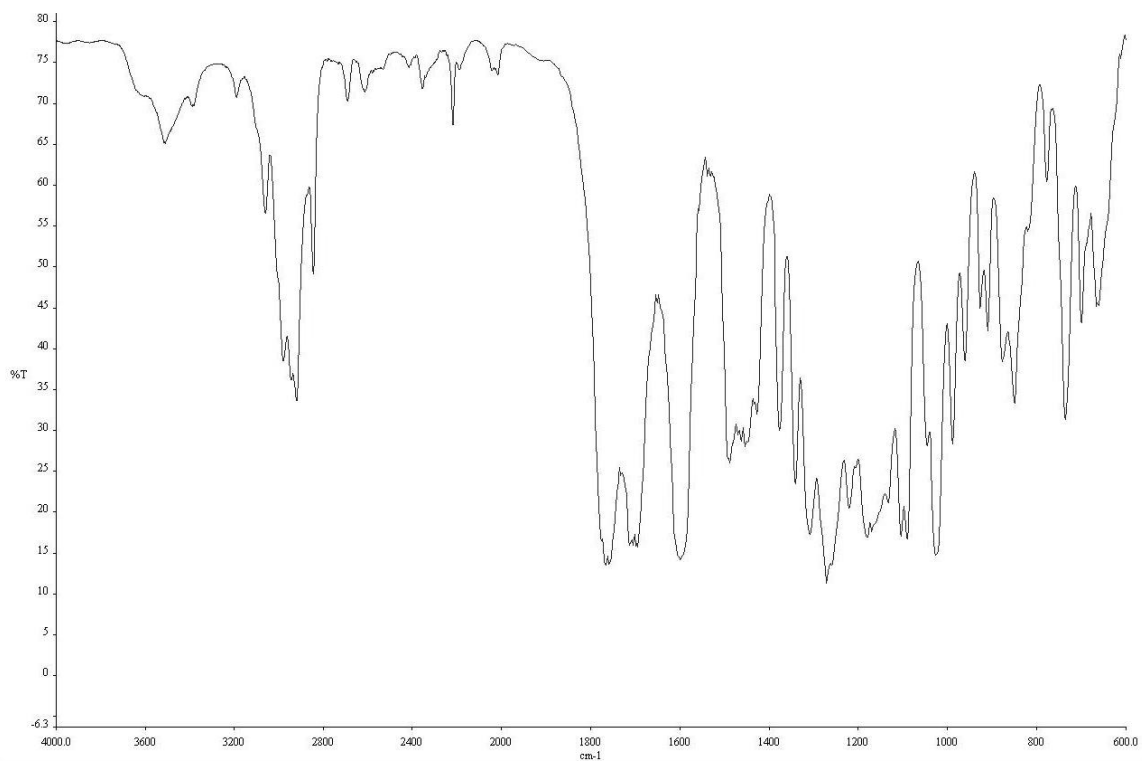***Figure A2.70*** ^{1}H NMR (400 MHz, CDCl$_3$) of compound **187b.**
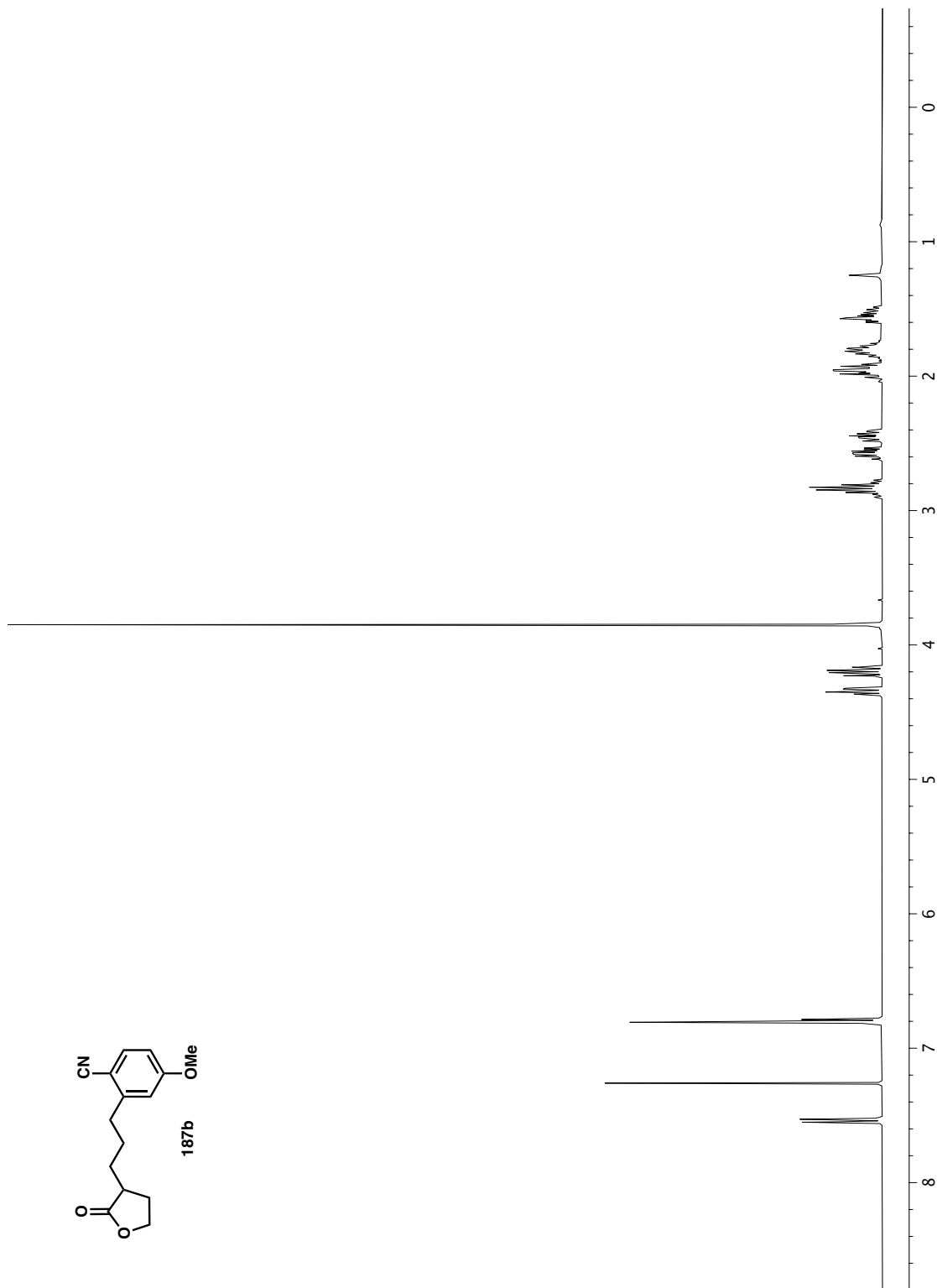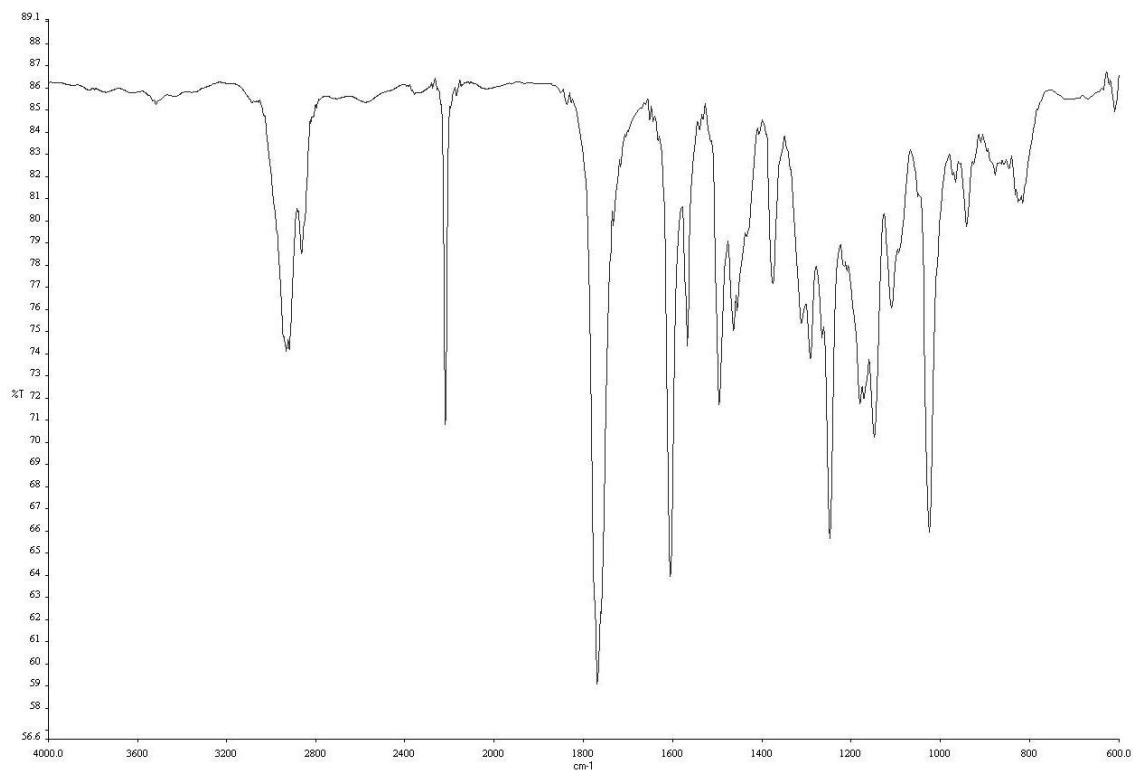
Figure A2.71 IR (NaCl, Thin Film) of compound **187b**.
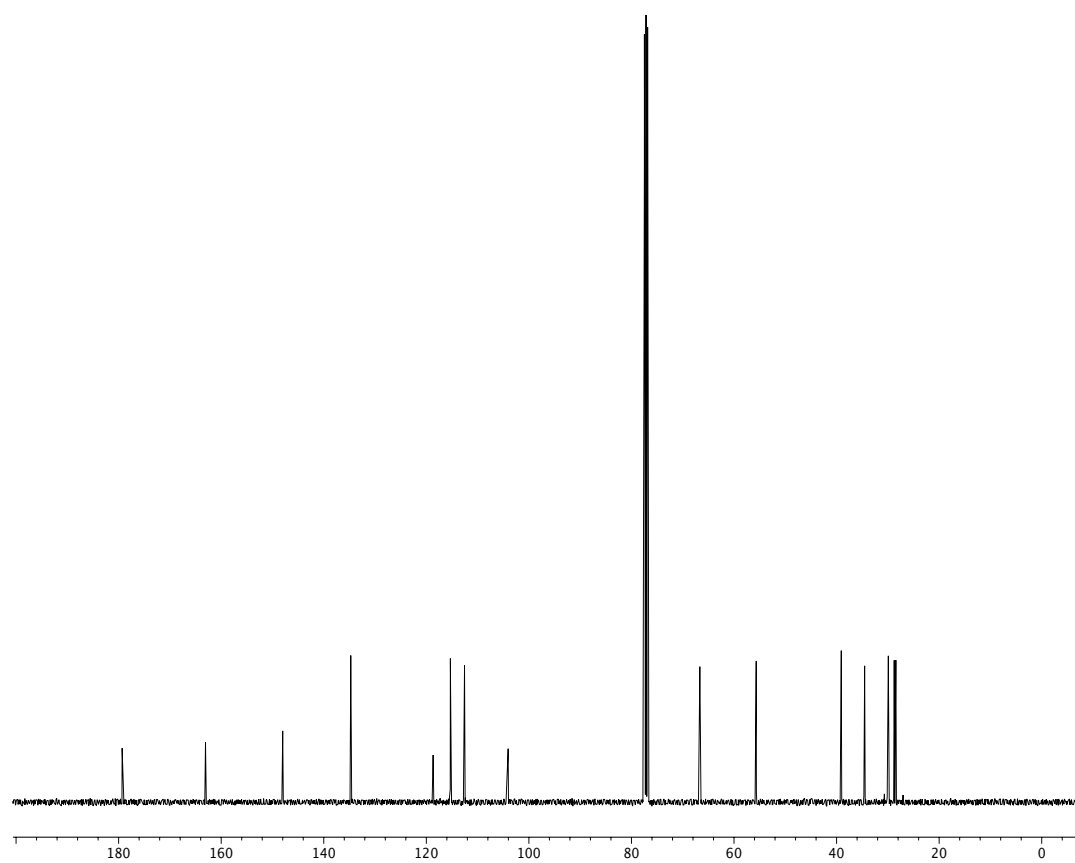
Figure A2.72 ^{13}C NMR (101 MHz, CDCl$_3$) of compound **187b**.
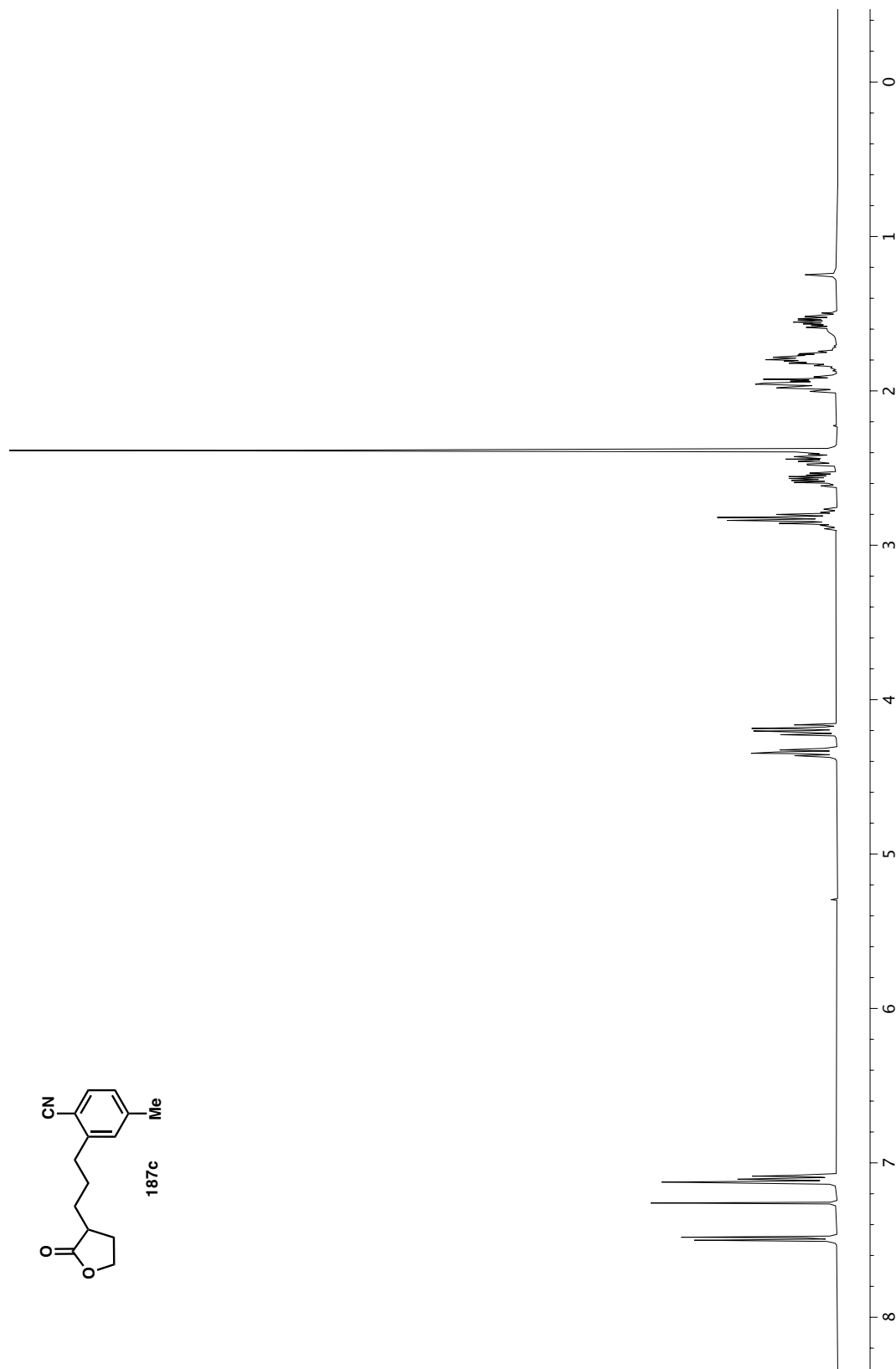
Figure A2.73 ^{1}H NMR (400 MHz, CDCl$_3$) of compound **187c.**
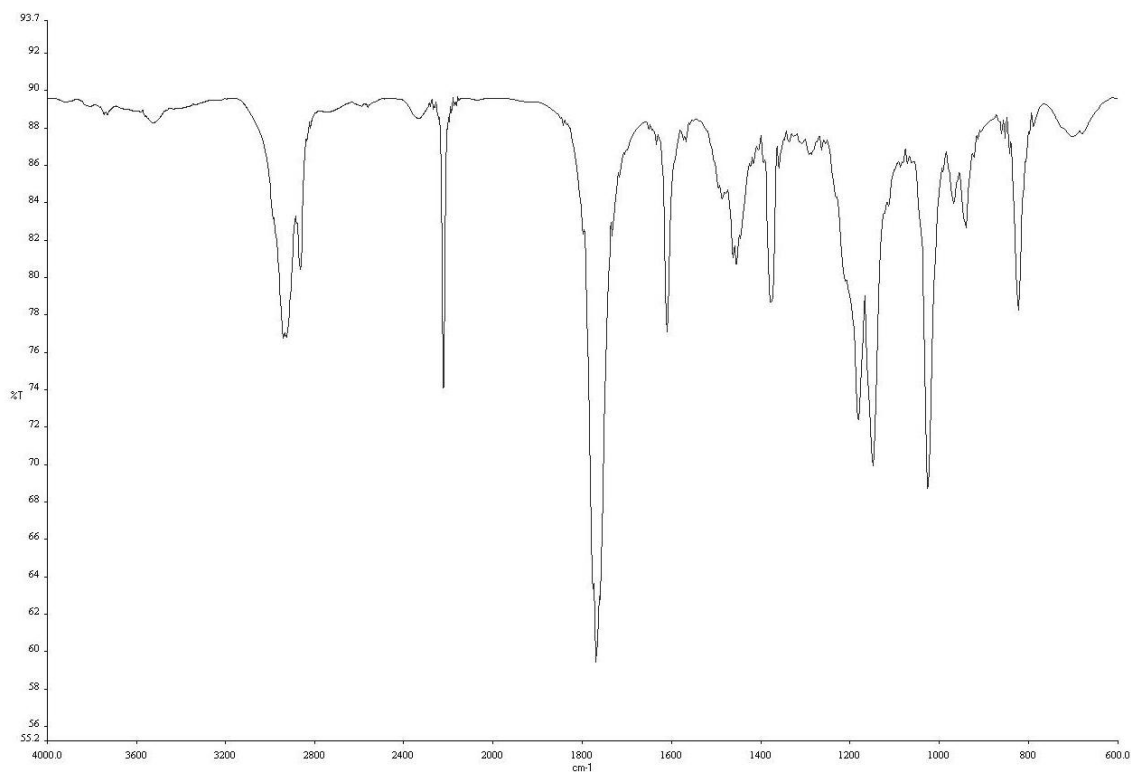
Figure A2.74 IR (NaCl, Thin Film) of compound **187c**.
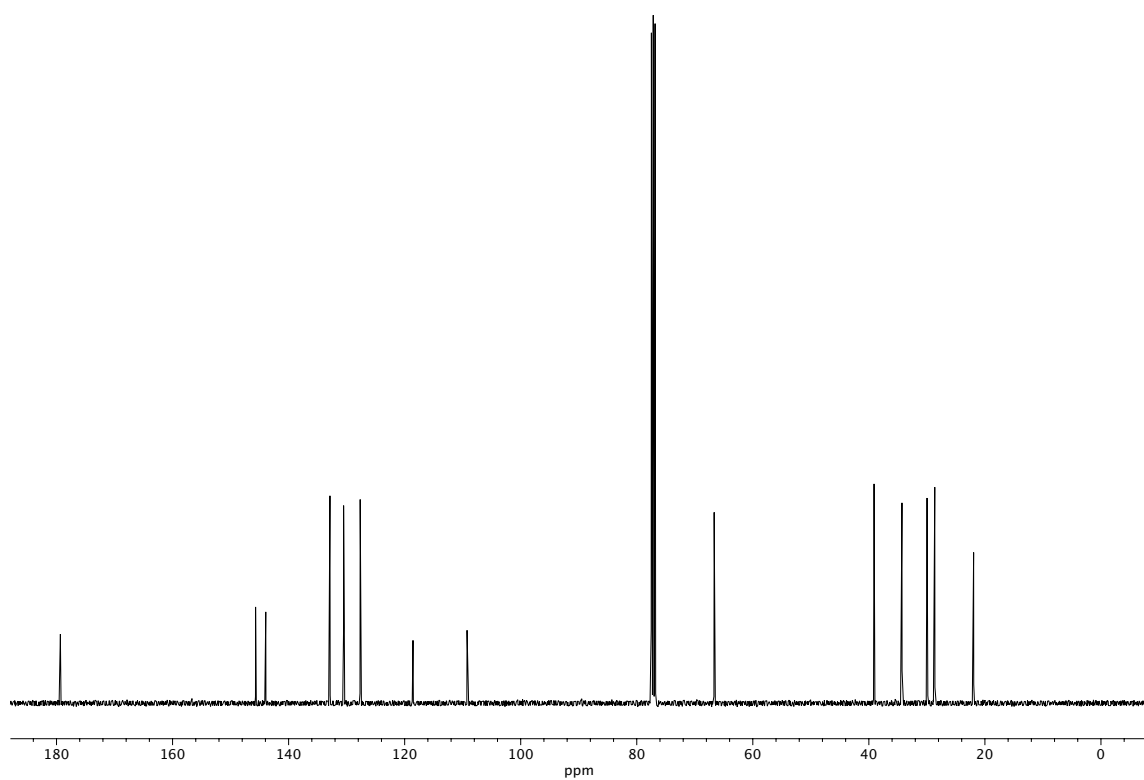
Figure A2.75 ^{13}C NMR (101 MHz, CDCl$_3$) of compound **187c**.
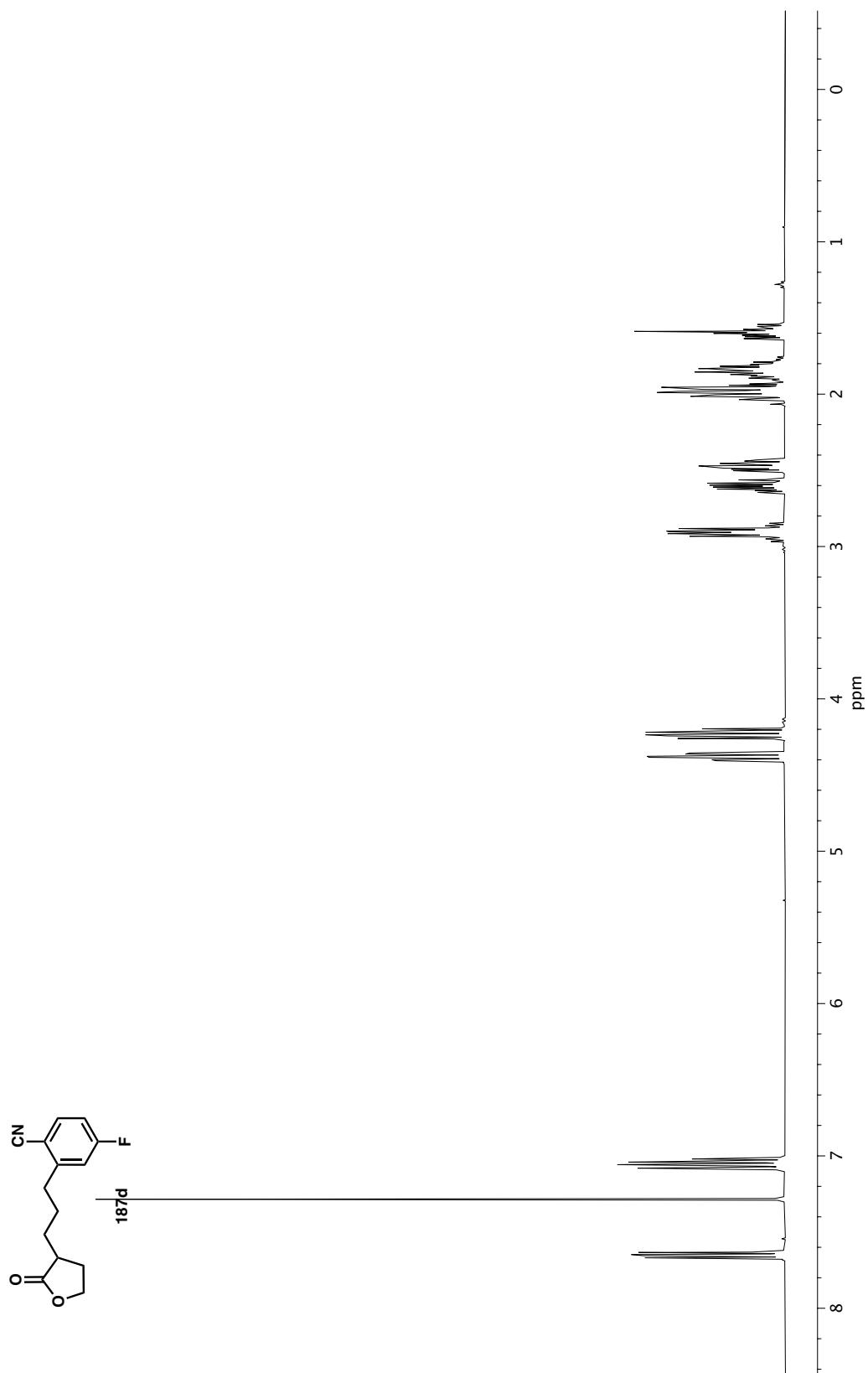
Figure A2.76 ¹H NMR (400 MHz, CDCl₃) of compound **187d.**
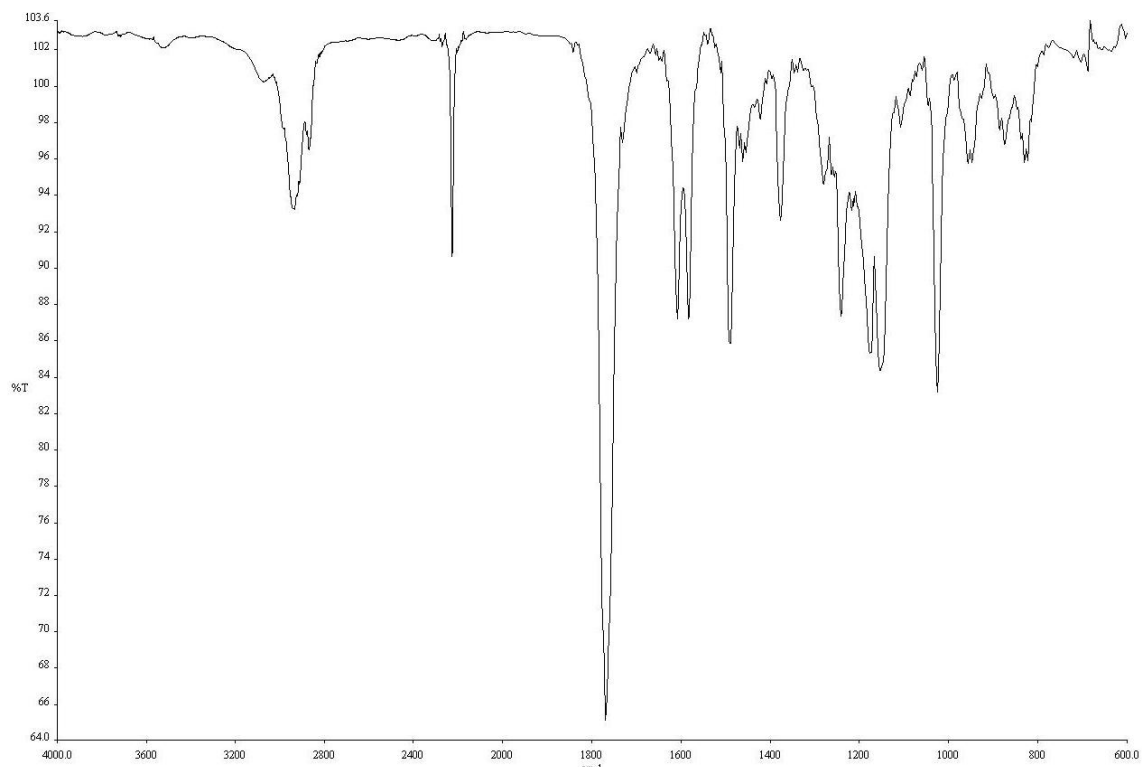
Figure A2.77 IR (NaCl, Thin Film) of compound **187d**.
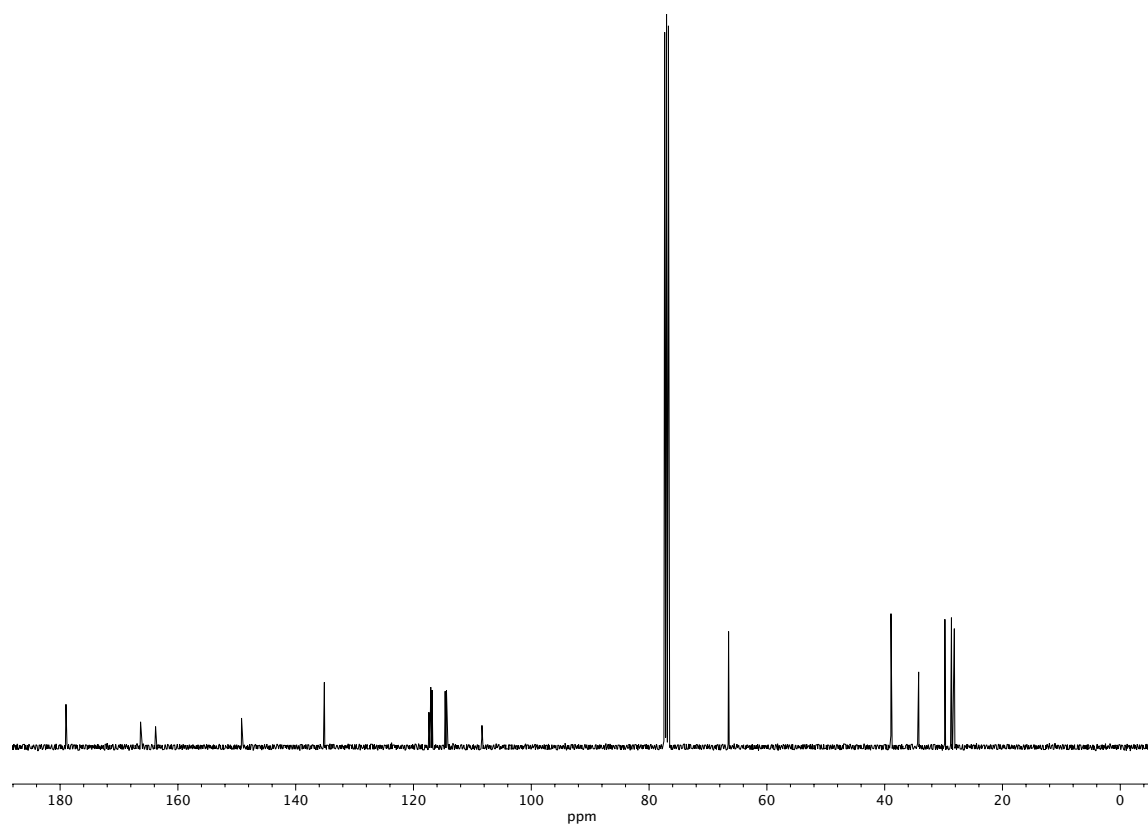
Figure A2.78 ¹³C NMR (101 MHz, CDCl₃) of compound **187d**.
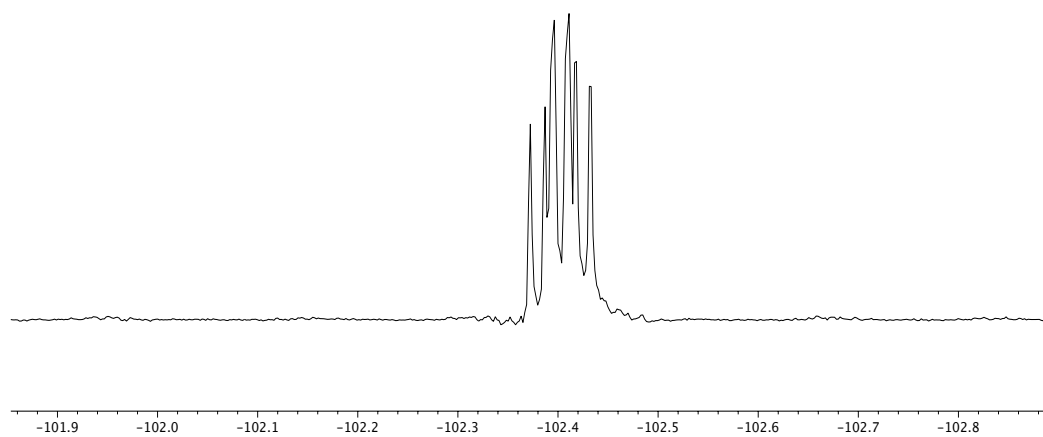
Figure A2.79 ^{19}F NMR (376 MHz, CDCl$_3$) of compound **187d**.
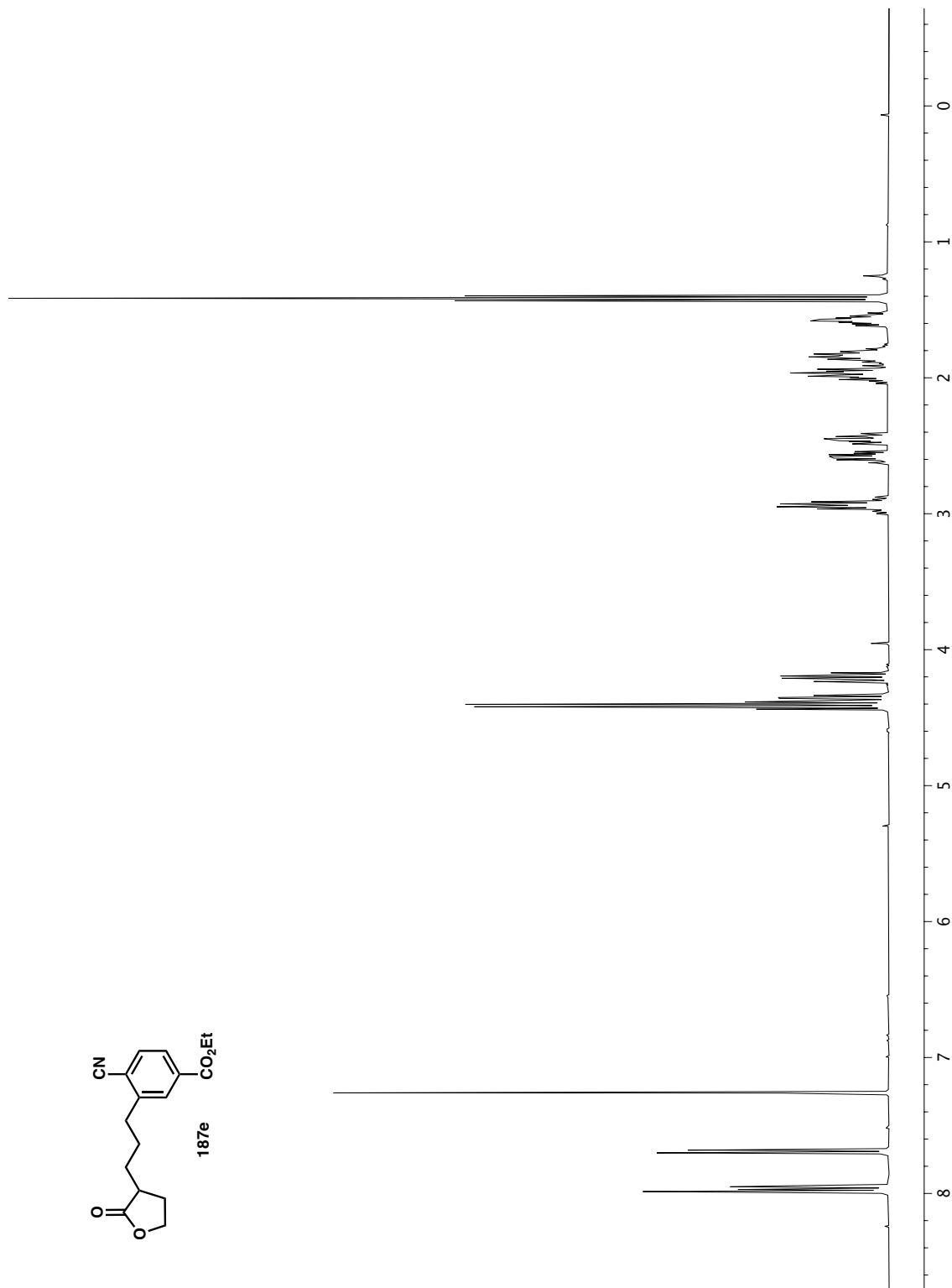
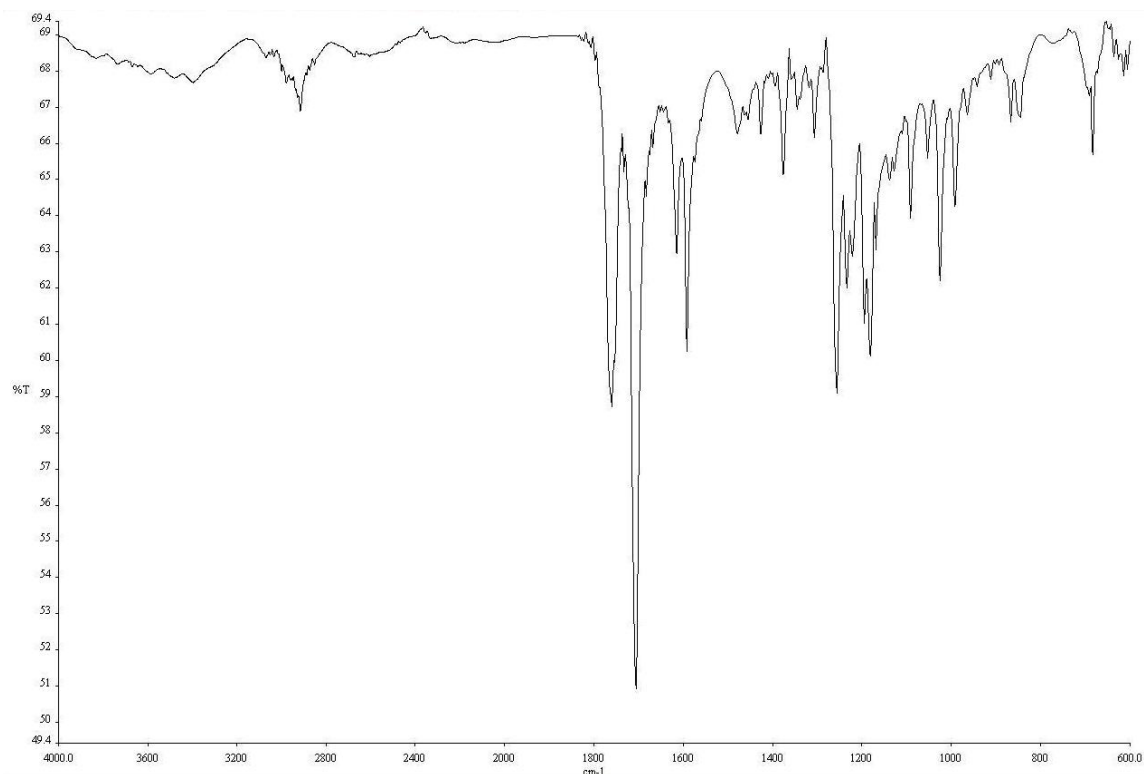*Figure A2.80* ^{1}H NMR (400 MHz, CDCl$_3$) of compound **187e.**
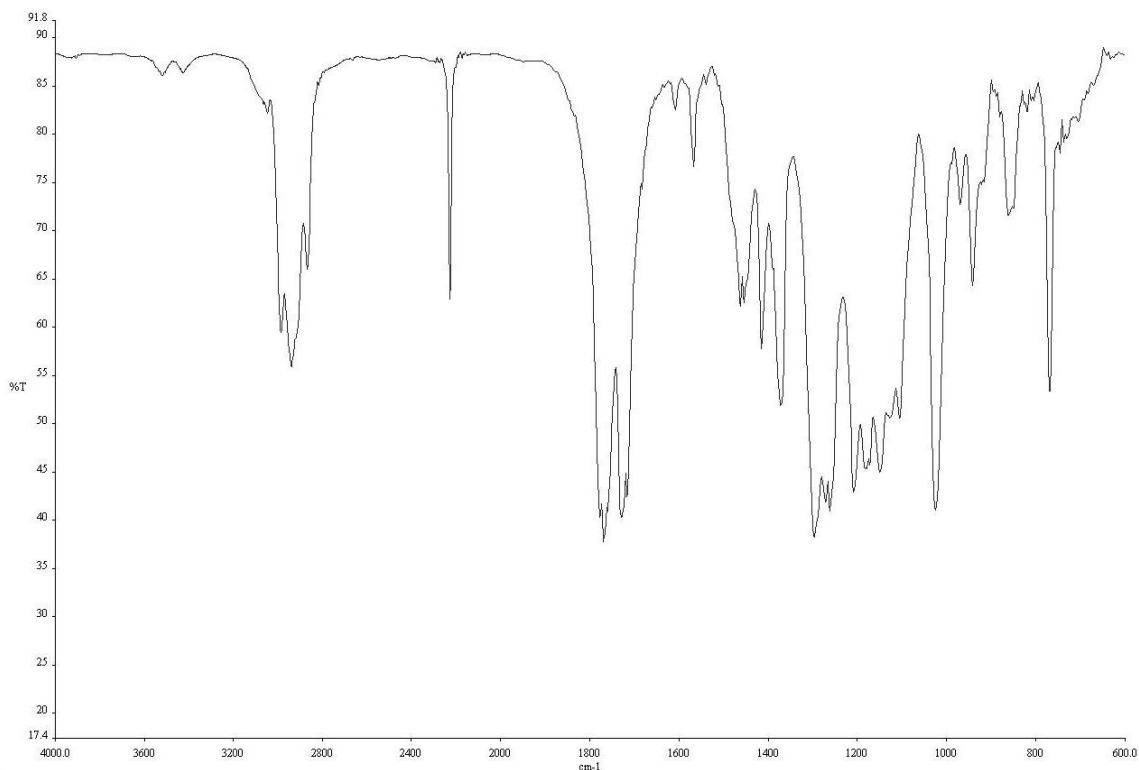
Figure A2.81 IR (NaCl, Thin Film) of compound **187e**.

Figure A2.82 ^{13}C NMR (101 MHz, CDCl$_3$) of compound **187e**.

Figure A2.83 ^{1}H NMR (400 MHz, CDCl$_3$) of compound **187f.**

Figure A2.84 IR (NaCl, Thin Film) of compound **187f**.
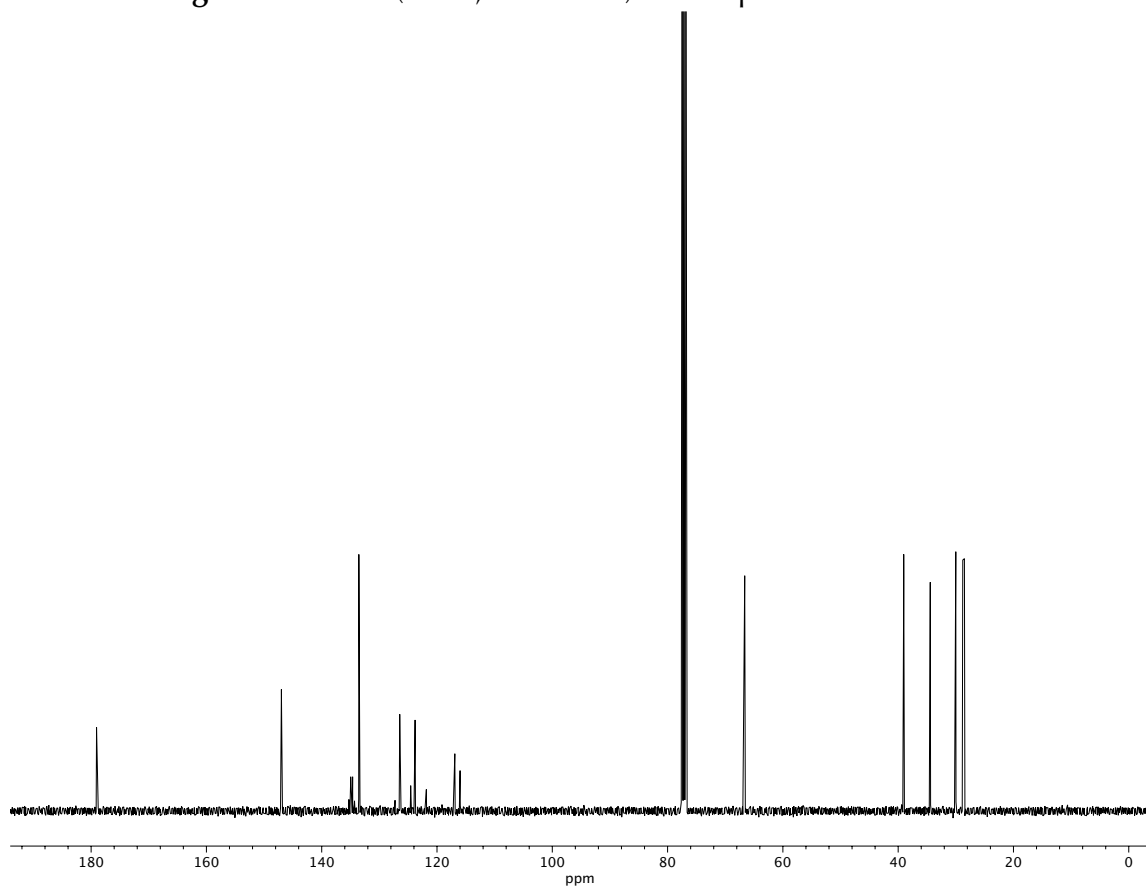
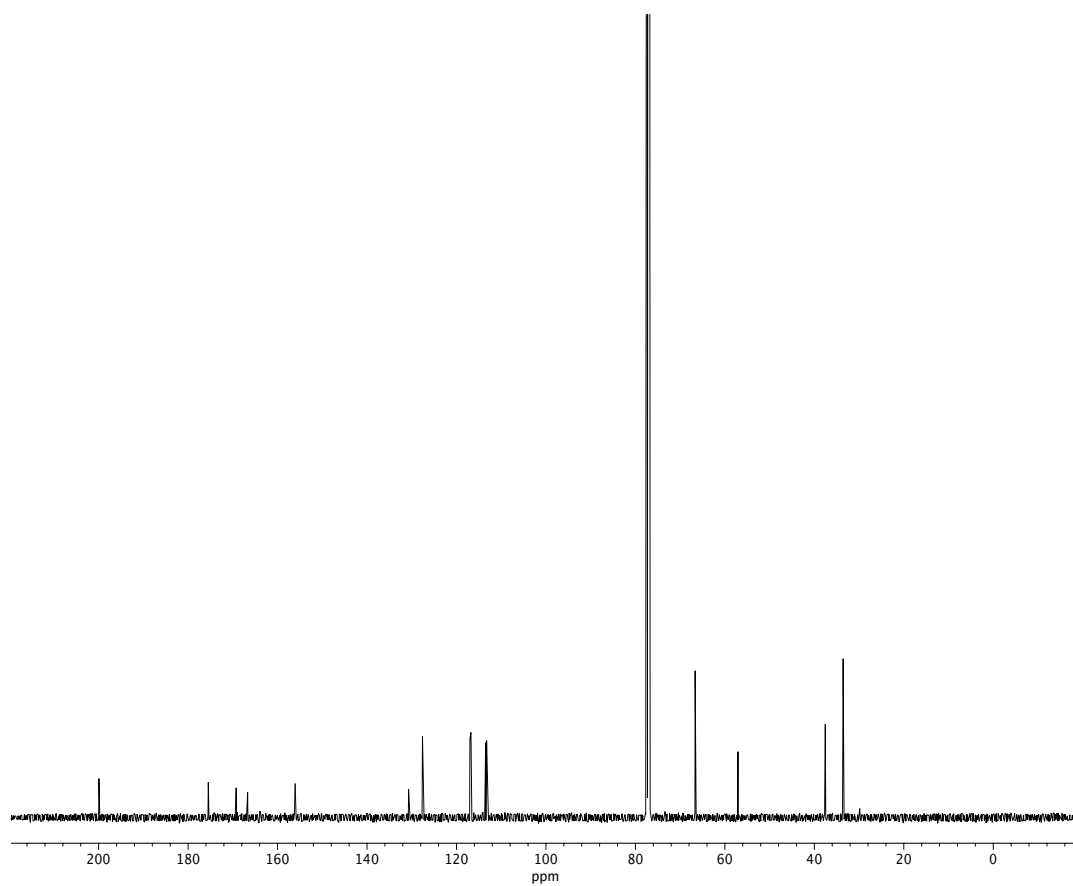***Figure A2.85*** ^{13}C NMR (101 MHz, CDCl$_3$) of compound **187f**.

Figure A2.86 ^{19}F NMR (376 MHz, CDCl$_3$) of compound **187f.**

Figure A2.87 ^{1}H NMR (400 MHz, CDCl$_3$) of compound **187g.**

Figure A2.88 IR (NaCl, Thin Film) of compound **187g**.
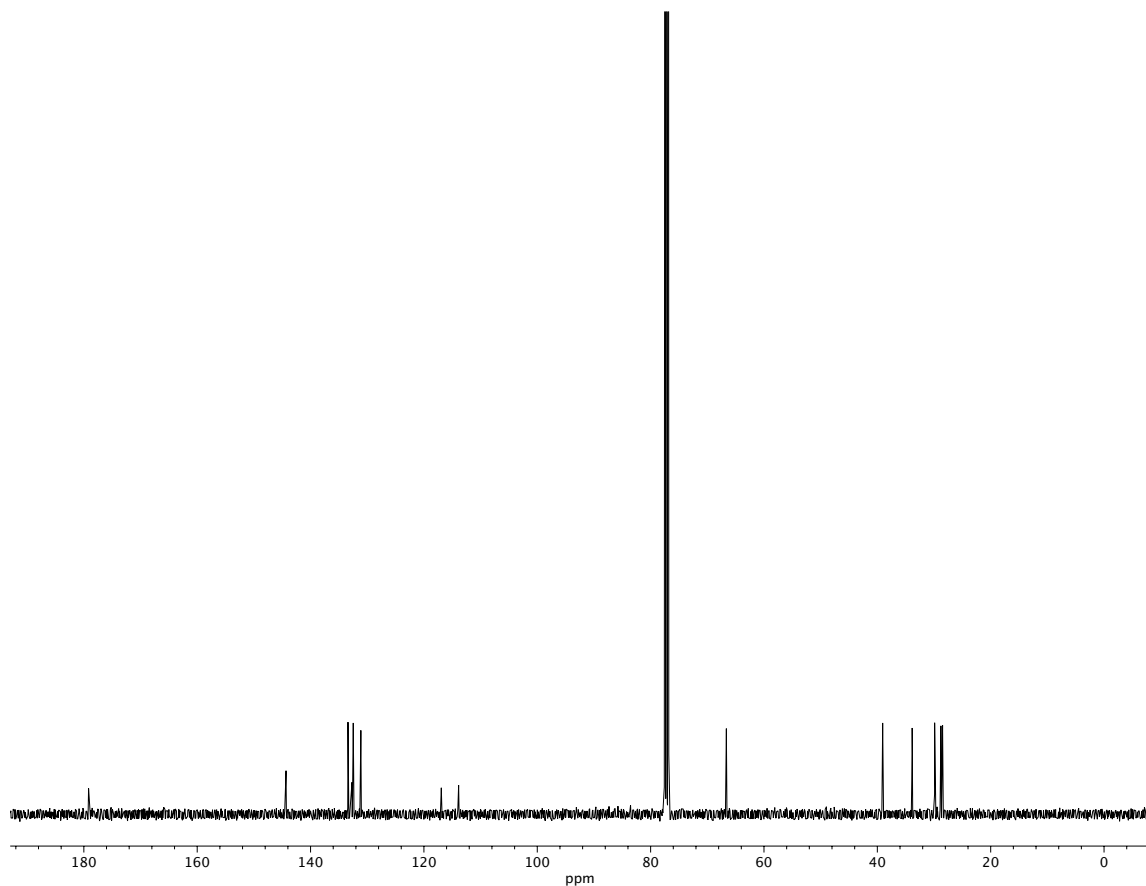
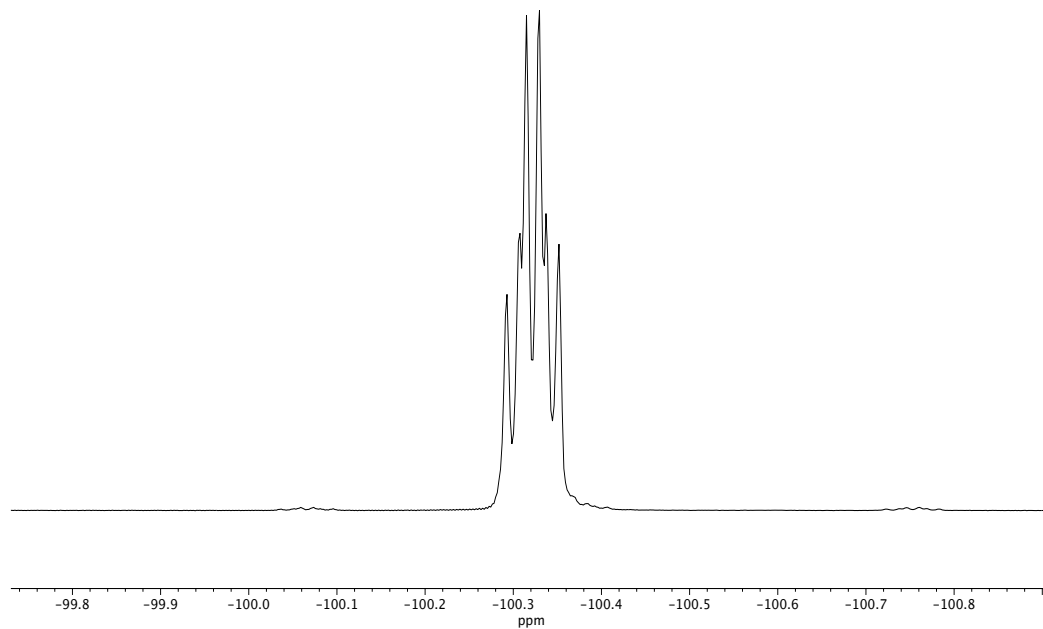***Figure A2.89*** ^{13}C NMR (101 MHz, CDCl$_3$) of compound **187g**.

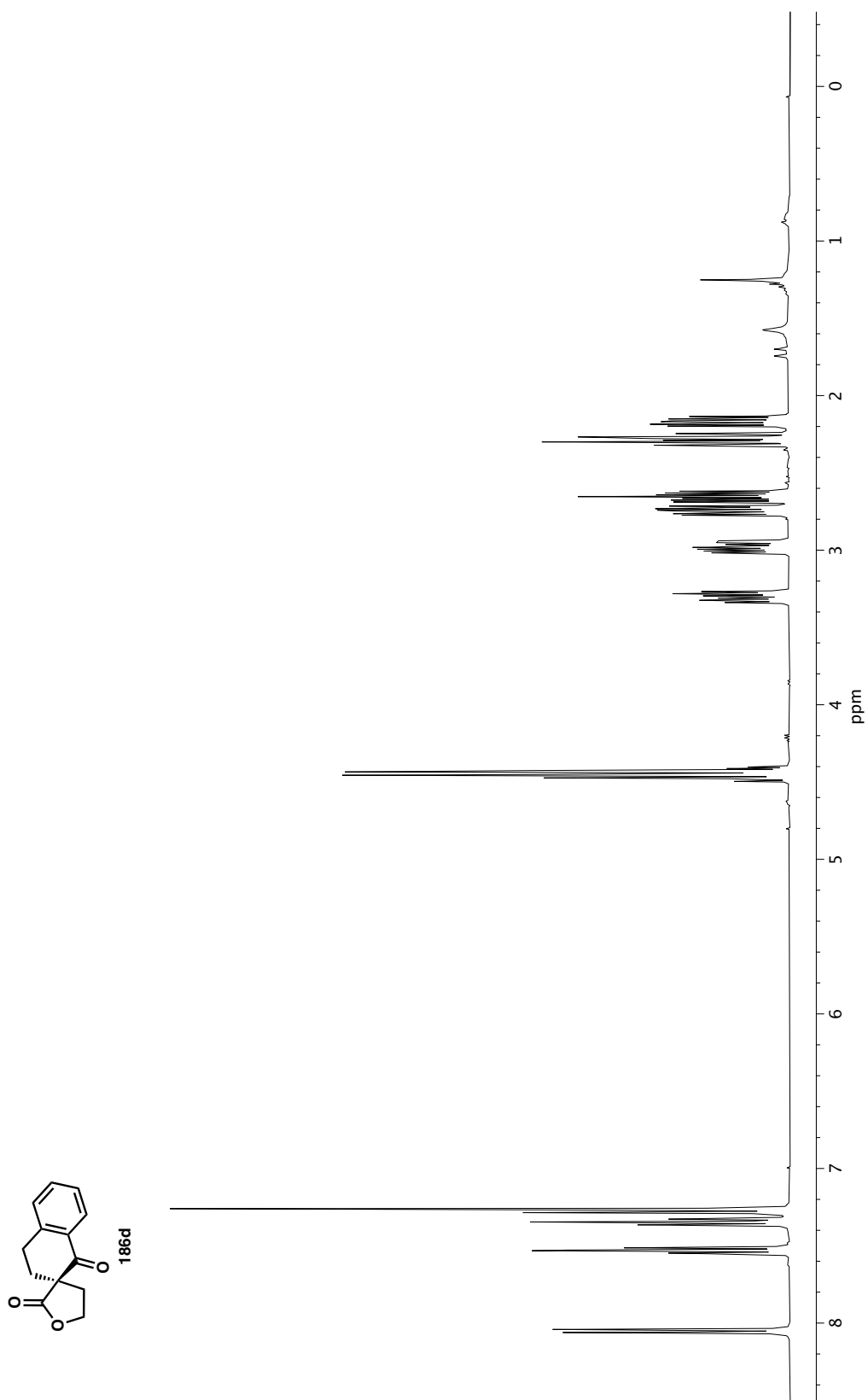**Figure A2.90** ^{1}H NMR (400 MHz, CDCl$_3$) of compound **S37.**

Figure A2.91 IR (NaCl, Thin Film) of compound **S37**.

Figure A2.92 ^{13}C NMR (101 MHz, CDCl$_3$) of compound **S37**.

Figure A2.93 ¹H NMR (400 MHz, CDCl$_3$) of compound **187h.**

Figure A2.94 IR (NaCl, Thin Film) of compound **187h**.

Figure A2.95 ^{13}C NMR (101 MHz, CDCl$_3$) of compound **187h**.
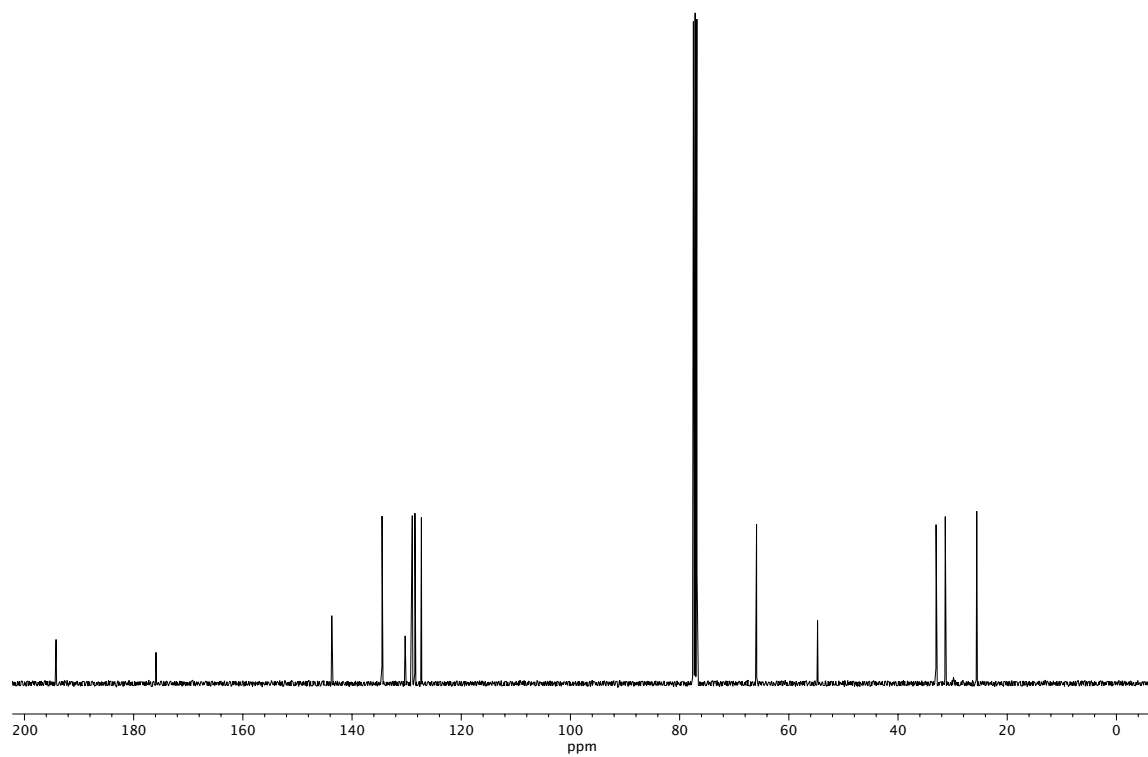
Figure A2.96 ¹H NMR (400 MHz, CDCl₃) of compound **S39.**

Figure A2.97 IR (NaCl, Thin Film) of compound **S39**.
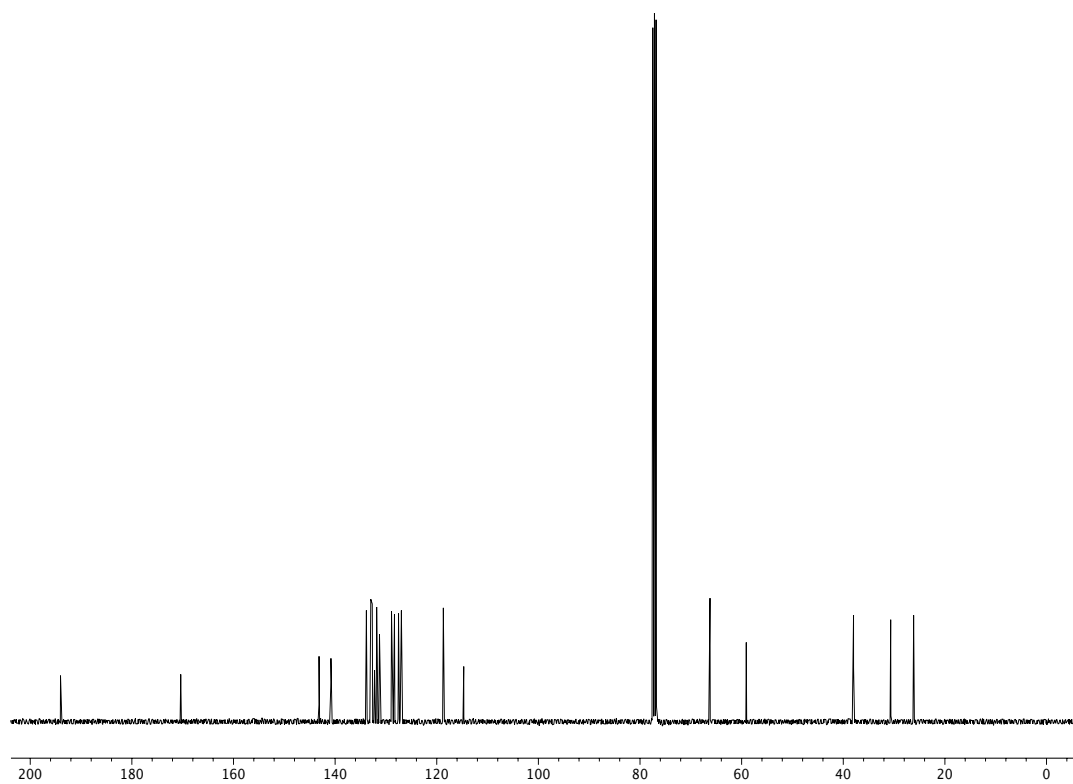
Figure A2.98 ^{13}C NMR (101 MHz, CDCl$_3$) of compound **S39**.

Figure A2.99 ^{1}H NMR (400 MHz, CDCl$_3$) of compound **192**.

Figure A2.100 IR (NaCl, Thin Film) of compound **192**.
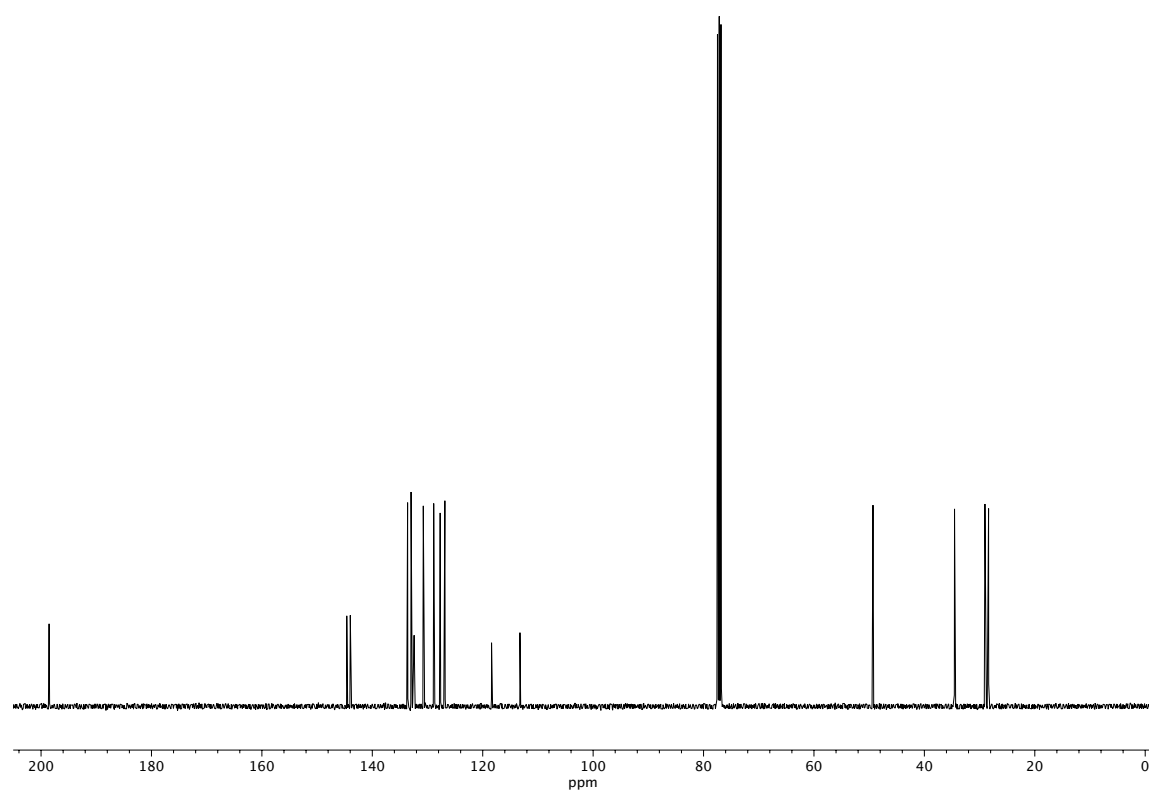
Figure A2.101 ^{13}C NMR (101 MHz, CDCl$_3$) of compound **192**.

Figure A2.102 ^{1}H NMR (400 MHz, CDCl$_3$) of compound **183.**

Figure A2.103 IR (NaCl, Thin Film) of compound **183**.
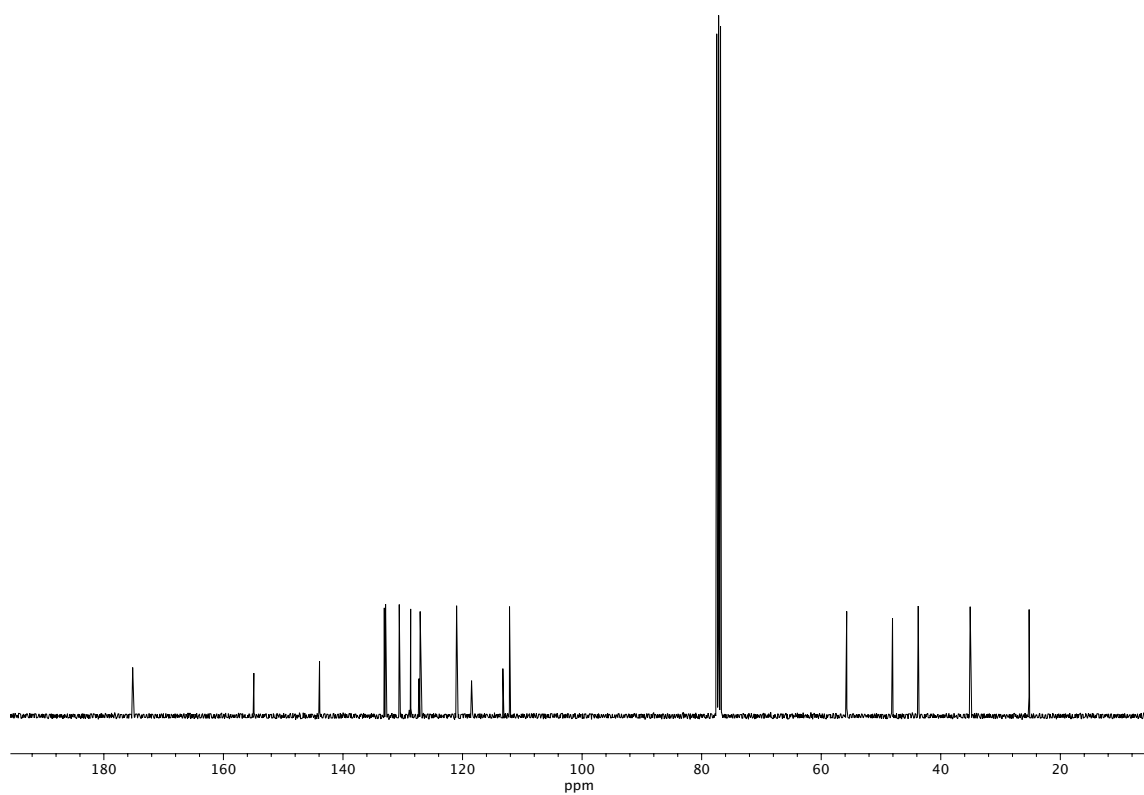
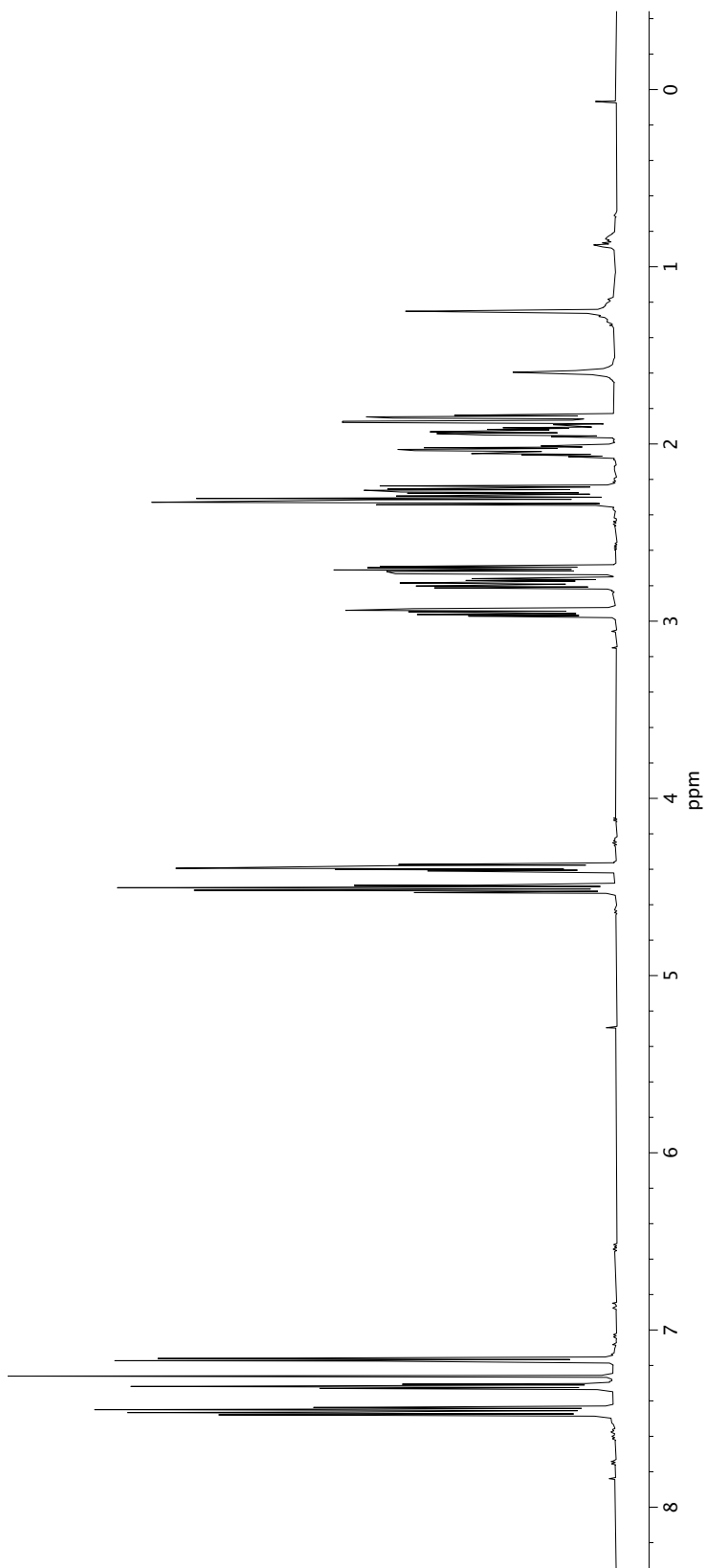**Figure A2.104** ^{13}C NMR (101 MHz, CDCl$_3$) of compound **183**.
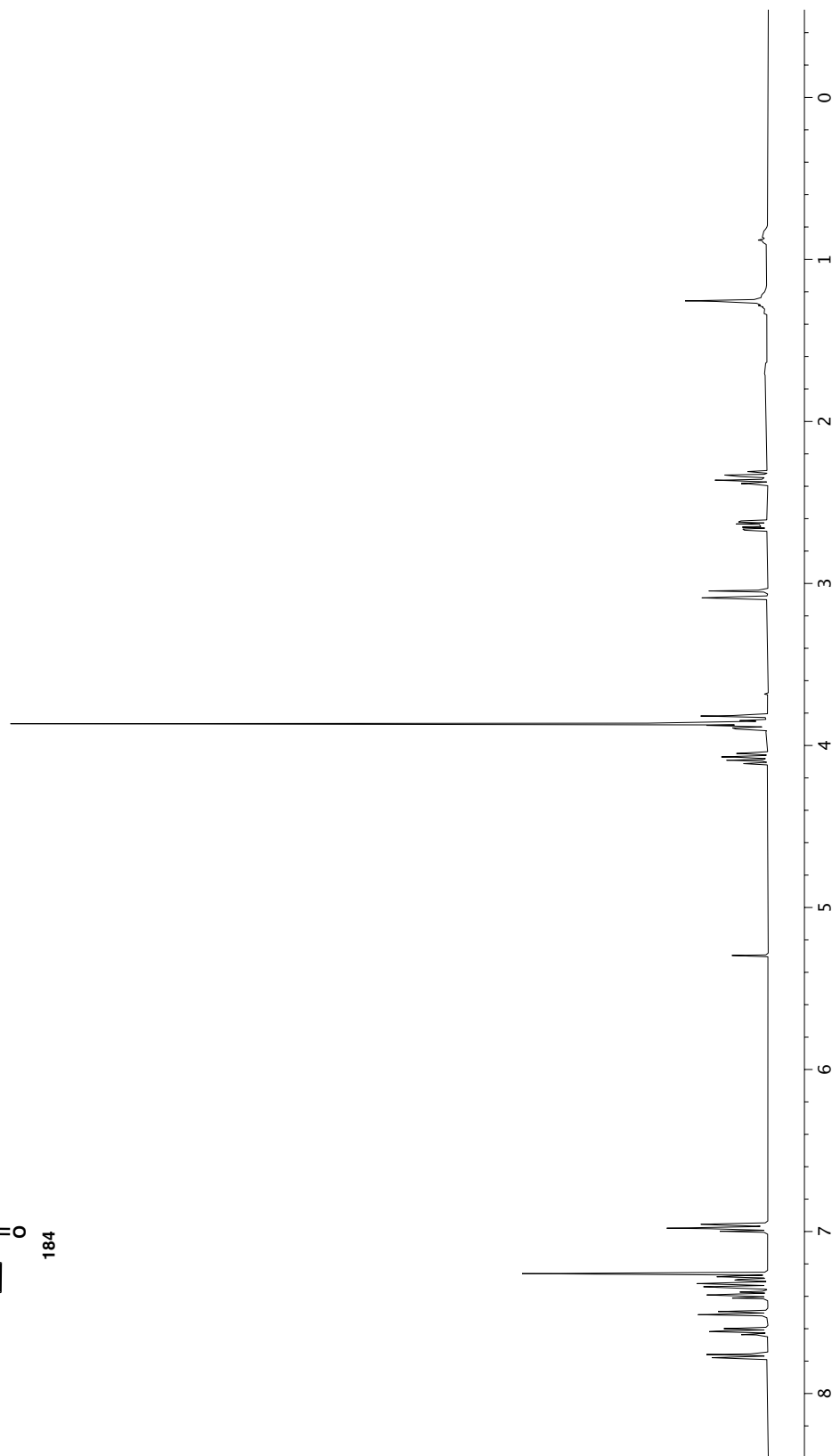
Figure A2.105 ^{1}H NMR (400 MHz, CDCl$_3$) of compound **184.**

Figure A2.106 IR (NaCl, Thin Film) of compound **184**.
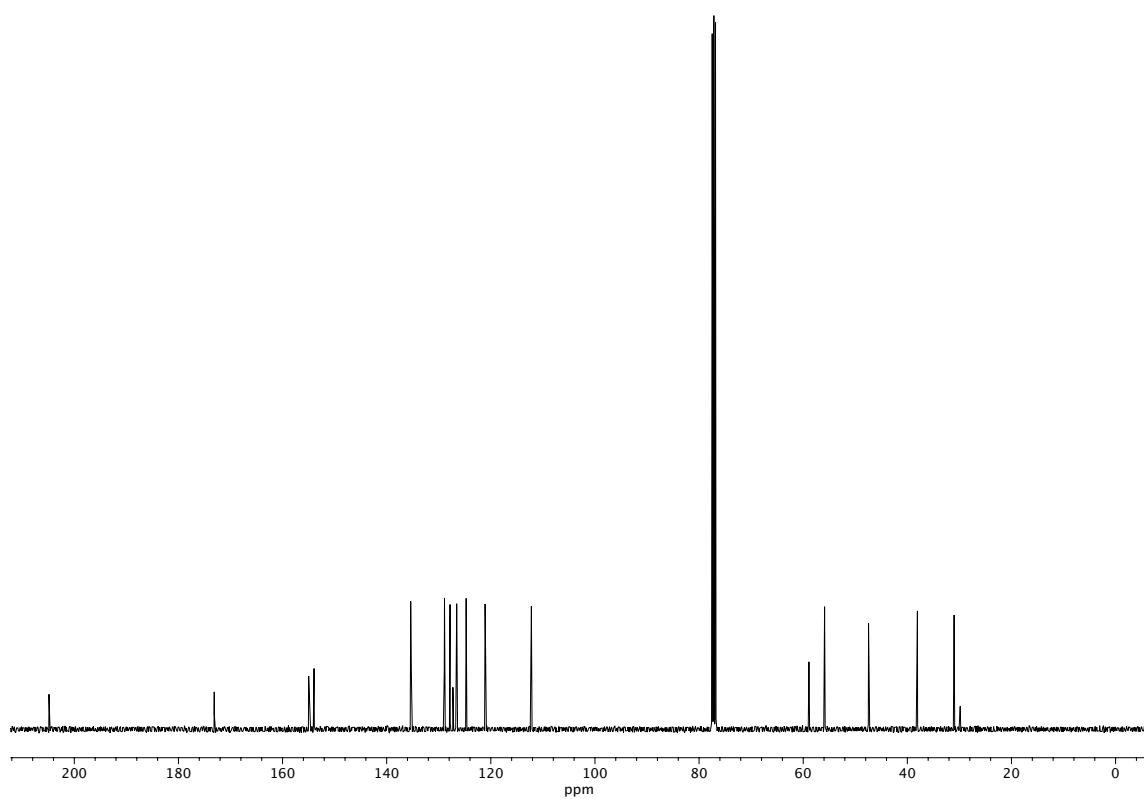
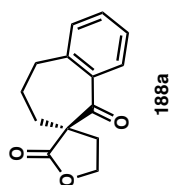***Figure A2.107*** ^{13}C NMR (101 MHz, CDCl$_3$) of compound **184**.

Figure A2.108 ^{1}H NMR (400 MHz, CDCl$_3$) of compound **186a**.
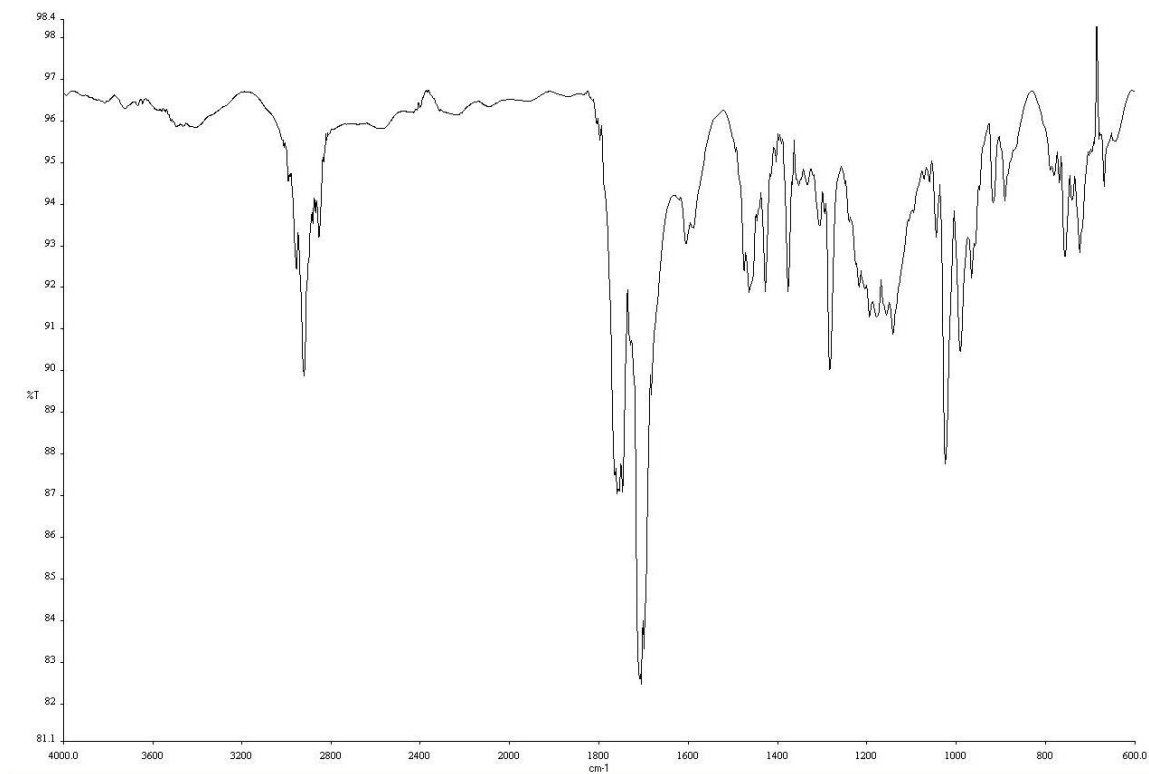
Figure A2.109 IR (NaCl, Thin Film) of compound **186a**.

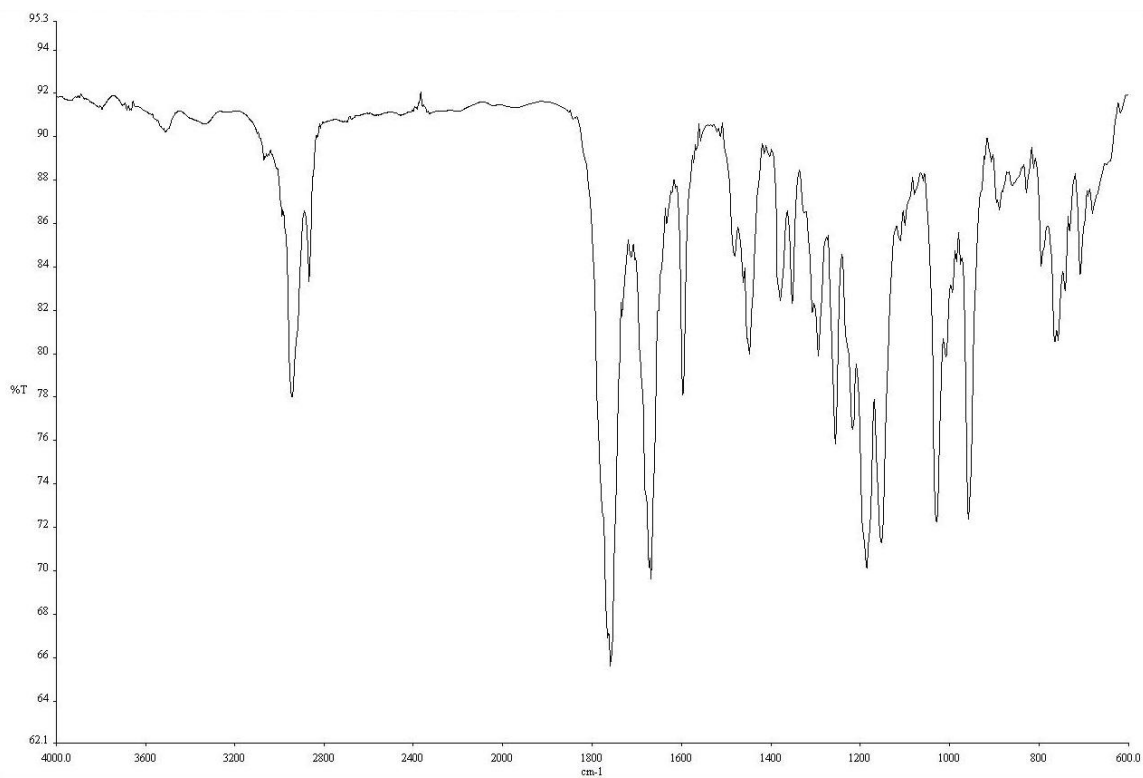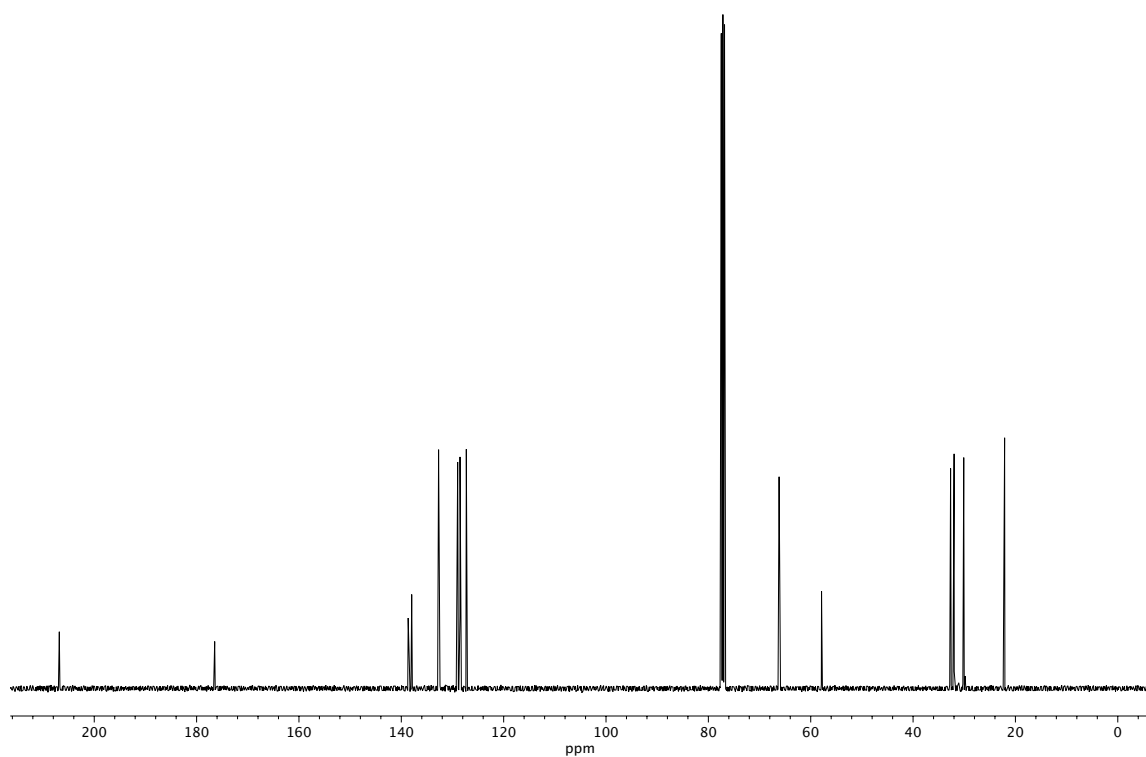**Figure A2.110** ^{13}C NMR (101 MHz, CDCl$_3$) of compound **186a**.

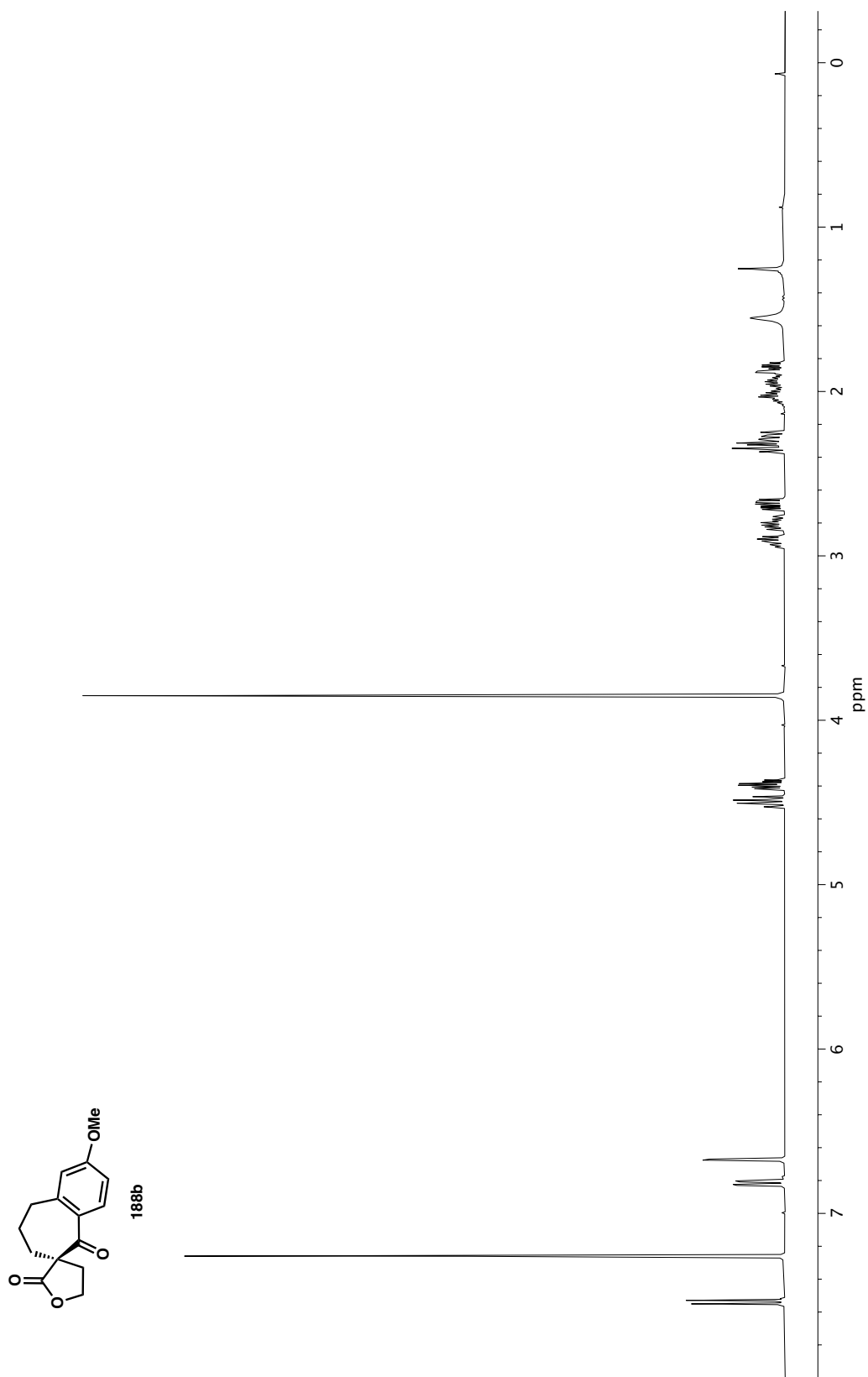***Figure A2.111*** ^{1}H NMR (400 MHz, CDCl$_3$) of compound **186b.**

Figure A2.112 IR (NaCl, Thin Film) of compound **186b**.
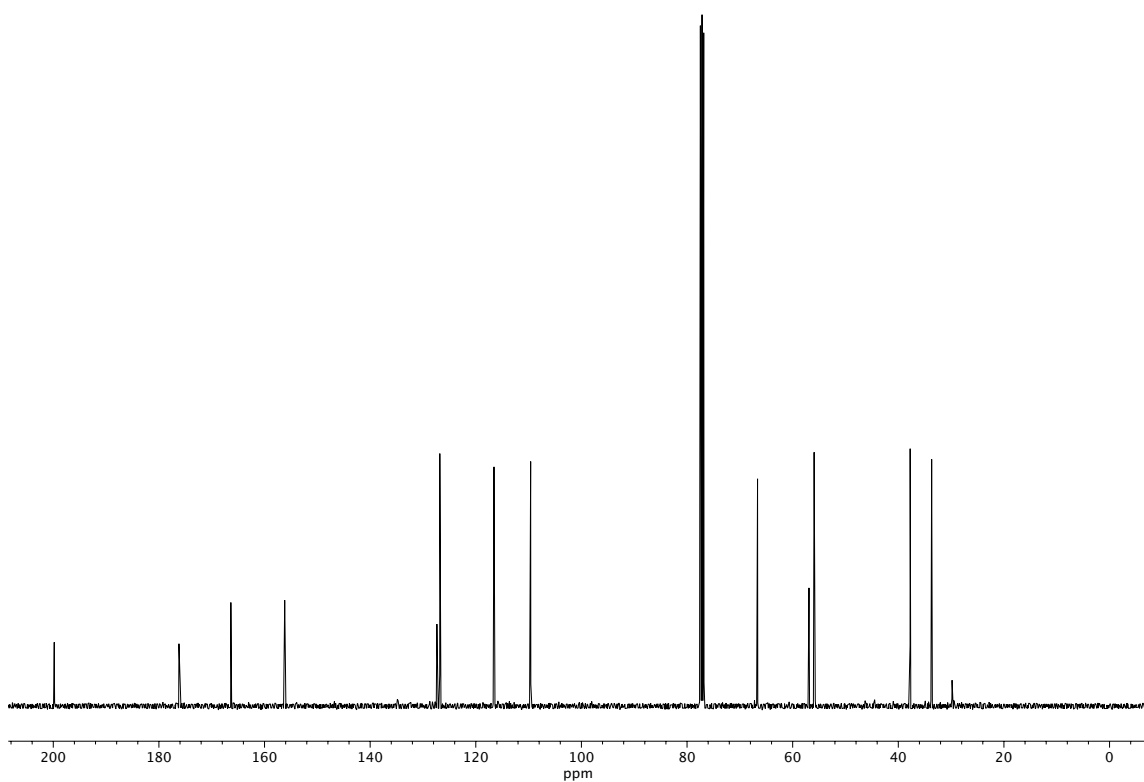
Figure A2.113 ^{13}C NMR (101 MHz, CDCl$_3$) of compound **186b**.
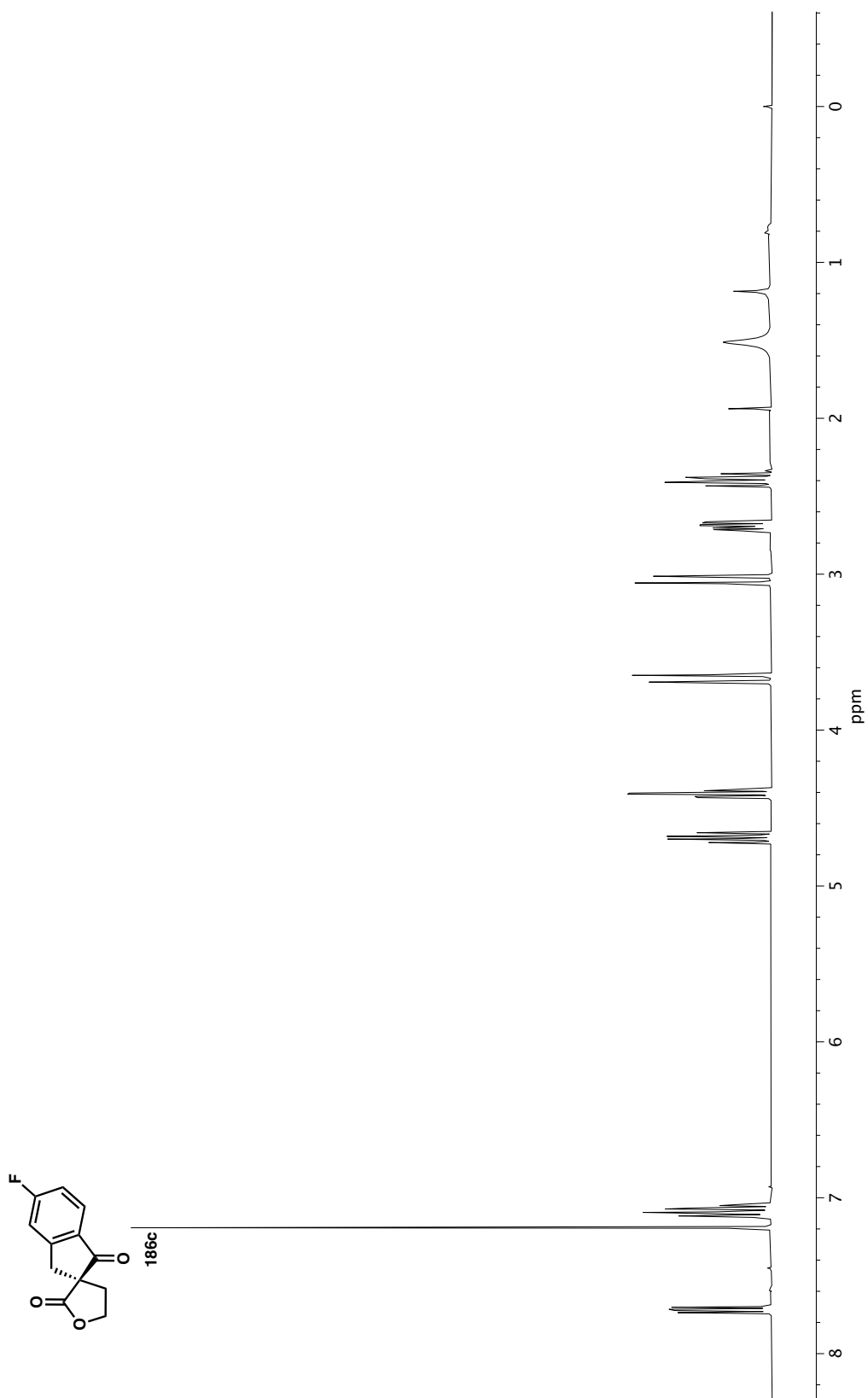
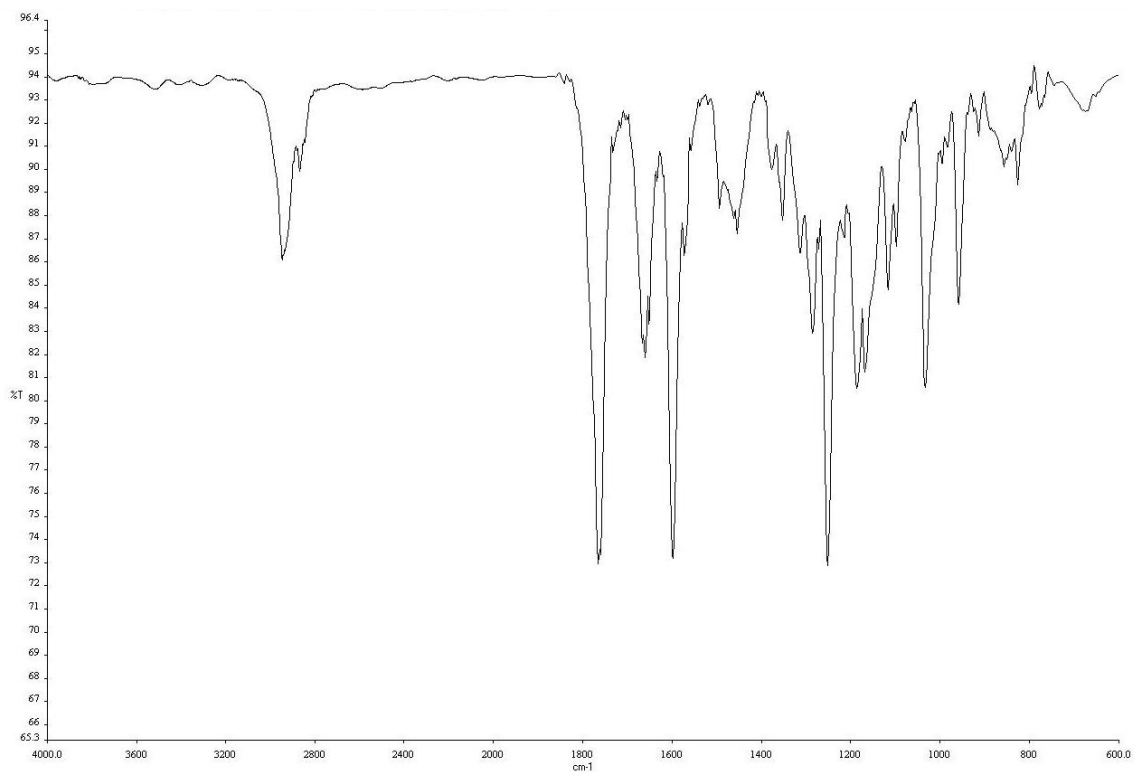**Figure A2.114** ^{1}H NMR (400 MHz, CDCl$_3$) of compound **186c.**

Figure A2.115 IR (NaCl, Thin Film) of compound **186c**.

Figure A2.116 ^{13}C NMR (101 MHz, CDCl$_3$) of compound **186c**.

Figure A2.117 ^{19}F NMR (376 MHz, CDCl$_3$) of compound **186c.**

Figure A2.118 ^{1}H NMR (400 MHz, CDCl$_3$) of compound **186d.**
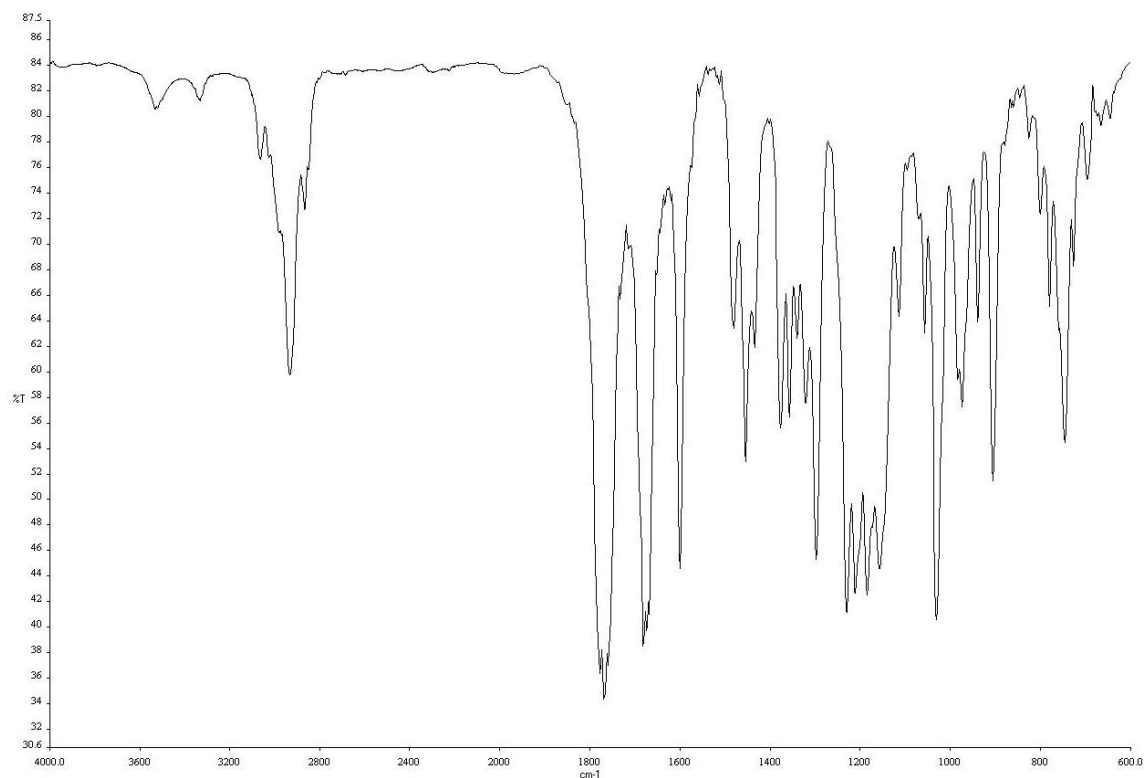
Figure A2.119 IR (NaCl, Thin Film) of compound **186d**.

Figure A2.120 ^{13}C NMR (101 MHz, CDCl$_3$) of compound **186d**.

Figure A2.121 ^{1}H NMR (400 MHz, CDCl$_3$) of compound **188a.**

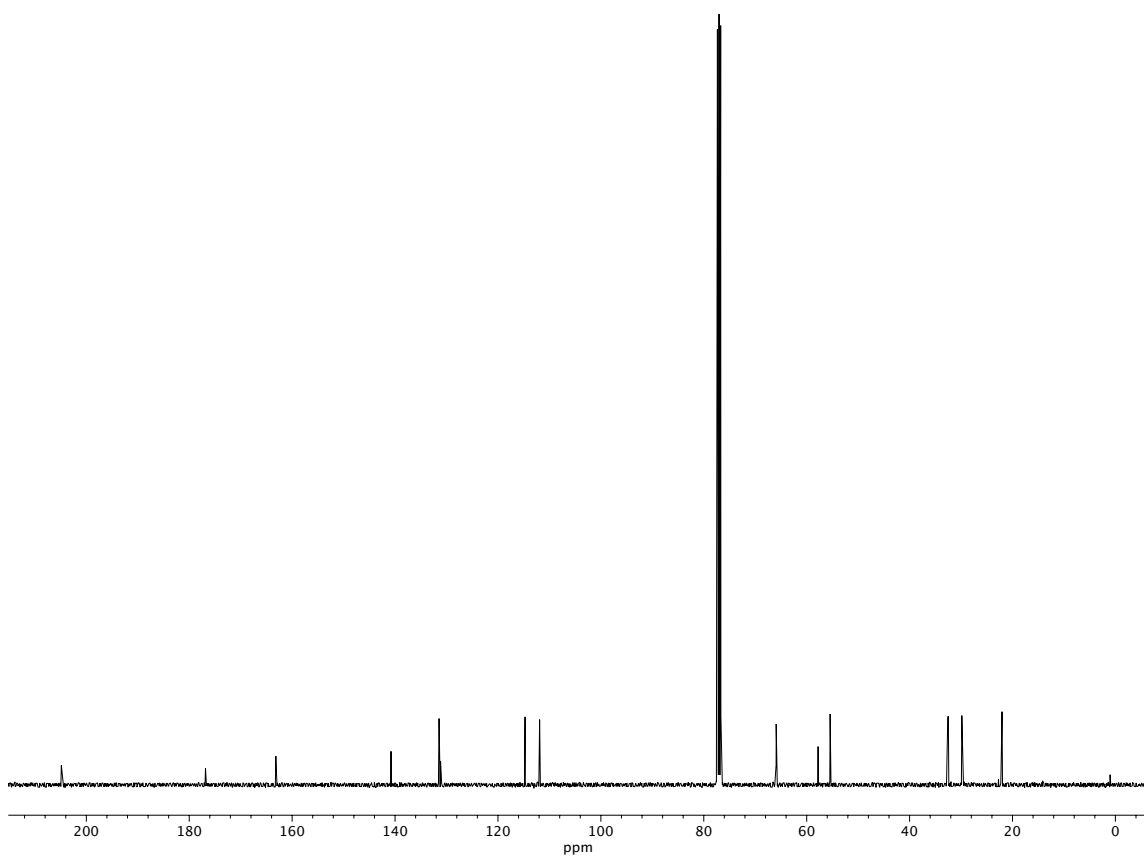**Figure A2.122** IR (NaCl, Thin Film) of compound **188a**.

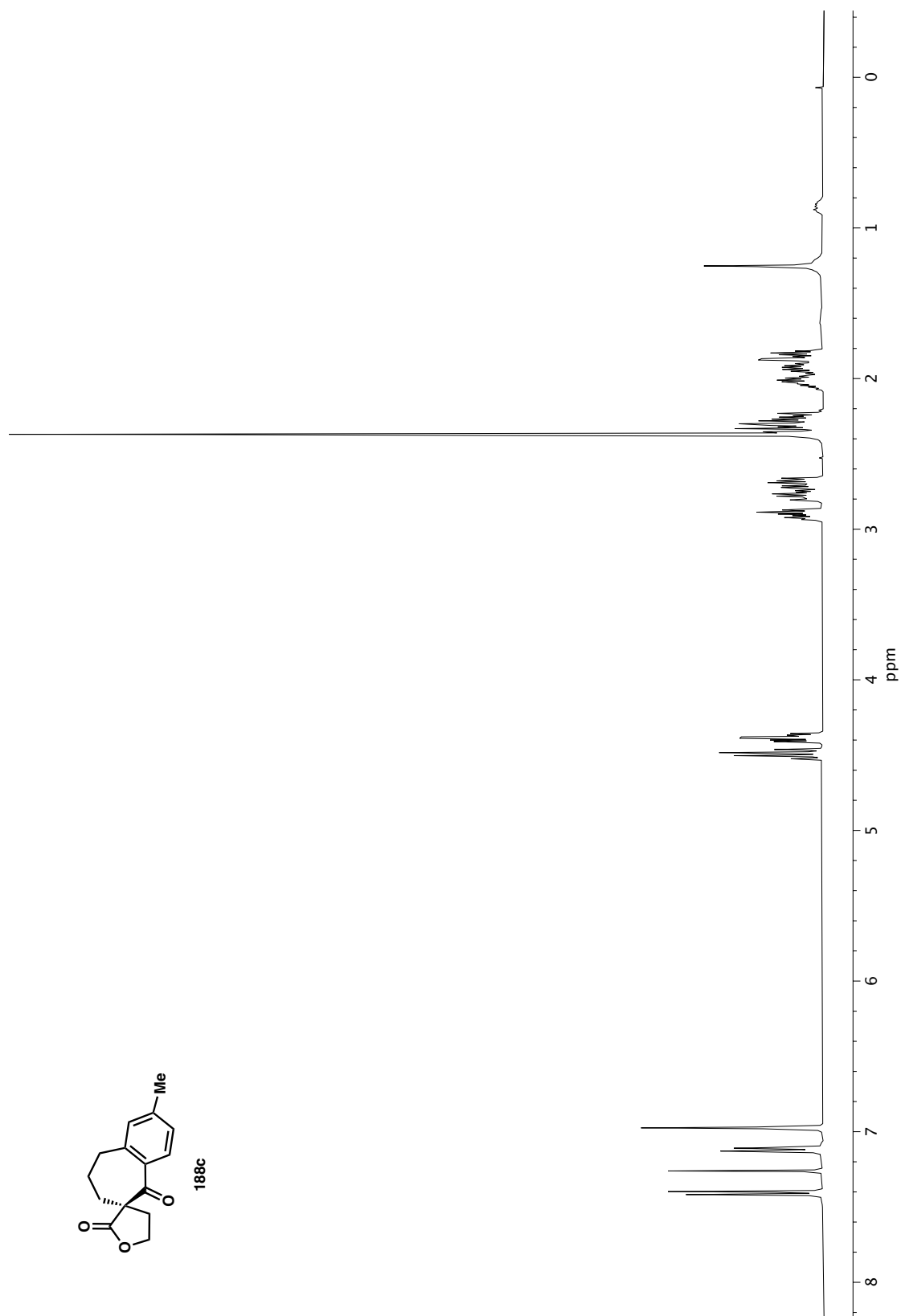**Figure A2.123** ^{13}C NMR (101 MHz, CDCl$_3$) of compound **188a**.

Figure A2.124 ^{1}H NMR (400 MHz, CDCl$_3$) of compound **188b.**

Figure A2.125 IR (NaCl, Thin Film) of compound **188b**.

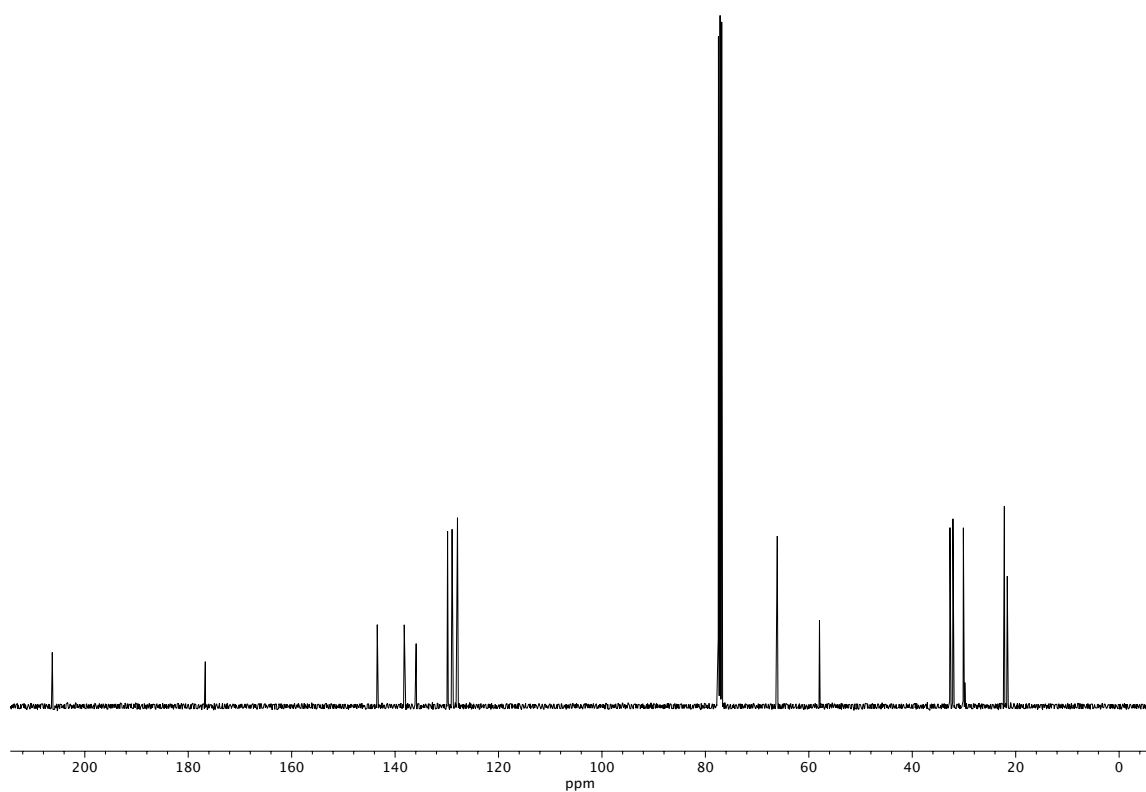***Figure A2.126*** ^{13}C NMR (101 MHz, CDCl$_3$) of compound **188b**.
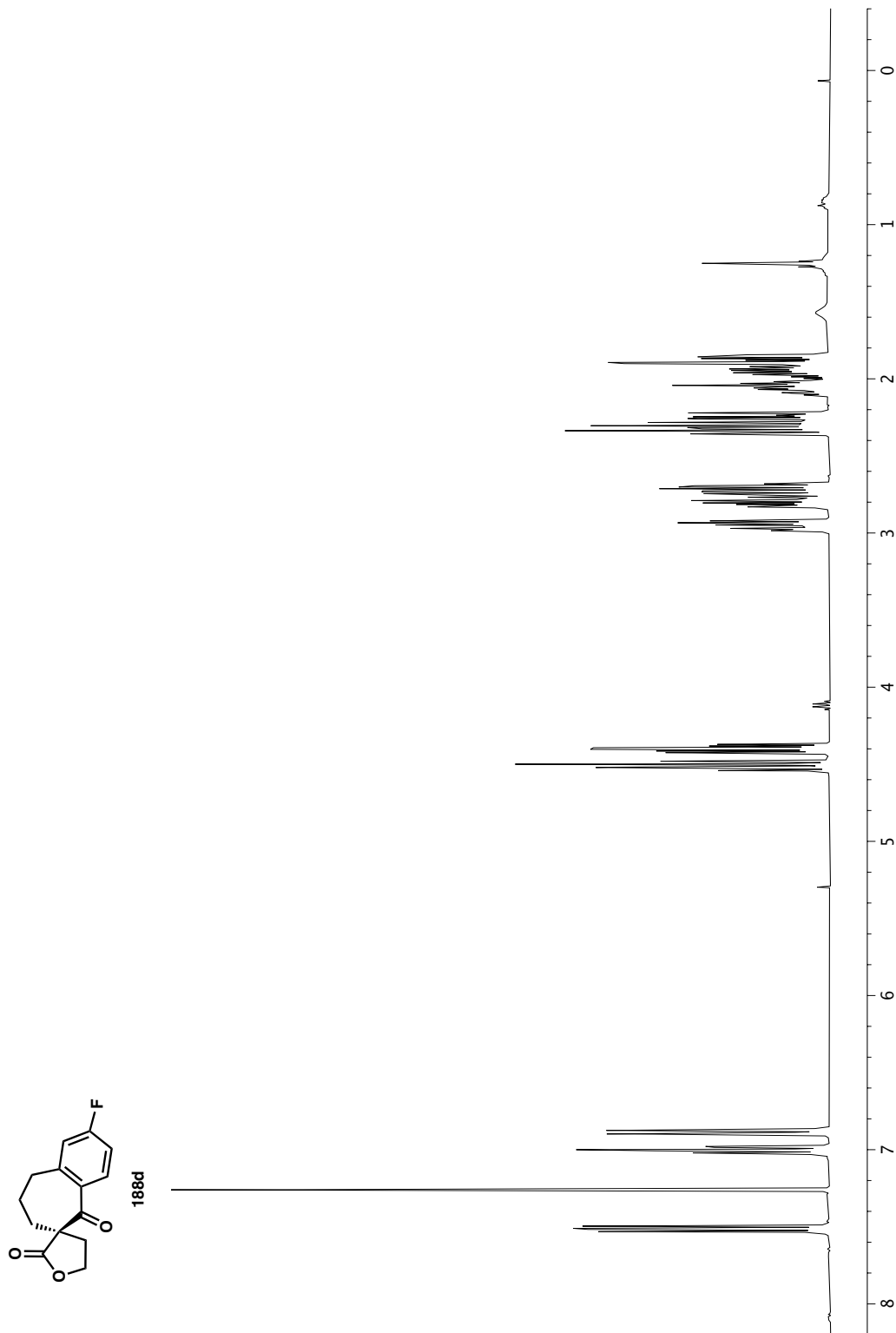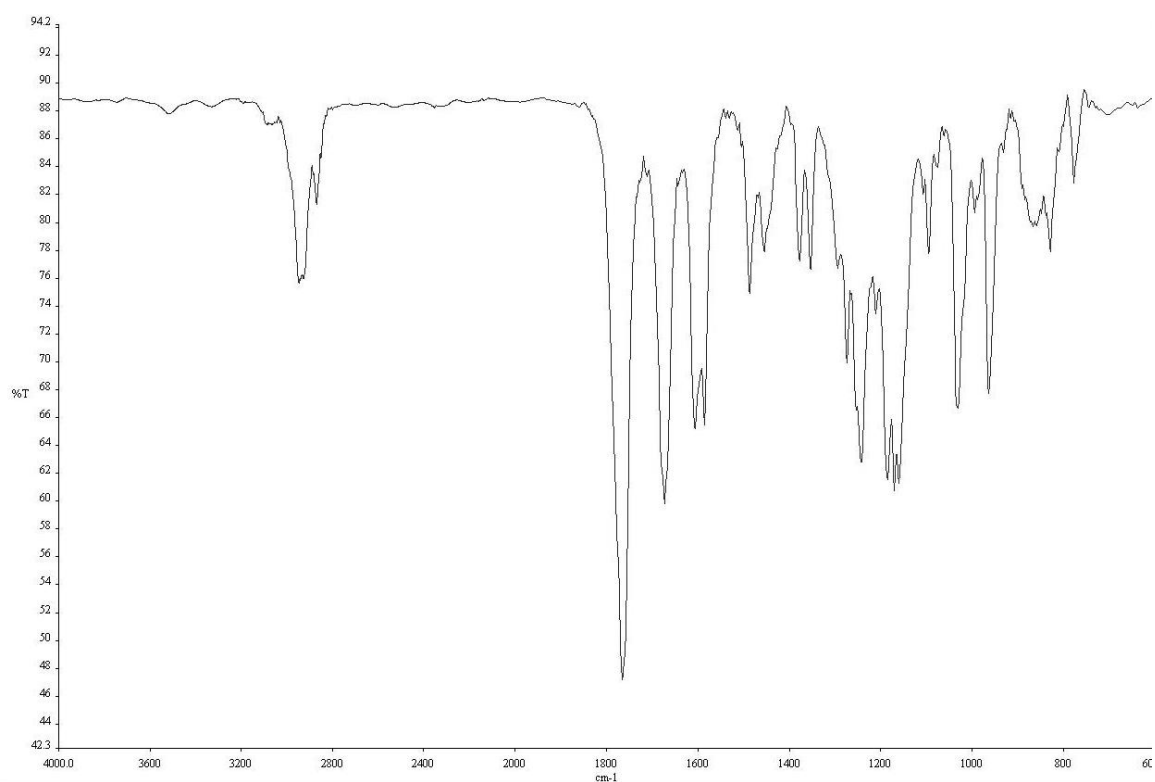
Figure A2.127 ^{1}H NMR (400 MHz, CDCl$_3$) of compound **188c.**

Figure A2.128 IR (NaCl, Thin Film) of compound **188c**.

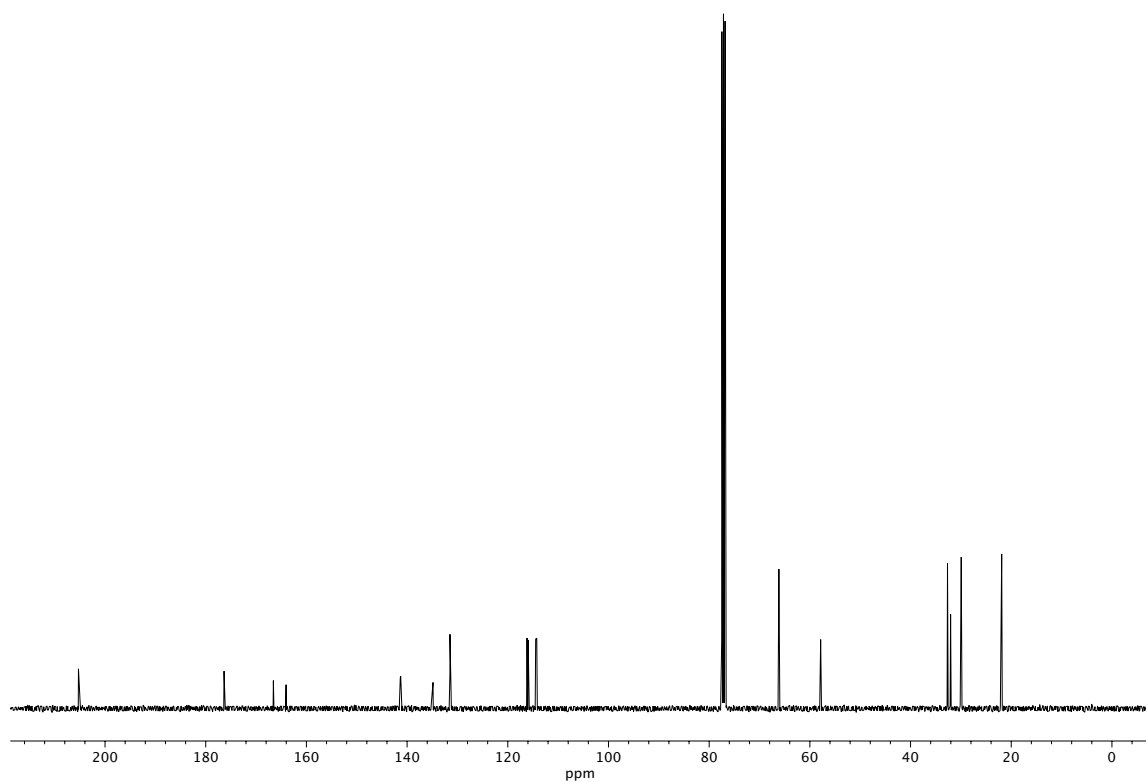*Figure A2.129* ^{13}C NMR (101 MHz, CDCl$_3$) of compound **188c**.

Figure A2.130 ¹H NMR (400 MHz, CDCl₃) of compound **188d.**

Figure A2.131 IR (NaCl, Thin Film) of compound **188d**.

Figure A2.132 ^{13}C NMR (101 MHz, CDCl$_3$) of compound **188d**.

Figure A2.133 ^{19}F NMR (376 MHz, CDCl$_3$) of compound **188d.**

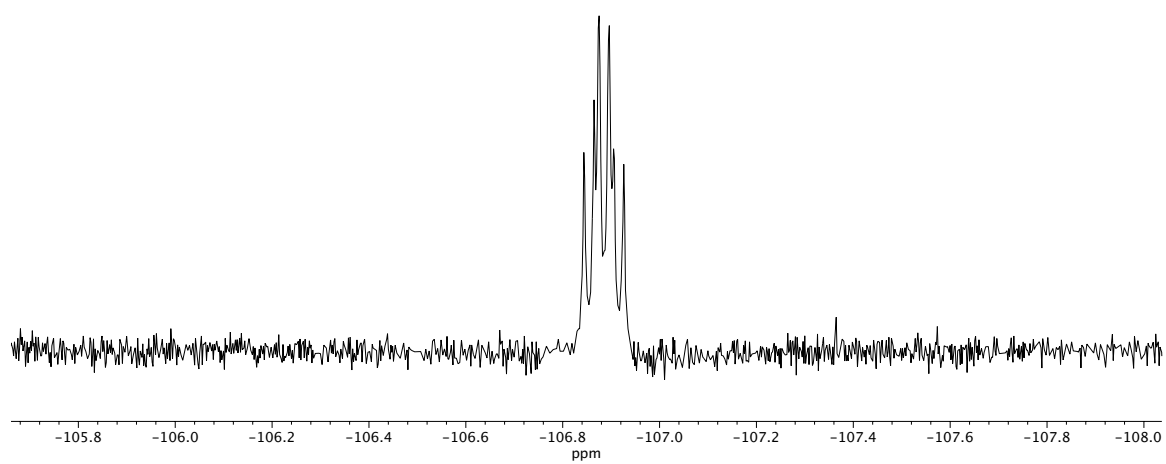**Figure A2.134** ^{1}H NMR (600 MHz, CDCl$_3$) of compound **188e**.

Figure A2.135 IR (NaCl, Thin Film) of compound **188e**.
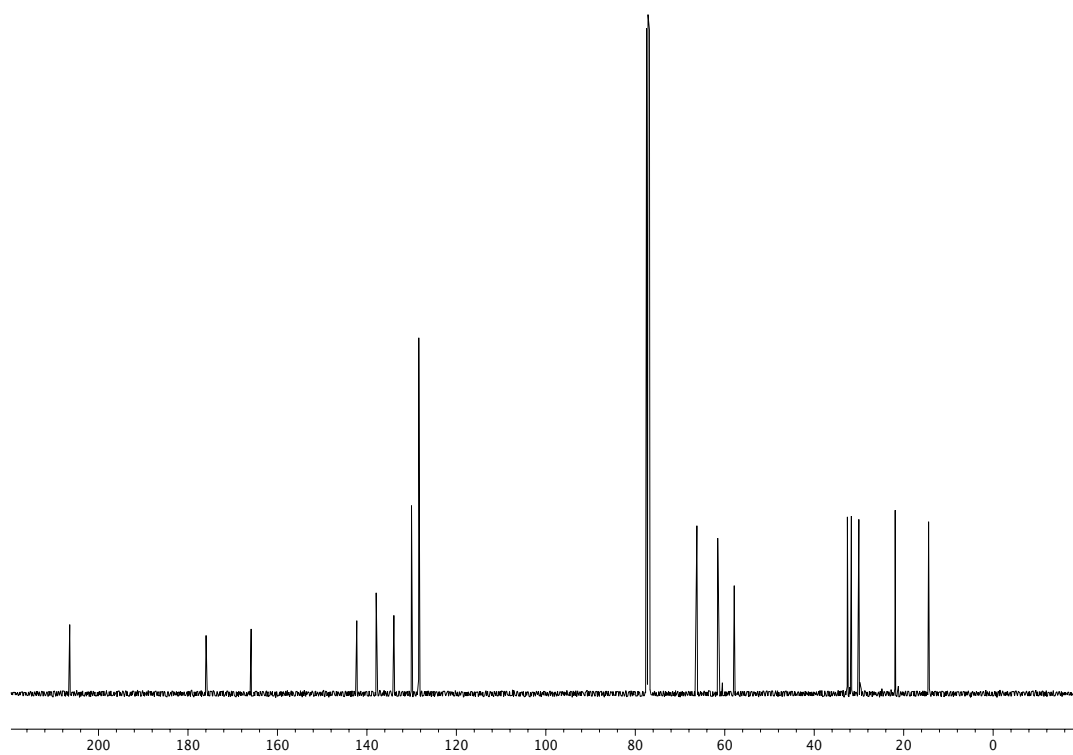
Figure A2.136 ^{13}C NMR (101 MHz, CDCl$_3$) of compound **188e**.

Figure A2.137 ^{1}H NMR (400 MHz, CDCl$_3$) of compound **188f.**

Figure A2.138 IR (NaCl, Thin Film) of compound **188f**.
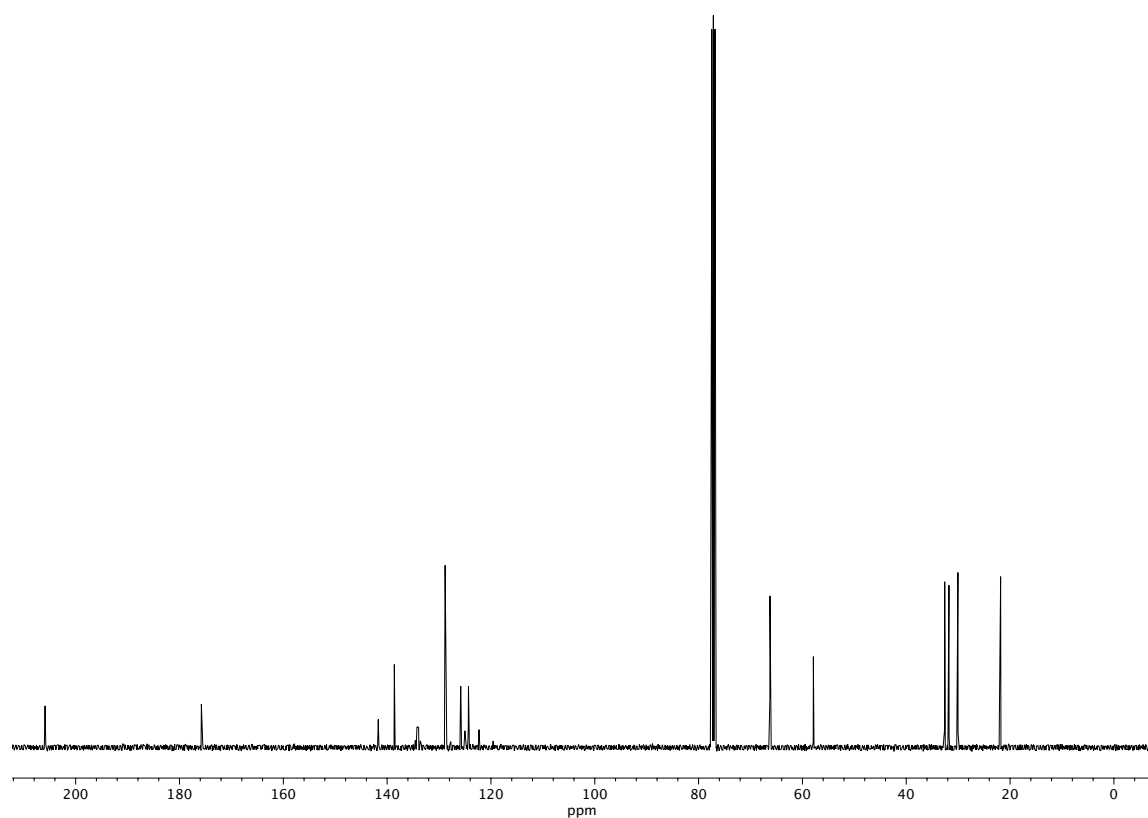
Figure A2.139 ^{13}C NMR (101 MHz, CDCl$_3$) of compound **188f**.

Figure A2.140 ^{19}F NMR (376 MHz, CDCl$_3$) of compound **188f.**

Figure A2.141 ^{1}H NMR (400 MHz, CDCl$_3$) of compound **188g**.
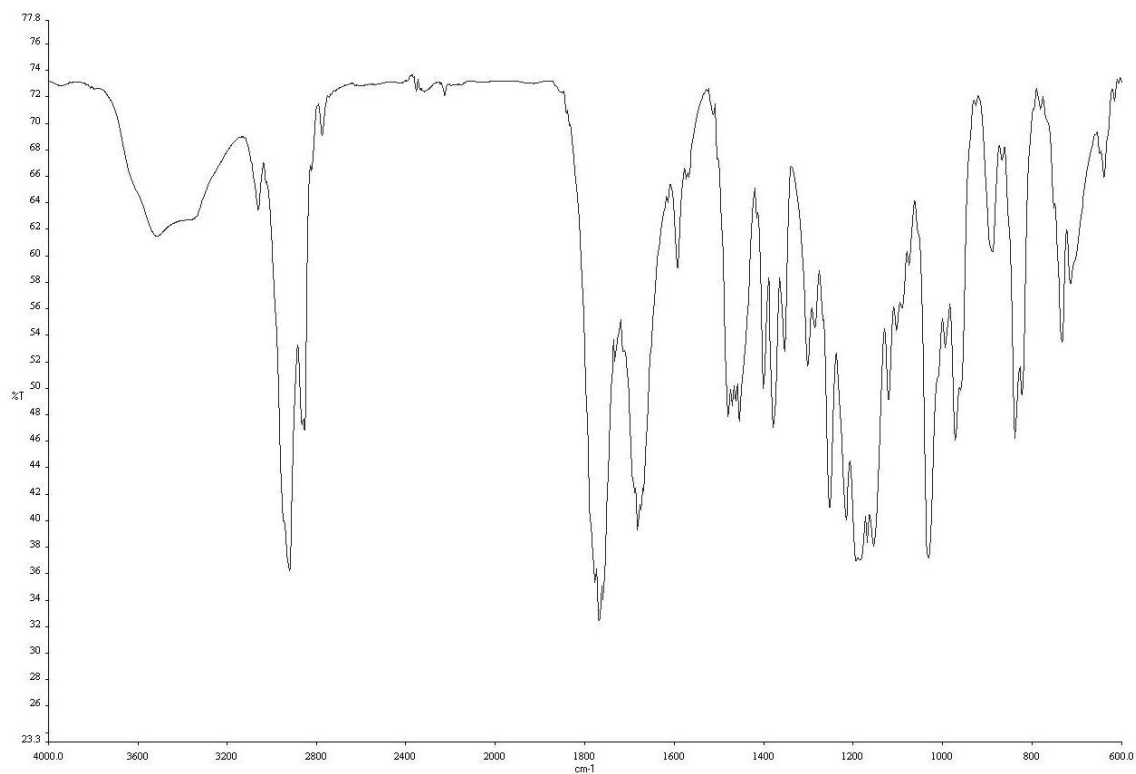
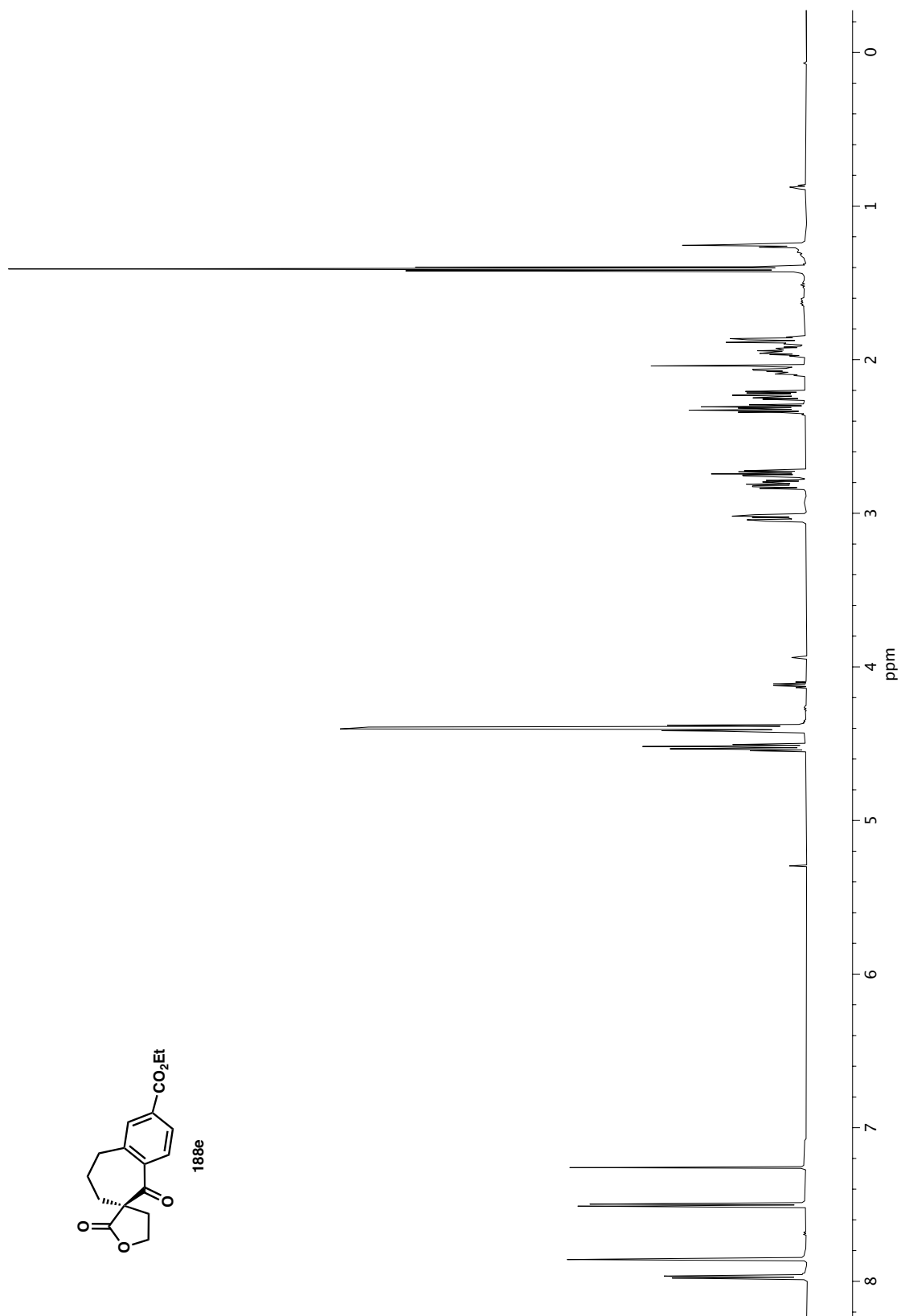***Figure A2.142*** IR (NaCl, Thin Film) of compound **188g**.
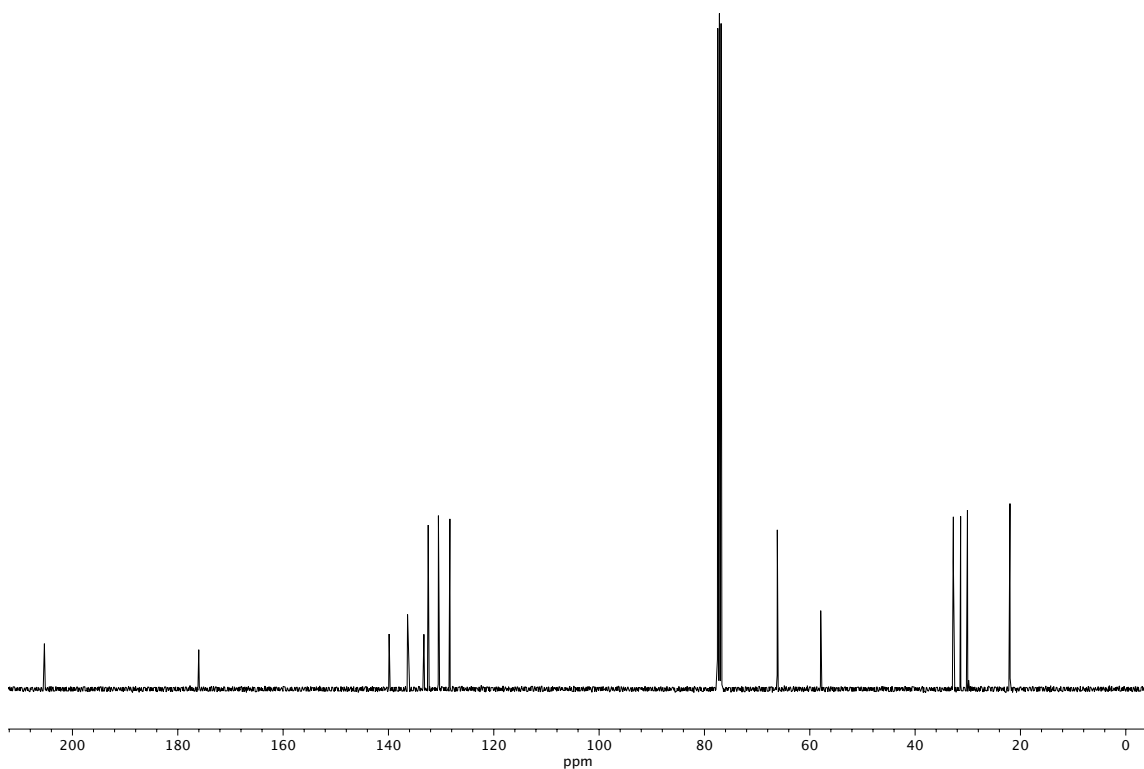
Figure A2.143 ^{13}C NMR (101 MHz, CDCl$_3$) of compound **188g**.

Figure A2.144 ¹H NMR (400 MHz, CDCl₃) of compound **188h.**

Figure A2.145 IR (NaCl, Thin Film) of compound **188h**.
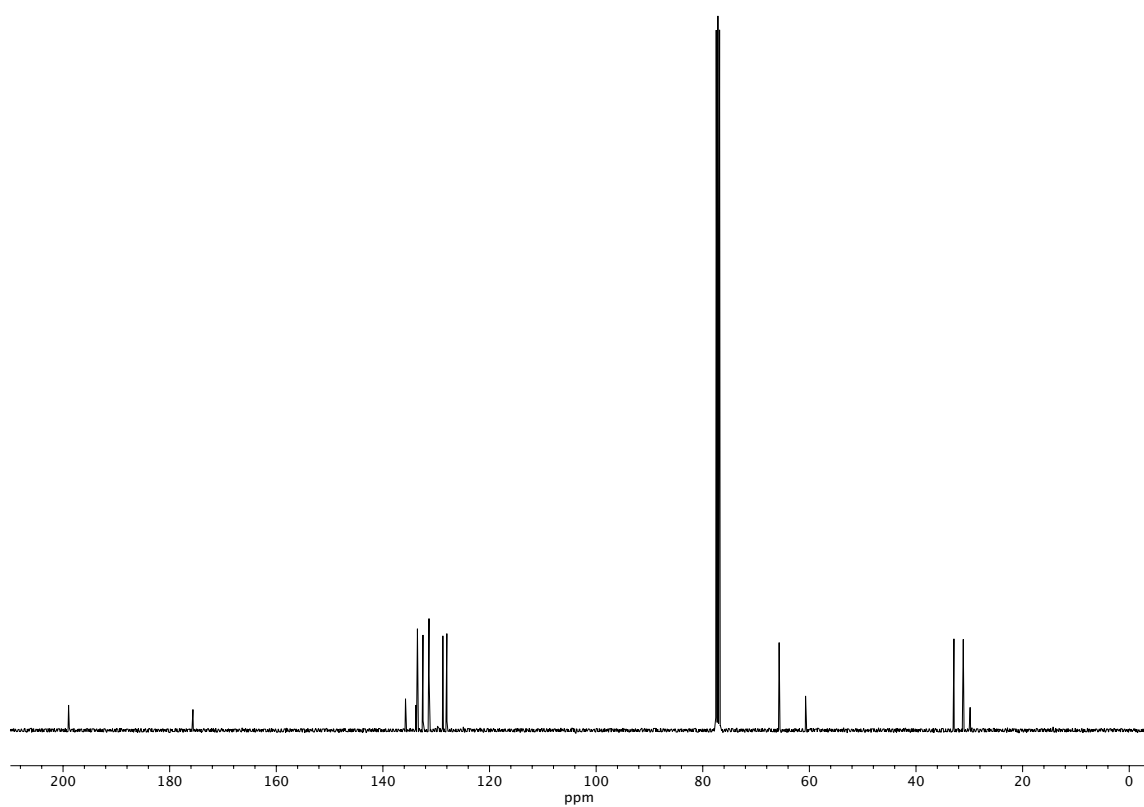
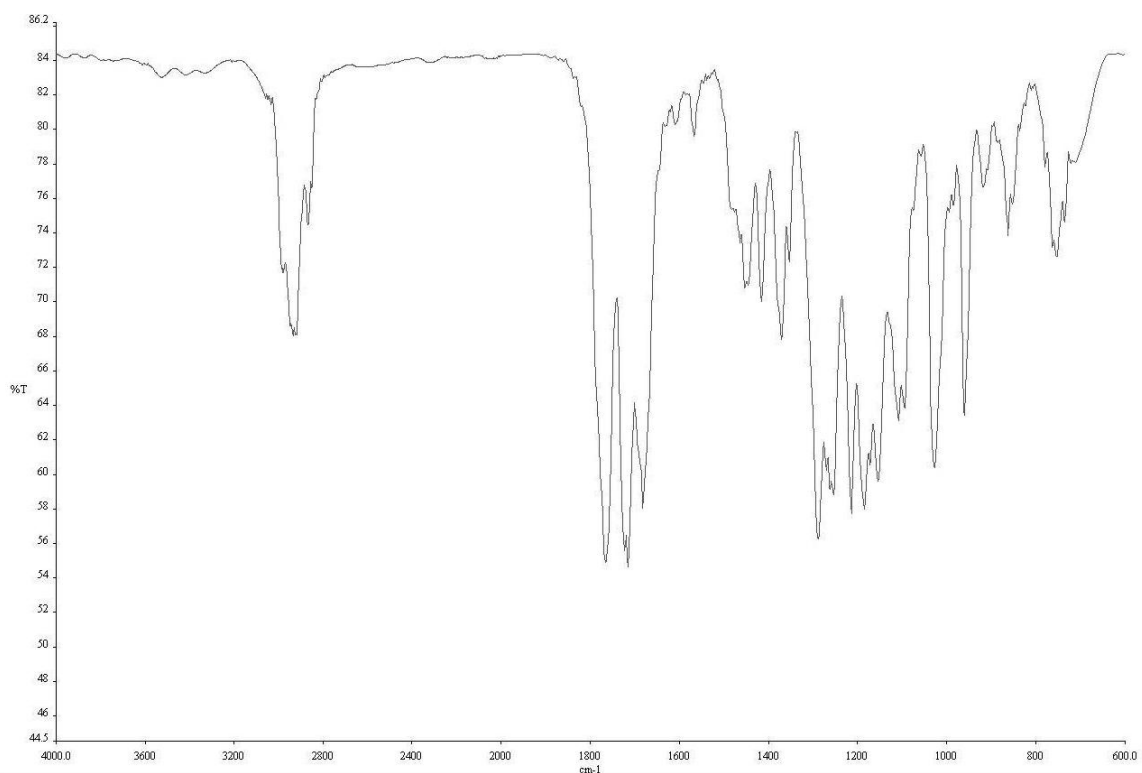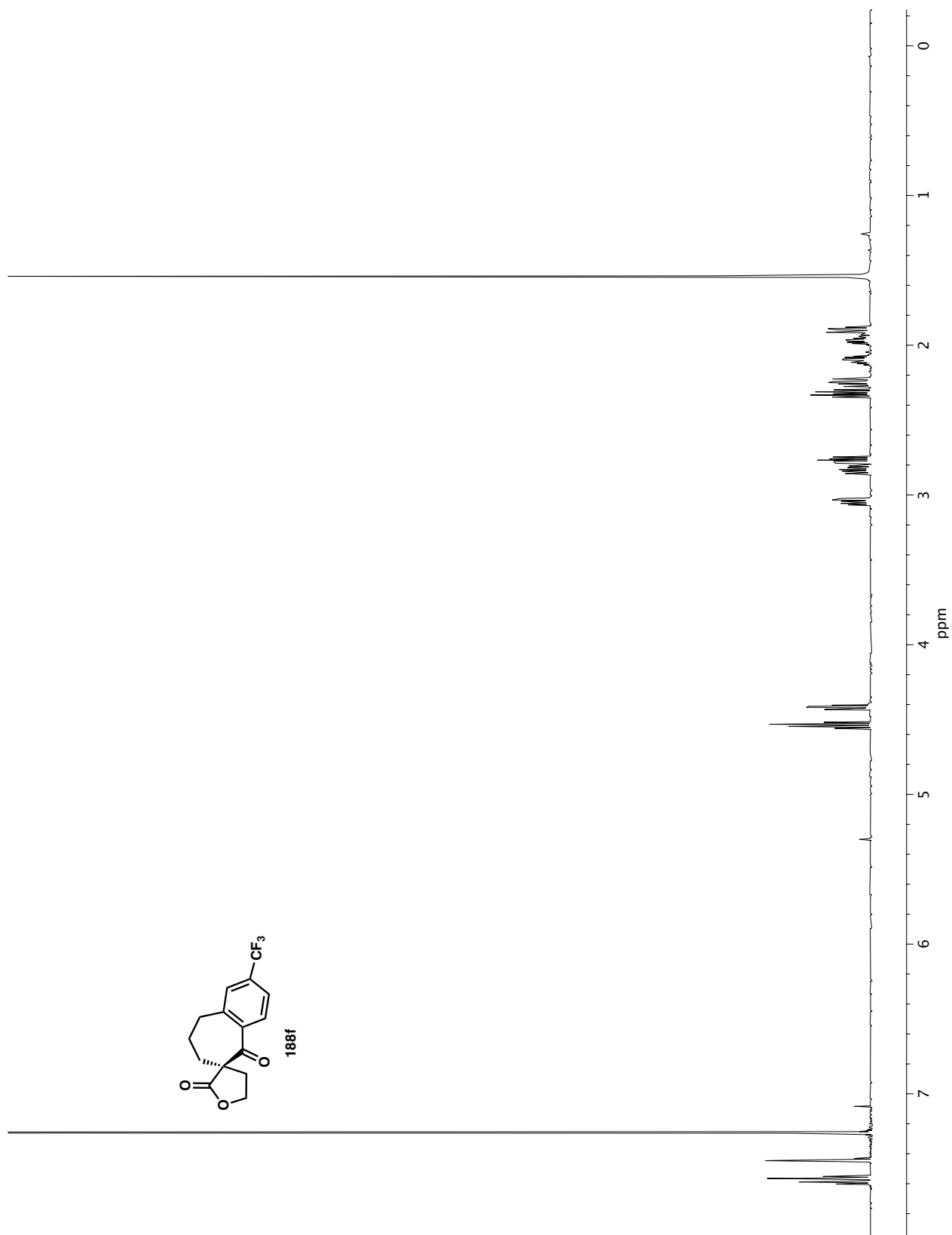**Figure A2.146** ^{13}C NMR (101 MHz, CDCl$_3$) of compound **188h**.
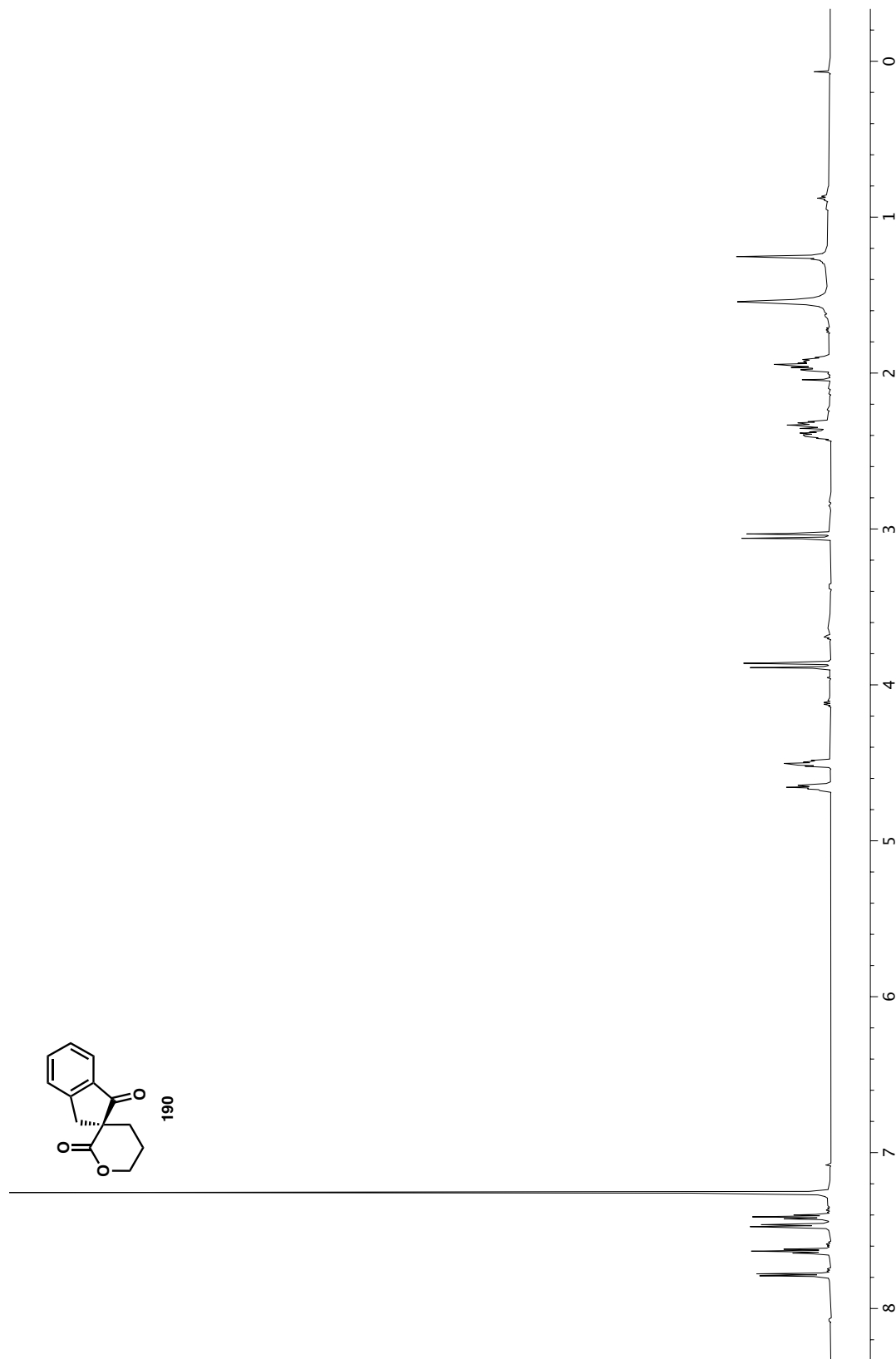
Figure A2.147 ^{1}H NMR (400 MHz, CDCl$_3$) of compound **190.**
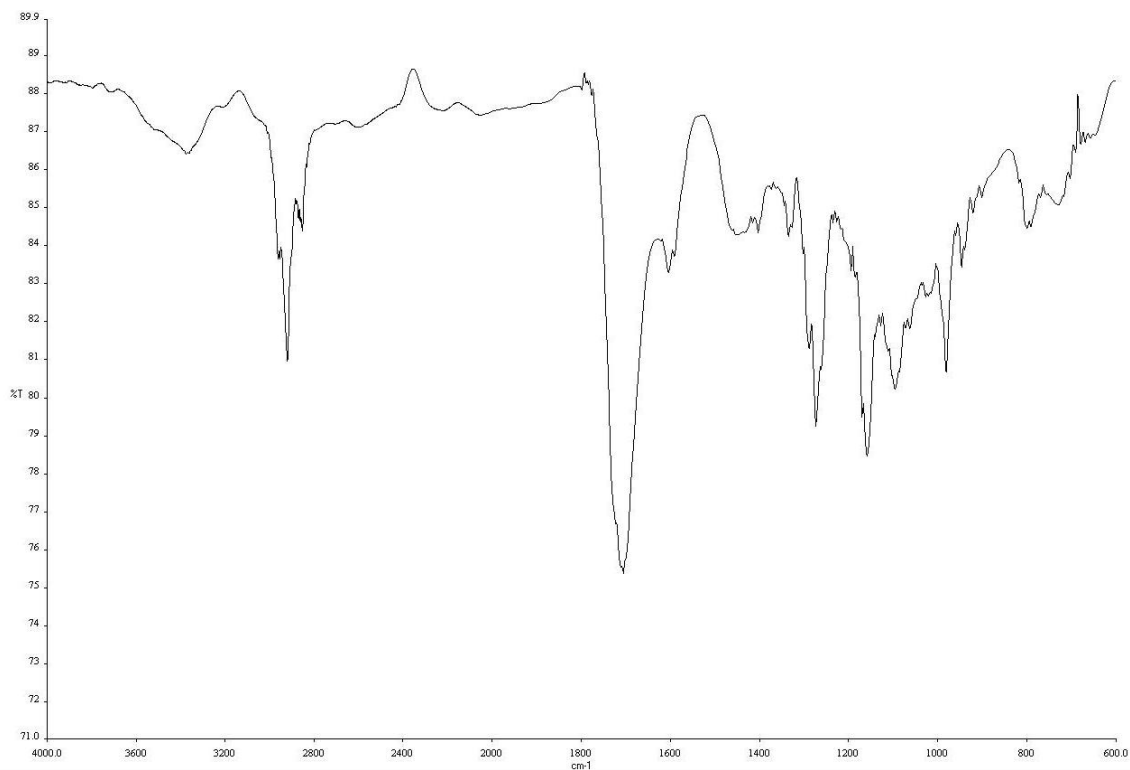
Figure A2.148 IR (NaCl, Thin Film) of compound **190**.
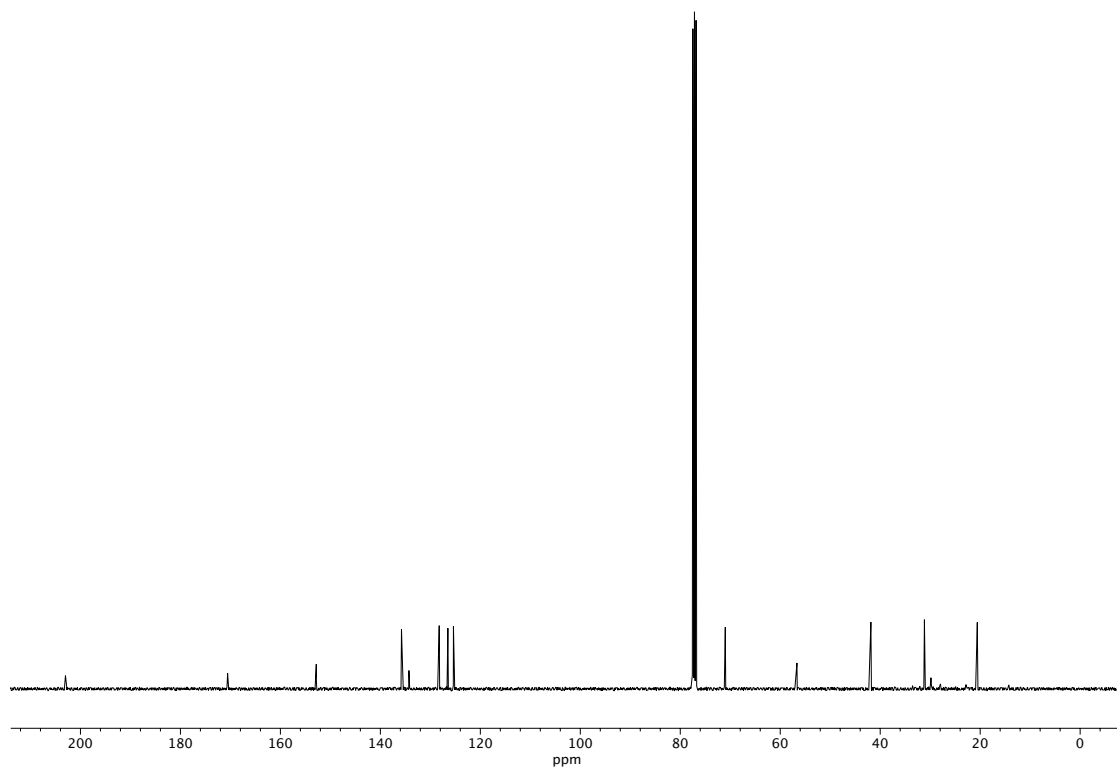
Figure A2.149 ^{13}C NMR (101 MHz, CDCl$_3$) of compound **190**.
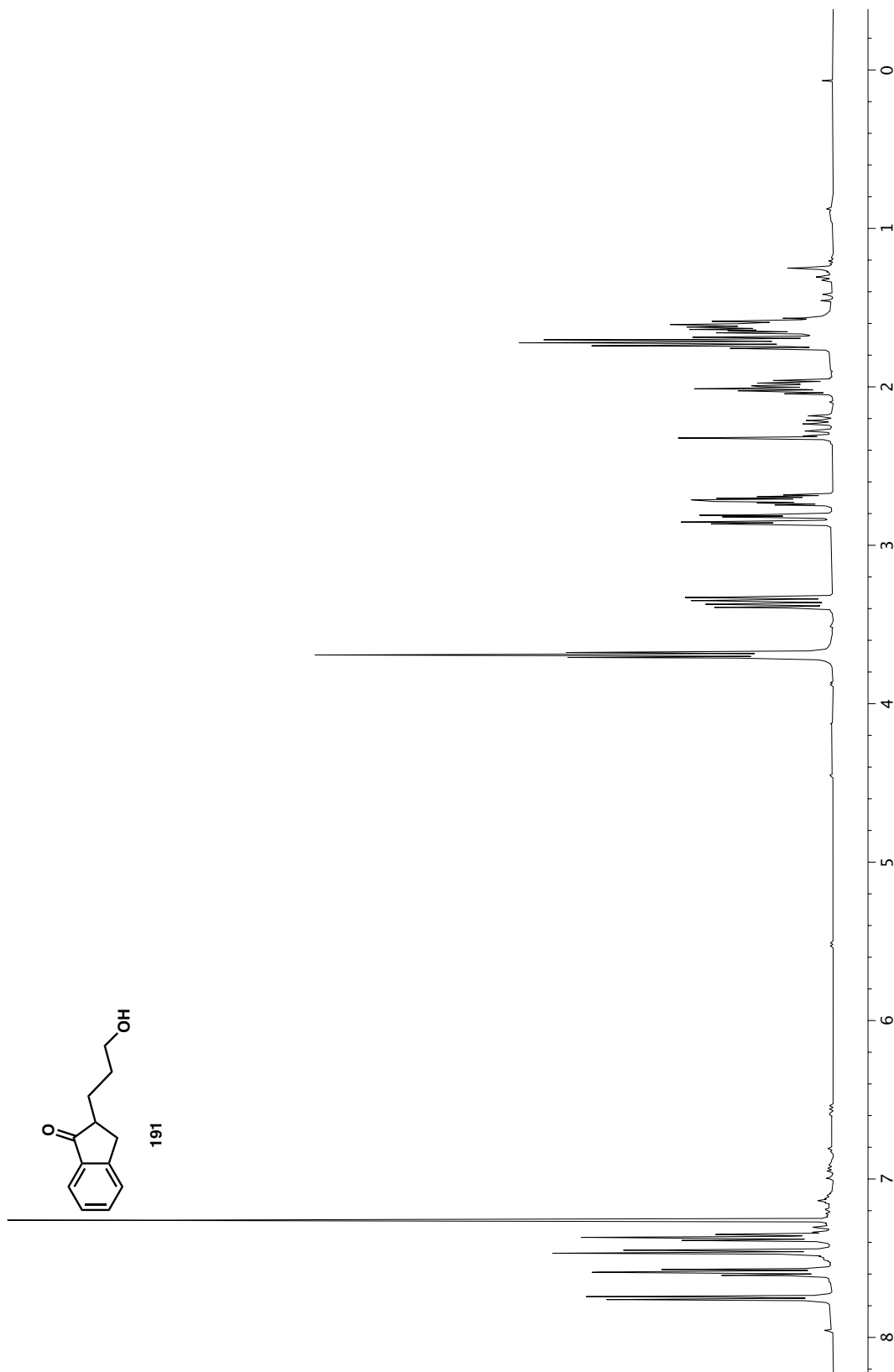
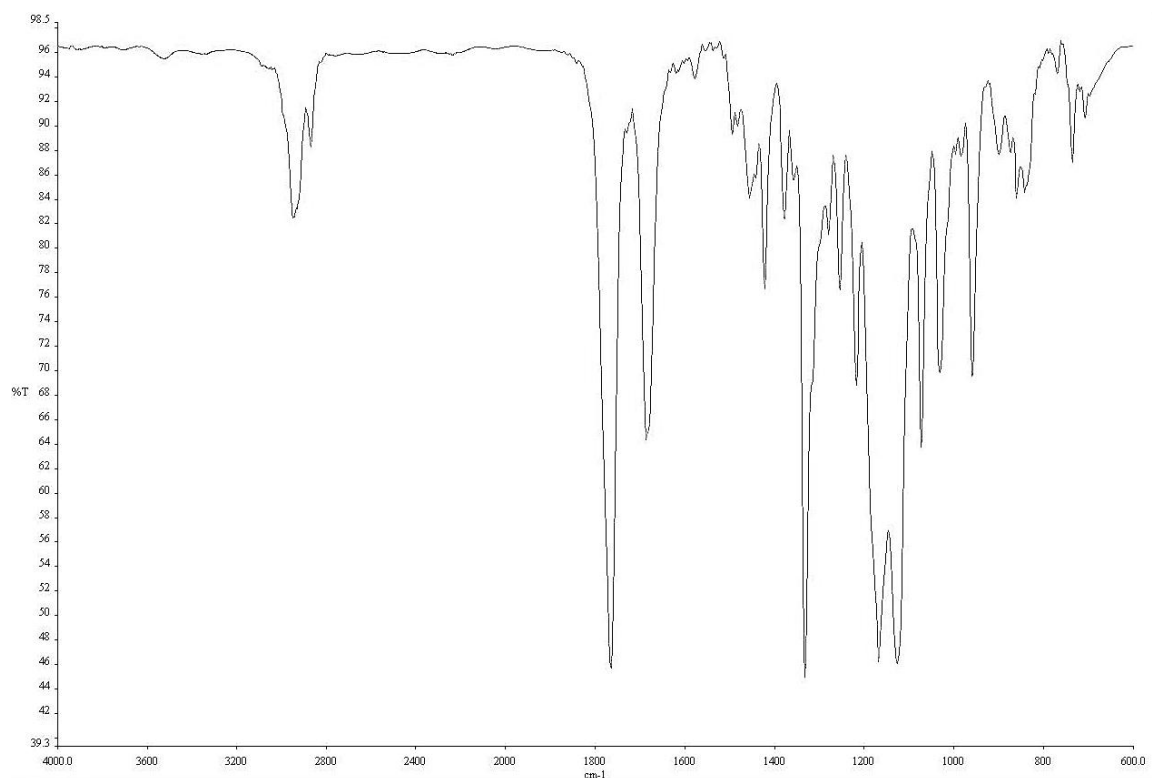**Figure A2.150** ^{1}H NMR (400 MHz, CDCl$_3$) of compound **191.**
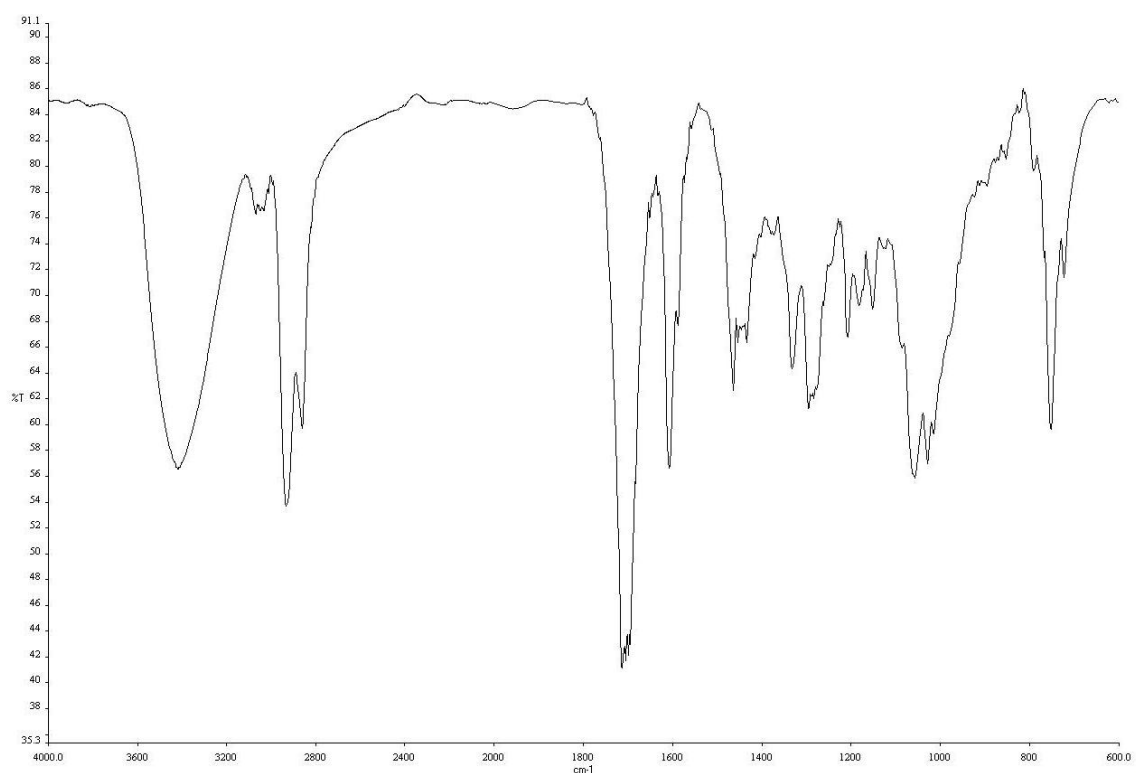
Figure A2.151 IR (NaCl, Thin Film) of compound **191**.
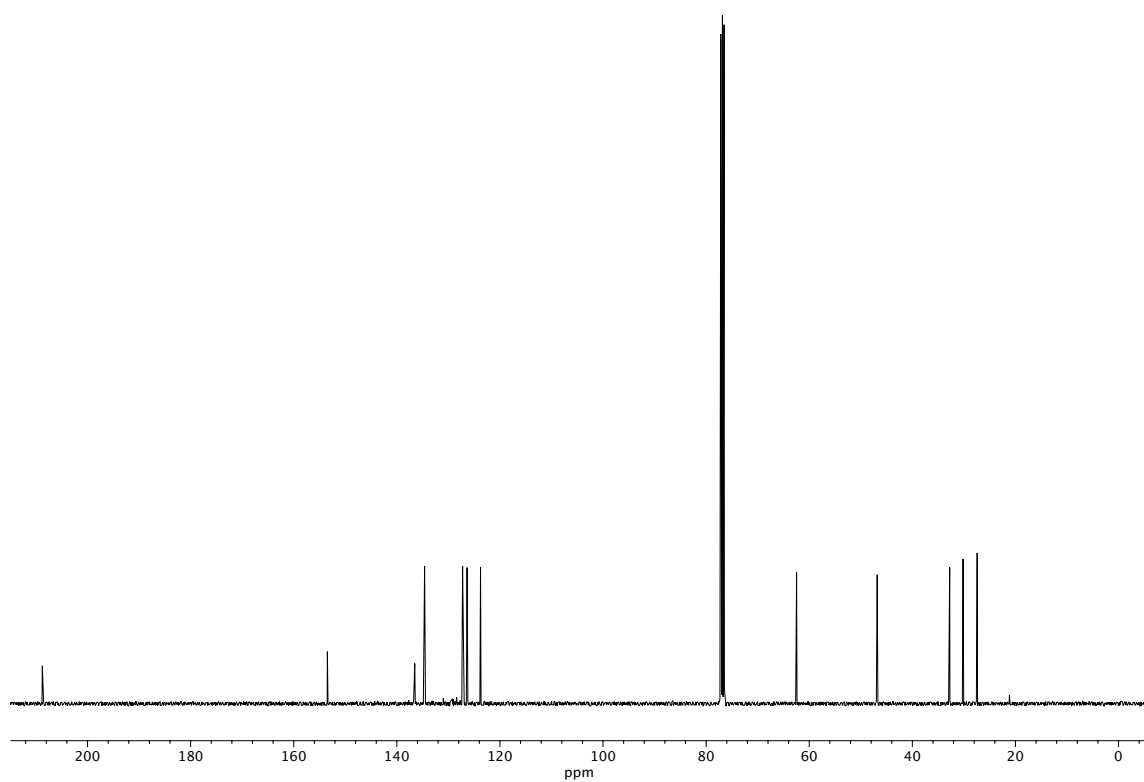
Figure A2.152 ^{13}C NMR (101 MHz, CDCl$_3$) of compound **191**.
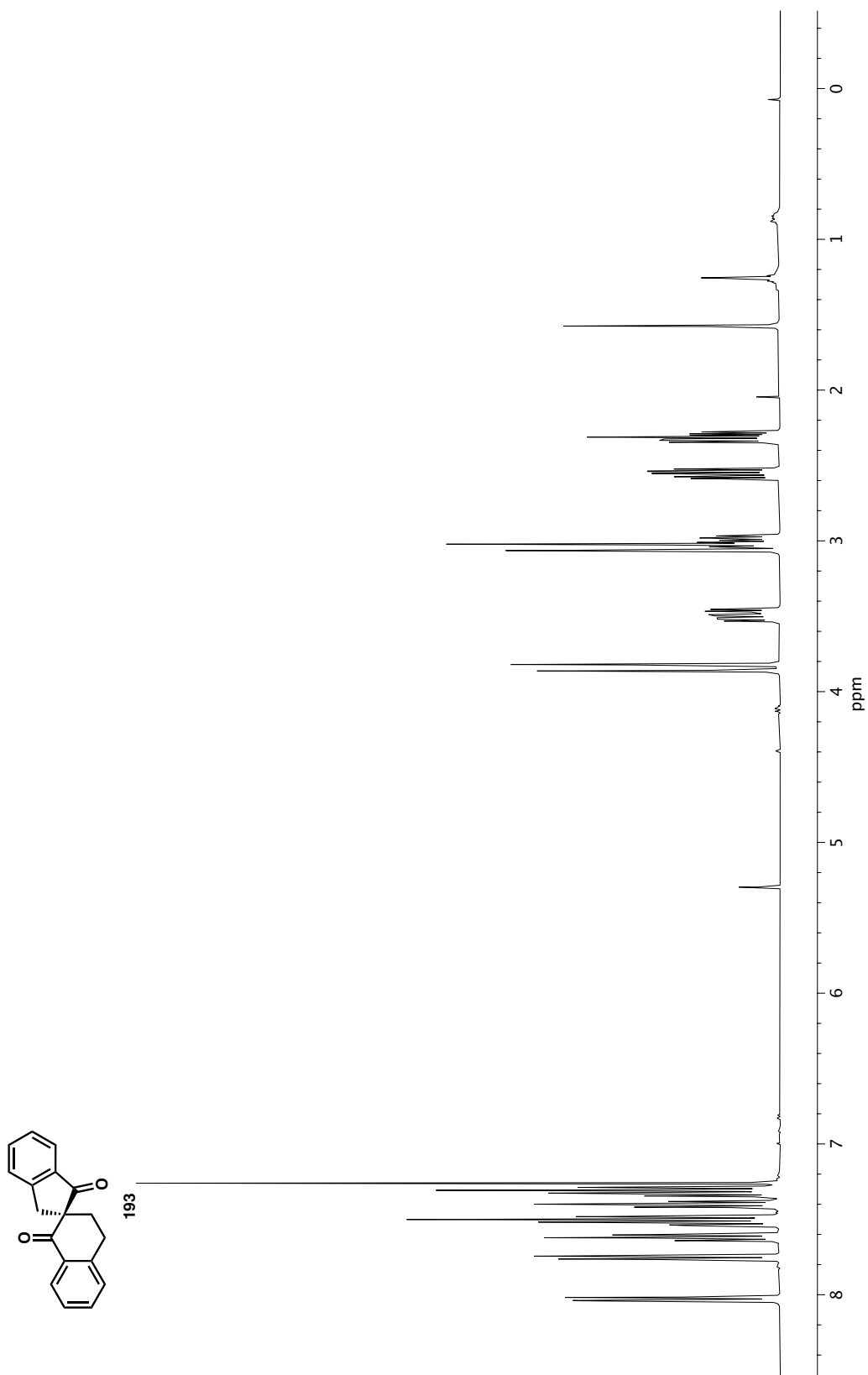
Figure A2.153 ¹H NMR (400 MHz, CDCl₃) of compound **193.**
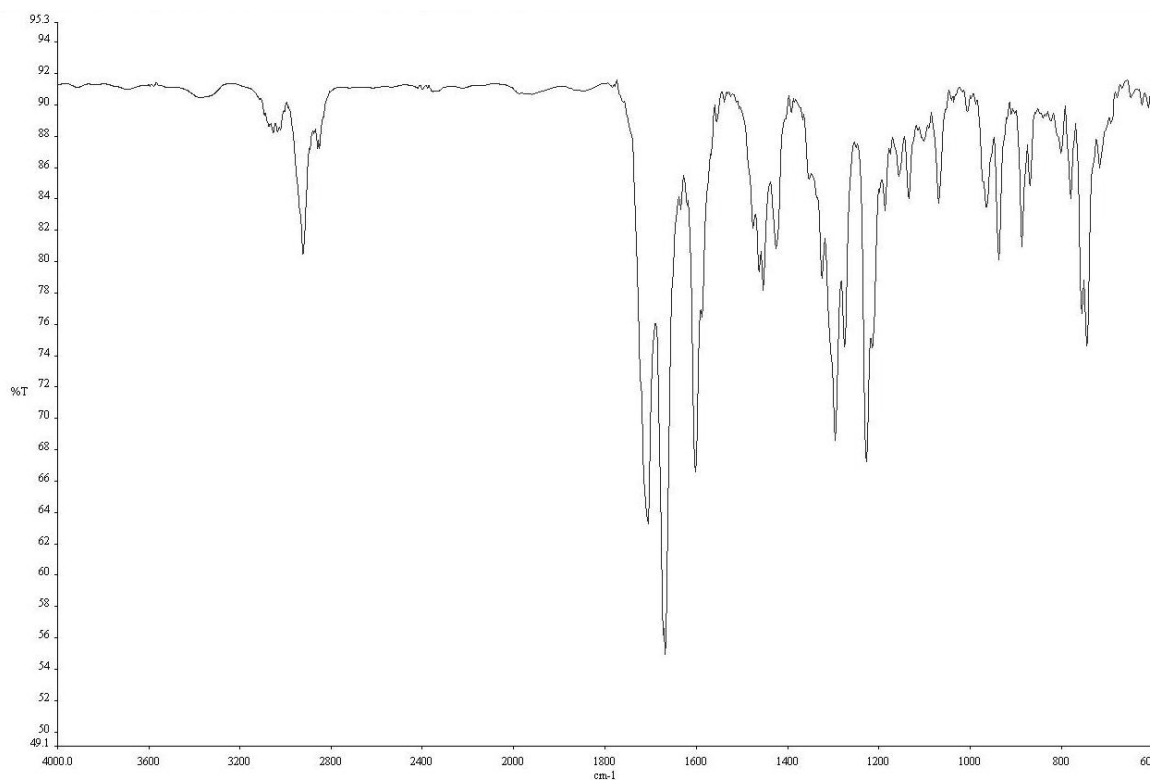
Figure A2.154 IR (NaCl, Thin Film) of compound **193**.
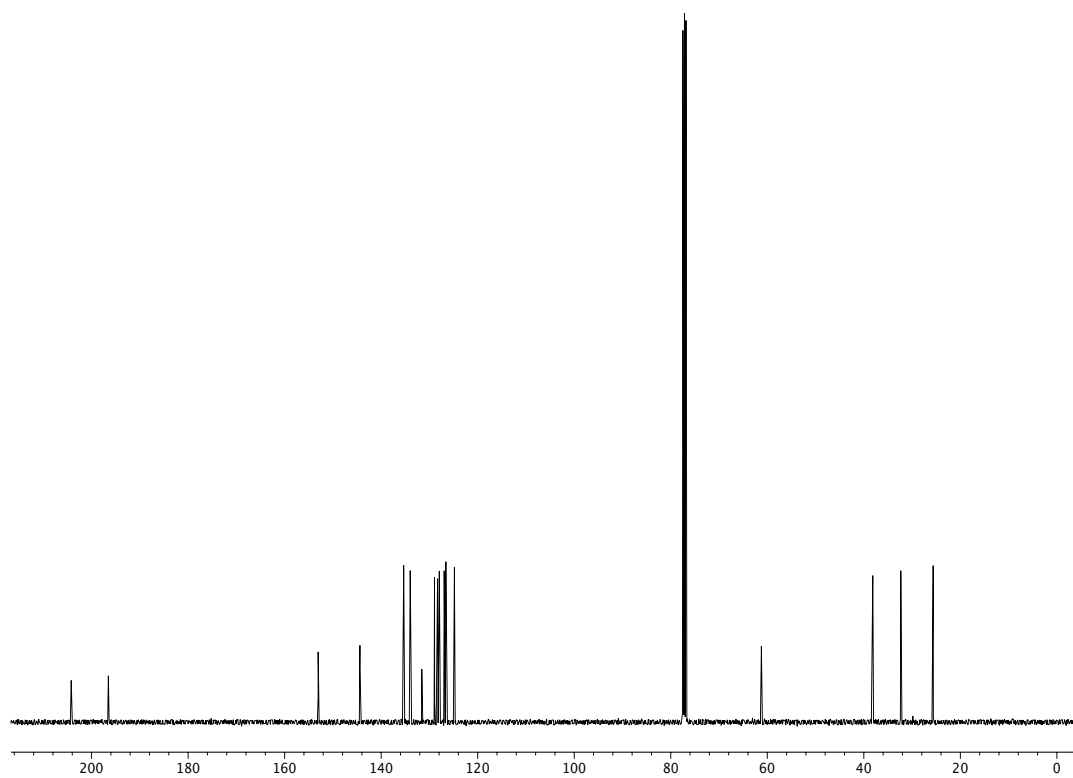
Figure A2.155 ^{13}C NMR (101 MHz, CDCl$_3$) of compound **193**.

Figure A2.156 ^{1}H NMR (400 MHz, CDCl$_3$) of compound **S41.**
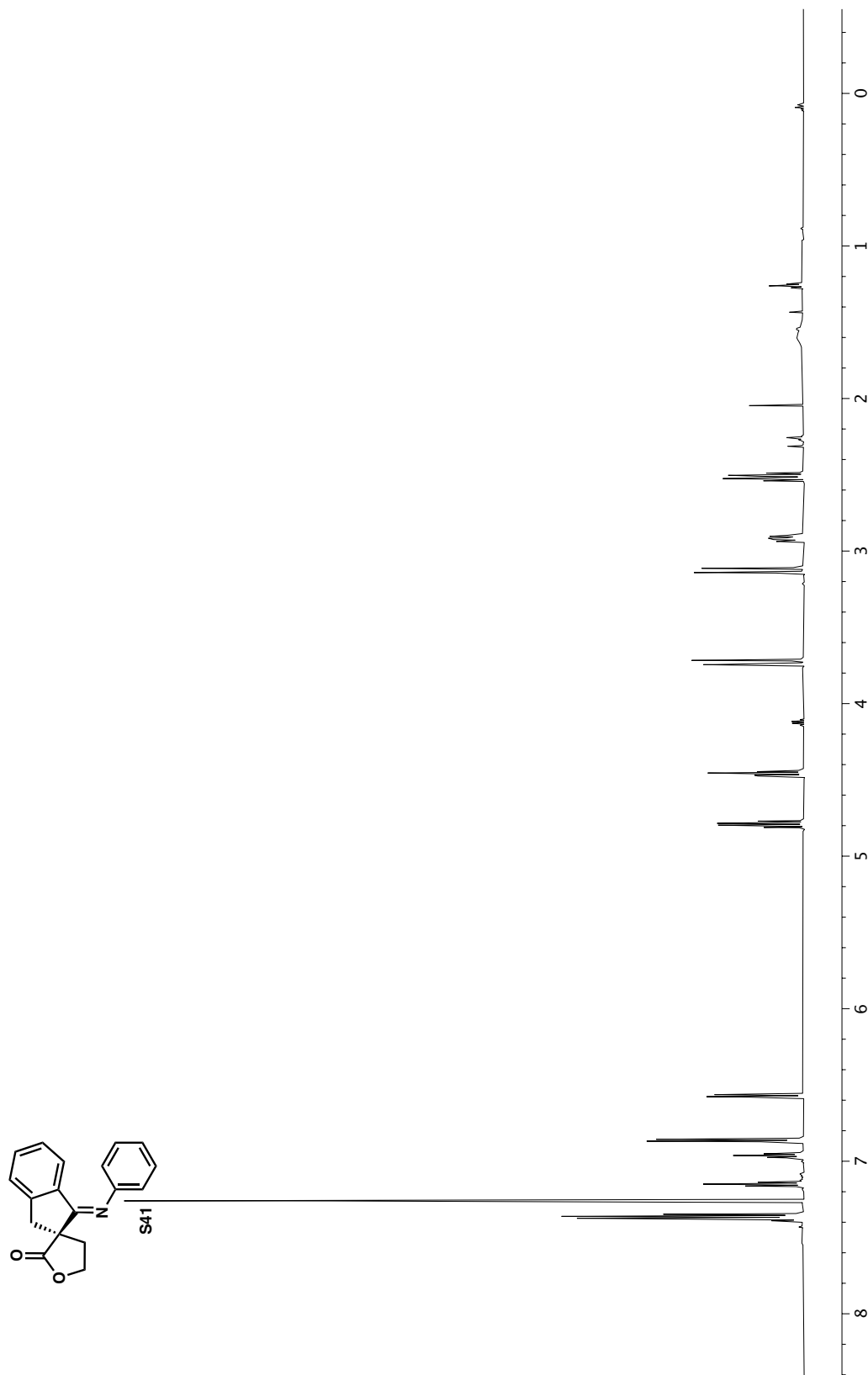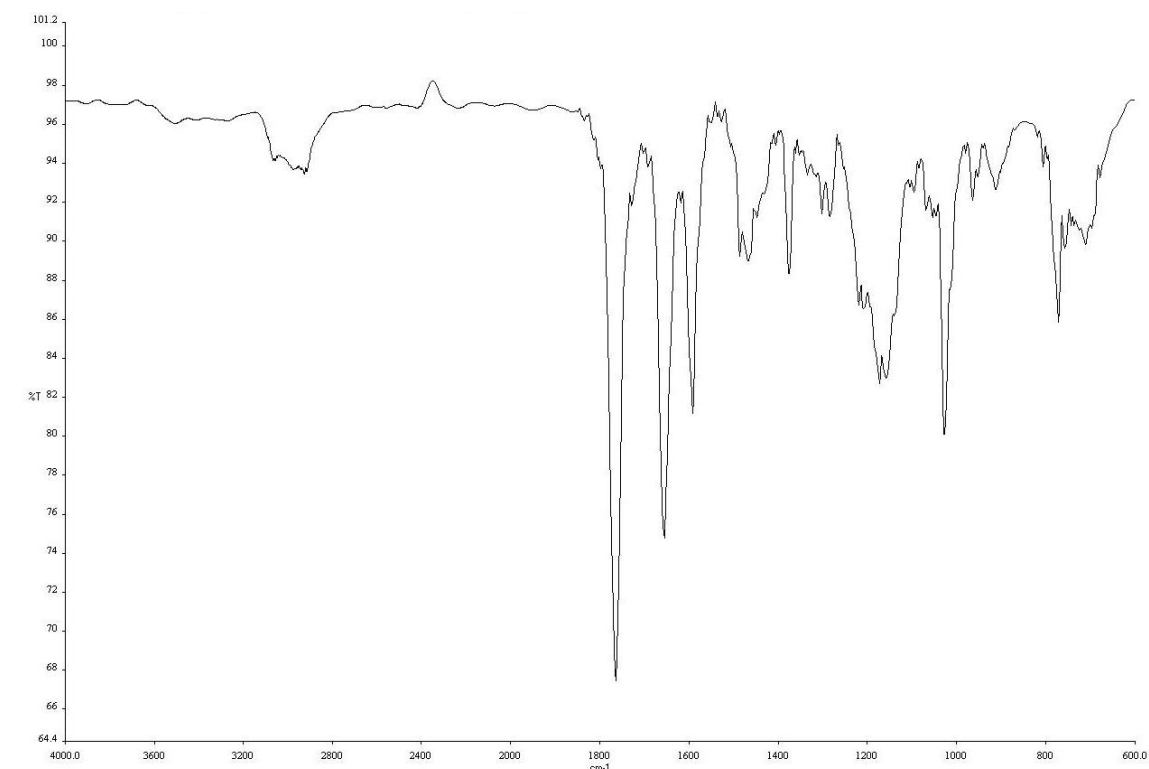
Figure A2.157 IR (NaCl, Thin Film) of compound **S41**.

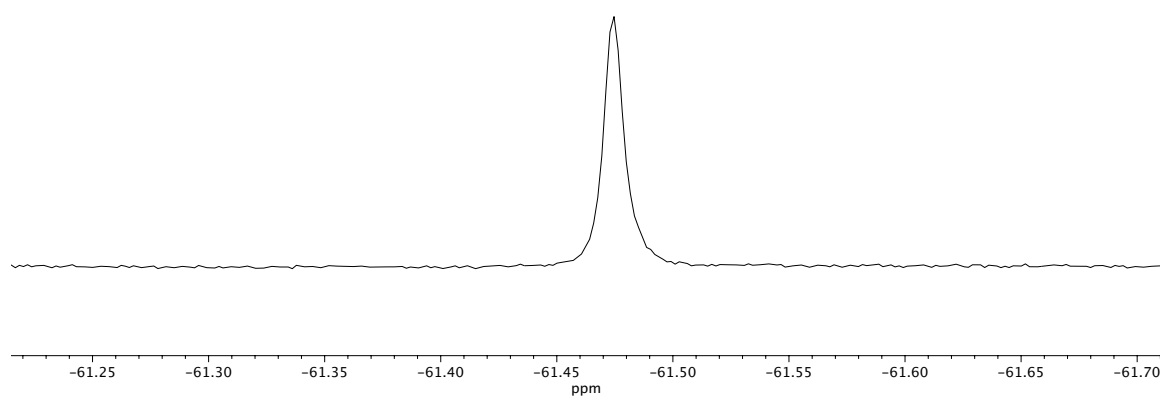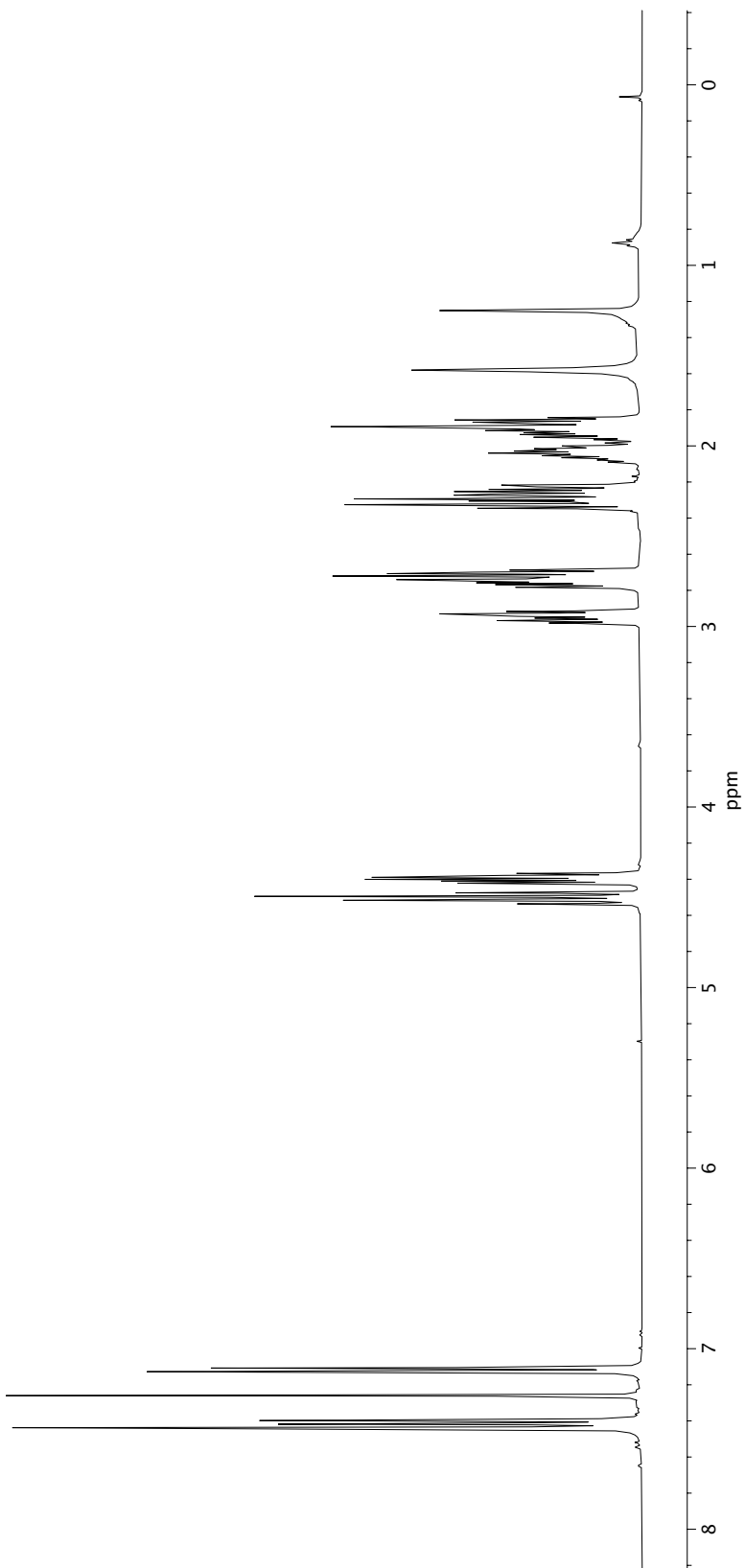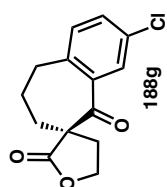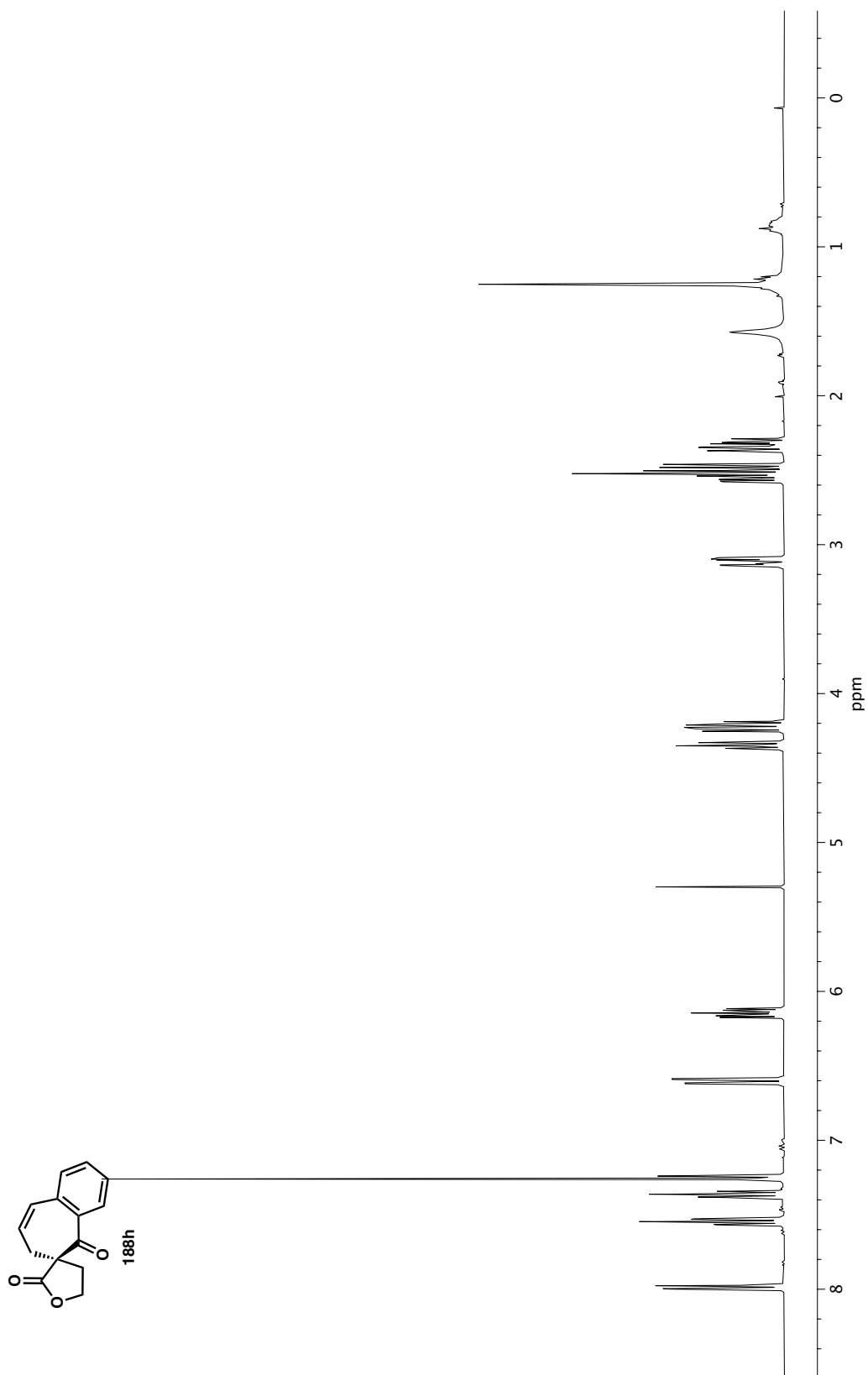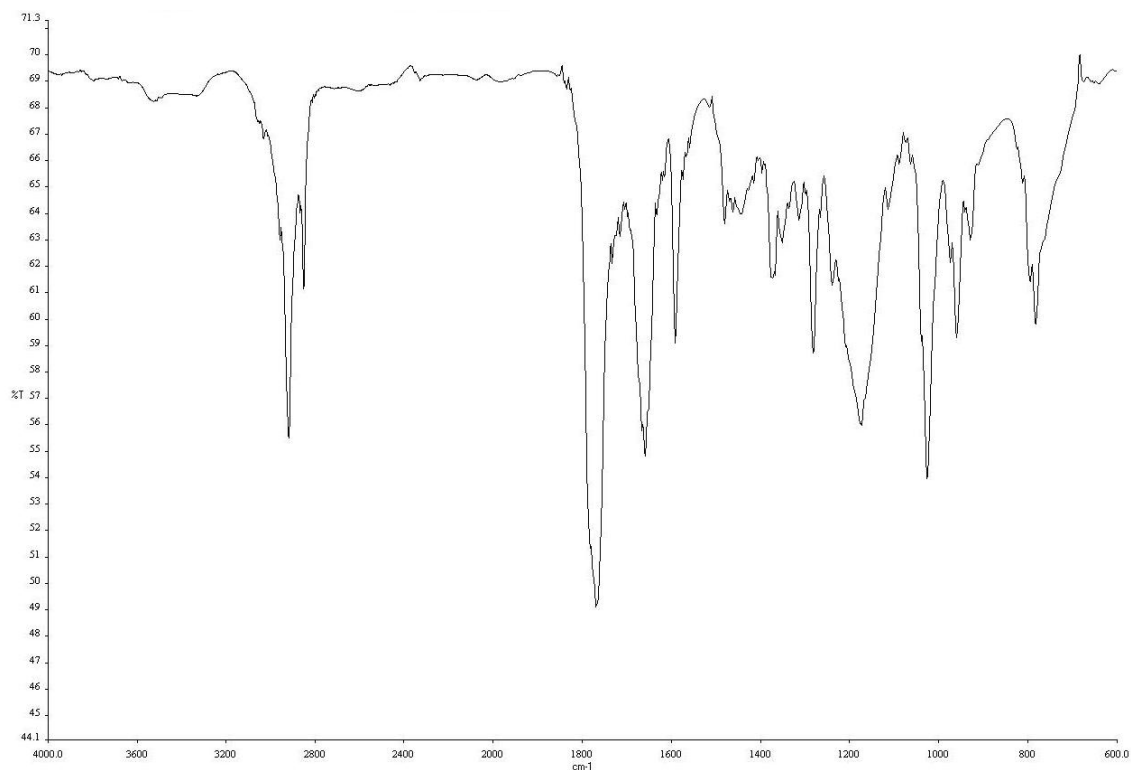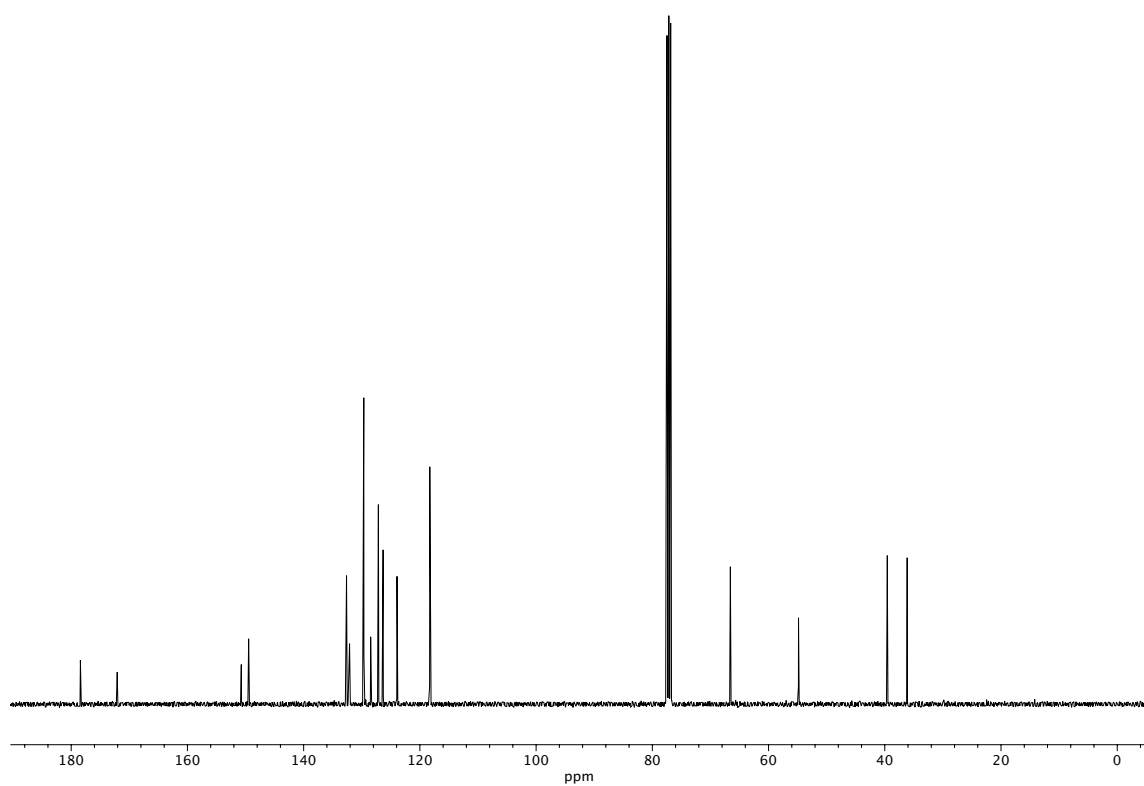**Figure A2.158** ^{13}C NMR (101 MHz, CDCl$_3$) of compound **S41**.

CHAPTER 4

Low Part-Per-Trillion, Humidity Resistant Detection of Nitric Oxide

Using Microtoroid Optical Resonators

4.1 INTRODUCTION

Systems for the selective and rapid detection of gases are important tools used to monitor environmental impacts,[1] occupational safety,[2] and human biomarkers.[3] Nitric oxide is a common byproduct of vehicle exhaust and industrial processes involving combustion, making it a main contributor to air pollution.[4] In fact, nitric oxide is a major industrial emission contributing to ozone layer depletion.[5] In the context of atmospheric chemistry, the detection of nitric oxide at the sub-ppb level is important for the study of climate history, air-snow interactions, and current atmospheric processes.[6–8] Additionally, nitric oxide detection in low ppt levels may have applications in determining the habitability of remote moons and exoplanets,[9] as NO is a biosignature of terrestrial life. In addition to its environmental impacts, nitric oxide also serves as an important biomarker of respiratory health. Higher concentrations of exhaled nitric oxide are associated with asthma and Chronic Obstructive Pulmonary Disease (COPD), and the exhaled nitric oxide (F_ENO) test is commonly administered in the diagnosis of these diseases.[10] Furthermore,

nitric oxide is easily oxidized in air to nitrogen dioxide, a common air pollutant which is highly corrosive and toxic and has been implicated as a danger to human respiratory health.[11] To mitigate injury due to gas exposure and monitor the environmental impacts of industrial processes, selective sensors for NO detection must be developed and deployed.[12] Additionally, for sensors to produce reliable and reproducible results in the field, resistance to external environmental factors such as humidity must be demonstrated.

A variety of sensors have been established for nitric oxide monitoring, including chemical electrode sensors,[13] chemiresistive gas sensors (CGS),[14–18] Rayleigh surface acoustic wave resonators (RSAW)[19] and chemiluminescence-based sensors.[20] The lowest limits of NO detection (sub-ppt) have been achieved with single-wall carbon nanotube (SWNT) based sensors, albeit with a lack of analyte specificity and lab-to-lab perturbations in sensitivity.[15] Semiconductor metal oxide based chemiresistive gas sensors have also demonstrated merit in NO sensing, however their practicality is limited by their extreme operating temperatures.[21] Additionally, chemiresistive gas sensors often display poor humidity tolerance due to the competitive absorption of water onto metal oxide semiconductor surfaces.[22] Recently, the development of humidity resistant materials for gas sensing has received much attention.[23–25] Highly practical, wearable, flexible, and humidity resistant NO/NO_2 gas sensors based on laser-induced graphene were recently reported by Yang and coworkers, displaying a LOD of 8.3 ppb for NO.[14] Despite this advance, there have been no reports of part-per-trillion level nitric oxide sensors that are selective as well as humidity resistant, a gap which we aimed to address through our research efforts.

Recently, our lab developed a platform for selective, ultra-sensitive gas sensing using whispering-gallery mode (WGM) microtoroid sensors coated with polymer brushes.[26] WGM optical microresonators have attracted intense interest in the past decades due to their high quality factors (Q) and small mode volumes, which cause enhanced light matter interaction. In WGM microresonators, photons will take hundreds of thousands of round trips while interacting with analytes on the surface, significantly increasing the optical sensing signal response to analytes. Since 2002, sensing based on WGM mode shift has developed a wide application area, including proteins,[27–30] gases,[26] exosomes,[31,32] nanoparticles,[27] viruses,[33] and even single molecules.[27,34] Frequency locked optical whispering evanescent resonator (FLOWER) is a sensing system that provides a lock-in method to track WGM resonances in real time with high (sub-femtometer) resolution.[27,30,35–38] This system allows us to further investigate the resonance shift of a WGM sensor at timescales as short as milliseconds when the sensor is placed in a continuously changing external environment. FLOWER provides advantages over plasmonic[39] or hybrid plasmonic-WGM sensors[40] in that it uses a bare microcavity, which enables a greater capture area and thus response time.[41]

In this research, we create a WGM gas-sensing platform to enable selective nitric oxide sensing in the low part-per-trillion range (6.4 ppt – 240 ppt). This is two orders of magnitude lower than what has previously been demonstrated with whispering gallery mode sensors for volatile organics such as DIMP, ammonia, and formaldehyde.[26] Co-polymers of 2-(methacryloyloxy) ferrocenecarboxylate (FcMA) and methyl methacrylate (MMA) were synthesized and deposited on the surface of the microtoroid in a polymer

brush. We propose that the selective binding of NO to the Fe centers in the poly(FcMA-MMA) co-polymer coating results in the formation of iron nitrosyl species within the polymer brush, causing brush swelling and a corresponding WGM resonance shift. While polymers of this type have been previously accessed via free-radical polymerization[42] and atom-transfer radical polymerization,[43] to the best of our knowledge, this is the first report of FcMA/MMA statistical co-polymers prepared via reversible addition fragmentation chain-transfer (RAFT) polymerization. Employing RAFT polymerization allowed us to access polymers with precise control over molecular weight while ensuring end-group fidelity. By testing polymeric coatings with various molecular weights and ferrocene content in our gas sensing experiments, we gauged the impacts of these factors on sensor performance. Additionally, our sensor displayed excellent specificity for NO, exhibiting no response greater than blank noise to volatile organics including benzene, hexanes, and diisopropyl methylphosphonate (DIMP). To evaluate the selectivity and practicality of our device, we tested it in different humidity environments, finding that sensor's response was consistent despite changes in humidity. Lastly, we discuss our proposed detection mechanism of NO and explain our sensor's high selectivity.

4.2   EXPERIMENTAL METHODS

Polymer Synthesis and Microtoroid Coating

Statistical co-polymers of 2-(methacryloyloxy) ferrocenecarboxylate and methyl methacrylate were prepared via RAFT polymerization (Scheme 4.1). Chain transfer agent CTA-OSu and radical initiator Int-OSu were employed to reliably install the desired

succinimide ester end group needed for toroid functionalization. Polymer A was prepared

by employing a 1: 10 ratio of FcMA to MMA, leading to a statistical co-polymer with a 1:

8.8 ratio of FcMA: MMA units (determined by ^{1}H NMR) and a M_n of 10.1 kDa, with

excellent polydispersity of M_n/M_w = 1.032. Polymer B was prepared in the same fashion,

however a 1: 20 ratio of FcMA to MMA was employed, leading to a polymer with M_n ~

8.5 kDa, M_n/M_w ~ 1.08 and a FcMA: MMA ratio of 1: 18.5.

Scheme 4.1 *Synthesis of statistical copolymers of 2-(methacryloyloxy) ferrocenecarboxylate and methyl methacrylate via RAFT polymerization.*
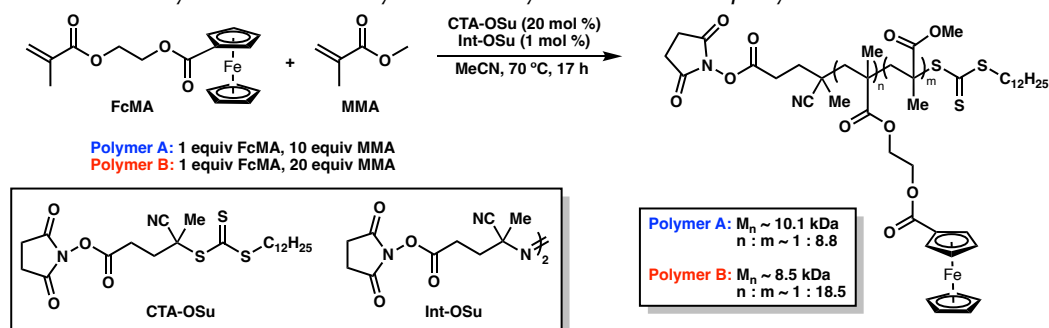
Microdisks were fabricated as previously described[27] in a cleanroom via

photolithography, patterning, and etching. Then, the silica microdisk was reflowed using a

carbon dioxide laser to form a microtoroid structure with a major radius of 100 μm in

diameter and a minor radius of 10 μm. Following plasma treatment of the microtoroid

surface, the chip was immersed in a glass vial containing a 1% solution of 3-(aminopropyl)

triethoxysilane (APTES) in 990 µL of chloroform, functionalizing the silica surface with

free amine groups (Scheme 4.2). The vial was placed on a nutator for 10 min and the chip

was then rinsed with chloroform and dried with nitrogen. Afterwards, the chip was

immersed in a 5 mM solution of either Polymer A or Polymer B for 2 hours, depositing the

polymer brush via an on-toroid amide coupling reaction. The chip was rinsed and blown-dry and then baked on a 100 °C hotplate for 30 min to evaporate most of the solvent and enhance the stability of the surface. Lastly, the chip was placed in a room-temperature vacuum overnight to thoroughly remove residual solvent.

Scheme 4.2 *Deposition of polymer brush onto microtoroid surface.*

(toroid following APTES coating)
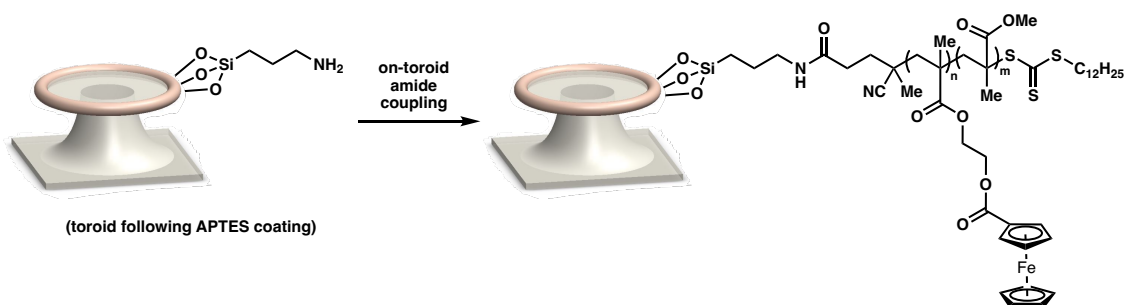
Gas Sensing

The chip was placed inside a small chamber (Figure 4.1a) enclosed inside a larger 20 cm × 10 cm × 10 cm stainless steel box connected to a vacuum to remove residual gas. A TEC element (Thorlabs TECD2S) was placed at the bottom of the small chamber. The small chamber was designed to reduce the space for diffusion and to make gas flow reach the microtoroid more evenly. A FlexStream™ Gas Standard Generator was connected to a flowmeter to read the exact flow rate into the chamber and then connected to the chamber to blow a target gas at a specific flow rate and concentration. The target gas was generated by mixing high concentration gas from a permeation tube and a gas carrier (either nitrogen or argon). This brings the gas to a secondary dilution system for further dilution to low part-per-trillion values. The concentration was controlled by adjusting the primary dilution

flow rate ,F_{pd}, the component gas flow rate, F_c, and diluted gas rate, F_{sd}, in the second dilution system. The final diluted gas concentration in ppm unit C_{ppmv} is given by:

$$C_{ppmv} = \frac{E_{ng/min} \times 22.41 \text{ L/mol}}{MW \times F_{pd}} \times \frac{F_c}{F_c + F_{sd}} \qquad (1)$$

where MW is molecule weight of target gas and $E_{ng/min}$ is the emission rate of the permeation tube. The flowmeter sets the flow rate after the second dilution system.

The FLOWER system uses a tunable laser (Velocity TLB-6700).The laser light polarization is adjusted by a polarization controller and goes through a 50:50 fiber splitter. One beam goes directly to a balanced photodetector (PD) while another goes through a tapered optical fiber. The balanced PD minimizes the effects of laser power fluctuations. A 24-bit data acquisition (DAQ) card collects the real time wavelength signal from both the laser and the temperature sensor. The fundamental mode was selected for tracking, as it exhibits the highest quality factors and greatest field area overlap with the polymer layer where the gas absorption is changing the optical properties of the layer (Figure 4.1c). Afterwards, the laser wavelength was locked-in to the selected fundamental mode and the DAQ monitored both the laser wavelength shift and the temperature sensor to give the raw data of WGM resonance and temperature.

Before testing the response to nitric oxide, argon was blown into the sample chamber for 30 minutes until thermal equilibration occurred. During an experiment, we cycled between blowing in pure argon for 10 minutes as a blank comparison and blowing in the mixed target gas and gas carrier for another 10 minutes. Argon was chosen as the carrier gas for the nitric oxide sensing experiments, as it is more dense than nitric oxide

and therefore can reliably displace it in between cycles. After completing one cycle, recording was stopped for several minutes until the residual waste gas was removed and the chamber re-filled with pure argon. (Figure 4.2)

Figure 4.1 *(a) Diagram of gas-sensing setup (b) Gas chamber with humidity sensor and coupled toroid. (c) Schematic of the coated microtoroid and nitric oxide binding process.*
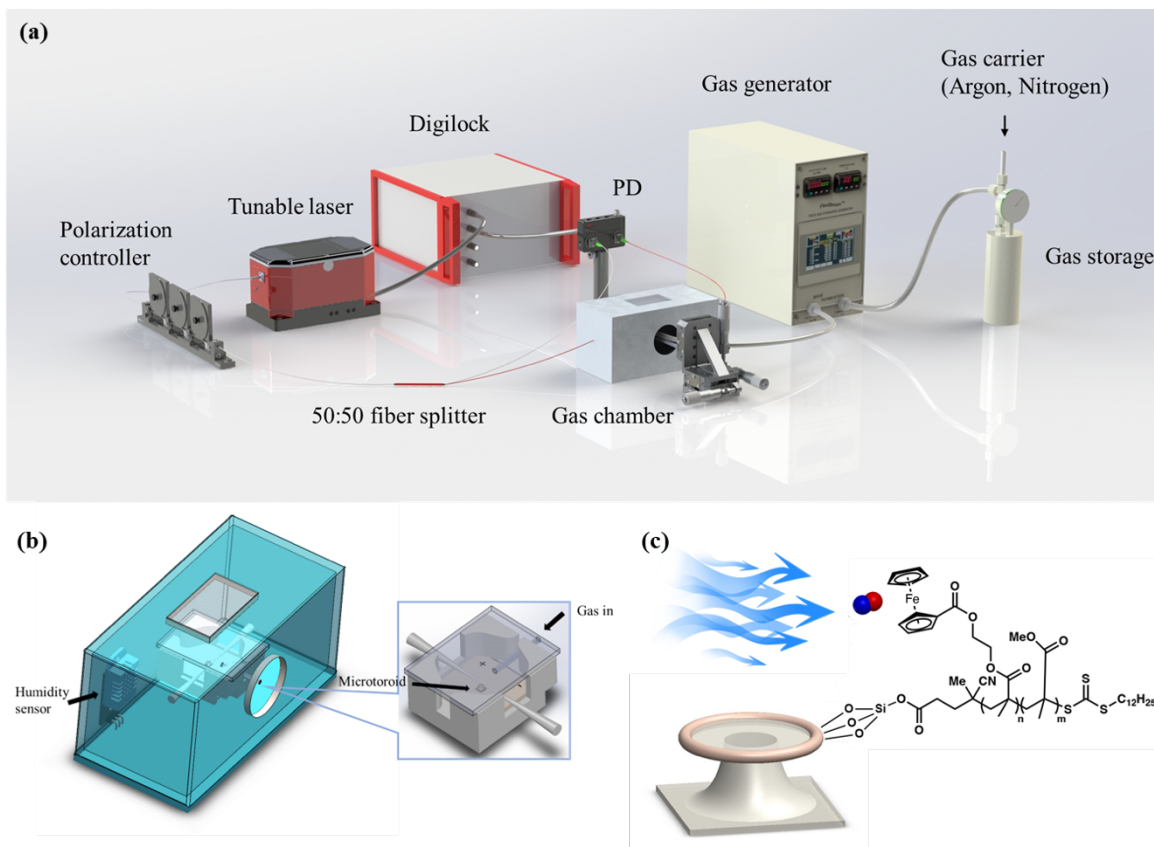
4.3   RESULTS AND DISCUSSION

The WGM resonance wavelength ($\Delta\lambda$) was measured in real time at concentrations from 6.4 ppt to 240 ppt (Figure 4.2). The chamber was purged with argon between each

concentration tested in order to release any NO absorbed in the polymer coating. Linear

fits were assigned to track the sensor's response during the intervals of Ar purging (white

intervals) and nitric oxide exposure (red intervals).

Figure 4.2 (a) FLOWER response to nitric oxide using a Polymer A as the toroid coating. (b) FLOWER response to nitric oxide sensing using Polymer B as the toroid coating.
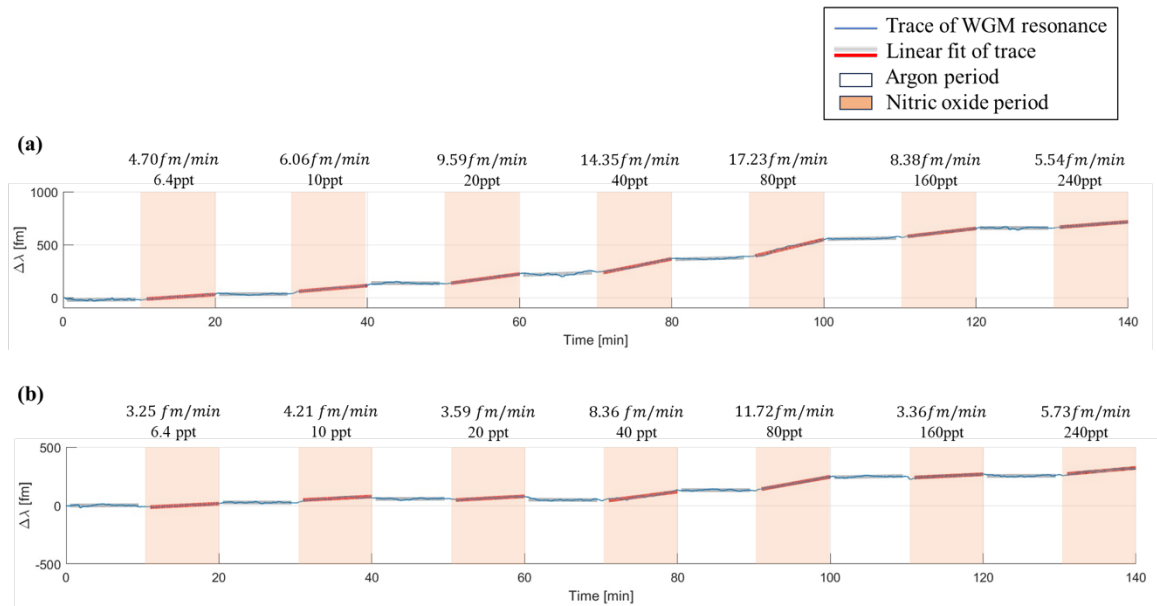
Nitric oxide detection real-time traces post temperature calibration are shown in

Figure 4.3, where the sensor's response is plotted against nitric oxide concentration. The

wavelength shift value ($\Delta\lambda$) is the relative wavelength shift from the starting point. The

slope of the wavelength shift over time is considered to be the target gas response.

Langmuir's theory of adsorption[44] is applied in our case to describe the molecule binding

dynamic and fit the curve of response. The two groups of data were fit to:

$$y = \frac{Bx}{\kappa_d + x} \qquad (2)$$

where B and κ_d are both fitting parameters (Figure 4.3b). By calculating the intersection point between the curve and the blank signal (1.5 fm/min), we derived the LOD (limit of detection) of the sensor for Polymer A to be 2.43 ppt and Polymer B to be 2.91 ppt. The response slope was relatively consistent across trials for concentrations from 0 to 100 ppt. Fluctuations observed at a given concentration between gas sensing trials were attributed to small differences in microtoroid size and polymer surface density. However, it was noted that the sensor's response began to decrease when concentrations above 100 ppt were tested, implying that the polymer coating on the toroid was quickly saturating with gas. The total wavelength shift since time zero is plotted in Figure 4.3d to show that binding continued above 100 ppt although the binding rate is attenuated by the reduced number of binding sites. Concentrations above 240 ppt could also be detected, although this causes the sensor to saturate (Figure S5, Supporting Information). This capability can be valuable for issuing early warnings, as it allows for the detection of NO concentrations within the 6.4 to 240 ppt range, while also indicating when larger concentrations are present. The sensor can also be recovered using heat, thus making it reusable after saturation (Figure S2, Supporting Information).

The impact of the chemical composition and molecular weight of the polymeric coating on the toroid was also evaluated. Polymer A, which contains a higher ratio of FcMA to MMA, displayed a higher response slope than Polymer B for concentrations between 0 and 100 ppt. Polymer A contains twice as many Fe binding sites for nitric oxide

Figure 4.3 *(a) Plot of the sensor response to the tested concentrations of nitric oxide. (b) One-site specific binding curve fit of each response trace. (c) Sensor coated with polymer A response to nitric oxide in different humidity environments. (d) Total wavelength shift since time zero.*
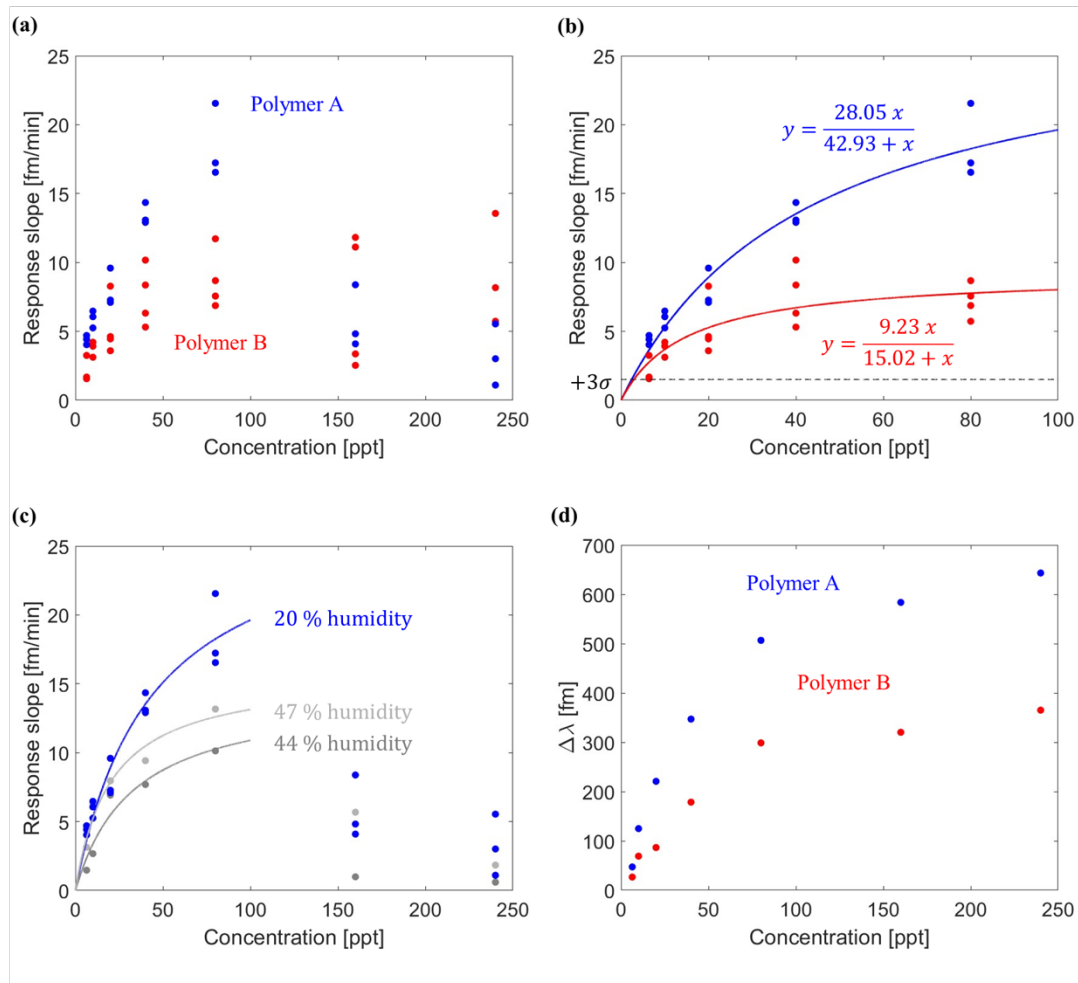
relative to Polymer B, thereby increasing the swelling of the polymer coating and producing a higher response slope. Polymer coatings of lower (~ 6.9 kDa) and higher (~ 19.2 kDa) molecular weights were also tested, but these either provided lower response slopes or saturated more quickly (Figure S4, Supporting Information). Additionally, a

polymer coating with low molecular weight (~ 5.0 kDa) but high FcMA content (1 : 5.7 ratio of FcMA:MMA) produced an irreversible response to NO at ppb-level concentrations (Figure S5b, Supporting Information). We propose that the molecular weight of the polymeric coating impacts the surface density of the polymer brush, which in turn impacts the magnitude of the sensor response. Lower response slopes are observed for polymers with lower molecular weights (5.0 kDa – 6.9 kDa), as there are fewer ferrocene binding sites on shorter chains. Conversely, we propose that larger polymers (~ 19.2 kDa) reduce the surface density of the polymer brush due to additional steric hindrance.[45,46]

To test the practicality of our sensor in the field, we also measured its response to NO in different humidity environments (Figure 4.3c). While competitive water absorption is a major challenge in the development of semiconductor metal oxide-based sensors[22], we hypothesized that the hydrophobic nature of the polymer coating on the microtoroid surface would protect against water absorption. We anticipated that our poly(FcMA/MMA) coatings would have similar water-resistant properties to that of poly(methyl methacrylate), due to their similar chemical composition. Despite being a hydrophobic polymer, poly(methyl methacrylate) can absorb up to 2% (w/w) water and experience a small degree of physical swelling[47]. However, this small amount of water absorption is only observed after the polymer is immersed in distilled water for 24 hours. Therefore, one would expect that the short-term exposure of our similar poly(FcMA-MMA) co-polymer to air with a relative humidity of 47% would not cause significant swelling, due to the polymer's hydrophobic nature. Accordingly, we anticipated the sensor's performance would remain consistent in different humidity environments. Indeed, the sensor displayed a similar

response at 44% or 47% humidity as compared to 20% humidity. The response slopes at higher humidity are largely unaffected at concentrations between 6.4 and 20 ppt, but at concentrations between 40 ppt and 80 ppt, the response slopes are slightly lower than those observed for Polymer A at 20% humidity. While this does slightly increase the error in NO concentration detected, we anticipate that in our future experimentation, we will be able to derive a mathematical model that could be applied to minimize this error. Notably, this constitutes the first report of a humidity resistant, part-per-trillion level nitric oxide sensor.

In addition to humidity resistance, the sensor reported herein also demonstrates excellent selectivity for nitric oxide when compared to other hazard gases including diisopropyl methylphosphonate (DIMP), hexane, and benzene (Figure 4a-c). None of these gases gave a response higher than the blank signal, even when tested at part-per-billion level concentrations.

We propose that the selective binding of NO to the Fe centers in the poly(FcMA-MMA) co-polymer coating results in the formation of iron nitrosyl species within the polymer brush, causing brush swelling and a corresponding WGM resonance shift. NO is an important biological signaling molecule, and the interaction between NO and Fe-containing enzymes is at the heart of many biosignaling pathways.[48] NO is a redox-active ligand that can change oxidation states when bound to a transition metal center. The geometric and electronic structure of metal nitrosyl complexes is a complex phenomenon that has been the subject of intense study, and structure often depends on both the oxidation level of a metal center and its spin state.[49]

Figure 4.4 *Selectivity demonstration of the FLOWER nitric oxide sensor. The sensor is tested in response to (a) DIMP, (b) hexane, (c) benzene. The grey and red line are linear fits to the blank (nitrogen) and the target gas response.*
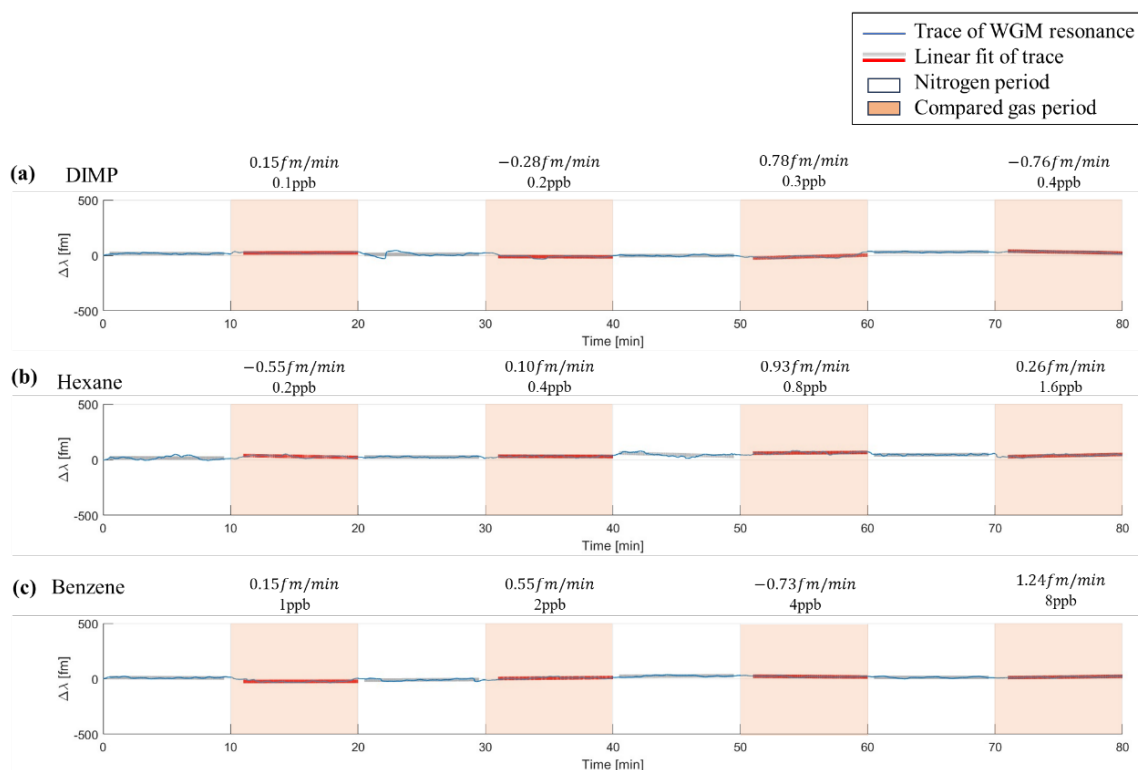
In the context of the nitric oxide sensor reported within, the geometric and electronic structure of the proposed iron nitrosyl species has yet to be elucidated. One possibility is that NO binds as a dative (L-type) ligand to the Fe center. As ferrocene is already an 18 electron complex, Cp ring slippage[50] would be necessary to generate a stable iron nitrosyl species that avoids an unfavorable 20-electron configuration (Figure S7, Supporting Information). To the best of our knowledge, ferrocene-nitrosyl complexes of this type have not yet been reported in the literature. Future studies are required to

determine the geometric and electronic structure of the iron nitrosyl species formed on the surface of the sensor.

One other mechanistic possibility we considered was a redox reaction between NO and ferrocene to form a ferrocenium hyponitrite species.[51–53] We hypothesized that a colorimetric change in the polymer coating associated with the oxidation of ferrocene (yellow) to ferrocenium (blue) could change the coating's refractive index, causing a WGM resonance shift. To test this hypothesis, we performed a solution-phase experiment wherein NO gas was bubbled through a solution of the poly(FcMA-MMA) co-polymer in MeCN. If the proposed oxidation occurred, we would have expected to observe a color change from yellow to blue. Instead, the solution stayed yellow even after 10 minutes of NO sparging, and no redox reaction was observed (Figure S21, Supporting Information). This experimental result does not support a redox mechanism; however, it cannot be ruled out at this time.

In comparison to existing technologies for nitric oxide sensing, the FLOWER sensor reported herein displayed the lowest experimentally detected concentration to date of 6.4 ppt, with an LOD of 2.43 ppt (Table 4.1). Slightly lower limits of detection were reported for carbon nanotube sensors,15 albeit with a lack of selectivity. Except for carbon nanotube sensors, our FLOWER sensor is the only other reported device that can measure nitric oxide in the low part-per-trillion range, and its humidity resistance and selectivity provide distinct advantages over existing nitric oxide sensors.

Table 1. Comparison of FLOWER-based NO sensor against existing technologies.

Sensing Technique	Calculated LOD	Concentration Range	Lowest Concentration Experimentally Detected	References
FLOWER	2.43 ppt	6.4 ppt – 240 ppt*	6.4 ppt	This paper
Carbon nanotube chemiresistor	590 ppq	10 ppt – 500ppm	10 ppt	[15]
Carbon nanotube chemiresistor	0.2 ppb	100 ppb – 5 ppm	100 ppb	[16]
Graphene chemiresistor		2 ppb – 420 ppb	2 ppb	[17]
LIG chemiresistor	8.3 ppb	20 ppb – 1 ppm	20 ppb	[14]
ZnO chemiresistor	10 ppb	10 ppb – 1 ppm	10 ppb	[18]
RSAW resonator	23 ppb	100 ppb –700ppb	100 ppb	[19]
RSAW resonator		1 ppb – 200 ppb	1 ppb	[54]
Chemical electrode	350 ppb	2.5 ppm – 10 ppm	2.5 ppm	[13]

* We can detect higher concentrations if the sensor is heated (Fig. S5)

4.4 CONCLUSION

In this paper, we exhibit low part-per-trillion level selective nitric oxide detection using WGM microtoroids functionalized with novel polymeric coatings. We synthesized ferrocene-containing polymers via RAFT polymerization that enable the sensor's selective responsive to nitric oxide, finding that more ferrocene-rich polymers with molecular weights around 10 kDa displayed the best sensing capabilities. With FLOWER real-time resonance tracking, we experimentally detected nitric oxide in concentrations as low as 6.4 ppt, the lowest experimentally demonstrated concentration reported in the literature, and we theoretically calculated an LOD of 2.43 ppt with a one-site binding model. Humidity resistance of the sensor was enabled by the hydrophobic nature of the polymer coatings

employed. Control experiments with several hazardous gases demonstrated the selectivity

of our sensor to nitric oxide.

4.5   EXPERIMENTAL SECTION

4.5.1 Temperature Calibration

Lock-in resonance shift raw data from FLOWER system and concurrent

temperature sensor trace data. This data is subtracted to give the final trace.

Figure 4.5. (a) Raw resonance shift data and real-time temperature trace. (b) Resonance shift after calibration.
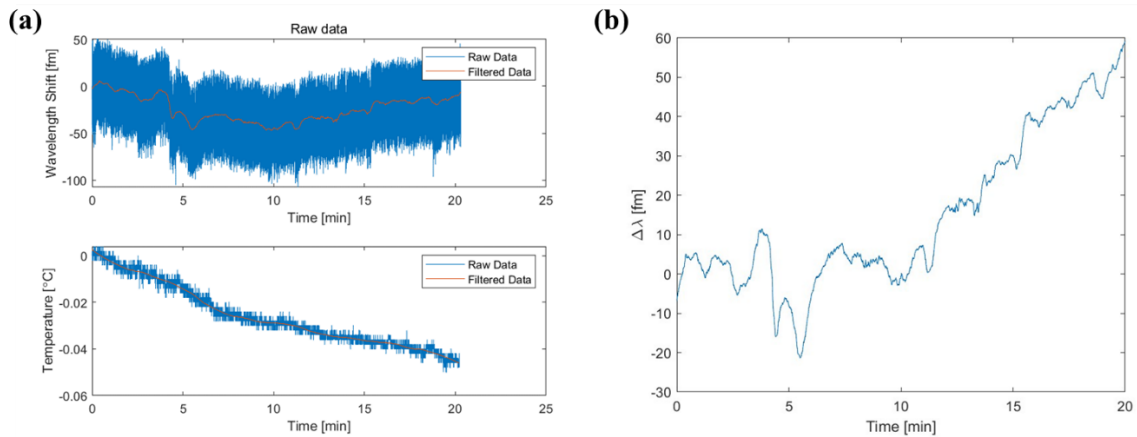
4.5.2 Sensor Recovery

After saturation was observed for polymer C, a TEC heating element was set to

100ºC to recover the signal. Sensor recovery was then observed.

Figure 4.6. *Sensor recovery experiment. The blue arrow points to the time that heating was applied. Comparing the response from 40 min to 60 min and 80 min to 100 min, heating can recover the sensor's performance.*
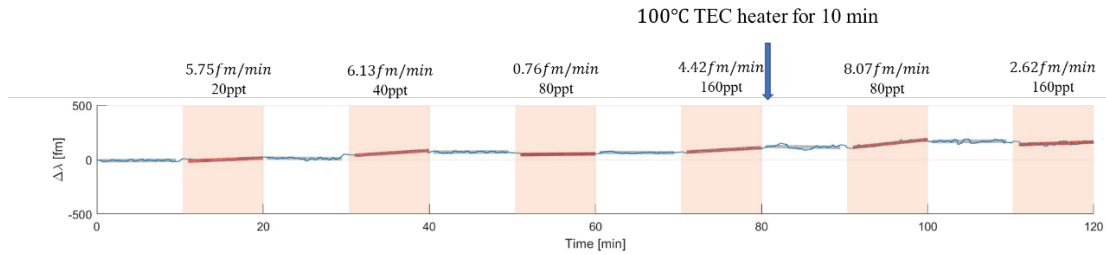
4.5.3 Control Experiments

To demonstrate the necessity of the FcMA/MMA copolymer coating, we also tested microtoroids coated with either a ferrocenyl monolayer or poly(methyl methacrylate) (PMMA) in our nitric oxide sensing experiments (Figure 4.7a). The ferrocenyl monolayer-coated microtoroid sensor displayed some response to nitric oxide at very low concentrations (6.4 ppt – 10 ppt) but quicky saturated (Figure 4.7a). The PMMA coated microtoroid did not provide a response above that of the control for concentrations from 6.4 ppt – 480 ppt (Figure 4.7b). Taken together, these results imply that the FcMA/MMA co-polymer coating is necessary to generate a sensitive and selective response of the sensor to nitric oxide.

Figure 4.7 *(a) Structures of ferrocenyl monolayer and PMMA attached to the microtoroid. (b) Sensor response to nitric oxide for microtoroid coated with a ferrocenyl monolayer. (c) Sensor response to nitric oxide for microtoroid coated with PMMA.*

(a)

Ferrocenyl monolayer
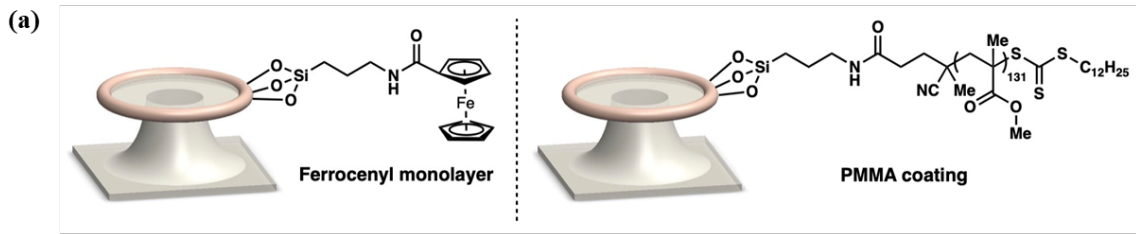
PMMA coating

(b)

Coating: Ferrocenyl monolayer
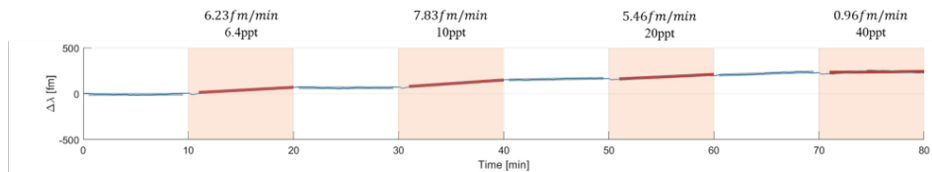
(c)

Coating: PMMA
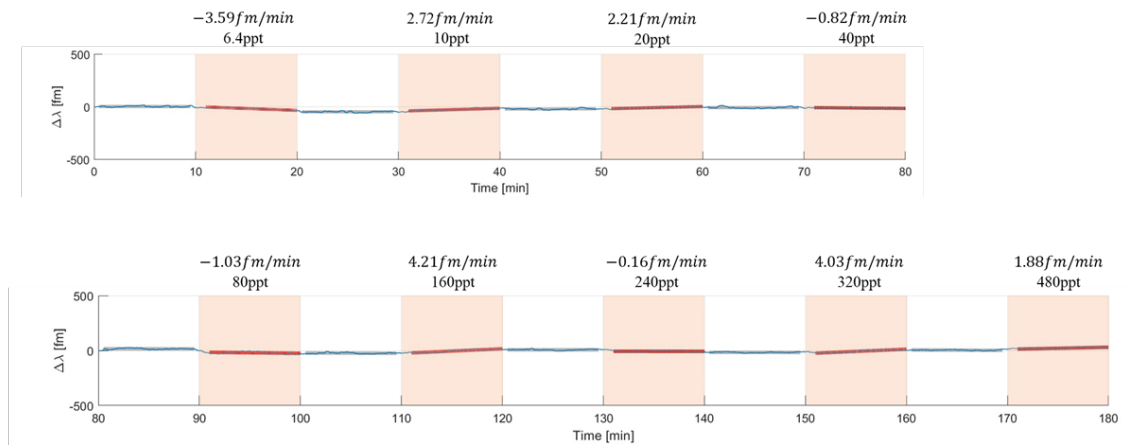
4.5.4 Effect of Polymer Molecular Weight on Sensing Capabilities

In addition to polymer A and B, we also evaluated the sensing capabilities of the polymeric coatings shown in Figure 4.8a. Polymers C and D contain similar FcMA content to Polymer B, but they differ in polymer chain length. Polymer E is a homopolymer of 2-(methacryloyloxy) ferrocenecarboxylate (FcMA) with a molecular weight of ~ 5.9 kDa. Figure 4.8b shows the response of a microtoroid coated with Polymer C to nitric oxide. Although a response was observed for concentrations from 6.4 ppt – 40 ppt, saturation

behavior was observed at a lower concentration of 40 ppt, whereas Polymer B saturated at

a higher concentration of 160 ppt. Polymer D has a similar n: m ratio with polymer C while

it has smaller molecule weight. However, the performance in Figure 4.8c shows that

polymer D has a higher response and saturation concentration. Polymer E, with a different

structure, showed some response to nitric oxide from 10 ppt to 80 ppt, but the response

slope was significantly lower at all concentrations measured. Interestingly, Polymer F, the

most ferrocene-rich polymer tested, displayed a lower response slope to NO for the

concentration range evaluated.

The response from different polymers indicates that the sensitivity is not simply

linearly related to either molecular weight of the polymer chain or the n: m ratio. For clarity,

plots of sensitivity versus the n: m ratio, molecular weight, and total number of ferrocene

binding sites are shown in Figure 4.8f. The values of the response at 40 ppt of Polymers A,

B, C, D, F divided by concentration are taken as sensitivity with units of fm/(min·ppt). The

number of ferrocene binding sites is roughly proportional to MW times the n: m ratio. From

Figure 4.8f we conclude that the sensitivity has a positive correlation with molecular

weight when the molecular weight is lower than 11 kDa. The larger polymers (~ 19.2 kDa)

reduce the surface density of the polymer brush due to additional steric hindrance. This

effect also has an impact on the sensitivity versus number of ferrocene binding sites.

Figure 4.8 *(a) Structures of Polymers C − E. (b) FLOWER response to nitric oxide*

using a coating of Polymer C. (c) FLOWER response to nitric oxide using a coating of

Polymer D. (d) FLOWER response to nitric oxide using a coating of Polymer E. (e)

FLOWER response to nitric oxide using a coating of Polymer F. (f) Sensitivity versus n: m ratio, molecular weight (MW) and number of ferrocene binding sites (represented as MW times n: m ratio).
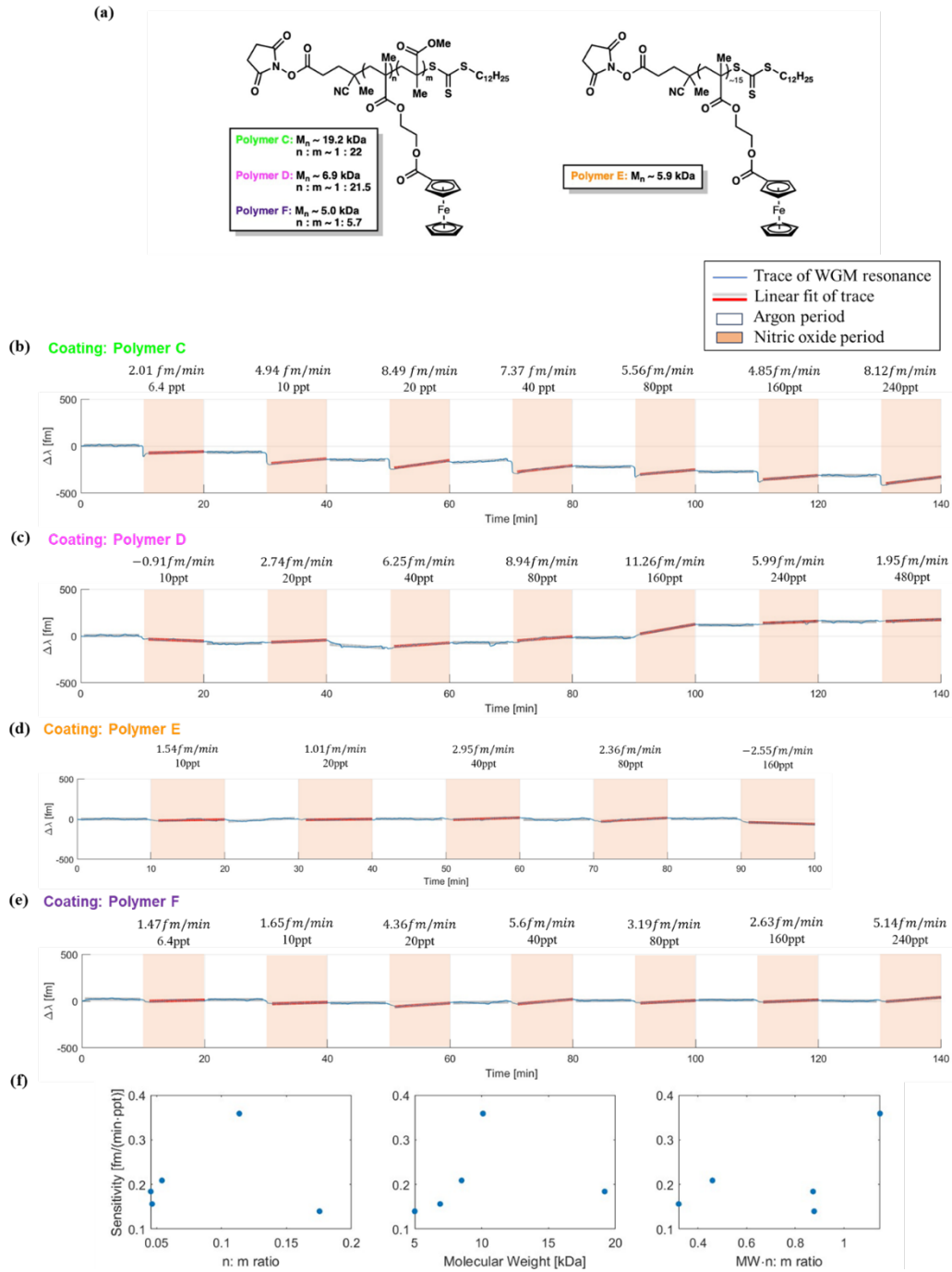
4.5.5 Sensor Performance at High Concentration

The sensors using Polymer B and Polymer F are tested at a higher concentration range. Both polymers showed saturation after the first concentration. For high concentration nitric oxide detection, a cleaning process is necessary if the sensor is to be used multiple times.

Figure 4.9 *(a) FLOWER response to nitric oxide using Polymer B from 0.26 to 1.5 ppb of NO. (b) FLOWER response to nitric oxide using Polymer F from 0.5 to 2 ppb.*
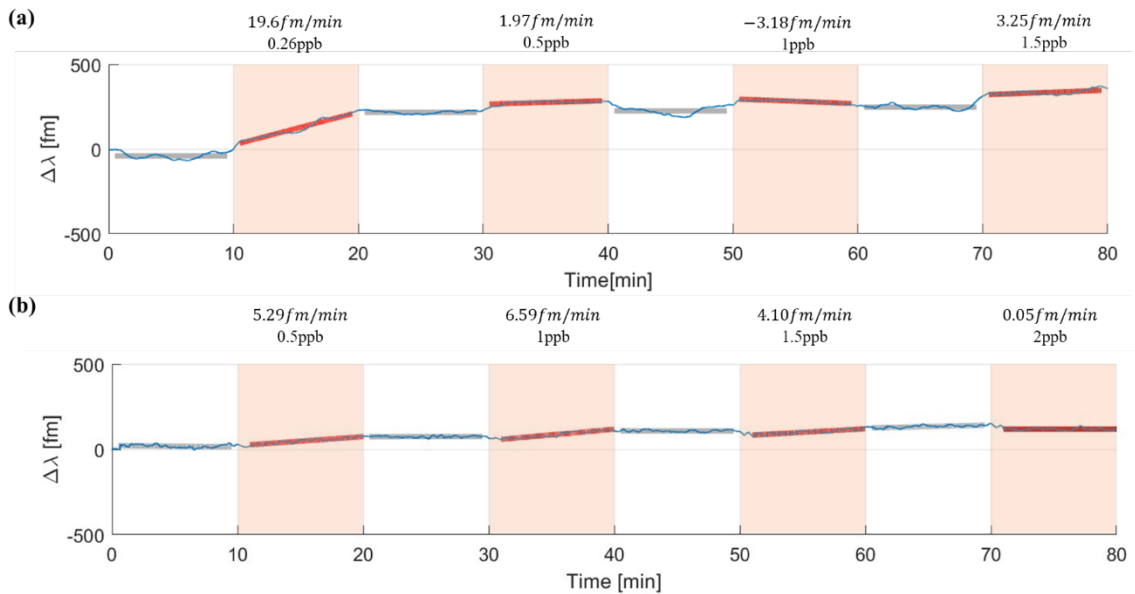
4.5.6 Humidity Sensing Experiments

High humidity environments were generated by putting water containers into the sample chamber (Figure 4.10). This approach was chosen to minimize noise generated by commercial humidifiers. A humidity sensor recorded the real-time humidity value in the chamber. This relatively sealed environment reached vapor-liquid equilibrium after over

an hour. After reaching equilibrium, temperature recording began and resonance shift tracking began.

Figure 4.10 *Top view of the big chamber. Water containers inside the chamber generate a humid environment. The chamber is covered during experimentation.*
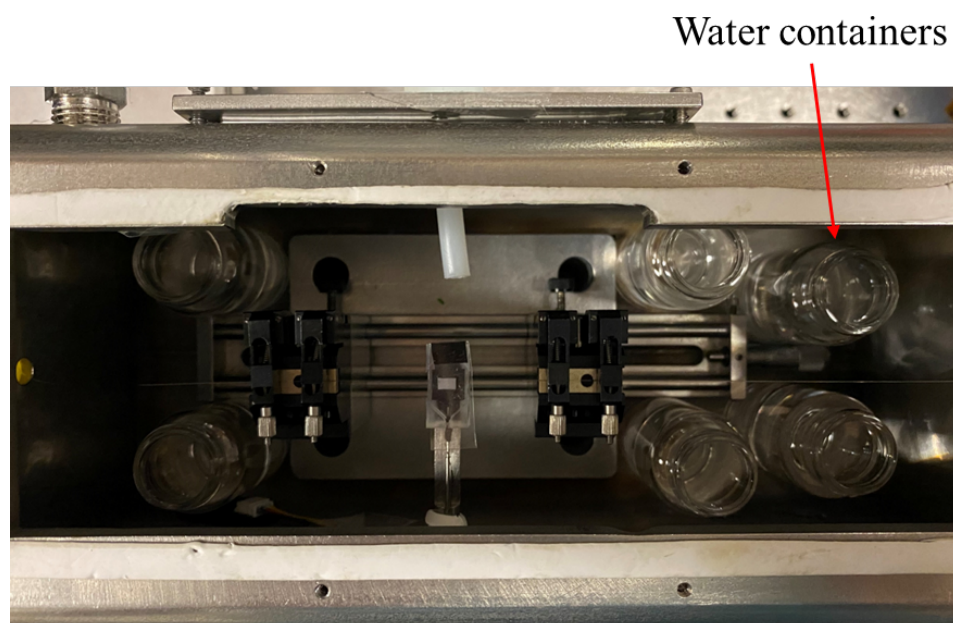
4.5.7 Hypothesized Mechanism of NO Binding

Figure 4.11 *Possible structure of iron nitrosyl complex formed upon binding of NO to the Fe centers embedded in the polymer.*
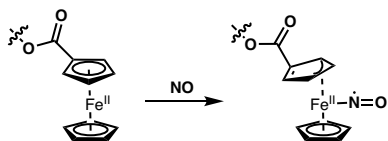
4.5.8 Polymer Synthesis and Characterization

All synthetic procedures were carried out using dry and degassed acetonitrile. CTA-OSu[55] and int-OSu[56] were prepared according to the literature protocol. FcMA was

prepared according to the literature protocol[43]. Methyl methacrylate (stabilized with 6-*tert*-Butyl-2,4-xylenol) was obtained from Tokyo Chemical Industry, and the inhibitor was removed immediately prior to polymerization via a short basic alumina plug. ^{1}H NMR spectra were collected with a 400 mHz Bruker spectrometer and reported relative to residual CHCl$_3$ (δ = 7.26 ppm). Size Exclusion Chromatography data were collected using an Agilent 1260 series pump equipped with two Agilent PLgel MIXED-B columns (7.5 x 300 mm), an Agilent 1200 series diode array detector, a Wyatt 18-angle DAWN HELEOS light scattering detector, and an Optilab rEX differential refractive index detector. The mobile phase was THF at a flow rate of 1 mL/min. The dn/dc value of the FcMA/MMA co-polymer at 25 ºC in THF was determined to be 0.094 mL/g via online calculation using injections of known concentration and mass.

Scheme 4.3 *Synthesis of poly(FcMA-MMA) via RAFT Polymerization*
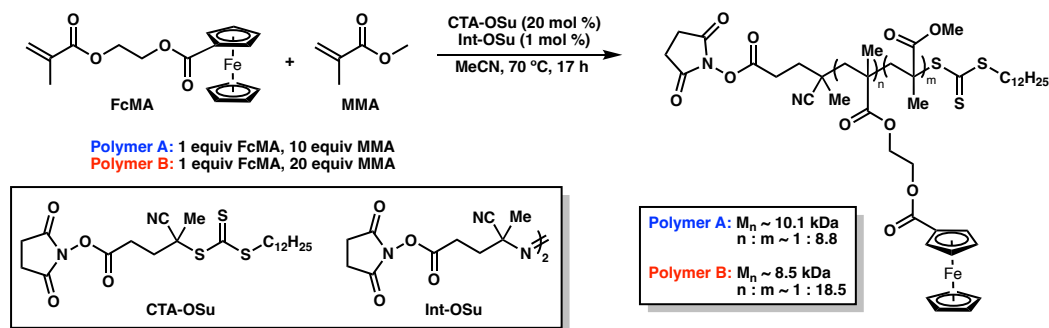
General Procedure for FcMA/MMA Co-polymer Synthesis

A 25 mL Schlenk tube was charged with a stir bar, CTA-OSu (0.2 equiv), int-OSu (0.01 equiv), and FcMA (1 equiv) as solids. Methyl methacrylate (10 **or** 20 equiv) was added via syringe, then dry MeCN (2.0 M in FcMA) was added via syringe. The flask was sealed and subjected to three freeze-pump-thaw cycles. After the final thaw, the flask was

not backfilled with inert gas. The reaction was placed in a 70 ºC oil bath, protected with a blast shield, and stirred for 17 h. The reaction was allowed to cool to 23 ºC, opened to air, and diluted with ~ 5 mL CHCl$_3$ and the resulting viscous orange polymer was dissolved by vortexing. The solution was added dropwise to a flask of Et$_2$O (150 mL) at -78 ºC with stirring to precipitate the FcMA/PMMA co-polymer. The solution was filtered through a medium porosity sintered glass frit, and the resulting sticky orange residue was re-dissolved in 2-5 mL of CHCl$_3$ and added dropwise to a flask of hexanes (150 mL) at -78 ºC with stirring to re-precipitate the polymer. The solution was filtered as described above and the filtrate was washed with ~ 60 mL of hexanes (3 x 20 mL portions). The resulting light orange powder was dried under high vacuum at 40 ºC overnight to remove any residual solvent.

Polymer A (n: m = 1: 8.8)

Polymer A was prepared as described by the general procedure above using 10 equiv of MMA relative to 1 equiv of FcMA. M$_n$ (GPC) ~ 10.1 kDa, PDI = 1.03. ^{1}H NMR (400 MHz, CDCl$_3$, 298 K) δ 4.84 (bs), 4.44 (bs, overlapped), 4.41 (bs, overlapped), 4.23 (bs, overlapped), 3.59 (bs), 3.23 (t), 2.85 (bs, overlapped), 1.80 (bm), 1.25 (bs), 1.02 (bs), 0.85 (bm). Note: many of the aliphatic signals below 2 ppm are indiscernible due to substantial overlap. However, signals attributable to the succinimide ester end group and ferrocenyl protons are clearly marked.

Polymer B (n: m = 1: 18.5)

Polymer B was prepared as described by the general procedure above using 20 equiv of MMA relative to 1 equiv of FcMA. M_n (GPC) ~ 8.5 kDa, PDI = 1.06. ^{1}H NMR (400 MHz, CDCl$_3$, 298 K) δ 4.94 (bs), 4.36 (bs, overlapped), 4.22 (bs, overlapped), 3.59 (bs), 2.85 (bs, overlapped), 1.80 (bm), 1.24 (bs), 1.01 (bs), 0.85 (bm). Note: many of the aliphatic signals below 2 ppm are indiscernible due to substantial overlap. However, signals attributable to the succinimide ester end group and ferrocenyl protons are clearly marked. Additionally, the use of different experimental parameters (number of scans and relaxation delay) in the collection of this spectra is responsible for the peak broadening observed.

Polymer C (n: m = 1: 22)

Polymer C was prepared as described by the general procedure above using 20 equiv of MMA relative to 1 equiv of FcMA, and 0.1 equiv of the CTA-OSu was used instead of 0.2 equiv. M_n (GPC) ~ 19.2 kDa, PDI = 1.05. ^{1}H NMR (400 MHz, CDCl$_3$, 298 K) δ 4.83 (bs), 4.44 (bs, overlapped), 4.40 (bs, overlapped), 4.22 (bs, overlapped), 3.58 (bs), 2.84 (bs, overlapped), 1.80 (bm), 1.24 (bs), 1.00 (bs), 0.83 (bm).

Polymer D (n: m = 1: 21.5)

Polymer D was prepared as described by the general procedure above using 20 equiv of MMA relative to 1 equiv of FcMA, and 0.4 equiv of the CTA-OSu were used instead of 0.2 equiv. M_n (GPC) ~ 6.9 kDa, PDI = 1.22. ^{1}H NMR (400 MHz, CDCl3, 298

K) δ 5.01 (bs), 4.42 (bs, overlapped), 4.33 (bs, overlapped), 4.21 (bs, overlapped), 3.59 (bs), 2.85 (bs, overlapped), 1.80 (bm), 1.25 (bs), 1.01 (bs), 0.85 (bm).

Polymer E

To a solid mixture of 2-(Methacryloyloxy)ethyl ferrocenecarboxylate (1.07 g, 3.12 mmol), CTA1 (100 mg, 0.2 mmol), and OSu initiator (4.3 mg, 0.010 mmol) was added anhydrous acetonitrile (2.5 mL). The resulting suspension was sealed in a thick walled reaction vessel fitted with a threaded PTFE high vacuum valve. The reaction mixture was degassed by three freeze-pump-thaw cycles. The reaction vessel was not backfilled with inert gas prior to heating. The reaction mixture was heated at 70 °C for 24 h. [Note: the reaction mixture was observed to become homogeneous within ca. 5 minutes of heating.] Upon cooling, an amorphous mass separated from the solution. Following exposure to air, the reaction mixture was dissolved into 10 mL of chloroform and precipitated into ca. 200 mL of methanol cooled to -78 °C. The resulting suspension was filtered through a medium porosity sintered glass frit, and the isolated solids were washed with room temperature methanol (3 x 20 mL). The resulting yellow solids were exposed to high vacuum at 40 °C overnight to remove residual volatiles. M_n (GPC) = 5.9 kDa, PDI = 1.04. ^{1}H NMR (400 MHz, CDCl$_3$, 298 K): δ 4.94 (bs), 4.74-3.99 (m), 3.21 (bs), 2.84 (s), 2.74 (bs), 2.17 (s, overlapped), 1.95 (bs), 1.80 (s), 1.62 (bs), 1.25 (s), 1.13 (s), 0.98 (bs), 0.92-0.84 (m).

Polymer F (n: m = 1: 5.7)

Polymer F was prepared as described by the general procedure above using 7.5 equiv of MMA relative to FcMA. M_n (GPC) = 5.0 kDa, PDI = 1.11. ^{1}H NMR (400 MHz,

CDCl$_3$, 298 K): δ 4.95 (bs), 4.36 (bs, overlapped), 4.23 (bs, overlapped), 3.59 (bs), 3.23 (bs), 2.85 (bs, overlapped), 1.81(bm), 1.25 (bs), 1.02 (bs), 0.88 (bm).

Polymer Stability Over Time

NMR of Polymer B After One Year of Storage at 23 ºC:

^{1}H NMR (400 MHz, CDCl$_3$, 298 K) δ 4.84 (bs), 4.44 (bs, overlapped), 4.40 (bs, overlapped), 4.23 (bs, overlapped), 3.59 (bs), 2.85 (bs, overlapped), 1.80 (bs), 1.24 (bs), 1.01 (bs), 0.84 (bm). Comparing to the spectrum taken immediately after isolation, there is no evidence of polymer chain scission or decomposition over time.

Figure 4.12 *^{1}H NMR spectrum of Polymer B after one year.*
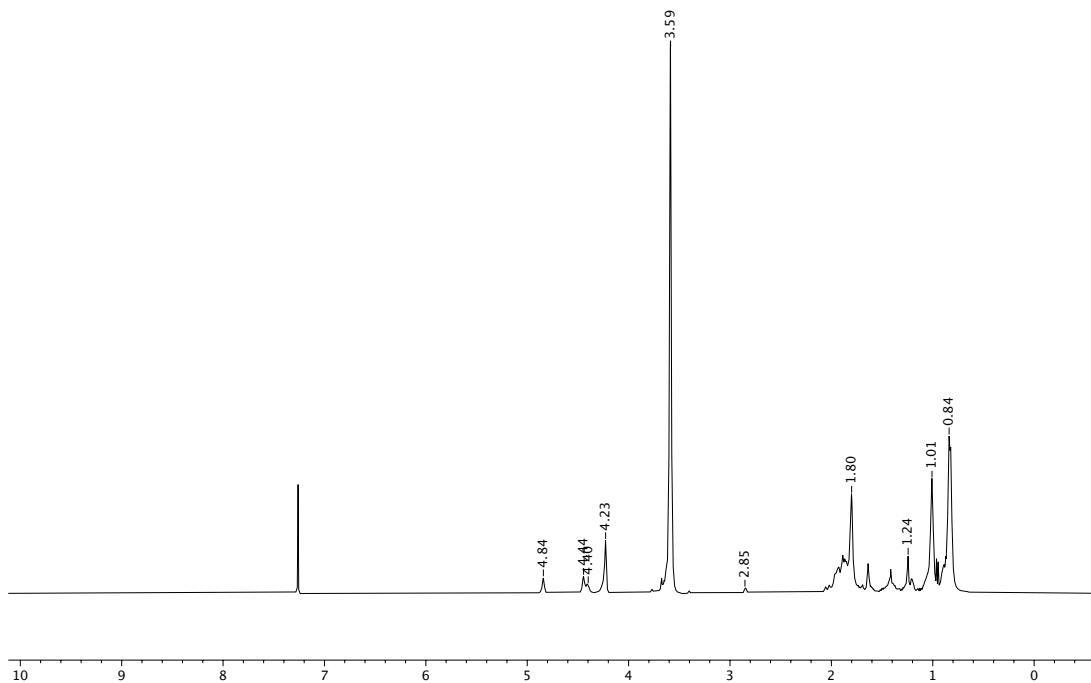
4.5.9 Testing Redox Reaction Mechanistic Hypothesis

Figure 4.13 *Testing redox reaction mechanism by sparging a solution of polymer with NO.*

| 0 minutes | 10 minutes |
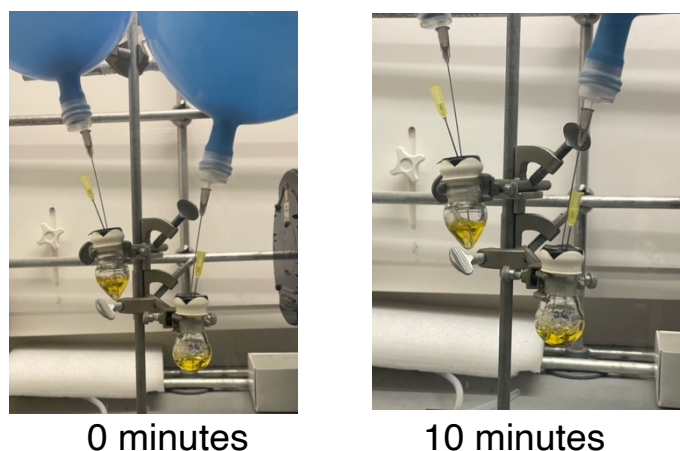
Procedure: A solution of Polymer A (~ 10 mg) in dry, degassed MeCN was sparged vigorously with 22 ppmv NO in N_2 for 10 minutes, and the color of the solution was monitored. No color change was observed.

4.6   REFERENCES

(1)   Dhall, S.; Mehta, B. R.; Tyagi, A. K.; Sood, K. A Review on Environmental Gas Sensors: Materials and Technologies. *Sensors International* **2021**, *2*, 100116.

(2)   Bag, A.; Lee, N.-E. Recent Advancements in Development of Wearable Gas Sensors. *Advanced Materials Technologies* **2021**, *6* (3), 2000883.

(3)   Privett, B. J.; Shin, J. H.; Schoenfisch, M. H. Electrochemical Nitric Oxide Sensors for Physiological Measurements. *Chem. Soc. Rev.* **2010**, *39* (6), 1925–1935.

(4)   Kampa, M.; Castanas, E. Human Health Effects of Air Pollution. *Environmental Pollution* **2008**, *151* (2), 362–367.

(5)   Ravishankara, A. R.; Daniel, J. S.; Portmann, R. W. Nitrous Oxide (N2O): The Dominant Ozone-Depleting Substance Emitted in the 21st Century. *Science* **2009**, *326* (5949), 123–125.

(6)   Dominé, F.; Shepson, P. B. Air-Snow Interactions and Atmospheric Chemistry. *Science* **2002**, *297* (5586), 1506–1510.

(7)   Honrath, R. E.; Lu, Y.; Peterson, M. C.; Dibb, J. E.; Arsenault, M. A.; Cullen, N. J.; Steffen, K. Vertical Fluxes of NOx, HONO, and HNO3 above the Snowpack at Summit, Greenland. *Atmospheric Environment* **2002**, *36* (15), 2629–2640.

(8)   Wang, F.; Lin, W.; Wang, J.; Zhu, T. NOx Release from Snow and Ice Covered Surface in Polar Regions and the Tibetan Plateau. *Advances in Climate Change Research* **2011**, *2* (3), 141–148.

(9)   Airapetian, V. S.; Jackman, C. H.; Mlynczak, M.; Danchi, W.; Hunt, L. Atmospheric Beacons of Life from Exoplanets Around G and K Stars. *Sci Rep* **2017**, *7* (1), 14141.

(10) Taylor, D. R.; Pijnenburg, M. W.; Smith, A. D. Exhaled Nitric Oxide Measurements: Clinical Application and Interpretation. *Thorax* **2006**, *61* (9), 817–827.

(11) Faustini, A.; Rapp, R.; Forastiere, F. Nitrogen Dioxide and Mortality: Review and Meta-Analysis of Long-Term Studies. *European Respiratory Journal* **2014**, *44* (3), 744–753.

(12) Ménil, F.; Coillard, V.; Lucat, C. Critical Review of Nitrogen Monoxide Sensors for Exhaust Gases of Lean Burn Engines. *Sensors and Actuators B: Chemical* **2000**, *67* (1), 1–23.

(13) Lin, C.-Y.; Chen, J.-G.; Hu, C.-W.; Tunney, J. J.; Ho, K.-C. Using a PEDOT:PSS Modified Electrode for Detecting Nitric Oxide Gas. *Sensors and Actuators B: Chemical* **2009**, *140* (2), 402–406.

(14) Yang, L.; Zheng, G.; Cao, Y.; Meng, C.; Li, Y.; Ji, H.; Chen, X.; Niu, G.; Yan, J.; Xue, Y.; Cheng, H. Moisture-Resistant, Stretchable NOx Gas Sensors Based on Laser-Induced Graphene for Environmental Monitoring and Breath Analysis. *Microsyst Nanoeng* **2022**, *8* (1), 1–12.

(15) Chen, G.; Paronyan, T. M.; Pigos, E. M.; Harutyunyan, A. R. Enhanced Gas Sensing in Pristine Carbon Nanotubes under Continuous Ultraviolet Light Illumination. *Sci Rep* **2012**, *2* (1), 343.

(16) Jeon, J.-Y.; Kang, B.-C.; Byun, Y. T.; Ha, T.-J. High-Performance Gas Sensors Based on Single-Wall Carbon Nanotube Random Networks for the Detection of Nitric Oxide down to the Ppb-Level. *Nanoscale* **2019**, *11* (4), 1587–1594.

(17) Li, W.; Geng, X.; Guo, Y.; Rong, J.; Gong, Y.; Wu, L.; Zhang, X.; Li, P.; Xu, J.; Cheng, G.; Sun, M.; Liu, L. Reduced Graphene Oxide Electrically Contacted Graphene Sensor for Highly Sensitive Nitric Oxide Detection. *ACS Nano* **2011**, *5* (9), 6955–6961.

(18) Singh, P.; Hu, L.-L.; Zan, H.-W.; Tseng, T.-Y. Highly Sensitive Nitric Oxide Gas Sensor Based on ZnO-Nanorods Vertical Resistor Operated at Room Temperature. *Nanotechnology* **2019**, *30* (9), 095501.

(19) Wang, S.-H.; Kuo, S.-H.; Shen, C.-Y. A Nitric Oxide Gas Sensor Based on Rayleigh Surface Acoustic Wave Resonator for Room Temperature Operation. *Sensors and Actuators B: Chemical* **2011**, *156* (2), 668–672.

(20) Robinson, J. K.; Bollinger, M. J.; Birks, J. W. Luminol/H2O2 Chemiluminescence Detector for the Analysis of Nitric Oxide in Exhaled Breath. *Anal. Chem.* **1999**, *71* (22), 5131–5136.

(21) Sun, Y.-F.; Liu, S.-B.; Meng, F.-L.; Liu, J.-Y.; Jin, Z.; Kong, L.-T.; Liu, J.-H. Metal Oxide Nanostructures and Their Gas Sensing Properties: A Review. *Sensors* **2012**, *12* (3), 2610–2631.

(22) Wang, Y.; Zhou, Y. Recent Progress on Anti-Humidity Strategies of Chemiresistive Gas Sensors. *Materials (Basel)* **2022**, *15* (24), 8728.

(23) Song, Z.; Huang, Z.; Liu, J.; Hu, Z.; Zhang, J.; Zhang, G.; Yi, F.; Jiang, S.; Lian, J.; Yan, J.; Zang, J.; Liu, H. Fully Stretchable and Humidity-Resistant Quantum Dot Gas Sensors. *ACS Sens.* **2018**, *3* (5), 1048–1055.

(24) Wang, J.; Yang, P.; Wei, X. High-Performance, Room-Temperature, and No-Humidity-Impact Ammonia Sensor Based on Heterogeneous Nickel Oxide and Zinc Oxide Nanocrystals. *ACS Appl. Mater. Interfaces* **2015**, *7* (6), 3816–3824.

(25) Yoon, J.-W.; Kim, J.-S.; Kim, T.-H.; Hong, Y. J.; Kang, Y. C.; Lee, J.-H. A New Strategy for Humidity Independent Oxide Chemiresistors: Dynamic Self-Refreshing

of In2O3 Sensing Surface Assisted by Layer-by-Layer Coated CeO2 Nanoclusters. *Small* **2016**, *12* (31), 4229–4240.

(26) Li, C.; Lohrey, T.; Nguyen, P.-D.; Min, Z.; Tang, Y.; Ge, C.; Sercel, Z. P.; McLeod, E.; Stoltz, B. M.; Su, J. Part-per-Trillion Trace Selective Gas Detection Using Frequency Locked Whispering-Gallery Mode Microtoroids. *ACS Appl. Mater. Interfaces* **2022**, *14* (37), 42430–42440.

(27) Su, J.; Goldberg, A. F.; Stoltz, B. M. Label-Free Detection of Single Nanoparticles and Biological Molecules Using Microtoroid Optical Resonators. *Light Sci Appl* **2016**, *5* (1), e16001–e16001.

(28) Luu, G. T.; Ge, C.; Tang, Y.; Li, K.; Cologna, S. M.; Godwin, A. K.; Burdette, J. E.; Su, J.; Sanchez, L. M. An Integrated Approach to Protein Discovery and Detection from Complex Biofluids. *Molecular & Cellular Proteomics* **2023**, *0* (0).

(29) Lu, T.; Su, T.-T. J.; Vahala, K. J.; Fraser, S. E. Split Frequency Sensing Methods and Systems. US8593638B2, November 26, 2013. https://patents.google.com/patent/US8593638B2/en (accessed 2022-10-13).

(30) Ozgur, E.; Roberts, K. E.; Ozgur, E. O.; Gin, A. N.; Bankhead, J. R.; Wang, Z.; Su, J. Ultrasensitive Detection of Human Chorionic Gonadotropin Using Frequency Locked Microtoroid Optical Resonators. *Anal. Chem.* **2019**, *91* (18), 11872–11878.

(31) Su, J. Label-Free Single Exosome Detection Using Frequency-Locked Microtoroid Optical Resonators. *ACS Photonics* **2015**, *2* (9), 1241–1245.

(32) Su, J. Label-Free Biological and Chemical Sensing Using Whispering Gallery Mode Optical Resonators: Past, Present, and Future. *Sensors* **2017**, *17* (3), 540.

(33) Shao, L.; Jiang, X.-F.; Yu, X.-C.; Li, B.-B.; Clements, W. R.; Vollmer, F.; Wang, W.; Xiao, Y.-F.; Gong, Q. Detection of Single Nanoparticles and Lentiviruses Using Microcavity Resonance Broadening. *Advanced Materials* **2013**, *25* (39), 5616–5620.

(34) Yu, X.-C.; Tang, S.-J.; Liu, W.; Xu, Y.; Gong, Q.; Chen, Y.-L.; Xiao, Y.-F. Single-Molecule Optofluidic Microsensor with Interface Whispering Gallery Modes. *Proceedings of the National Academy of Sciences* **2022**, *119* (6), e2108678119.

(35) AU - Su, J. Label-Free Single Molecule Detection Using Microtoroid Optical Resonators. *JoVE* **2015**, No. 106, e53180.

(36) Hao, S.; Su, J. Noise-Induced Limits of Detection in Frequency Locked Optical Microcavities. *Journal of Lightwave Technology* **2020**, *38* (22), 6393–6401.

(37) Hao, S.; Suebka, S.; Su, J. Single 5-Nm Quantum Dot Detection via Microtoroid Optical Resonator Photothermal Microscopy. arXiv September 14, 2023.

(38) Luu, G. T.; Ge, C.; Tang, Y.; Li, K.; Cologna, S. M.; Godwin, A. K.; Burdette, J. E.; Su, J.; Sanchez, L. M. An Integrated Approach to Protein Discovery and Detection From Complex Biofluids. *Molecular & Cellular Proteomics* **2023**, *22* (7).

(39) Nguyen, P.-D.; Zhang, X.; Su, J. One-Step Controlled Synthesis of Size-Tunable Toroidal Gold Particles for Biochemical Sensing. *ACS Appl. Nano Mater.* **2019**, *2* (12), 7839–7847.

(40) Li, C.; Chen, L.; McLeod, E.; Su, J. Dark Mode Plasmonic Optical Microcavity Biochemical Sensor. *Photon. Res., PRJ* **2019**, *7* (8), 939–947.

(41) Suebka, S.; Nguyen, P.-D.; Gin, A.; Su, J. How Fast It Can Stick: Visualizing Flow Delivery to Microtoroid Biosensors. *ACS Sens.* **2021**, *6* (7), 2700–2708.

(42) Droulia, M.; Anastasaki, A.; Rokotas, A.; Pitsikalis, M.; Paraskevopoulou, P. Statistical Copolymers of Methyl Methacrylate and 2-Methacryloyloxyethyl Ferrocenecarboxylate: Monomer Reactivity Ratios, Thermal and Electrochemical Properties. *Journal of Polymer Science Part A: Polymer Chemistry* **2011**, *49* (14), 3080–3089.

(43) Kim, B. Y.; Ratcliff, E. L.; Armstrong, Neal. R.; Kowalewski, T.; Pyun, J. Ferrocene Functional Polymer Brushes on Indium Tin Oxide via Surface-Initiated Atom Transfer Radical Polymerization. *Langmuir* **2010**, *26* (3), 2083–2092.

(44) Swenson, H.; Stadie, N. P. Langmuir's Theory of Adsorption: A Centennial Review. *Langmuir* **2019**, *35* (16), 5409–5426.

(45) Tawade, B. V.; Apata, I. E.; Pradhan, N.; Karim, A.; Raghavan, D. Recent Advances in the Synthesis of Polymer-Grafted Low-K and High-K Nanoparticles for Dielectric and Electronic Applications. *Molecules* **2021**, *26* (10), 2942.

(46) Yan, J.; Bockstaller, M. R.; Matyjaszewski, K. Brush-Modified Materials: Control of Molecular Architecture, Assembly Behavior, Properties and Applications. *Progress in Polymer Science* **2020**, *100*, 101180.

(47) N'Diaye, M.; Pascaretti-Grizon, F.; Massin, P.; Baslé, M. F.; Chappard, D. Water Absorption of Poly(Methyl Methacrylate) Measured by Vertical Interference Microscopy. *Langmuir* **2012**, *28* (31), 11609–11614.

(48) Lehnert, N.; Kim, E.; Dong, H. T.; Harland, J. B.; Hunt, A. P.; Manickas, E. C.; Oakley, K. M.; Pham, J.; Reed, G. C.; Alfaro, V. S. The Biologically Relevant

Coordination Chemistry of Iron and Nitric Oxide: Electronic Structure and Reactivity. *Chem. Rev.* **2021**, *121* (24), 14682–14905.

(49) Enemark, J. H.; Feltham, R. D. Principles of Structure, Bonding, and Reactivity for Metal Nitrosyl Complexes. *Coordination Chemistry Reviews* **1974**, *13* (4), 339–406.

(50) O'Connor, J. M.; Casey, C. P. Ring-Slippage Chemistry of Transition Metal Cyclopentadienyl and Indenyl Complexes. *Chem. Rev.* **1987**, *87* (2), 307–318.

(51) Mary Vergheese, T.; Berchmans, S. Selective NO Reduction Using Blue Ferrocenyl Cation. *Electrochimica Acta* **2006**, *52* (2), 567–574.

(52) Mathi, S.; Gupta, P. K.; Kumar, R.; Nagarale, R. K.; Sharma, A. Ferrocenium Ion Confinement in Polyelectrolyte for Electrochemical Nitric Oxide Sensor. *ChemistrySelect* **2019**, *4* (13), 3833–3840.

(53) Sudhesh, P.; T., B.; Berchmans, S. Insights into Ferrocene-Mediated Nitric Oxide Sensing – Elucidation of Mechanism and Isolation of Intermediate. *Electrochimica Acta* **2016**, *210*, 321–327.

(54) Wang, S.-H.; Shen, C.-Y.; Su, J.-M.; Chang, S.-W. A Room Temperature Nitric Oxide Gas Sensor Based on a Copper-Ion-Doped Polyaniline/Tungsten Oxide Nanocomposite. *Sensors* **2015**, *15* (4), 7084–7095.

(55) Smith, A. A. A.; Zuwala, K.; Pilgram, O.; Johansen, K. S.; Tolstrup, M.; Dagnæs-Hansen, F.; Zelikin, A. N. Albumin–Polymer–Drug Conjugates: Long Circulating, High Payload Drug Delivery Vehicles. *ACS Macro Lett.* **2016**, *5* (10), 1089–1094.

(56) Wang, H.; Chen, Z.; Xin, L.; Cui, J.; Zhao, S.; Yan, Y. Synthesis of Pyrene-Capped Polystyrene by Free Radical Polymerization and Its Application in Direct

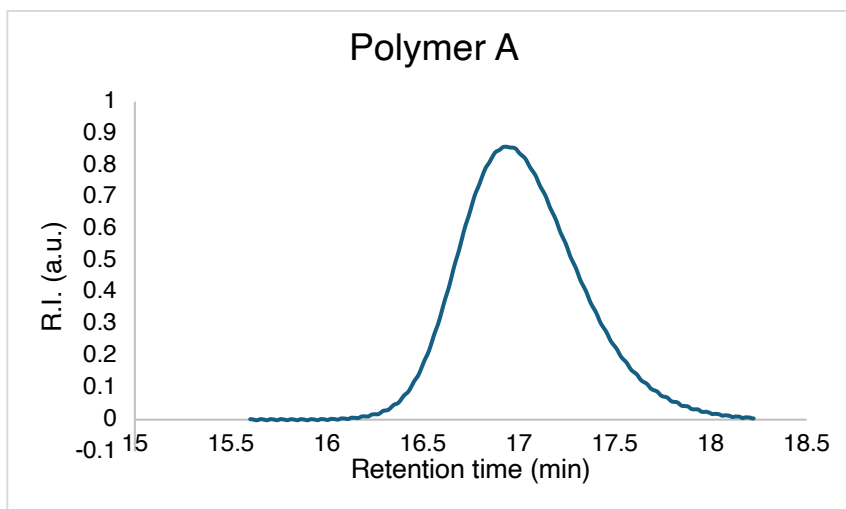Exfoliation of Graphite into Graphene Nanosheets. *Journal of Polymer Science Part A: Polymer Chemistry* **2015**, *53* (18), 2175–2185.

APPENDIX 3

Spectra Relevant to Chapter 4: Low Part-Per-Trillion, Humidity

Resistant Detection of Nitric Oxide Using Microtoroid Optical
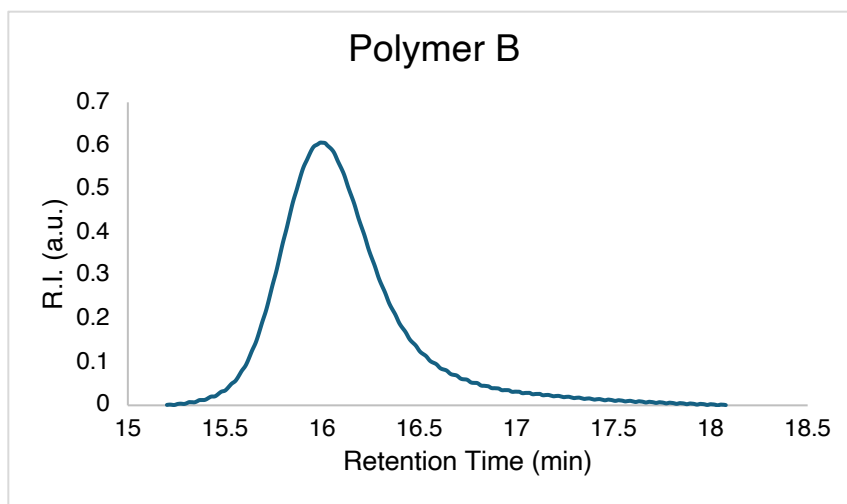
Resonators

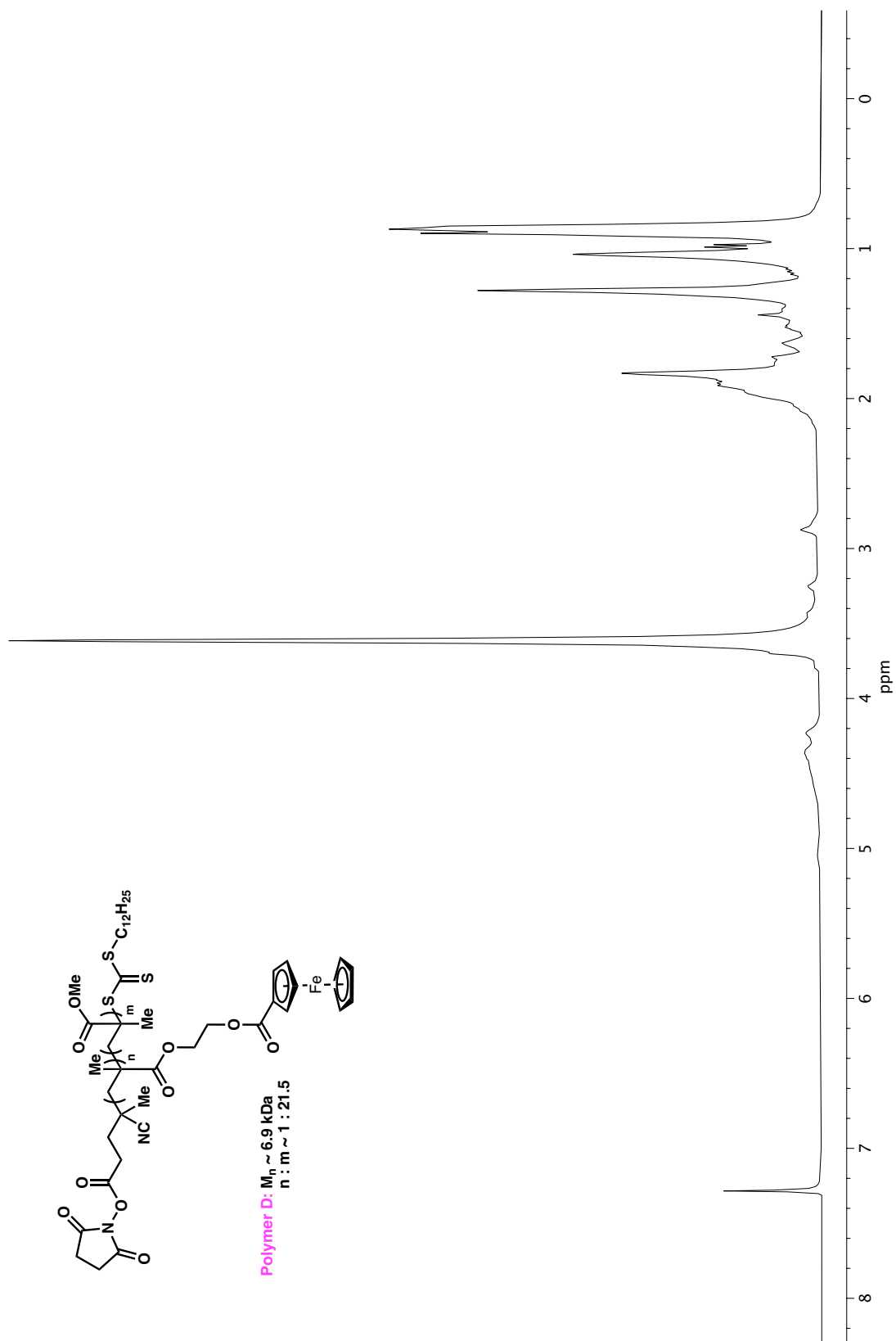***Figure A3.1*** ^{1}H NMR (400 MHz, CDCl$_3$) of Polymer A.

Figure A3.2 SEC trace of Polymer A.

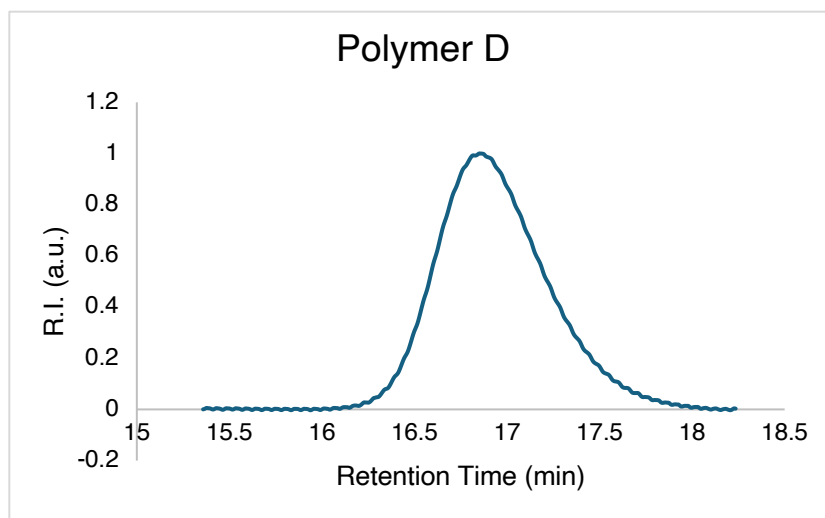***Figure A3.3*** ^{1}H NMR (400 MHz, CDCl$_3$) of Polymer B.

Figure A3.4 SEC trace of Polymer B.
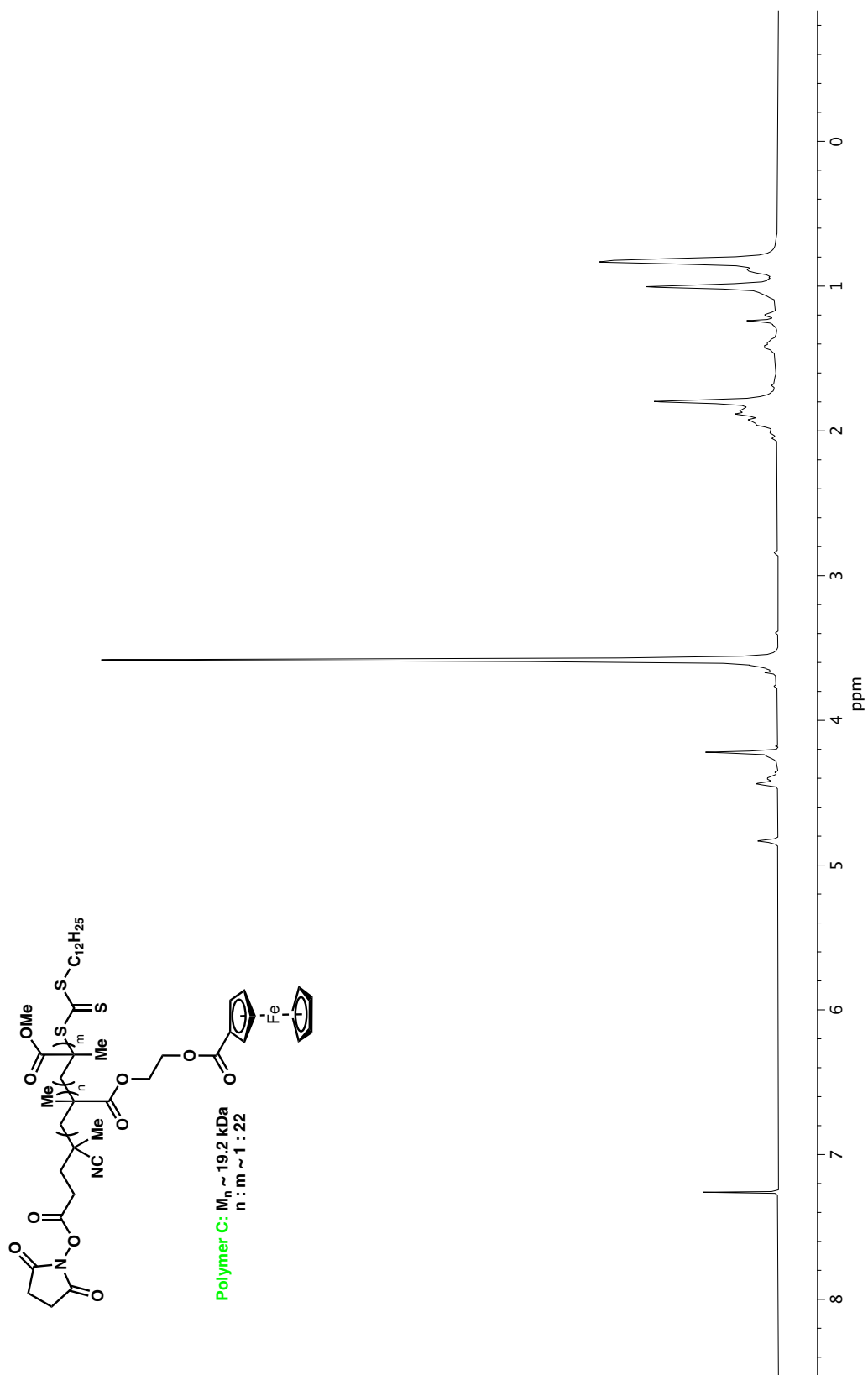
Figure A3.5 ^{1}H NMR (400 MHz, CDCl$_3$) of Polymer C.
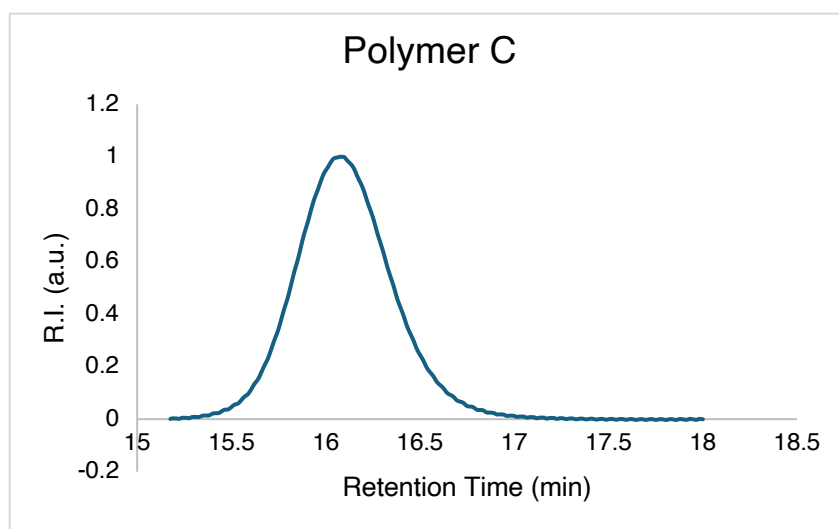
Figure A3.6 SEC trace of Polymer C.

Figure A3.7 ^{1}H NMR (400 MHz, CDCl$_3$) of Polymer D.
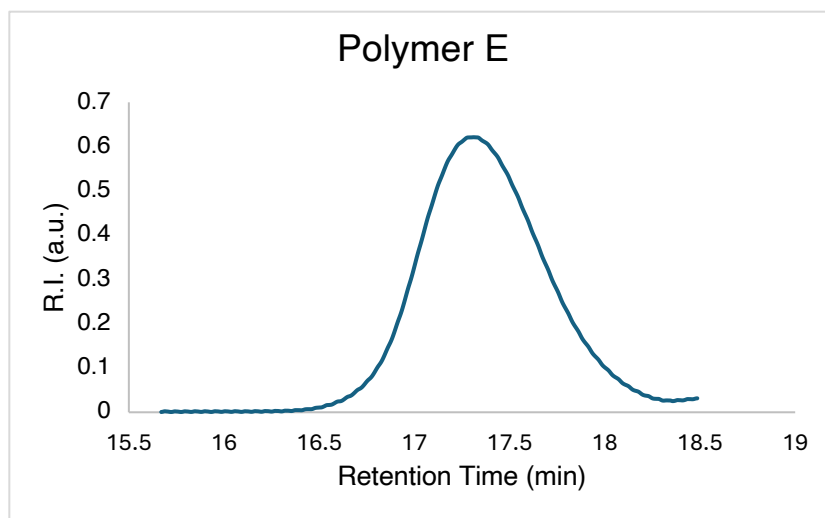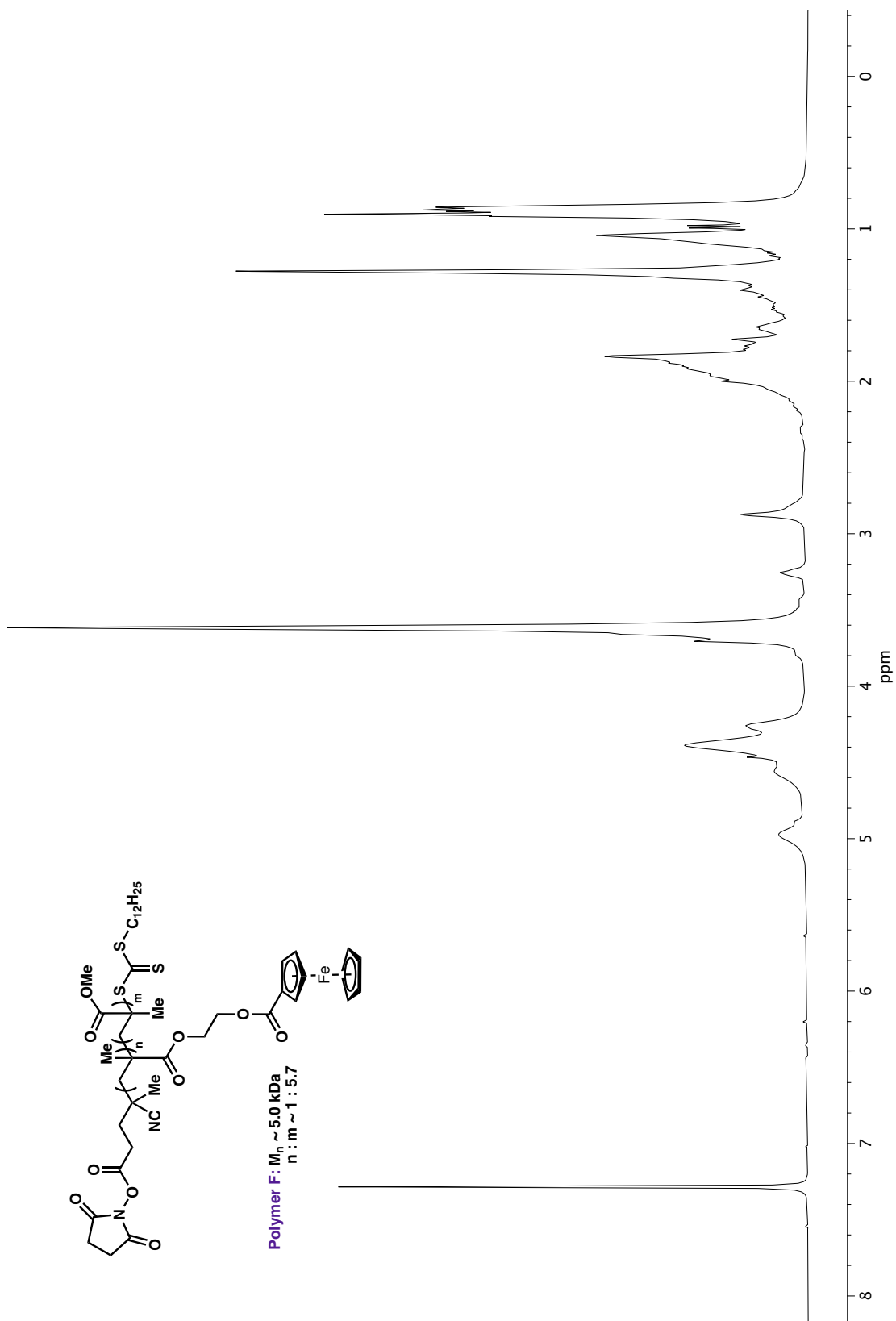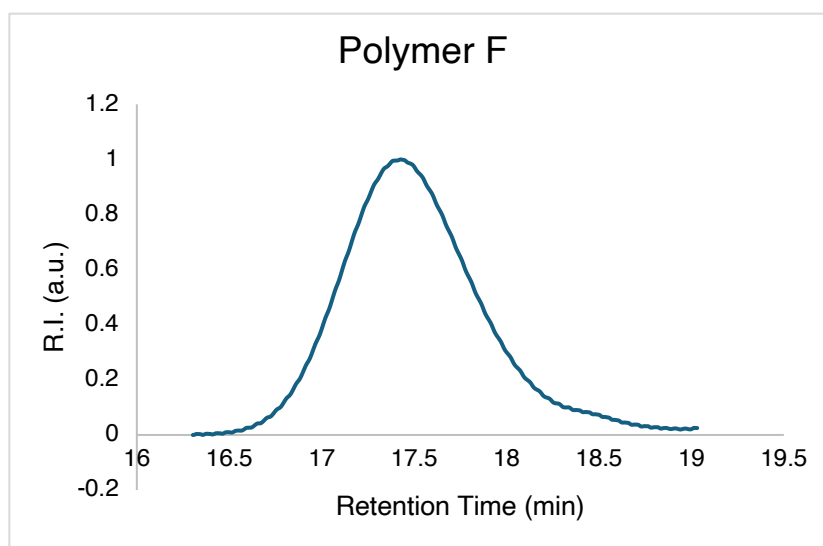
Figure A3.8 SEC trace of Polymer D.
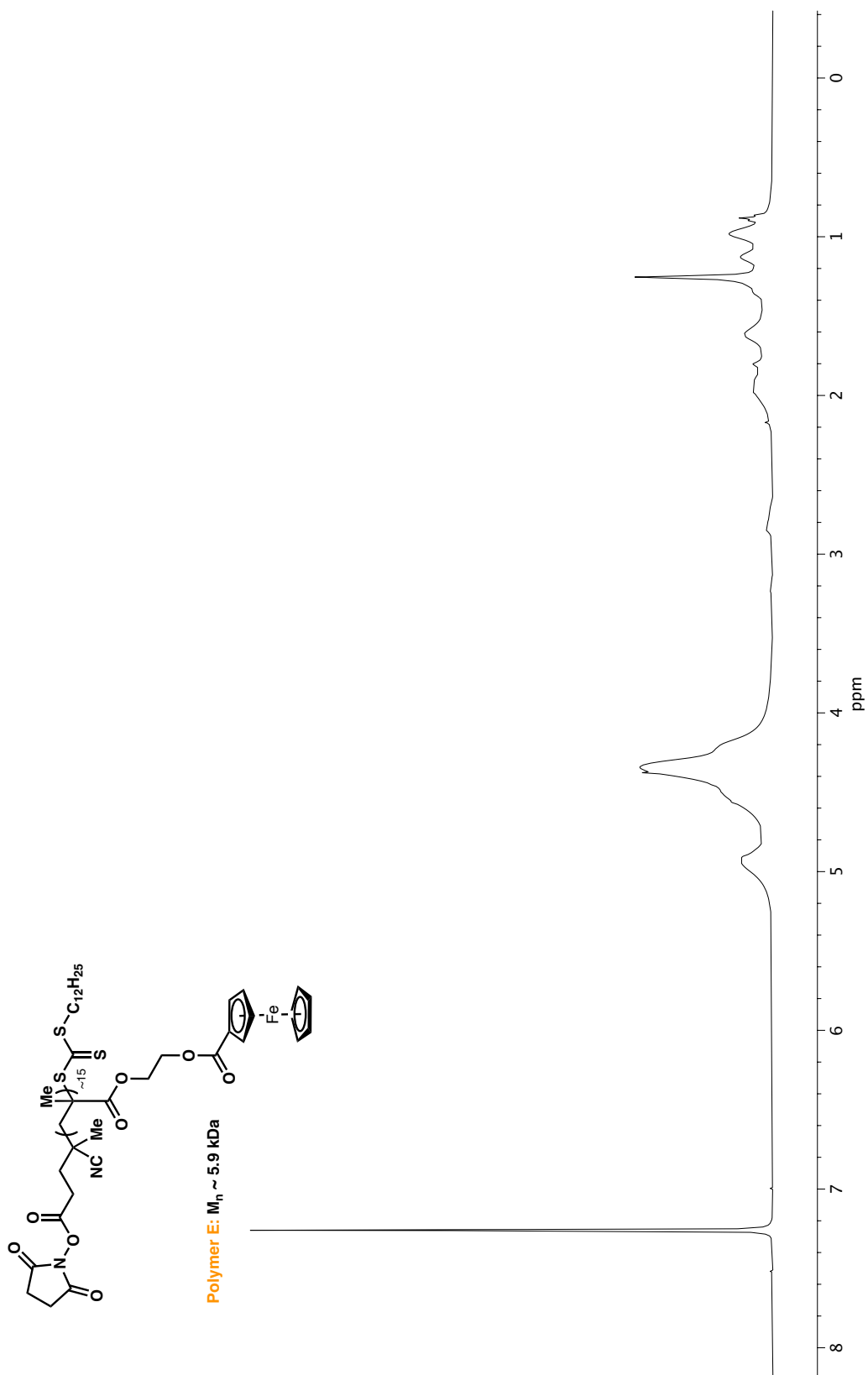
Figure A3.9 ^{1}H NMR (400 MHz, CDCl$_3$) of Polymer E.

Figure A3.10 SEC trace of Polymer E.

Figure A3.11 ^{1}H NMR (400 MHz, CDCl$_3$) of Polymer F.

Figure A3.12 SEC trace of Polymer F.

ABOUT THE AUTHOR

Allison (Ally) Michelle Stanko was born in Buffalo, NY on March 1st, 1997. She is the daughter of Susan and Michael Stanko, and the younger sister of Dr. Elizabeth Stanko. Ally was raised in Grand Island, NY, and she attended high school at Nardin Academy in downtown Buffalo. In her teenage years, Ally was a competitive figure skater on the regional and state level, and she is a United States Figure Skating Association Gold Medalist.

After graduating from Nardin, Ally moved to Rochester, NY, where she originally began her studies in Biomedical Engineering at the University of Rochester. After discovering her love for organic chemistry during her sophomore year, she became a Chemistry major, eventually earning her Bachelor of Science in Chemistry in 2019. During her time at the University of Rochester, she conducted research in the lab of Professor Alison Frontier, where she worked on the application of the Halo-Prins and Halo-Nazarov reactions to the total synthesis of Rocaglamide. Her memorable experience in the Frontier lab fostered her love of experimental work and inspired her to pursue a PhD in Chemistry.

In 2019, Ally moved to Pasadena, California, to pursue her PhD at the California Institute of Technology. She joined the lab of Professor Sarah Reisman, where she worked on the development of a novel palladium-catalyzed cascade cyclization. In her third year, Ally departed the Reisman group and joined the laboratory of Professor Brian Stoltz. During her time in the Stoltz group, Ally worked on projects in the areas of asymmetric transition metal catalysis and polymer synthesis. Following graduation, Ally will begin her career as a Scientist on the Platform Chemistry team at Terray Therapeutics in Monrovia, CA.

Ally currently lives in Altadena, CA, with her fiancé Alexander Ferreira and their dog, Astra. Her hobbies include rock climbing, camping, skiing, hula hooping, and rollerskating.